(PRE-)IONIC AND/OR CHIRAL ALKENE AND ALKYNE METATHESIS CATALYSTS OF GROUP 6

Von der Fakultät Chemie der Universität Stuttgart

zur Erlangung der Würde eines

Doktors der Naturwissenschaften (Dr. rer. nat.)

genehmigte Abhandlung

vorgelegt von

Iris Elser

aus Stuttgart

Hauptberichter:	Prof. Dr. M. R. Buchmeiser
1. Mitberichter:	Prof. Dr. B. Plietker
2. Mitberichter:	Prof. Dr. D. Gudat

Tag der mündlichen Prüfung: 05.09.2018

Institut für Polymerchemie der Universität Stuttgart

2018

©1993 Waterson Dist. by Universal Press Syndicate, Calvin and Hobbes, December 29, 1993, Bill Waterson.

This work was carried out from April 2014 to June 2018 at the Institute of Polymer Chemistry (University of Stuttgart, Germany) under the supervision of Prof. Dr. M. R. Buchmeiser.

Erklärung über die Eigenständigkeit der Dissertation

Ich versichere, dass ich die vorliegende Arbeit mit dem Titel

Ionische und/oder chirale Alken- und Alkin-Metathese Katalysatoren der Gruppe 6 und deren Präkursoren

selbständig verfasst und keine anderen als die angegebenen Quellen und Hilfsmittel benutzt habe; aus fremden Quellen entnommene Passagen und Gedanken sind als solche kenntlich gemacht.

Declaration of Authorship

I hereby certify that the dissertation entitled

(Pre-)Ionic and/or Chiral Alkene and Alkyne Metathesis Catalysts of Group 6

is entirely my own work, unless indicated otherwise. Passages and ideas from other sources have been clearly indicated.

Name/Name: Iris Elser

Unterschrift/Signed: _____

Datum/Date: _____

DANKE

Dank geht zunächst an Herrn Prof. Dr. M. R. Buchmeiser für die Übernahme der Betreuung meiner Doktorarbeit, für die großartigen Arbeitsbedingungen sowie für die interessanten Themen, und die Unterstützung beim „character-building“. Vor allem auch für die Teilnahme am ISOM und an der Katalytikertagung in Weimar, sowie für die stets zeitnahe Unterstützung und Korrektur bei der Anfertigung von Publikationen und dieser Doktorarbeit. Auch Herrn Prof. Dr. B. Plietker und Herrn Prof. Dr. D. Gudat sei für die Übernahme der Gutachtertätigkeit und des Prüfungsvorsitzes gedankt.

Dank geht ebenfalls an Dongren Wang, der stets mit Rat und Tat zur Seite stand und ohne den die meisten Geräte und damit auch der Rest schon lange nicht mehr laufen würden.

Danken möchte ich an dieser Stelle auch Dr. Wolfgang Frey und Dr. Klaus Wurst für das Messen von Kristallstrukturen, sowie Barbara Förtsch für das Messen unzähliger Elementaranalysen und der Analytik-Abteilung des Instituts für Organische Chemie für die Messung von Massespektren.

Dank geht selbstverständlich an alle ehemaligen und gegenwärtigen Mitglieder des Arbeitskreises Buchmeiser. Besonderer Dank geht hier an:

Patrick, König des schlechten Humors, für technischen und moralischen Support, oft auch in Kombination. Kai M. für alles und im Besonderen für Erheiterung in Sachen Isoamylacetat. Jonny (den gar nicht mehr so Erlauchten) für entspannende Boulder-Abende und heiße Zitrone. Meliten für gute Gespräche und immer lustige Abende an Berliner Luft. Geri for being so incredibly geri and a lot of fun in Stuttgart and Budapest. Suman, for many evenings with non-spicy indian food, mango lassi and inputs concerning chemistry. Mathis (die Gabel Gottes), Phil (1 Pommes-1€), Julian (Tschorle) und Kai H. (den Pflanzenretter) für interessante Konversationen zu unaussprechlichen Themen, die oft eine willkommene Abwechslung im Büro waren. Max K. für großartige und problemlose Zusammenarbeit an der Glove Box und am Paper sowie für das Bereiten fragwürdiger musikalischer Erlebnisse mit Margarete. Flixi für „wiiiirkliiiich“ überragende Unterstützung in Sachen Silika. Roman, für Support in chemischen Fragen, vor allem wenn wirklich gar nichts mehr ging, das bereitwillige Teilen von Chemikalien und für den Titel meines zukünftigen Buches „Fifty Shades of Brown-Mein erstes Jahr als Doktorand“. Elx und Felx für Spiel und Spaß in der Kaffeepause. Mike (den Erretter der Glove Box und der Pumpen) für die Gelegenheit dem Rekord im Pizzaessen beiwohnen zu dürfen. Tim für schnelle und kompetente Hilfe bei der BET. Erna für Spaß mit fluoreszierenden Fasern und gute Unterhaltungen. Sir Raccoon (moralischer Kompass) für gemeinsames kranen in Sonne und Sonne sowie für stets erheiternde gemeinsame Unternehmungen wie zum Beispiel den Besuch im Mineralbad Leuze. Die Gesamtheit der Muhwi+shisha-Crew für sprachlich stets korrekte Unterhaltung. Die Kaffeemaschine, ohne deren immerwährende Unterstützung so manches Paper zu spät abgeliefert worden wäre.

Auch die von mir betreuten Bachelorstudenten Andi H., Benni, Chris, Leonard und Andi F. seien dankend erwähnt.

Isa, treue Begleiterin seit dem ersten Semester, ohne Mensa-Donnerstage und Not-Kaffee wäre es vermutlich nichts geworden. Der Blocksberg steht.

Danke an Simon, mit dessen Unterstützung alles läuft wie geschnürt, sowie an Shan, Marius, Kai Y., Kai B., Jörg, Axel und Dana (!) für Ausgleich bei Essen, Sport, Bang, Saboteur, Wizard, Urlaub und Pyjamapartys.

Danke an Mama, Papa, Anne, Ceasar, Baf und Schär für Zufluchtsorte mit gutem Essen, Unterhaltungen und vor allem ausdauernder Unterstützung!

CONTENTS

1 LIST OF ABBREVIATIONS

1.1 GENERAL

$\%V_{bur}$	Buried Volume in Percentage
1,2-DCE	1,2-Dichloroethane
5-Me-Cl_2	4,5-Cl_2-1,3-Me_2-imidazol-2-ylidene
ACM	Alkyne Cross-Metathesis
Ad	Adamantyl
ADIMET	Acyclic Diyne Metathesis
ADMET	Acyclic Diene Metathesis
Ar	Aryl, Aromatic Substituent
ARCM	Asymmetric Ring-Closing Metathesis
AROM	Asymmetric Ring-Opening Metathesis
ATR	Attenuated Total Reflection (IR mode)
$B(Ar^F)_4$	Tetrakis(3,5-trifluoromethylphenyl)borate
BINOL	1,1´-Binaphth-2,2´-ol
Bitet	3,3´-Dibromo-2´-(*tert*-butyldimethylsilyloxy)-5,5´,6,6´,7,7´,8,8´-octahydro-1,1´binaphth-2-ol
CAAC	Cyclic Alkyl Amino Carbene
CCDC	Cambridge Crystallographic Data Centre
CM	Cross-Metathesis
DCM	Dichloromethane
DCPD	Dicyclopentadiene
DFT	Density Functional Theory
Dipp	2,6-Diisopropylphenyl
DME	1,2-Dimethoxyethane
DMSO	Dimethylsulfoxide
DSC	Differential Scanning Calorimetry
E_{dim}	Dimerization Energy
$E_{fit,dim}$	Calculated Dimerization Energy
equiv.	Equivalents
ESI	Electrospray Ionization
E_{S-T}	Energy Difference between Singulet and Triplet State
Et	Ethyl, C_2H_5
et al.	et alia

GC	Gas Chromatography
GC-MS	Gas Chromatography coupled with Mass Spectrometry
GPC	Gel Permeation Chromatography
HIPTOH	Hexaisopropylterphenol, 2,6-(2,4,6-triisopropylphenyl)phenol
HM	Homometathesis
HMTOH	Hexamethylterphenol, 2,6-(2,4,6-trimethylphenyl)phenol
HOMO	Highest Occupied Molecular Orbital
HPLC	High Performance Liquid Chromatography
HRMS	High Resolution Mass Spectrometry
ICP-OES	Inductively Coupled Plasma-Optical Emission Spectrometry
ICy	1,3-Dicyclohexylimidazol-2-ylidene
IMes	1,3-Dimesitylimidazol-2-ylidene
$IMesH_2$	1,3-Dimesitylimidazolin-2-ylidene
iPr	Isopropyl
IR	Infrared
it	*Isotactic*
I*t*Bu	1,3-Di-*tert*-butylimidazol-2-ylidene
J	Coupling Constant
KHMDS	Potassium Hexamethyldisilazid
LUMO	Lowest Unoccupied Molecular Orbital
MAC	Mono Alkoxide Chloride
MAP	Mono Alkoxide Pyrrolide
MCB	Metallacyclobutane
Me	Methyl, CH_3
MeCN	Acetonitrile
Mes	Mesityl, 2,4,6-Trimethylphenyl
MIC	Mesoionic Carbene
MMC	Macromonocyclization
M_n	Number-average molecular weight
m/z	Mass-to-charge ratio
MS	Mass Spectrometry
NCAM	Nitrile Cross Alkyne Metathesis
NHC	*N*-Heterocyclic Carbene
NMR	Nuclear Magnetic Resonance
Np	Neopentyl
OHIPT	Hexaisopropylterphenoxide, 2,6-(2,4,6-triisopropylphenyl)phenolate

OHMT	Hexamethylterphenoxide, 2,6-(2,4,6-trimethylphenyl)phenolate
PDI	Polydispersity Index
PG	Protecting Group
Ph	Phenyl, C_6H_5
Picolyl	2-Pyridylmethyl
ppm	Parts per Million
Py	Pyridine
Pyr	Pyrrole
RCAM	Ring-Closing Alkyne Metathesis
RCM	Ring-Closing Metathesis
RIM	Reaction Injection Molding
rt	Room temperature
ROAMP	Ring-Opening Alkyne Metathesis Polymerization
ROCM	Ring-Opening Cross-Metathesis
ROMP	Ring-Opening Metathesis Polymerization
SHOP	*Shell* Higher Olefin Process
SILP	Supported Ionic Liquid Phase
SP	Square Pyramidal
st	*Syndiotactic*
TAM	Terminal Alkyne Metathesis
TBP	Trigonal Bipyramidal
*t*Bu	*Tert*-Butyl, 2-Methylpropyl
T_c	Coalescence Temperature
TEP	*Tolmans* Electronic Parameter
THF	Tetrahydrofuran
TMS	Trimethylsilyl
TON	Turnover Number
TRAM	Terminal Ring-Closing Alkyne Metathesis
V_{bur}	Buried Volume
VE	Valence Electrons
V/V	Volume-to-volume ratio
WCA	Weakly Coordinating Anion

1.2 UNITS

Å	Angstrom, 10^{-10} m
°C	Degree Celsius

g	Gram
h	Hour
Hz	Hertz
L	Liter
m	Meter
min	Minute
mol	Mole
s	Second

1.3 PREFIXES FOR SI-UNITS

p	Pico, 10^{-12}
n	Nano, 10^{-9}
µ	Micro, 10^{-6}
m	Milli, 10^{-3}
k	Kilo, 10^{3}
M	Mega, 10^{6}
G	Giga, 10^{9}

2 OBJECTIVE

Organometallic catalysts have become ubiquitous in chemistry and enable highly sophisticated chemical transformations. Metal-catalyzed carbon-carbon and carbon-heteroatom bond formation[1] and *CH*-activation[2] provide access to a multitude of organic compounds.[3] Organometal-catalyst-based industrial applications further highlight the impact on everyday life. Prominent examples are the *Shell Higher Olefin Process* (*SHOP*, production of linear α-olefins), the *Wacker* process (transformation of ethylene to acetaldehyde) or the synthesis of tons of poly(ethylene) and poly(propylene) by *Ziegler-Natta* catalysts.[4] Catalyst development has come a long way since the 1950s, especially due to the elucidation of mechanisms and active species, which were rewarded by several Nobel Prices (1963: *K. Ziegler*, *G. Natta*; 1973: *E. O. Fischer*, *G. Wilkinson*; 2001: *K. B. Sharpless, W. Knowles*, *R. Noyori*; 2005: *R. R. Schrock*, *R. H. Grubbs*, Y. Chauvin; 2010: *R. F. Heck*, *E. Negishi*, *A. Suzuki*).[5] However, many issues remain to be addressed. Catalyst stability, catalyst removal from products, catalyst costs, catalyst recycling, reduction of catalyst loadings, and the synthesis of catalysts for especially challenging substrates and applications (functional group tolerance, stereoselectivity, latency) represent constant challenges to the organometallic chemist. The aim of this work was to contribute solutions to some of those issues in the prominent field of olefin and alkyne metathesis[4b,5a,6] by the synthesis and application of new molybdenum- and tungsten-based alkene and alkyne complexes, as well as by mechanistic studies. The work presented herein builds on previous publications and the knowledge included therein, outlined in the theoretical introduction, by transferring well-established methods to the occurring query. Catalyst removal and catalyst recycling in molybdenum- and tungsten-based olefin metathesis were approached by exploitation of a biphasic reaction setup and the synthesis of the required catalysts. Catalyst stability, closely entangled with the reduction of catalyst loadings and the synthesis of latent catalysts, were supposed to be addressed by profiting from stabilization through the chelate effect[7] and strong σ-donor ligands by the introduction of bidentate ligands and *N*-heterocyclic carbenes (NHCs)[8]. To enrich the library of stereoselective molybdenum- and tungsten-based olefin metathesis catalysts,[6a,9] the development of synthesis routes to chiral molybdenum imido alkylidene NHC complexes was pursued. Furthermore, investigations of structure-productivity relations in novel molybdenum trisalkoxy alkylidyne NHC complexes[10] in model alkyne metathesis reactions were envisioned to gain valuable insights on the active species and the activation mechanisms.

3 ZUSAMMENFASSUNG

Seit ihren Anfängen in den 1950er Jahren hat sich die Organometall-Katalyse stark weiterentwickelt. Dennoch bestehen noch diverse Herausforderungen. Die Katalysatorstabilität, die Stabilität der aktiven Spezies, ein breites Substratspektrum (z.B. bezüglich funktioneller Gruppen), Stereoselektivität und die Verringerung der Katalysatormenge sowie die Rückgewinnung des Katalysatorsystems stellen nur einige dieser Herausforderungen dar. Die Olefin- und Alkinmetathese repräsentieren die Klasse der Organometall-katalysierten Reaktionen.[6,9b,11] Sowohl die organische als auch die Polymerchemie profitieren von der Vielfalt der durch die Metathese zugänglichen chemischen Strukturen.[11d,12] Hierbei stützt sich die breite Anwendbarkeit der Olefin- und Alkinmetathese vor allem auf eine gut aufgestellte Katalysatorbibliothek. Sowohl Ruthenium-, als auch Molybdän- und Wolfram-basierte Katalysatorsysteme ermöglichen die Synthese komplexer organischer Moleküle und Polymere. Ziel dieser Arbeit ist es, zu dieser Katalysatorbibliothek beizutragen um neue Anwendungen für Olefin- und Alkinmetathese zu ermöglichen und einige der oben genannten Herausforderungen zu adressieren.

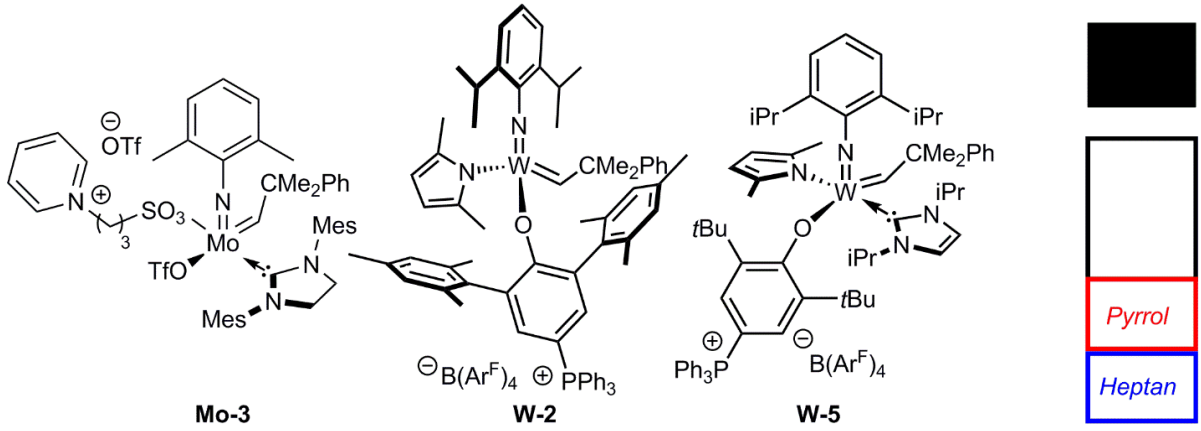

Abbildung 1: Beispielhafte Molybdän- und Wolfram-basierte Katalysatorsysteme **Mo-3**, **W-2** und **W-5** mit Betainliganden. Schematische Darstellung des zweiphasigen Lösemittelsystems, bestehend aus Heptan und Pyrrol. ($B(Ar^F)_4$ = Tetrakis(3,5-trifluormethylphenyl)borat).

Eine Möglichkeit zur Vermeidung von Katalysatorrückständen in Olefinmetathese-Produkten ist die Verwendung eines zweiphasigen Lösemittelsystems.[13] In dieser Arbeit wird die Synthese der ersten Molybdän- und Wolfram-basierten Olefinmetathese-Katalysatoren mit Betainliganden und ihre Anwendung in der Zweiphasen-Katalyse beschrieben.[14] Kommerziell erhältliche, sowie neu entwickelte alkoxid-, sulfonat- und aminbasierte Betainliganden kommen zum Einsatz. Sowohl die Klasse der Mono Alkoxid Pyrrolid (MAP)-Katalysatoren als auch die der Molybdän und Wolfram Imido Alkyliden Komplexe mit *N*-heterozyklischen Carbenen (NHC) sind vertreten (beispielhafte Katalysatoren **Mo-3**, **W-2** und **W-5**, Abbildung

1). Eine Zweiphasenkatalyse in Mischungen aus Pyrrol und Heptan (Lösemittelsystem entwickelt durch *Roman Schowner*[15]) ermöglichte die Synthese metallfreier Olefinmetathese-Produkte (<2 ppm) durch einfaches Abtrennen der polaren Katalysatorphase. Die erreichten Aktivitäten waren vergleichbar mit den in herkömmlichen Lösemitteln beobachteten Werten. Zudem konnten Molybdän Imido Alkyliden NHC Komplexe mit einer kationischen Ladung am Metall und dem schwach koordinierenden $B(Ar^F)_4$-Anion erfolgreich in der Zweiphasenkatalyse verwendet werden ($B(Ar^F)_4$ = Tetrakis(3,5-trifluormethylphenyl)borat).

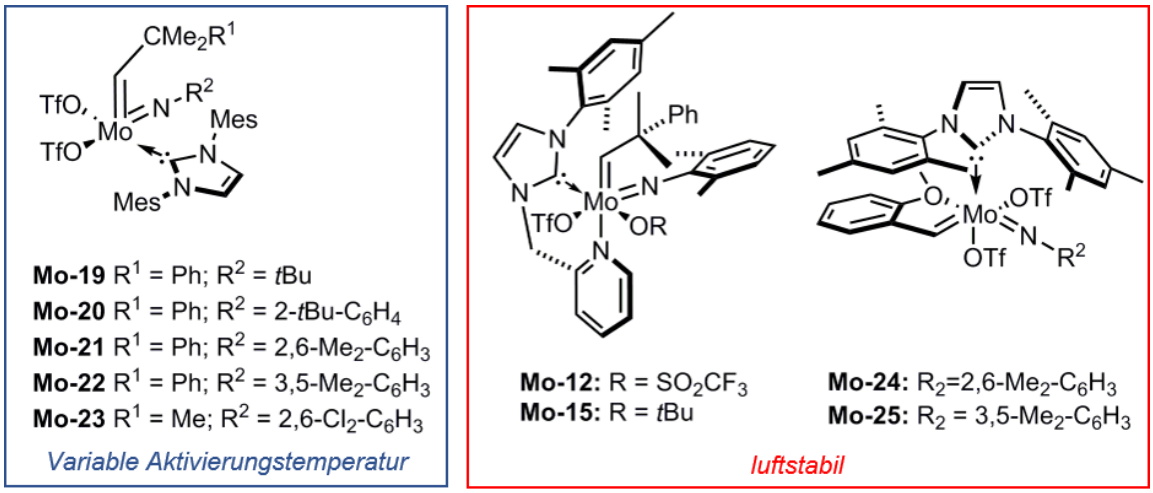

Abbildung 2: Fünf- und sechsfach koordinierte Molybdän Imido Alkyliden NHC Komplexe für die latente ringöffnende Metathesepolymerisation (ROMP) von Dizyklopentadien (DCPD).

Durch die Verwendung eines chelatisierenden NHCs (*N*-Mesityl-*N*-(2-picolyl)-imidazol-2-yliden) mit einer zusätzlichen neutralen Donoreinheit sollte die Stabilität von vor allem kationischen Molybdän Imido Alkyliden NHC Komplexen erhöht werden. Hierbei sollten die Stabilisierung durch den Chelateffekt und die Möglichkeit eines hemilabilen Verhaltens genutzt werden.[16] Die resultierenden neutralen oktaedrischen und fünffach koordinierten kationischen Komplexe zeigten zwar eine hohe Stabilität, jedoch nur eine zu vernachlässigende Aktivität in der Ringschlussmetathese (RCM) von 1,7-Oktadien. Jedoch konnten die oktaedrischen Komplexe **Mo-12** und **Mo-15** in der ringöffnenden Metathesepolymerisation (ROMP) von Dizyklopentadien (DCPD) verwendet werden. Die Synthese von Poly(DCPD) ist ein industriell relevanter Zweig der Olefinmetathese.[4b,4c] Die Beobachtung, dass **Mo-12** und **Mo-15** als Feststoffe für einen Zeitraum von mindestens zwölf Stunden Stabilität an Luft aufweisen, führte zur Synthese von Molybdän Imido Alkyliden NHC Komplexen mit einer chelatisierenden Alkyliden-Einheit (**Mo-24**, **Mo-25**, Abbildung 2).[17] Aufbauend auf vorhergehenden Arbeiten[17-18] wurden fünf- (**Mo-19**-**Mo-23**, Abbildung 2, blau) und sechsfach koordinierte (**Mo-12**, **Mo-15**, **Mo-24**, **Mo-25**, Abbildung 2, rot) Molybdän Imido Alkyliden NHC Komplexe bezüglich ihres Verhaltens in der latenten ROMP von DCPD verglichen. Analyse der Katalysator-DCPD-Mischungen erfolgte hier mittels dynamischer

Differenzkalorimetrie (DSC). Poly(DCPD) mit variierenden Glasübergangstemperaturen T_g und Vernetzungsgraden war zugänglich. Je nach Wahl der Liganden waren Aktivierungstemperaturen T_{onset} von 65 bis 140°C zugänglich. Auch **Mo-24** und **Mo-25** waren als Feststoffe für mindestens zwölf Stunden luftstabil, vergleichbar mit strukturell verwandten Ruthenium-basierten *Grubbs Hoveyda* Katalysatoren. Im Gegensatz zu bereits publizierten luftstabilen Katalysatoren,[19] können die Katalysatorsysteme rein thermisch aktiviert werden. Ein Zusatz von Additiven ist nicht nötig.

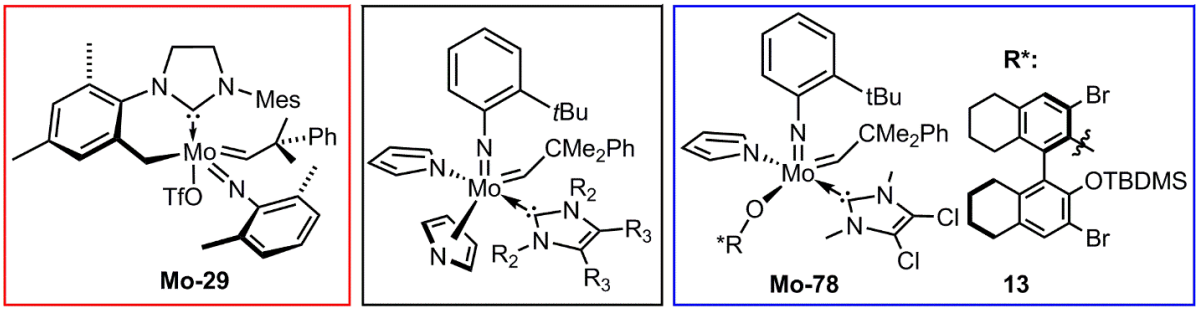

Abbildung 3: Wichtige Intermediate in der Entwicklung verschiedener Syntheserouten für chirale Molybdän Imido Alkyliden NHC Komplexe. Isolierter *CH*-aktivierter Komplex **Mo-29** (rot). Bispyrrolid NHC Komplexe als Präkursoren für chirale Komplexe (schwarz). Isolierter chiraler Molybdän Imido Alkyliden NHC Komplex **Mo-78** (blau).

Des Weiteren wurde die Entwicklung von Syntheserouten für chirale Molybdän Imido Alkyliden NHC Komplexe angestrebt. Ziel war es, die Bibliothek chiraler Ruthenium-, Wolfram- und Molybdän-basierter stereoselektiver Katalysatoren zu erweitern.[9b,20] Basierend auf mechanistischen Überlegungen der Gruppen *Eisenstein* und *Copéret*[21] wurde die stereochemische Information über den Alkoxid-Liganden eingeführt. Unzählige Reaktionen zwischen 3,3´-Dibromo-2´-(*tert*-butyldimethylsilyloxy)-5,5´,6,6´,7,7´,8,8´-octahydro-1,1´-binaphth-2-olat (**13**) und diversen Molybdän Imido Alkyliden NHC Komplexen zeigten, dass *CH*-Aktivierung eine Synthese der gewünschten Komplexe erschwerte. Ein *CH*-aktivierter Komplex Mo(*N*-2,6-Me_2-C_6H_3)(CHCMe_2Ph)(1-mesityl-3-(C_9H_{10})-imidazol-2-yliden)(OTf) (**Mo-29**, Abbildung 3, rot) mit einem *C*-chelatisierenden NHC konnte isoliert und die einzigartige Struktur mittels Einkristall-Röntgen-Strukturanalyse verifiziert werden.[16] Sowohl der sterische Anspruch, als auch die Basizität der chiralen Alkoxide wurden als problematisch identifiziert. Daher wurde eine alternative Syntheseroute entwickelt. Molybdän Imido Alkyliden Bispyrrolid Komplexe bieten die Möglichkeit Alkoxid-Liganden durch einfaches Protonieren eines Pyrrolid-Liganden in ihrer protonierten Form einzuführen.[22] Die Bildung basischer Alkoxide und die daraus resultierende *CH*-Aktivierung oder das Deprotonieren der aziden *CH*-Alkyliden-Bindung sollten somit vermieden werden. Daher wurden Molybdän Imido Alkyliden NHC Bispyrrolid Komplexe Mo(*N*-2-*t*Bu-C_6H_3)(CHCMe_2Ph)(NC_4H_4)$_2$(NHC) und ihre

kationischen Analoga [Mo(*N*-2-*t*Bu-C_6H_3)(CHCMe$_2$Ph)(NC_4H_4)(NHC)][B(Ar^F)$_4$] mit diversen Carbenen (NHC = 1,3-Diisopropylimidazol-2-yliden, 4,5-Dichloro-1,3-dimethylimidazol-2-yliden, 1,3,4-Triphenyl-1,2,4-triazol-5-yliden) als mögliche Präkursoren für chirale Komplexe synthetisiert (Abbildung 3, schwarz). Tatsächlich konnten (chirale) sterisch anspruchsvolle und basische Alkoxide durch Protonieren eines Pyrrolidliganden mit dem jeweiligen Alkohol eingeführt werden. Der chirale Komplex Mo(*N*-2-*t*Bu-C_6H_4)(CHCMe$_2$Ph)(NC_4H_4)(4,5-Cl_2-1,3-Dimethylimidazol-2-yliden)(**13**) (**Mo-78**, Abbildung 3, blau) und Mo(*N*-2-*t*Bu-C_6H_4)(CHCMe$_2$Ph)(NC_4H_4)(1,3-Diisopropylimidazol-2-yliden)(OHMT) mit einem sterisch anspruchsvollen Alkoxid (**Mo-77**, OHMT = 2,6-Bis(2,4,6-trimethylphenyl)phenoxid, Abbildung 3, blau) konnten erfolgreich hergestellt werden.

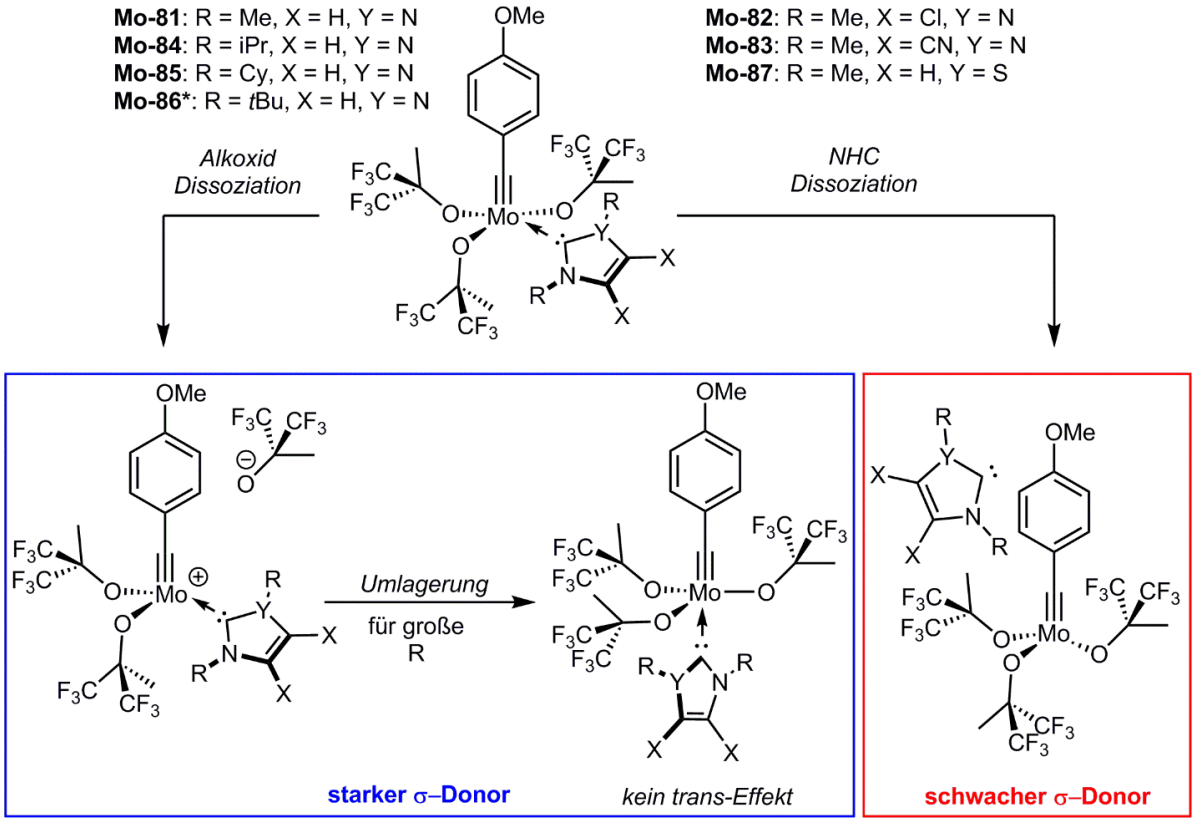

Abbildung 4: Vorgeschlagener Mechanismus für die Bildung der aktiven Spezies in der Alkin-Metathese mit Molybdän Alkylidin NHC Komplexen in Abhängigkeit des NHCs. Alkoxid Dissoziation für starke σ-Donoren (blau) und NHC Dissoziation (rot) für schwache σ-Donoren. *****1,3-Di-*tert*-butylimidazol-2-yliden in **Mo-86** bindet abnormal.

Zudem wurden zuvor synthetisierte Molybdän Trisalkoxy Alkylidin NHC Komplexe **Mo-81** - **Mo-87**[10] bezüglich der Bildung der in der Alkinmetathese aktiven Spezies untersucht. Als Model-Reaktion wurde die Selbstmetathese von 1-Phenyl-1-propin gewählt.[23] Tatsächlich wurde ein Zusammenhang zwischen den elektronischen und sterischen Eigenschaften des jeweiligen koordinierten NHCs und der Aktivität der Komplexe hergestellt (Abbildung 4, *vide supra*). Komplexe mit schwachen σ-Donoren (hohe *Tolman* elektronische Parameter [24] (TEP), **Mo-82**, **Mo-83**, **Mo-87**, Abbildung 4, rot) scheinen bevorzugt das NHC zu dissoziieren,

wohingegen Komplexe mit starken σ-Donoren (niedrige TEP[24], **Mo-81**, **Mo-84**-**Mo-86,** Abbildung 4, blau) das Alkoxid zu geringen Anteilen dissoziieren können. Zudem wurde beobachtet, dass Komplexe mit starken σ-Donoren und hohem sterischen Anspruch (**Mo-84** und **Mo-85**) seitens des NHCs in koordinierenden Lösemitteln (MeCN) Umlagerungen von quadratisch pyramidalen (SP) zu trigonal bipyramidalen (TBP) Geometrien eingehen. Diese Umlagerung konnte für Komplexe mit sterisch weniger anspruchsvollen und stark elektronenschiebenden NHCs nicht beobachtet werden (**Mo-81** und **Mo-86** (NHC abnormal gebunden)).

4 ABSTRACT

Organometallic catalysis has highly evolved since the early 1950´s. Yet, it still suffers from various shortcomings. Amongst them are the stability of the catalyst and the active species, narrow substrate scopes (functional groups), stereoselectivity, reduction of catalyst loadings and removal of catalyst residues from the products. Olefin and alkyne metathesis catalyzed by transition metal alkylidene and alkylidyne catalysts are famous representatives of organometal-catalyzed reactions.[6,9b,11] The formation of new carbon-carbon double and triple bonds has widened the scope of both, organic and polymer chemistry.[11d,12] A large library of catalyst systems, mainly based on ruthenium, molybdenum and tungsten, provides access to the synthesis of complex organic (natural) products and polymers. This work aims to add to this catalyst library, thereby broadening the general applicability of olefin and alkyne metathesis catalysts. Furthermore, some of the issues inherent in organometallic catalysis (*vide infra*) were to be addressed.

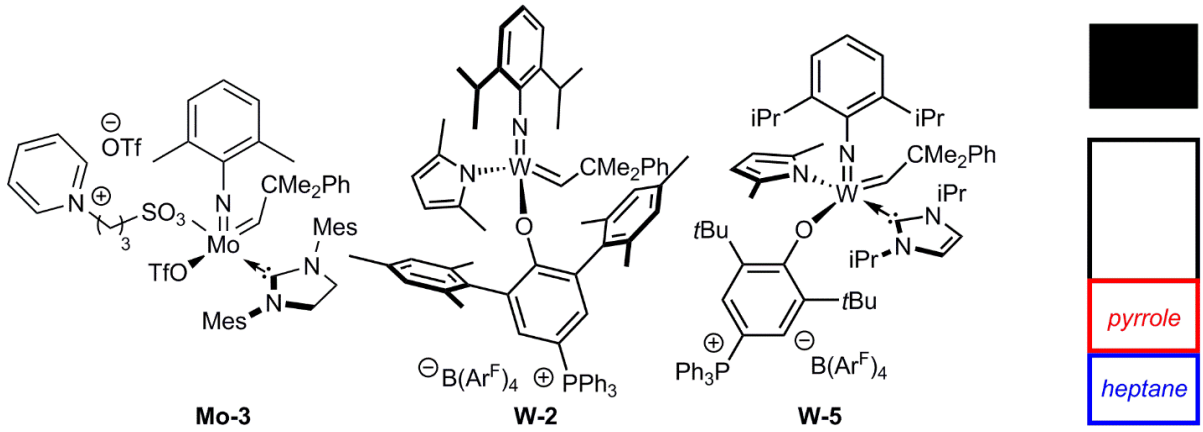

Figure 1: Exemplary molybdenum- and tungsten-based catalysts **Mo-3**, **W-2** and **W-5** bearing betaine-type ligands. Schematic view of the biphasic reaction setup consisting of pyrrole and heptane. ($B(Ar^F)_4$ = tetrakis(3,5-trifluoromethylphenyl)borate).

Catalyst contamination of products in organometal-catalyzed chemistry can be overcome by biphasic reactions setups.[13] This work describes the synthesis of the first molybdenum and tungsten olefin metathesis catalysts bearing betaine-type ligands and their application in biphasic olefin metathesis.[14] The catalysts are based on commercially available or newly developed betaine-type alkoxides, sulfonates and amines. The cationically tagged metal complexes are distributed amongst mono alkoxide pyrrolide (MAP)-type and *N*-heterocyclic carbene (NHC) molybdenum and tungsten imido alkylidene catalysts (exemplary catalysts **Mo-3**, **W-2** and **W-5**, Figure 1). Their usage in a biphasic reaction setup (first introduced by *Roman Schowner*[15]) consisting of pyrrole and heptane provides access to metal-free

products (<2 ppm) by simple removal of the catalyst-containing polar phase. Turnover numbers (TONs) in the biphasic system were comparable to those in standard organic solvents. The solvent system was also applicable to cationic-at-metal molybdenum imido alkylidene NHC complexes with the weakly coordinating anion $B(Ar^F)_4$ ($B(Ar^F)_4$ = tetrakis(3,5-trifluoromethylphenyl)borate).

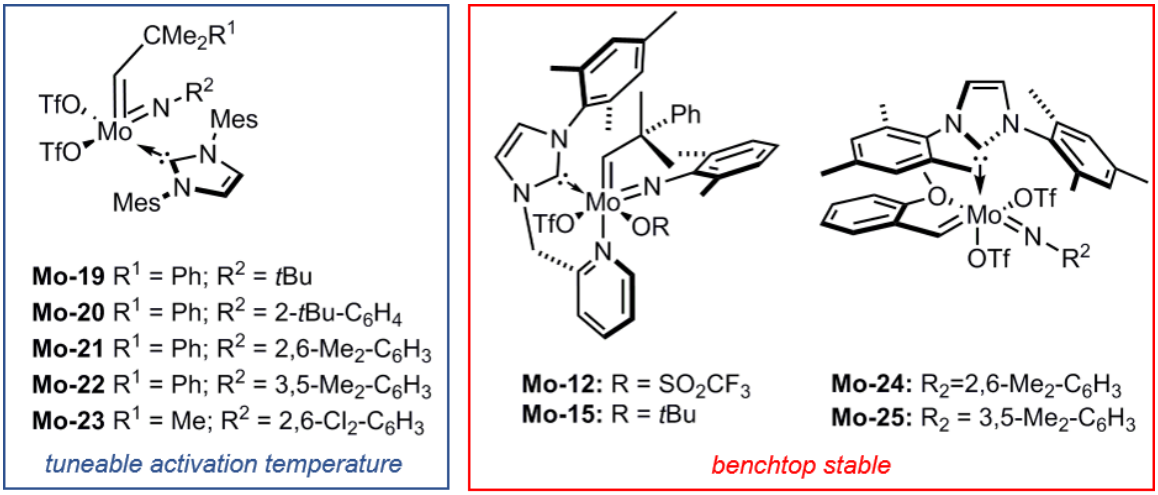

Figure 2: Penta- (blue) and hexacoordinated (red) molybdenum imido alkylidene NHC complexes for latent ring-opening metathesis polymerization (ROMP) of dicyclopentadiene (DCPD).

In addition, catalyst stability of molybdenum imido alkylidene NHC complexes has been addressed by the introduction of chelating *N*-mesityl-*N*-(2-picolyl)-imidazol-2-ylidene with an additional neutral donor to Mo(*N*-2,6-Me_2-C_6H_3)($CHCMe_2Ph$)$(OTf)_2$(DME). The aim was to exploit the chelate effect and potential hemi-lability of the chelating NHC.[16] However, the derived neutral octahedral and cationic pentacoordinated complexes, while highly stable, show only reduced activity in ring-closing metathesis (RCM) of 1,7-octadiene. Nevertheless, the octahedral complexes **Mo-12** and **Mo-15** can be used in industrially relevant latent ring-opening metathesis polymerization (ROMP) of dicyclopentadiene (DCPD).[4b,4c] Due to their air stability in the solid state for at least up to twelve hours they triggered the synthesis of molybdenum imido alkylidene complexes with a chelating alkylidene moiety (**Mo-24**, **Mo-25**, Figure 2).[17] Building on preliminary work,[17-18] pentacoordinated (**Mo-19**-**Mo-23**, Figure 2, blue) and hexacoordinated (**Mo-12**, **Mo-15**, **Mo-24**, **Mo-25**, Figure 2, red) molybdenum imido alkylidene *N*-heterocyclic carbene complexes were compared with respect to their ROMP behavior for DCPD by differential scanning calorimetry (DSC) measurements. They provided poly(DCPD) with different glass transition temperatures and different degrees of crosslinking. Furthermore, the pentacoordinated catalysts showed tuneable activation temperatures (65°C < T_{onset} < 140°C). It should be highlighted that, similar to ruthenium-based *Grubbs Hoveyda*-type systems,[25] the 2-methoxystyrene coordinated octahedral catalysts are air stable in the

solid state. Beneficially, in contrast to previously published catalysts,[19] they can easily be thermally activated without addition of scavengers.

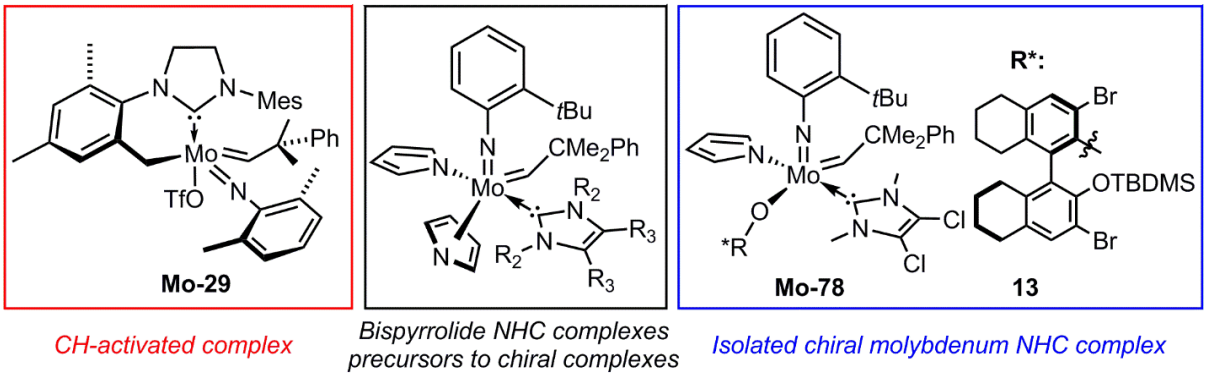

Figure 3: Important intermediates in the development of synthetic routes to chiral molybdenum imido alkylidene NHC complexes. Isolation of a *C*-chelated complex **Mo-29** resulting from *CH*-activation (red). Bispyrrolide NHC complexes as precursors to chiral complexes (black). Proof of concept: Isolated chiral complex **Mo-78** (blue).

Furthermore, the synthesis of chiral molybdenum imido alkylidene NHC complexes was pursued to enrich the library of stereoselective olefin metathesis catalysts.[9b,20] Due to mechanistic considerations published by the *Copéret* and *Eisenstein* group,[21] chirality was introduced *via* the alkoxide ligand rather than the NHC or the imido ligand. Extensive studies on the reaction of monoprotected 3,3´-dibromo-2´-(*tert*-butyldimethylsilyloxy)-5,5´,6,6´,7,7´,8,8´-octahydro-1,1´-binaphth-2-olate (**13**) with molybdenum imido alkylidene NHC bistriflate catalysts revealed *CH*-activation on the NHC as the limiting factor in the synthesis of the desired catalysts. The *CH*-activated complex Mo(*N*-2,6-Me_2-C_6H_3)(CHCMe_2Ph)(1-mesityl-3-(C_9H_{10})-imidazol-2-ylidene)(OTf) (**Mo-29**, Figure 3, red) with a *C*-chelating NHC was successfully isolated and the structure was confirmed by single crystal X-ray crystallography.[16] Since, apart from steric bulk, basicity of the chiral alkoxides was identified as a main drawback, a new synthetic protocol was developed. Bispyrrolide molybdenum imido alkylidene complexes offer the possibility to introduce alkoxide ligands in their protonated form.[22] Thereby, the formation of free basic alkoxides and *CH*-activation or deprotonation of the acidic alkylidene proton can be avoided. In consequence, molybdenum imido alkylidene NHC bispyrrolide complexes Mo(*N*-2-*t*Bu-C_6H_4)(CHCMe_2Ph)(NC_4H_4)$_2$(NHC) and their cationic counterparts [Mo(*N*-2-*t*Bu-C_6H_4)(CHCMe_2Ph)(NC_4H_4)(NHC)][B(Ar^F)$_4$] with varying carbene (NHC = 1,3-diisopropylimidazol-2-ylidene, 4,5-dichloro-1,3-dimethylimidazol-2-ylidene, 1,3,4-triphenyl-1,2,4-triazol-5-ylidene) were synthesized to probe their utility as precursors to chiral molybdenum imido alkylidene NHC complexes (Figure 3, black). Indeed, introduction of bulky chiral ligands by simple protonation of one pyrrolide with the respective alcohols was successful and lead to the isolation of chiral complex Mo(*N*-2-*t*Bu-C_6H_4)(CHCMe_2Ph)(NC_4H_4)(4,5-Cl_2-1,3-dimethylimidazol-2-ylidene)(**13**) (**Mo-78**, Figure 3, blue). Also, Mo(*N*-2-*t*Bu-C_6H_4)(CHCMe_2Ph)(NC_4H_4)(1,3-diisopropylimidazol-2-

ylidene)(OHMT) with a sterically demanding and basic alkoxide (**Mo-77**, OHMT = 2,6-bis(2,4,6-trimethylphenyl)phenoxide) was isolated.

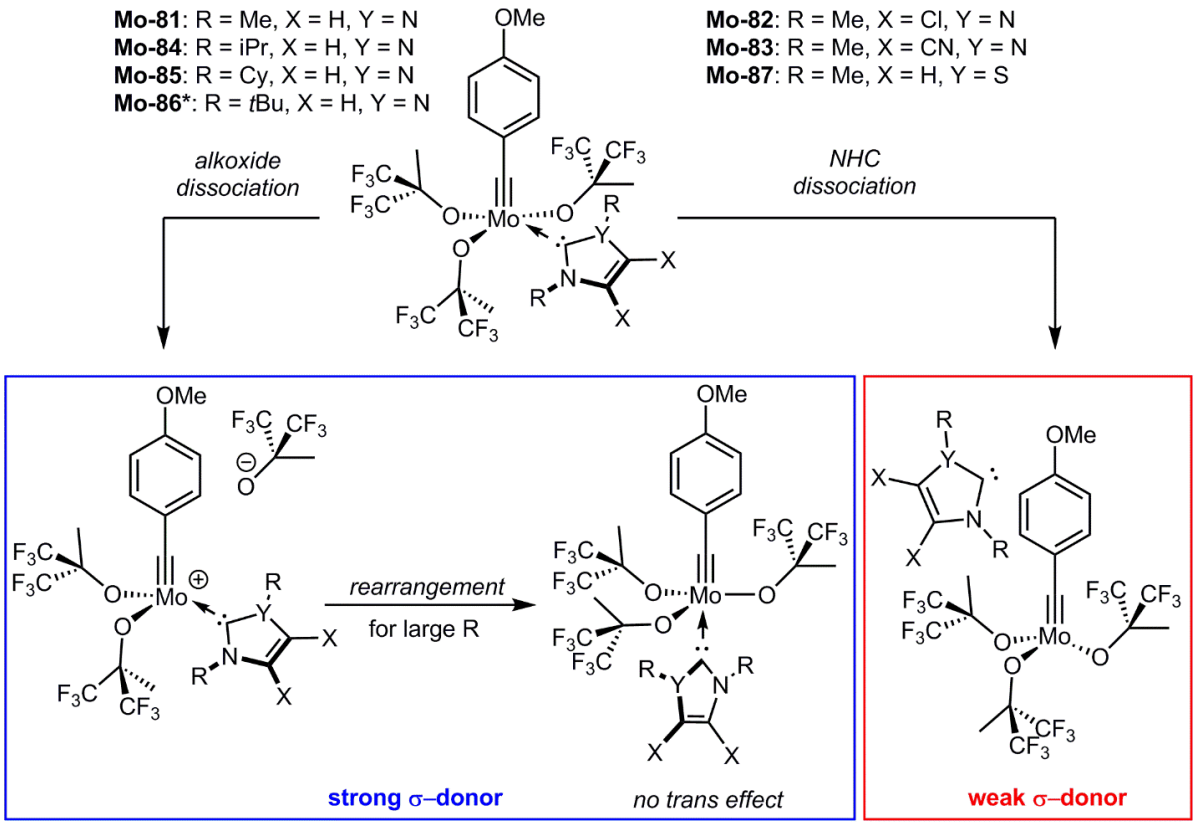

Figure 4: Proposed NHC-dependant formation of active species in alkyne metathesis for molybdenum alkylidyne NHC complexes. Alkoxide dissociation for strong σ-donors (blue) and NHC dissociation (red) for weak σ-donors. *****1,3-Di-*tert*-butylimidazol-2-ylidene in **Mo-86** binds in an abnormal fashion.

Next, previously synthesized molybdenum alkylidyne NHC complexes[10] **Mo-81** - **Mo-87** were investigated concerning their activation mechanism in homometathesis (HM) of 1-phenyl-1-propyne.[23] Interestingly, the active species most likely depends on the electronic and steric nature of the incorporated NHC. Complexes with weak σ-donors (high *Tolman* electronics parameter[24] (TEP), **Mo-82**, **Mo-83**, **Mo-87**) dissociate the NHC (Figure 4, red), whereas complexes containing stronger σ-donors (low TEP,[24] **Mo-81**, **Mo-84**-**Mo-86**) dissociate small amounts of the alkoxide ligand (Figure 4, blue). Complexes with stronger σ-donors can be divided into those with high and low steric constraint: **Mo-84** and **Mo-85** with sterically demanding NHCs have been shown to undergo rearrangements from square pyramidal (SP) to trigonal bipyramidal (TBP) geometries in coordinating solvents (MeCN, Figure 4). This rearrangement was not observed for complexes **Mo-81** and **Mo-86** (carbene is bound in an abnormal fashion) bearing smaller NHCs.

5 THEORY

5.1 CARBENES

Carbenes have emerged as a powerful ligand class, outrivalling the previously used phosphines in many aspects[8,26]. The fact that carbenes have almost replaced phosphines as spectator ligands in numerous relevant transition metal catalyzed reactions, such as palladium-catalyzed coupling reactions and ruthenium-catalyzed olefin metathesis, is mostly due to their superior σ-donor properties. They are defined as neutral species with a carbon atom featuring only six valence electrons. A special class of carbenes that has gained a lot of attention are *N*-heterocyclic carbenes (NHCs). NHCs bear at least one nitrogen atom directly adjacent to the carbene center.

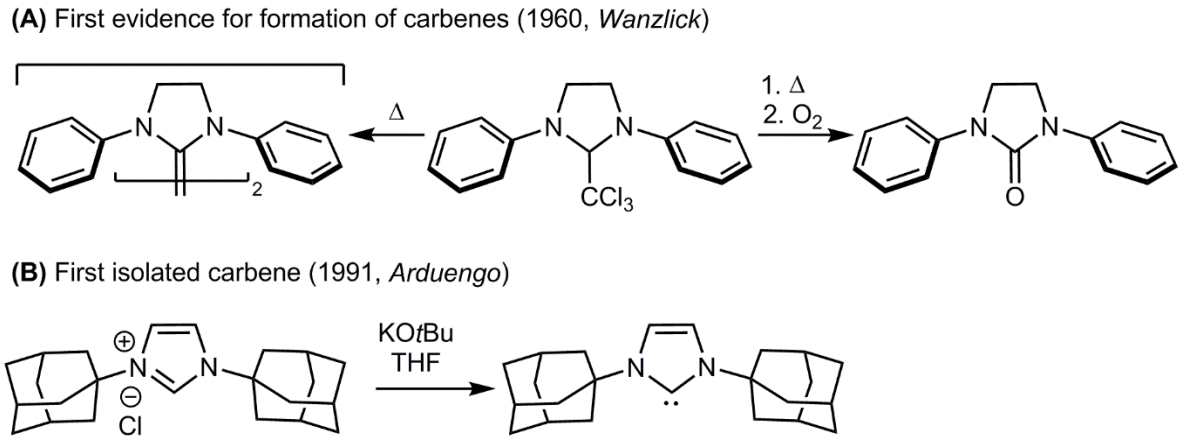

Scheme 1: **(A)** First evidence for the formation of carbenes by *Wanzlick*[27] and **(B)** first isolated carbene by *Arduengo*[28].

First evidence for the existence of carbenes was provided by *Wanzlick* through the isolation of 1,3-diphenylimidazolin-2-on[27a] and the respective carbene dimers[27b] (*Wanzlick* equilibrium) from heated solutions of 1,3-diphenyl-2-trichloromethylimidazolin (Figure 5, **(A)**). Also, *Wanzlick*[29] and *Öfele*[30] were able to trap carbenes with metal fragments, leading to metal carbene complexes. However, it was the first isolation of an NHC with sterically demanding adamantyl substituents by *Arduengo et al.* in 1991[28] (Figure 5, **(B)**) that triggered an increasing application of NHCs as ligands in transition metal catalysis and in organocatalysis. The depicted syntheses, deprotonation of imidazolium salts with strong bases (KO*t*Bu, KHMDS) as well as abstraction of small molecules ($CHCl_3$, MeOH, CO_2) from carbene adducts, still represent the most common routes to carbenes. Many routes to their precursor imidazolium salts and NHC-adducts are published.[31] Often, bulky groups on the nitrogen atoms (e.g. adamantyl or mesityl substituents) provide kinetic stability to the carbon center by preventing dimerization. The main contribution to the stability of NHCs however, lies in their special

electronic structure. Carbenes can either exist in a triplet (two unpaired electrons) or a singlet (all electrons paired) ground state.[32] Which ground state a certain carbene prefers mainly depends on its chemical environment. NHCs are mostly singlet carbenes, which renders them especially stable. Four different electronic configurations can be envisioned for NHCs (Figure 5, top).[32] A singlet $^1A_1$ state with both electrons in the σ-orbital (HOMO: highest occupied molecular orbital), a singlet $^1A_1$ state with both electrons in the p-orbital (LUMO, lowest unoccupied molecular orbital), a singlet $^1B_1$ state and a triplet $^3B_1$ state, each with one electron in the σ- and the p-orbital, respectively (Figure 5, top). Most NHCs are in the $^1A_1(\sigma^2)$ singlet ground state because the σ-electron-withdrawing properties of the nitrogen atom(s) stabilize the HOMO and lower its energy ($E_{S\text{-}T}$, Figure 5) resulting in an increase in the HOMO-LUMO gap (ΔE, Figure 5). The higher ΔE and $E_{S\text{-}T}$ get, the more favored is the $^1A_1(\sigma^2)$ singlet ground state. The singlet $^1B_1(\sigma^1p_\pi^1)$ and the triplet $^3B_1(\sigma^1p_\pi^1)$ configuration become competitive when the energy difference between the HOMO and the LUMO (ΔE, Figure 5, bottom) is small. The $^1A_1(p\pi^2)$ configuration can usually be neglected under standard conditions. The stability of NHCs therefore correlates with ΔE between the $\sigma(sp^2)$- (HOMO) and the p_π-orbital (LUMO). If the energy gap between the triplet and the singlet configuration of the carbene, $E_{S\text{-}T}$ (Figure 5, bottom), exceeds approximately 40 kcal/mol, the singlet ground state is favored.[32]

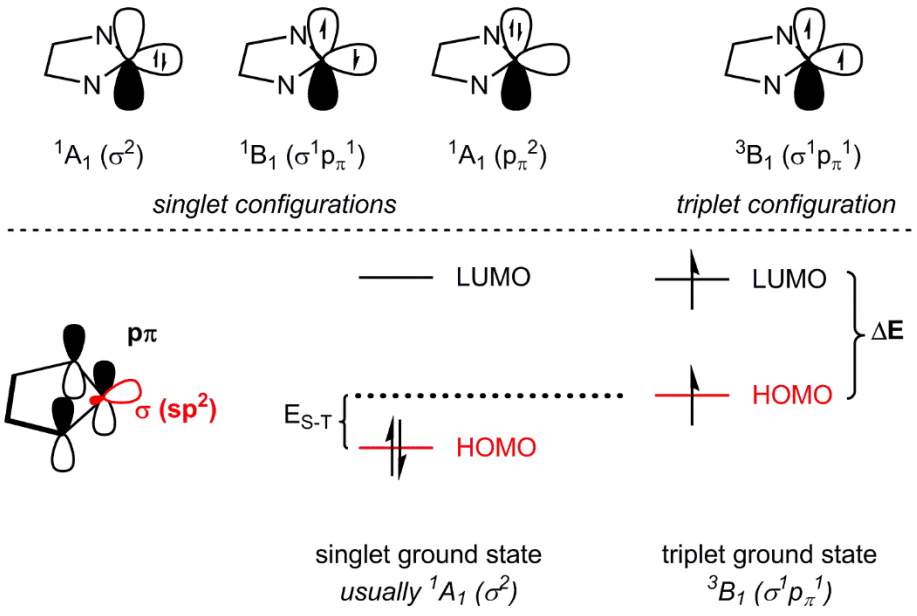

Figure 5: Top: Possible electronic configurations of NHCs. Singlet ground state configuration $^1A_1(\sigma^2)$ and singlet configurations $^1B_1(\sigma^1p_\pi^1)$ and $^1A_1(p_\pi^2)$ as well as rivalling triplet ground state $^3B_1(\sigma^1p_\pi^1)$. Bottom: Stabilization of HOMO ($E_{S\text{-}T}$) by electron-withdrawing properties of nitrogen atoms, leading to an increase in the HOMO-LUMO gap (ΔE), therefore favoring the singlet ground state $^1A_1(\sigma^2)$ over the triplet ground state $^3B_1(\sigma^1p_\pi^1)$. [32]

Another factor favoring the singlet ground state in NHCs is the cyclic structure, forcing the carbene atom to adopt a bent, sp^2 like structure. It should also be noted that aromatic carbenes are more stabilized than their non-aromatic counterparts (e.g. imidazol-2-ylidenes *vs.*

imidazolidin-2-ylidenes) and can therefore be isolated with less bulky substituents on the nitrogen atoms. Further electronic stabilization is provided by π-donation of the nitrogen lone pairs into the empty p-orbital.

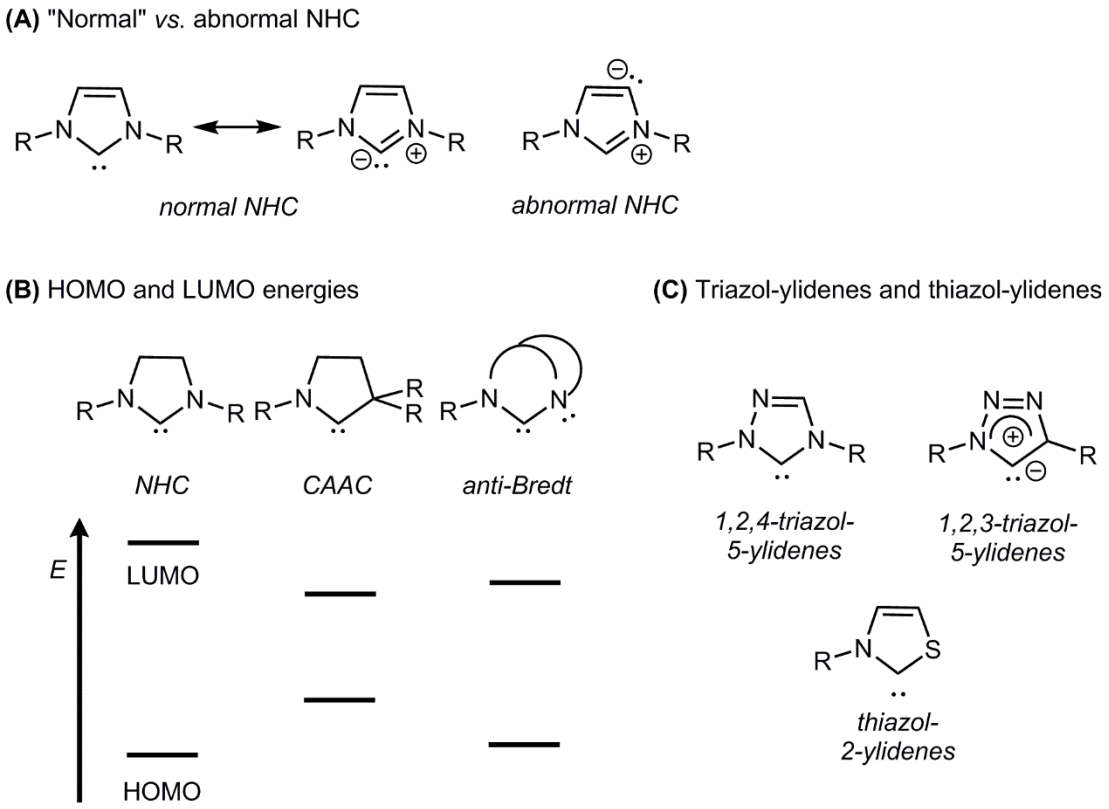

Figure 6: Special classes of NHC: **(A)** Normal *vs.* abnormal (mesoionic) NHCs with charge separation.[32] **(B)** Comparison of HOMO and LUMO energies in "normal" carbenes, cyclic alkyl amino carbenes (CAAC)[33] and anti-Bredt carbenes[34] with pyramidalized nitrogen atoms. **(C)** Multiple heteroatom containing carbenes (triazol- and thiazol-ylidenes).[35]

Lately, also other classes of stable carbenes have been prepared. Abnormal (mesoionic, MIC)[36] carbenes, cyclic alkyl amino carbenes (CAAC)[33] and anti-Bredt carbenes[34], and their respective metal complexes have been isolated (Figure 6). MICs, in contrast to "normal" carbenes, are carbenes that have no neutral mesomeric structure but can only be written with negative and positive partial charges (Figure 6, **(A)**). They are often synthesized by blocking the *C*2-carbon to prevent deprotonation at the more acidic *C*2-position. In some cases, abnormal carbenes form by rearrangements when the corresponding carbene is coordinated to a sterically encumbered metal center.[36] CAAC are carbenes with only *one* nitrogen atom adjacent to the carbene carbon. Instead, one of the electronegative nitrogen atoms is replaced by a σ-donating (not π-donating) alkyl group, which renders CAACs better σ-donors and better π-acceptors than normal NHCs with two nitrogen atoms next to the carbene (Figure 6, **(B)**). In addition, the quaternary carbon atom in direct proximity to the carbon center provides them with a unique steric profile.[33] Anti-Bredt carbenes are cyclic diamino carbenes featuring a pyramidalized nitrogen atom.[34] The pyramidalization prohibits the nitrogen atom from donating

electron density to the p-orbital of the carbene carbon, therefore only lowering the energy of the LUMO and not effecting the HOMO energy (Figure 6). The resulting carbene therefore shows increased electrophilicity in comparison to a “normal” NHC but only negligible changes in nucleophilicity[34]. Also, carbenes with more than two heteroatoms and heteroatoms other than nitrogen and their metal complexes have been synthesized. Amongst them are 1,2,4-triazol-5-ylidenes[35a] and 1,2,3-triazol-5-ylidenes (MIC)[35b] as well as thiazol-2-ylidenes[35c,35d] (Figure 6).

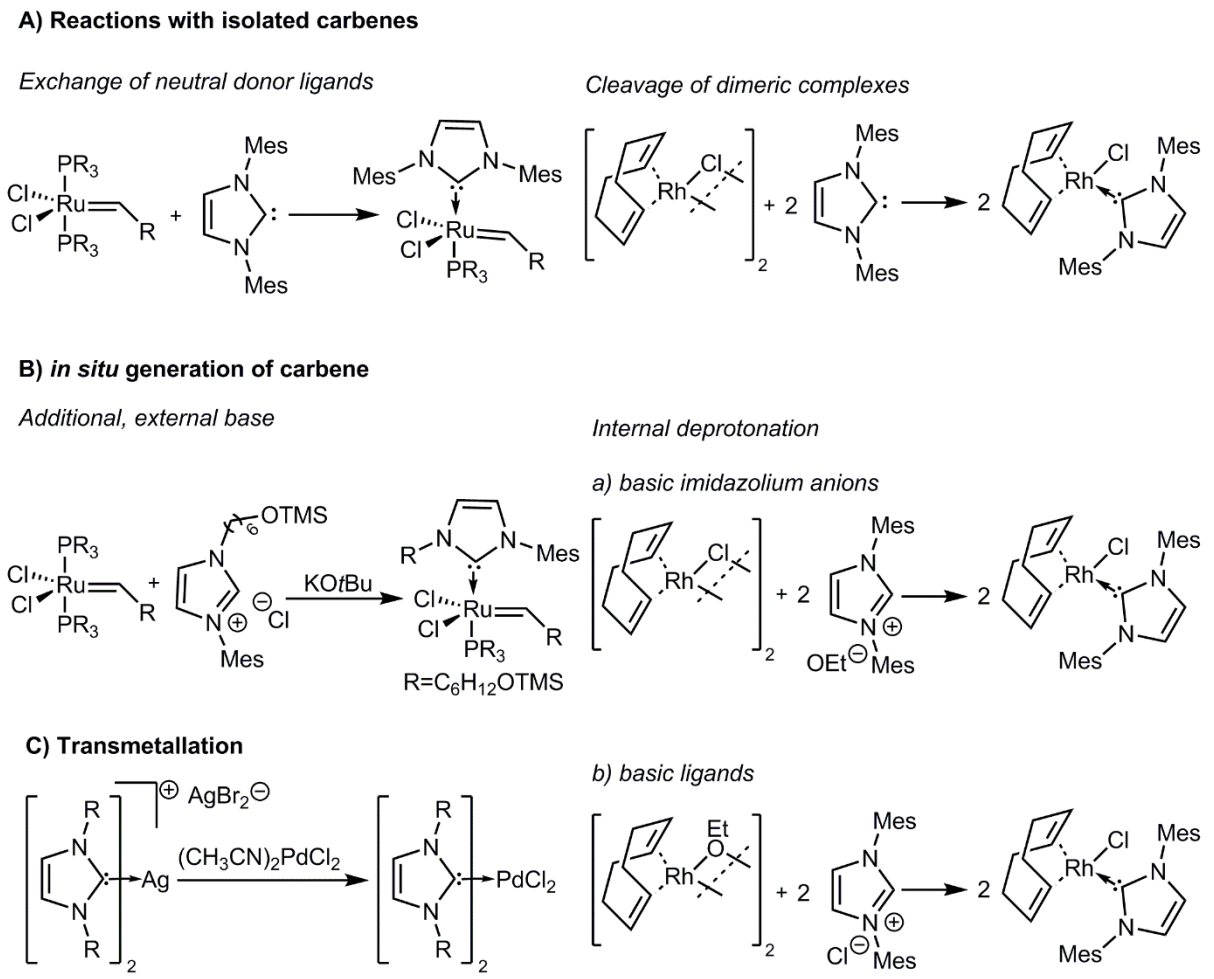

Scheme 2: Synthesis of metal NHC complexes.[37] **(A)** Reactions with free carbenes either proceed by substitution of neutral donor ligands or by cleavage of dimeric complexes. **(B)** The carbene is generated *in situ*, either by addition of an external base or by internal deprotonation. **(C)** Transmetallation with e.g. silver NHC complexes.

NHC (transition) metal complexes find a variety of applications throughout organic chemistry. Many different approaches to their syntheses have been explored (Scheme 2).[37] In many cases, complexes can be synthesized by replacement of another neutral donor ligand (e.g. phosphine, THF) by the free carbene or by cleavage of a dimeric metal complex with the free carbene (Scheme 2, **(A)**). However, in case the carbene is unstable, it can be generated *in situ* in presence of the precursor complex, with an external or internal (proton transfer to a ligand of the metal complex or to the anion of the imidazolium salt) base (Scheme 2, **(B)**). Also,

transfer of carbenes from silver or gold complexes to other transition metals is a viable approach (Scheme 2, **(C)**).

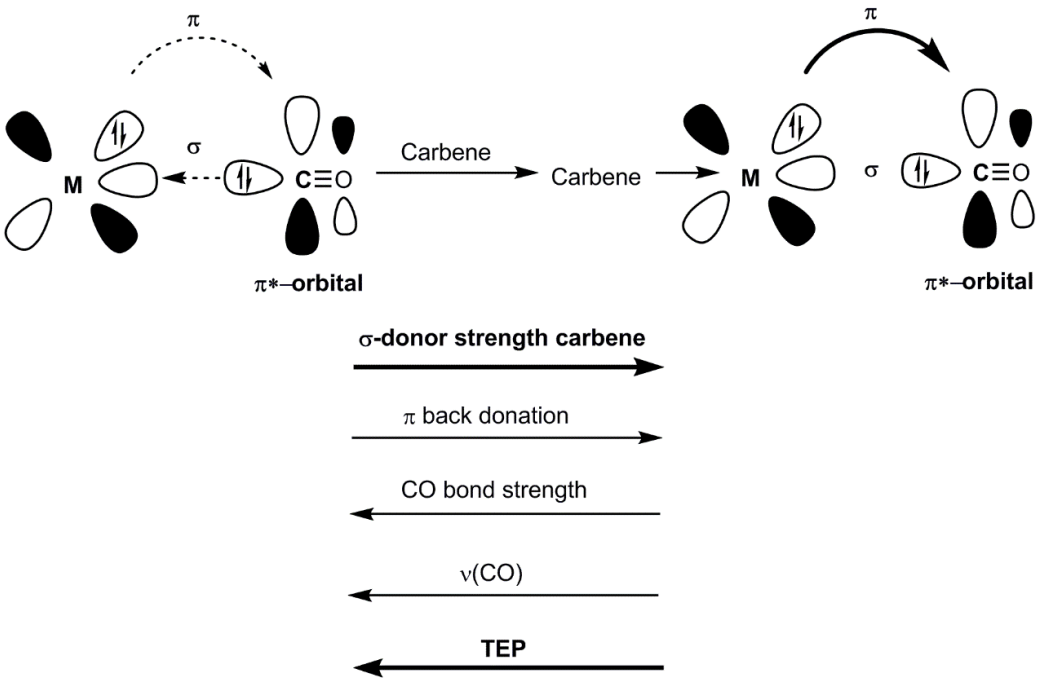

Scheme 3: Determination of TEP of a carbene by measurement of the A_1 C≡O vibrational mode of the respective iridium, rhodium[38] or nickel[24] carbonyl complex. The stronger the σ-donation from the carbene to the metal center, the higher the amount of π back donation from the metal into the anti-bonding π*-orbital is. A decrease in C≡O bond strength leads to a decrease in vibration frequency, translating into a lower TEP. Strong σ-donors have a low TEP and *vice versa*.[39]

Since the σ-donor strength of carbenes is highly important for their reactivity and the reactivity of the corresponding carbene complexes, several ways to measure this property have been developed.[8] The *Tolman* electronic parameter (TEP, Scheme 3) has emerged as a prominent parameter to determine and compare σ-donor properties of phosphines as well as carbenes.[39] TEP is derived from the frequency of the A_1 C≡O vibrational mode of mostly nickel[24], iridium or rhodium[38] complexes (Scheme 3). C≡O is a σ-donor/ π-acceptor ligand, the metal C≡O bond consist of a σ-bond from the carbonyl ligand to the metal center and a π back bond from the metal center into a low lying π*-orbital of C≡O. If the overall electron density on the metal center increases, for example through σ-donation from another ligand, π back donation from the metal into the anti-bonding orbital is increased, resulting in a weaker C≡O bond and a lower frequency. The lower the frequency and the lower the TEP, the higher the σ-donor strength of the corresponding carbene is. TEP can also be retrieved from computational methods. Some general trends can be concluded from the measurements made so far, although, as always, there are exceptions.[8,24] In terms of heteroatoms adjacent to the carbene center, the σ-donor strength decreases from cyclic alkyl amino carbenes (CAAC) over NHCs and oxazol-ylidenes to thiazol-ylidenes. Also, TEP increases from 5- to 7-membered NHCs and is highly dependent

on the substituents on the nitrogen atoms. Evidently, not only electronic but also steric influences of the carbene have a great impact on the catalytic properties of the carbene metal complex. Sterics in NHCs can be described with the cone angle that has been developed for phosphines[39b,40]; but today sterics are mainly characterized in terms of buried volume (V_{bur}).[41] V_{bur} has been defined as the space a ligand takes up in the first ligand sphere of a central (metal) atom. The coordination sphere is constructed with a given radius *R* around the central atom (Figure 7). The coordinating atom of the ligand is then placed in the distance *d* from the metal center on the z-axis (Figure 7). For the determination of V_{bur} the geometry of the ligand must be known, either from computational methods such as density functional theory (DFT) optimizations or from single-crystal X-ray analysis.

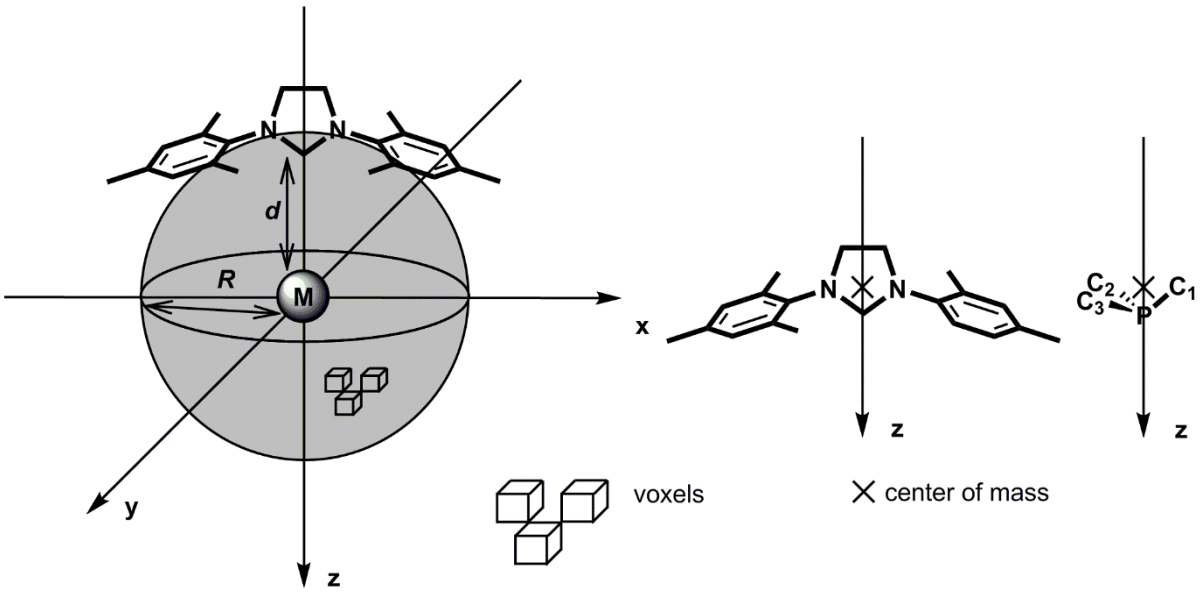

Figure 7: Determination of buried volume (V_{bur}) by calculating the space the ligand takes up in the first coordination sphere (radius *R*) of the metal center in the distance *d*.[41a,41b]

Furthermore, the distance between the coordinating atom and the central atom (*d*, Figure 7) has a high impact on the buried volume of a ligand. Of course, the buried volume of one NHC can differ greatly in different metal complexes. *Sambvca2* (former *Sambvca*), developed by *Cavallo et al*., presents an online tool for the determination of buried volume.[41a,41b] The software requires the geometry of the ligand and the distance between the coordinating atom and the metal atom to determine the buried volume. The coordination sphere is set 3.5 Å in the default settings but can be changed by the user. The buried volume is then determined by dividing the coordination sphere into voxels (3D pixels, Figure 7). Every voxel within the *van-der-Waals* radius of a ligand atom belongs to the V_{bur}. Buried volume is usually given as percentage of the complete coordination sphere ($\%V_{bur}$). Buried volume in combination with the energy gap between the singlet and the triplet state $E_{S\text{-}T}$ of a given carbene has been utilized to predict if a carbene is stable towards dimerization.[32a] The dimerization energy E_{dim}

is defined as the sum of an electronic contribution $NHC_{electronic}$ and a steric contribution NHC_{steric}. The electronic contribution has been reduced to the singlet-triplet energy gap $E_{S\text{-}T}$, whereas the steric contribution has been coupled to the buried volume. This allows for calculations of the theoretical values for the dimerization energy ($E_{fit,dim}$) of a range of NHCs. Good accordance with experimental dimerization energies E_{dim} could be obtained and an operating window of $E_{fit,dim}$ for stable monomeric NHCs was postulated. For $E_{fit,dim}$>-3 kcal/mol carbenes are proposed to be stable in their monomeric form, whereas for carbenes with $E_{fit,dim}$<-22 kcal/mol dimerization will occur.[41e]

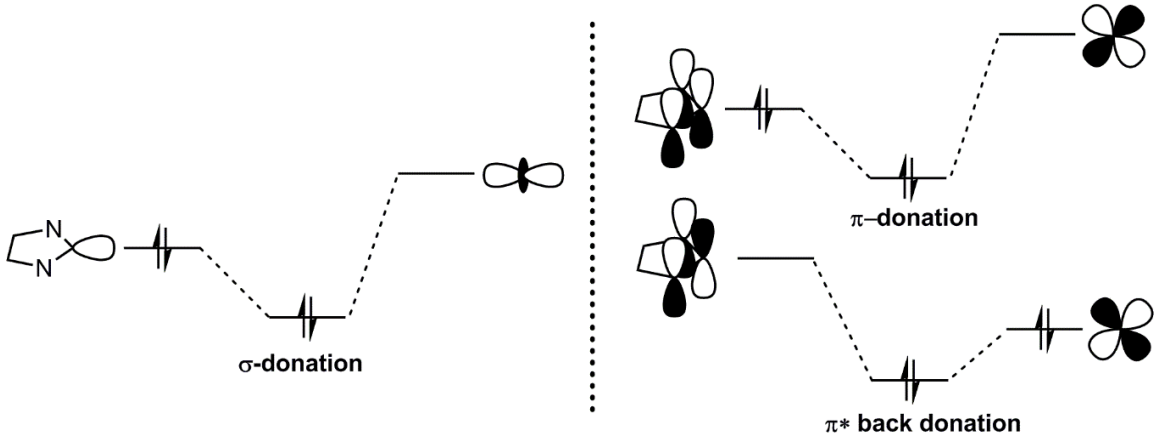

Figure 8: The metal carbene bond. Left: σ-donation from the sp^2 hybrid orbital into the d_z-orbital (arbitrarily chosen). Right: π-donation from the carbene to the metal as well as π back donation from metal orbitals into π*-orbitals of the carbene. [32a]

The NHC metal bond is mainly characterized by a σ-bond from the carbene-carbon into empty d-orbitals at the metal center. Nevertheless, also π back donation from the metal into an empty π*-orbital at the carbene and π-donation from the carbene into empty d-orbitals at the metal are to be discussed[32a]. In fact, studies on a multitude of NHC-metal complexes with different NHCs and different d-electron count at the metal center revealed, that π-contributions mainly depend on the d-electron count. The more d-electrons on the metal, the higher the π back donation into the carbene orbitals (average π-contribution of 20% in d^{10} systems, average of 10% in d^0 systems; 100%: all orbital interactions). On the other hand, σ- and π-donation from carbene to metal increase with decreasing d-electron count. Of course, also electrostatic interactions contribute to the carbene metal bond, although they are not easily accessible. For neutral d^0-complexes and cationic complexes, electrostatic interactions play a more crucial role. As already discussed for the dimerization energy of carbenes, steric repulsion also has an impact on the stability of the metal carbene bond.

(A) Carbenes with stereocenters

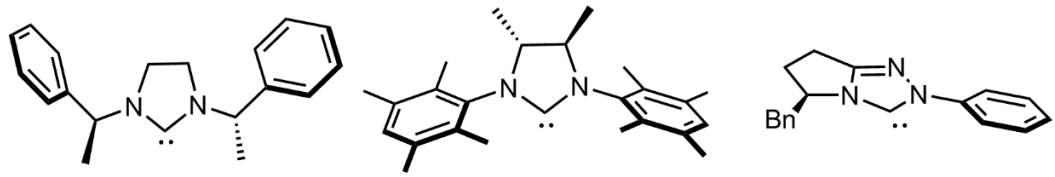

(B) Carbenes with elements of axial chirality and planar chirality

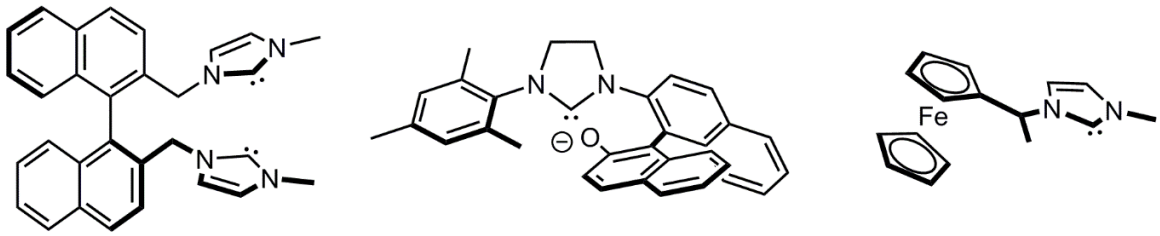

Figure 9: Exemplary chiral carbenes with stereocenters **(A)** and axial chirality as well as planar chirality **(B)**.[42]

Apart from electronic stabilization, NHCs also offer the possibility to introduce chirality. NHCs with one or several stereocenters, axial chirality and planar chirality have been synthesized and coordinated to metal centers.[42] Imidazolium salts and their respective carbenes containing chiral stereocenters on the nitrogen substituents as well as in the backbone of the NHC have been isolated (Figure 9, **(A)**). Chiral residues in the backbone, even though not in proximity to the central metal atom, influence the orientation of the NHC wingtips, which in turn have direct impact on the stereochemistry of the metal center.[42a] Amongst others, *3,3´*-substituted biphenols and 1,1´-binaphthyl-2,2´-diamine or 2-amino-2'-hydroxy-1,1'-binaphthalene[43] have been used to introduce axial chirality to NHCs (Figure 9, **(B)**). Especially chiral ferrocene derivatives[44] have been utilized to gain planar chirality (Figure 9, **(B)**), comparable to commonly used phosphine ligands (eg. Josiphos[45]). Furthermore, *trans*-1,2-diamino cyclohexane has been widely applied as an element of chirality in NHCs.[42]

Another means to dramatically influence the coordination chemistry of NHC metal complexes is the incorporation of chelating bidentate or pincer carbenes (Figure 10, top).[46] Bidentate carbenes bear a second coordinating group, which is tethered to the imidazol-2-ylidene core. The second donor can either be charged or neutral. Pincer-type carbenes feature two additional chelating groups, thereby having the ability to block three coordination sites on a metal center. Famous examples for chelating carbenes with anionic tethers are alcoholates[47], thiolates[48], amines[49] and sulfonates[48,50] (Figure 10, *exemplary anionic donors*). Neutral donors are often phosphines[51], imines[49], (thio)ethers[48] and aromatic heterocycles[52] (Figure 10, *exemplary neutral donors*). Through variations in the linker length[53] and the rigidity of the system, carbenes with different properties are accessible. Especially in the case of neutral

additional donors, the concept of hemilability emerges.[54] In hemilabile complexes, the donor can easily dissociate and recoordinate, thereby blocking or opening coordination sites. This becomes particularly interesting in the case of instable complexes and transition states. A special class of chelating carbenes are bis-carbenes.[55] Apart from influencing the coordination sphere, bidentate and pincer carbenes enhance stability through the chelate effect.[7]

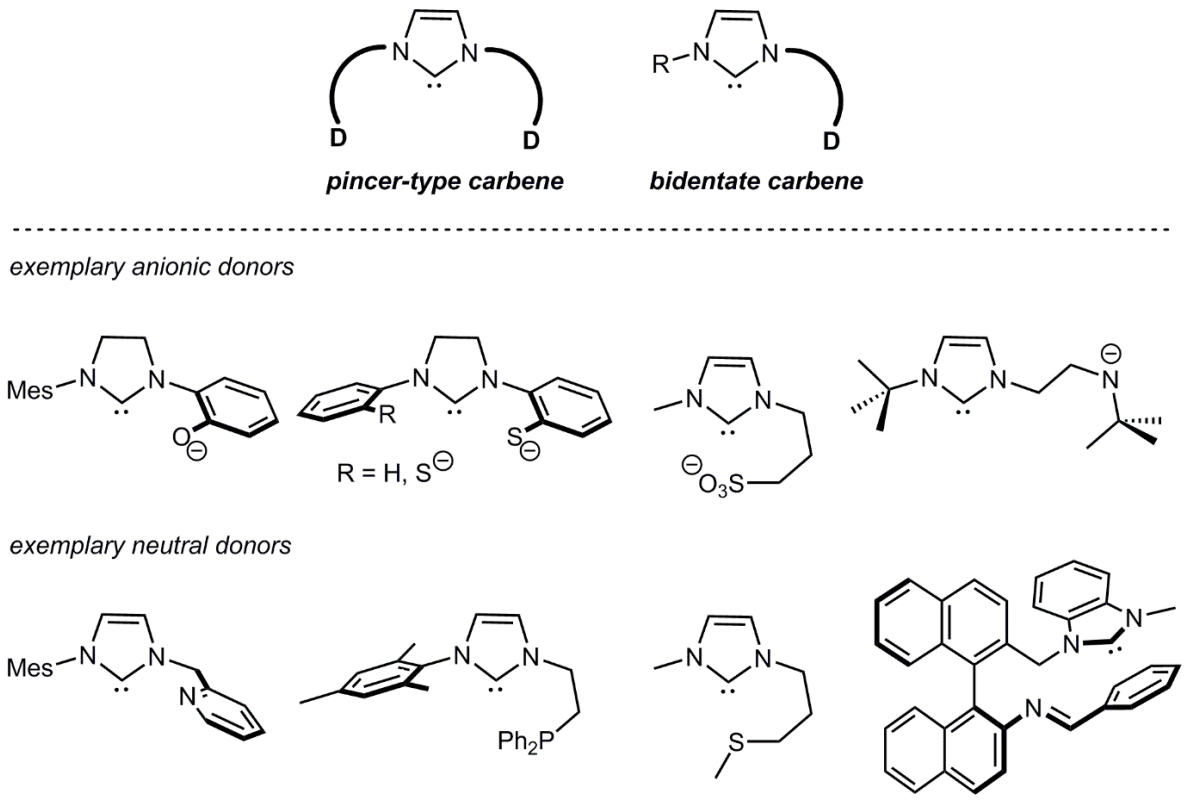

Figure 10: Bidentate and pincer carbenes bearing additional anionic or neutral donor functionalities.[46]

5.2 METATHESIS

Metathesis, apart from (palladium catalyzed) coupling reactions, is one of the most prominent pathways to the formation of new carbon-carbon bonds[11d,56]. Carbon-carbon bond formation is highly important in organic, as well as in polymer chemistry and provides access to products with pharmaceutical and industrial impact[4b,4c]. Metathesis reactions can be divided into olefin metathesis, alkyne metathesis and alkane metathesis[57].

5.2.1 OLEFIN METATHESIS

Olefin metathesis is the catalytic formation of new carbon-carbon double bonds from internal and terminal (cyclic olefins). On can distinguish between several different types of olefin metathesis reactions (Scheme 4).[6a,58]

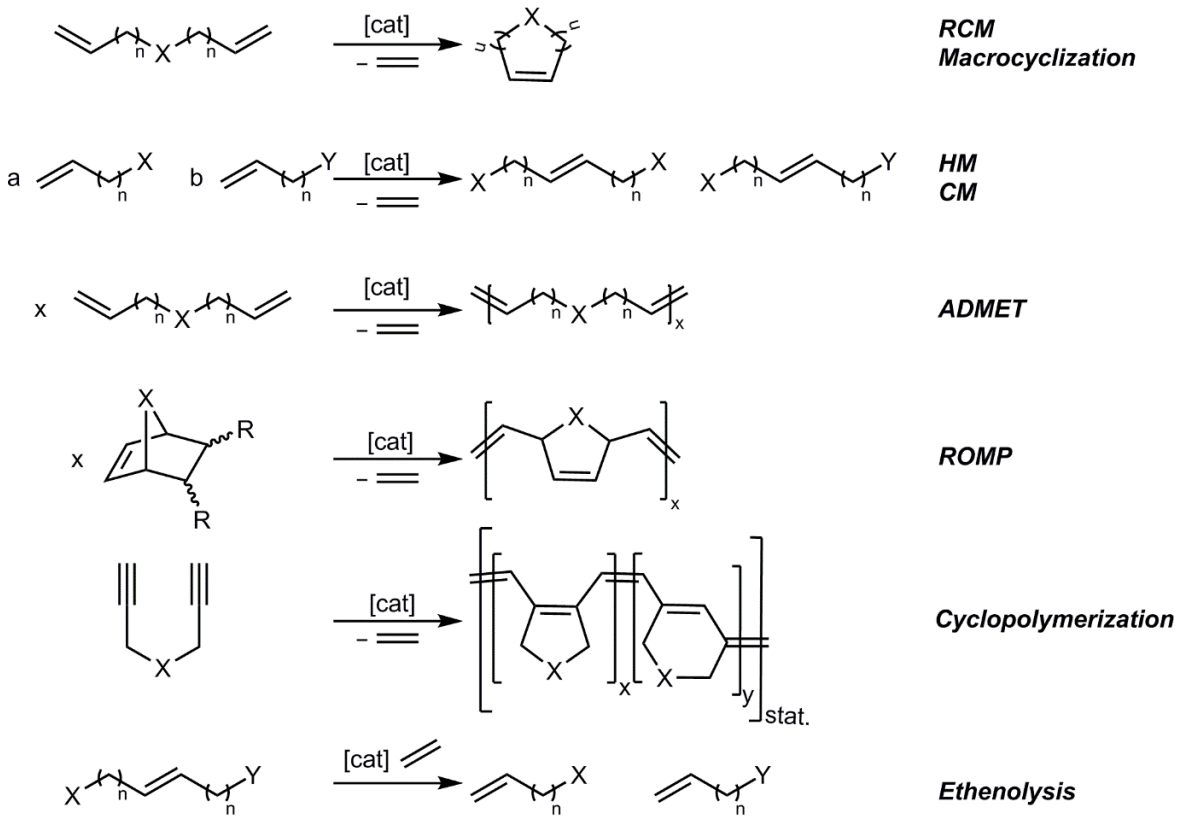

Scheme 4: Exemplary types of metathesis reactions leading to unsaturated rings (RCM, macrocyclization), short- or long-chain alkenes (HM, CM, ethenolysis) and unsaturated polymers (ADMET, ROMP, cyclopolymerization).[6a,58]

Ring-closing metathesis (RCM), cross-metathesis (CM), homometathesis (HM), cyclopolymerization, ring-opening metathesis polymerisation (ROMP) and acyclic diene metathesis polymerization (ADMET) are some prominent examples (Scheme 4). All metathesis reactions are reversible. In RCM, terminal dienes are ring-closed to form cyclic alkenes.[59] The competing reaction to RCM is ADMET. Here, the terminal dienes are coupled via their terminal double bonds to form polymer chains. Importantly, ADMET is a step growth

polymerization, not a chain polymerization. Therefore, reaction conditions have to be adjusted accordingly[60] (high boiling solvents or bulk polymerization under high vacuum). RCM is preferred over ADMET when 5-, 6- or 7-membered rings are formed. The longer the alkylic chain between the double bonds, the more pronounced ADMET becomes. In consequence, macrocyclizations[12c] (RCM of long chain dienes) are achieved by working under highly dilute conditions[61], leading to a preferred intramolecular reaction. In CM, the substituents of two (internal or terminal) olefins are exchanged. Homometathesis, which is the cross-metathesis of one olefin with itself, in most cases is observed as competing reaction.[62] Usually, when electronically distinct double bonds are present, by careful adjustment of the stoichiometric factors a and b (Scheme 4), the yield of the cross-metathesis product can be maximized. Often, the less reactive olefin is used in excess. The ring-opening of strained cyclic olefins (usually norbornenes, norbornadienes or comparable cycloalkenes) under the formation of unsaturated polymer chains is called ring-opening metathesis polymerization (ROMP).[12b,63] The driving force of ROMP is the release of ring strain, whereas for RCM, HM and CM the release of low boiling side products such as ethylene favors product formation. The reverse reaction to all above described reactions is ethenolysis[64], where internal alkenes are split into terminal alkenes under ethylene pressure.

Olefin metathesis is a transition metal catalyzed chemical transformation and is closely connected to the rise of organometallic chemistry.[5a,5b] First evidence was provided by *Ziegler*, who found that 1-butene could be formed from ethylene as a by-product in polyethylene formation when traces of nickel were present. Further work by, amongst others, the *Ziegler* and *Natta* groups resulted in the finding, that titanium and zirconium halides together with alkyl aluminium compounds would lead to the polymerization of ethylene and propylene to yield polyethylene or polypropylene. Both were awarded the Nobel Prize in 1963. Application of those systems in the polymerization of norbornene[65] at the *DuPont* group lead to the unexpected formation of an unsaturated ring-opened polymer. *Natta* observed the same when using molybdenum or tungsten halides in the polymerization of cyclopentene.[66] Also, *Banks* and *Bailey* observed the formation of 2-butene and ethylene as by-products of propylene polymerization.[67] Nevertheless, at this time, the nature of the active species was unclear and ill-defined catalysts were frequently used. Obviously, these systems were far from optimum.

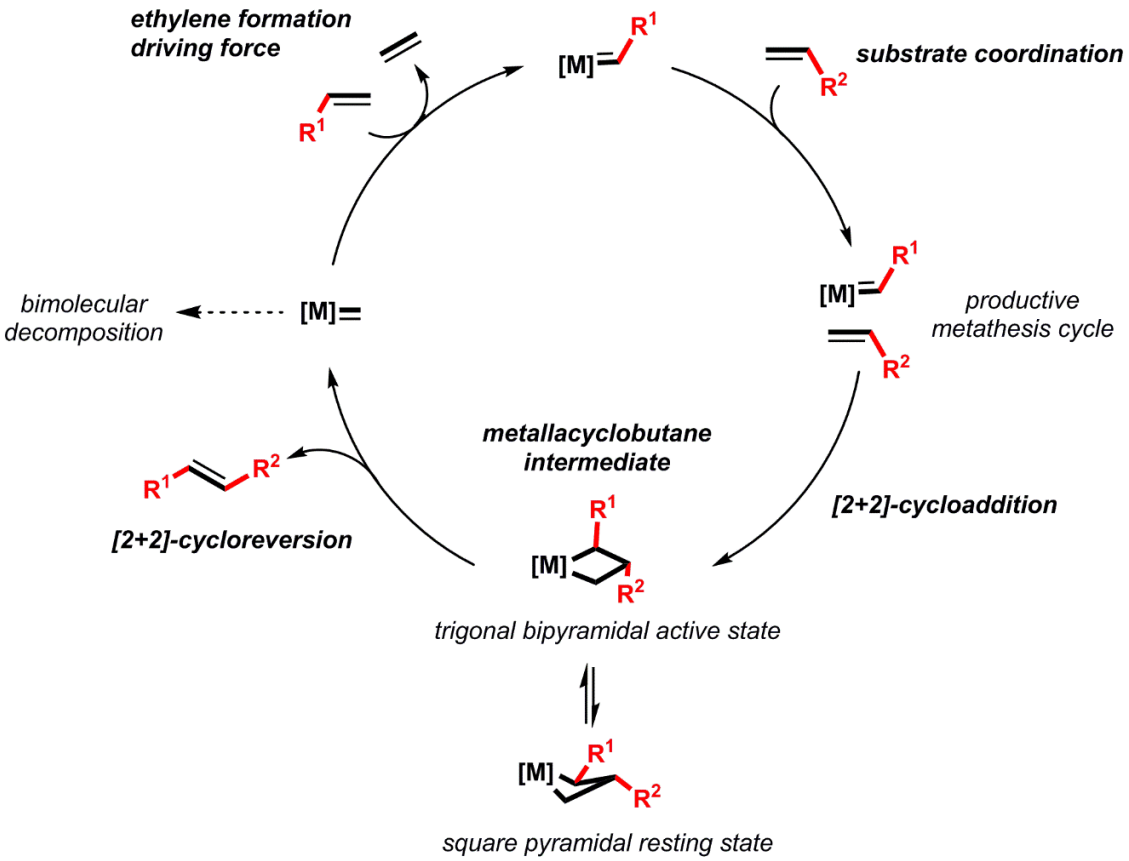

Scheme 5: Productive metathesis cycle consisting of substrate coordination to the *Lewis* acidic metal center; [2+2]-cycloaddition; a metallacyclobutane intermediate; [2+2]-cycloreversion and formation of the initial starting alkylidene under release of ethylene. All reactions are reversible. Arrows for back-reactions have been omitted for clarity.[68]

Especially the elucidation of the unique [2+2]-cycloaddition/cycloreversion mechanism based on metal alkylidenes as the active species proposed by Nobel laureate *Yves Chauvin*[68], that was later supported by the isolation of the first metallacyclobutanes (MCBs)[69], improved catalyst development (Scheme 5). First, the olefin coordinates to the *Lewis* acidic metal center. Then, in a [2+2]-cycloaddition, the metallacyclobutane intermediate is formed. Subsequently, the four-membered ring opens under release of the corresponding product olefin and a metal methylidene, which, after an additional [2+2]-cycloaddition/cycloreversion process reforms the starting alkylidene. What made the mechanism so intriguing, was the metallacyclobutane intermediate as well as the metal alkylidene as active species. Metallacyclobutanes have been found to exist in two geometries for molybdenum and tungsten imido as well as tungsten oxo alkylidene complexes. The metallacyclobutane can either take up a TBP (trigonal bipyramidal) or a SP (square pyramidal) structure (Scheme 5). For ruthenium-based catalysts, the SP form has not been observed so far. The trigonal bipyramidal structure has been found to be the metathesis-active species, whereas the square pyramidal structure represents an inactive resting state and, in addition, has been found to be prone to decomposition.[21c] Quite recently, studies showed that the activity of a metallacyclobutane can be deduced from the ^{13}C NMR chemical shift tensors of the α/α´- and β- carbon atoms in the MCB.[70] Metathesis-active

metallacyclobutanes display chemical shift tensors for the α- and β- carbon atom of 100 and 0 ppm and have rather short M-$C_{\alpha/\alpha}$ and M-C_{β} bonds. The $C_{\alpha/\alpha}$ -C_{β} bonds are rather long. This is postulated to be a direct consequence of a low-lying empty orbital in the plane of the metallacyclobutane that shows local π*(M-$C_{\alpha/\alpha}$) character, meaning that the α-carbons still have alkylidene character.

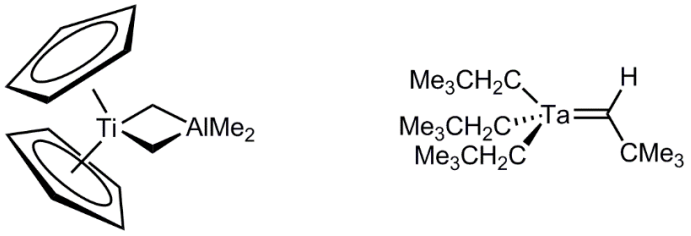

Tebbe reagent *first Schrock carbene*

Figure 11: Milestones in the development of olefin metathesis catalysts. The first isolated metathetically active *Tebbe* reagent[71] (left) and the first isolated *Schrock* carbene[5a] (right).

Apart from the isolation of metallacyclobutanes, the *Chauvin* mechanism was further supported, when *Schrock* showed that metal carbene complexes could indeed be formed under the conditions applied to synthesize *Ziegler Natta* catalysts.[5a] He reported the first stable high oxidation state tantalum-based transition metal complex with a metal carbon double bond. $(Me_3CCH_2)_3Ta(=CHCMe_3)$ was the first representative of a new class of compounds, today termed *Schrock* carbenes (Figure 11). One of the first well-defined metathesis-active complexes was the *Tebbe* reagent[71], a titanium metallocene complex (Figure 11).

The nature of the metal-carbon double bond in *Schrock* carbenes can best be described by setting it apart from another group of metal-carbon double bonds, *Fischer* carbenes (Figure 12).[72] *Schrock*-type carbenes usually feature a transition metal in a high oxidation state and alkyl or hydrogen residues on the carbene, whereas *Fischer* carbenes are based on transition metals in low oxidation states and bear electron-withdrawing heteroatoms adjacent to the carbene atom. The two types of metal carbenes differ in reactivity. Whereas *Fischer*-type carbenes are rather electrophilic, *Schrock*-type carbenes are rather nucleophilic. This difference can be explained by taking a deeper look into the respective metal carbene bonds. *Fischer*-type carbenes are thought to be the result of the combination of a singlet carbene and a singlet metal fragment. Factors that favor low spin configurations on the metal fragment (e.g. π-acceptor ligands) and low spin configurations on the carbene carbon (e.g. π-donor substituents like amines or ethers), lead to the formation of *Fischer* carbene complexes.

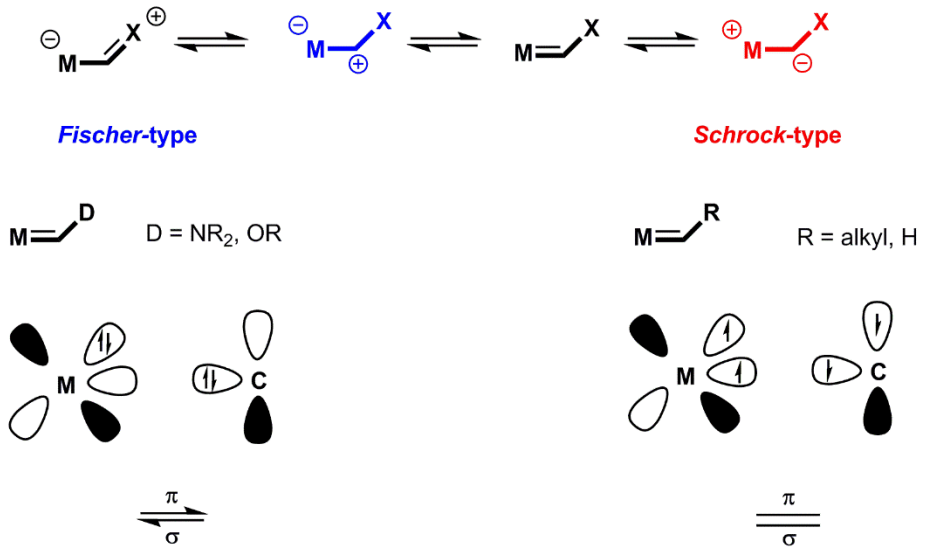

Figure 12: *Fischer*- and *Schrock*-type carbenes. Bond description as combination of two dative bonds (π and σ) resulting from pairing of a singlet carbene and a singlet metal fragment leading to a positive partial charge on the carbene (electrophilic carbene) in *Fischer* type carbenes. Two non-polar covalent bonds resulting from pairing of a triplet carbene with a triplet metal fragment resulting in a negative or no partial charge on the carbene (nucleophilic carbene) in *Schrock* carbenes.[72]

The metal carbene double bond can therefore be described as the formal overlapping of two dative bonds, one σ-bond from the carbene to the metal and one π-bond from the metal to the carbene. Since the σ-donating properties of the carbene are stronger than the π-acceptor properties, a formal positive partial charge on the carbene carbon can be deduced (blue structure, Figure 12). On the other hand, *Schrock*-type carbenes are thought to derive from the combination of a metal fragment in its triplet state and a carbene in its triplet configuration thereby leading to two non-polar covalent bonds. A nucleophilic (red structure, Figure 12) or neutral resonance structure can be assumed to be the favored structure. However, this is a quite crude approach, and the two described metal carbene bonds can be seen as the two extremes of metal carbene double bonds. When singlet carbenes are paired with triplet metal fragments or *vice versa*, the bonding situation becomes more complicated and reactivity must be investigated.

A further milestone in the synthesis of olefin metathesis catalysts based on molybdenum and tungsten was the finding, that bimolecular decomposition (especially of methylidene complexes), as one of the main decomposition pathways, can be prohibited by the introduction of sterically demanding imido ligands.[11c] This gave rise to *Schrock*-type catalysts, which are tetracoordinated species with an imido ligand, an alkylidene moiety and two alkoxide ligands.

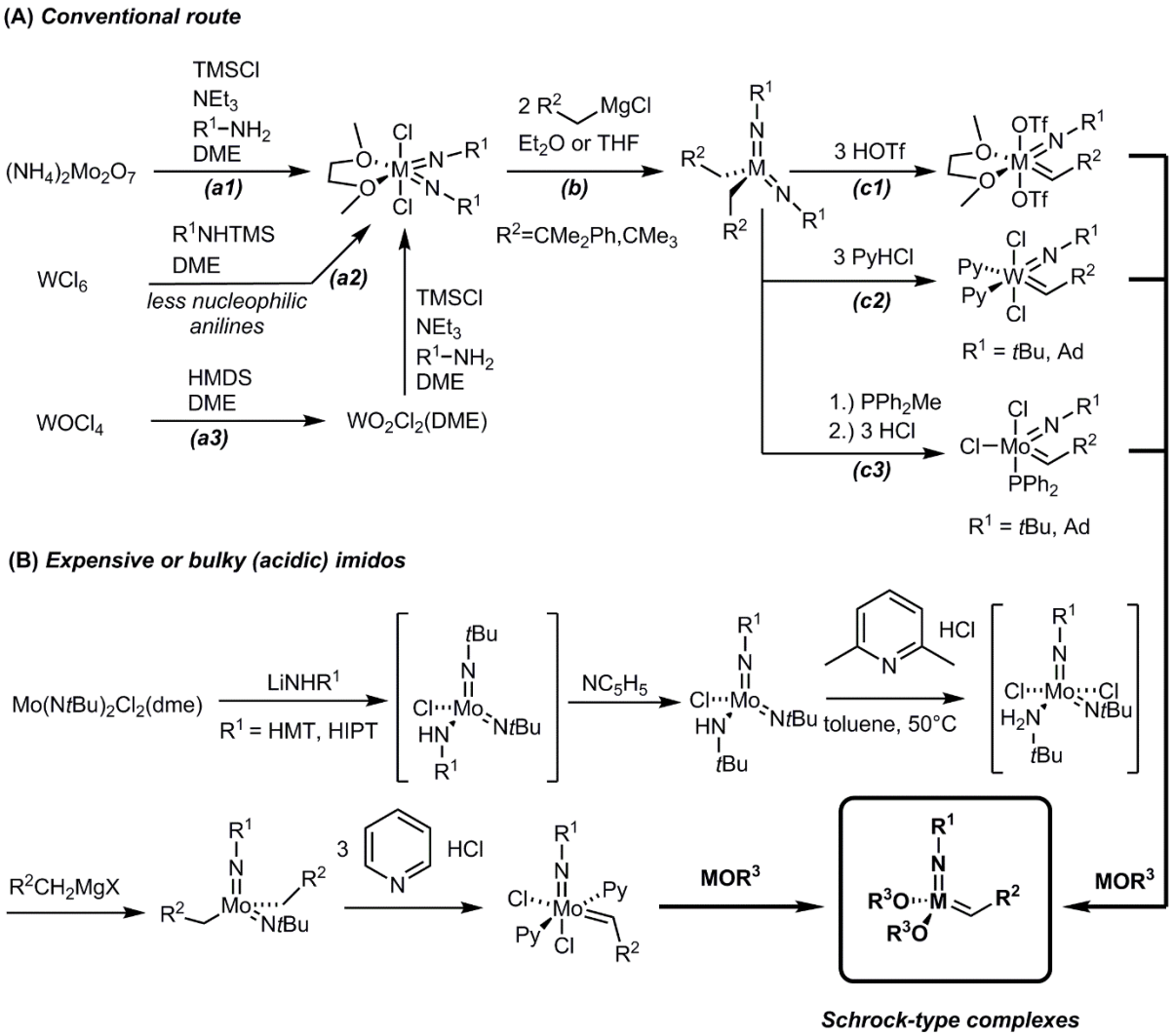

Scheme 6: Synthetic routes to *Schrock*-type complexes. **(A)** Conventional route starting from metal salts[73]and **(B)** late introduction of expensive and/or bulky imido ligands using a sacrificial *tert*-butyl imido ligand.[74]

The most prominent, general route to *Schrock*-type catalysts starts from molybdenum (usually molybdates) and tungsten salts ($WO_2Cl_2(DME)$[73a]) in high oxidation states to yield $M(NR^1)Cl_2(DME)$ complexes (Scheme 6, **(A)**, **a1** and **a3**). The synthesis proceeds over alkylation of the bischloro bisimido DME species (Scheme 6, **(A)**, **b**) and α-hydrogen abstraction to yield bisalkyl bisimido complexes (Scheme 6, **(A)**, **c1-3**).[73b] The universal precursors are $M(NR^1)(CHR^2)(OTf)_2(DME)$ complexes, which upon treatment with two equivalents of metal alkoxides, usually at low temperatures, react to the tetracoordinated desired metal imido bisalkoxide alkylidene complexes. Protonation of the bisalkyl bisimido complexes is usually carried out with triflic acid (Scheme 6, **(A)**, **c1**) but can also be realized with pyridinium hydrochloride[73c] (Scheme 6, **(A)**, **c2**) or PPh_2Me/HCl[73d] (Scheme 6, **(A)**, **c3**), as well as with acidic (highly fluorinated) alcohols[75]. In the case of tungsten, for electron withdrawing imido ligands, a special route starting from tungsten hexachloride was developed (Scheme 6, **(A)**, **a2**)[73e], since the usual procedure employing triethyl amine, TMSCl and the

respective aniline was unsuccessful. Most probably, the decreased nucleophilicity of the anilines results in incomplete replacement of the two oxo ligands in WO_2Cl_2(DME). Instead, tungsten hexachloride was reacted with the already TMS-protected aniline in DME, leading to the desired bisimido bischloro DME species in good yields and high purity (Scheme 6, **(A)**, **a2**).[73e] If expensive and/or bulky and rather acidic imido ligands are desired, to prevent usage of one sacrificial imido ligand, another route has been elaborated. Here, the high basicity of the *tert*-butyl imido ligand is exploited (Scheme 6, **(B)**). The imido ligand of choice is introduced as its lithium salt. Prominent examples, synthesized according to this route, are the HMT imido (hexamethylterphenyl, 2,6-(2,4,6-Me_3-C_6H_2)-C_6H_3) and the HIPT imido (hexaisopropylterphenyl, 2,6-(2,4,6-iPr_3-C_6H_2)-C_6H_3) metal alkylidene complexes.[74]

Another, particularly interesting feature of *Schrock*-type metathesis catalysts is the bond between the metal center and the imido ligand as well as the orientation of the imido ligand and the alkylidene moiety to one another. *Schrock*-type catalysts can exist in two forms, the *syn*-configuration, where the alkylidene hydrogen is pointing away from the imido ligand and the *anti*- configuration where the opposite is the case. Rotamer formation originates from the fact that there are two residual orbitals (d) at the metal center capable to engage in a metal-carbon π-bond, but the one that is vertical to the MNC plane is more accessible, since the π-orbital in the MNC plane is more likely to form a second π-bond to the imido ligand (*syn*-B vs. transition state, Scheme 7).[76] This is also reflected in a close to linear Mo=N-C_{ipso} bond for both, *syn*- and *anti*-isomer. The *syn*-isomer is more stable due to an agostic interaction between a metal orbital and the carbon-hydrogen bond (*syn*-C, Scheme 7). Agostic interactions are described as two-electron-three-center bonds. In *Schrock*-type catalysts (tetrahedral) as well as in their base adducts (TBP), all non-bonding (low energy) orbitals on the metal center in the MNC plane, that can engage in an agostic interaction, point away from the imido ligand, resulting in the observed higher stability of the *syn*-isomer.[76c] On the other hand, *anti*-isomers have been shown to be more reactive due to the increased *Lewis* acidity of the metal center resulting from the lack of agostic interaction.[77] Preferred formation of the *anti*-isomer can be encouraged by the introduction of sterically demanding imido ligands or by the employment of rigid ligand architectures such as bidentate ligands.[74,78] *Schrock et al.*[77] and *Davis et al.*[76a] demonstrated, that *syn*- and *anti*-alkylidenes can be interconverted into one another by irradiation with UV light (preferably 366 nm) or thermally. *Syn*-/*anti*-isomer interconversion rates have been determined by ^{1}H NMR spectroscopy and several trends could be identified.[77]

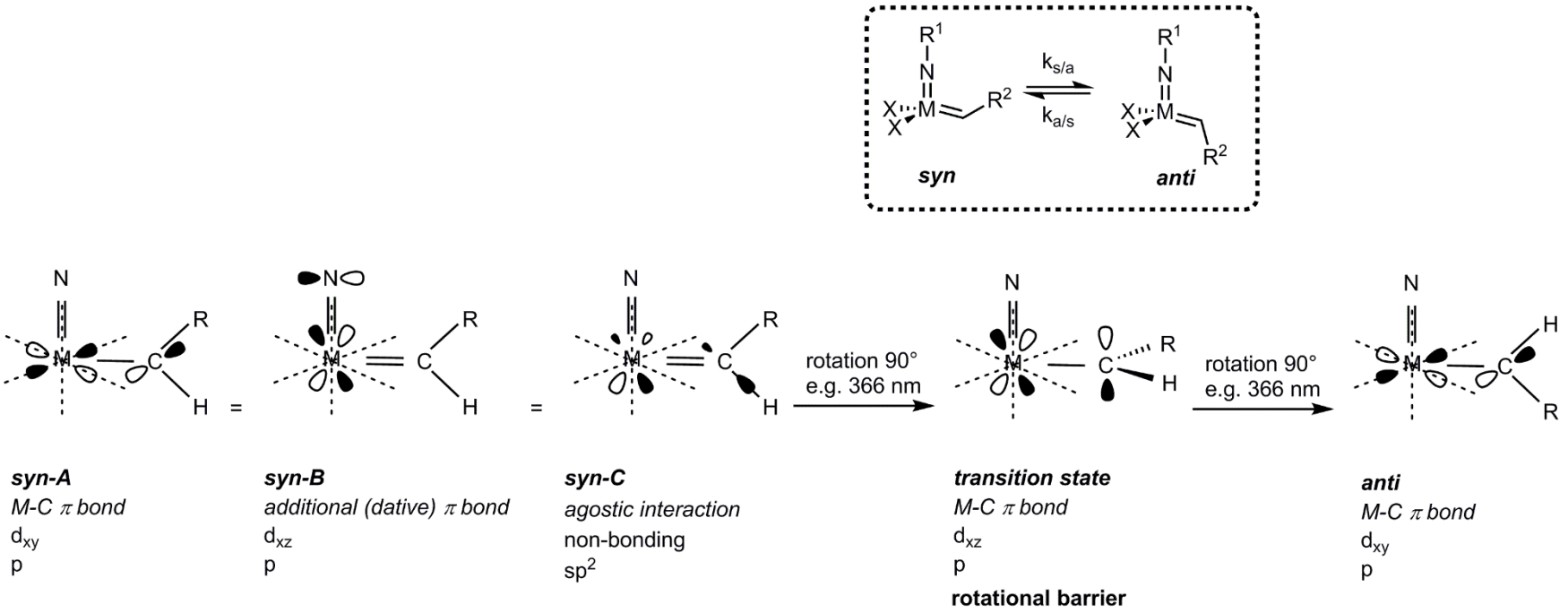

Scheme 7: *Syn-anti*-interconversion in *Schrock*-type metal complexes. Interactions that lead to preferred formation of *syn-*/*anti*-isomers (***syn*-B**) *vs*. transition state and interactions that lead to higher stability of *syn- vs- anti-* isomer (***syn*-C**).[76]

Anti-isomers are usually found approximately 1 ppm downfield from the corresponding *syn*-isomers in ^{1}H NMR spectra and display $^1J_{CH}$ coupling constants of the alkylidene proton between 145 and 155 Hz, whereas *syn*-isomers showed $^1J_{CH}$ values of 115 to 125 Hz.[76c] In tungsten complexes the increase in $^1J_{CH}$ in the *anti*-isomer is accompanied by a decrease in $^1J_{WC}$. Both can be explained by considering that the missing agostic interaction weakens the *WC* bond and strengthens the *CH* bond. Several trends for *anti*- to *syn*-interconversion were published. First, $k_{a/s}$ decreased with increasing fluorine content β to the oxygen of the alkoxide ligand.[77a] The increased *Lewis* acidity on the metal center leads to an increase in π-donation from the imido nitrogen to the metal center, resulting in a higher activation barrier for the formation of the intermediate 90° rotated double bond. Second, coordinating solvents like THF or DME decrease *anti*- to *syn*-interconversion.[76c,77b] *Schrock et al*. concluded that *syn*/*anti*-interconversion takes place in tetracoordinated species.[76c] Also, the neophylidene ligand was found to rotate only marginally slower than the neopentylidene ligand. The *syn*-/*anti*-interconversion rate $k_{s/a}$ was calculated from the equilibrium constant K_{eq} ($k_{a/s}$/$k_{s/a}$).

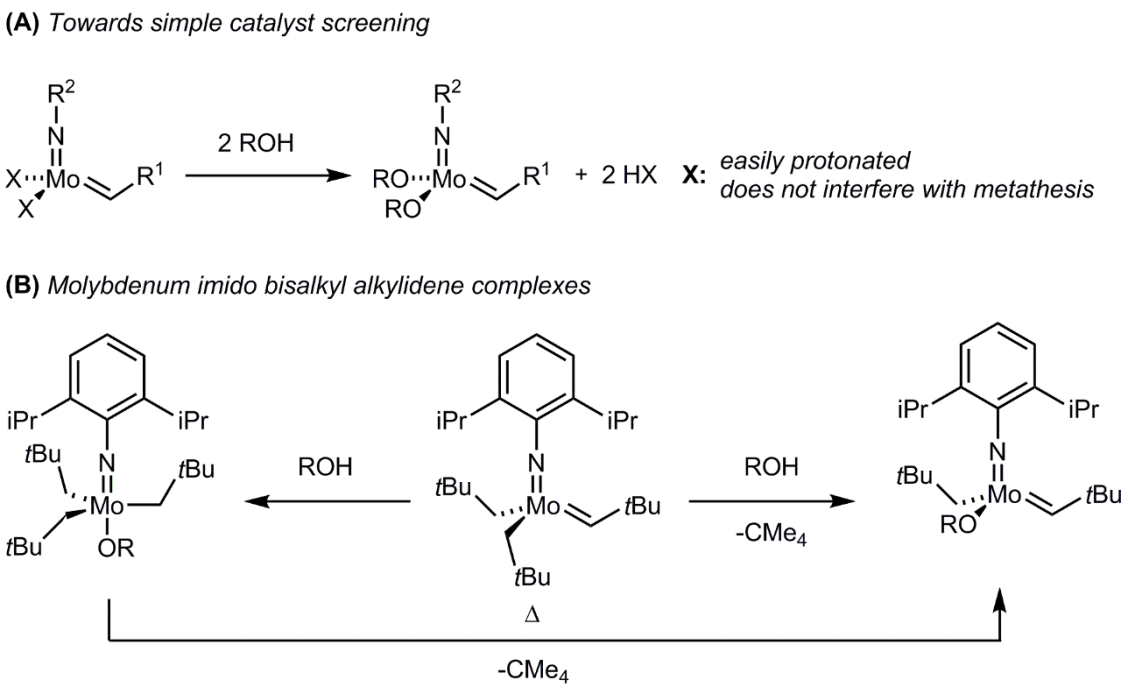

Scheme 8: **(A)** Precursors for *in situ* synthesis of molybdenum imido bisalkoxide complexes. **(B)** First attempts for precursors: molybdenum imido bisalkyl alkylidene complexes.[79]

Several criteria must be met if olefin metathesis catalysts should become suitable for industrial applications. For one, catalyst screening for tailored applications must be simple. Therefore, *Schrock et al.* investigated additional routes to standard metal imido alkylidene bisalkoxide complexes, where isolation of the catalysts would be unnecessary. In consequence, the product HX resulting from replacement of the X ligands in complexes M(NAr)($CHCMe_2R^1$)$(X)_2$ by other ligands, like terphenoxides or chiral alkoxides has to meet two criteria. First, HX

should not interfere with the metathesis reaction and second it should be easily separated from the product (Scheme 8, **(A)**). First attempts included the synthesis of molybdenum bisalkyl alkylidene complexes (Scheme 8, **(B)**). Unfortunately, protonation of both alkyl residues proved to be challenging and in some cases the alkylidene was protonated by the alcohol to yield molybdenum trialkyl complexes.[79] In contrast, the development of bispyrrolide complexes M(NAr)(CHCMe$_2$R)(NC$_4$H$_4$)$_2$ was promising.[22b,80]

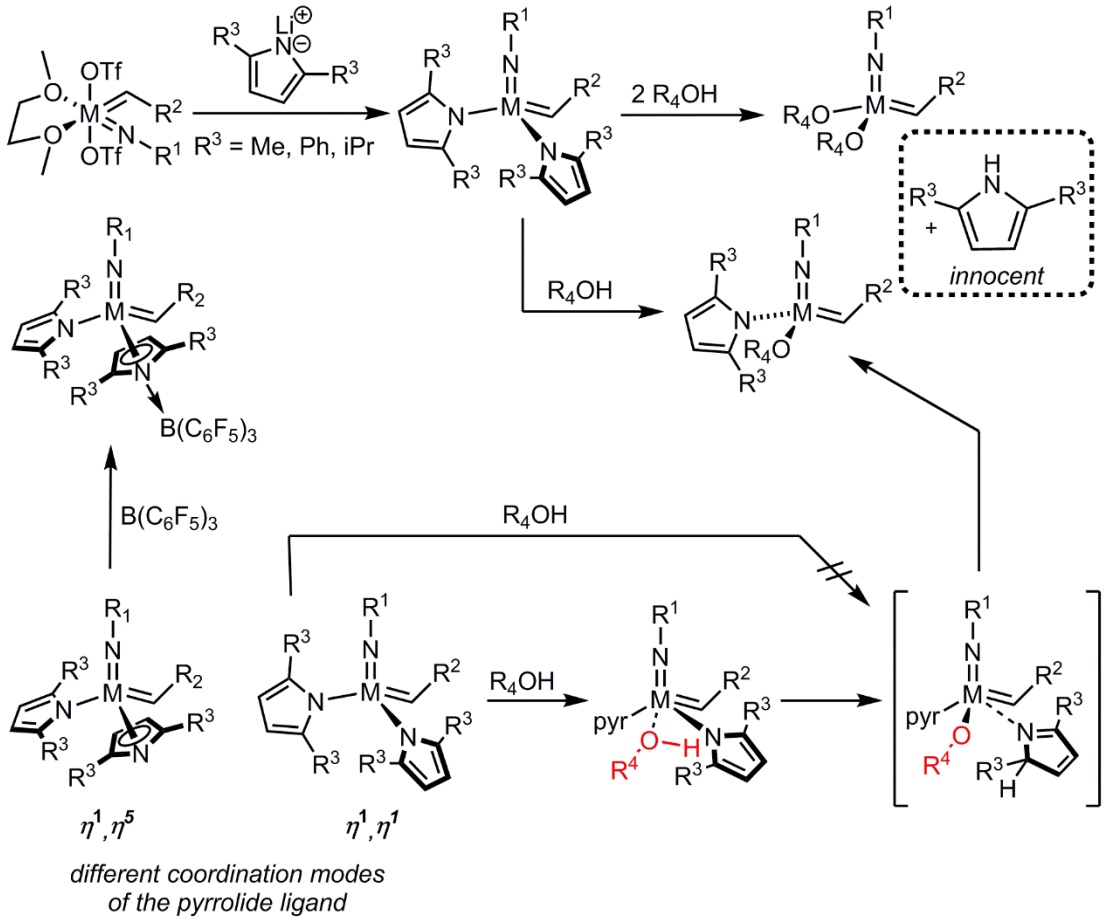

Scheme 9: Group 6 bispyrrolide imido alkylidene complexes: Synthesis from M(NR^1)(CHR^2)(OTf)$_2$(DME) complexes[22a], proposed mechanism for their formation[22a] and reactivity towards *Lewis* acids[22b].

Bispyrrolides are easily accessible *via* the conversion of the universal bistriflate precursors with two equivalents lithium pyrrolide in diethyl ether or toluene (Scheme 9). Both pyrrolides could easily be replaced with alkoxides by protonation with the corresponding alcohol, rendering the synthesis of metal alkoxides obsolete. In addition, complexes that were inaccessible before could be prepared by this approach. Bispyrrolide complexes containing the parent pyrrolide ligand often proved to be dimers.[22b] The pyrrolide ligand is isoelectronic to the cyclopentadienyl ligand, and similarly can coordinate either η^1 or η^5 (Scheme 9) to a metal center. The crystal structure of a dimer of a parent pyrrolide complex showed, that one pyrrolide ligand was coordinated η^5 to one metal center and η^1 via the nitrogen to the other

metal center. The η^5 coordination mode can be trapped by the addition of a *Lewis* acid.[22b] To circumvent dimer formation, bispyrrolide complexes with more sterically demanding pyrrolides, bearing methyl or even bigger groups (e.g. mesityl) adjacent to the nitrogen atom, were synthesized.[22a] Especially the 2,5-dimethylpyrrolide complexes proved to be superior due to increased stability and easier isolation while maintaining the favorable reactivity towards alcohols. The replacement of only one pyrrolide ligand by an alkoxide led to the next generation of *Schrock*-type complexes, so called mono alkoxide pyrrolide (MAP)-type complexes (Scheme 9). The reactivity of the bispyrrolides towards alcohols seems to depend on the accessibility of the η^1,η^1 species at room temperature. The ratio between η^1,η^1 species and η^1,η^5 species is temperature-dependent and is sensitive towards subtle changes in the steric environment. Furthermore, an associative pathway for the replacement of pyrrolide by alkoxide was proposed.[22a] First, an alcohol adduct of the η^1,η^1 bispyrrolide is formed, then the proton is transferred to one of the carbon atoms adjacent to the nitrogen atom of pyrrolide under formation of a pyrrolenin intermediate, before pyrrole is released (Scheme 9). Phosphine adducts of MAP-type complexes showed coordination of PR_3 *trans* to the pyrrolide ligand.[22a] *Eisenstein* and co-workers predicted, that stereogenic-at-metal complexes bearing one donor and one acceptor ligand would result in highly effective metathesis catalysts.[21a,21b,21e] The acceptor ligand ensures sufficient *Lewis* acidity at the metal center, facilitating substrate coordination. The donor ligand serves several, maybe more important, features. First, a donor ligand can facilitate distortion of the previously tetrahedral complex into a TBP geometry, where olefin coordination is more prone to occur. The distorted, olefin coordinated complex is stabilized best, when the olefin is coordinated *trans* to the donor (Scheme 10).

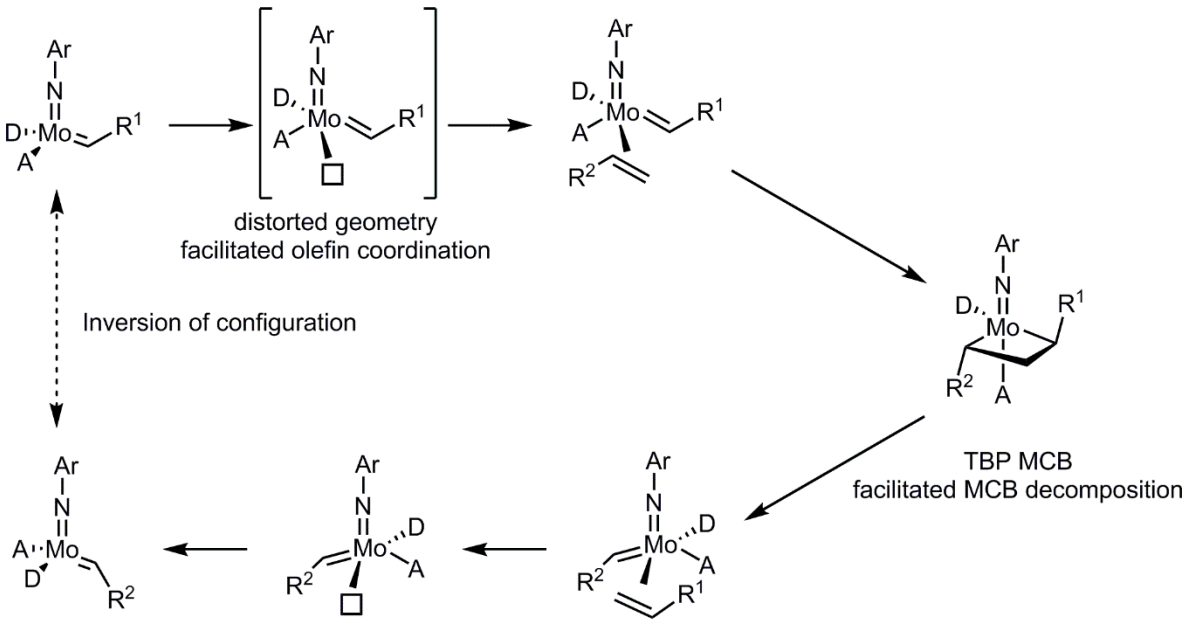

Scheme 10: Influence of the introduction of two electronically distinct ligands into an SP molybdenum imido alkylidene complex. Donor ligand (D) facilitates distortion of the metal complex and metallacyclobutane (MCB) decomposition. Acceptor ligand (A) ensures decent reactivity.[21a,21b,21e]

The olefin, the alkylidene and the donor ligand should occupy equatorial positions, whereas the imido ligand and the acceptor ligand should be in the axial positions of the distorted TBP structure. Second, the donor ligand facilitates metallacyclobutane decomposition under release of olefin by destabilization of the MCB intermediate resulting in a lowering of the activation barrier. Also, the electronegative nitrogen atom disfavors MCB decomposition via β-hydride elimination.[81] By taking a more careful look into the above described process, another interesting feature of MAP-type catalysts, relevant to stereoselective metathesis, becomes apparent. The stereogenic-at-metal complexes show inversion of configuration ((*R*) to (*S*) or *vice versa*) at the metal center after each olefin metathesis step (Scheme 10).[82] However, for stereoselective RCM, involving two metathesis events, the initial configuration is regained after one substrate turnover (translating into two metathesis steps). Considering the TBP structure of the MCB complex with metallacyclobutane and donor in the plane and the imido ligand and the acceptor ligand in the apex, in case stereoselective metathesis is wanted, it is most suitable to introduce steric information in the acceptor ligand. MAP-type complexes containing sterically demanding alkoxides, e.g. terphenoxides or 3,3´-substituted 5,5´,6,6´,7,7´,8,8´-octahydro-1,1´-bi-2-naphthols (8H-BINOL), were successfully applied in (*Z*)-selective olefin metathesis reactions, amongst others in the synthesis of epothilone C, yuzu lactone, epilachnene and nakadomarin A.[21d,61b-d,75,83]

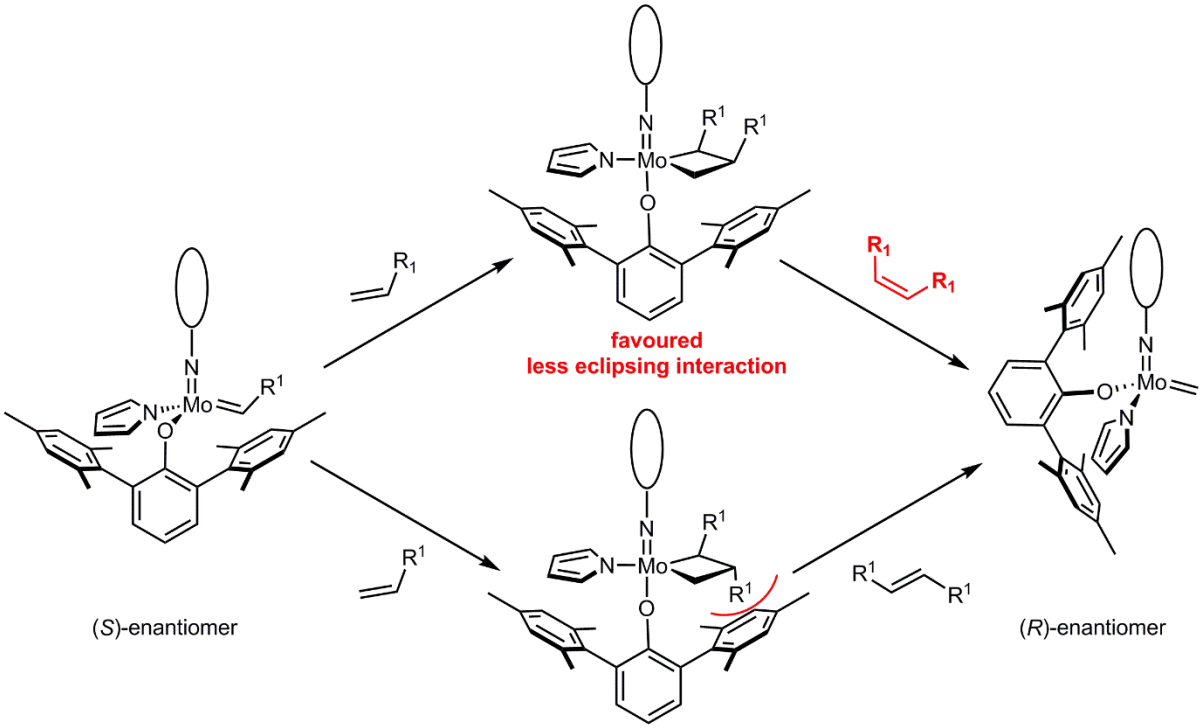

Scheme 11: (*Z*)-selective olefin metathesis. Inversion of configuration at the metal center within one metathesis step. Eclipsing interactions in the TBP metallacyclobutane intermediates leading to the favored formation of (*Z*)-products.[84]

The high (*Z*)-selectivity of the catalyst systems stems from a careful choice of acceptor and imido ligand. If the imido ligand in the TBP metallacyclobutane complex is small and the alkoxide ligand is sterically demanding (or *vice versa*), orientation of both substituents in the metallacyclobutane towards the small ligand is energetically favored, leading to primarily (*Z*)-products (Scheme 11). Of course, since olefin metathesis is a reversible process, the energetically disfavored (*Z*)-products can re-enter the metathesis cycle, interfering with overall selectivity. Therefore, formation of (*Z*)-products over reaction time must be carefully monitored and ethylene is usually removed since it severely competes with the substrate and leads to instable metal methylidenes.[84]

Stereoselectivity plays a crucial role in macrocyclization, since the stereoisomers often have different smells. Macrocyclization is a branch of olefin metathesis relevant to for example fragrance industry since several macrocycles are used as fragrances in perfumes. Isoambrettolide and ambrettolide are prominent examples. Macrocyclization still provides some challenges in terms of reaction control. As already outlined above, RCM is only favorable if small cycles (approx. 5-8 carbon atoms) are formed. In the case of bigger cycles, ADMET or oligomerization become competitive (Scheme 12).

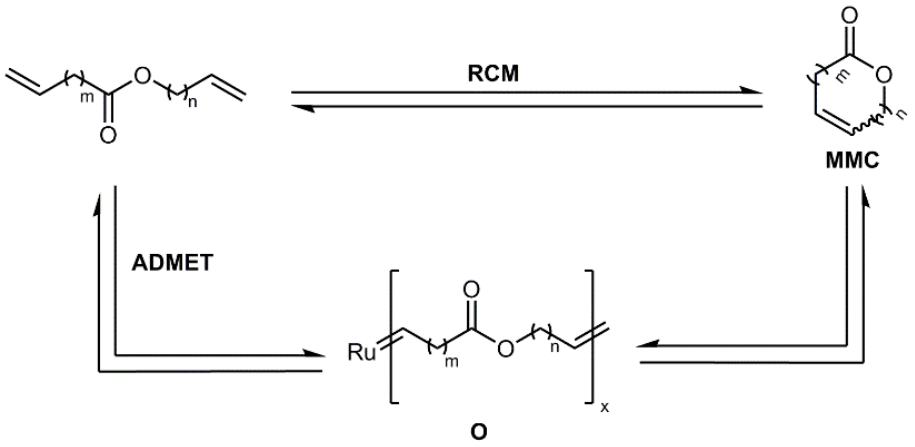

Scheme 12: Competing ADMET and RCM in macrocyclization of long chain dienes. Formation of oligomers (O) *vs*. formation of macrocycle (MMC).[85]

Macrocyclization proceeds *via* formation of (macrocyclic) oligomers, which are then, over time, cyclodepolymerized to form the desired macrocyclic species.[85] Therefore, RCM of long chain dienes requires high dilutions and long reaction times. Several groups published on the (*Z*)-selective formation of multiple macrocycles employing MAP-type catalysts or *CH*-activated ruthenium based catalysts in 1,2-dichloroethane under static vacuum and at a substrate concentration of 3-5 mM.[61a,61c,61d,86] It was also shown that (*E*)-/(*Z*) mixtures of macrocycles can be transferred into almost exclusively (*E*)-isomer by selective ethenolysis of a (*Z*)-macrocycle.

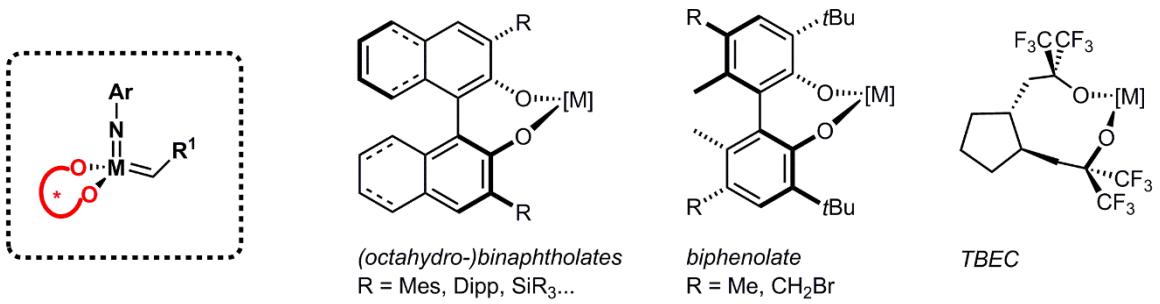

Figure 13: Exemplary chiral chelating diolate ligands for molybdenum and tungsten imido alkylidene olefin metathesis catalysts.[9a,20,87]

The first synthesized chiral olefin metathesis catalysts contained chiral chelating diolate ligands (Figure 13).[88] The diolates were usually based on (3,3´-substituted-) biphenolates or binaphtholates. One chiral catalyst with a (1*R*,2*R*)-2´,2´,2´´,2´´-tetrakis(trifluoromethyl)-1,2-bis(2´-hydroxyethyl)cyclopentane ligand was isolated by *Grubbs et al.*[89], although the corresponding catalyst showed only moderate enantioselectivity (Figure 13). Apart from the synthesis of highly tactic polymers[88a] (*vide infra*), those catalyst were primarily employed in the asymmetric RCM (ARCM) of racemic dienes or achiral trienes.[9,90] Further frequently used asymmetric olefin metathesis reactions are tandem asymmetric ring opening/ cross-

metathesis (AROM/CM) and AROM/RCM.[91] Racemic dienes are transferred into the enantioenriched substrates and the enantioenriched products with inverse configuration by chiral resolution (Scheme 13). Several criteria must be met if chiral resolution is desired. First, two chiral transition states with significantly different energies should be formed. Second, the interconversion between those two species has to be much faster than the follow-up reaction (Scheme 13).[92] Considering reaction rates that translates into $k_{2A} >> k_{2B}$ (or *vice versa*) and $k_{2X} >> k_{3X}$ (**(A)**, Scheme 13). Differences in the energies of the transition states can arise from subtle differences in steric interactions in the MCB transition state (**(B)**, Scheme 13). Olefins usually approach an olefin metathesis catalyst *via* one of the CNO faces.[93] In a chiral metal complex two different CNO faces are present, one side is typically blocked by a sterically demanding group, thereby leading to differences in reaction rates. ARCM of achiral symmetrical trienes offers access to chiral molecules. Here, the formation of one of the two possible enantiomers is preferred.

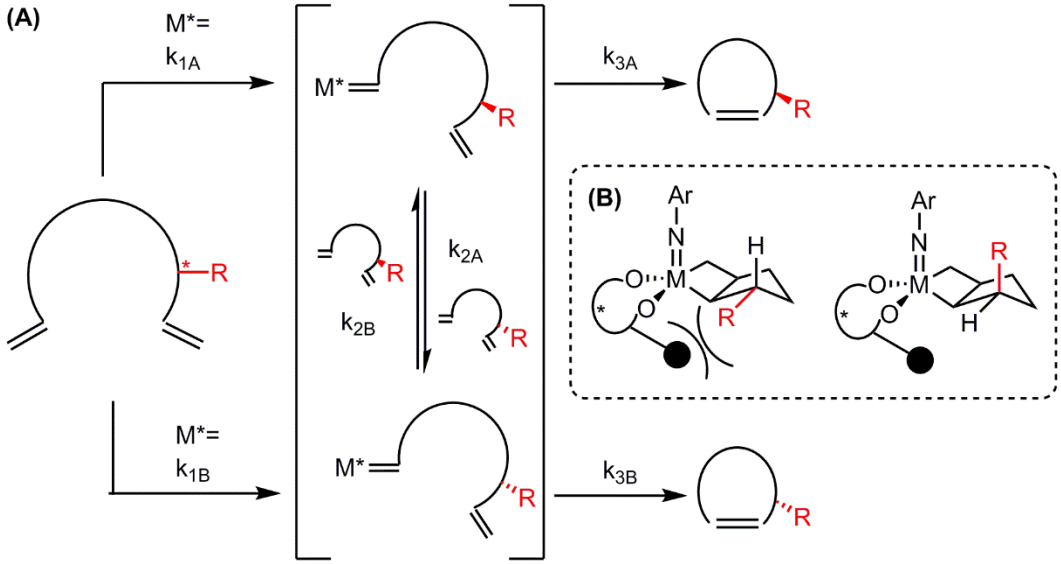

Scheme 13: Chiral resolution of racemic dienes. **(A)** Relevant steps. **(B)** Transition states with different energies due to differing steric interactions.[92]

Hoveyda et al. developed a model to explain enantioselectivities in the ARCM of symmetrical enol ethers (Scheme 14).[94] During the formation of the first metal-carbon double bond with a substrate, formation of *syn*- and *anti*-alkylidenes is possible. Due to the higher *Lewis* acidity the *anti*-isomer is more reactive. The approach of the second double bond to the metal center *prior* to ring-closing therefore preferably takes place at the *anti*-isomer. In the *anti*-isomer (as well as in the *syn*-isomer), different approaches of the olefin to the preferred CNO face lead to different steric interactions, resulting in different activation barriers. In the case of enol ethers, a *syn*-pentane interaction was postulated to be the cause for the preferred orientation of the second incoming double bond.

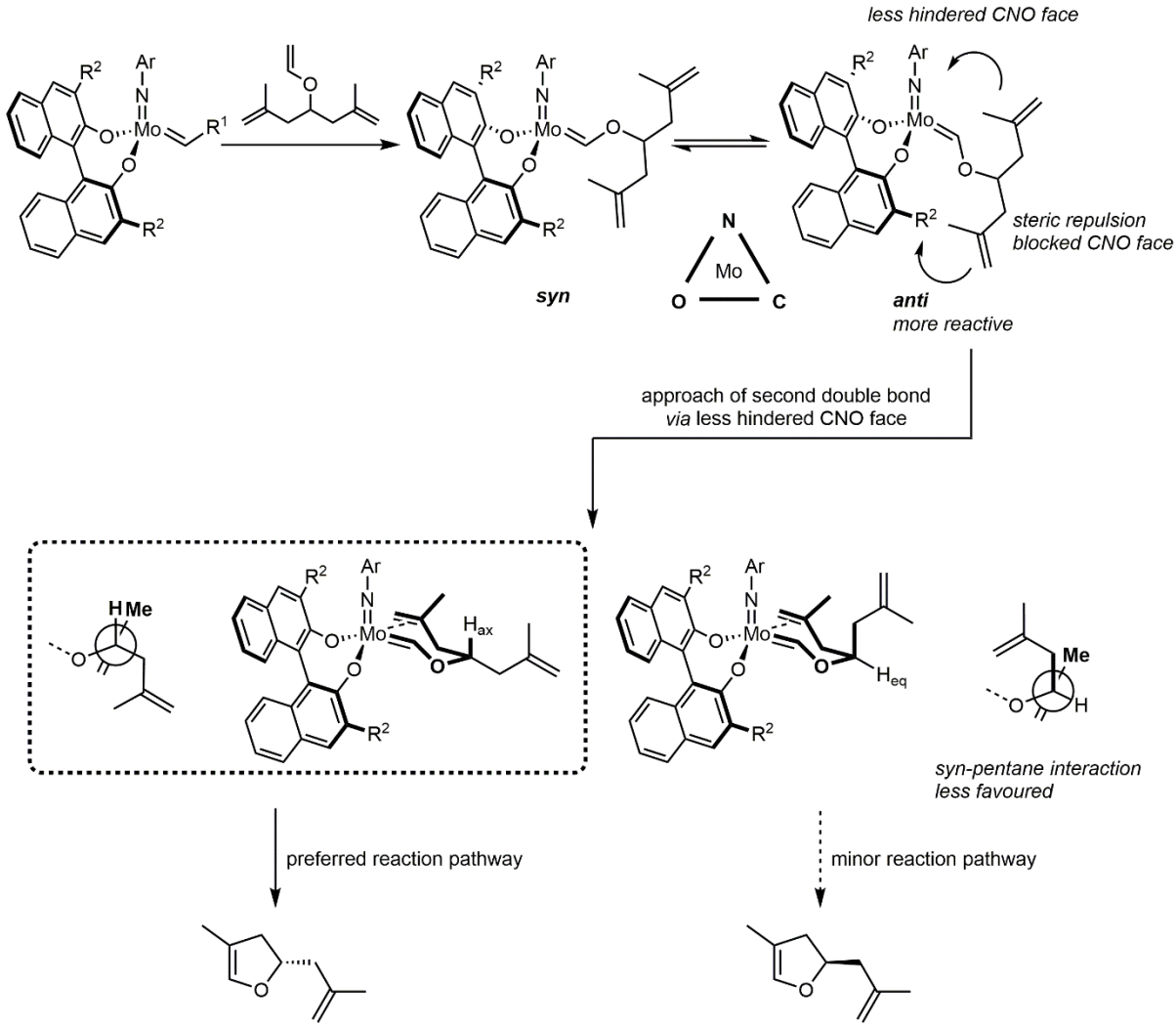

Scheme 14: ARCM of achiral symmetrical enol ethers. Preferred coordination of the second double bond *via* the less hindered CNO face of the more reactive *anti*-isomer. *Syn*-pentane interaction leads to favorable formation of one enantiomer. [94]

The kinetic resolution of racemic dienes is an excellent example to demonstrate, that there is not a single catalyst that will catalyze every reaction. For example, biphenolate ligands, in many cases, lead to high conversions and enantioselectivities in the ARCM of 1,6-dienes[95], whereas binaphtholate ligands are usually more likely to provide good reactivitiy and selectivity in the ARCM of 1,7-dienes.[96] 8H-BINOL ligands, which were designed as hybrids between biphenolates and binaphtholates, also show a unique reactivity profile.[97] This underlines the need for large catalyst libraries and fast catalyst screening provided by MAP-type catalysts. Also, the reactivity of chiral catalysts with chelating diolate ligands was comparably low, which was postulated to result from highly strained and therefore high-energy metallacyclobutanes.[21d]

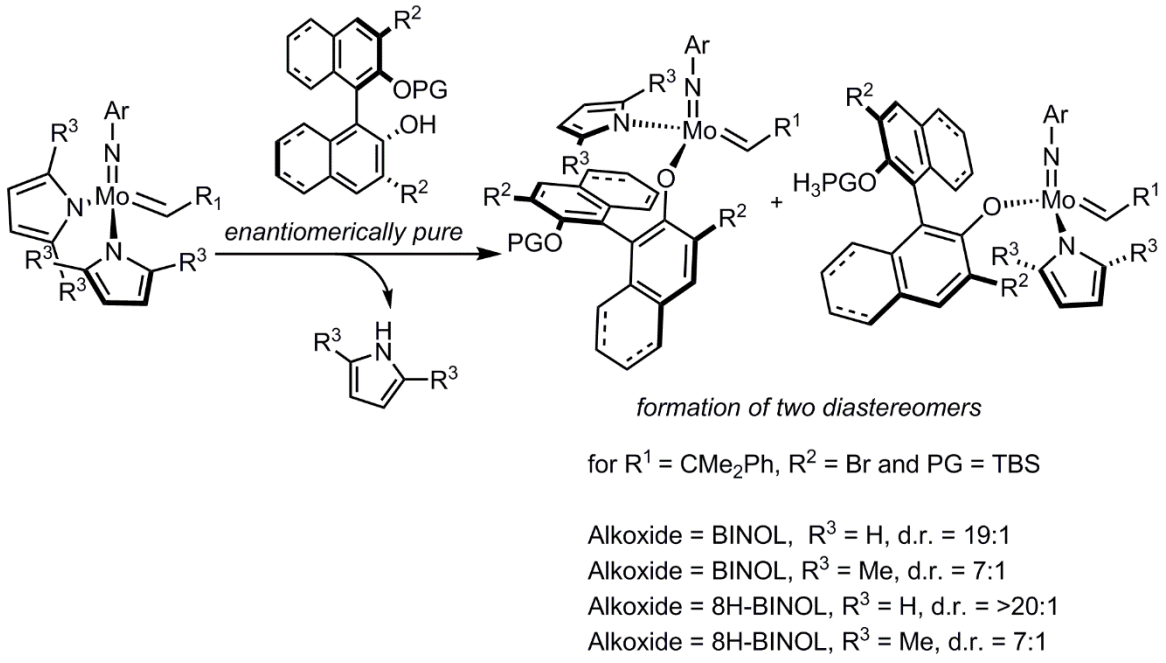

Scheme 15: Diastereoselectivity in the formation of chiral MAP type catalysts from metal bispyrrolides and enantiomerically pure (8H-)BINOLS.[21d,21e,98]

In fact, chiral MAP-type catalyst featuring mono-protected 8H-BINOLs have been prepared and successfully used in asymmetric olefin metathesis reactions.[21d,21e,98] Results were comparable to, or better than those obtained for the previously used diolate catalysts. The MAP-type species can be prepared *in situ* from the corresponding mono-protected chiral alcohol and the metal imido alkylidene bispyrrolide species (Scheme 15). In case enantiomerically pure mono-protected (8H-)BINOLs are coordinated to bispyrrolide species, two diastereomers are formed. However, when catalysts are used *in situ* and without separation of the diastereomers by crystallization, it is crucial that preferably one diastereomer is formed.[21e] Diastereoselectivity in the catalyst formation, amongst other factors, depends on the choice of the imido ligand, the alkoxide ligand and the 2,5-substituents of the pyrrolide ligand. If the 3,3´-substituents are hydrogen atoms, diastereoselectivity in catalyst synthesis drops and formation of bisalkoxides instead of MAP-type catalysts is observed, even when only one equivalent alcohol respective to metal bispyrrolide is used.[21e] No interconversion between the two diastereomers was observed in solution up to one month.[21e] 8H-BINOLs offer various possibilities to electronically or sterically tune the ligand system. The 3,3´-substituents for example have been altered from the electron-withdrawing halogens[21d,61c,98c] (I, Br, Cl, and F) to methyl[98a] and to methoxy[98a] and the influence of protecting groups[98a] was investigated.

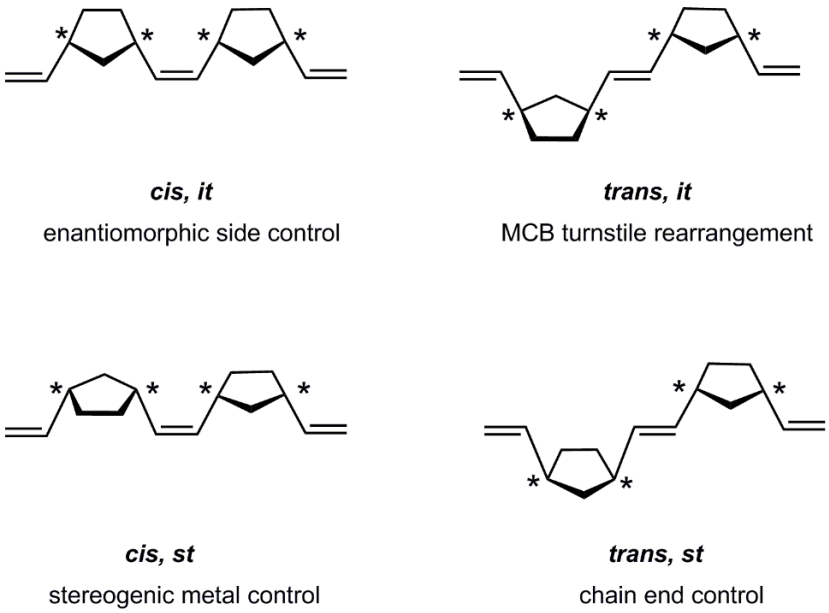

Figure 14: Four possible stereoregular structures for ROMP derived polymers and the so far identified mechanisms leading to their formation.[12a]

As already mentioned, chiral olefin metathesis catalysts also found widespread application in the ROMP of strained cyclic olefins. The primary structure of stereoregular ROMP-derived polymers is defined by the double bond configuration (*cis* or *trans*) and by tacticity.[12a] A given polymer is termed “isotactic” (*it*) when all chiral carbon atoms in the repeat unit have the same configuration throughout the polymer. In a syndiotactic (*st*) polymer, chiral atoms in neighbouring repeat units display opposite chirality. The formation of a polymer with a single structure translates into the presence of only one propagation step (or a sequence of propagation steps that is repeated) which is at least twenty times faster than all other imaginable propagation steps. In total, four different stereoregular structures can be envisioned, namely *cis*,*it*; *cis*,*st*; *trans*,*it* and *trans*,*st* (Figure 14). Control over polymer structure is crucial because primary, secondary and tertiary orientations have a huge impact on physical properties. Four pathways to ROMP polymers with defined structures have been identified so far.[12a] Chain end control (*trans*, *st* polymers), enantiomorphic site control (*cis*, *it*), stereogenic-metal control (*cis*,*st*) and a turnstile-type rearrangement of the metallacyclobutane (*trans*,*st*). Before going into detail for each pathway, the key factors, leading to *cis*- and *trans*-double bonds, as well as *it*- or *st*-structures must be defined.

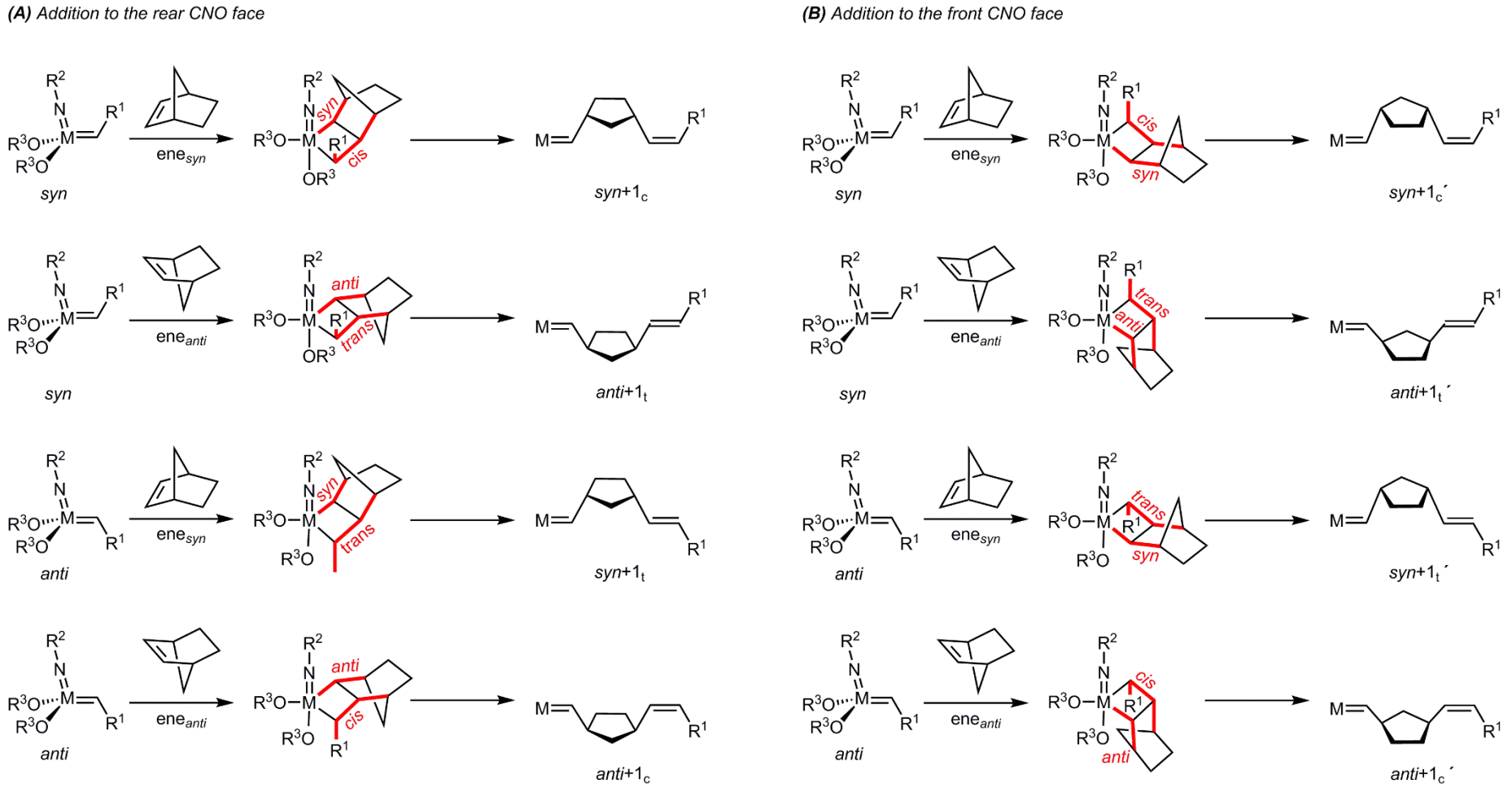

Scheme 16: First insertion products of norbornene addition from the rear **(A)** and front **(B)** CNO face to *syn*- and *anti*-isomers of a metal alkylidene.[12a]

When a substrate adds to the metal alkylidene bond it adds *via* one of the CNO faces[93] (not *via* COO). If one CNO face is favored and the starting alkylidene is in its *syn*-configuration, norbornene can add with its ring structure pointing in the same (ene_{syn}) or opposite (ene_{anti}) direction compared to the substituent of the imido ligand, leading to *syn*+1_c (*syn* alkylidene, *cis*-double bond) and *anti*+1_t (*anti* alkylidene, *trans*-double bond) insertion products (Scheme 16, **(A)**). Approach of the substrate via the same CNO face but to the *anti*- instead of the *syn*-isomer leads to *syn*+1_t and *anti*+1_c. Approach of the substrate from the other CNO face (Scheme 16, **(B)**) leads to the mirror images of the four above described structures, *syn*+1_c´, *anti*+1_t´, *syn*+1_t´ and *anti*+1_c´. When an additional substrate is inserted, eight possible propagation pathways are possible since the two CNO faces are distinct due to the chiral β-carbon. Each stereoregular structure can therefore be formed by two different pathways. For example, a *trans*,*st* polymer structure is accessible *via* chain end control (Scheme 17). Chain end control means that the favored CNO side is determined by the polymer structure, in detail by the configuration of the C_β-carbon atom. A *trans*,*st* polymer structure can be achieved, when in addition to chain end control, either the *syn*-isomer is the reactive isomer and the ene always approaches *anti* to the imido ligand or when the *anti*-isomer reacts and an ene_{anti} approach is preferred. If one CNO face of a metal alkylidene bearing a chiral (racemic) C_2-symmetric diolate ligand is preferred over the other due to for example steric constraint, this is termed enantiomorphic site control. Formation of *cis*,*it* structures by enantiomorphic site control is achieved when an *anti*-isomer reacts via the ene_{anti} approach or an *syn*-isomer via the ene_{syn} approach (Scheme 18, **(A)**). Chiral (racemic) MAP-type catalysts on the other hand enable the synthesis of *st* polymers, since the configuration at the metal center inverts after each monomer insertion and the monomer will always approach *trans* to the pyrrolide ligand. This is called stereogenic metal control and differs from enantiomorphic site control and chain end control since selectivity originates from electronic rather than steric factors. When a bulky aryloxide and a small imido ligand are employed the ene will always insert *syn* to the imido ligand (Scheme 18, **(B)**). This will ultimately result in *cis*,*st* structures.

(A) chain end control, only syn-isomer reacts

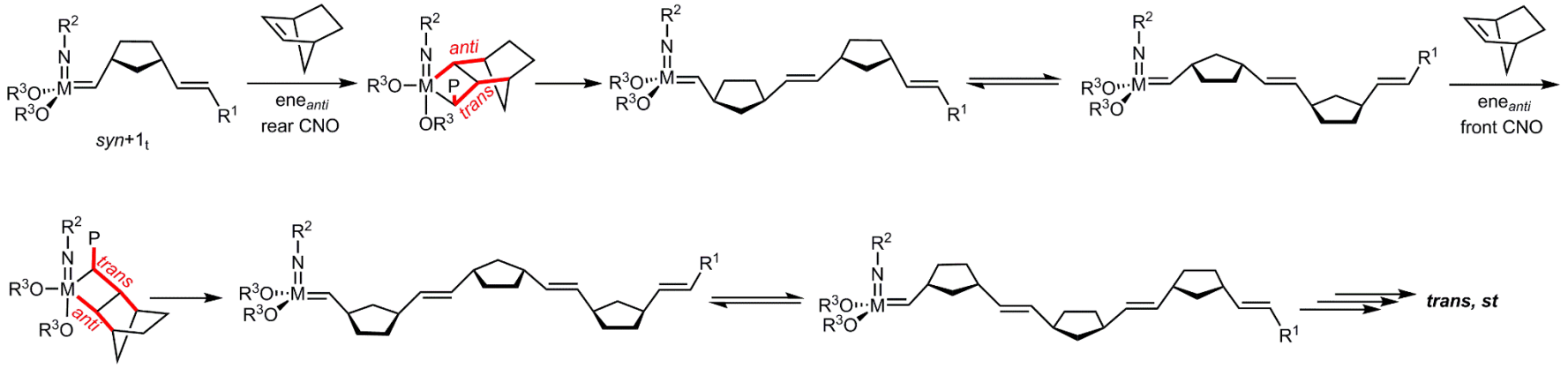

(B) chain end control, only anti-isomer reacts

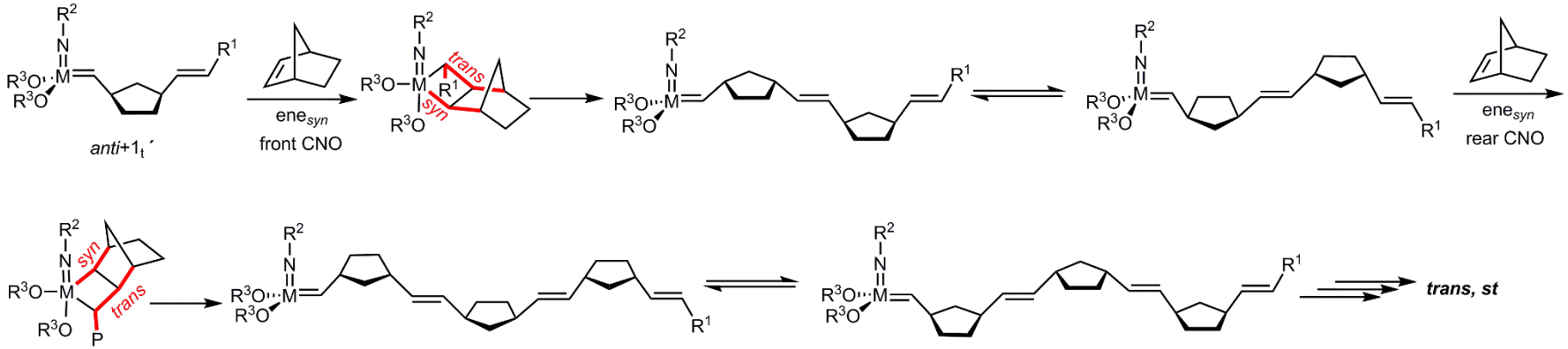

Scheme 17: Two different pathways leading to a *trans*,*st* polymer structure. **(A)** *syn*-isomer is the reactive isomer, ene$_{anti}$ approach and chain end control; **(B)** *anti*-isomer is the reactive isomer, ene$_{syn}$ approach, chain end control.[12a]

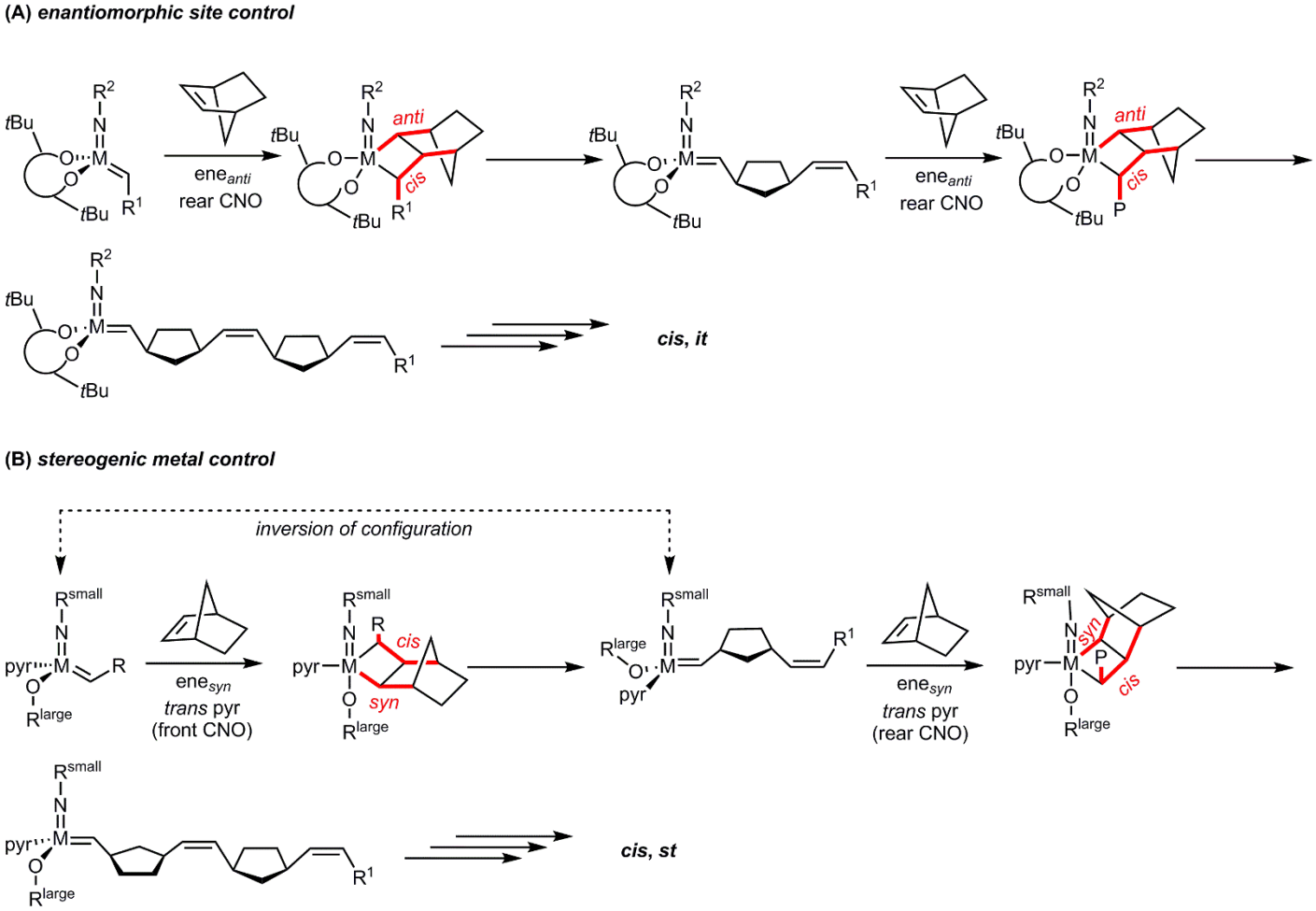

Scheme 18: **(A)** Exemplary pathway to the formation of *cis*, *it* structures by enantiomorphic site control with the *anti*-isomer being the reactive isomer and ene$_{anti}$ approach. **(B)** Formation of *cis*,*st* structures by stereogenic metal control with chiral (racemic) MAP-type catalysts.[12a]

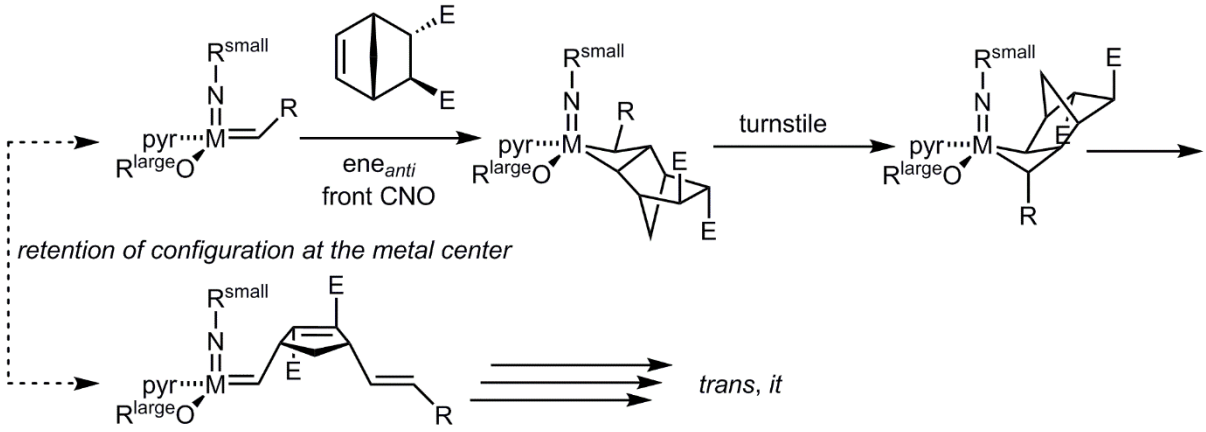

Scheme 19: Proposed mechanism for the formation of poly(DCMNBE) trans,*it* dyads with the key step being a turnstile rearrangement of the metallacyclobutane, leading to retention of configuration at the metal center.[99]

In 2012 *Schrock et al.* published on the formation of poly(2,3-dicarbomethoxy-norbornadiene) (poly(DCMNBE)) consisting of *cis*,*st* and *trans*,*it* dyads in a ratio of approximately 8:92.[99] They proposed a mechanism leading to *trans,it* dyads relying on *anti* monomer insertion to a *syn*-isomer followed by a turnstile rearrangement in the metallacyclobutane which leads to retention of configuration at the metal center (Scheme 19).[99] They preferred this mechanism over one that is based on alternating *anti*+ene$_{syn}$ and *syn*+ene$_{anti}$ approach to the CNO face *trans* to the pyrrolide ligand since this would include two different propagating steps.

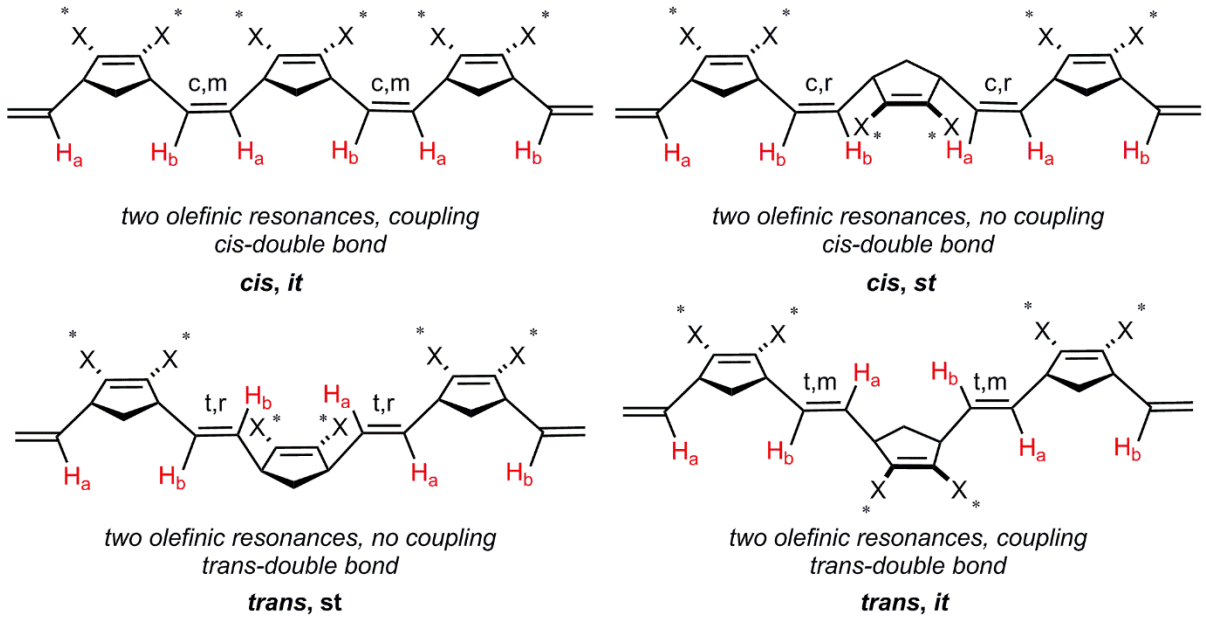

Figure 15: Four possible stereoregular structures of poly(2,3-dicarboalkoxy-norbornadienes).[88b]

Tacticitiy in the above described structures has been determined by polymerization of, for example, norbornadienes with enantiomerically pure alkyl esters in 2- and 3-position and transferring the obtained results to other polymers.[88b] A *cis*,*it* polymer and a *trans*,*it* polymer should display two olefinic resonances that are coupled (doublet of doublets, often pseudo-

triplets) whereas *cis* and *trans*,*st* polymers should display two olefinic resonances that are not coupled (Figure 15).

Another issue in metathesis reactions is the selective synthesis of pure *(E)*-products. *Schrock* and *Hoveyda* recently published on the selective formation of thermodynamically less favored (*E*)-alkenyl halides from cross-metathesis of (*E*)-1,2-dihaloalkenes with MAP-type catalyst bearing sterically demanding aryl oxides.[100] (*E*)-selectivity can be reasoned by a similar approach as described before for (*Z*)-selectivity with MAP-type catalyst by considering favorable interactions in the respective metallacyclobutanes (Figure 16).

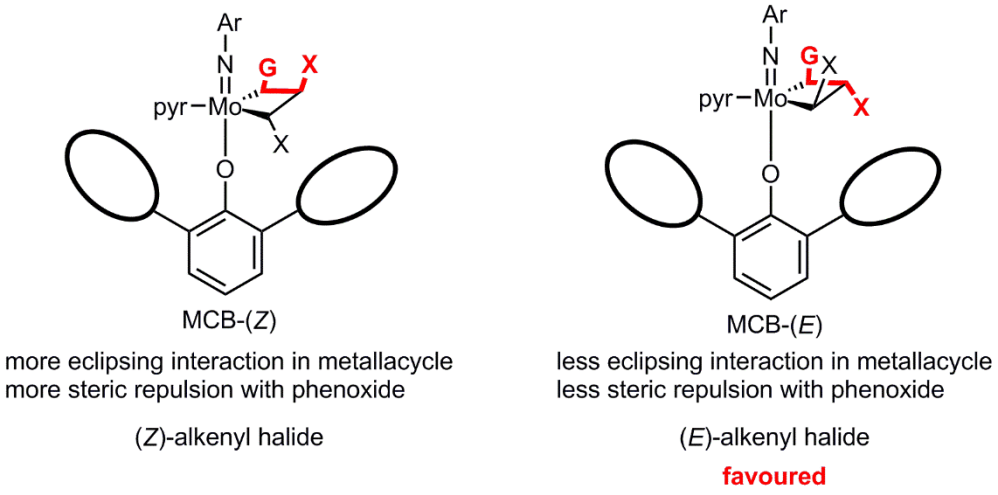

Figure 16: Eclipsing interaction and steric repulsion in metallacyclobutanes of MAP-type catalysts with 1,2-dihaloalkenes leading to (*Z*)- or (*E*)-alkenyl halides.[100]

In MCB-(*Z*), which would collapse into the (*Z*)-alkenyl halide, there is a strong eclipsing interaction between the chloride on the β-metallacyclobutane carbon and G, whereas in MCB-(*E*) the eclipsing interaction between the two substituents on the α carbons is reduced. Also, the steric repulsion between the large aryloxide and the α-*C*-substituent in MCB-(*Z*) is stronger than the repulsion between the aryl oxide and the β-*C*-substituent in MCB-(*E*). Especially MAP-type catalysts with aryl oxides bearing 3,5-substituents on the phenyl wingtips proved to be active and (*E*)-selective in cross-metathesis reactions with (*E*)-alkenyl halides. No substituents on the alkoxides phenyl wingtips lead to high (*E*)-selectivity but a strong decrease in conversion, most probably due to bimolecular decomposition.

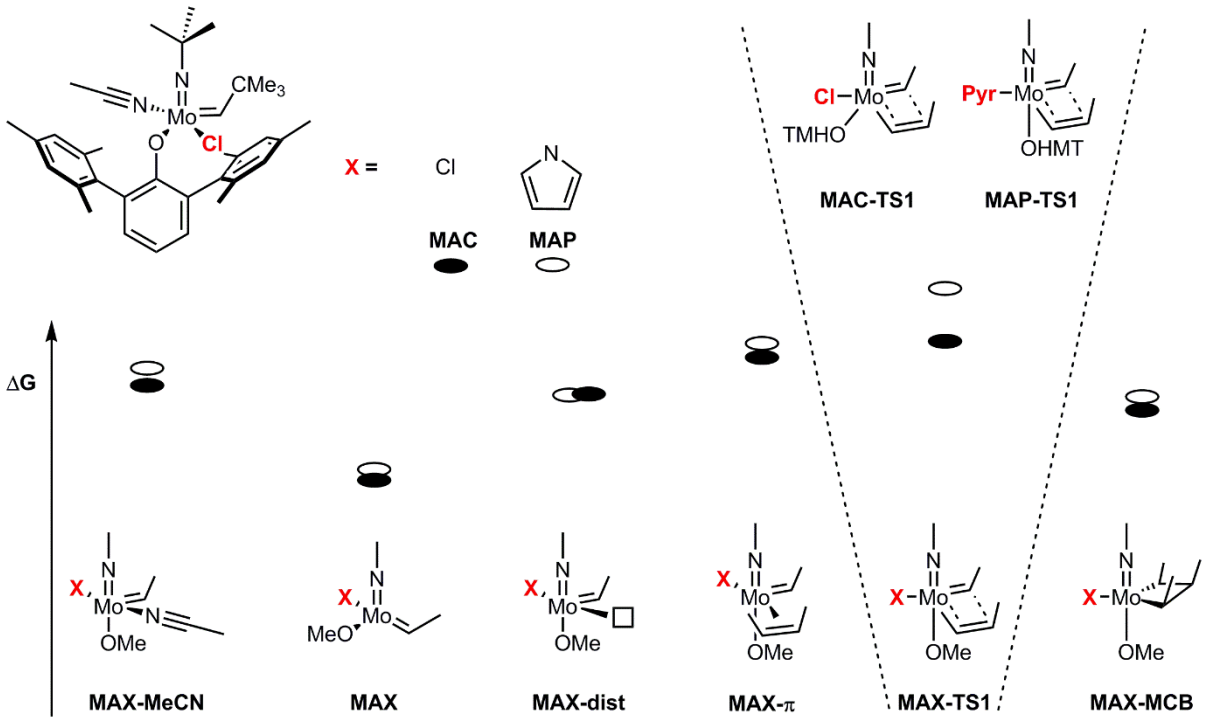

Figure 17: Comparison of MAC-type and MAP-type molybdenum alkylidene complexes in metallacyclobutane formation. Higher activity of MAC- *vs*. MAP-type complexes can be explained by the lower total energy barrier from **MAC→MAC-MCB** *vs.* **MAP→MAP-MCB**.[101]

In 2017 the *Schrock* and the *Hoveyda* group published on molybdenum imido mono alkoxide chloride alkylidene complexes (MAC) that showed remarkable activity and selectivity towards the higher energy *(Z)*-isomers in cross-metathesis reactions with *(Z)*-1,1,1,4,4,4-hexafluoro-2-butene, as well as in cross-metathesis reactions with *(Z)*-1,2-dichloro- and dibromoethane.[101] Density functional theory (DFT) calculations on several methoxy ligated complexes, including MAP-type complexes, were carried out to explain the high activity of MACs as well as their *(Z)*-selectivity and preferred formation of cross-metathesis *vs.* homometathesis products (Figure 17). The high activity can be traced back to a rather small total energy barrier of 12.5 kcal/mol from the monoalkoxide chloride imido alkylidene complex **MAC** over the distorted complex with a free coordination site *trans* to the chloride **MAC-dist** and over the π-olefin complex **MAC-π** to metallacyclobutane formation **MAC-MCB** (Figure 17). For comparison, MAP complexes display an overall energy barrier from the starting complex **MAP** to the metallacyclobutane **MAP-MCB** of 14.1 kcal/mol and 14.0 kcal/mol for parent pyrrolide and 2,5-dimethylpyrrolide, respectively. The low energy transition state **MAC-TS1** accounts mainly for the comparably low barrier. The energy barrier to the transition state **MAC-TS1** correlates with the carbon carbon double bond activation in **MAX-π** derived from the respective C=C bond length which is longer for the more *Lewis* acidic MAC complexes (stronger chelation leads to less double bond character and a longer C=C bond). Previous investigations on less substituted metallacyclobutanes suggested that the stronger σ-donor

renders a *trans* coordination site more readily available.[21a,21b] The difference between the overall energy barrier (**MAX→MAX-MCB**) of MAC and MAP complexes becomes even more distinct when a more sterically demanding OHMT ligand is considered. This is due to the fact, that in the MAC catalyst, the phenoxide ligand can increase its distance to the double bond carbon atoms by shifting towards the less sterically demanding chloride ligand, resulting in a lower energy for **MAC-TS1** *vs*. **MAP-TS1**.

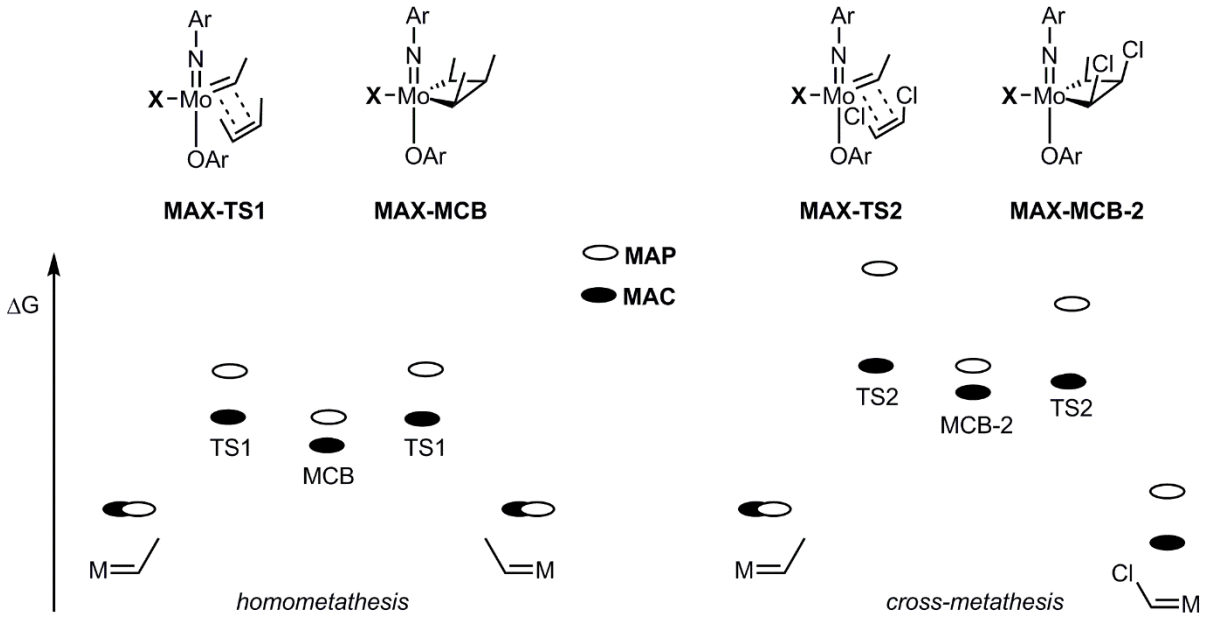

Figure 18: Comparison of MAC- and MAP-type molybdenum imido alkylidene complexes in metallacyclobutane formation. The comparably high yield of cross-metathesis product for MAC-type complexes *vs*. MAP-type complexes can be deduced from the fact that the energy difference between the transition states **MAC-TS1** and **MAC-TS2** is lower than that in the MAP-type complex (**MAP-TS1** and **MAP-TS2**).[101]

The fact that for MAC complexes cross-metathesis (alkene/alkene halide) is more favored over homometathesis (alkene/alkene) than for the MAP complexes was claimed to originate from differences in chemoselectivity. For MAC complexes the energy barrier to **MAC-TS1** (alkene/alkene, 12.3 kcal/mol) and **MAC-TS2** (alkene/alkene halide, 14.5 kcal/mol), respectively is almost the same, whereas for MAP complexes the energy gap between **MAP-TS1** (alkene/alkene, 17.3 kcal/mol) and **MAP-TS2** (alkene/alkene halide, 23.0 kcal/mol) is substantial (Figure 18). The high *(Z)*-selectivity obtained with MAC in cross-metathesis reactions with alkene halides was postulated to be a consequence of slow *(Z)*- to *(E)*-isomerization.

The development of tungsten oxo alkylidene complexes, which are thought to be the active species in “classical”, ill-defined catalyst systems, had been neglected for a long time, since, in these systems, deactivation due to bimolecular decomposition was more prominent. Consequently, reports on tungsten oxo alkylidene complexes are sparse.[102] However, when MAP-type catalysts bearing sterically demanding aryl oxides in combination with small imido ligands had been shown to result in the preferred formation of (*Z*)-double bonds (*vide infra*), tungsten oxo complexes shifted back into focus. The comparably low steric demand of the oxo vs. any imido ligand made them promising targets. An improved synthesis route to tungsten oxo alkylidene complexes was published by *Schrock et al*. (Scheme 20).[103] Previously, the alkylidene moiety was transferred from tantalum to tungsten[104] and the starting material was changed from $W(O)Cl_4$ to WCl_6.

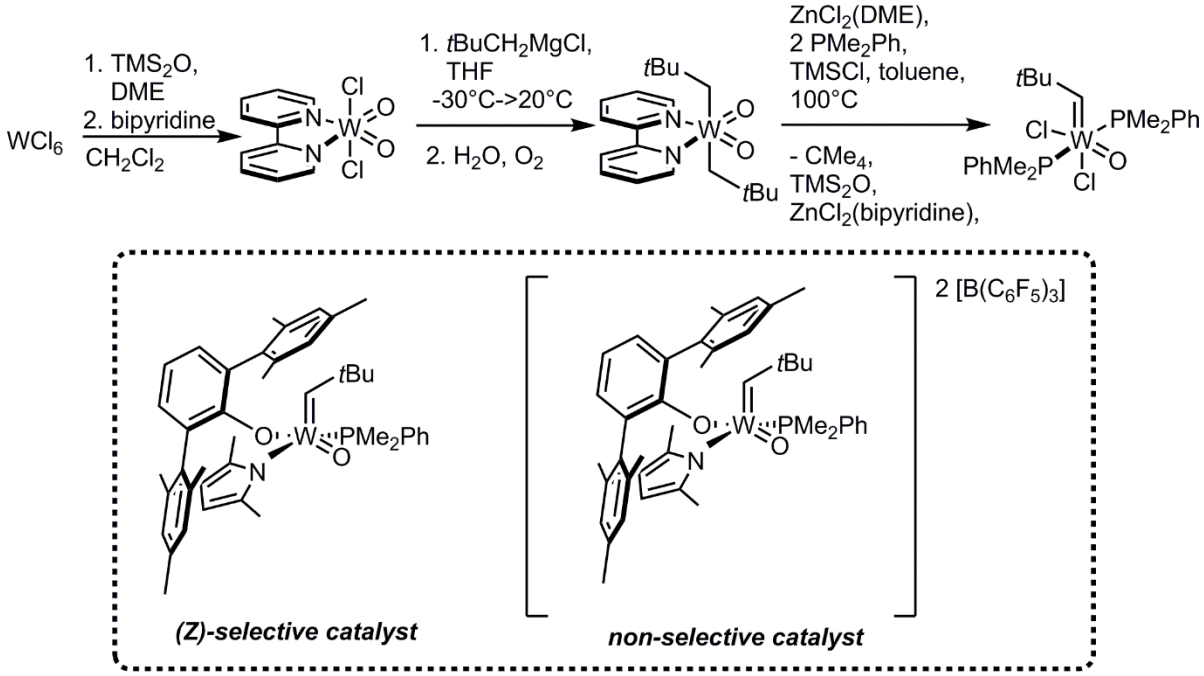

Scheme 20: Improved synthesis route to tungsten oxo alkylidene complexes published by *Schrock et al.* Prevention of bimolecular decomposition by introduction of sterically demanding OHMT ligand. Exemplary (*Z*)-selective tungsten oxo alkylidene complex and the corresponding non-selective *Lewis* acid activated catalyst.[103,105]

The key factor to prevent bimolecular decomposition in tungsten oxo alkylidene species was the introduction of sterically demanding aryl oxide ligands, e.g. OHMT or OHIPT.[103,105b,106] In fact, a tungsten oxo alkylidene complex W(O)(CH*t*Bu)Cl(OHMT)(PMe_2Ph) has been shown to catalyze the (*Z*)-selective coupling of several terminal olefins (Scheme 20).[105b] For the activity of tungsten oxo alkylidene complexes, activation by *Lewis* acids plays a crucial role. The *Lewis* acid is thought to bind to the oxo ligand and in consequence activate the metal center (Scheme 20). Tungsten oxo alkylidene complexes bearing $B(C_6F_5)_3$ have been observed by proton NMR spectroscopy. $B(C_6F_5)_3$ coordination has been shown to accelerate both, metallacyclobutane formation and metallacyclobutane rearrangement.[105] In consequence, the more active, *Lewis*

acid-coordinated tungsten oxo complexes resulted in the formation of thermodynamic mixtures of (*E*)- and (*Z*)- products.

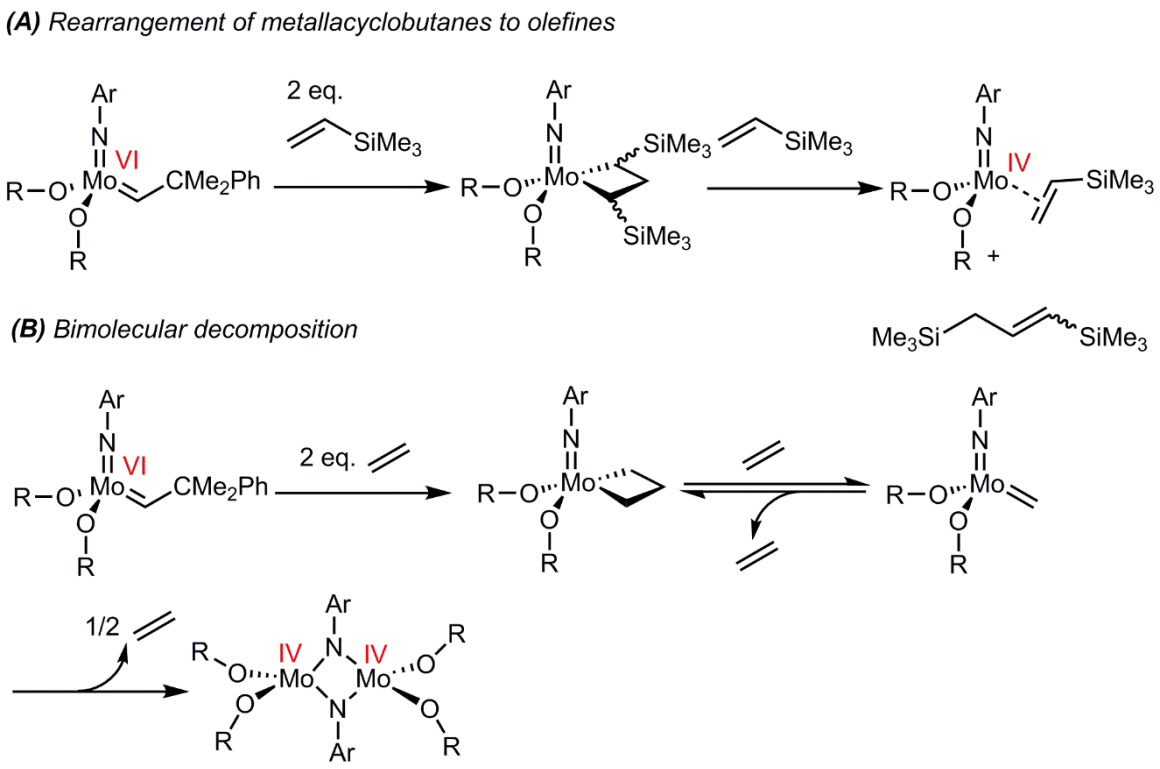

Scheme 21: Main decomposition pathways for Mo(VI) olefin metathesis catalysts under formation of Mo(IV) species. **(A)** Rearrangement of metallacyclobutanes under elimination of an olefin and formation of a Mo(IV) olefin π-complex. **(B)** Bimolecular decomposition in the presence of ethylene under formation of bimetallic nitrogen bridged Mo(IV) complexes.[58]

Molybdenum- and tungsten(VI)-based metathesis catalysts generally decompose under the formation of M(IV) species.[58] Two main decomposition pathways have been reported. First, metallacyclobutanes can rearrange under formation of olefins (Scheme 21, **(A)**) and second, bimolecular decomposition through coupling of two metal alkylidene species can occur (Scheme 21, **(B)**).[58] Bimolecular decomposition is fastest for metal methylidenes, due to low steric constraint and the release of ethylene. Other studies on enantiomerically pure binaphtholate coordinated molybdenum imido alkylidene complexes showed, that the concentration of ethylene (by-product if terminal olefins are converted) is a crucial factor.[90e] They first observed propylene as a byproduct of catalyst decomposition which might result from ß-hydride-elimination in a metallacyclobutane accompanied by formation of a metal hydride species. The investigations also showed, that many more, minor, not yet identified pathways for catalyst deactivation take place.[90e] However, since the major decomposition pathways lead to formation of reduced species, it is important to stabilize the high oxidation state by for example strongly donating ligands, such as carbenes.

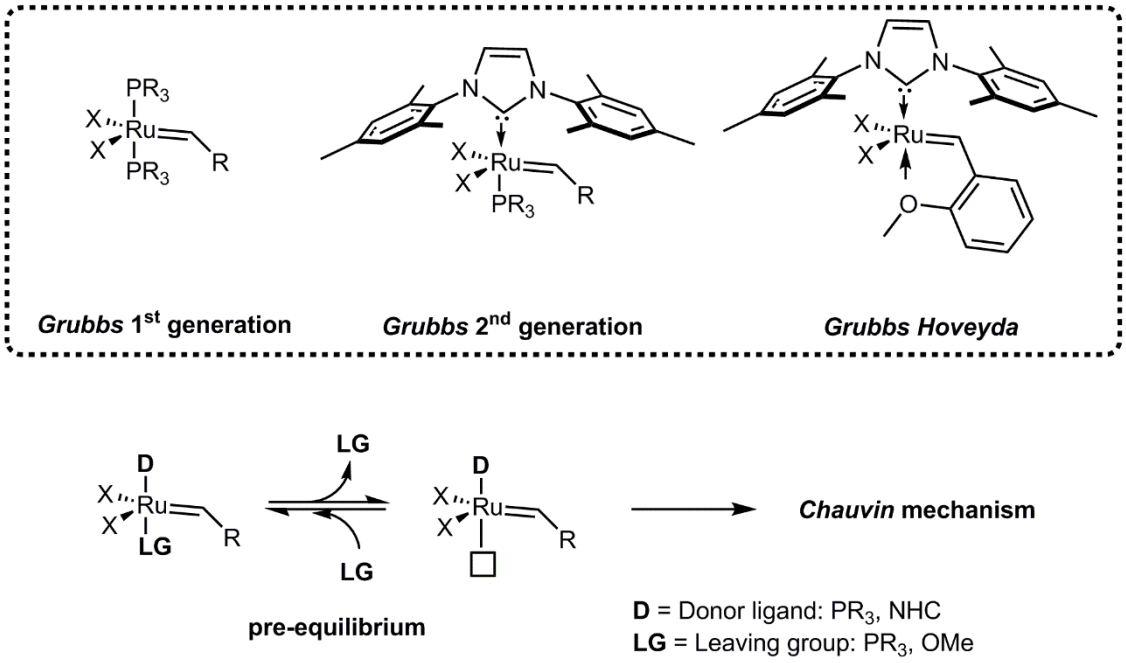

Figure 19: *Grubbs* catalysts of the 1st and 2nd generation. *Grubbs Hoveyda*-type catalyst with a chelating alkylidene ligand. Pre-equilibrium (phosphine dissociation) *prior* to a productive metathesis cycle.[11f,11g,25,107]

The success story of olefin metathesis would not be complete without mentioning the ruthenium-based alkylidene metathesis catalysts, developed by the third Nobel laureate *Robert Grubbs*, that enrich the library of metathesis catalysts. *Grubbs* catalysts of the first generation bear one alkylidene ligand, two X-type ligands (halides, pseudo halides[108]) and two phosphine ligands.[11f] Metallacyclobutane formation as well as [2+2]-cycloaddition and [2+2]-cycloreversion occur similar to *Schrock*-type systems. Nevertheless, *Grubbs*-type systems, in contrast to the tetracoordinated molybdenum and tungsten complexes, must dissociate one phosphine ligand prior to substrate coordination.[11g] The active species therefore is a tetracoordinated complex. The pre-equilibrium between the initiator and the phosphine-free active complex has a direct impact on the molecular weight of ROMP derived polymers, the observed value is usually higher than the theoretical one. Phosphine dissociation is facilitated when strong σ-donors are coordinated *trans* to the leaving group. The replacement of one phosphine ligand by an NHC in the *Grubbs* second generation catalysts therefore leads to a dramatic enhancement of activity.[109] Beforehand, *Hermann et al.* had replaced both phosphine ligands in the early systems by NHCs, however, those bis-NHC-complexes only showed moderate activity due to the decreased propensity of carbenes *vs*. phosphines to dissociate from a metal center.[107] More recently, more sophisticated carbenes like CAAC[110] (cyclic alkyl amino carbenes) and anti-Bredt carbenes[111] have been incorporated into the *Grubbs* second-type structure, leading to unique reactivity profiles.

Another class of unprecedented catalysts, that deserve attention, are the *Grubbs* 2nd generation catalysts bearing *C*-chelating NHCs (Figure 20).[112] *CH*-activation occurs at one of the nitrogen substituents of the NHC resulting in *C*-chelating carbenes.

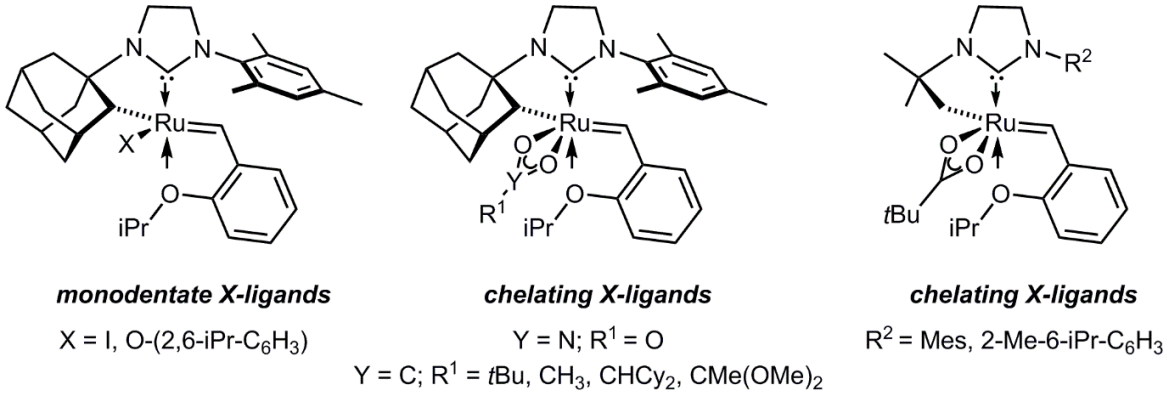

Figure 20: Unprecedented ruthenium-based metathesis catalysts with *C*-chelating NHCs.[112]

N-substituents that have been shown to undergo *CH*-activation are (amongst others[112c]) the *tert*-butyl[113], the adamantyl[114] and the mesityl[112a] group (Figure 20). The catalysts can be used in stereoselective metathesis, like for example in the (*Z*)-selective macrocyclization of long-chain terminal dienes[61a] as well as in (Z)-selective ROCM[112b] or in ethenolysis. A further improvement in handling *Grubbs*-type systems was introduced by the *Hoveyda* group[25] by replacement of the alkylidene ligand with *o*-methoxystyrene, acting as a chelating ligand. Those so-called *Grubbs Hoveyda*-type catalysts show high activity and are, in many cases, stable under air. The increase in activity can be explained, if easy back coordination of the phosphine ligand in the *Grubbs* first and second-generation catalysts is considered. It should be noted, that apart from molybdenum- and tungsten-based stereoselective catalysts, ruthenium-based catalysts have gained some attention.[20,87]

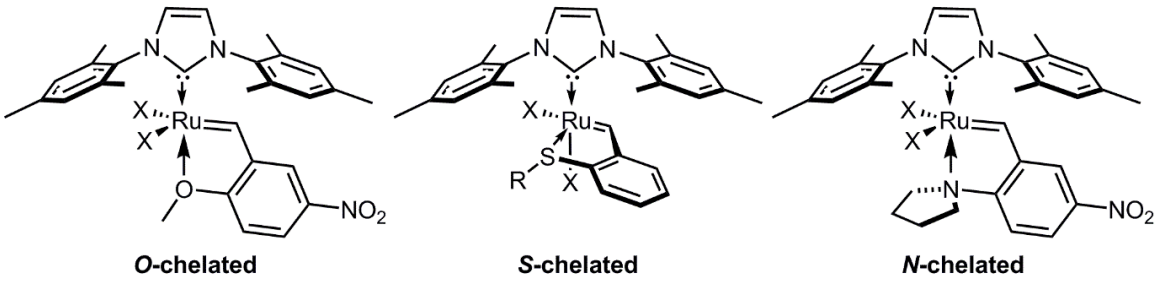

Figure 21: Latent ruthenium-based olefin metathesis catalyst containing chelating alkylidene moieties.[115]

The development of latent ruthenium-based systems for reaction injection molding (RIM) of dicyclopentadiene lead to a large library of especially *Grubbs Hoveyda*-type systems.[116] Especially the *Lemcoff* group published on a variety of *Grubbs Hoveyda*-type catalysts with different chelating alkylidene ligands for latent ROMP.[115] The chelating alkylidene moiety has

been altered from alkyl and aryl (thio)ethers[117] over phosphines[118], sulfoxides[115a,119], secondary amines[120], imines[121] and heterocycles[115a,121-122] to carbonyls[122-123] in order to tune activity or achieve thermally or chemically induced latency. [115a,117b,124] Apart from thermal activation, latent *Grubbs Hoveyda*-type catalysts have been activated chemically (e.g. by changing pH) or by UV light.[115,125] Also, latent catalysts with chelating ligands other than alkylidenes have been published.[117c,126]

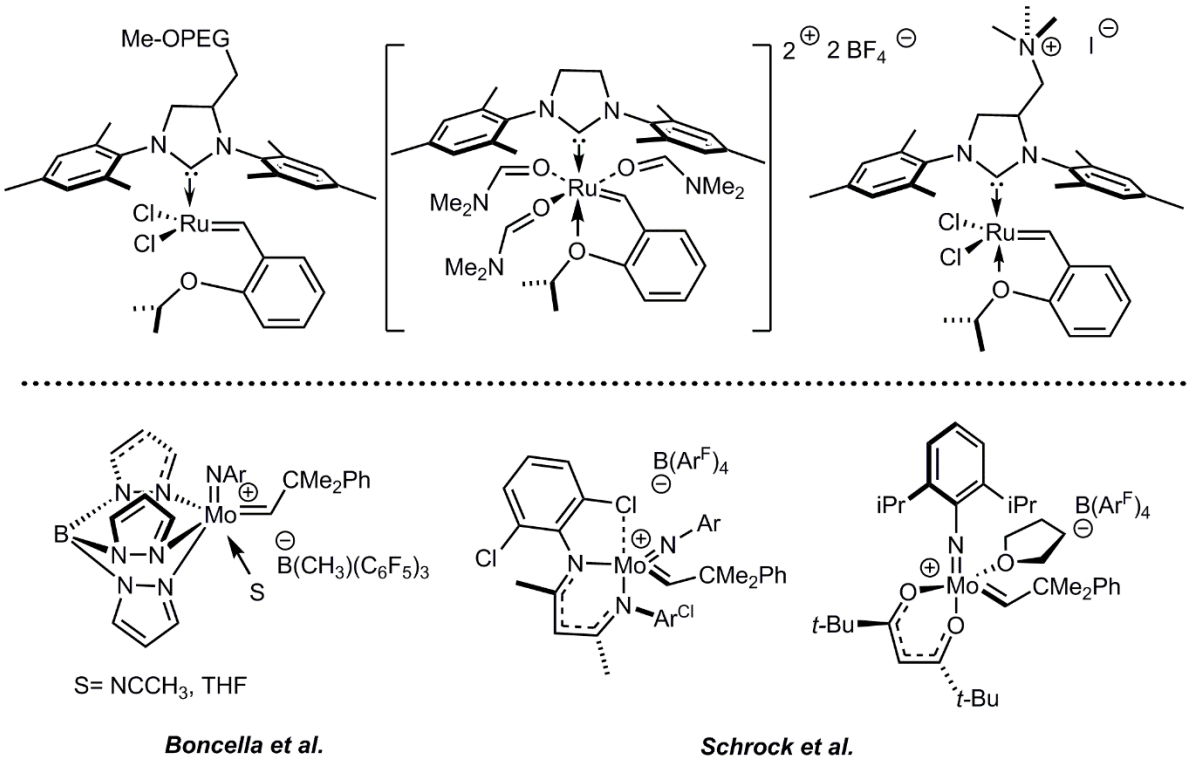

Figure 22: Top: Exemplary *Grubbs*-type catalysts for biphasic olefin metathesis, bearing hydrophilic or cationic tags, as well as cationic charge on ruthenium.[127] Bottom: State of the art cationic molybdenum imido alkylidene complexes with strong donor ligands and non-coordinating anions.[128]

To overcome issues inherent to organometallic catalysis like metal contamination, catalyst recycling and substrate inhibition, biphasic metathesis reactions have been explored by several research groups. Especially *Grubbs*- and *Grubbs Hoveyda*-type catalysts have been extensively used under biphasic conditions in ionic liquids[127a] or even water.[129] Mostly, solubility of the catalyst in the polar phase has been ensured by introduction of an ionic or highly polar group into the catalyst structure. Cationically tagged NHCs[127b], X-type ligands[127c] and alkylidene ligands[130] have been attached to the metal core.[127a,129b] The *Buchmeiser* group even published on a ruthenium complex with the cationic charge on the metal center, applicable under biphasic conditions in ionic liquids.[131] However, no biphasic metathesis reactions with cationic *Schrock*-type catalysts were published at the time this work was started. This was most probably due to the fact, that almost no ionic molybdenum- or tungsten-based alkylidene complexes were known. First publications on ionic group 6 metal alkylidenes

appeared in 1995, when *Boncella et al.* published on a cationic molybdenum alkylidene complex stabilized by tris(pyrazolylborate) with a weakly coordinating anion.[128a] Later, *Schrock et al.* published on cationic molybdenum imido alkylidene complexes with sterically demanding β-diketonate and β-diketiminate ligands[128b] and on cationic molybdenum imido alkylidene pyrrolide complexes with coordinating solvents (THF, lutidine).[128c] However, those catalysts were instable when exposed to substrates and therefore found no application in metathesis reactions. Nevertheless, those publications already showed that cationic group 6 metal alkylidenes were accessible via stabilization of the metal center with good donor ligands and using weakly coordinating borate-based anions.

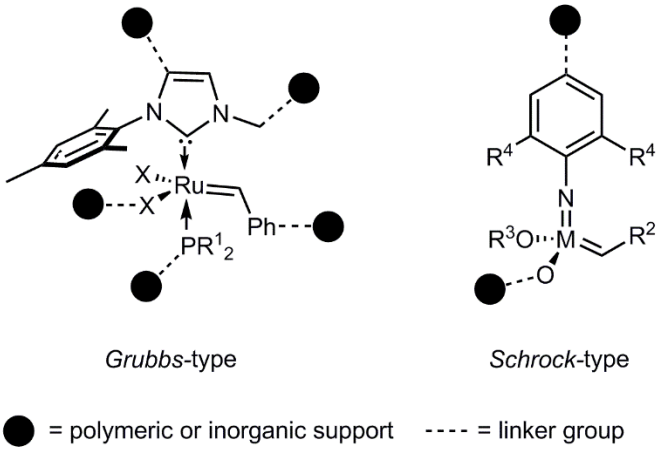

Figure 23: Possible immobilization sites in standard *Grubbs*- and *Schrock*-type olefin metathesis catalysts.[132]

Group 6, as well as ruthenium-based metathesis catalysts, have been immobilized on various supports.[132] Immobilization offers several opportunities. On the one hand, immobilized catalysts can easily be separated from reaction mixtures by simple filtration, and therefore allow for the isolation of metal-free products. Furthermore, the solid support incorporating the catalyst can be filled into columns or similar reaction vessels and applied continuously. Specially manufactured supports, e.g. materials with defined pore sizes or tortuosity, can be used to solve issues that cannot be addressed by catalyst design. For example, by restricting catalyst poisoning species entry to the pores. Additionally, *Schrock*-type, as well as *Grubbs*-type catalysts have been immobilized on inorganic supports as well as on organic monolithic structures, by either molecularly linking the catalyst to the support or by the exploitation of adhesive effects[133]. Group 6 metal alkylidenes have been covalently immobilized via the imido[134] and the alkoxide[135] ligand. [132] Ruthenium-based systems, in addition, have been immobilized *via* the phosphine or pyridine[136] ligand and the heterocyclic carbene[137] as well as *via* the alkylidene ligand[138] (Figure 23). Furthermore, *Grubbs*-type catalysts have been immobilized by the supported ionic liquid phase (SILP) technology.[139] In the SILP technology an ionic liquid is immobilized on the support. The ionically tagged catalyst dissolves in the

immobilized ionic liquid. The ionic charge of the catalyst prevents the active complex to be washed out by the solvent carrying the substrate.

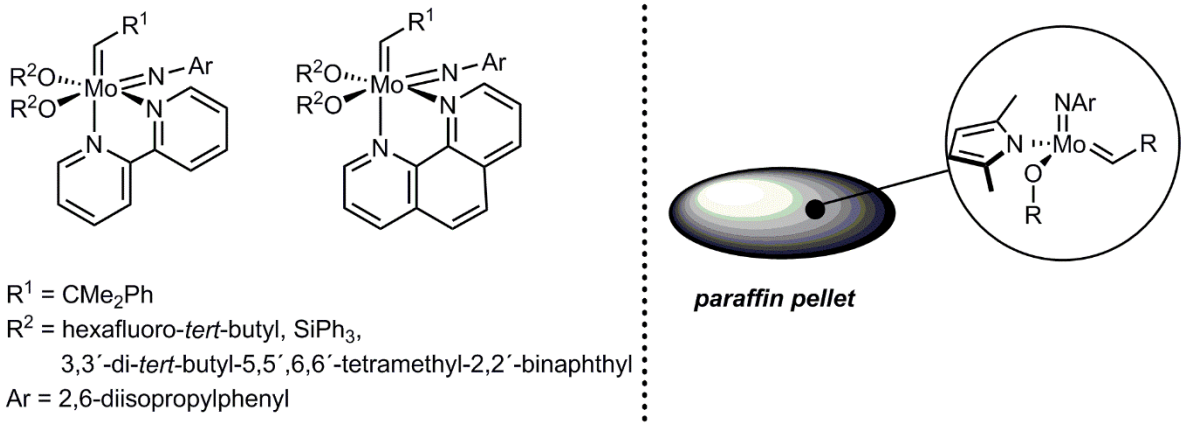

Figure 24: Approaches to render high oxidation state metal alkylidene complexes air stable. Left: Introduction of chelating ligands.[19] Right: Immobilization in a paraffin matrix (right).[120]

A further issue that prevents molybdenum- and tungsten-based metathesis catalysts from frequent use in organic chemistry is their general sensibility towards air and moisture.[119] Whereas ruthenium-based catalysts, especially of the *Grubbs Hoveyda*-type, often show high stability and in some cases can even be stored on the bench, molybdenum and tungsten catalysts require the strictly anhydrous and oxygen-free conditions of a glove box. This issue has been tackled by several groups and the introduction of chelating ligands such as bipyridine and phenanthroline to standard *Schrock*-type bisalkoxide imido alkylidene complexes has led to benchtop stable compounds.[19] However, to form an active catalyst, zinc chloride must be added to the reaction mixture as a scavenger. Also, immobilization of MAP-type catalysts in a paraffin matrix[120] presents an excellent solution, however hampered by parrafin removal from the products.

5.2.2 *ALKYNE METATHESIS*

As outlined above, another important branch of metathesis is alkyne metathesis, the coupling of two alkynes under the formation of a new alkyne. In analogy to olefin metathesis, alkyne metathesis can be divided into special reaction patterns. Alkyne cross-metathesis (ACM), ring-closing alkyne metathesis (RCAM), ring-opening alkyne metathesis polymerization (ROAMP) and acyclic diyne metathesis polymerization (ADIMET) can be applied to form new carbon-carbon triple bonds (Scheme 22).

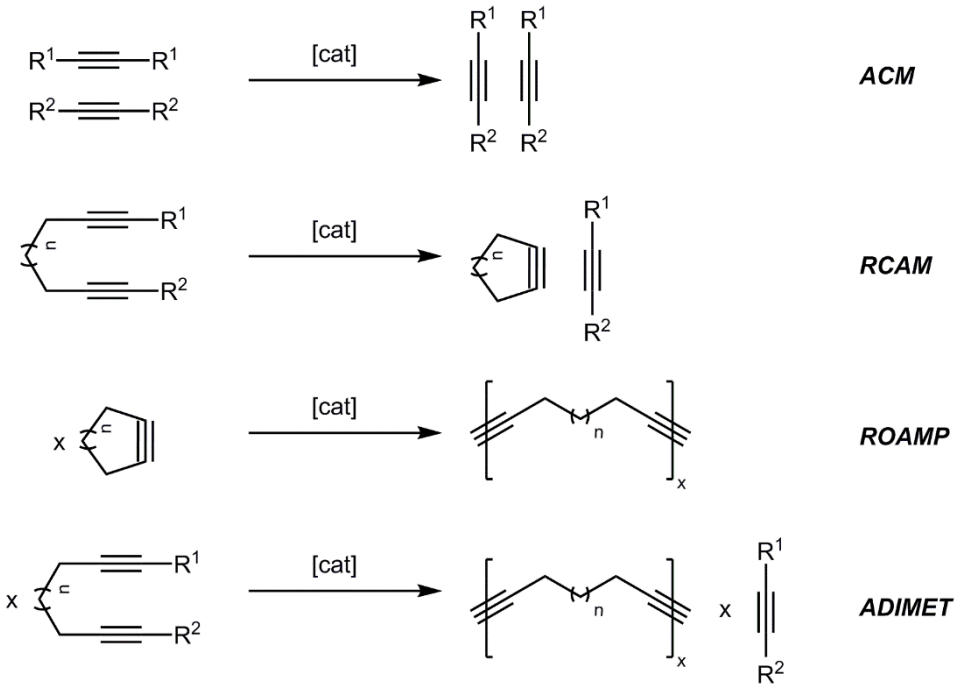

Scheme 22: Different types of alkyne metathesis reactions. Alkyne cross-metathesis (ACM), ring-closing alkyne metathesis (RCAM), ring-opening alkyne metathesis polymerization (ROAMP) and acyclic diyne metathesis (ADIMET).[6b,6d]

In contrast to olefin metathesis, alkyne metathesis usually is performed with internal alkynes, sometimes leading to non-volatile by-products, which must be removed selectively to ensure complete conversion.[11e] The *Fürstner* group proposed the usage of 5 Å molecular sieves to remove small alkynes, such as butyne, from reaction mixtures.[140] This allowed for higher yields and higher reaction rates.

The analogy between alkyne and olefin metathesis also holds in terms of mechanism. For one, the corresponding reactive species are metal alkylidynes. Furthermore, alkyne metathesis proceeds according to the *Katz* mechanism (Scheme 23) under formation of metallacyclobutadiene complexes by a [2+2]-cycloaddition.[11e] Those metallacyclobutadienes then decompose in a [2+2]-cycloreversion step to form (in case of a productive metathesis event) a new metal alkylidyne and a new alkyne.

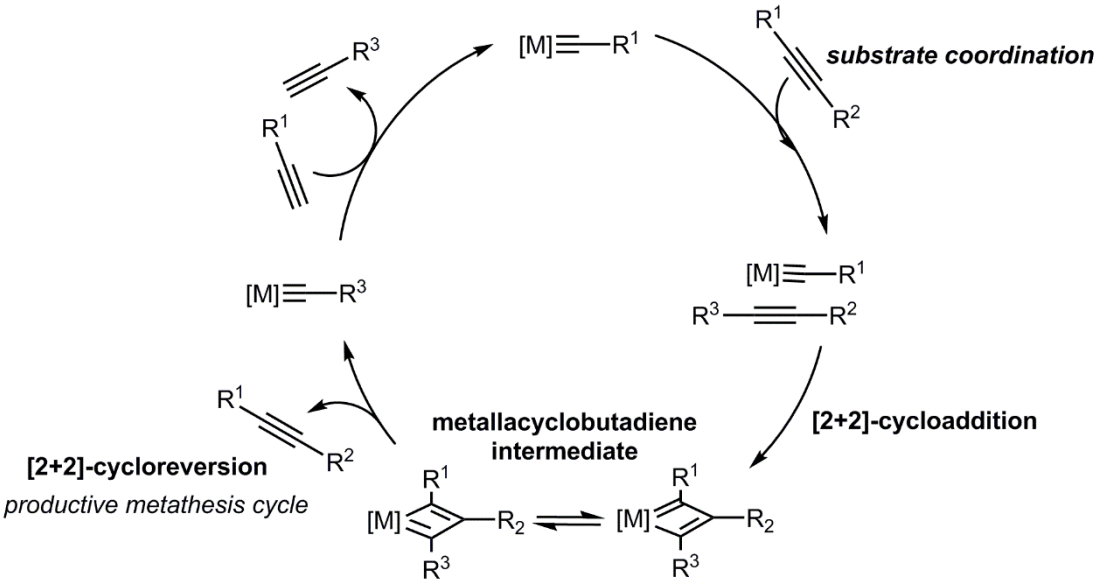

Scheme 23: *Katz* mechanism. Alkyne metathesis proceeds *via* [2+2]-cycloaddition, formation of a metallacyclobutadiene and subsequent [2+2]-cycloreversion. All reactions are reversible, arrows for back-reactions have been omitted for clarity.[6b,6d]

Importantly, the metallacyclobutadiene must rearrange to release the desired new alkyne. One difference between alkene and alkyne metathesis is, that in alkene metathesis terminal olefins can be converted, whereas this often is a problem in alkyne metathesis. If terminal alkynes are used polymerization can be observed as competitive pathway after a few minutes.[141] Terminal alkyne metathesis (TAM) leads to metallacyclobutadienes (Scheme 24) with hydrogen substituents in α- and/or β-position. Elimination of one (basic) X-type ligand and the acidic β-proton in the metallacyclobutadiene under formation of HX results in the key intermediate for alkyne polymerization, a so-called deprotio-metallacycle (Scheme 24, **(A)**). Coordination of another alkyne substrate to the deprotio-metallacycle then leads to reduction of W(VI) to W(IV) and to the formation of a metal alkylidene. The metal alkylidene then polymerizes alkynes under formation of unsaturated polymers *via* metallacyclobutene intermediates.

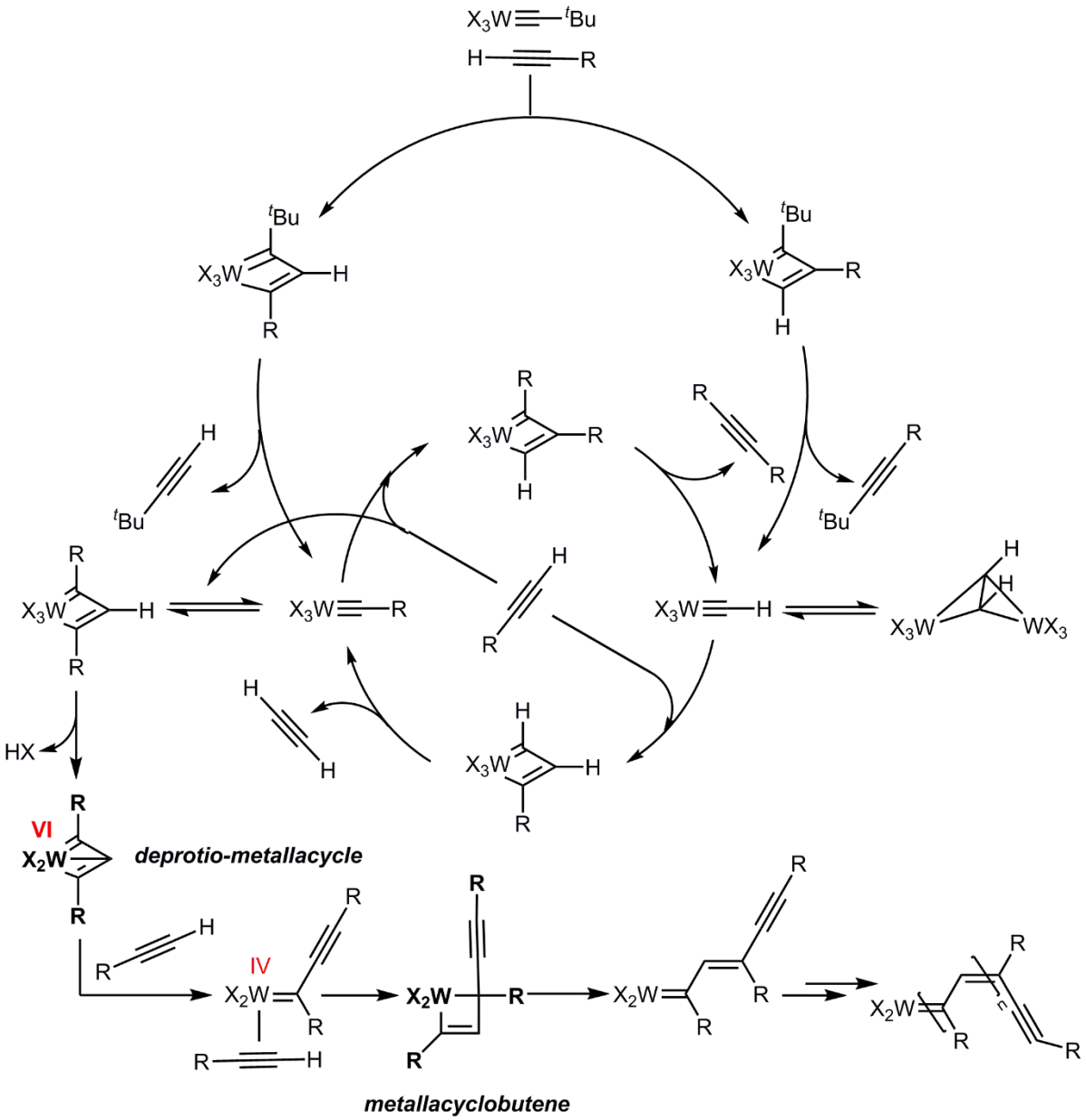

Scheme 24: Competitive pathways to alkyne metathesis: In the presence of terminal alkynes deprotio-metallacycles can form by elimination of HX (deprotonation) from the complex. Subsequently, under coordination of a further substrate, W(VI) is reduced to W(IV) under formation of an alkylidene. The alkylidene can then polymerize alkynes via metallacyclobutenes.[141]

Also, cyclotrimerization[142], resulting from metallacyclobutadiene-ring-expansion, was observed for (mono-)substituted alkynes, when chlorides instead of alkoxides were used as X-type ligands (Scheme 25). Upon cyclotrimerization, reduced cyclopentadienyl complexes of W(IV) are formed. Since, similar to olefin metathesis, undesired reaction pathways seem to lead to reduced W(IV) species, coordination of stabilizing ligands could lead to improved catalyst performance.

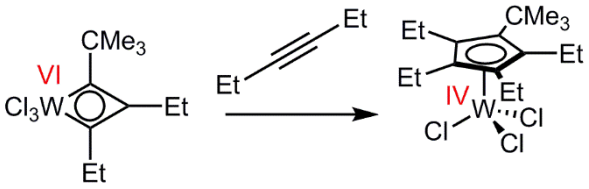

Scheme 25: Competitive pathways to alkyne metathesis: Cyclotrimerization under formation of a reduced, substituted cyclopentadienyl W(IV)-complex.[142]

Comparable to metal alkylidenes, metal alkylidynes can be divided into *Schrock* and *Fischer* carbynes.[143] In *Schrock* carbynes, the carbyne is in the quartet configuration (three unpaired electrons in the sp-, p_y- and p_z-orbital), whereas in the *Fischer* carbynes, the carbyne is in the dublett configuration (two paired electrons in the sp- and one electron in an empty p-orbital). Consequently, the bonding situation in *Schrock* carbynes can be described by three dative bonds. For *Fischer* carbynes, σ- donation from the carbyne sp- into empty metal orbitals plus one covalent bond, as well as back donation into the empty carbyne p-orbital must be considered.

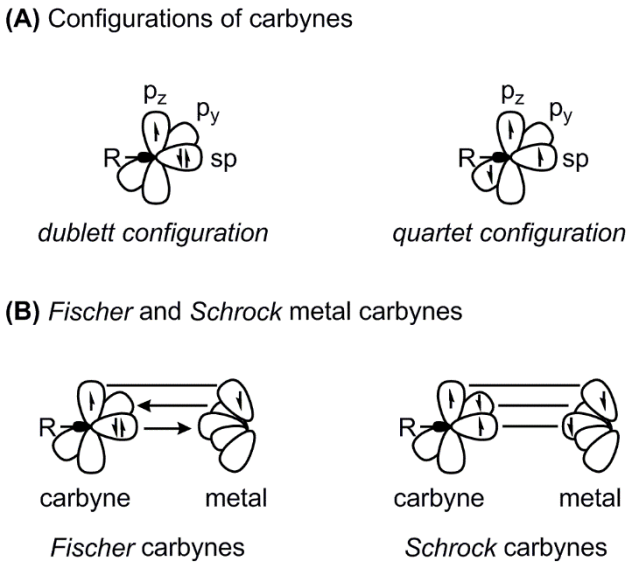

Figure 25: **(A)** Dublett and quartet configuration of carbynes. **(B)** Bonding situation in *Fischer*- and *Schrock*- type carbynes.[143]

Metathesis-active group 6 metal alkylidyne complexes can be divided into five sub-groups.[6b-d] On the one hand, ill-defined catalysts based on silica-immobilized metal trioxides[144] or mixtures of $Mo(CO)_6$ and phenols have been applied. Huge efforts in this field have been made by *Mortreux et al*. On the other hand, the well-defined catalyst systems can be split into the *Schrock*-type catalysts and the more recently developed *Fürstner*- and *Tamm*-type complexes. The *Cummins-Fürstner-Moore* systems belong to both groups, the active species are either well-defined catalysts or are generated *in situ* from well-defined pre-catalysts by additives.

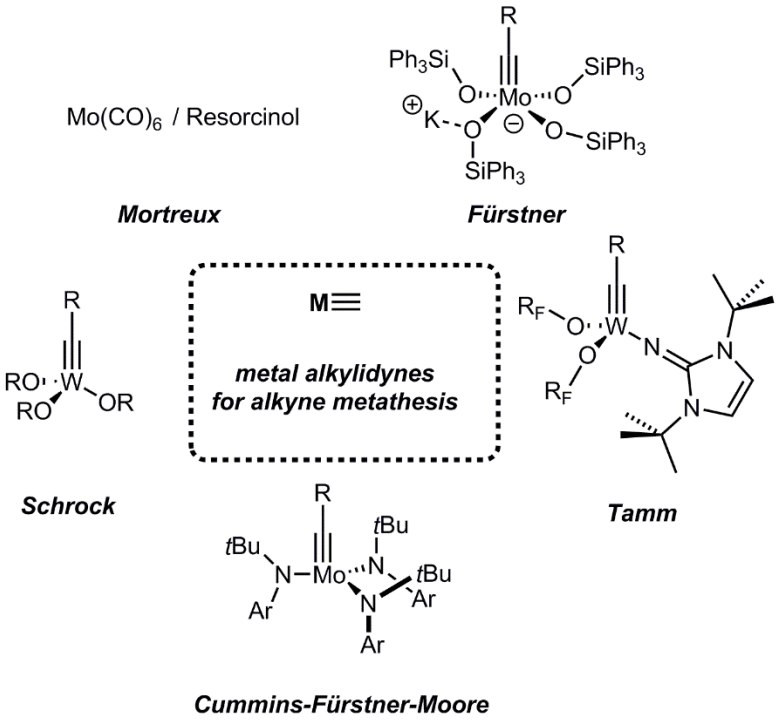

Figure 26: Metathesis-active group 6 metal alkylidynes. Important catalyst systems developed by the *Mortreux*, *Cummins*, *Fürstner*, *Schrock* and *Tamm* groups.

As for alkene metathesis, the development of suitable catalyst systems was a process that started with ill-defined, supported transition metal salts. In 1968, *Bailey et al.* published on the first alkyne disproportionation catalyzed by silica-supported tungsten trioxide.[144a] Later, in 1972 *Mortreux et al*. reported that the same was true for molybdenum trioxide supported on silica.[144b] Then, in 1974, the *Mortreux* group introduced a catalyst system based on molybdenum hexacarbonyl and phenols (resorcinol, α-napthalin) that successfully catalyzed alkyne metathesis.[142] Despite its intolerance towards functional groups and the ill-defined active species, this system has been extensively used and empirically optimized through additives by several groups. This demonstrates the lack of a decent library of alkylidyne catalysts in comparison to alkene metathesis catalysts in the early days of metathesis.

(A) High-oxidation state routes

a) *alkylidyne generation by α-hydrogen abstraction*

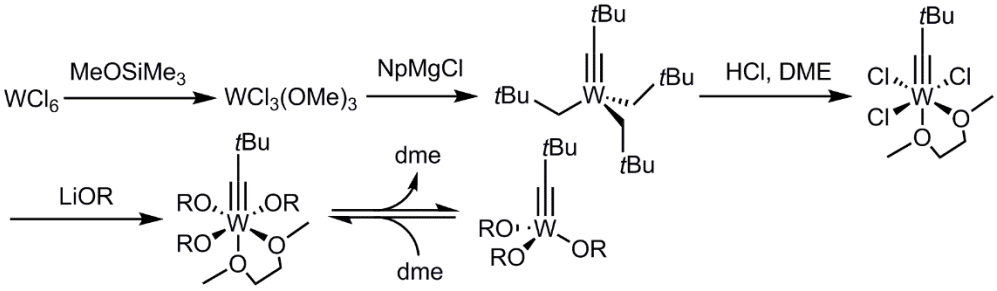

b) *scission of acetylenes or nitriles by a binuclear tungsten complex*

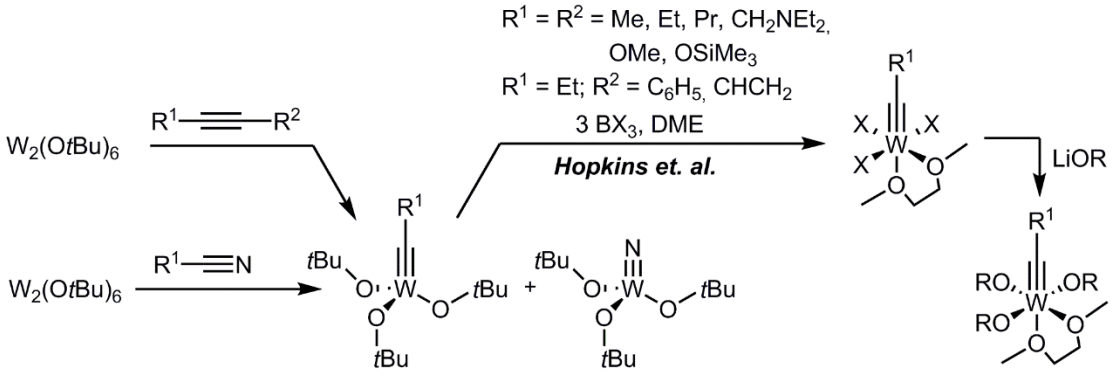

c) *conversion of nitrides to alkylidynes*

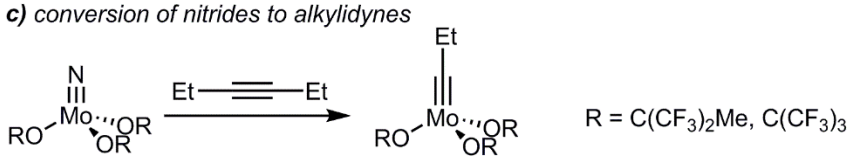

(B) Low-oxidation state route

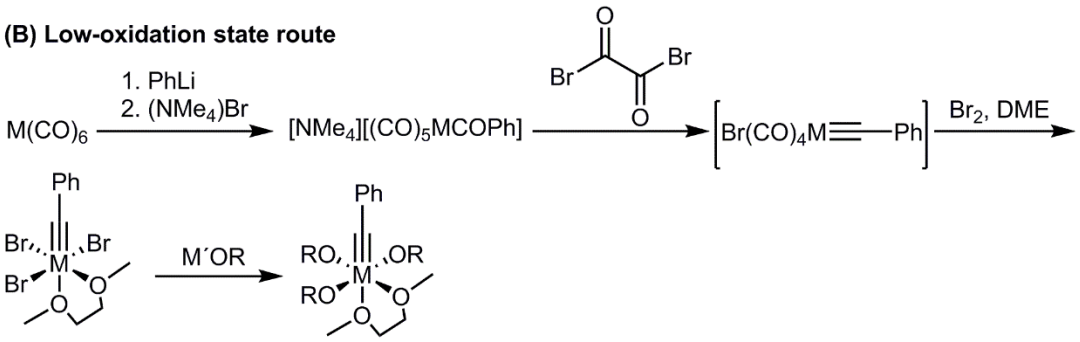

Scheme 26: High- and low-oxidation state routes to group 6 metal alkylidynes. **(A)** High-oxidation state routes including the synthesis of **a)** neopentylidyne complexes by α-hydrogen abstraction[145], **b)** cleavage of alkynes or nitriles with binuclear tungsten hexa-*tert*-butoxide[146] and **c)** exchange of nitride by alkyne ligands.[147] **(B)** Low-oxidation state route starting from tungsten hexacarbonyl by oxidative transformation of $Br(CO)_4M{\equiv}R$ into $Br_3M{\equiv}R(DME)$ with bromine.[148]

The well-defined *Schrock* type systems[145] usually take up the form $M{\equiv}R(X)_3(DME)$ and can be prepared *via* different synthesis routes (Scheme 26). Complexes of the type $W{\equiv}R(O\mathit{t}Bu)_3$ can be synthesized *via* the high oxidation state route (Scheme 26, **(A)**, **a)**) from tungsten hexachloride. First, WCl_6 is converted with three equivalents of methoxytrimethylsilane into $WCl_3(OMe)_3$, which is in turn reacted with neopentylmagnesium chloride to give

W≡C*t*Bu(CH_2CMe_3)$_3$.[145] Subsequently, the alkylidyne alkyl complex is protonated with HCl in DME to yield W≡C*t*BuCl_3(DME). Different alkoxides can be introduced by reaction with lithium alkoxides.[145] Disadvantages of this route are the restriction of the alkyne to substituents without β-hydrogen as well as the low yield of W≡C*t*Bu(CH_2CMe_3)$_3$. Another published route, although restricted to *tert*-butoxide ligands, is the cleavage of acetylenes by ditungsten hexa-*tert*-butoxide (Scheme 26, **(A)**, **b)**).[146] The same binuclear tungsten complex also enables cleavage of nitriles to form the desired tungsten alkylidyne complex and stoichiometric amounts of tungsten nitride complex (Scheme 26, **(A)**, **b)**). An interesting expansion of this route by the *Hopkins* group, overcoming the limitation to the *tert*-butoxide ligand, is the possibility to convert the received W≡R(O*t*Bu)$_3$ species into W≡R$(X)_3$ complexes by reacting them with BX_3 in DME.[149] This provides access to alkylidyne complexes with modularity in the alkylidyne and alkoxide ligand. In addition, *Johnson et al*. published on the possibility to introduce alkylidyne ligands to molybdenum nitride complexes by simple conversion with internal alkynes (Scheme 26, **(A)**, **c)**).[147] A further, highly modular route to high-oxidation state group 6 metal alkylidynes with respect to accessible alkylidyne ligands was developed by *McDermott et al*. starting from tungsten hexacarbonyl (Scheme 26, **(B)**).[148] This so-called "low-oxidation state route" relies on low-oxidation state $X(CO)_4$M≡R complexes previously synthesized by *Fischer*. The key step is the oxidative transformation of $X(CO)_4$M≡R with bromine in DME to afford Br_3M≡R(DME) complexes, that can be converted to $(OR)_3$M≡R(DME) catalysts by treatment with the corresponding lithium or potassium alkoxides.

The *Fürstner-Cummins-Moore* system is based on triamido ligands and profits from a stabilization of the metal center by nitrogen lone-pair donation. The first metathesis-active complexes of this kind were introduced by the *Fürstner* group.[150] They cleaved CH_2Cl_2 with Mo(N(*t*Bu)Ar)$_3$ complexes (first synthesized by *Cummins et al.* [151]), leading to the methylidyne complex Mo≡CH((N(*t*Bu)Ar)$_3$ and the chloro complex MoCl(N(*t*Bu)Ar)$_3$ (Scheme 27).[150] *Fürstner*, counterintuitively, claimed the chloro complex to be the active species, since the methylidyne was shown to be inactive.[6c] On the other hand, *Schrock* proposed that the formation of mixed species of the type Mo(CH)$(NArR)_{3-x}Cl_x$ leads to the observed catalyst activity.[6c] In addition, *Moore et al.* transferred the synthesis protocol to complexes bearing different alkynes (Mo≡CMe(N(*t*Bu)Ar)$_3$ and Mo≡CEt(N(*t*Bu)Ar)$_3$). *Moore et al.* significantly improved the synthesis with a newly developed reductive recycling strategy.[152] The application of magnesium successively lead to complete conversion of Mo(N(*t*Bu)Ar)$_3$ to the desired alkylidyne species by converting the chloride-complex into the educt which then in turn could again be transformed into desired product and by-product (Scheme 27).

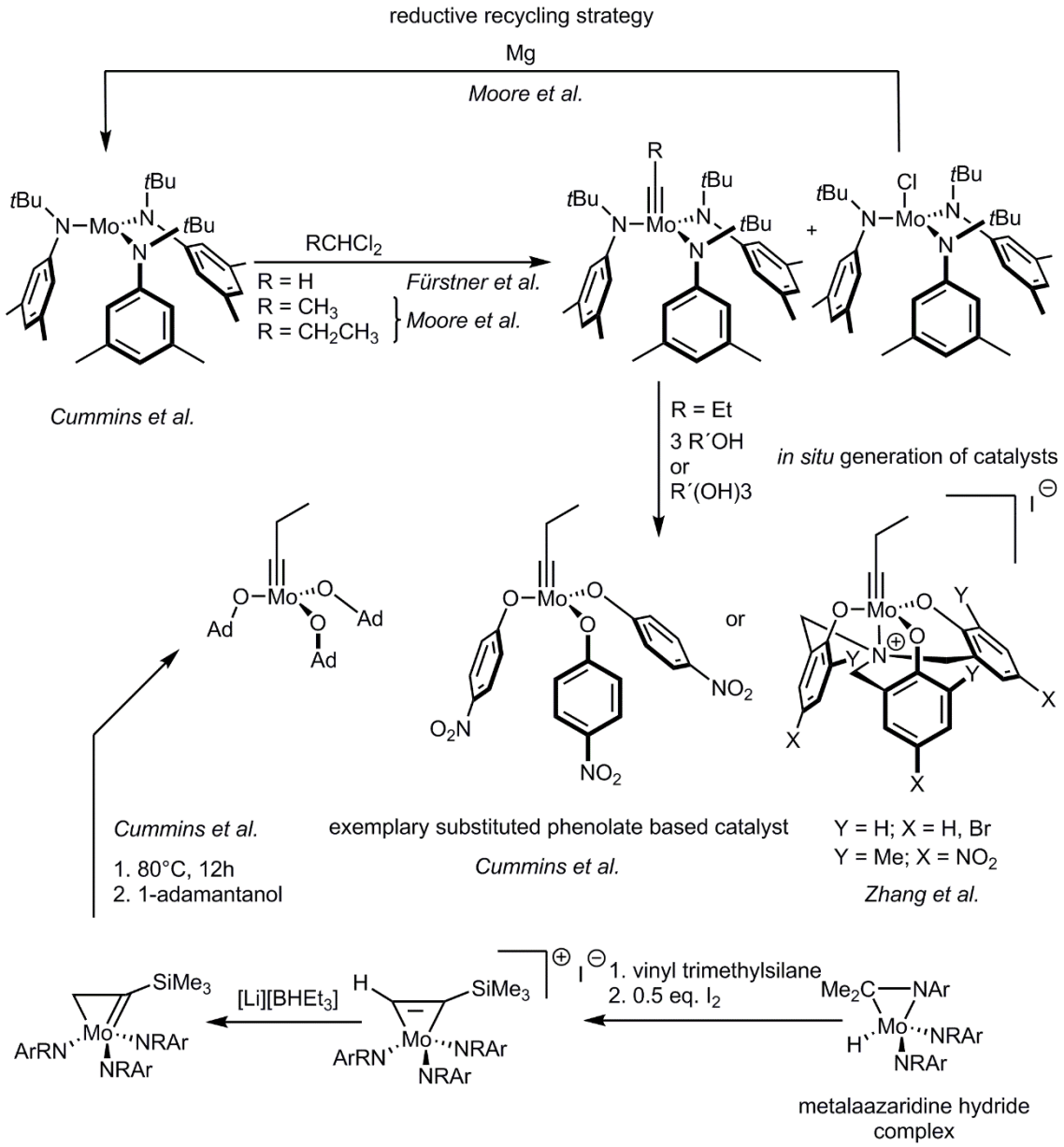

Scheme 27: Development of alkyne metathesis catalysts involving triamido ligated molybdenum alkylidynes by the groups *Cummins*, *Fürstner* and *Moore*. [150-153]

Immobilization on silica resulted in efficient alkyne metathesis catalysts. Also, *in situ* protonation of amido ligands in Mo≡CEt(N(*t*Bu)Ar)$_3$ with various phenols, especially *para*-nitro-phenol (*Cummins et al.*) resulted in active alkyne metathesis catalysts.[152] Several complexes bearing tridentate triphenolamines were described by *Zhang et al.*[153a] Most probably, addition of phenols leads to the partial protonation of the amine ligands and active phenolate complexes. In support of this hypothesis, *Cummins et al.* published on the synthesis of tris-alkoxide molybdenum alkylidyne complexes from a metalaazaridine hydride complex (Scheme 27, bottom).[153b] In the last synthesis step, the amido ligands were removed by protonation with 1-adamantanol, which lead to well-defined alkyne metathesis catalysts.

The *Fürstner* group synthesized a library of siloxide-based alkyne metathesis catalysts.[140,154] The complexes are either isolated as pentacoordinated neutral complexes of the type M≡R(OSiR´)$_3$·(HOSiR´) (***silanol adduct***, Scheme 28), M≡R(OSiR´)$_3$·MeCN or in the form of ate complexes of the type [M≡R(OSiR´)$_4$]$^-$K$^+$ (***ate-DME*** and ***ate-Et$_2$O***, Scheme 28). However, in all cases the neutral tetracoordinated M≡R(OSiR´)$_3$ complexes are believed to be the active species. If three equivalents of KOSiPh$_3$ are used, mixtures of the above described species (and additional non-identified products) are formed, whereas with >4 equivalents, the ate complexes are formed exclusively.

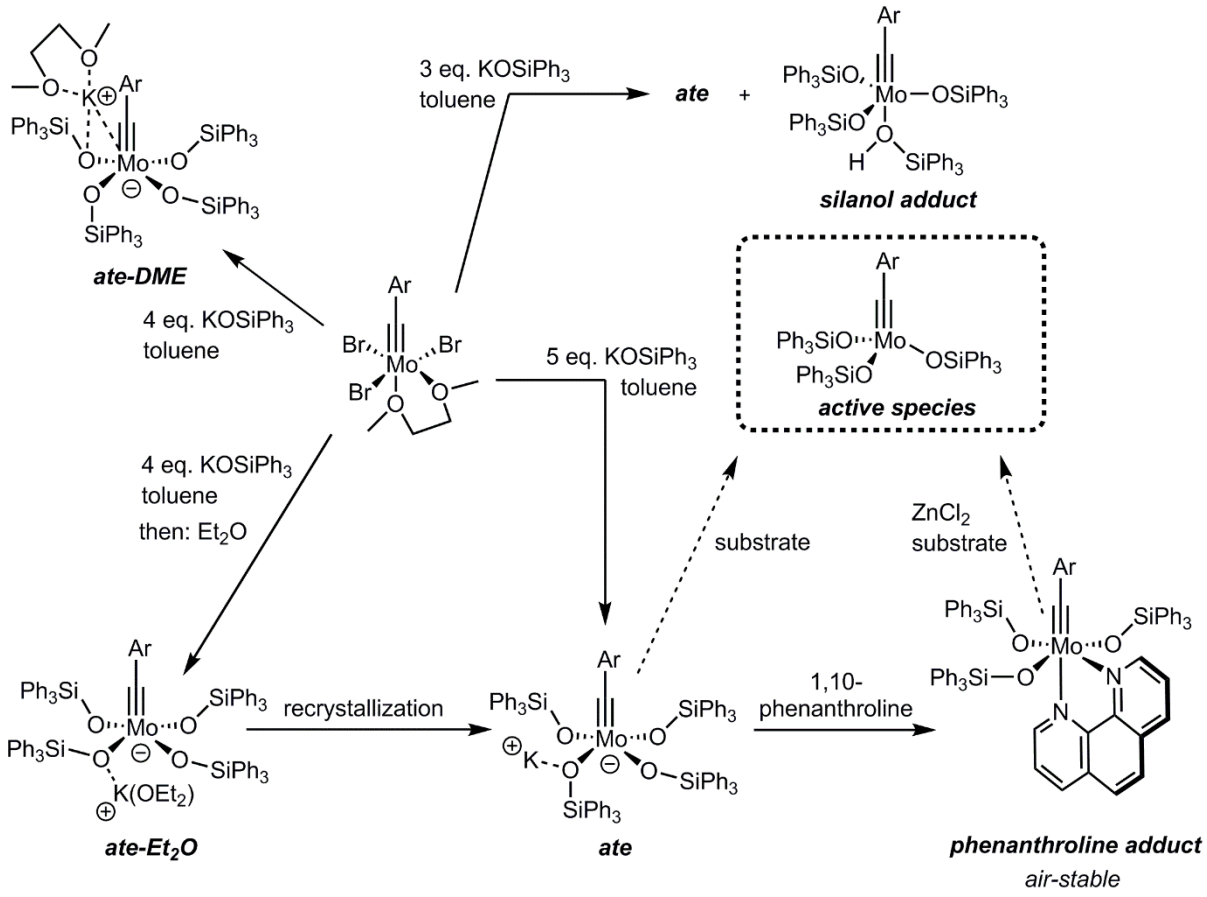

Scheme 28: Siloxide-based catalysts developed by *Fürstner et al*. Synthesis route to and variable structures of siloxide-based catalysts.[140,154]

Upon addition of bipyridine or phenanthroline the catalysts do not only loose one silanolate ligand but also become air stable (***phenanthroline adduct***, Scheme 28). Although, as to be expected, inactive in alkyne metathesis, those air stable adducts can easily be activated to form the active M≡R(OSiR´)$_3$ species *in situ* by addition of ZnCl$_2$. Siloxides are special ligands in terms of steric as well as electronic properties. Whereas the triphenylsiloxide ligand provides enough steric protection to prevent bimolecular decomposition, it does not hinder coordination of substrate (except maybe for extremely bulky ones).

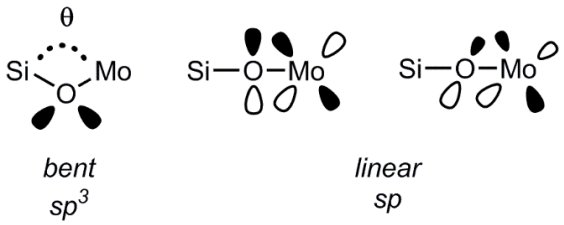

Figure 27: Visualization of orbital interactions and hybridization for a bent (sp^3) and a linear (sp) Si-O-Mo bond.[154]

Siloxides in sum are weaker donors than alkoxides, since $p_\pi \rightarrow$d-donation competes with back donation from the metal d-orbitals into the low-lying Si-C σ*-orbital. Furthermore, they are electronically flexible since donation into the metal d-orbitals is highly dependent on the Mo-O-Si angle Θ. Donation reaches its maximum for Θ = 180° (sp hybridization, Figure 27), since both orthogonal p_π-orbitals can engage in donation to metal d-orbitals. *Fürstner* postulated, that this angle is not static in solution, but might adapt to the requirements of each intermediate of the catalytic cycle, therefore explaining the high activity and stability of the siloxide based systems.[154]

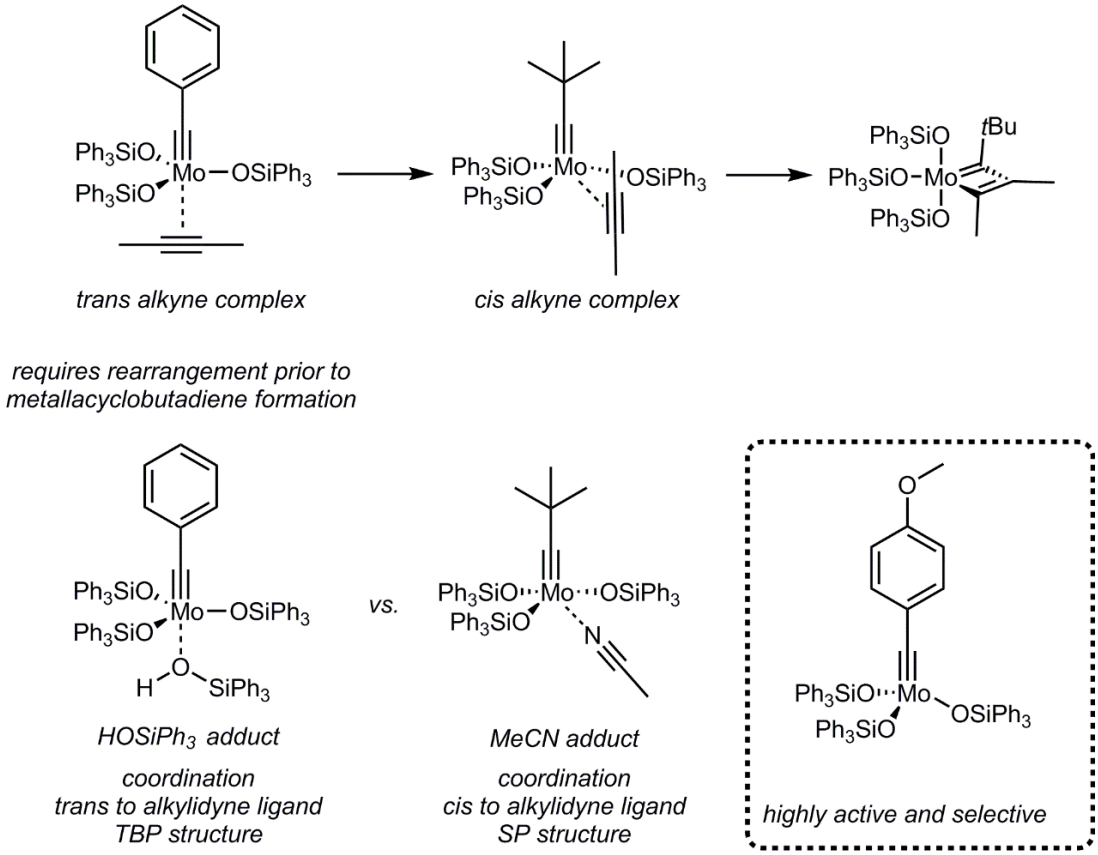

Figure 28: *Left:* Hypothetical alkyne adducts (top) and isolated neutral adducts of proposed active species (bottom). Metallacyclobutadiene formation requires a *cis* orientation of the alkyne substrate to the alkylidyne ligand. *Right, in dashed frame:* Highly active and selective tetracoordinated alkylidyne metathesis complex.[140,154]

Since neutral adducts with square-pyramidal (*MeCN adduct*, Figure 28) and trigonal bipyramidal (*$HOSiPh_3$ adduct*, Figure 28) geometries have been observed, it is still unclear, whether alkyne coordination takes place *cis* or *trans* to the alkylidyne in the *Fürstner*-type systems (Figure 28, left, bottom). Metallacyclobutadiene formation requires a *cis* orientation of alkyne to alkylidyne (*cis alkyne complex*, Figure 28). In one case a tetracoordinated, neutral complex with the above proposed structure for the active species with a *p*-methoxy-benzylidyne ligand was successfully isolated (Figure 28, in dashed frame). This complex is one of the most reactive and selective alkyne metathesis catalysts up to date. *Fürstner et al*. furthermore developed a route to complexes of the type $M{\equiv}N(OSiAr)_3$ starting from Na_2MoO_4 in a straightforward three-step procedure, which can be converted into alkylidynes according to the protocol introduced by *Johnson et al.* (vide supra, (Scheme 26, **(A)**, **c)**). [147]

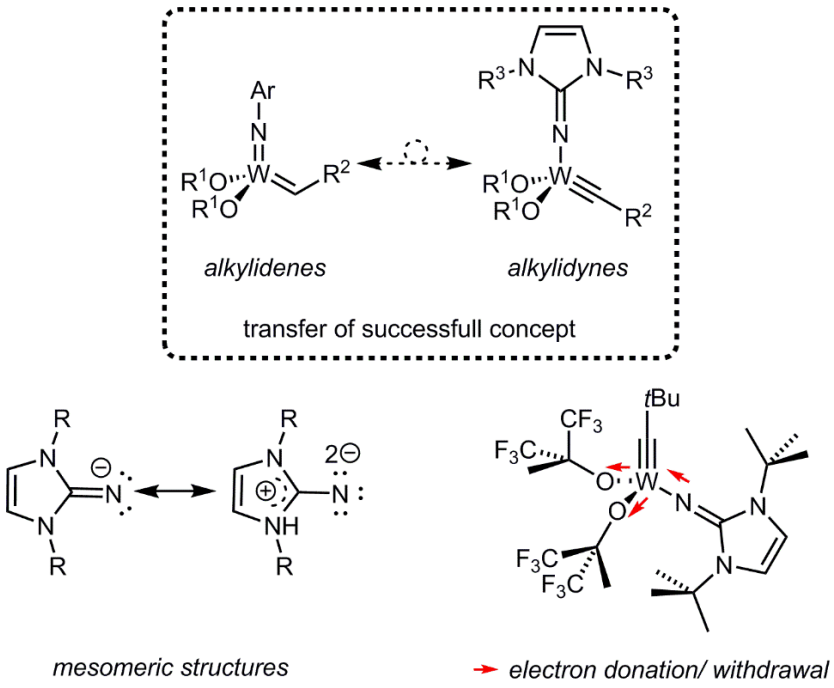

Figure 29: Design strategy for imidazoline-2-iminato coordinated alkyne metathesis catalysts developed by the *Tamm* group. Imidazolin-2-iminato ligands as monoanionic analogues to imido ligands in alkene metathesis catalysts and push-pull electronics on the metal center.[155]

Tamm et al. synthesized alkylidyne complexes of imidazolin-2-iminato ligands (Figure 29).[155] They transferred the concept to stabilize high oxidation state metal centers with sterically demanding dianionic ligands from alkene metathesis catalysts (imido ligand) to alkynes (Figure 29). They proposed that the imidazolin-2-iminato ligand presents a monoanionic analogue of an imido ligand. Complexes were received from the conversion of imidazolin-2-iminato ligands with trisalkoxy alkylidyne molybdenum and tungsten complexes under replacement of one alkoxide. Installation of electron-withdrawing alkoxides at the metal center was essential to create a favorable push-pull system (Figure 29). The catalysts were

successfully used in various alkyne metathesis reactions, such as ACM[156], RCAM[157] and ROAMP[158] of cyclooctyne at room temperature. An isolated metallacyclobutadiene complex confirmed that the *Katz* mechanism was operative.

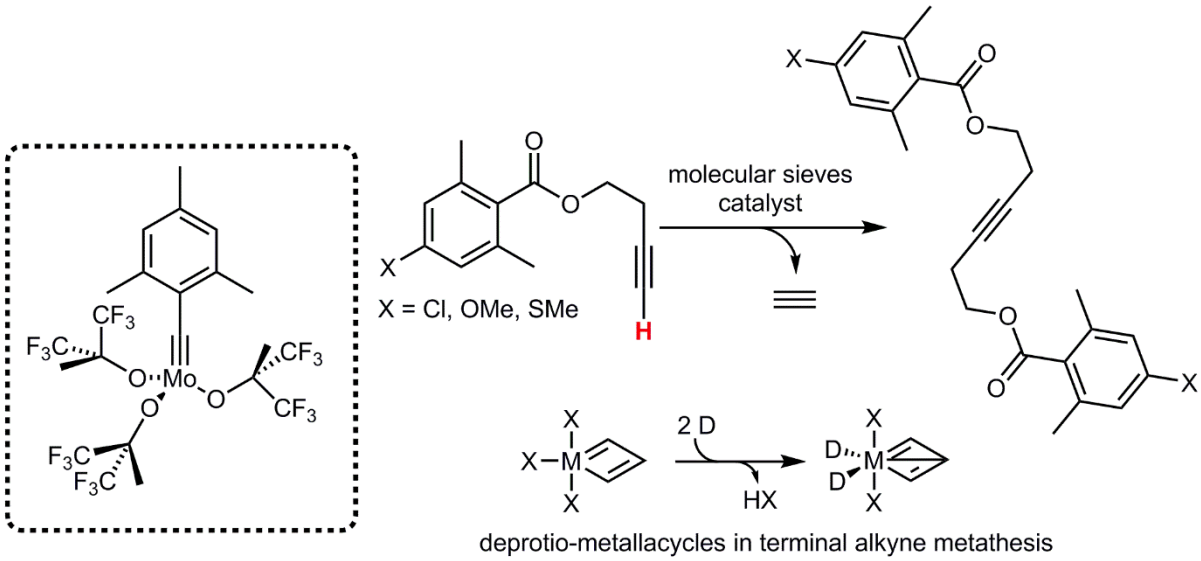

Scheme 29: First effective catalyst for terminal alkyne metathesis (TAM) and donor ligand promoted formation of deprotio-metallacyclobutadienes.[159]

The *Tamm* group also reported on the first catalysts that efficiently promote terminal alkyne metathesis (TAM, Scheme 29) and terminal ring-closing metathesis (TRAM).[159] The complex is a common molybdenum-based *Schrock*-type alkylidyne with three hexafluoro-*tert*-butoxide ligands and a 2,4,6-trimethylbenzylidyne ligand (Scheme 29). The high acidity of the fluorinated alkoxide and its resulting reduced propensity to take up a proton account for the fact that no polymerization of terminal alkynes was observed for this catalyst.[159] Polymerization proceeds *via* formation of deprotio-metallacycles (*vide infra*, Scheme 24) which is in turn facilitated by basic donor ligands. Lately, they also published on derivates of the successful 2,4,6-benzylidyne complex with longer chain fluorinated alkoxides of molybdenum and tungsten.[160]

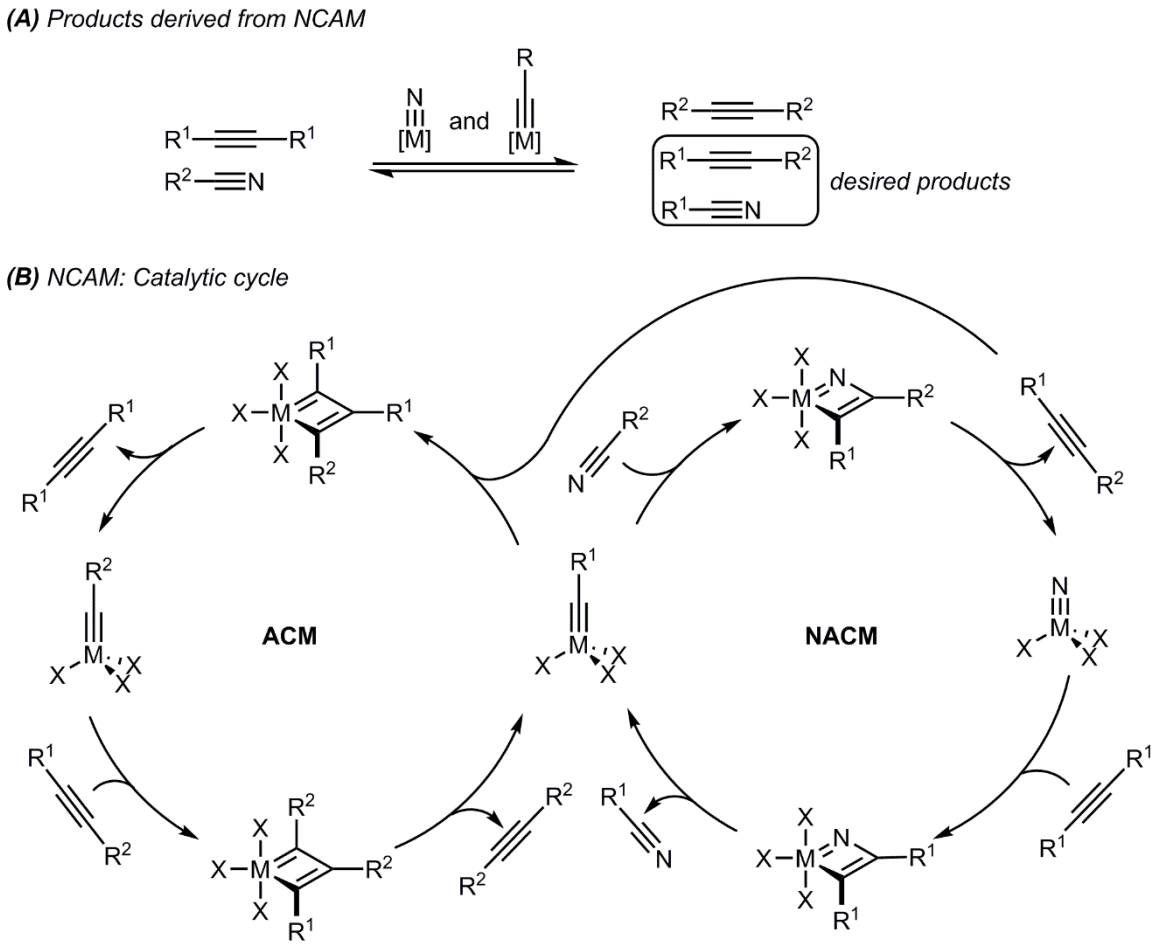

Scheme 30: **(A)** Products derived from NCAM and **(B)** catalytic cycles of nitrile alkyne cross-metathesis (NCAM) and competing alkyne cross-metathesis (ACM).[161]

In 2007 *Johnson et al.* published on the first catalytic nitrile-alkyne cross-metathesis (NCAM).[161a] In NCAM, nitriles are converted with internal alkynes to yield all possible alkyne cross nitrile metathesis products. However, competing alkyne cross-metathesis results in low conversion to the desired products (Scheme 30, **(A)**). Metal nitrides as well as metal alkylidynes are proposed to be the active species (Scheme 30, **(B)**). Studies showed, that the initially formed unsymmetrical alkyne is not accumulated but instantly consumed, indicating that alkyne metathesis proceeds faster than NACM.[161] Hence, although NACM presents an interesting new playground for chemists, a lot of progress must be made until it will become applicable for a wide range of substrates.

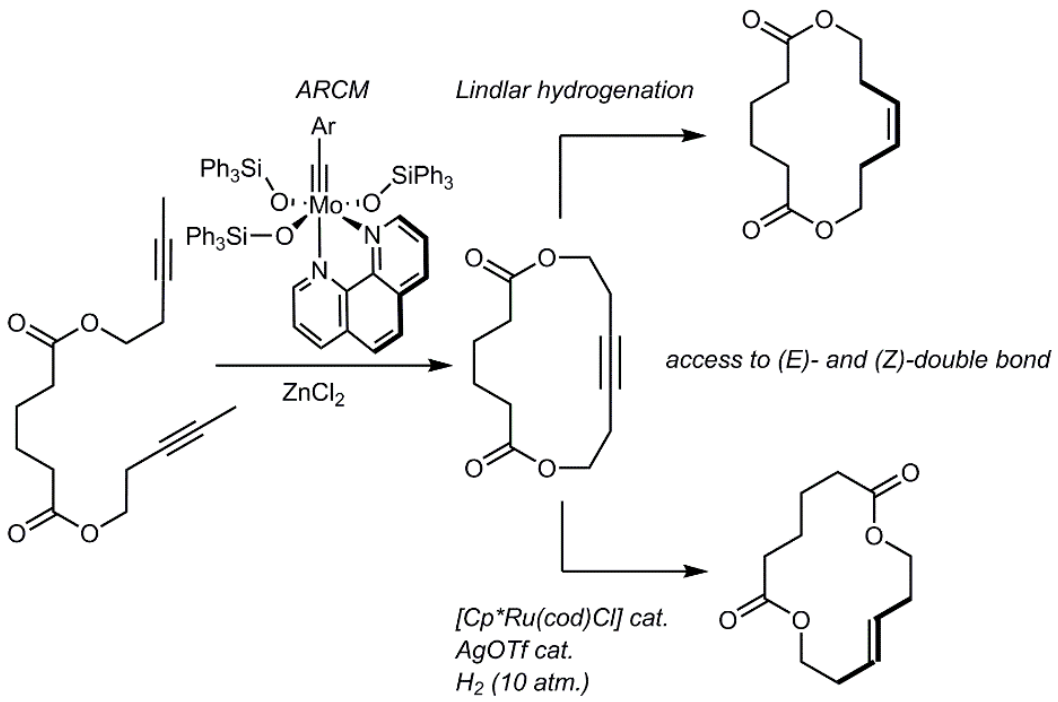

Figure 30: Stereoselective access to (*E*)- and (*Z*)-double bonds by combination of ARCM and stereoselective hydrogenation.[9a,162]

In many instances, especially in drug synthesis, stereoselective synthesis of (*E*)- or (*Z*)-double bonds is crucial. Although (*E*)- and (*Z*)-double bonds are now in many cases accessible through stereoselective RCM (MAP-type catalysts, *vide supra*), an interesting alternative was highlighted by *Fürstner* and co-workers.[9a,162] They successfully combined ARCM with stereoselective hydrogenation (Figure 30). Through careful choice of the hydrogenation catalyst both, (*E*)- and (*Z*)-isomer, can be gained from the ARCM product. Even though alkynes are often more expensive than alkenes, the described methodology offers the advantage that many alkyne metathesis catalysts don´t attack double bonds, thereby widening the scope to substrates with additional olefinic moieties.

5.3 PENTACOORDINATED METAL COMPLEXES

Pentacoordinated metal complexes play a key role in many transition metal catalyzed reactions, since they can arise from substrate coordination to a tetrahedral ML_4 complex (e.g. in olefin metathesis) or from dissociation of one ligand in especially stable octahedral ML_6 complexes to provide a coordination site (dissociative substitution, e.g. in hydrogenation reactions).[163]

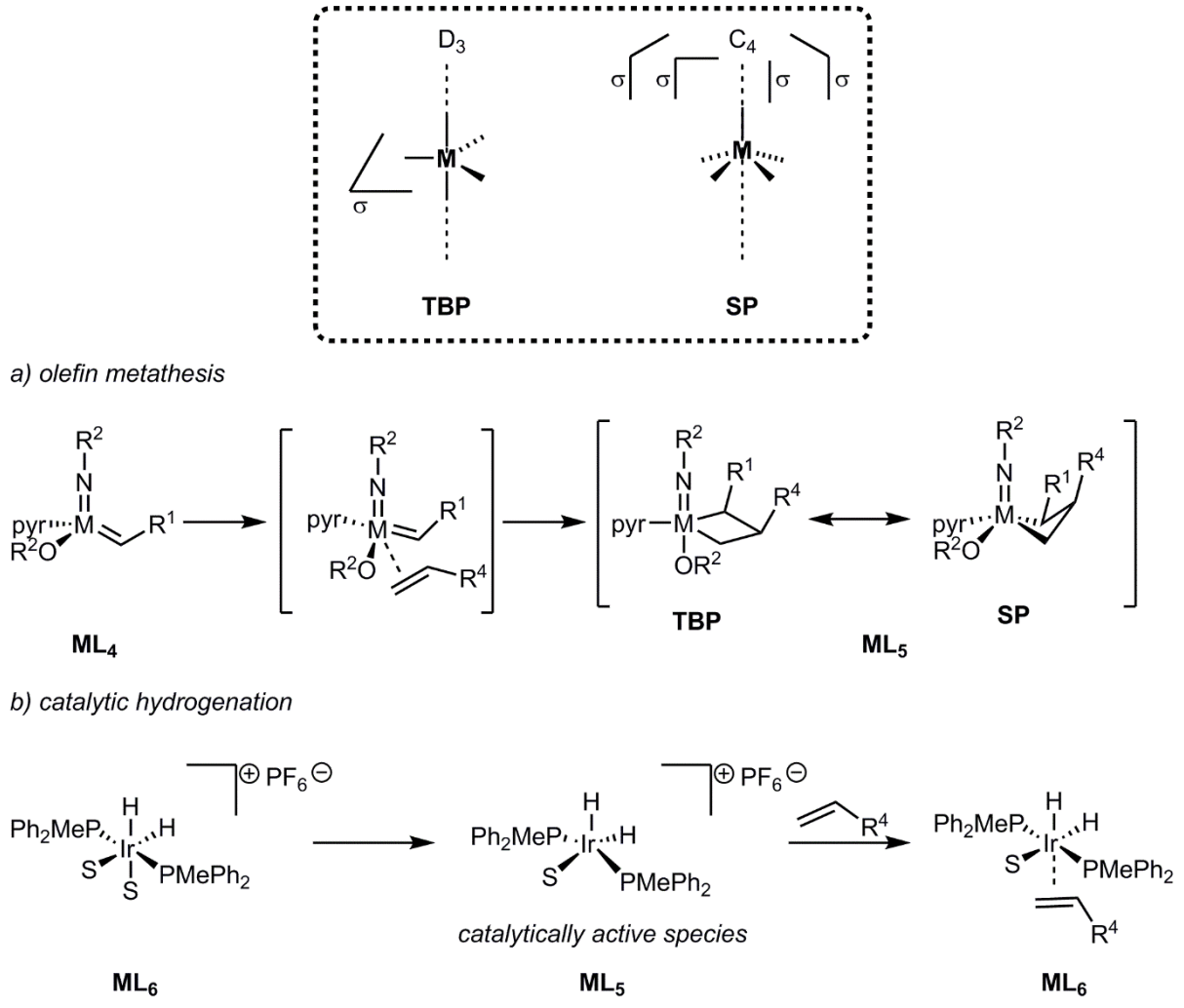

Figure 31: Trigonal bipyramidal (TBP) and square pyramidal (SP) geometry of pentacoordinated metal complexes and significance in *a)* olefin metathesis and *b)* catalytic hydrogenation.[163]

They can either take up a trigonal bipyramidal coordination sphere (TBP) or a square pyramidal geometry (SP). TBP complexes have a D_{3h} symmetry (one D_3 (threefold) axis of rotation and one symmetry plane (σ) orthogonal to it), whereas SP complexes show a C_{4v} symmetry (one C_4 (fourfold) axis of rotation and four planes of symmetry (σ) that contain this axis).

Addison et. al proposed the geometry index τ as a means of determining whether a given complex is closer to the trigonal bipyramidal or the square pyramidal geometry. τ ranges between 0 (SP) and 1 (TBP)[164] and is calculated by subtracting the two biggest angles present in the complex and dividing by 60°.

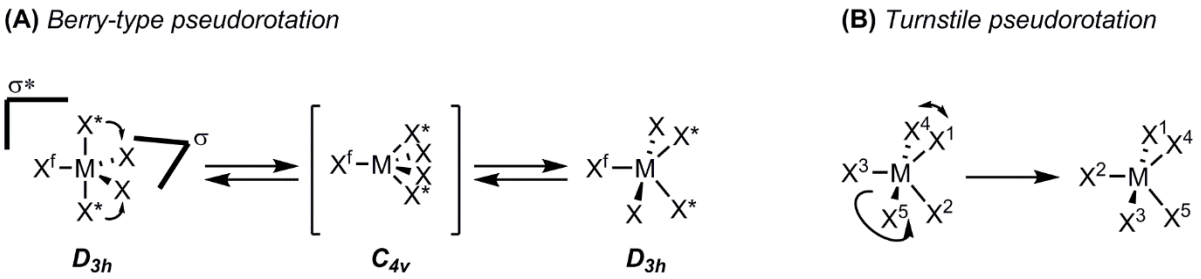

Figure 32: Pseudorotation in pentacoordinated metal complexes. **(A)** *Berry*-type pseudorotation and **(B)** turnstile pseudorotation.[165]

Pentacoordinated molecules are often fluxional and engage in pseudorotations[165], e.g. in the *Berry*-type pseudorotation or the turnstile pseudorotation (Figure 32). In the *Berry*-type pseudorotation axial and equatorial ligands change places (Figure 32, **(A)**). One ligand, X^f, stays fixed, the primarily apical ligands X* undergo a bending displacement in the plane σ* (containing X^f and X*) from 180 to 120°. The two ligands X also undergo a bending displacement in the plane σ (containing X^f and X) from 120 to 180°. A C_{4v} (SP) transition state is passed. Another pseudorotation described for pentacoordinated molecules is the turnstile pseudorotation (Figure 32, **(B)**). Here, the ligands X^2, X^3 and X^5 apparently rotate on an approximate local C_3 axis comparable to a turnstile, whereas X^4 and X^1 interchange on an approximate local C_2 axis. Another description includes two superimposed movements. On the one hand, X^1 and X^4 tilt at approximately 9° and X^2 and X^5 undergo a relative bending motion, comparable to a scissor, until their angle becomes 90°. On the other hand, X^3 and X^4 as well as X^1, X^2 and X^5 undergo an internal rotation. Due to fluxionality and the existence of two favored geometries (TBP and SP), pentacoordinated complexes exhibit a multitude of optical isomers (Figure 33).[166] TBP complexes of the type M[abcde] are chiral if a≠b≠c and d≠e, whereas SP complexes are chiral when a≠c and b≠d and either b≠c (if a=d) oder a≠b (if c=d). For a M[abcde] system with five different ligands, 25 optical isomers plus their corresponding enantiomers are hypothetically accessible. Of course, in many cases, certain restrictions due to electronic properties of the ligands in the respective geometry can be made, thereby lowering the number of optical isomers.

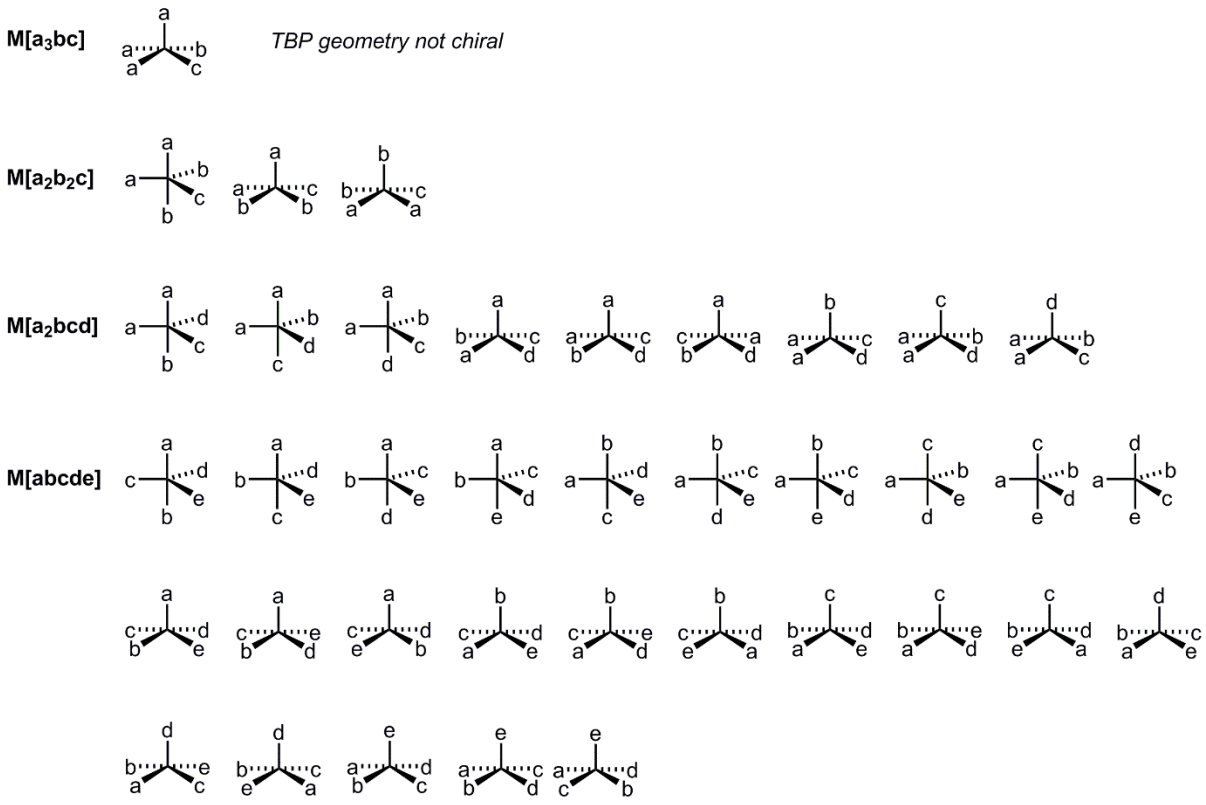

Figure 33: TBP and SP optical isomers of pentacoordinated complexes. Only one enantiomer is depicted.[166]

5.4 GROUP 6 *N*-HETEROCYCLIC CARBENE METAL ALKYLIDENE COMPLEXES

With the aim to synthesize cationic metal alkylidenes, *Buchmeiser et al.* coordinated *N*-heterocyclic carbenes to *Schrock*s´ molybdenum imido bistriflate alkylidene DME (1,2-dimethoxyethane) complexes, resulting in 16-VE pentacoordinated complexes[167].

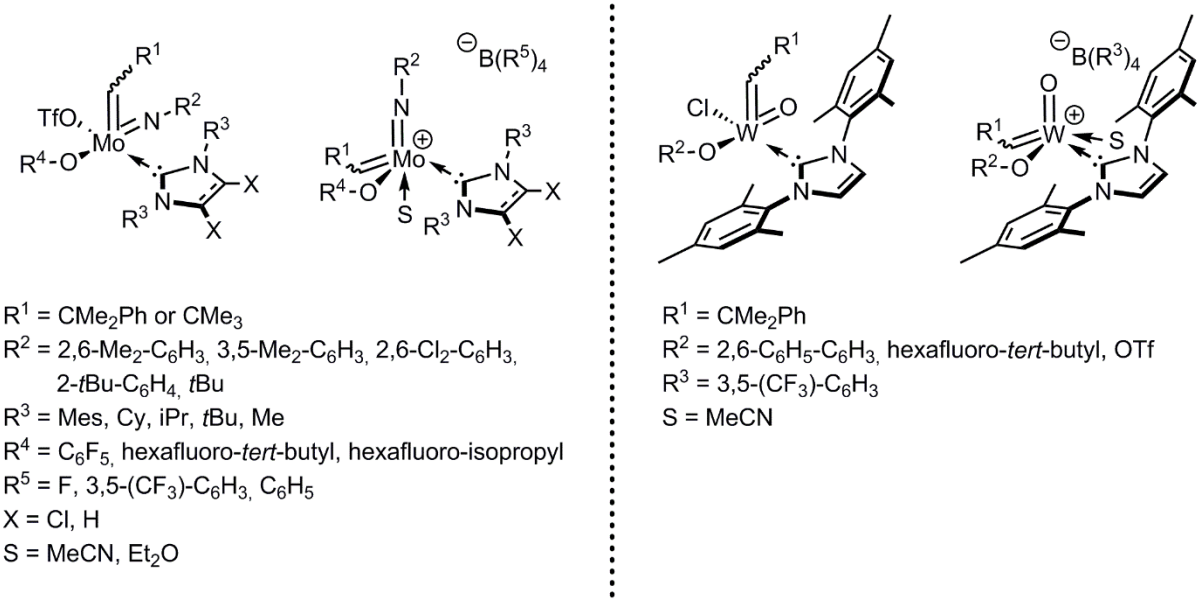

R^1 = CMe_2Ph or CMe_3
R^2 = 2,6-Me_2-C_6H_3, 3,5-Me_2-C_6H_3, 2,6-Cl_2-C_6H_3, 2-*t*Bu-C_6H_4, *t*Bu
R^3 = Mes, Cy, iPr, *t*Bu, Me
R^4 = C_6F_5, hexafluoro-*tert*-butyl, hexafluoro-isopropyl
R^5 = F, 3,5-(CF_3)-C_6H_3, C_6H_5
X = Cl, H
S = MeCN, Et_2O

R^1 = CMe_2Ph
R^2 = 2,6-C_6H_5-C_6H_3, hexafluoro-*tert*-butyl, OTf
R^3 = 3,5-(CF_3)-C_6H_3
S = MeCN

Figure 34: Cationic and neutral group 6 metal imido alkylidene NHC complexes.[17b,167-168]

The complexes of the general formula Mo(NAr)($CHCMe_2R^1$)$(OTf)_2$(NHC) proved to be active in olefin metathesis reactions. This was somewhat unexpected since 16-VE complexes were not thought to be reactive, due to decreased *Lewis* acidity on the metal center and the formation of stable octahedral complexes upon substrate coordination. In fact, when the metathesis reaction of Mo(*N*-2,6-Me_2-C_6H_3)($CHCMe_3$)$(OTf)_2$(1,3-dimesitylimidazolin-2-ylidene) with a norbornene derivative was monitored via *in situ* ^{19}F NMR spectroscopy, the formation of weakly coordinated triflate was observed.[167] Apparently, an intermediate with a weakly coordinated triflate anion was formed during the metathesis reaction either *via* an associative (substrate coordination triggers triflate dissociation) or a dissociative (triflate dissociation *prior* to substrate coordination) pathway (Scheme 31). Current results imply, that the reaction mechanism (associative or dissociative) is highly substrate dependant.[169] Variation of the NHC and alkoxide ligand in the pentacoordinated complexes showed an impact on reactivity. Replacement of one triflate ligand by an alkoxide ligand like *tert*-butoxide, hexafluoro-*tert*-butoxide or pentafluorophenoxide showed, that more electron-donating alkoxides lead to facilitated triflate dissociation whereas more electron-withdrawing ligands result in hindered loss of triflate. The influence of the NHC can best be verified by measuring the coalescence temperature of the two triflate ligands in molybdenum imido bistriflate NHC ligands.[168e] It was defined as the temperature at which the two triflate signals begin to coalesce in ^{19}F NMR spectroscopy. The coalescence temperature was postulated to be a direct consequence of the formation of an intermediate species with a triflate acting as weakly coordinating anion (WCA), where the bound and the WCA triflate exchange rapidly. Two enantiomers can be envisioned for pentacoordinated molybdenum imido bistriflate NHC complexes. The enantiomers can interconvert into each other in a *Berry*-type pseudo rotation *via* a SP intermediate, where the *trans*-effect of the NHC on the triflate ligand is at its maximum.

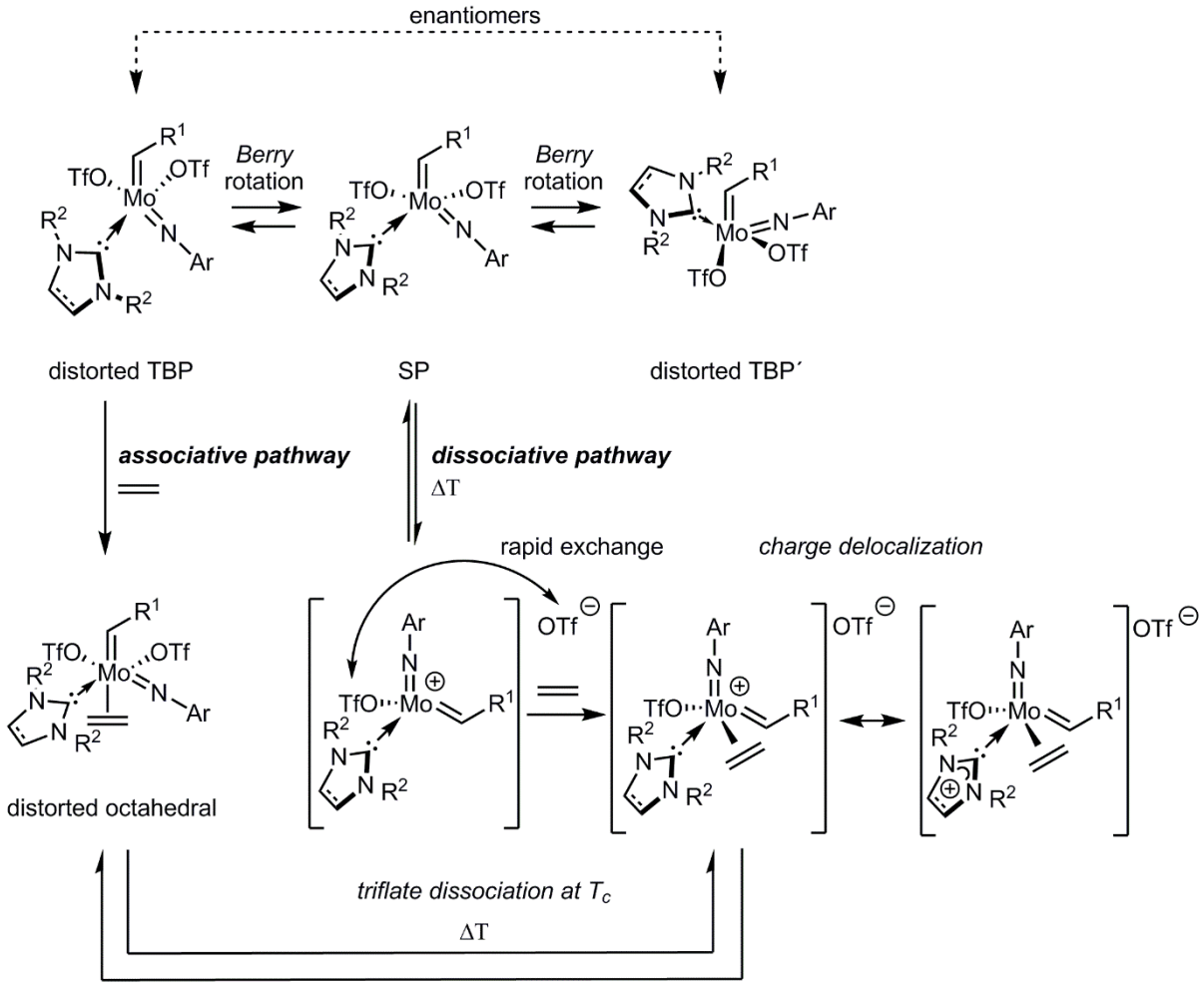

Scheme 31: Substrate coordination to molybdenum imido alkylidene NHC complexes. *Associative pathway*: Substrate coordination *prior* to ion pair formation. *Dissociative pathway*: Triflate dissociation *prior* to substrate coordination.[17b,168e]

The triflate ligand acting as WCA was exchanged by weakly coordinating boron-based anions, resulting in the first highly active cationic molybdenum imido alkylidene complexes capable of catalyzing metathesis reactions.[16,23,78,167-168,168d] Most of the cationic complexes can only be isolated when bearing an additional solvent molecule like diethyl ether or acetonitrile. In accordance with the molybdenum-based catalysts also tungsten oxo- and imido-based NHC catalysts have been synthesized and showed interesting properties in metathesis reactions.[168b,168f] Especially a tungsten oxo NHC alkylidene complex immobilized on silica showed extraordinary activity.[170] Molybdenum imido alkylidene NHC complexes have also been immobilized on silica *via* the NHC ligand and showed comparable activity to their homogeneous analogues, displaying no molybdenum residues in the product.[168a]

6 RESULTS AND DISCUSSION

6.1 GROUP 6 METAL ALKYLIDENES BEARING IONIC LIGANDS

Parts of the following chapter have already been published. Reprinted (adapted) with permission from (I. Elser, R. Schowner, W. Frey, M. R. Buchmeiser, *Chem. Eur. J.* **2017**, *23*, 6398-6405). Copyright (2017) John Wiley and Sons. And reprinted (adapted) with permission from (D. A. Imbrich, I. Elser, W. Frey, M. R. Buchmeiser, *ChemCatChem* **2017**, *9*, 2996-3002). Copyright (2017) John Wiley and Sons.

6.1.1 WORKING HYPOTHESIS

A major drawback in catalysis with organometallic compounds is the presence of metal residues in the final products.[171] This can be avoided by the application of biphasic reaction setups, where the substrate and the catalyst display distinct solubilities. Biphasic reaction setups containing fluorinated solvents and ionic liquids or other highly polar solvents (even water) in combination with standard solvents have been reported for a multitude of catalytic reactions.[13,172] Even olefin metathesis in biphasic reaction media has been described, however, at the time this study emerged, reports were restricted to ruthenium-catalyzed reactions.[127a,127b,129c,131] No molybdenum- and tungsten-based catalysts bearing ionic ligands had been described. Ruthenium and high oxidation state molybdenum and tungsten metathesis catalysts exhibit differences in terms of catalytic activity and tolerance of functional groups.[62,173] Hence, the synthesis of ionic molybdenum- and tungsten-based olefin metathesis catalysts for biphasic olefin metathesis shifted into focus. Since the aim was to use a mixture of a highly polar (polar organic or ionic liquid) and a nonpolar solvent, introduction of polar or ionic groups to the catalysts was mandatory to ensure exclusive solubility of the catalyst in the polar phase. When considering the introduction of ionic ligands to standard molybdenum or tungsten imido alkylidene complexes like MAP-type or bisalkoxide complexes it is evident, that introduction of the ionic charge *via* the alkoxide ligand is favorable over the introduction of the ionic charge *via* the imido or alkylidene ligand (Figure 35).

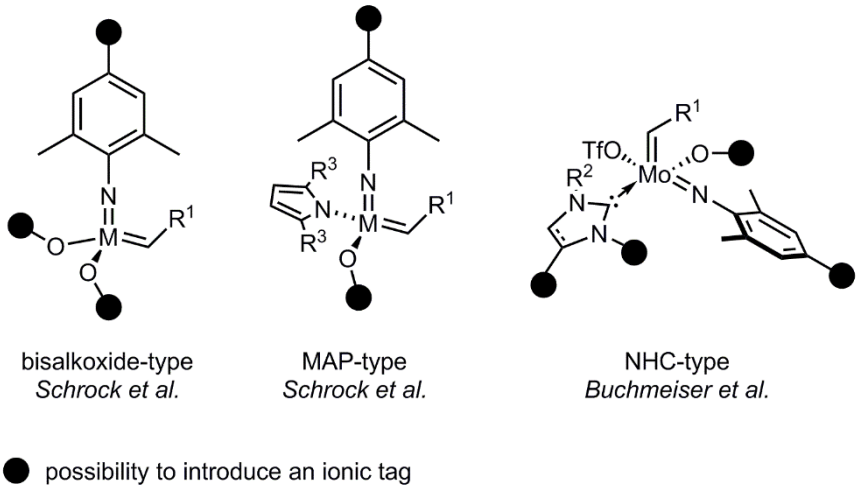

Figure 35: Opportunities to introduce an ionic tag to standard molybdenum- or tungsten-based olefin metathesis catalysts.

An ionic charge on the alkylidene ligand might be useful in some occasions, but certainly not when the preferred solubility in the polar phase ought to be maintained, since it leaves the active complex in the first productive metathesis step. The imido ligand on the other hand would be suitable for introduction of an ionic charge but is, in contrast to the alkoxide ligand, already present in the first stage of catalyst preparation. Furthermore, the synthesis of molybdenum imido alkylidene bistriflate DME precursor complexes is accompanied with the formation of inorganic salts, that might be hard to separate from an ionic metal complex.[73b] Therefore, suitable ionic (betaine-type) alkoxide ligands were synthesized or purchased from standard suppliers and tested in the synthesis of ionic group 6 metal complexes. Previous results had indicated, that the synthesis of chiral BINOL-based ligands in which the cationic charge of the ionic tag is not in conjugation with the prospective alcoholate is favorable. Otherwise hardly soluble quinoid structures can form upon deprotonation.[174] If, however, it is inevitable that the positive charge is in conjugation with the anionic charge, less electronegative phosphorous cations might be favorable over nitrogen cations. For molybdenum imido alkylidene NHC complexes the introduction of an ionic NHC provides an additional pathway. Also, recently published cationic-at-metal complexes[168a,168c,168e] bearing an NHC might be used under biphasic conditions. It should be noted, that for bisalkoxide standard *Schrock*-type complexes two ionic ligands must be introduced, since mixed alkoxide metal complexes are known to undergo ligand scrambling.[175] Anions for the conceptualized metal complexes and ligands must be carefully chosen. The weakly coordinating anion (WCA) tetrakis(3,5-trifluoromethylphenyl)borate) ($B(Ar^F)_4$) was chosen due to the sterically demanding trifluoromethyl groups. They ensure shielding of the anionic boron center, thereby preventing coordination of the anion to the metal center which was expected to result in reduction of catalyst activity.

6.1.2 SYNTHESIS OF LIGANDS

6.1.2.1 Synthesis of ionically tagged alcohols

Four ionic analogues to already established ligand systems in olefin metathesis were identified as target structures. Established ligand systems are sterically encumbered fluorinated alkoxides,[175] sterically demanding terphenoxides[82-83,105b,176] and axially chiral biphenolates or binaphtholates[21d,21e,90a,90d,95-96,177] (Figure 36). Terphenoxides are usually applied in (*Z*)-selective olefin metathesis whereas axially chiral biphenolates and binaphtholates are additionally used in enantioselective olefin metathesis reactions.

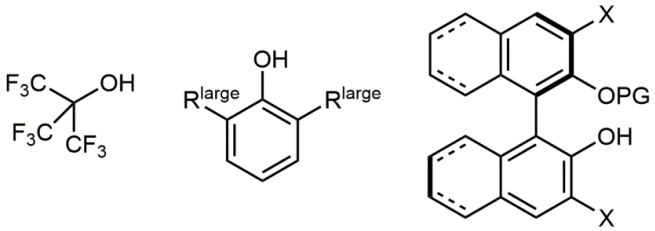

Figure 36: Ligand types commonly used in olefin metathesis. From left to right: Sterically demanding fluorinated alkoxides, sterically demanding terphenoxides and axially chiral binaphtholates.

Two 2,6-disubstituted phenoxides were synthesized as ionic mimics of the successful OHMT ligands usually applied in (*Z*)-selective metathesis.[61c,75,83a,178] Synthesis of [(3,5-di-*tert*-butyl-4-hydroxy-phenyl)triphenylphosphonium][$B(Ar^F)_4$] (**1**) was developed by *Roman Schowner*[14-15] and starts from commercially available 2,6-di-*tert*-butyl-4-bromo-phenol **1a**. The first synthesis step is a $Pd_2(dba)_3$-catalyzed (dba = dibenzylideneacetone) coupling reaction of **1a** with triphenyl phosphine in ethylene glycol at 130 °C and leads to the phosphonium ion tagged phenol **1b** which was purified by column chromatography (silica, MeOH/CH_2Cl_2, 1/10, V/V) and isolated in 95% yield. **1b** was easily transformed into the anion exchanged product **1** in 85% yield by conversion with $Na(BAr^F)_4$ in CH_2Cl_2 and a few drops of diethyl ether (ensures solubility of $Na(BAr^F)_4$) and can be purified by crystallization from CH_2Cl_2.

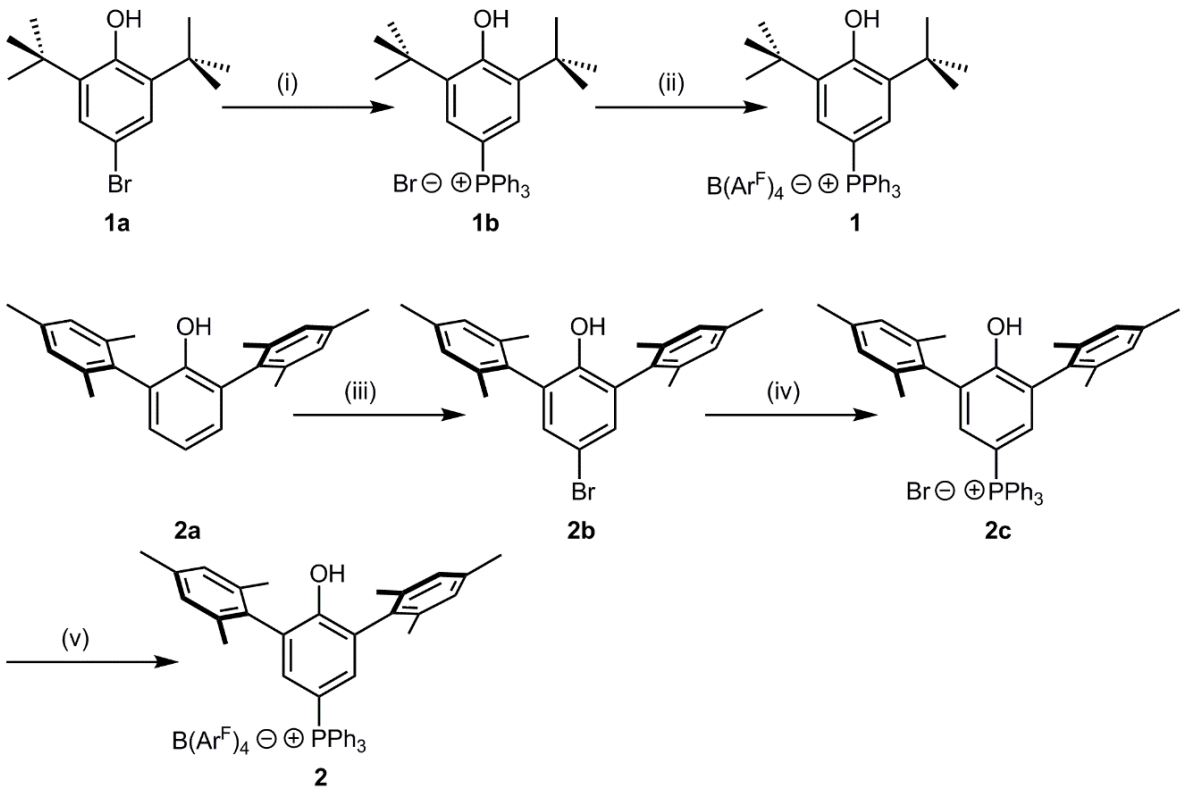

Scheme 32: Synthetic protocols for the preparation of the ionically tagged phenols **1** and **2**. (i) $Pd_2(dba)_3$, ethylene glycol, 130 °C (95% yield); (ii) $NaB(Ar^F)_4$, CH_2Cl_2/diethyl ether, room temperature (85% yield); 81% overall yield; (iii) Br_2, glacial acetic acid, -10 °C-> room temperature (not isolated); (iv) $Pd_2(dba)_3$, ethylene glycol, 130 °C (60% yield); (v) $NaB(Ar^F)_4$, CH_2Cl_2/diethyl ether, room temperature (78% yield); 47% overall yield.

Furthermore, [(3,5-dimesityl-4-hydroxy-phenyl)triphenylphosphonium][$B(Ar^F)_4$] (**2**) was synthesized *via* an analogous synthetic protocol. 2,6-(2,4,6-Trimethylphenyl)-phenol (**2a**, hexamethylterphenoxide, HMTOH) was prepared in a multi-step synthesis starting from commercially available 1,3-dichlorobenzene according to a literature-known procedure (Scheme 33).[179] **2a** was then brominated with bromine in glacial acetic acid to yield 4-bromo-2,6-(2,4,6-trimethylphenyl)-phenol (**2b**). Unfortunately, despite several efforts (working in high dilution, slow addition of bromine, less than one equivalent of bromine), **2b** always contained minor amounts of doubly brominated by-products (up to 3%, as observed by GC-MS). Consequently the crude product was applied in the follow-up reaction. Pure [(3,5-dimesityl-4-hydroxy-phenyl)triphenylphosphonium][Br] (**2c**) was isolated in 60% yield after a $Pd_2(dba)_3$-catalyzed coupling reaction with triphenyl phosphine in ethylene glycol at 130 °C and subsequent column chromatography (silica, MeOH/ CH_2Cl_2, 1/10, V/V), which allowed for removal of the doubly phosphonium tagged species. Anion exchange with $NaB(Ar^F)_4$ in a mixture of CH_2Cl_2 and diethyl ether lead to the desired phenol **2** in 78% yield after filtration of a solution of the crude product in CH_2Cl_2 over dry silica.

Also, the phosphonium-tagged ionic ligand [(4-(1-hydroxy-ethyl)phenyl)triphenyl-phosphonium] [$B(Ar^F)_4$] **3** was synthesized as a mimic for alkylic alcohols, comparable to *tert*-butoxide or hexafluoro-*tert*-butoxide, commonly used as ligands in *Schrock*-type olefin metathesis catalysts.[175] **3a** was employed in its racemic form. As described for above procedures, **3** was synthesized by coupling of **3a** with triphenyl phosphine to give **3b** (87% yield after column chromatography, silica, methanol/ CH_2Cl_2, 1/20 -> 1/10, V/V) followed by anion exchange with $NaB(Ar^F)_4$ to provide **3** (91% yield).

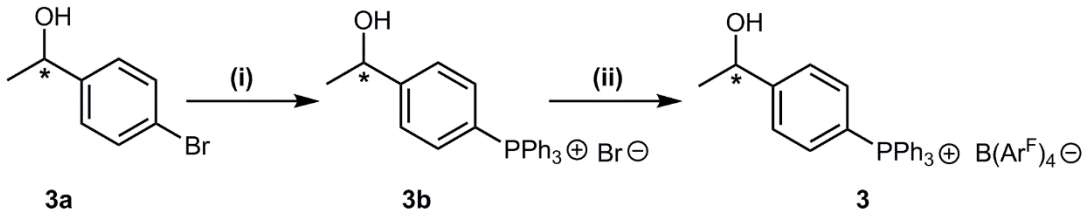

Scheme 33: Synthesis of ionic ligand **3**. (i) $Pd_2(dba)_3$, ethylene glycol, 120 °C (87% yield); (ii) $NaB(Ar^F)_4$, acetonitrile/ CH_2Cl_2, room temperature (91% yield); 79% overall yield.

Finally, starting from (*S*)-1,1´-binaphth-2,2´-ol (**4a**) the ionically tagged chiral ligand [2-((2´-hydroxy-1,1´-binapth-2-oxy)methyl)-*N*-methylpyridinium][$B(Ar^F)_4$] (**4**) was accessed as an analogue to monoprotected C_2-symmetric ligands commonly used in enantioselective metathesis.[21d,21e] The synthesis of **4b** is literature-known[180], however the protection and deprotection step were omitted and an alternative synthesis route was explored. First, **4a** was reacted with one equivalent of 2-picolyl hydrobromide to selectively etherify one hydroxyl group in a mixture of water and acetone at 65°C with potassium carbonate as a base for 48 hours (**(i)**, Scheme 34).

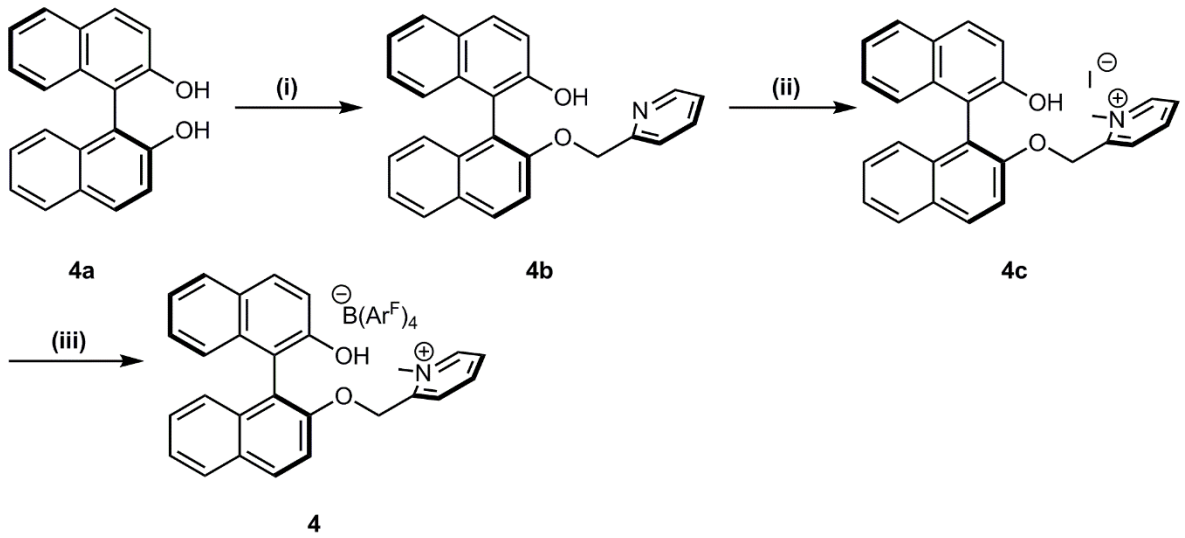

Scheme 34: Synthesis of chiral ligand **4** starting from commercially available (*S*)-BINOL. (i) 2-Picolyl hydrobromide, K_2CO_3, 65 °C, water/acetone, 48 hours, 74% yield; (ii) methyl iodide, acetone, reflux, 80% yield; (iii) $NaB(Ar^F)_4$, acetonitrile/ CH_2Cl_2, 92 % yield; 55% overall yield.

The crude product was purified by column chromatography (silica, diethyl ether) to provide 2-((2´-hydroxy-1,1´-binaphth-2-oxy)methyl)-pyridine (**4b**) in 74% yield. **4b** was methylated with methyl iodide in acetone under reflux. [2-((2´-hydroxy-1,1´-binaphth-2-oxy)methyl)-*N*-methyl-pyridinium][I] **4c** precipitates from the reaction mixture and can easily be separated by filtration. Analytically pure **4c** was available in 80% yield by simple washing of the crude product with diethyl ether. The anion exchange from **4c** to **4** was carried out in a mixture of acetonitrile and CH_2Cl_2 with $NaB(Ar^F)_4$. **4** was isolated as a sticky foam after filtration of a solution of the crude product in CH_2Cl_2 over Celite® in 92% yield.

6.1.2.2 Synthesis of (pre-)ionic N-heterocyclic carbene(-precursor)s

In addition to the ionically tagged alkoxides, two NHC ligands for the prospective introduction to molybdenum imido alkylidene bistriflate complexes were synthesized according to literature-known procedures (Scheme 35).[127b,181] On the one hand, **5** was chosen because of its ionizable group and because it had been coordinated to ruthenium-based metathesis catalysts: *Skowerski et al*. synthesized a cationically tagged complex by simple methylation of the dimethylamino group with methyl iodide.[127b] The introduction of the ionic charge after the coordination of the ligand, by for example methylation with methyl iodide, methyl triflate or comparable alkylating agents, was to be investigated.

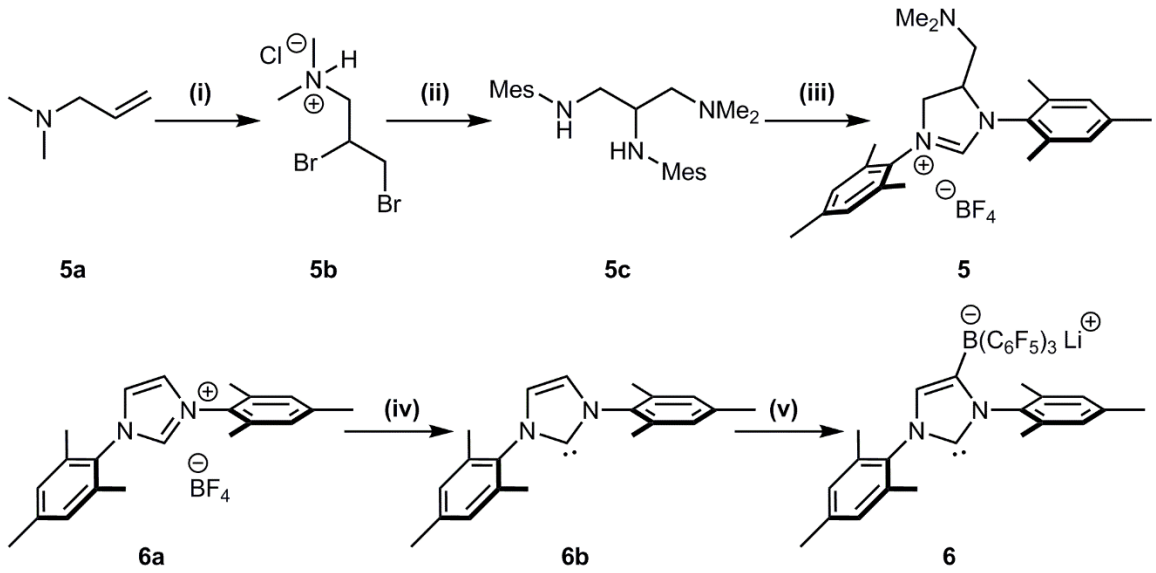

Scheme 35: Synthesis of an imidazolium salt with an ionizable group (**5**) and an anionically tagged NHC ligand (**6**) according to literature-known procedures. (i) 1.) HCl, H_2O, 2.) Br_2, 50 °C, 57% yield (literature: 66%); (ii) 1.) 2,4,6-trimethylaniline (excess), 125 °C, 24 hours, 2.) NaOH, 75% yield (literature: 70%); (iii) ammonium tetrafluoroborate, triethyl orthoformat, 120 °C, 3 hours, 40% yield (literature: 62%); 17% overall yield. (iv) KO*t*Bu, THF, 12 hours, 79% yield; (v) 1.) *n*-BuLi, toluene, 12 hours, 2.) $B(C_6F_5)_3$, toluene, 12 hours, 66% yield (literature: 70%); 52% overall yield.

On the other hand, NHC **6**[181] bearing a WCA, was selected to examine whether there are advantages of an anionic tag *vs.* a cationic tag. Both ligands were easily accessible on the published routes in yields comparable to those described in literature.

6.1.3 SYNTHESIS OF COMPLEXES WITH IONICALLY TAGGED LIGANDS

6.1.3.1 Synthesis of complexes with ionically tagged alkoxides

With the above-mentioned tagged alkoxide ligands at hand the synthesis of molybdenum- and tungsten-based olefin metathesis catalysts was pursued. Consequently, ligands **1**, **2**, **3** and **4** were reacted with different classes of molybdenum (and tungsten) imido alkylidene complexes employing different bases, solvents and reaction temperatures. Only successful reactions or exemplary reactions leading to valuable insights will be discussed in detail. An overview on additional reactions is provided in the experimental section (Table 11, experimental section).

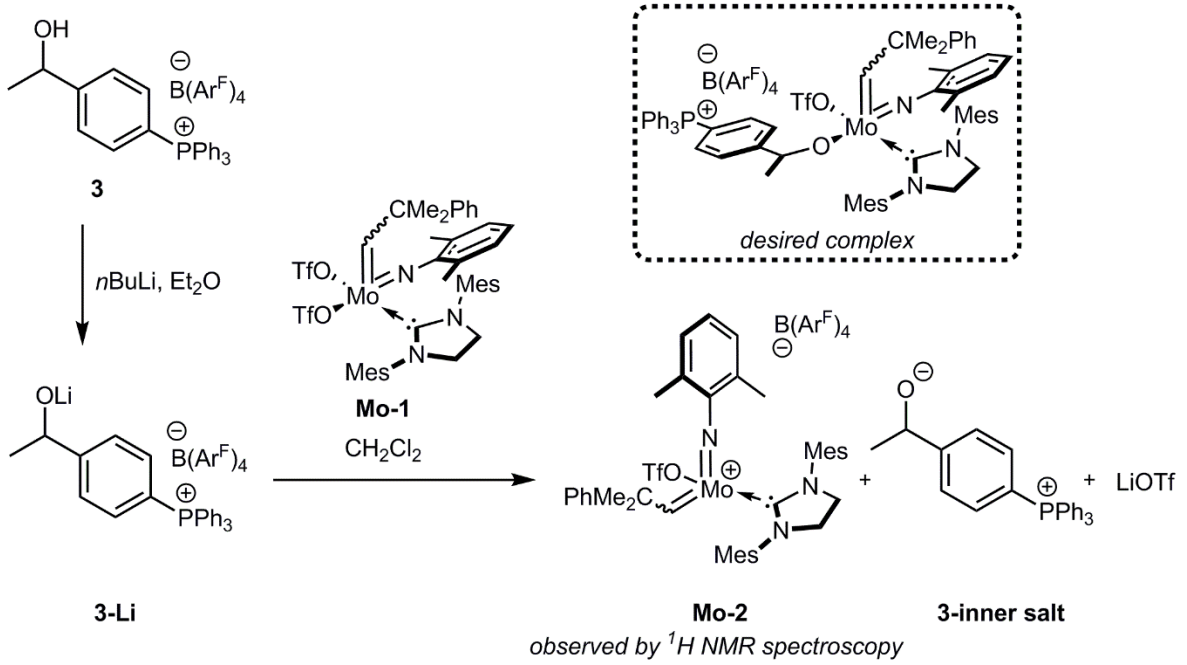

Scheme 36: Reaction of **3-Li** with **Mo-1** under formation of a cationic-at-metal complex **Mo-2**, **3-inner salt** and lithium triflate instead of the desired complex containing the cationically tagged ligand **3**.

To introduce **3** to **Mo-1**, **3** was *in situ* deprotonated with *n*-BuLi in diethyl ether. Diethyl ether was removed, the residue was dissolved in CH_2Cl_2, and added to a solution of **Mo-1** in CH_2Cl_2 at -35 °C. After filtration the crude reaction mixture did not show any ligand signals, however, formation of a salt was observed during the reaction. It was therefore suspected, that one of the triflate ligands in **Mo-1** had been removed under formation of cationic complex **Mo-2**, **3-inner salt** and lithium triflate (Scheme 36). Indeed, all NMR-signals of **Mo-2** (synthesized for comparison by reaction of **Mo-1** with $NaB(Ar^F)_4$ in CH_2Cl_2[168a]), were observed in the crude reaction mixture. The same was true for comparable reactions with **4**. Consequently, to avoid the formation of stable and apparently inert or highly insoluble inner salts, the ligands were reacted with molybdenum imido bispyrrolide complexes and a tungsten imido NHC bispyrrolide complex. The addition of alcohols to molybdenum imido alkylidene bispyrrolides

is supposed to proceed by alcohol coordination *prior* to proton transfer to the pyrrolide ligand (Scheme 37).[22a] Therefore, the formation of inner salts should be circumvented.

Issue:

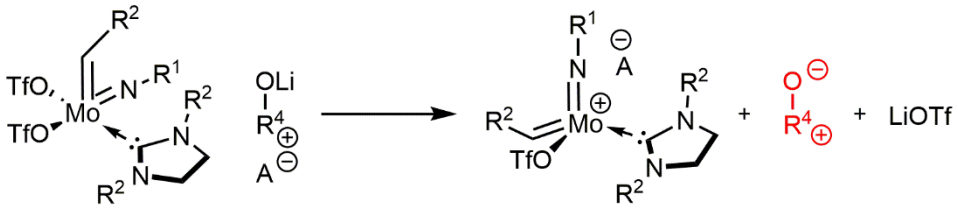

Driving force: Formation of extremely stable compounds and insoluble salts

Approach:

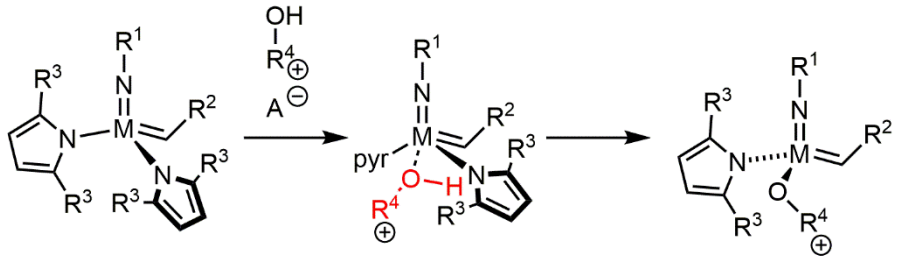

No formation of inner salts

Scheme 37: Problematic formation of inner salts during reaction of cationically tagged lithium alkoxides with molybdenum imido alkylidene NHC complexes. Approach to prevent formation of inner salts by introduction of ionically tagged alcohols to bispyrrolide (NHC) complexes.

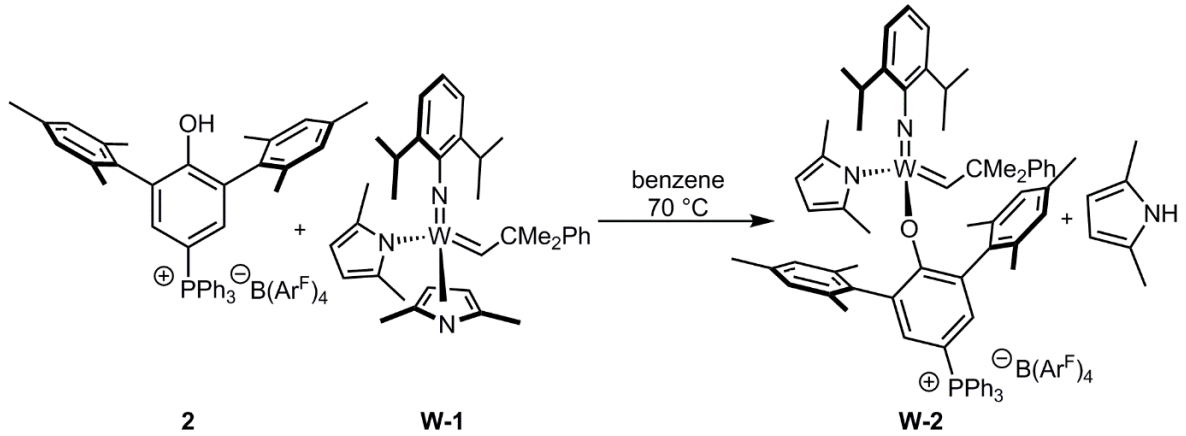

Scheme 38: Synthesis of ionic tungsten-based MAP-type complex **W-2** (quantitative yield) by reaction of **W-1** with **2**.

For **3** and **4** no conversion was observed when the alcohols were reacted with literature-known bispyrrolide complex W(*N*-2,6-iPr$_2$-C$_6$H$_3$)(CHCMe$_2$Ph)(2,5-Me$_2$-NC$_4$H$_2$)$_2$ (**W-1**). However, for the reaction of **2** with **W-1** in benzene at 70 °C, the desired ionically tagged MAP-type complex W(*N*-2,6-iPr$_2$-C$_6$H$_3$)(CHCMe$_2$Ph)(2,5-Me$_2$-NC$_4$H$_2$)(**2**) (**W-2**) could be isolated after simple washing with pentane to remove 2,5-dimethylpyrrole in quantitative yield (Scheme 38). **W-2** is the first isolated ionically tagged MAP-type alkylidene complex.

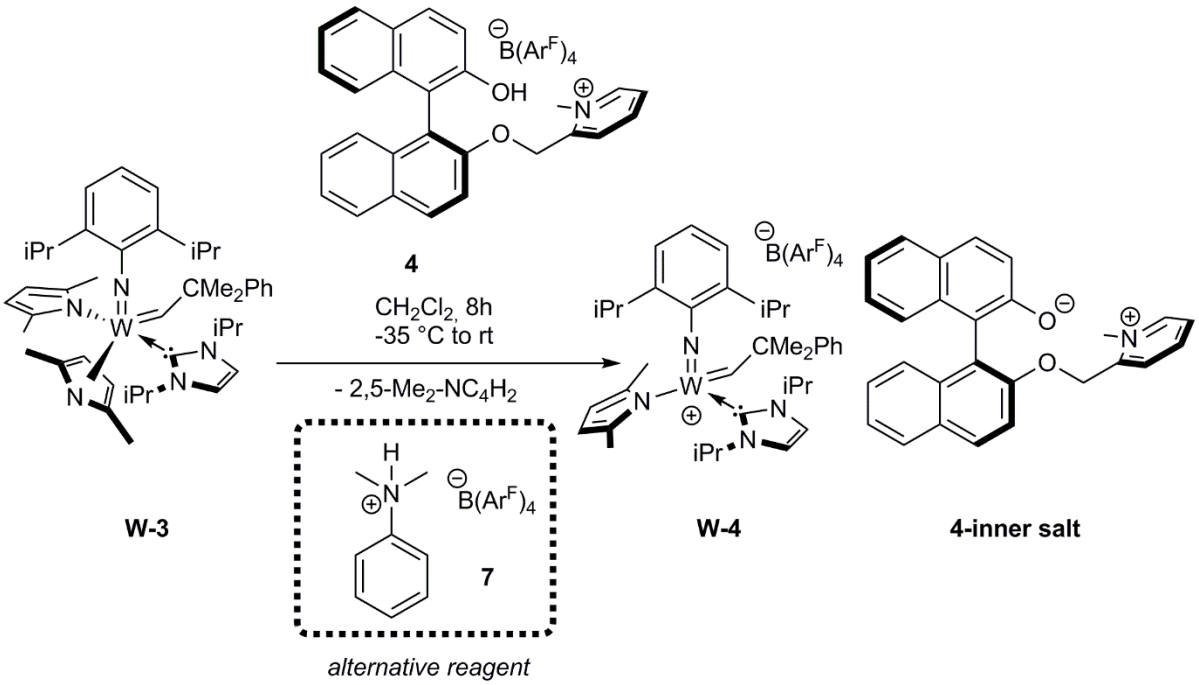

Scheme 39: Unexpected synthesis of cationic-at-metal complex **W-4** by reaction of **W-3** with **4**. *N,N*-dimethyl anilinium B(Ar^F)$_4$ (**7**) can be applied as a substitute for **4** (92% yield).

Next, W(*N*-2-6-iPr$_2$-C$_6$H$_3$)(CHCMe$_2$Ph)(2,5-Me$_2$-NC$_4$H$_2$)$_2$(1,3-diisopropylimidazol-2-ylidene) (**W-3**) was synthesized from the literature-known bispyrrolide complex **W-1** in 85% yield by reaction with 1,3-diisopropylimidazol-2-ylidene in diethyl ether according to a synthetic protocol first developed by *Dominik Imbrich.*[168f,182] When **4** was reacted with **W-3**,

interestingly, no replacement of a pyrrolide ligand by the alkoxide was observed (Scheme 39). Instead, the cationic monopyrrolide complex **W-4** was isolated. Again, the formation of **4-inner salt** was favored over coordination of the alkoxide to the cationic electron deficient tungsten center. **W-4** is also preparable by application of easily accessible *N,N*-dimethylanilinium $B(Ar^F)_4$ (**7**) as proton source in 92% yield. The by-product *N,N*-dimethyl aniline is easily removed by washing with pentane.

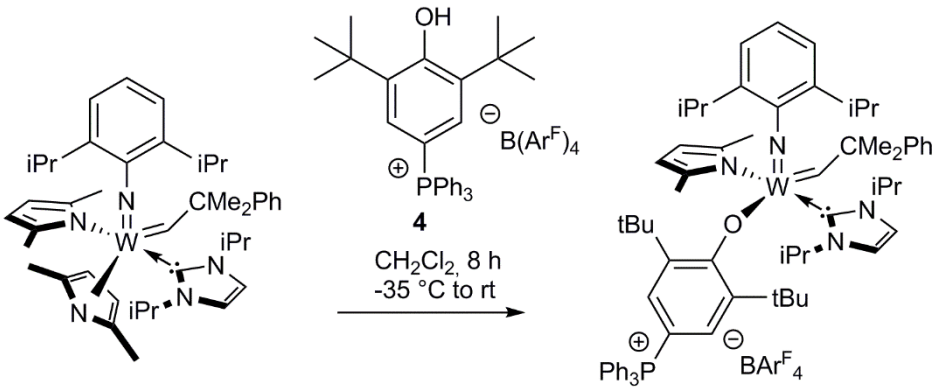

W-3 **W-5**

Scheme 40: Synthesis of the first tungsten imido alkylidene NHC pyrrolide complex **W-5** with a phosphonium tagged alkoxide **4** (79% yield) from **W-3** and **4**.

On the other hand, reaction of **4** with **W-3** resulted in the isolation of the expected complex **W-5** in 79% yield. **W-5** was not expected to show high catalytic activity, due to its 16-VE structure, and because, in contrast to published molybdenum imido NHC alkylidene bistriflate complexes[168a,168c,168e,183], **W-5** does not contain a good leaving group. Unfortunately, attempts to activate **W-5** by selective protonation of the pyrrolide ligand with **7**, to afford a more *Lewis* acidic cationic-at-metal complex, led to decomposition. Eventually, unselective protonation of all ligands occurs.

Since the synthesis of metathesis-active complexes with alkoxide-based cationically tagged ligands suffered from the formation of inert inner salts, incapable of reacting with the high oxidation state molybdenum and tungsten alkylidenes, another type of ligand was investigated. Commercially available 3-(1-pyridinium)-1-propanesulfonate **8** was chosen as a cationically tagged triflate mimic.

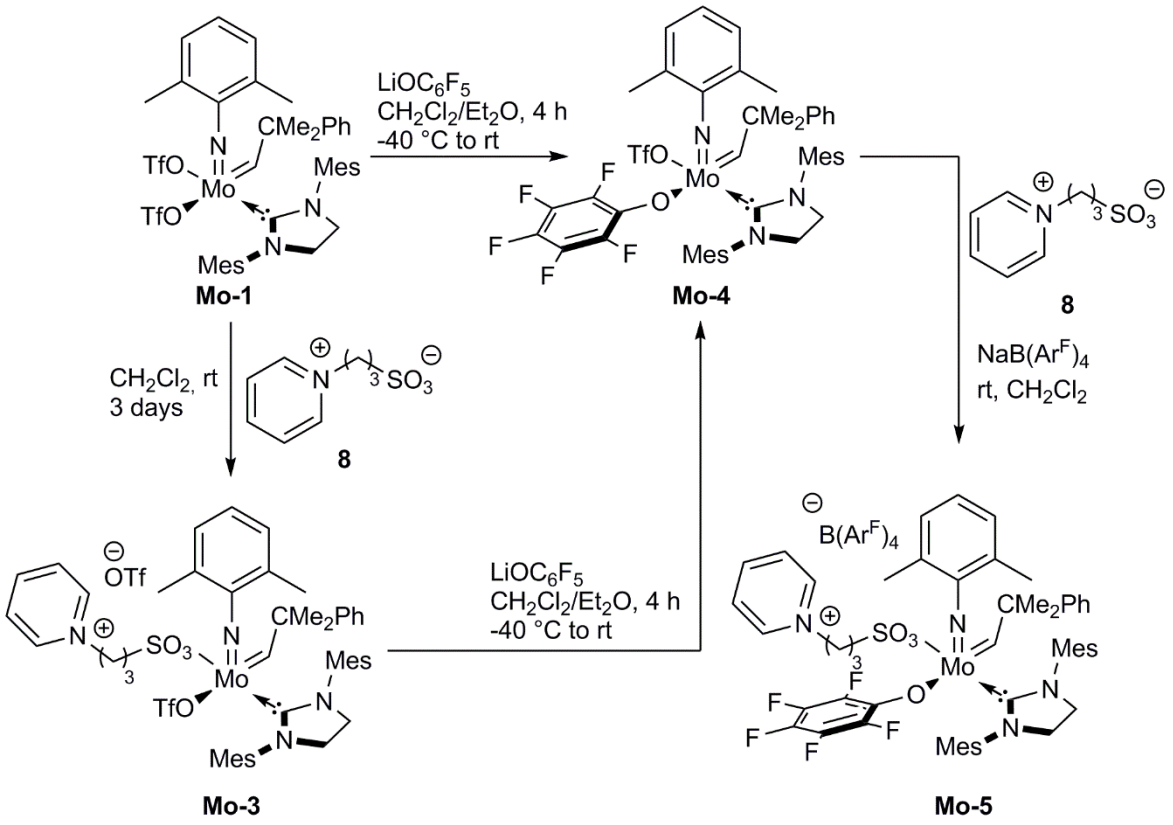

Scheme 41: Synthesis of the first cationically tagged molybdenum imido NHC complexes **Mo-3** and **Mo-5** in 82 and 87% yield by conversion of the precursor complexes **Mo-1** and **Mo-4** with triflate mimic **8**.

Reaction of Mo(*N*-2,6-Me_2-C_6H_3)(CHCMe_2Ph)(OTf)$_2$(IMesH_2) **Mo-1**[168a] with **8** yielded the ionically tagged complex Mo(*N*-2,6-Me_2-C_6H_3)(CHCMe_2Ph)(OTf)(**8**)(IMesH_2) (**Mo-3**, Scheme 41, IMesH_2 = 1,3-dimesitylimidazolin-2-ylidene) in 82% yield by replacement of one of the triflate ligands. Crystals of **Mo-3** suitable for single-crystal X-Ray analysis were grown out of a mixture of CH_2Cl_2, diethyl ether and pentane. Compound **Mo-3** (Figure 37) crystallizes in the monoclinic space group $P2_1/c$, a = 1646.60(10) pm, b = 2744.17(17) pm, c = 1377.85(9) pm, α = γ = 90 °, β = 105.358(2)°. The ligands adopt a distorted square pyramidal geometry (τ = 0.11)[164] with the alkylidene moiety occupying the apical position. The triflate ligand is situated *trans* to the NHC ligand, whereas the ionically tagged sulfonate is located trans to the imido ligand. The Mo-triflate distance (Mo-O4, 216.0(3) pm) in **Mo-3** is longer than the one in complex **Mo-1** (214.79(10) pm).[168a]

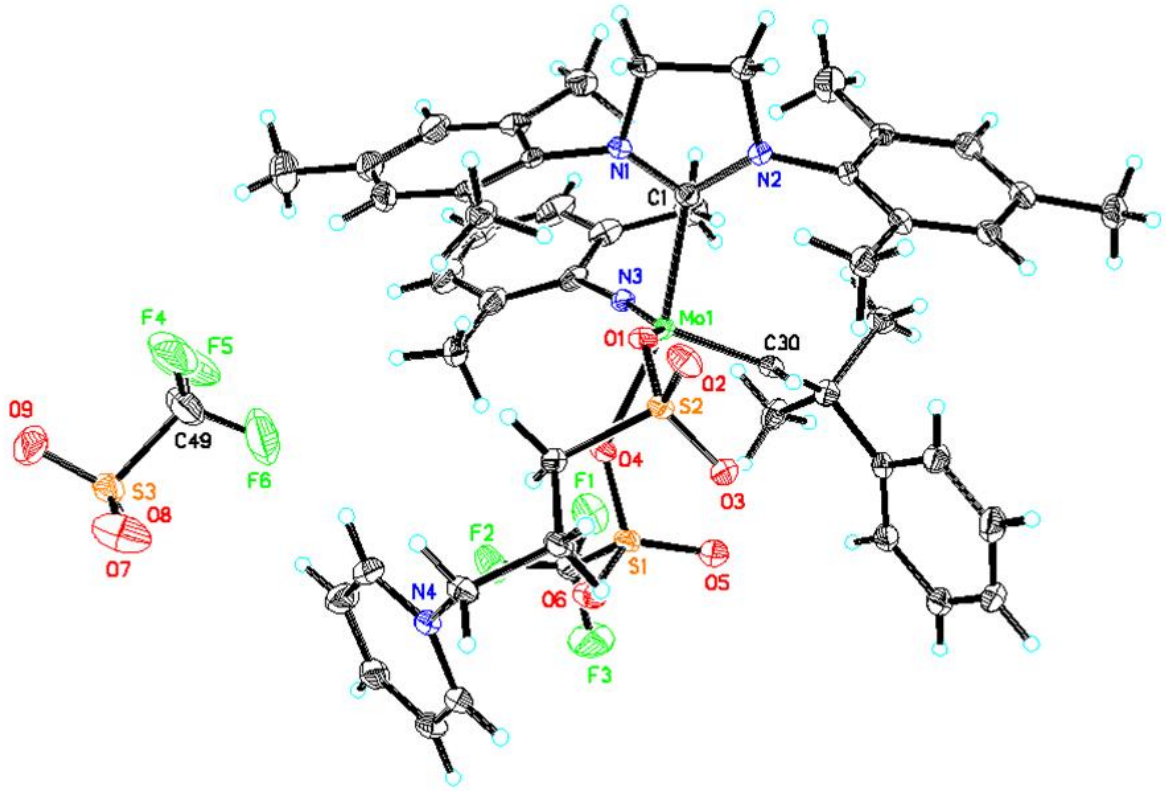

Figure 37: Single-crystal X-ray structure of **Mo-3**. Selected bond lengths [pm] and angles [°]: Mo1-N3 173.3(3), Mo1-C30 187.6(4), Mo1-O1 208.2(3), Mo1-O4 216.0(3), Mo1-C1 222.6(4); N3-Mo1-C30 103.63(16), N3-Mo1-O1 146.66(13), C30-Mo1-O1 109.71(14), N3-Mo1-O4 95.46(12), C30-Mo1-O4 96.69(13), O1-Mo1-O4 80.36(10), N3-Mo1-C1 96.66(14), C30-Mo1-C1 103.31(14), O1-Mo1-C1 76.50(12), O4-Mo1-C1 153.39(12).

In **Mo-3**, ^{19}F NMR reveals a rapid exchange between free and Mo-bound triflate in solution at room temperature. The ^{19}F NMR spectrum shows only one signal at δ = -78.52 ppm for both triflate ligands, indicating a coalescence temperature (T_c) < 25 °C. T_c was defined as the temperature at which the two triflate ligands begin to coalesce in ^{19}F NMR spectroscopy. Molybdenum imido alkylidene NHC complexes were postulated to have an active species in which the triflate ligand is almost completely dissociated and behaves more like a WCA.[167,168e] For a biphasic reaction setup, it is crucial that the triflate but not the ionic ligand dissociates from the metal to form an active cationic species. To confirm this, a ^{1}H NMR study of the ROMP reaction of complexes **Mo-1** and **Mo-3** with 5,6-bis(pentyloxymethyl)bicyclo[2.2.1]hept-2-ene **M1** (catalyst:substrate = 1:5) in $CDCl_3$ was performed. *In situ* ^{1}H NMR spectroscopy of the polymerization showed that the two complexes had different main propagating species (Figure A35, Appendix). This suggest formation of the active species in **Mo-3** proceeds via dissociation of the triflate, not the ionic ligand. With catalyst **Mo-3**, poly(**M1**) was obtained in quantitative yield with an M_n of 21,900 g/mol ($M_{n,theo}$ = 14,700 g/mol) and a PDI of 3 (70 % *trans*). Exchange of the X-type ligand in **Mo-3** to lithium pentafluorophenoxide resulted in the quantitative exchange of the betaine but not the triflate ligand by pentafluorophenoxide yielding Mo(*N*-2,6-Me_2-C_6H_3)(CHCMe_2Ph)(IMesH_2)(OTf)(OC_6F_5) (**Mo-4**).[168a,168e] However, in

Mo-4 replacement of one triflate by betaine **8** could be achieved by addition of sodium tetrakis(3,5-trifluoromethylphenyl)borate ($NaB(Ar^F)_4$), affording **Mo-5** as a $B(Ar^F)_4$ salt instead of a triflate salt in 87% yield (Scheme 41).

6.1.3.2 Synthesis of complexes with ionically tagged N-heterocyclic carbenes

Reactions of imidazolium salt **5** and NHC **6** with metal precursors did not lead to the isolation of ionically tagged molybdenum- or tungsten-based olefin metathesis catalysts. For **5**, which was *in situ* deprotonated with a variety of bases (potassium *tert*-amylate, KHMDS, LiHMDS, *n*-BuLi, KH), conversion with the bistriflate precursors (**Mo-P1** - **Mo-P5**, *vide infra*) and the bispyrrolide complexes (**Mo-P6** - **Mo-P9**, *vide infra*) was observed, however no pure products were isolated. Eventually, the dimethyl amino group causes the resulting products to decompose. For **6** no reactivity was observed with a variety of molybdenum imido alkylidene bistriflate DME (**Mo-P1** - **Mo-P5**) complexes in toluene. This was surprising since the NHC was shown to be a strong donor compared to 1,3-dimesitylimidazol-2-yliden (IMes), which can conveniently be introduced to most molybdenum imido alkylidene bistriflate DME complexes.[167-168,168e] Maybe the reduced reactivity is a consequence of increased steric bulk. Literature research on ionically tagged NHCs led to 1,4-diphenyl-4H-[1,2,4]-triazol-3-yl)phenylamine (nitron, **9**, Scheme 42). *Färber* and his research group reported that nitron can act as a carbene *via* its NHC-type tautomer (**9-tautomer**) and isolated the corresponding ruthenium(III) complex.[184] **9** is commercially available and was therefore thought to be an interesting candidate for the synthesis of ionically tagged molybdenum imido NHC alkylidene complexes. Reacting Mo(*N*-2,6-Me_2-C_6H_3)(CHCMe_2Ph)$(OTf)_2$DME (DME = 1,2-dimethoxyethane) **Mo-P1** with *one* equivalent of **9** resulted in the formation of a new complex and the educt in a ratio of 1:1. This indicated the formation of complex **Mo-6** (Scheme 42) by replacement of both existent triflate ligands in **Mo-P1** by the amido ligand. In fact, when **Mo-P1** was reacted with *two* equivalents of **9**, **Mo-6** could be obtained by simple filtration in quantitative yield.

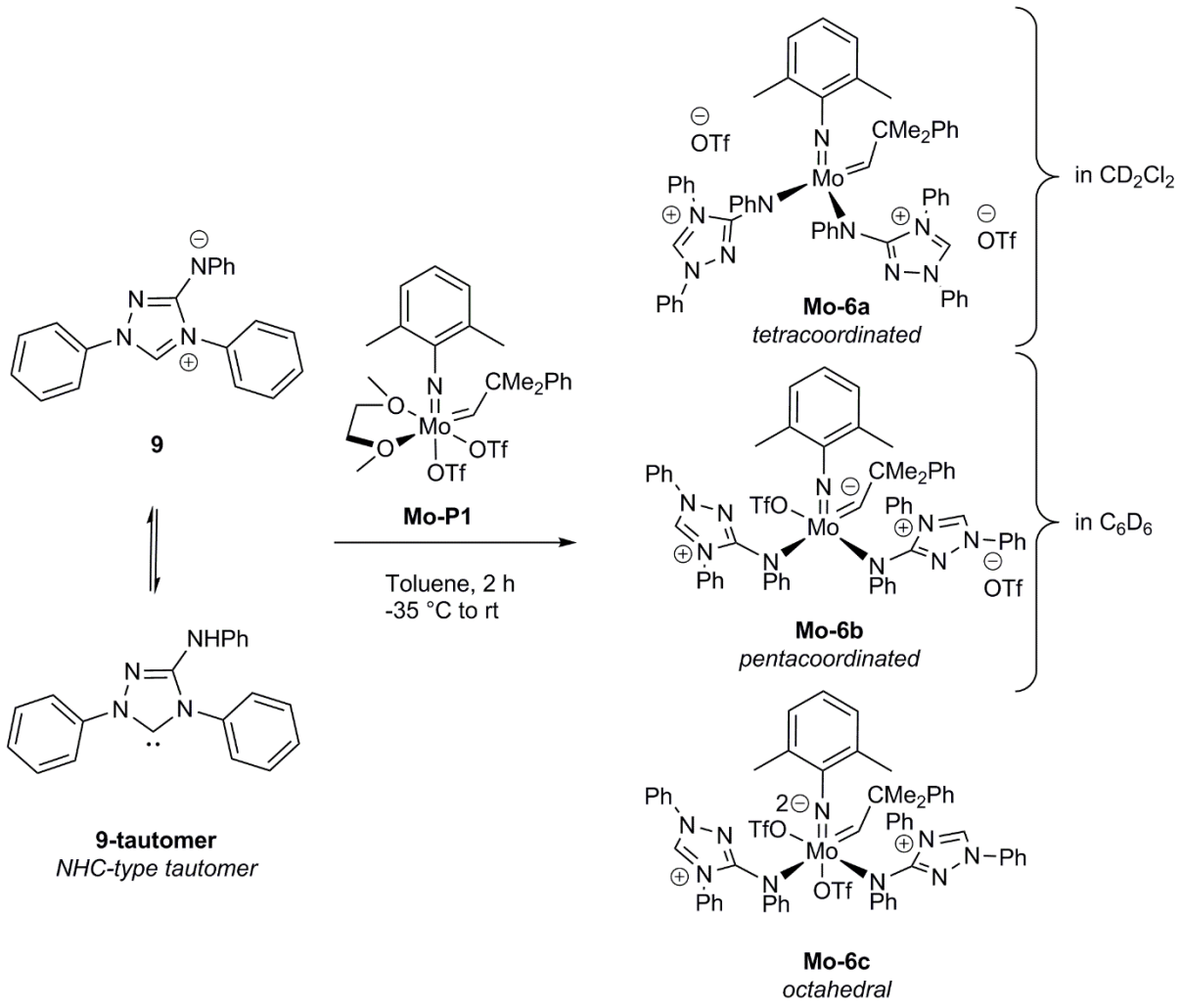

Scheme 42: Synthesis of complex **Mo-6** from nitron **9** and the bistriflate precursor **Mo-P1** in quantitative yield. Solvent dependent envisioned structures **Mo-6a** (in CD_2Cl_2), **Mo-6b** (in C_6D_6) and **Mo-6c** (not found).

Here, however, the ligand binds *via* the anionic amido group in the backbone of the nitron. The characteristic signal for the acidic triazolium proton was observed at δ = 9.11 ppm in CD_2Cl_2. There are several possibilities for the structure of **Mo-6**, which in fact turned out to be solvent-dependent. Either both triflate ligands are attached to an octahedral dianionic molybdenum center (**Mo-6c**) or both triflates leave the complex to form a tetracoordinated complex (**Mo-6a**) that is neutral at the metal center. Another possibility is that one triflate ligand is attached to a monoanionic molybdenum center (**Mo-6b**). The ^{19}F NMR spectrum of **Mo-6** in CD_2Cl_2 showed only one resonance at δ = -78.6 ppm indicating two anionic triflates, therefore hinting to structure **Mo-6a**. In C_6D_6, however, two resonances at δ = -77.75 and -77.93 ppm became visible, pointing towards the monoanionic structure **Mo-6b** with one triflate attached to the molybdenum center or to structure **Mo-6c** with the triflates in two distinct positions of the octahedron. The ^1H NMR spectrum of **Mo-6** in C_6D_6, showed broad signals suggesting a fast exchange between two triflates, maybe one attached to molybdenum and an anionic one, as present in **Mo-6b**. Attempts to activate **Mo-6** by replacing the coordinating triflate anion with

$B(Ar^F)_4$ by conversion of **Mo-6** with two equivalents $NaB(Ar^F)_4$ in CH_2Cl_2 failed due to decomposition of the resulting products. Most probably the amido ligands do not provide sufficient stability to the high oxidation state metal center.

6.1.4 (Biphasic) catalysis with betaine containing group 6 metal alkylidenes

All complexes were tested for their metathesis activity in a set of standard RCM and HM reactions. For a full understanding, the complexes were tested in a common organic solvent (such as toluene or 1,2-dichloroethane) and under biphasic conditions. First tests were done with catalysts **Mo-3** and **Mo-5**. Ring closing metathesis (RCM) and homo metathesis (HM) reactions of standard substrates catalyzed by **Mo-3** and **Mo-5** were carried out in 1,2-dichloroethane at 80 °C. Notably, **Mo-5** turned out to be highly active in standard RCM and HM reactions in 1,2-dichloroethane at 80 °C (Table 1). For 1,7-octadiene, complete conversion to cyclohexene was observed at room temperature after two hours using a catalyst loading of 0.1 mol-%. Using 100,000 equiv. of substrate with respect to **Mo-5**, a TON of 32,700 was achieved. Catalysts **Mo-3** and **Mo-5** were also tested in RCM and HM reactions under biphasic conditions using pyrrole as the polar and heptane as the nonpolar phase (Table 1). The two solvents are immiscible at room temperature but miscible at higher temperatures (solvent system first introduced by *Roman Schowner*[15]). For all substrates, the reactivity in the biphasic system was comparable to the one in 1,2-dichloroethane. Both catalysts tolerate ethers, thioethers, and esters under biphasic reaction conditions. To test the stability of the catalysts in pyrrole, stock solutions of **Mo-3** and **Mo-5** in pyrrole were stored at -35 °C for one day and then subjected to the RCM of 1,7-octadiene. For both catalysts, **Mo-3** and **Mo-5**, TONs were virtually the same as for a freshly prepared stock solution, i.e. 730/750 and 1000/1000, respectively. While the major goal of the biphasic setup was the production of metal-free products, the recyclability of the catalysts was investigated, too. After one cycle the nonpolar layer was removed, and new substrate and heptane were added. For **Mo-5**, reactivity was observed in the second cycle, however, the TON significantly decreased from 1000 to 450. For **Mo-3**, no reactivity was observed in the second cycle. To ensure metal-free products, once the reactions were complete, the metal content of the nonpolar heptane phase was determined by inductively coupled plasma-optical emission spectroscopy (ICP-OES) after microwave-assisted digestion with *aqua regia* (Table 10, experimental section). No molybdenum residues (< 2 ppm) were detected in the nonpolar phase for both catalysts in the reactions with 1,7-octadiene, 1-hexene and diallyldiphenylsilane. Next, three additional molybdenum imido alkylidene NHC complexes, **Mo-7**, **Mo-8** and **Mo-9**, first synthesized, characterized and provided by *Roman Schowner*,[14-15] bearing commercially available 2,6-Ph-4-(2,4,6-Ph-pyridinio)phenolate were investigated concerning their activity.

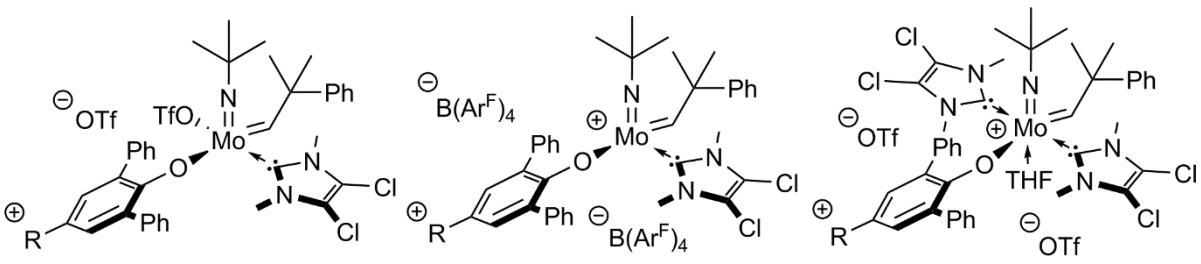

Mo-7 **Mo-8** **Mo-9**

R = (2,4,6-Ph)NC_5H_2

Figure 38: Molybdenum imido alkylidene NHC complexes, **Mo-7**, **Mo-8** and **Mo-9**, first synthesized and characterized by *Roman Schowner*, bearing commercially available 2,6-Ph-4-(2,4,6-Ph-pyridinio)phenolate.

Catalyst **Mo-7** was tested in RCM and HM reactions at 80 °C both in 1,2-dichloroethane and in pyrrole/heptane. Reasonable activities were observed in both solvent systems. **Mo-8** performed better than **Mo-7** in most of the tested metathesis reactions even though the reactions with **Mo-8** were run at room temperature (Table 1). The increased activity can directly be deduced from the cationic charge on molybdenum in **Mo-8**. In comparison to silica-supported molybdenum imido alkylidene NHC complexes (**I1**, Table 1) previously published by our group,[168a] the biphasic reaction setup provides higher TONs, while maintaining the access to the desired metal-free products.

Table 1: Productivities expressed in turnover numbers (TONs) in RCM and HM reactions with catalysts **Mo-3**, **Mo-5**, **Mo-7**, **Mo-8** and **I1** in 1,2-dichloroethane (1,2-DCE) and under biphasic conditions (pyrrole/heptane).

	catalyst **Mo-3** [a]		catalyst **Mo-5**[a]		catalyst **Mo-7**[a]		catalyst **Mo-8**[b]		**I1**[d]
substrate	biphasic	1,2-DCE	biphasic	1,2-DCE	biphasic	1,2-DCE	biphasic	1,2-DCE	1,2-DCE
RCM									
diallyldiphenylsilane	280	510	590	240	0	540	50	610	90
diallyl ether	80	90	680	730	280	460	450	870	
diethyl diallylmalonate	120	280	500	290	0	120	180	210	
1,7-octadiene	740	350	1000[b] (32700[c])	1000[b]	470	340	640	1000	530
diallyl sulfide	130	0	1000	800	240	120	180	190	
HM									
allyltrimethylsilane	150	160	190	210	440	370	0	0	550
1-octene	400	420	510	630	500 (37/63)	240 (25/75)	310 (51/49)	530 (7/93)	
allylbenzene	140	270	620	670	130 (55/45)	30 (77/23)	320 (47/53)	410 (82/18)	
1-hexene	200	230	850	510	-	-	-	-	

*[a] 80 °C, dodecane as internal standard, 6 hours, catalyst: substrate 1:1000. [b] Room temperature, dodecane as internal standard, 6 hours, catalyst:substrate = 1:1000. [c] Room temperature, dodecane as internal standard, 6 hours, catalyst:substrate = 1:100000. [d] Results for comparison from previous publication[168a], **I1**: Mo(N-2,6-Me_2-C_6H_3)(CHCMe_2Ph)(2-(silica-O-methylene)-imidazoline-2-ylidene)(OTf)$_2$, 80 °C, dodecane as internal standard, 4 hours, catalyst:substrate = 1:1000.*

Notably, **Mo-9** showed increased reactivity under biphasic conditions compared to the reactions in 1,2-dichloroethane at 80 °C (Table 2). This behavior could originate from the fact that the weak donor solvent pyrrole can stabilize the active cationic molybdenum center and therefore elevate productivity. Again, ICP-OES measurements of the nonpolar phase did not reveal any leaching of molybdenum for all three catalysts.

Table 2: Productivities of **Mo-9** expressed in TONs in 1,2-dichloroethane (1,2-DCE) and under biphasic conditions (pyrrole/heptane) at 80 °C.[a]

substrate	biphasic	1,2-DCE
RCM		
diallyldiphenylsilane	550	0
diallyl ether	0	0
diethyl diallylmalonate	160	50
1,7-octadiene	990	230
diallyl sulfide	150	10
HM		
allyltrimethylsilane	540	190
1-octene	440 (10/90)	120 (43/57)
allylbenzene	380 (52/48)	60 (59/41)

[a] Dodecane as internal standard, 6 hours, catalyst:substrate = 1:1000. Values in brackets: (E/Z)-isomer ratio. E/Z-ratios were determined by GC-MS.

Mo-6 showed moderate activity in the RCM of 1,7-octadiene and diallyldiphenylsilane with TONs of 220 and 650 at 60 °C in toluene. **Mo-6** was inactive in the RCM of diallyl ether, diethyl diallylmalonate (DEDAM) and diallyl sulfide as well as in the HM of 1-hexene, 1-octene and allyl benzene. The observed activity is in accordance with the assumption that the complex bears an anionic charge at molybdenum, which results in a decreased electrophilicity. This reactivity is in accordance with the reactivity observed for anionic tungsten imido alkylidene complexes.[185] ICP-OES measurements of the nonpolar phases of the reaction of **Mo-6** with diallyldiphenylsilane again did not show any leaching of molybdenum into the heptane phase (< 2 ppm). Catalyst **W-5** did not show any activity in selected RCM (diallyldiphenylsilane, diallyl ether, 1,7-octadiene) and HM (1-hexene, allyltrimethylsilane, 1-octene) reactions at 80 °C in 1,2-dichloroethane. The low activity can be explained by the poor leaving group properties of the 2,5-dimethylpyrrolide ligand compared to triflate.

Catalyst **W-2**, designed as a mimic for (*Z*)-selective MAP-type catalysts,[61c,75,80,83a,178] was investigated in RCM and HM reactions under biphasic and homogeneous conditions (Table 3). Unfortunately, TONs were comparably low, most probably due to steric constraint on the tungsten center. With **W-2**, additional biphasic reactions with an ionic liquid (**IL1**, 1-methyl-2-ethylimidazolium tris(pentafluoroethyl)trifluorophosphate) were done by *Roman Schowner*[15] and demonstrated the high stability of ionically tagged MAP-type complexes in ionic liquids. **W-2** indeed showed (*Z*)-selectivity in HM of 1-octene (94-98% (*Z*)-product) and allyl phenyl

sulfide (93-95% (*Z*)-product). (*Z*)-selectivity was observed irrespective of the solvent used, indicating that neither pyrrole nor the IL interfere with metathesis.

Table 3: Productivities expressed in TONs in RCM and HM reactions with catalyst **W-2** using different solvent systems.

substrate	**toluene[a]**	**pyrrole/heptane[b]**	**IL1/heptane[c]**
1,7-octadiene	515	840	780
1-hexene	250	120	170
allyl benzene	50 (97/3)	60 (99/1)	30 (87/13)
allyl trimethylsilane	250	280	210
1-dodecene	150	200	230
1-octene	220 (2/98)	240 (3/97)	280 (6/94)
allyl phenyl sulfide	120 (5/95)	150 (5/95)	115 (7/93)

[a] 25 °C, dodecane as internal standard, 6 hours, catalyst:substrate = 1:1000.[b] pyrrole:heptane (2:3), 25 °C, dodecane as internal standard, 6 hours, catalyst:substrate = 1:1000. [c] Reactions were done by Roman Schowner,[15] IL1:heptane (1:3), 25 °C, mesitylene as internal standard, 6 h, catalyst:substrate = 1:1000; ***IL1*** *= 1-methyl-3-ethylimidazolium tris(pentafluoroethyl)trifluorophosphate. Values in brackets: (E/Z)-isomer ratio. E/Z-ratios were determined by GC-MS.*

Additionally, RCM, HM and polymerizations (ROMP and cyclopolymerization) with the tungsten based mono pyrrolide NHC complex **W-4** were investigated (Figure 39). All reactions were done at 80°C for six hours. RCM and HM revealed overall moderate activity (Table 4). However, in the RCM of 1,7-octadiene, TONs of 1000 (catalyst/ substrate 1/1000) and 14700 (catalyst/substrate 1/100000) were achieved.

Table 4: Productivities of **W-4** expressed in TON in 1,2-dichloroethane.

substrate	**TON**
diallyl diphenyl silane[a)]	340
1-octene [a)]	600 (21/79)
diethyl diallyl malonate [a)]	60
ethyl oleate [a)]	260 (*Z*/*E*: 9-octadecene: 20/ 80; dimethyl 9-octadecene-1,18-dioate: 8/92)
1,7-octadiene [a),b)]	1000[a)] (14700[b)])

Reaction conditions: a) 80°C, catalyst: substrate = 1:1000, 3 hours, internal standard: dodecane; b) 80 °C, catalyst: substrate = 1:100000, 3 hours, internal standard: dodecane. Values in brackets: (E/Z)-isomer ratio. E/Z-ratios were determined by GC-MS.

Polymerizations showed moderate to excellent yields and substantial functional group tolerance. Polymerizations were done at 80°C for six hours and the polymers were isolated by precipitation into either pentane or methanol and subsequent centrifugation and drying under high vacuum overnight. For **M1** (quantitative), **M2** (64%), **M3** (18%), **M4** (23%), **M5** (quantitative), **M6** (16%), **M7** (quantitative), **M8** (28%) and **M9** (quantitative) the corresponding polymers could be obtained (Figure 39). Catalyst **W-4** showed high functional group tolerance versus alcohol, acid, nitrile and sulfide moieties. **W-4** provided poly(**M1**), poly(**M2**) and poly(**M3**) with a *trans*-content of 70, 94 and 77%, respectively. Unfortunately, most of the cyclopolymerization-derived polymers could only be characterized by UV/Vis and IR spectroscopy because they were insoluble in common deuterated NMR solvents.

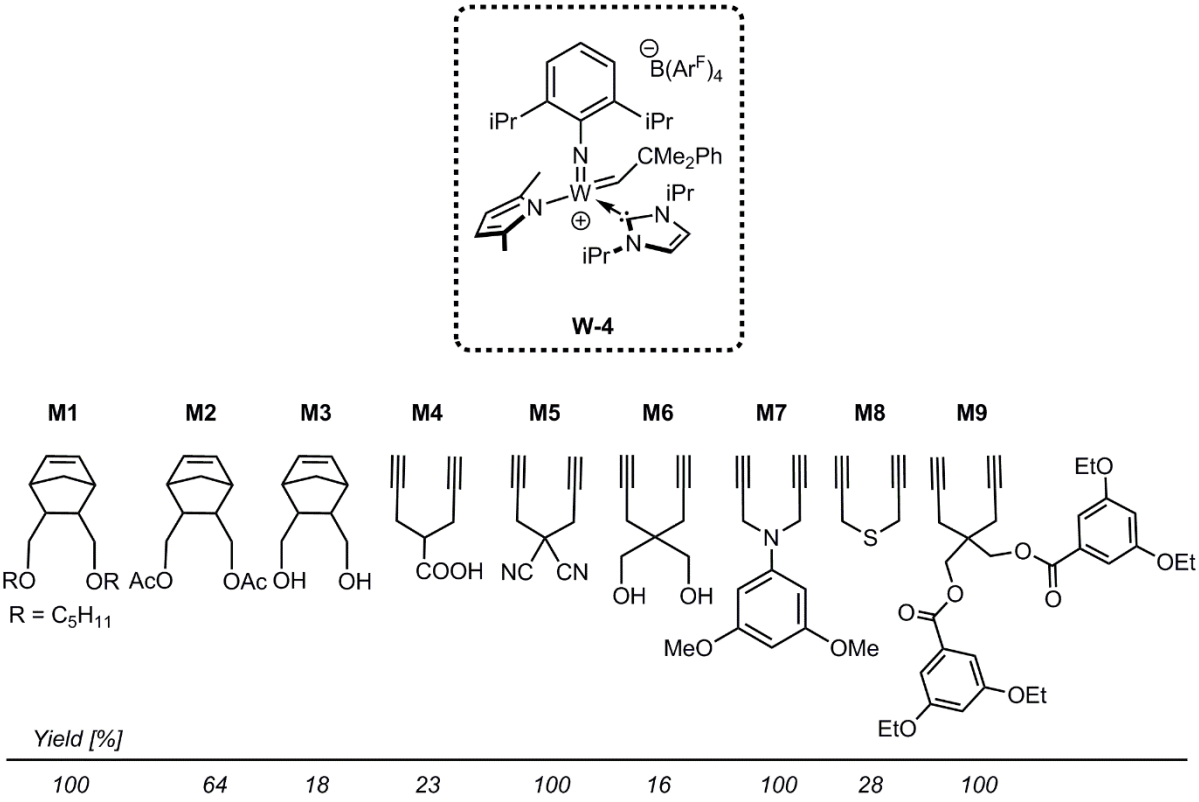

Figure 39: ROMP (**M1-M3**) and cyclopolymerization (**M4-M9**) of different (functionalized) monomers with the tungsten-based cationic-at-metal catalyst **W-4**. Isolated polymer yields after six hours at 80 °C.

6.1.5 *CATIONIC-AT-METAL MOLYBDENUM IMIDO ALKYLIDENE NHC COMPLEXES IN BIPHASIC REACTIONS*

Once a biphasic reaction setup for molybdenum imido alkylidene NHC complexes and MAP-type complexes bearing betaine-type ligands consisting of a mixture of pyrrole and heptane had been developed[186], the applicability of catalysts bearing a cationic charge on molybdenum came into focus.

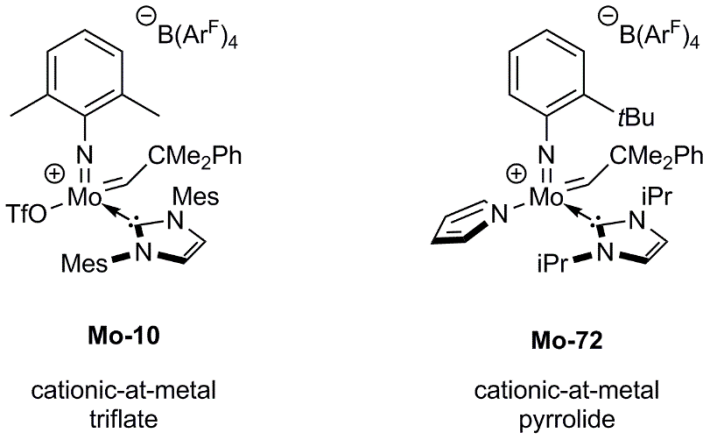

Figure 40: Cationic-at-metal complexes **Mo-10** and **Mo-72** for application in biphasic reactions.

Therefore, two representative cationic complexes, namely one for molybdenum imido alkylidene monotriflate $B(Ar^F)_4$ complexes **Mo-10** and one for molybdenum imido alkylidene NHC pyrrolide $B(Ar^F)_4$ complexes **Mo-72**, were tested in metathesis reactions under biphasic conditions. **Mo-10** was prepared according to a literature-known procedure[168e] and **Mo-72** was synthesized according to a procedure described below. Both, **Mo-10** and **Mo-72**, showed reasonable activity in the biphasic mixture, although activity was somewhat reduced compared to the reaction in 1,2-dichloroethane (Table 5). Nevertheless, in RCM of 1,7-octadiene TONs of 990 and 860 were reached with **Mo-10** and **Mo-72** respectively. Beneficially, no molybdenum residues were detected in the nonpolar phase *via* ICP-OES (< 2 ppm).

Table 5: Productivities in TON for biphasic metathesis in a mixture of pyrrole/heptane (biphasic) and in 1,2-dichloroethane (1,2-DCE) for catalysts **Mo-10** and **Mo-72**.

	Mo-10		**Mo-72**	
substrate	biphasic	1,2-DCE	biphasic	1,2-DCE
diallyl diphenyl silane	120	550	180	629
1,7-octadiene	990	1000	860	1000
1-octene	310	510	210	500
allyl benzylether	0	0	460	320
allyl benzene	90	412	360	430

Reaction conditions: room temperature, cat:substrate 1:1000, internal standard for GC analysis: dodecane, 6 hours.

6.1.6 *Outlook*

Since the synthesis of metal-free products is particularly important for pharmaceutical industry, and stereoselectivity plays a major role in this field, MAP-type catalysts similar to **W-2**, are an interesting target. The observed low activity of **W-2** (Table 3) should easily be overcome by usage of smaller or more electron-withdrawing imido ligands, such as *N*-*tert*-butylimido or *N*-pentafluorophenylimido, that facilitate substrate coordination compared to the 2,6-diisopropylphenylimido ligand (**Mo-11** and **W-6**, Figure 41). Also, the (4-hydroxy-2,6-(2,4,6-triisopropylphenyl)-phenyl)-triphenylphosphonium $B(Ar^F)_4$ (**2***, Figure 41) ligand might be interesting in terms of improving (*Z*)-selectivity. The increase in steric bulk introduced by the isopropyl *vs*. the methyl groups should increase unfavorable steric interactions in the (*E*)-MCB intermediate and therefore result in higher (*Z*)-selectivity.[83a,178] The synthesis of the intermediate 4-bromo-2,6-(2,4,6-triisopropylphenyl)phenol is literature-known[187], and coupling with triphenylphosphine and anion exchange to the WCA $B(Ar^F)_4$ should proceed as described above for ligand **2**.

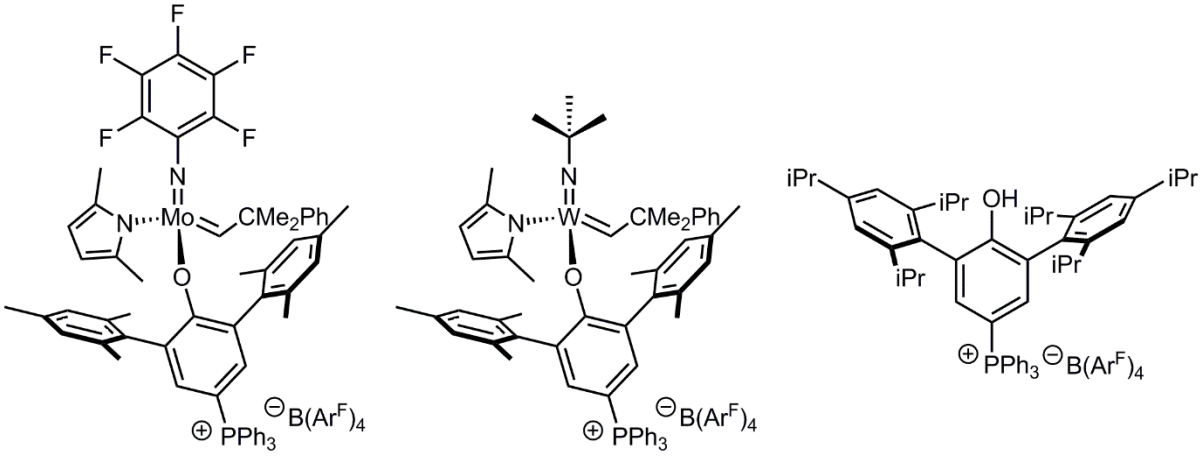

Mo-11 **W-6** **2***

Figure 41: Target structures for potentially (*Z*)-selective cationically tagged **Mo-11** with an electron-withdrawing imido ligand and **W-6** with a smaller imido ligand for more reactivity. Proposed cationic HIPTOH-derivative **2***.

6.2 MOLYBDENUM IMIDO ALKYLIDENE COMPLEXES WITH CHELATING *N*-HETEROCYCLIC CARBENES

Parts of the following chapter have already been published. Reprinted (adapted) with permission from (I. Elser, W. Frey, K. Wurst, M. R. Buchmeiser, *Organometallics* **2016**, *35*, 4106-4111). Copyright (2016) American Chemical Society.

6.2.1 WORKING HYPOTHESIS

Recently developed cationic molybdenum imido alkylidene complexes $[Mo(NR^1)(CHCMe_2Ph)(OR^2)(NHC)][B(Ar^F)_4]$ with weakly coordinating anions (WCA) are the first well-defined cationic metathesis-active complexes.[168a,168e] In most cases the catalysts bear an additional donor solvent (e.g. acetonitrile or diethyl ether) in their coordination sphere.[167-168,168c,168e,183] Sometimes the donor solvent is even necessary for the abstraction of the X-type ligand by $NaB(Ar^F)_4$ or similar reagents. Even though the catalysts are remarkably stable, in particular in comparison to previously published complexes by the *Schrock* group,[128b,128c] further stabilization to increase productivity was pursued. The introduction of chelating *N*-heterocyclic carbenes was thought to result in a stabilization of the cationic species because of the chelate effect.[7]

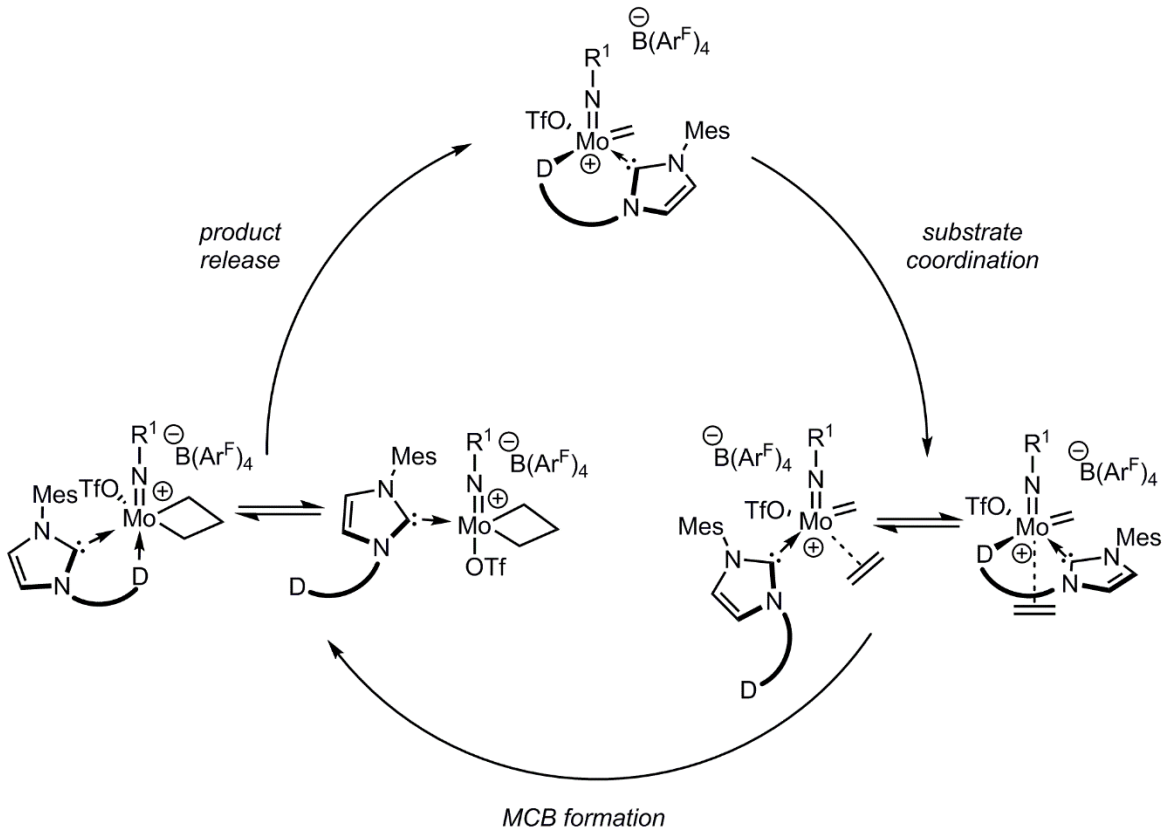

Scheme 43: Schematic view of olefin metathesis catalytic cycle with a cationic-at-metal molybdenum imido alkylidene complex bearing a chelating NHC. Stabilizing influence of the hemi-labile ligand.

Especially the introduction of a hemi-labile neutral donor moiety with the propensity to dissociate and then again coordinate during the metathesis cycle was expected to result in higher stability and increased catalyst life-times. A pyridyl-donor was chosen, since (bi)pyridine is known to coordinate to group 6 imido alkylidene complexes.[19,73c,188] Furthermore, catalysts bearing dangling ligands provide the possibility to study the coordination of donors to molybdenum imido alkylidene NHC complexes to extract information on, for example, the preferred coordination site.

6.2.2 *Results and Discussion*

N-Mesityl-*N*-(2-picolyl)-imidazolium bromide (**10**) was synthesized according to a literature-known procedure[52d] from *N*-mesitylimidazole. As precursor, the easily accessible Mo(*N*-2,6-Me_2-C_6H_3)($CHCMe_2Ph$)$(OTf)_2$(DME) complex (**Mo-P1**) was chosen, since it was the precursor that was best explored at that time.[167-168] **10** was deprotonated with potassium hexamethyldisilazid (KHMDS) in benzene, directly *prior* to metal complex formation.

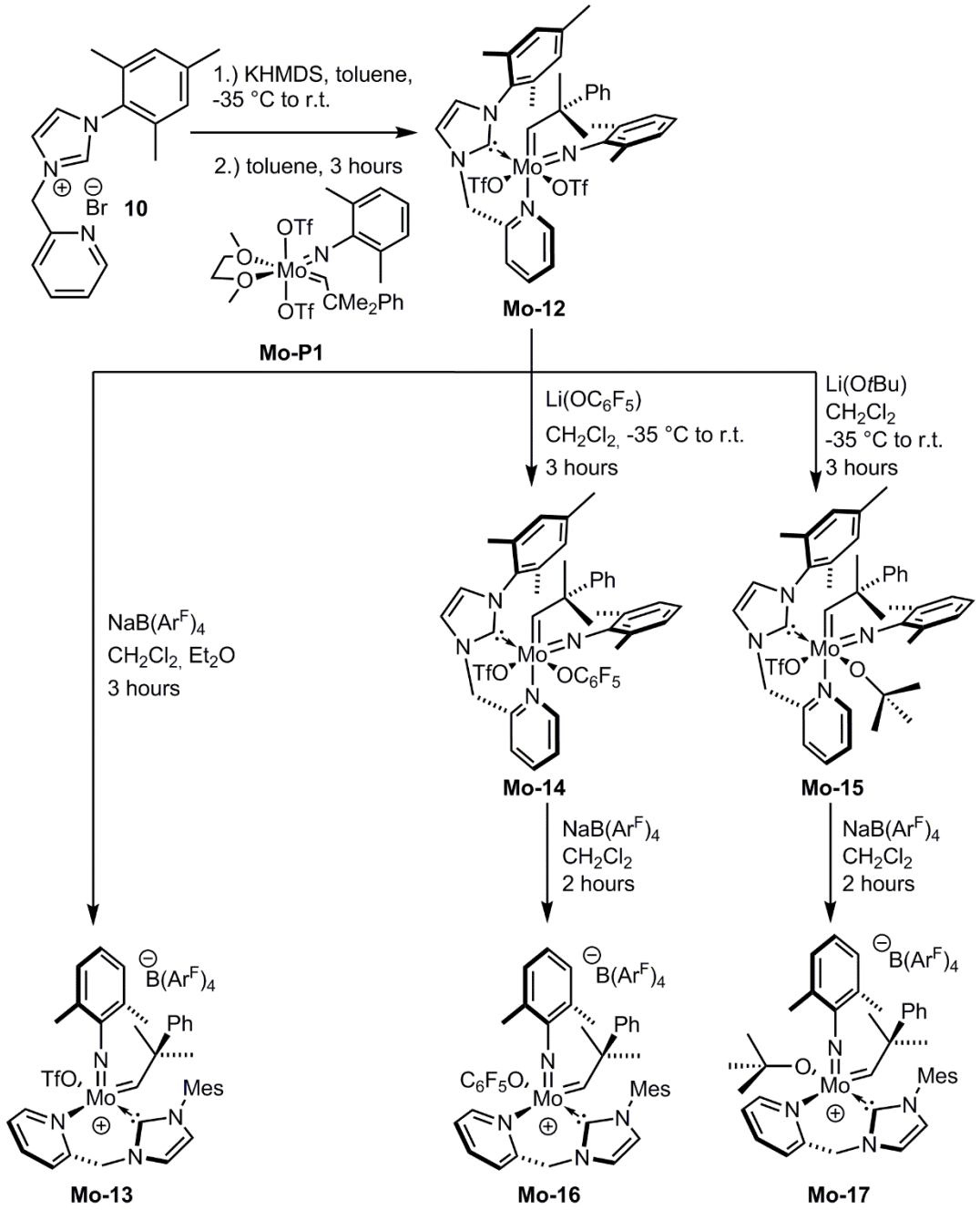

Scheme 44: Synthesis of complexes **Mo-12** - **Mo-17**. (Yields: **Mo-12**: 52%, **Mo-13**: 91%, **Mo-14**: 96%, **Mo-15**: 57%, **Mo-16**: 77%, **Mo-17**: 81%)

The *in situ* generated NHC was reacted with the precursor in benzene or toluene at -35°C and was warmed to room temperature. Either immediately, or after a short time the formation of Mo(*N*-2,6-Me_2-C_6H_3)(CHCMe_2Ph)(OTf)$_2$(*N*-mesityl-*N*-(2-picolyl)-imidazol-2-ylidene) (**Mo-12**) in the form of a yellow precipitate or in some cases a yellow oil was observed. After three to six hours the precipitate was filtered off, washed with diethyl ether and dried *in vacuo* to afford the desired complex **Mo-12** in a moderate isolated yield of 52 %. When an oil was observed, the solution was decanted, and the oil was treated with diethyl ether until it solidified.

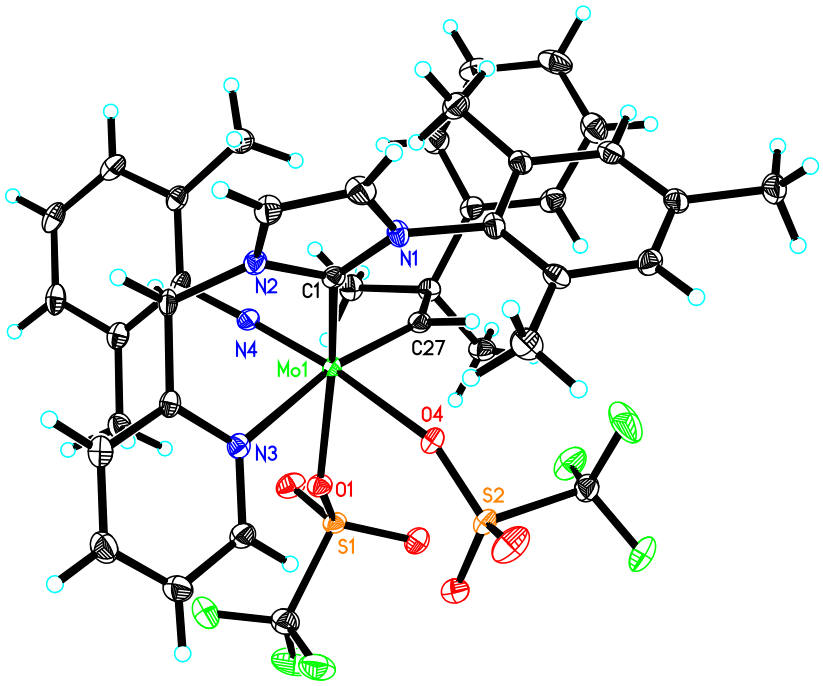

Figure 42: Single-crystal X-ray structure of **Mo-12**. Selected bond lengths [pm] and angles [°]:Mo1-N4 172.98(19), Mo1-C27 194.1(2), Mo1-O1 215.43(15), Mo1-C1 220.5(2), Mo1-O4 220.85(15), Mo1-N3 241.36(19); N4-Mo1-C27 98.04(9), N4-Mo1-O1 96.49(7), C27-Mo1-O1 97.80(8), N4-Mo1-C1 95.42(8), C27-Mo1-C1 102.58(9), O1-Mo1-C1 154.66(7), N4-Mo1-O4 173.03(7), C27-Mo1-O4 88.81(8), O1-Mo1-O4 81.42(6), C1-Mo1-O4 84.26(7), N4-Mo1-N3 93.36(8), C27-Mo1-N3 168.42(8), O1-Mo1-N3 78.87(6), C1-Mo1-N3 78.17(7), O4-Mo1-N3 79.74(6).

Crystals of **Mo-12** suitable for single crystal X-ray crystallography were grown from a mixture of CH_2Cl_2 and pentane. The crystal structure revealed a distorted octahedral structure with the NHC and one of the triflate ligands in the apical positions. The angle between the NHC ligand and the triflate ligand *trans* to the NHC is 154.66(7) °. The Mo-triflate bond with the triflate group *trans* to the NHC is significantly longer than for the one *trans* to the pyridine (215.43(15) pm *vs.* 220.85(15) pm). The 18-VE complex **Mo-12** can be regarded as the pyridine adduct of a 16-VE molybdenum imido alkylidene bistriflate NHC complex. The single crystal X-ray structure clearly shows coordination of the pyridine *trans* to the alkylidene moiety. Notably, this provides the first evidence for the analogous approach of an olefin to (distorted) square pyramidal 16-VE Mo-imido alkylidene NHC complexes, under formation of a quasi-cationic complex with WCA triflate. This was previously postulated as activation mechanism for molybdenum imido alkylidene bistriflate NHC complexes in olefin metathesis. ^{1}H NMR studies

of solutions of **Mo-12** in CD_2Cl_2 at room temperature showed that, over time, a new alkylidene signal forms at δ = 14.67 ppm. This alkylidene signal is assigned to the cationic complex with triflate as WCA (Figure 43).

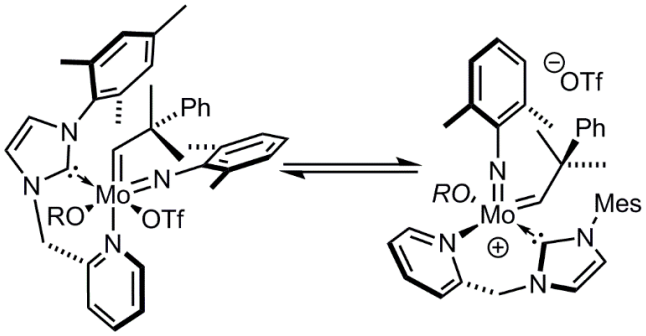

Figure 43: Equilibrium between octahedral neutral and cationic pentacoordinated complex with WCA triflate. Equilibrium strongly depends on alkoxide.

Formation of a sharp peak at δ = -77.94 ppm in the ^{19}F NMR spectrum supports this hypothesis. After twelve hours in CD_2Cl_2 the ratio between the cationic and the neutral complex is 1:1. To investigate the influence of the X-type ligand on complex structure, reactivity and the equilibrium between neutral and cationic species, one triflate in **Mo-12** was replaced by different alkoxides. For that purpose, the electron-withdrawing pentafluorophenoxide and the electron-donating *tert*-butoxide were chosen (Scheme 44). Mo(*N*-2,6-Me_2-C_6H_3)(CHCMe_2Ph)(OTf)(OC_6F_5)(*N*-mesityl-*N*-(2-picolyl)-imidazol-2-ylidene) (**Mo-14**) was obtained by conversion of **Mo-12** with lithium pentafluorophenoxide in CH_2Cl_2 in 96% isolated yield. The ^1H NMR spectrum of **Mo-14** in CD_2Cl_2 shows two alkylidene signals at δ = 14.01 and 13.79 ppm. In the ^{19}F NMR spectrum, two triflate signals are visible at δ = -77.0 and -78.9 ppm. This indicates the existence of two species in solution, a neutral one with the triflate bound to molybdenum and a cationic one with triflate as anion (1:10 mixture). No change in the ratio of cationic to neutral complex was observed for twelve hours. Mo(*N*-2,6-Me_2-C_6H_3)(CHCMe_2Ph)(OTf)(O*t*Bu)(*N*-mesityl-*N*-(2-picolyl)-imidazol-2-ylidene) (**Mo-15**) was isolated in 57% yield by the same protocol using lithium *tert*-butoxide instead of the fluorinated alkoxide. The ^1H NMR spectrum of **Mo-15** in CD_2Cl_2 exclusively showed free triflate at δ = -78.9 ppm. The electron-donating property of the *tert*-butoxide ligand obviously renders the complex more prone to the dissociation of triflate.

The proposal that the newly observed alkylidene signal of **Mo-12** in solution belongs to the cationic species was further verified by the isolation of the cationic complex [Mo(*N*-2,6-Me_2-C_6H_3)(CHCMe_2Ph)(OTf)(*N*-mesityl-*N*-(2-picolyl)-imidazol-2-ylidene)][B(Ar^F)$_4$] (**Mo-13**). **Mo-13** was synthesized in 91% yield by replacing one triflate in **Mo-12** with the WCA B(Ar^F)$_4$ (Scheme 44). **Mo-13** and **Mo-12** show the same alkylidene shift at δ = 14.73 ppm, thus underlining the assumption that triflate is serving only as WCA. Compound **Mo-13** (Scheme 44) crystallizes in the triclinic space group, a = 1005.81(6) pm, b = 1703.05(8) pm, c = 2188.89(12) pm, α = 77.026(3) °, β = 86,625(4) °, γ = 80.441(3) °. Compared to **Mo-12**, in **Mo-13** the molybdenum-pyridine bond length decreased significantly from 241.3(6) pm to 230.2(3) pm, clearly emphasizing the high electrophilicity of the cationic molybdenum center. All other molybdenum ligand bonds decrease in length as well, however not to such an extent (Figure 44).

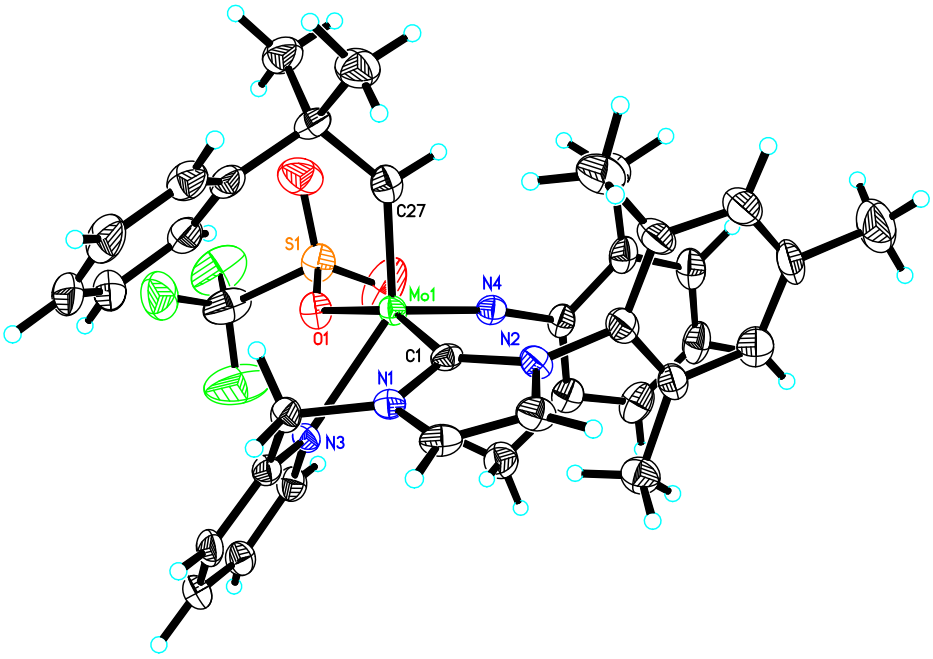

Figure 44: Single-crystal X-ray structure of **Mo-13**. Selected bond lengths [pm] and angles [°]: Mo1-C27 192.3(4), Mo1-O1 213.3(3), Mo1-C1 219.7(4), Mo1-N3 230.2(3), Mo1-N4 170.7(4); N4-Mo1-C27 98.46(18), N4-Mo1-O1 96.34(14), C27-Mo1-O1 99.74(15), N4-Mo1-C1 96.28(16), C27-Mo1-C1 95.75(16), O1-Mo1-C1 158.32(13), N4-Mo1-N3 123.10(14), C27-Mo1-N3 138.44(16), O1-Mo1-N3 76.98(12), C1-Mo1-N3 81.37(14). The WCA B(Ar^F)$_4$ has been omitted for clarity.

Also, both **Mo-14** and **Mo-15** were converted to their cationic analogues by reaction with NaB(Ar^F)$_4$ in a mixture of CH_2Cl_2 and diethyl ether. The corresponding complexes **Mo-16** and **Mo-17** were isolated in 77 and 81 % yield, respectively. The activity of cationic complexes **Mo-13**, **Mo-16** and **Mo-17** in the ring-closing metathesis (RCM) of 1,7-octadiene in 1,2-dichloroethane was investigated at 80 °C. Complexes **Mo-16** and **Mo-17** showed no activity at all. Interestingly, **Mo-13** provided cyclohexene from 1,7-octadiene with a TON of 170. However, **Mo-13** did not show any activity in the RCM of diallyldiphenylsilane, diallyl ether and diethyl diallylmalonate. The low activity is not surprising, since **Mo-13**, **Mo-16** and **Mo-17** are

16-VE complexes; coordination of substrate consequently leads to the formation of unreactive 18-VE complexes. The finding that complex **Mo-13** proved to be more reactive than complex **Mo-16** deserves attention since the electron-withdrawing character of the fluorinated alkoxide should decrease the electron density at the molybdenum center leading to a more electron-deficient and therefore more reactive catalyst. An explanation could be that upon coordination of substrate the remaining triflate in **Mo-13** as good leaving group can dissociate to form a two-fold cationic species while the pentafluorophenoxide cannot.

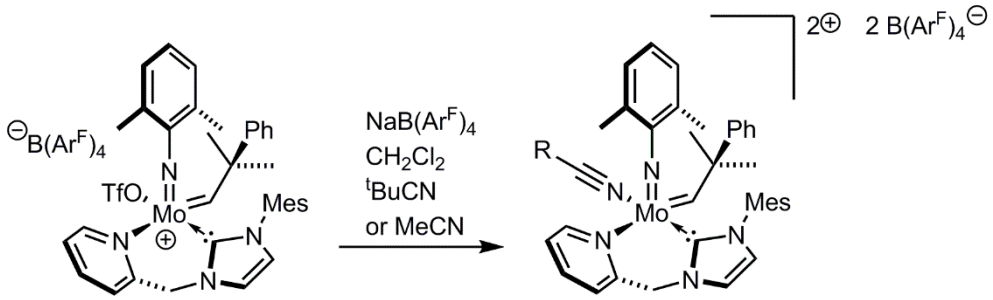

Mo-13

Mo-18-RCN
R= *t*Bu or Me
not isolated

Scheme 45: *In situ* removal of one triflate in **Mo-13** with $NaB(Ar^F)_4$ in the presence of coordinating solvents (*tert*-BuCN, MeCN) to yield **Mo-18**. **Mo-18** was not isolated.

To further support this hypothesis, **Mo-13** was reacted with $NaB(Ar^F)_4$ in CH_2Cl_2 (Scheme 45). No formation of **Mo-18** was observed. However, if a coordinating solvent (acetonitrile) was added to the reaction mixture, the formation of a new alkylidene signal was observed in the ^1H NMR spectrum. The ^{19}F NMR spectrum of the crude product did not show any resonance for a triflate ligand, therefore excluding that the shift in the alkylidene resonance results from simple acetonitrile coordination. Also, comparison of the crude ^1H NMR spectrum of **Mo-18·MeCN** in CD_2Cl_2 and a spectrum of **Mo-13** in CD_2Cl_2 with two drops of acetonitrile showed different resonances (Figure A 85). Until now, **Mo-18** could not be isolated in pure form, since crystallization was unsuccessful. Nevertheless, 1,7-octadiene was converted with crude **Mo-18-*t*BuCN**. After six hours in CH_2Cl_2 at 80°C the observed TON was 370. In view of the postulate that **Mo-18** is a dicationic molybdenum imido alkylidene NHC complex, this is a rather low activity. An explanation is, that *tert*-butylnitrile is a better ligand than 1,7-octadiene and is therefore not replaced easily by this substrate. Despite the preliminary assumptions, no hemi-lability of the pyridyl donor could be observed, most probably due to the entropic stabilization of the chelate 6-ring. Even attempts to break the pyridine molybdenum bond by addition of triflic acid or *N*,*N*-dimethylanilinium $B(Ar^F)_4$ to **Mo-12** and **Mo-13** as well as boron based Lewis acids (BF_3, $B(C_6F_5)_3$) and $ZnCl_2$ to **Mo-13**, **Mo-16** and **Mo-17** were unsuccessful.

6.2.3 OUTLOOK

The observed low activity of the cationic complexes could be overcome if the pyridyl-donor would exhibit hemi-labile behavior. Hemi-lability could be achieved by the introduction of sterically demanding groups adjacent to the pyridyl-donor. Examples in literature have shown that a systematic increase of the steric bulk at the carbon atom α to the pyridyl nitrogen results in an increase in the nitrogen metal bond length and therefore in a weakened bond.[52d] That could enable replacement of the pyridyl donor by the substrate and lead to an increase in activity while at the same time retaining stability by back coordination in other stages of the catalytic cycle (*vide infra*, Scheme 43).

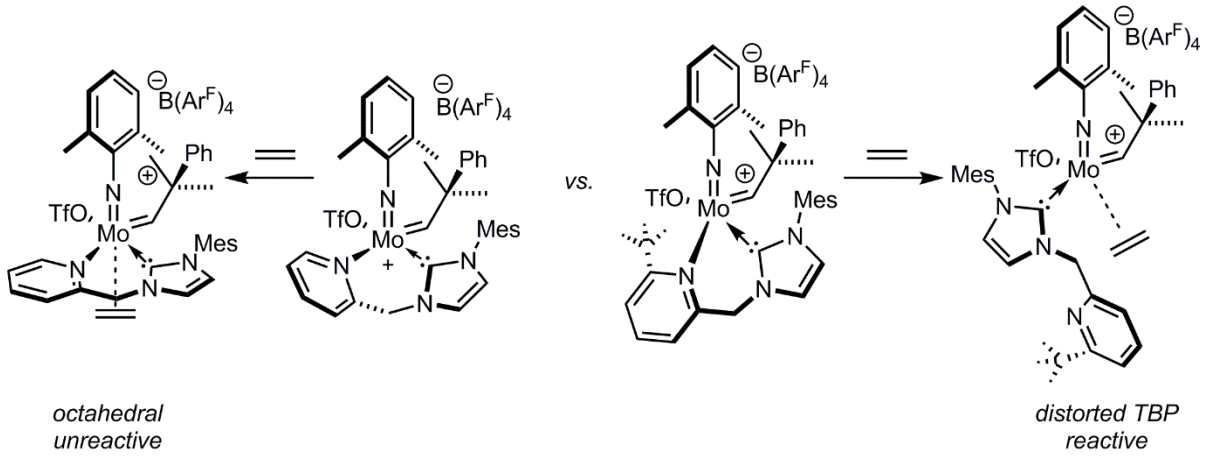

Scheme 46: Hypothetical influence of a sterically demanding *tert*-butyl group adjacent to the pyridyl-donor. Octahedral unreactive ethylene complex *vs.* reactive TBP complex enabled by dissociation of the pyridyl-donor (hemi-lability).

Also, the synthesis of dicationic molybdenum imido alkylidene complexes stabilized by chelating NHC seems attractive since, due to their electrophilicity, they should be highly reactive, if they could be synthesized without a coordinating solvent or one that is easily replaced by incoming substrate.

6.3 (PRE-)CATALYSTS FOR LATENT RING-OPENING METATHESIS POLYMERIZATION OF DICYCLOPENTADIENE

Parts of the following chapter are incorporated in a publication: I. Elser, B. R. Kordes, W. Frey, K. Herz, R. Schowner, L. Stöhr, H. J. Altmann, M. R. Buchmeiser, *Chem. Eur. J.*, Latent and Air Stable Pre-Catalysts for the Polymerization of Dicyclopentadiene: From Penta- to Hexacoordination in Molybdenum Imido Alkylidene *N*-Heterocyclic Carbene Complexes, *accepted paper*.

6.3.1 WORKING HYPOTHESIS

ROMP of dicyclopentadiene (DCPD) by reaction injection molding (RIM) is an industrially relevant field of chemistry.[4b,4c] Here, the catalyst is formed *in situ*, by mixing of two components, which immediately react with the monomer. State of the art catalyst mixtures are air sensitive and require inert conditions. Depending on the catalyst used and on the reaction temperature applied, either linear or crosslinked poly(DCPD) with different properties and applications are accessible (Scheme 47).[4b,4c] Generally, more active catalysts and high reaction temperatures result in ring-opening of the remaining five-membered ring.

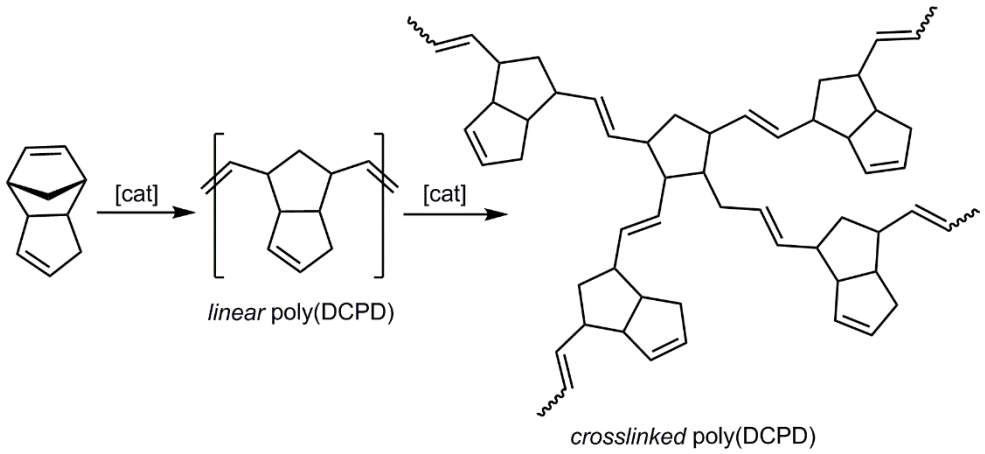

Scheme 47: Synthesis of poly(DCPD) with olefin metathesis catalysts. Poly(DCPD) is accessible in its linear and crosslinked form depending on the catalyst used and the reaction temperature.

Thermally or photochemically latent catalysts systems provide an alternative to RIM. The obvious advantage of latent systems is the storability of the stable catalyst/DCPD mixtures. Several ruthenium-based olefin metathesis catalysts are latent in ROMP of DCPD.[117c,121,125a,126,189] Catalyst design usually entails a *Grubbs Hoveyda*-type structure (chelating alkylidene) or other chelating ligands.[115a,117c,121,125a,126,189] Those catalyst systems are easily tuned by careful choice of the chelating group and the chelate ring size. Lately, *Buchmeiser et al.* showed that molybdenum imido alkylidene NHC complexes containing for example 1,2,4-triazol-5-ylidenes form stable mixtures with DCPD, that can be polymerized

upon heating.[18] Latency of those systems stems from the propensity of the pre-catalysts to dissociate one of the triflate ligands to form the active species at a given, catalyst-dependent temperature T_c (coalescence temperature, Scheme 48). One aim of this work was to reveal structure-reactivity relationships of molybdenum imido alkylidene bistriflate NHC complexes in terms of activation temperature in ROMP of DCPD. Here, especially the influence of X-type and imido ligand were of interest. Of course, focus also was on the polymer properties (swelling propensity and glass transition temperature T_g).

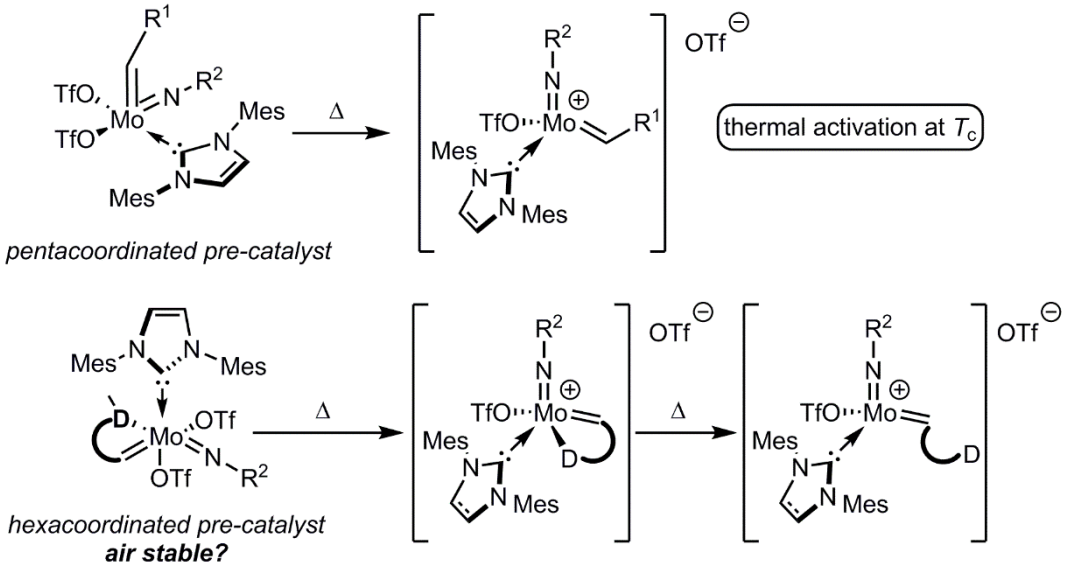

Scheme 48: Model for the activation of penta- and hexacoordinated molybdenum imido NHC bistriflate pre-catalysts.

Also, another challenge in olefin metathesis was addressed. Air stable pre-catalysts would provide crucial advantages to industry. In contrast to ruthenium-based systems[119] reports on air stable molybdenum- and tungsten-based olefin metathesis catalysts are scarce.[19,120] On the one hand, immobilization of standard MAP-type complexes in a paraffin matrix led to catalyst pellets that can be handled under air. On the other hand, coordination of bipyridine and 1,1-phenanthroline resulted in benchtop-stable complexes. However, both methods are disadvantageous for the application in ROMP of DCPD. Either paraffin or $ZnCl_2$, applied to remove bipyridine and phenanthroline, will remain in the polymer. Hence, the synthesis and application of thermally latent *and* air stable hexacoordinated molybdenum imido alkylidene NHC complexes, comparable to above described complexes **Mo-12** and **Mo-15**, was envisioned. The 18-VE structure of the compounds in combination with a chelating ligand and the NHC was envisioned to result in air stable and latent catalysts. In addition to testing the pyridyl-NHC coordinated complexes, the introduction of a chelating alkylidene was pursued. A chelating alkylidene ligand, in contrast to the chelating NHC, offers the advantage that the chelating moiety leaves the complex after the first monomer insertion and instead is

incorporated in the resulting polymer. Consequently, the activation barrier for dissociation of the chelating ligand only must be overcome once. Moreover, the chelating alkylidene ligand was expected to increase the activation temperature T_{onset} for ROMP of DCPD (Scheme 48). Even though high activation temperatures are expected to correlate with superior latency, an activation temperature T_{onset} > 140°C was suspected to result in overheating since polymerization of DCPD is an exothermal reaction. Therefore, at first, precursors with low T_{onset} had to be determined.

6.3.2 *Pentacoordinated molybdenum imido alkylidene NHC bistriflate complexes*

Molybdenum imido alkylidene NHC complexes featuring the 1,3-dimesitylimidazol-2-ylidene (IMes) ligand were identified as promising targets. First, they are easily accessible in good yields with differing imido ligands. Also, IMes displays a low TEP which favors triflate dissociation. On top, the IMes ligand is commercially available and stable, resulting in good storability. IMes complexes **Mo-19** - **Mo-23** with varying imido ligands were synthesized to test the impact of the imido ligand on latency in ROMP of DCPD. **Mo-19**, **Mo-20**, **Mo-21**, **Mo-22** and **Mo-23** were synthesized from **Mo-P2**, **Mo-P3**, **Mo-P1**, **Mo-P4** and **Mo-P5**, respectively, by conversion of the precursors with IMes in benzene or toluene (Scheme 49).

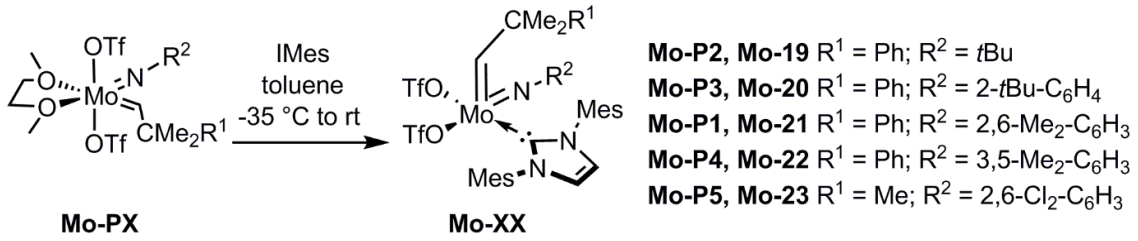

Scheme 49: Synthesis of molybdenum imido alkylidene IMes complexes **Mo-19** - **Mo-23** with varying imido ligands.

The synthesis of **Mo-21**[168a], **Mo-22**[190]and **Mo-23**[168a] was previously described in the literature. The synthesis of **Mo-19** was first developed by *Roman Schowner*[15], whereas the synthesis of **Mo-20** was first developed by *Laura Stöhr*[191]. Comparison of the single crystal X-Ray structures of **Mo-20** - **Mo-23**, revealed structure-reactivity relationships in the ROMP of DCPD. **Mo-20**, **Mo-21**[183], **Mo-22**[190] as well as **Mo-23**[183], which all show a distorted SP structure, display comparable bond lengths, angles and geometry in the solid state. For **Mo-20**, **Mo-21**[183] and **Mo-23**[183] the longest Mo-OTf bond is coordinated *trans* to the NHC, whereas for **Mo-22** [19] the longest Mo-OTf bond is situated *trans* to the imido ligand (Table 6). **Mo-22** is also closest to a square pyramidal structure as indicated by the smallest τ value. As anticipated, this correlates with the lowest coalescence temperature, T_c, for **Mo-22** (T_c = 60°C). T_c is the temperature at which the two triflate ligands in the complexes begin to coalesce in ^{19}F NMR spectroscopy. This was postulated to be a consequence of the formation of a quasi-cationic complex in which the weakly coordinated triflate and the one bound to molybdenum

exchange rapidly. For **Mo-20** and **Mo-21**, T_c increases with decreasing Mo-OTf bond length (triflate *trans* to the NHC,Table 6).

Table 6: Geometry (τ), important bond lengths and angles, coalescence temperatures T_c and temperature for the onset of polymerization $T_{onset,TScan}$ for catalysts **Mo-19**-**Mo-23**.[183,190]

catalyst	geometry (□)	Mo-OTf [pm](i)	NHC or imido-Mo-OTf [°]	T_c [°C] (iv)	$T_{onset,TScan}$ [°C](v)
Mo-20	distorted SP (0.325)	216.97(17)	157.34(9)(ii)	79	80
Mo-21	distorted SP (0.298)	215.3(5)	157.5(2) (ii)	85	90
Mo-22	distorted SP (0.229)	214.7(4)	162.87(18) (iii)	60	65
Mo-23	distorted SP (0.243)	213.80(14)	156.54(6) (ii)	-	115

*(i) Longest Mo-OTf bond, trans to NHC for **Mo-20**, **Mo-21**, **Mo-23** or trans to imido for **Mo-22**; (ii) angle for NHC-Mo-OTf; (iii) angle for imido-Mo-OTf; (iv) coalescence temperature T_c previously determined by variable temperature ^{19}F NMR spectrosopy in deuterated 1,2-dichlorobenzene[190]; (iv) determined by DSC temperature scan measurements.*

Next, the propensity of molybdenum imido alkylidene bistriflate IMes complexes **Mo-19** - **Mo-23** to polymerize DCPD was investigated in differential scanning calorimetry (DSC) measurements. As outlined above, the aim was to find the most suitable candidates for the introduction of a chelating alkylidene *with a low T_{onset}*.

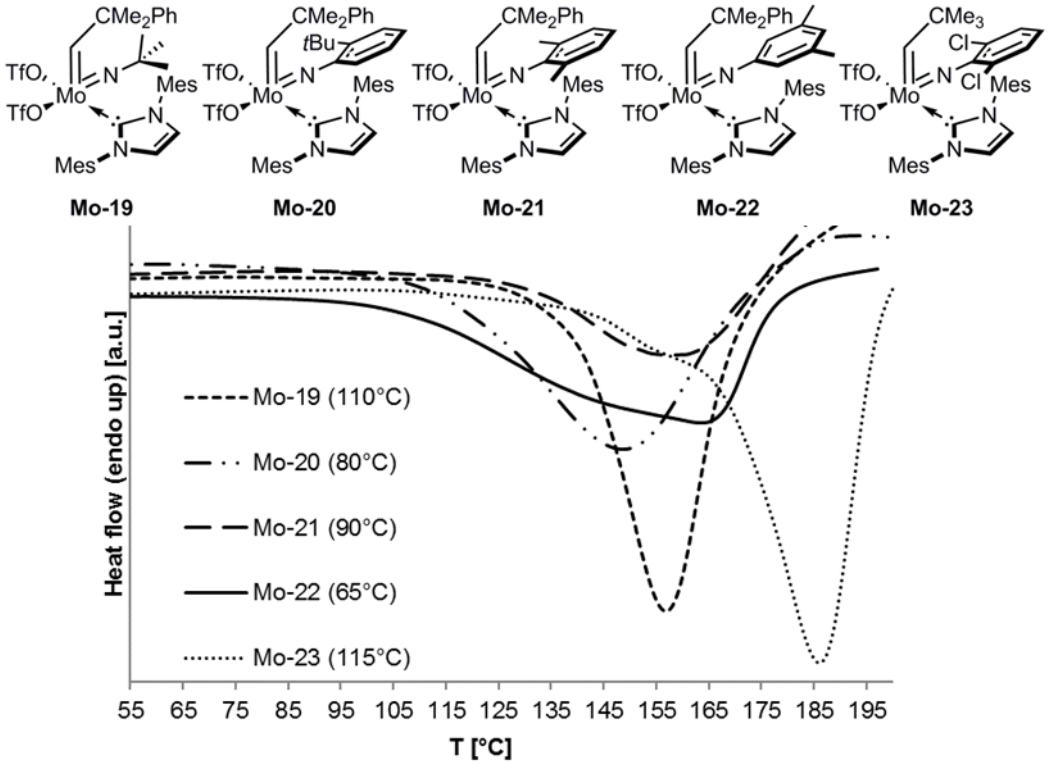

Figure 45: DSC curves of the temperature scan DSC measurements of **Mo-19** - **Mo-23**. Catalyst/ CH_2Cl_2/DCPD 1 equiv./10 µL/500 equiv. *Heating program:* 0°C for one minute, 0 °C → 200 °C (10 $K \cdot min^{-1}$). Values in brackets: $T_{onset,TScan}$.

All complexes except **Mo-22** formed stable mixtures with DCPD for several hours. For **Mo-22**, polymerization occurred within several minutes despite the observed $T_{onset,TScan}$ of 65°C. $T_{onset,TScan}$ was defined as the temperature at which the exothermal curing reaction started. A clear influence of the imido ligand on $T_{onset,TScan}$ was observed by DSC (Figure 45). The *tert*-butylimido ligand in **Mo-19** ($T_{onset,TScan}$ = 110°C) is less electron donating than the alkyl substituted aromatic imido ligands in complexes **Mo-20** - **Mo-22** ($T_{onset,TScan}$= 65, 80 and 90°C, respectively). As anticipated, **Mo-23**, with the electron-withdrawing chloro-substituents at the aromatic imido ligand, displays the highest $T_{exo,max}$ = 186°C and $T_{onset,TScan}$ = 115°C of all screened bistriflate catalysts. In fact, $T_{onset,TScan}$ for **Mo-20** - **Mo-22** also correlated with their previously published coalescence temperature T_c = 60°C (**Mo-22**), T_c = 79°C (**Mo-20**) and T_c = 85°C (**Mo-21**) in deuterated 1,2-dichlorobenzene (Table 6).[190] Poly(DCPD) derived from the polymerization with catalysts **Mo-19** (T = 110°C), **Mo-21** (T = 110°C) and **Mo-22** (T = 80°C) showed swelling of 25, 45 and 50% in toluene. Highly crosslinked poly(DCPD), showing no swelling in toluene at all, was isolated from polymerizations with **Mo-20** (T = 80°C) and **Mo-23** (T = 150°C) (Table 24, experimental section). Despite the high curing temperature of 110°C, the comparably low degree of crosslinking of poly(DCPD) prepared by ROMP with **Mo-21** correlates with a lower ΔH of -210 $J \cdot g^{-1}$ (Table 12, experimental section) observed in temperature scan DSC measurements. The high degree of crosslinking observed for **Mo-23** can be explained by the high curing temperature applied. In turn the rather low curing temperature used with **Mo-22** accounts for the observed low degree of crosslinking. These findings highlight the impact of the imido ligand on the activity of molybdenum imido alkylidene NHC complexes and underline the systems´ modularity in terms of activation temperatures T_{onset}. Also, the *N*-2,6-dimethylphenylimido and the *N*-3,5-dimethylphenylimido complexes **Mo-21** and **Mo-22** were identified as best targets for the introduction of a chelating alkylidene ligand due to their rather low $T_{onset,TScan}$ (65 and 90°C, respectively) for reasons outlined above.

6.3.3 Hexacoordinated molybdenum imido alkylidene NHC bistriflate complexes with a chelating alkylidene moiety

The results reported above were provided as the basis for a bachelor thesis with the aim to synthesize thermally latent *and* air stable hexacoordinated molybdenum imido alkylidene bistriflate NHC complexes with chelating ligands. Indeed, the bachelor thesis of *Benjamin Kordes* resulted in the synthesis of complex **Mo-25** (Scheme 50) with a chelating alkylidene.[17a] Additional catalyst **Mo-24** (synthesis developed by *Katharina Herz*[169]) and **Mo-25**, based on the most promising precursor complexes, were shown to be latent in DCPD polymerization. As anticipated, **Mo-24** and **Mo-25** were air stable.[17a] They thereby add to the very small group of air stable group 6 olefin metathesis catalysts. With those preliminary results at hand, the latent behavior of catalysts **Mo-12**, **Mo-15**, **Mo-24** and **Mo-25** was

systematically investigated by DSC measurements and compared with the respective pentacoordinated precursor-complexes **Mo-21** and **Mo-22**.

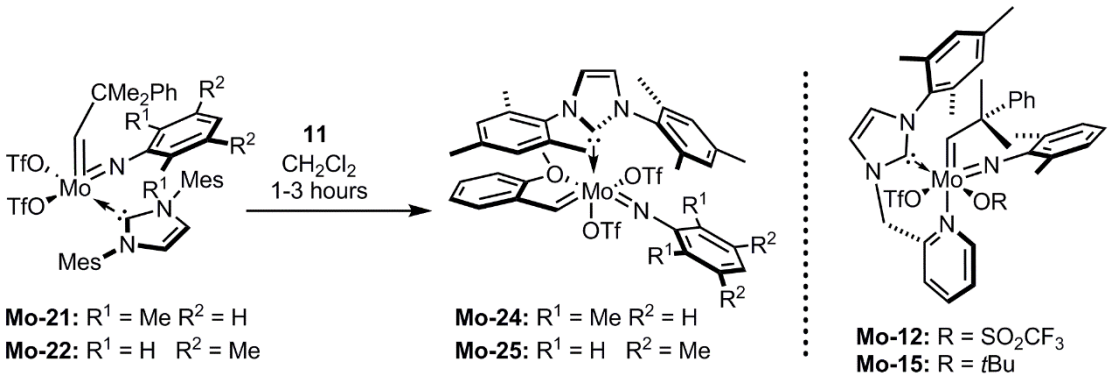

Scheme 50: Left: Synthesis of octahedral complexes **Mo-24** and **Mo-25** by replacement of the neophylidene moiety by 2-methoxystyrene **11** in the corresponding molybdenum imido alkylidene bistriflate IMes complexes **Mo-21** and **Mo-22** (yield: 95 and 61%). [17a,169] Right: Previously synthesized complexes **Mo-12** and **Mo-15**.

Mo-24 and **Mo-25** can conveniently be synthesized from **Mo-21** and **Mo-22** in 95 and 61% yield. Also, additional catalysts **Mo-27** and **Mo-28** were synthesized, to investigate the influence of the electron-donating and electron-withdrawing properties of the X-type ligand on the ROMP behavior for DCPD. **Mo-27** contains an electron-donating phenoxide ligand instead of the second triflate. This was expected to result in a reduced T_{onset}. Interestingly, reaction of **Mo-25** with lithium phenoxide did not lead to any conversion. Instead, the triflate ligand in the precursor complex **Mo-22** had to be replaced by a phenoxide, leading to the monotriflate monoalkoxide complex **Mo-26** in 68 % isolated yield. Subsequently, the chelating alkylidene moiety was introduced by reaction of **Mo-26** with **11**, to yield **Mo-27** in 66 % isolated yield (Scheme 51).

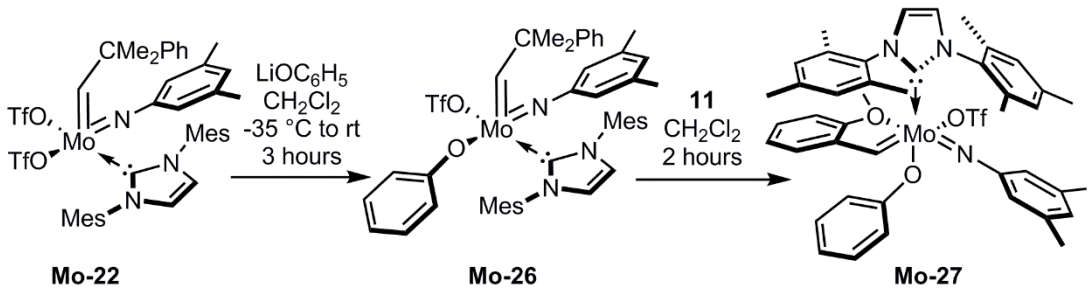

Scheme 51: Synthesis of octahedral complex **Mo-27** by replacement of the neophylidene moiety by 2-methoxystyrene **11** in the corresponding molybdenum imido alkylidene monotriflate monophenoxy IMes complex **Mo-26** (yield: **Mo-26**: 68%; **Mo-27**: 66%).

The carboxylate coordinated catalyst **Mo-28** was synthesized from **Mo-21**, by reaction of **Mo-21** with lithium pentafluorobenzoate in CH_2Cl_2 and diethyl ether. Pentafluorobenzoate was chosen because of its chelating ability and the electron-withdrawing character. Both properties were expected to render the catalyst system latent. **Mo-28** was isolated after recrystallization

from a mixture of CH_2Cl_2 and pentane in 67% isolated yield. **Mo-28** showed varying amounts of *anti*-isomer and even allowed for the isolation of samples with all *anti*-configuration.

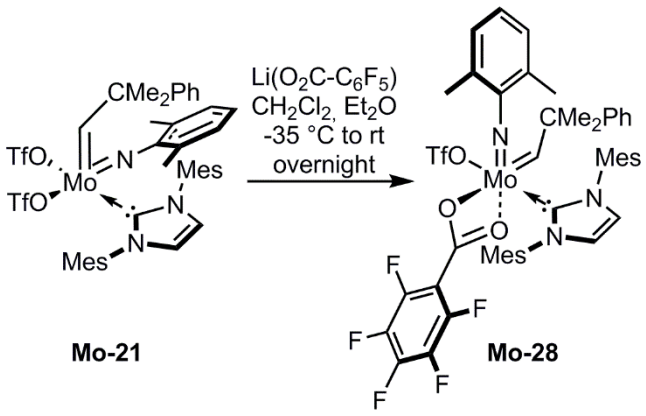

Scheme 52: Synthesis of a carboxylate-based catalyst, **Mo-28,** from **Mo-21** by conversion with lithium pentafluorobenzoate in CH_2Cl_2 in 67% yield.

First, complexes **Mo-12** and **Mo-15**[192] bearing a pyridyl-substituted NHC (Scheme 5) were investigated in the polymerization of DCPD since they presented an excellent opportunity to probe the hypothesis that an octahedral geometry, resulting from the incorporation of a chelating ligand into molybdenum imido alkylidene NHC bistriflate complexes, would offer access to highly stable and latent olefin metathesis catalysts. In fact, DSC measurements of mixtures of **Mo-12** with DCPD revealed an onset of polymerization at $T_{onset,TScan}$ = 80°C. The exothermal maximum was observed at $T_{exo,max}$ = 115 °C using a heating rate of 5 $K \cdot min^{-1}$ (**Fehler! Verweisquelle konnte nicht gefunden werden.**). Small amounts of 1,2,4-trichlorobenzene (TCB) had to be added to enable ROMP of DCPD.

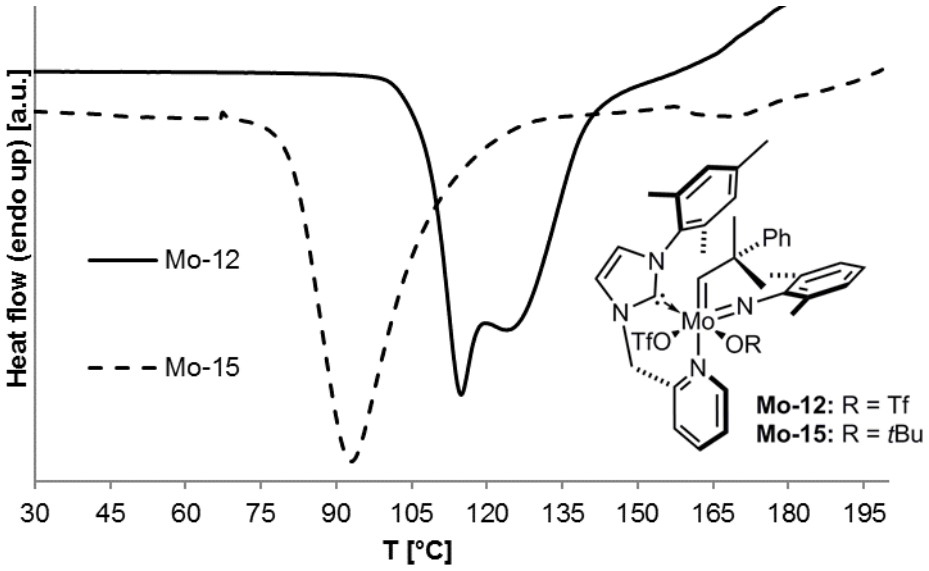

Figure 46: DSC curves of temperature scan DSC measurements of pre-catalysts **Mo-12** and **Mo-15** with 1,2,4-trichlorobenzene and DCPD. Catalyst/TCB/DCPD 1/10/100. *Heating program*: 0 °C for 1 minute, 0 °C to 200 °C (10 $Kmin^{-1}$). **Mo-12**: $T_{exo,max}$ = 115 °C; $T_{onset,TScan}$ = 80 °C. **Mo-15**: $T_{exo,max}$ = 98 °C; $T_{onset,TScan}$ = 70 °C.

Notably, such mixtures of **Mo-12**/TCB/DCPD could be stored at room temperature for at least one day without any polymerization of DCPD. Latency was proven by temperature scan DSC measurements of the aged mixture after one day and comparison of the measured reaction enthalpy with the one of a freshly prepared mixture (Table 17, Figure 85, experimental section). Notably, **Mo-12** was air stable for at least two hours in the solid state (Figure 85, experimental section). Catalyst **Mo-15**, based on an electron-donating *tert*-butoxide ligand, was also tested in latent DCPD polymerization. A lower value for $T_{onset,TScan}$ and an increase in activity was expected due to a facilitated release of triflate because of the higher electron density at molybdenum. And indeed, a decrease in $T_{onset,TScan}$ to 70°C and in $T_{exo,max}$ to 98°C was confirmed. Because of its higher reactivity compared to **Mo-12**, which produced poly(DCPD) that also contained soluble, non-cross-linked poly(DCPD), pre-catalyst **Mo-15** was only latent for approximately three hours at room temperature as judged from DSC measurements of **Mo-15** /TCB/DCPD mixtures (Figure A 45, Table A 6, appendix). However, like **Mo-12**, pre-catalyst **Mo-15** was also stable under air for twelve hours in the solid state (Figure 86, experimental section). The lower degree of swelling in toluene (8%) observed for poly(DCPD) polymerized with **Mo-12** compared to poly(DCPD) polymerized with **Mo-15** (34%) can be explained by the higher curing temperature that was applied (110°C vs 80°C). Catalysts **Mo-12** and **Mo-15**, when exposed to higher monomer loadings, decomposed before complete monomer consumption, as indicated by the cracking of non-polymerized DCPD in the DSC curves. We attribute this finding to the back coordination of the pyridyl moiety to the active species, leading to an activation barrier for each metathesis step.

To overcome this obstacle, above described catalysts **Mo-24**, **Mo-25**, **Mo-27** bearing a chelating alkylidene ligand were applied. With such systems, back coordination of the donor-moiety is almost impossible after the first insertion step (*vide supra*).

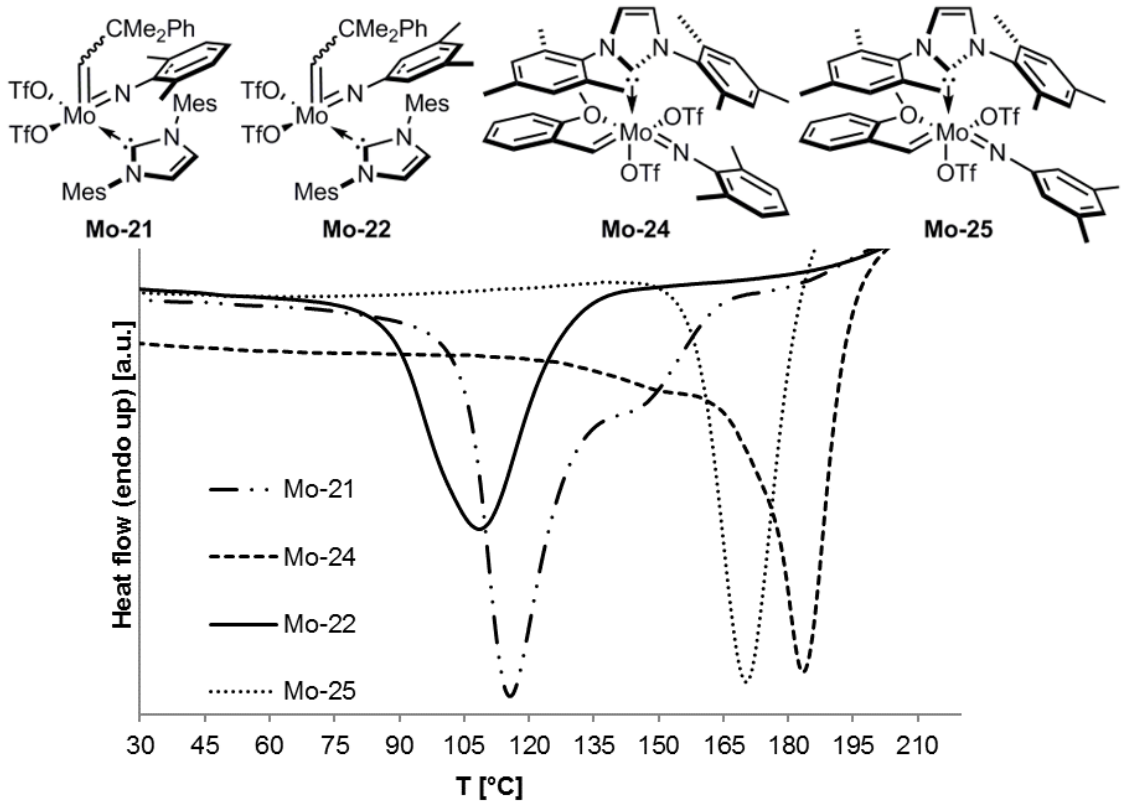

Figure 47: DSC curves of the temperature scan DSC measurements of pentacoordinated precursor complexes **Mo-21** and **Mo-22** in comparison to the chelated hexacoordinated catalysts **Mo-24** and **Mo-25**. Catalyst/TCB/DCPD 1/10/100. *Heating program:* 0 °C for one minute, 0 °C → 200 °C or 220 °C (5 $Kmin^{-1}$).

Temperature scan DSC measurements of mixtures of **Mo-24**, TCB and DCPD showed a $T_{exo,max}$ of 183 °C and a $T_{onset,TScan}$ of 120 °C (Figure 47). Isothermal DSC measurements for 30 minutes at T = 80, 100, 120 and 140°C revealed a $T_{onset,iso}$ > 140°C (Table 14, Figure 82, experimental section).

Table 7: $T_{exo,max}$, $T_{onset,iso}$ in ROMP of DCPD and air stability of pentacoordinated complexes **Mo-21**, **Mo-22** in comparison to hexacoordinated complexes **Mo-24** and **Mo-25**.

catalyst	$T_{exo,max}$ [°C][(i)]	$T_{onset,iso}$ [°C] [(ii)]	air stable [(iii)]
Mo-21	115	100	no
Mo-24	183	>140	yes
Mo-22	98	60	no
Mo-25	168	100	yes

(i) $T_{exo,max}$: Exothermal maximum in the DSC curve of a temperature scan measurement. Heating program: 0°C for one minute, 0 °C → 200 °C or 220 °C (5 $Kmin^{-1}$). (ii) $T_{onset,iso}$: Maximum temperature a sample could be heated at for thirty minutes without polymerization. (iii) Catalyst was stored under air in the solid form for twelve hours. Stability was confirmed by NMR spectroscopy in dry deuterated solvents.

With **Mo-25** containing the *N*-3,5-dimethylphenylimido ligand, both temperatures could be reduced to $T_{onset,iso}$ = 100 °C and $T_{exo,max}$ = 168 °C (Table 16, Figure 80, Figure 84, experimental section). The decrease in the onset of polymerization from the *N*-2,6- to the *N*-

3,5-dimethylphenylimido ligand is tentatively attributed to a facilitated approach of substrate to the metal center in case of the less sterically demanding imido ligand. Both, **Mo-24** and **Mo-25**, were thermally fully latent at room temperature for at least three days as demonstrated by temperature scan DSC measurements after one, two and three days and by comparison of the obtained reaction enthalpies with those of freshly prepared reference mixtures (Figure 88, Figure 89, Table 20, Table 21, experimental section). Poly(DCPD) prepared by the action of these pre-catalysts did not show any swelling in toluene, indicating a high degree of crosslinking. Air stability of catalysts **Mo-24** and **Mo-25** was measured by storing them under air for twelve hours in the solid state on a glass plate. Both were air stable, as verified by ^{1}H NMR spectroscopy in dry deuterated solvents, which did not reveal any detectable catalyst decomposition (Figure A 113, Figure A 114, appendix). However, under the same conditions, the precursor catalysts **Mo-21** and **Mo-22** showed decomposition (Figure A 111, Figure A 112, appendix). Surprisingly, **Mo-21**, with the sterically more shielded metal center, was less stable in the presence of air than **Mo-22**. Three different catalyst to monomer ratios (1/100, 1/175, 1/250) were investigated for both **Mo-24** and **Mo-25** in the ROMP of DCPD. The amount of TCB was kept constant. No significant changes in the DSC temperature scan curves were observed (Figure 90, Figure 91, experimental section); the determined enthalpies were in the range between 260 and 300 $J \cdot g^{-1}$ (Table 23, experimental section). T_g values of poly(DCPD) derived from the polymerization of DCPD with **Mo-19**- **Mo-25**, **Mo-12** and **Mo-15** ranged between 130 and 170°C (Table 25, experimental section).

Additionally, complexes **Mo-27** and **Mo-28** were applied in ROMP of DCPD. As expected, the phenoxy ligand in **Mo-27** had a strong influence on activity, leading to immediate polymerization of DCPD at room temperature. The change from triflate to phenoxide therefore leads to a drastic decrease in T_c of approximately 75°C. The same was true for complex **Mo-28,** regardless of the electron-withdrawing carboxylate and its potentially chelating character. Eventually, the observed high amounts of *anti*-isomer in samples of **Mo-28** account for the high activity.

6.3.4 OUTLOOK

One issue neglected so far is the low solubility of the catalysts in dicyclopentadiene. Small amounts of solvent must be added to enable polymerization. The introduction of long alkyl chains should lead to increased solubility. Alkylic chains in the back-bone of the NHC are unfavorable, since NHC synthesis would become substantially more time consuming, whereas long chain alkylic alcohols or alkyl chain tagged phenols are commercially available (e.g. 2-methyl-2-butanol or 4-octyl phenol). Therefore, the easiest way to introduce alkylic substituents is the alkoxide ligand.

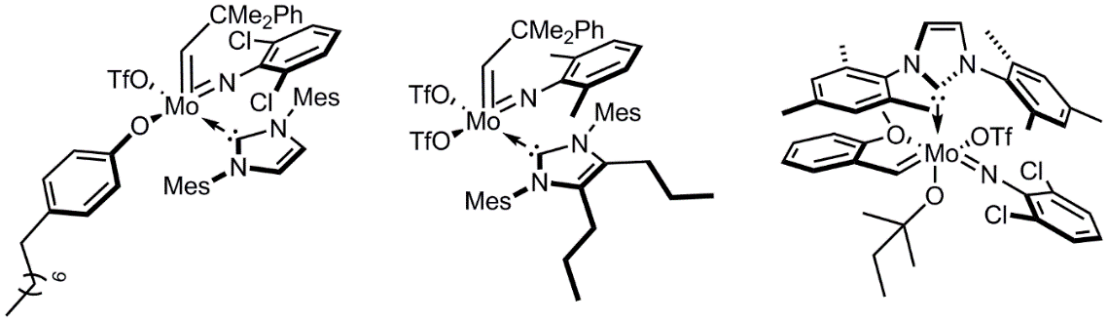

Figure 48: Examples for catalysts with additional alkylic chains to provide better solubility in dicyclopentadiene, rendering usage of additional solvents obsolete.

However, electronic factors must be carefully balanced, since donating alkoxides have shown to increase reactivity towards dicyclopentadiene. To counterbalance the increased electron donation from the alkoxide, the *N*-2,6-dichlorophenylimido or the *N*-*tert*-butylimido ligand could be used due to their observed high T_{onset}. Furthermore, large scale experiments should be done to test applicability of the catalysts in industry and investigate the material properties.

6.4 SYNTHETIC ROUTES TO CHIRAL MOLYBDENUM IMIDO ALKYLIDENE *N*-HETEROCYCLIC CARBENE COMPLEXES

Parts of the following chapter have already been published. Reprinted (adapted) with permission from (I. Elser, W. Frey, K. Wurst, M. R. Buchmeiser, *Organometallics* **2016**, *35*, 4106-4111). Copyright (2016) American Chemical Society.

6.4.1 WORKING HYPOTHESIS

Chiral molybdenum imido alkylidene NHC complexes could be of special interest in the synthesis of chiral functionalized molecules. Especially in the synthesis of natural products, where functional groups are omnipresent, the usage of NHC coordinated complexes could render uneconomic protection and deprotection steps obsolete. Molybdenum imido NHC alkylidene complexes offer three opportunities to introduce chirality. Chiral imidos, *N*-heterocyclic carbenes and alkoxides could be employed. Chiral imido ligands, however, are introduced in an early step of catalyst synthesis, which results in high consumption of usually expensive chiral amines. Even though introduction of chirality *via* the NHC seems viable, *Eisenstein* and co-workers claimed that the metallacyclobutane is formed *trans* to the strongest donor, which in this case would be the NHC, and therefore has only a small impact on stereoselectivity in the metallacyclobutane.[21a,21b,21d] The alkoxide however, should take up the apical position in the TBP transition state and in consequence should have a high impact on sterics in the MCB (Figure 49).

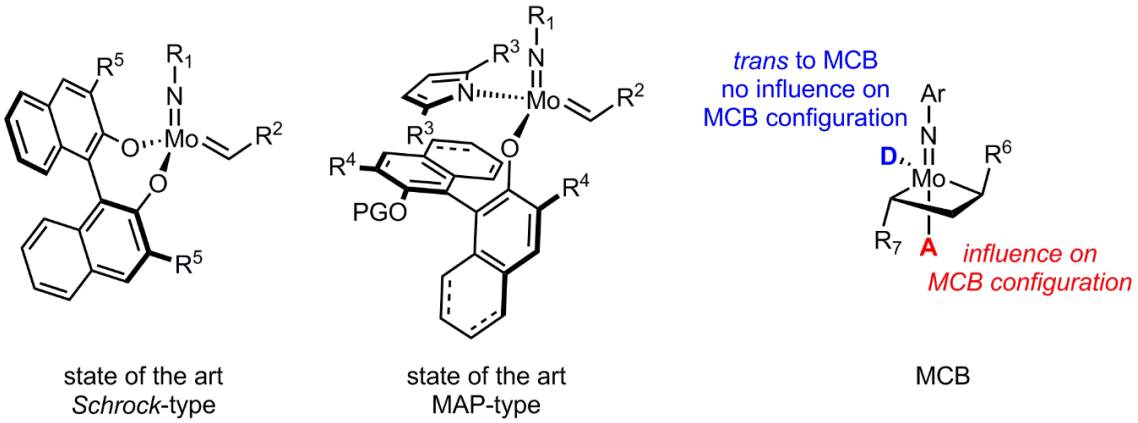

Figure 49: State of the art chiral *Schrock*- and MAP-type catalysts with 1,1´-binapthol-2,2´-ate- or octahydro-1,1´-binapthol-2,2´-ate-derived ligands. Metallacyclobutane (MCB) with donor (D) and acceptor (A) ligand. Only A has an influence on steric configuration in the MCB.

Chiral 1,1´-biphenolates, binaphtholates and octahydrobinaphtholates have successfully been used as ligands in enantioselective (metathesis) reactions and are in some cases even commercially available (Figure 49).[9a,20,21e,92,96,193] Hence, they have been chosen as key elements of chiral induction in the investigations on chiral molybdenum imido alkylidene NHC complexes presented in this work. Since metal centers coordinated by electronically distinct

ligands had been calculated to be more active than their symmetrically coordinated counterparts (MAP *vs*. normal *Schrock*-type bisalkoxide[21a,21b]), the mono-protected forms of the diols were used. As outlined in the theoretical introduction, pentacoordinated complexes have a multitude of optical isomers.[166] The target Mo(NR^1)(CHR^2)(OTf)(OR)(NHC) complexes have four optical isomers, if a SP geometry and an apical position of the alkylidene ligand, as well as a *cis* configuration of the alkoxide and triflate ligand are considered (Figure 50). All assumptions are based on single crystal X-ray analyses of Mo(NR^1)(CHR^2)(OTf)(OR)(NHC) complexes.[17b,167-168,168c,168e,183]

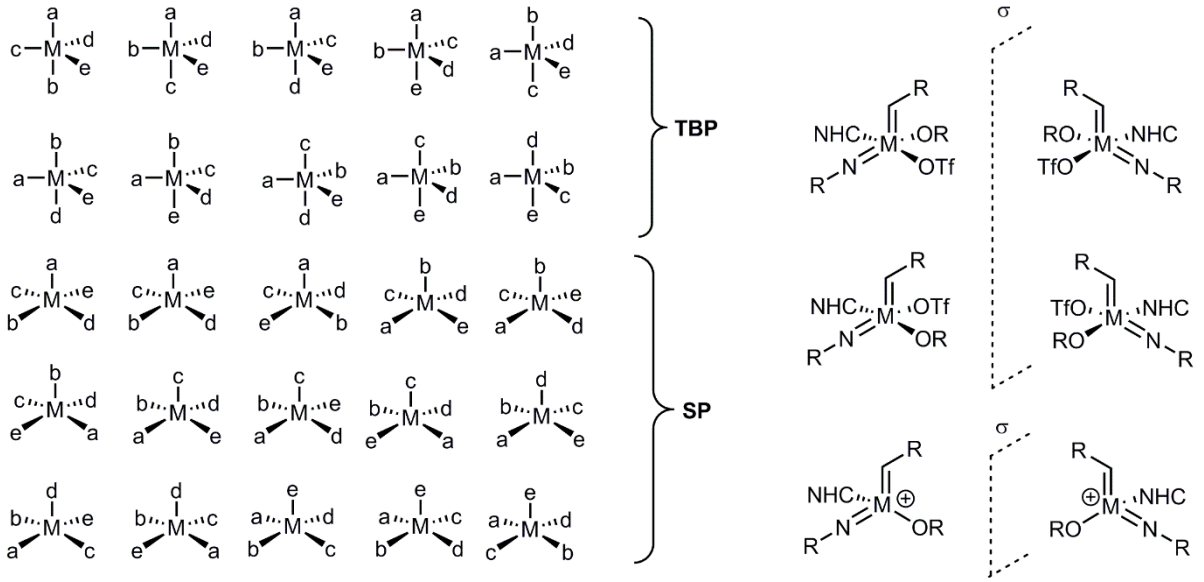

Figure 50: *Left*: All possible isomers for pentacoordinate complexes of the M(abcde)-type. Only one enantiomer depicted if enantiomers are present. *Right:* Optical isomers for pentacoordinated Mo(NR^1)(CHR^2)(OTf)(OR)(NHC) complexes and tetracoordinated cationic [Mo(NR^1)(CHR^2)(OR)(NHC)][B(Ar^F)$_4$] complexes (anion omitted for clarity).

In view of the fluxionality of pentacoordinate complexes[165] and the multitude of possible isomers, as well as in view of catalytic activity, it would be favorable to have cationic molybdenum imido alkylidene NHC complexes bearing chiral alkoxides. Here, only two diastereomers are possible (Figure 50).

6.4.2 Synthesis of ligands, substrates and the derived racemic products

The ligands (*S*)-3,3´-dibromo-2´-(*tert*-butyldimethylsilyloxy)-1,1´-binaphthalen-2-ol **12**[21e], (*R*)-3,3´-dibromo-2´-(*tert*-butyldimethylsilyloxy)-5,5´,6,6´,7,7´,8,8´-octahydro-1,1´-binaphth-2-ol **13**[21e] and (*R*)-2´-trimethylsilyloxy-3,3´-di(*tert*-butyl)-5,5´,6,6´-tetramethyl-1,1´-biphen-2-ol **14**[178] were synthesized according to literature starting from commercially available (*S*)-1,1´-binapth-2,2´-ol, (*R*)-5,5´,6,6´,7,7´,8,8´-octahydro-1,1´-binaphth-2,2´-ol and (*R*)-3,3´-di-*tert*-butyl-5,5´,6,6´-tetramethyl-1,1´-biphen-2,2´-ol, respectively.

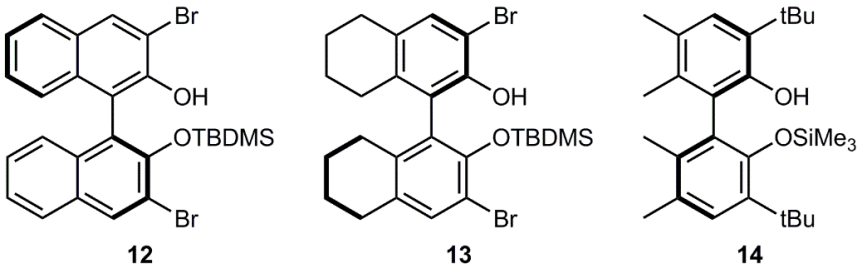

Figure 51: Mono-protected chiral C2-symmetric ligands **12**, **13** and **14** for the synthesis of chiral molybdenum imido alkylidene NHC complexes.

Five bench-mark substrates were chosen to evaluate the performance of potential chiral molybdenum imido alkylidene NHC complexes in enantioselective metathesis (Figure 52). **15**[96], **16**[177a], **17**[177b], **18**[177b] and **19**[194] were synthesized according to literature. Substrates **15**, **16**, **17** and **18** are chiral and can be used in catalytic kinetic resolution, whereas substrate **19** is prochiral and can be applied in catalytic desymmetrization reactions. Substrates leading to 5- (**21**, **24**) and 6-ring (**20**, **22**, **23**) heterocycles were chosen. Although the ultimate goal are substrates incorporating unprotected amines, alcohols and similar challenging moieties, work focused on enantioselectivity in first place, not on functional group tolerance.

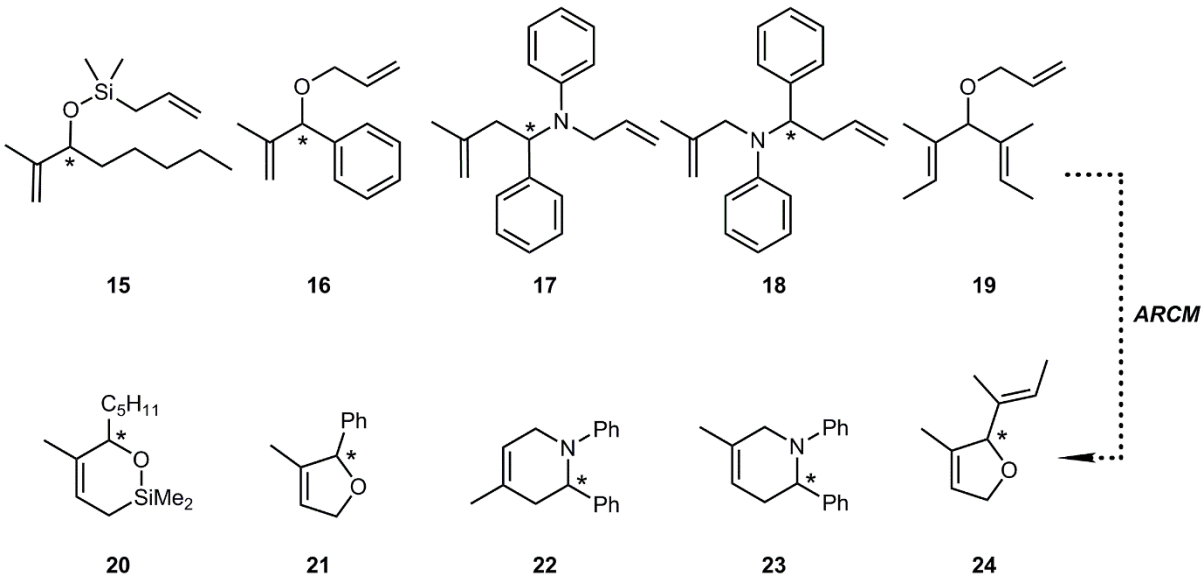

Figure 52: *Top:* Synthesized racemic chiral bench-mark substrates **15**, **16**, **17** and **18** for catalytic kinetic resolution by asymmetric olefin metathesis and non-chiral substrate **19** for catalytic enantioselective triene desymmetrization by ARCM. *Bottom*: Derived heterocyclic ARCM-products **20**, **21**, **22**, **23** and **24**.

The substrates were reacted with one of two non-chiral standard metathesis catalysts (*Grubbs* 2nd catalyst for **15**, **16** and **19** or *Schrock*-type Mo(*N*-2,6-iPr_2-C_6H_3)($CHCMe_2Ph$)($OCCH_3(CF_3)_2)_2$ for **17** and **18**) to develop GC-MS and analytical HPLC methods on chiral columns for separation of educt and the respective product enantiomers **20**, **21**, **22**, **23** and **24** (Figure 52). All product enantiomers were successfully separated by analytical HPLC (**22**, **23**) or GC-MS (**20**, **21**, **24**) on chiral columns (HPLC: *AD-H, Chiral Technologies Europe*, 250

x 4.6 mm ID; GC-MS: *Beta Dex™-120*, *Supelco*, 30m x 0.25 mm x 0.25 µm). Detailed parameters are provided in the experimental section (Table 26 and Table 27).

6.4.3 *Reactions with molybdenum imido alkylidene N-heterocyclic carbene bistriflate complexes- CH-activation Issue*

The standard protocol for introduction of alkoxides to molybdenum imido alkylidene bistriflate NHC complexes is replacement of one triflate with a lithium alkoxide in CH_2Cl_2. Therefore, first attempts to coordinate chiral alkoxides to molybdenum imido NHC alkylidene complexes included the reaction of a variety of NHC complexes with the respective metal alkoxides of **12**, **13** and **14**. Several imido ligands were chosen. Mainly $IMesH_2$ and IMes complexes were employed, since those had proven to be the most reactive complexes due to facilitated release of triflate encouraged by the good σ-donor ligands (TEP[24] = $IMesH_2$: 2051.2 and IMes: 2050.5). Although extensive effort was made by changing solvent, reaction temperature and time, as well as going from lithium to potassium or sodium alkoxides, the desired products could not be isolated. A detailed overview on all reactions is provided in the experimental section (Table 28).

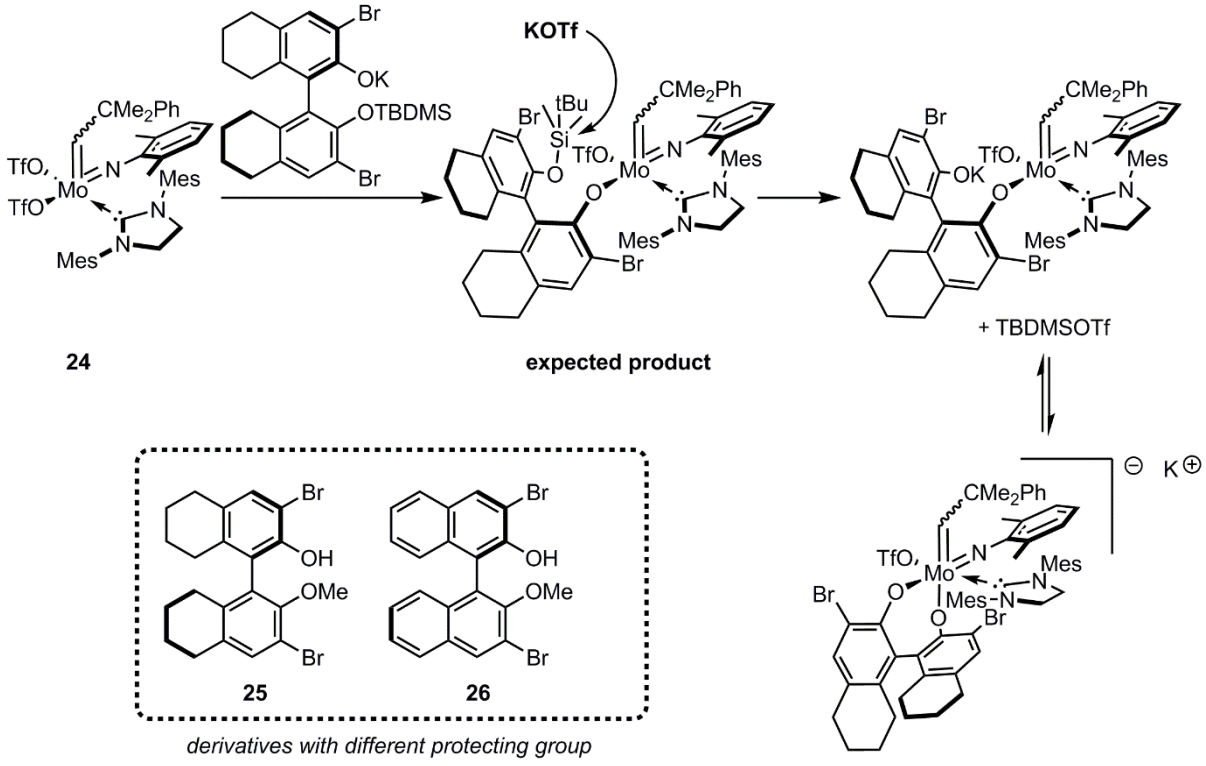

Scheme 53: Proposed mechanism for reaction of formed triflate anion with TBDMS protecting group and additional ligands **25** and **26** synthesized to test the hypothesis.

It was suspected that the TBDMS protecting group on the chiral ligand might be attacked by the leaving triflate anion and could cause failure of the reactions. Consequently, a more stable methyl-protecting group (**25**[195] and **26**[196]) was introduced to 3,3´-dibromo-5,5´,6,6´,7,7´,8,8´-

octahydro-1,1´-binaphth-2,2´-ol and 3,3´-dibromo-1,1´-binapth-2,2´-ol and the resulting ligands were employed in the reaction with complex **24** under the same reaction conditions. Unfortunately, this again did not lead to any improvement, therefore negating the hypothesis. Also, cationic [Mo(*N*-2,6-Me_2-C_6H_3)(CHCMe_2Ph)(OTf)(IMes)][B(Ar^F)$_4$] **Mo-2** was employed in the reaction with the deprotonated ligands, however, no pure compounds could be isolated.

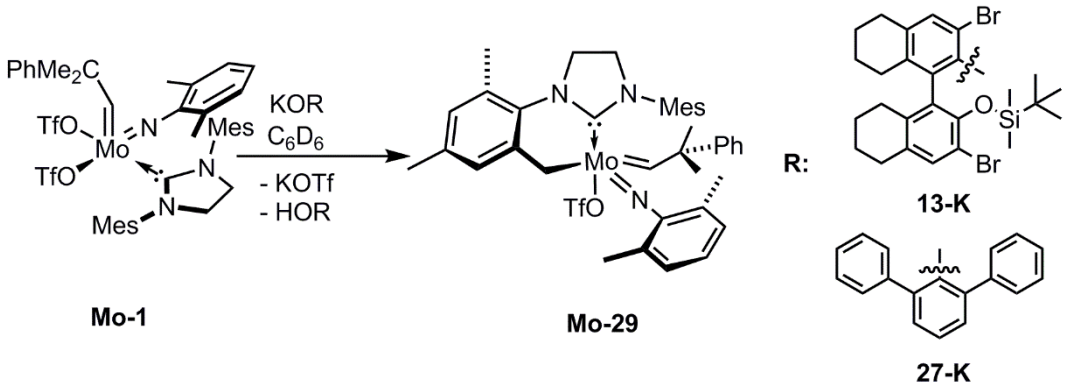

Scheme 54: Isolation of molybdenum imido alkylidene NHC complex **Mo-29** with a *C*-chelating *N*-heterocyclic carbene by deprotonation of **Mo-1** with sterically hindered potassium bases **13-K** or **27-K**.

Interestingly, in case of the reaction of **Mo-1** with **13-K** in benzene (Scheme 54) and filtration of the reaction mixture, intensive red crystals could be obtained after crystallization of the crude residue from a mixture of CH_2Cl_2, diethyl ether and pentane. Crystallization from other solvents and solvent mixtures proved to be ineffective. Also, the reaction was only successful if benzene or toluene were used as reaction medium. ^{1}H NMR spectroscopy of **Mo-29** in C_6D_6 revealed the absence of the ligand **13**.

Interestingly, the for aromatic protons of the mesityl residues of the NHC could be observed as four distinct signals at δ = 7.48, 6.67, 6.28 and 5.89 ppm (Figure 53, left). In addition, two doublets were observed at δ = 3.22 ($^3J_{HH}$ = 8.7 Hz) and 3.09 ($^3J_{HH}$ = 8.7 Hz) ppm (Figure 53). Consequently, a structure containing a chelating methylene bridge between one of the mesityl methyl groups and the molybdenum center (**Mo-29**, Figure 53) was postulated and later proven by single crystal X-ray analysis. To find a less expensive, non-chiral base, for the synthesis of **Mo-29**, several bases were tested in the reaction with **Mo-1**. Addition of *n*-butyl lithium resulted in decomposition and reaction with potassium *tert*-butoxide lead to the expected exchange of one triflate ligand by the *tert*-butoxide ligand. However, the use of the sterically demanding base K(O(2,6-$Ph_2(C_6H_3)$)) **27-K** again resulted in the formation of the *CH*-activated complex **Mo-29**.

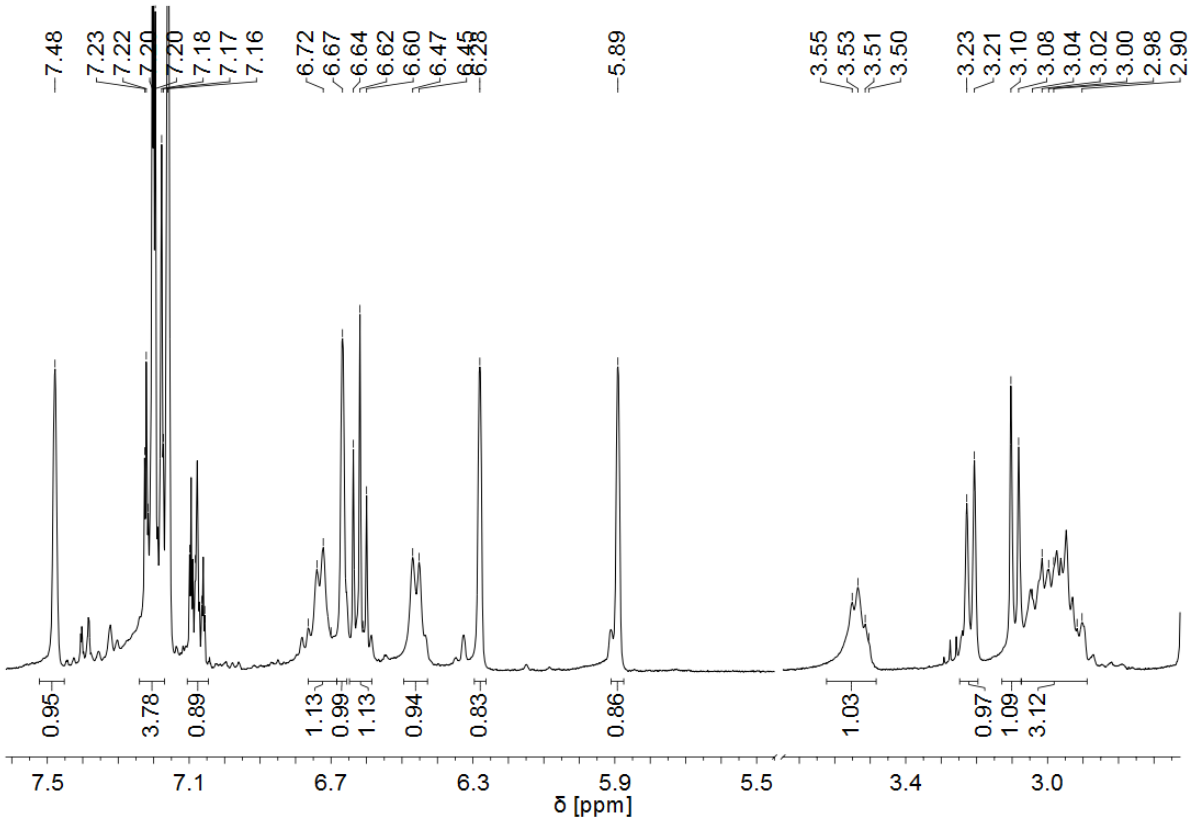

Figure 53: Zoom into aromatic (left) and alkylic (right) region of the ^{1}H NMR spectrum of **Mo-29** in C_6D_6. Aromatic mesityl protons at δ = 7.48, 6.67, 6.28 and 5.89 ppm and protons of the methylene molybdenum bridge at δ = 3.22 ($^3J_{HH}$ = 8.7 Hz) and 3.09 ($^3J_{HH}$ = 8.7 Hz) ppm.

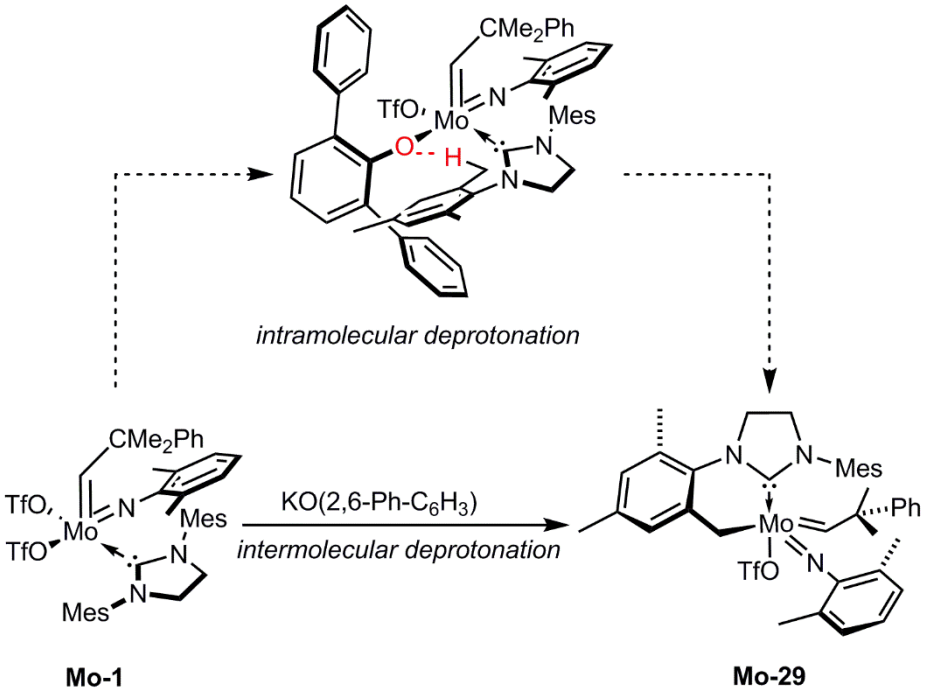

Scheme 55: Inter- *vs*. intramolecular (coordination of ligand *prior* to proton transfer) deprotonation of the methyl group by phenoxide in the formation of **Mo-29**.

To shed light on the mechanism of the formation of **Mo-29**, an *in situ* NMR study of the reaction between **Mo-1** and **27-K** in C_6D_6 was made. The question was, whether **Mo-29** forms *via* intramolecular deprotonation or *prior* to ligand coordination by intermolecular deprotonation (Scheme 55). The ^{1}H NMR spectrum of the reaction mixture of **Mo-1** and K(O(2,6-Ph_2(C_6H_3))) **27-K** in C_6D_6 immediately showed the appearance of the phenolic proton of HO(2,6-Ph_2(C_6H_3))) **27** at δ = 5.17 ppm. No additional alkylidene signals apart from the educt and the product alkylidene signal were observed (Figure A 119, appendix). Hence, coordination of the bulky ligands does not seem to occur (at least on the NMR time scale). Instead, immediate deprotonation of the NHC at the mesityl substituents seems to take place.

The structure of **Mo-29** was unambiguously proven by single crystal X-Ray analysis. **Mo-29** (Figure 54) crystallizes in the triclinic space group with a = 1135.66(5) pm, b = 1136.94(4) pm, c = 1916.87(8) pm and α = 103.513(2)°, β = 91.108(2)° and γ = 118.335(2)°. The triflate ligand is coordinated *trans* to the NHC and the angle between the two ligands is 151.72(13)°. The molybdenum methylene bond is 220.1(4) pm.

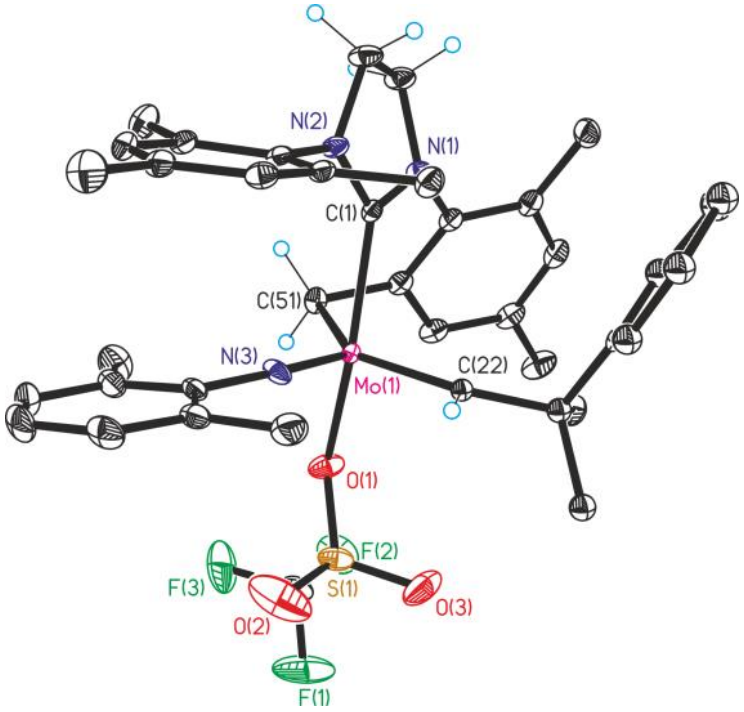

Figure 54: Single crystal X-ray structure of **Mo-29**. Selected bond lengths [pm] and angles [°]: Mo1-N3 172.3(3), Mo1-C22A 186.4(8), Mo1-C22 195.5(7), Mo1-O1 214.5(3), Mo1-C1 217.8(4), Mo1-C51 220.1(4); N3-Mo1-C22A 116.7(4), N3-Mo1-C22 97.4(3), O1-Mo1-C1 151.72(13), N3-Mo1-O1 99.78(14), C22A-Mo1-O1 93.4(3), C22-Mo1-O1 100.1(2), N3-Mo1-C1 100.59(14), C22A-Mo1-C51 137.3(3), O1-Mo1-C51 77.69(13), C1-Mo1-C51 74.57(14). Positional disorder of nearly 1:1 of the benzylcarbene group C22-C31. C26 (exact overlying) and C25 and C25A were refined with anisotropic displacement parameters. All other carbon atoms of this group were refined isotropically, because of nearly overlying positions. Hydrogens at C22 and C22A were found and refined isotropically with bond restraints (d=94 pm).

Mo-29 was tested in a simple set of olefin metathesis reactions. RCM and HM reactions of 1,7-octadiene, diallyl diphenylsilane, diallyl ether, 1-hexene and 1-octene with **Mo-29** in toluene at 80 °C did not lead to the desired products. Instead, in case of 1-octene and 1,7-octadiene isomerization of the double bond was observed. For 1,7-octadiene, complete isomerization into 1,6- and 2,6-octadiene was observed. For 1-octene, isomerization to 2-octene and 3-octene was noticed. For both substrates the ratio between the isomerization products varied, although in all experiments 1,6-octadiene and 2-octene were the main products. At room temperature, no reaction took place. Attempted removal of the remaining triflate ligand in **Mo-29** with $NaB(Ar^F)_4$ to eventually alter reactivity resulted in decomposition.

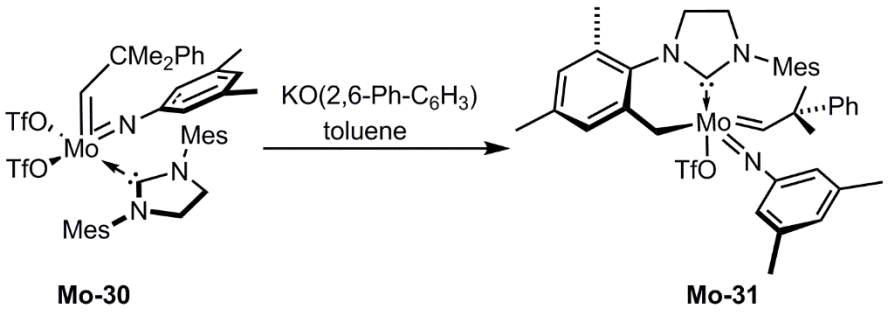

Scheme 56: *CH*-activation in molybdenum imido alkylidene NHC complexes. Synthesis of Mo(*N*-3,5-Me_2-C_6H_3)(CHCMe_2Ph)(OTf)(1-mesityl-3-(C_9H_{10})-imidazolin-2-ylidene) **Mo-31** by deprotonation of **Mo-30** with a sterically hindered potassium base **27-K** in toluene.

To gain more insights, the protocol for the synthesis of *CH*-activated **Mo-29** was applied to further molybdenum imido alkylidene bistriflate NHC complexes. And indeed, the same *CH*-activation process was observed if the *N*-3,5-dimethylphenylimido ligand (**Mo-30**, Scheme 56) was applied in the reaction with **27-K** instead of the *N*-2,6-dimethylphenylimido ligand (**Mo-1**, Scheme 54). This was surprising, since the 3,5-dimethylphenylimido ligand was expected to take up less space in the ligand sphere and therefore result in less steric constraint in the precursor complex.

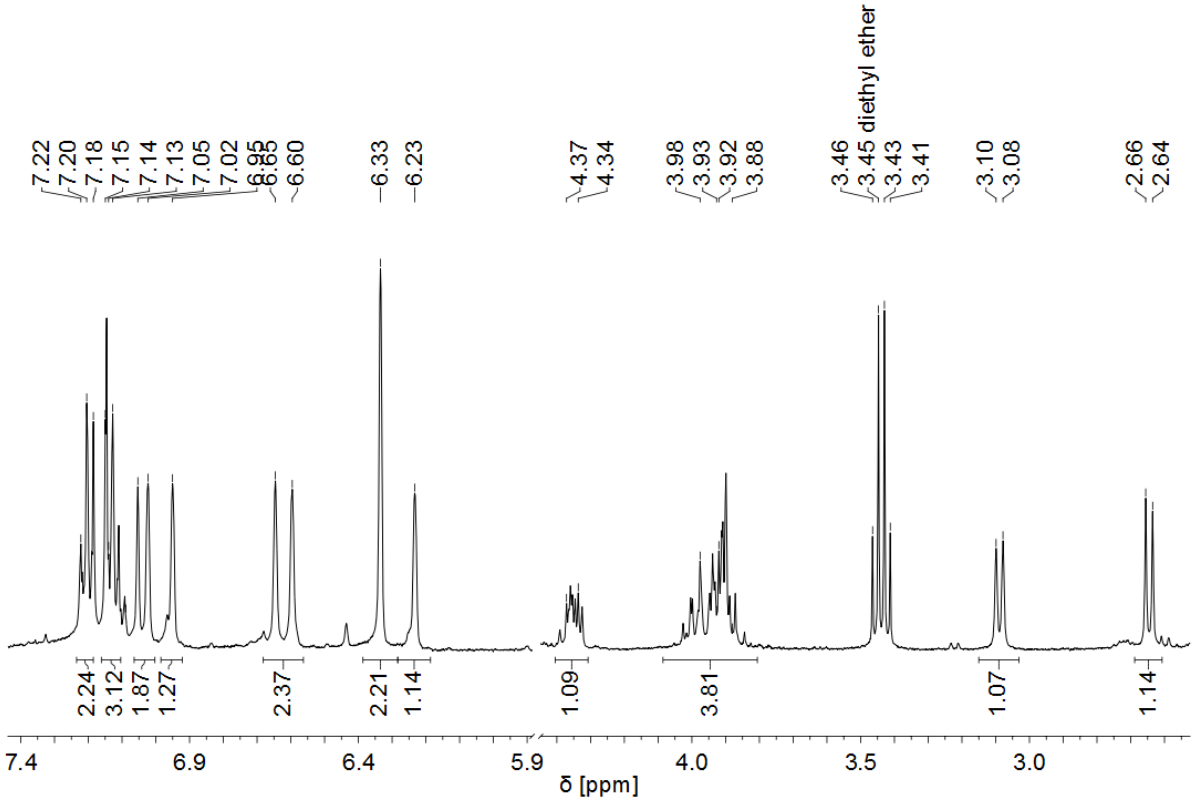

Figure 55: Details of the ^{1}H NMR spectrum of **Mo-31** in CD_2Cl_2. *Left:* aromatic region with four inequivalent mesitylene protons at δ = 6.95, 6.65, 6.60 and 6.23 ppm. *Right:* Doublets of the methylene-molybdenum bond at δ = 3.09 and 2.65 ppm.

Mo-31 could be obtained by crystallization from CH_2Cl_2, diethyl ether and pentane and so far, only has been characterized by ^1H and ^{19}F NMR spectroscopy. The ^1H NMR spectrum of **Mo-31** in CD_2Cl_2 clearly shows the four distinct aromatic protons of the mesityl residues as singulet signals at δ = 6.95, 6.65, 6.60 and 6.23 ppm (Figure 55, left). Additionally, the diastereotopic methylene protons of **Mo-31** are visible at δ = 3.09 and 2.65 ppm (Figure 55, right).

6.4.4 Buried volume of imido ligands

Since *CH*-activation or alkylidene ligand deprotonation in the synthesis of molybdenum imido alkylidene NHC complexes appeared to be a consequence of steric constraint in combination with high basicity of the employed alkoxide, steric factors of the individual ancillary ligands came into focus. One way to describe the sterics of ligands in coordination chemistry is the buried volume V_{bur}. A still increasing library of buried volumes of common NHC ligands has already been published,[8,41f] however, no comparison of the buried volumes of different aryl and alkylimido ligands in metathesis catalysts was accessible at this time. Buried volume (V_{bur}) is a measure of the space that a ligand takes up in the first coordination sphere of a central atom.[41b].

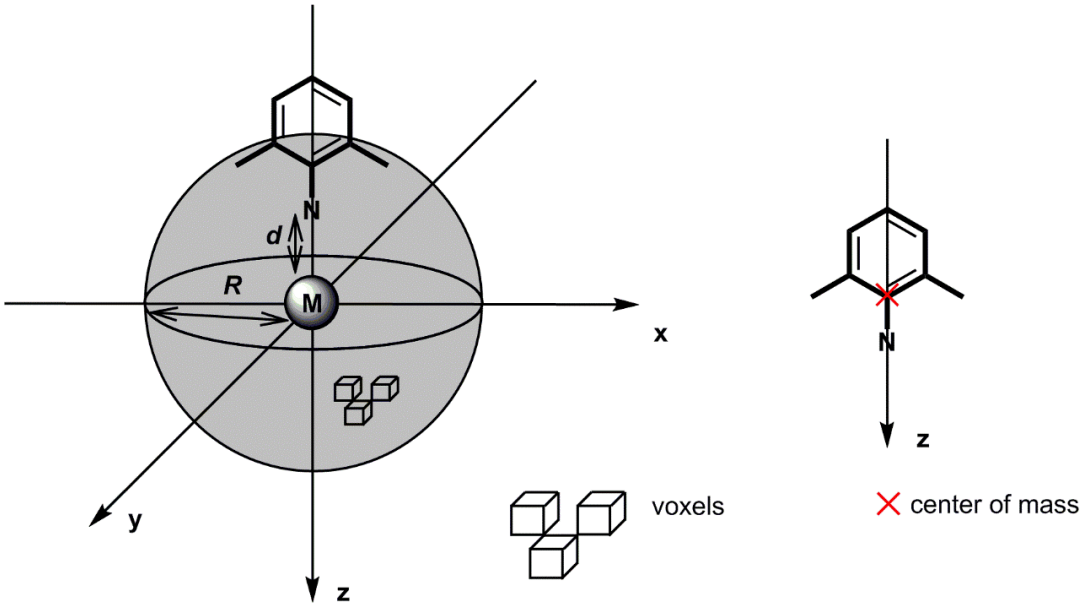

Figure 56: Schematic view: *Left*: Buried volume of an imido ligand in the first coordination sphere (grey sphere) of a central metal atom. *Right*: Orientation of imido on the z-axis through the center of mass.

The coordination sphere is constructed with a given radius *R* around the central atom. The coordinating atom of the ligand is then placed in the distance *d* from the metal center on the z-axis. For the determination of V_{bur}, the geometry of the ligand must be known, either from computational methods such as DFT optimizations or from the crystal structure (Figure 56). Furthermore, the distance between the coordinating atom and the central atom has a high impact on the buried volume of a ligand. Of course, the buried volume of one imido ligand can

differ in diverse metal complexes (e.g. resulting from different bond lengths and geometries). *Sambvca2*[41a] (former *Sambvca*[41b]), developed by *Cavallo et al*., is an online tool for the determination of V_{bur}. The software requires the geometry of the ligand and the distance between the coordinating atom and the metal atom for calculations. The radius of the coordination sphere is 3.5 Å in the default settings but can be changed by the user. The buried volume is then determined by dividing the coordination sphere into voxels (3D pixels) and adding up every voxel that is within the van der Waals radius of a ligand atom. The sum of all voxels is defined as V_{bur}. Buried volume is usually given as percentage of the complete coordination sphere $\%V_{bur}$. All available crystal structures of molybdenum imido alkylidene complexes in the *Buchmeiser* group have been used to determine quantitative differences in the steric demand of commonly used imido ligands.[14-16,17b,18,78,167-168,168f,169-170,183,191]

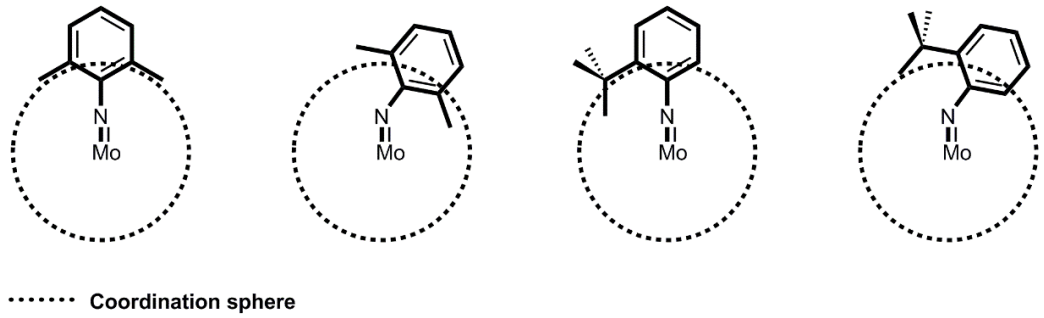

Figure 57: Influence of Mo-N_{Imido}-$C_{1,Imido}$ angle on buried volume in asymmetrically and symmetrically substituted imido ligands.

$\%V_{bur}$ was once determined for the actual M-N_{imido} bond length and once for the average M-N_{imido} bond length to account for eventual differences (Figure 58 and Table 8). As expected, the *tert*-butylimido and the adamantly imido ligand display decreased $\%V_{bur}$ in comparison to the aryl based imido ligands. Interestingly, for the aryl based ligands, the parameter with the highest impact on the buried volume, irrespective of the 2,6-substituents is the angle between Mo-N_{Imido}-$C_{1,Imido}$ (Figure 57). For symmetrically substituted imido ligands (*N*-2,6-Cl_2-C_6H_3, *N*-2,6-Me_2-C_6H_3, *N*-2,6-iPr_2-C_6H_3) $\%V_{bur}$ decreases with increasing Mo-N_{Imido}-$C_{1,Imido}$ angle. For the asymmetrically substituted 2-*tert*-butylphenylimido ligand $\%V_{bur}$ decreases with decreasing Mo-N_{Imido}-$C_{1,Imido}$ angle, since the substituent can point away from the coordination sphere. Of course, all those values only hold up in the solid state, in solution rotational processes take place.

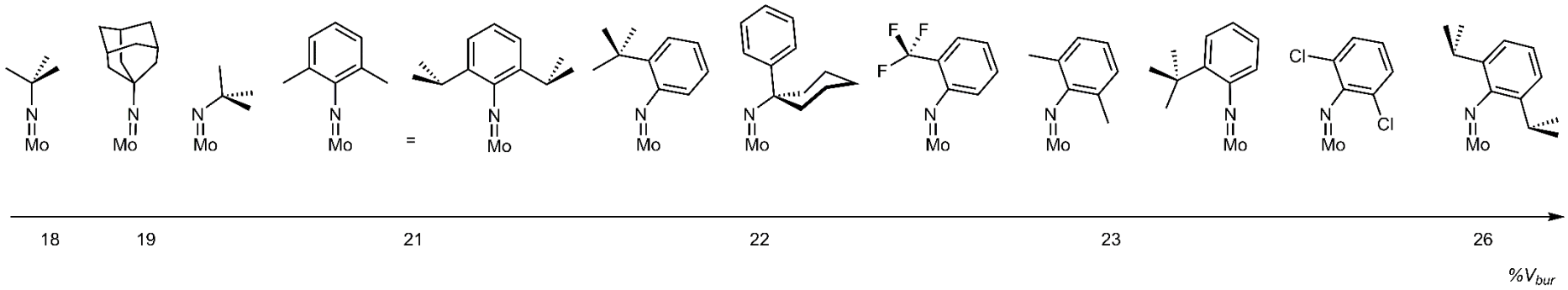

Figure 58: Schematic view of $\%V_{bur}$ of imido ligands, listed according to increasing $\%V_{bur}$ in Table 8 (distance = 1.73 Å) from left to right. Influence of the Mo-N_{Imido}-C_{imido} angle. For the aryl based ligands, the parameter with the highest impact on the buried volume, irrespective of the 2,6-substituents is the angle between Mo-N_{Imido}-$C_{1,Imido}$. For symmetrically substituted imido ligands (*N*-2,6-Cl_2-C_6H_3, *N*-2,6-Me_2-C_6H_3, *N*-2,6-iPr_2-C_6H_3) $\%V_{bur}$ decreases with increasing Mo-N_{Imido}-$C_{1,Imido}$ angle. For the asymmetrically substituted 2-*tert*-butylphenylimido ligand $\%V_{bur}$ decreases with decreasing Mo-N_{Imido}-$C_{1,Imido}$ angle, since the substituent can point away from the coordination sphere.

Table 8: Buried volume *%V_{bur}* for complexes of the type Mo(NR^1)(CR^2)(OTf)(OR^3)(NHC), listed according to imido ligand.[14-16,17b,18,78,167-168,168f,169-170,183,191]

Formula	#	Mo-N_{Imido}-C_{Imido} [°][a]	%V_{bur} for M-N_{Imido} = 2 Å[b]	%V_{bur} for M-N_{Imido} = 1.73 Å[b,c]	%V_{bur} for actual M-N_{Imido}[b]	M-Imido [Å] [a]
Mo**(N-2,6-Cl_2-C_6H_3)**($CHCMe_3$)($OTf)_2$(IMes)	**Mo-23**	154.8314	23.8	27.2	27.2	1.73
Mo**(N-2,6-Cl_2-C_6H_3)**($CHCMe_3$)($OTf)_2$($IMesH_2$)	**Mo-32**	156.0214	23.7	27	27	1.73
Mo**(N-2,6-iPr_2-C_6H_3)**($CHCMe_2Ph$)(OTf)(*N*-Dipp-*N*'-2-O-C_6H_4)	**Mo-33**	153.9717	25.8	29.6	29.5	1.74
Mo**(N-2,6-iPr_2-C_6H_3)**($CHCMe_2Ph$)($OC_6F_5)_2$($IMesH_2$)	**Mo-34**	172.82	20.7	24.1	23.9	1.75
Mo**(N-2,6-iPr_2-C_6H_3)**($CHCMe_2Ph$)(OC_6F_5)(*N*-dipp-*N*'-2-O-C_6H_4)	**Mo-35**	158.36	23.1	26.8	26.7	1.74
Mo**(N-2,6-Me_2-C_6H_3)**($CHCMe_2Ph$)(OTf)(*N*-Mes-*N*'-2-O-C_6H_4)	**Mo-36**	156.23	22.6	25.9	25.7	1.74
Mo**(N-2,6-Me_2-C_6H_3)**(CH-o-OMe-Ph) ($OTf)_2$(IMes)	**Mo-24**	170.43	21.4	24.7	24.9	1.71
[Mo**(N-2,6-Me_2-C_6H_3)**($CHCMe_2Ph$)(OTf)(IMes-Pic)][$B(Ar^F)_4$]	**Mo-13**	169.43	21.5	27.3	25.1	1.71
Mo**(N-2,6-Me_2-C_6H_3)**($CHCMe_2Ph$)($OTf)_2$(IMes-Pic)	**Mo-12**	177.64	20.9	24.2	24.2	1.73
Mo**(N-2,6-Me_2-C_6H_3)**($CHCMe_2Ph$)($OTf)_2$(I*t*Bu)	**Mo-37**	176.81	21	24.3	24.5	1.72
[Mo**(N-2-CF_3-C_6H_4)**($CHCMe_2Ph$)(ODFT)(5-Me-Cl_2)][$B(Ar^F)_4$]	**Mo-38**	167.5	22.6	25.8	25.6	1.75
[Mo**(N-2-*t*Bu-C_6H_4)**($CHCMe_2Ph$)(OTf)(IMes)][$B(Ar^F)_4$]	**Mo-39**	172.0213	21.7	25.2	25.2	1.73
Mo**(N-2-*t*Bu-C_6H_4)**($CHCMe_2Ph$)($OTf)_2$(IMes)	**Mo-20**	174.7518	23.2	26.5	26.5	1.73
Mo**(N-2-*t*Bu-C_6H_4)**($CHCMe_2Ph$)($OTf)_2$(ICy)	**Mo-40**	168.321	22.1	25.6	25.6	1.73
Mo**(N-PhCy)**($CHCMe_2Ph$)($OTf)_2$(IMes)	**Mo-41**	163.02	22	25.6	26	1.70
Mo**(N-Ad)**($CHCMe_2Ph$)($OTf)_2$(ICy)	**Mo-42**	169.611	19.1	22.3	22.6	1.70
[Mo**(N-*t*Bu)**($CHCMe_3$)(OHIPT)(5-Me-Cl_2)][$B(Ar^F)_4$]	**Mo-43**	176.55	18.7	21.8	21.7	1.74
Mo**(N-*t*Bu)**($CHCMe_3$)($OC_6F_5)_2$(5-Me-Cl_2)	**Mo-44**	164.5118	19.4	22.6	22.6	1.73

[a] *Data from single crystal X-ray crystallography;* [b] *Data derived from calculation with Sambvca2[41a];* [c] *1.73 Å is the average M-N_{imido} bond length taken from all available crystal data of molybdenum imido NHC alkylidene complexes in the Buchmeiser group. IMes: 1,3-dimesitylimidazol-2-ylidene, $IMesH_2$: 1,3-dimesitylimidazolin-2-ylidene, ICy: 1,3-diicyclohexylimidazol-2-ylidene, ItBu: 1,3-di-tert-butylimidazol-2-ylidene, 5-Me-Cl2: 4,5-Cl_2-1,3-Me_2-imidazol-2-ylidene, Dipp: 2,6-diisopropylphenyl, Pic: 2-pyridylmethyl, Ad: adamantyl, ODFT: decafluoroterphenoxide, OHIPT: 2,6-(Dipp)-phenol.*

6.4.5 *Coordination of N-heterocyclic carbenes to MAP-type complexes*

Since a multitude of chiral MAP-type complexes bearing the chiral monoprotected ligand **13** were already published, attempts were made to coordinate NHCs to literature-known chiral catalysts.[21d,21e,91b] It was suspected, that MAP-type complexes are electrophilic enough to take up a further σ-donor (NHC). The aim was to first introduce the NHC and then remove the residual pyrrolide ligand by protonation with *N*,*N*-dimethyl anilinium $B(Ar^F)_4$ to afford cationic chiral molybdenum imido alkylidene NHC complexes. Syntheses of the MAP-type complexes **Mo-48** - **Mo-50**, based on the *N*-2,6-diisopropylphenyl, *N*-2-*tert*-butylphenyl and the *N*-*tert*-butylimido ligand, started from the corresponding bispyrrolide complexes **Mo-P6** - **Mo-P8**.[21d,21e,98b] **Mo-P6** - **Mo-P8** were synthesized from the bistriflate precursors $Mo(NR^1)(CHR^2)(OTf)_2(DME)$ in accordance with the literature.[22a] However, no conversion of the MAP-type complexes **Mo-48** – **Mo-50** with 1,3-diisopropylimidazol-2-ylidene and IMes was observed in all cases (Scheme 57), irrespective of the solvent (toluene, diethyl ether) and temperature (room temperature and 60°C) applied.

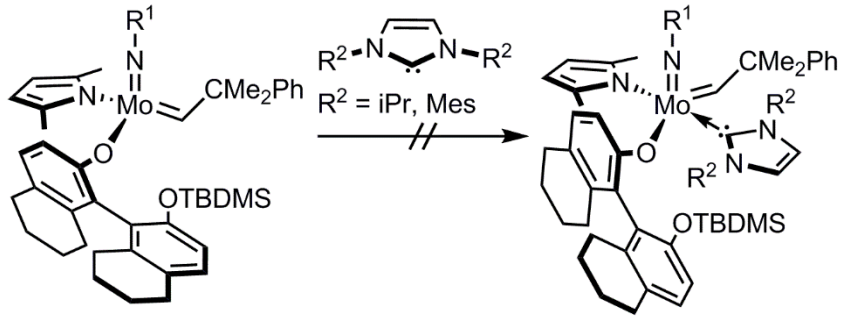

Mo-48: R^1 = 2,6-iPr_2-C_6H_3 **Mo-51**: R^1 = 2,6-iPr_2-C_6H_3, R^2 = iPr **Mo-54**: R^1 = 2,6-iPr_2-C_6H_3, R^2 = Mes
Mo-49: R^1 = 2-*t*Bu-C_6H_4 **Mo-52**: R^1 = 2-*t*Bu-C_6H_4, R^2 = iPr **Mo-55**: R^1 = 2-*t*Bu-C_6H_4, R^2 = Mes
Mo-50: R^1 = *t*Bu **Mo-53**: R^1 = *t*Bu, R^2 = iPr **Mo-56**: R^1 = *t*Bu, R^2 = Mes

Scheme 57: Attempted synthesis of chiral molybdenum imido alkylidene NHC complexes **Mo-51** - **Mo-53** by conversion of literature-known chiral MAP-type complexes **Mo-48** - **Mo-50** with NHCs.

Apart from that, coordination of NHCs to MAP-type complexes has been further pursued with other chiral alkoxides by *Andreas Hans* in his bachelor thesis.[197] He in fact succeeded in the synthesis of one chiral molybdenum imido alkylidene NHC complex, however with a different, less sterically demanding fenchol-derived alkoxide ligand (Figure 59).

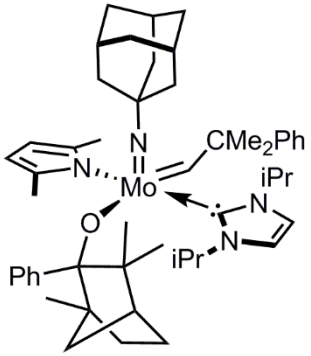

Mo-57

Figure 59: First molybdenum imido alkylidene NHC complex **Mo-57** containing a chiral fenchol derivative synthesized by *Andreas Hans* during his Bachelor thesis.

Unfortunately, **Mo-57** showed low activity and provided only one of the bench-mark substrates in low yield in a racemic mixture (according to GC-MS). In addition, A. Hans observed *CH*-activation in case alkoxide introduction was attempted *via* attachment of the lithium alkoxide to a molybdenum imido alkylidene bistriflate NHC complex.

6.4.6 *Molybdenum imido alkylidene bispyrrolide N-heterocyclic carbene complexes*

Apart from the usage of small imido and NHC ligands, another attempt to introduce sterically demanding, chiral, monoprotected biphenolates and binaphtholates to molybdenum imido alkylidene NHC complexes was pursued. The molybdenum imido alkylidene bispyrrolide complexes published by *Schrock et al.* in 2006 offer the possibility to introduce alkoxides as alcohols by selective protonation of one pyrrolide ligand.[21d,22b,82-83,198] The same approach should be viable for bispyrrolide NHC complexes. Here, not alkoxides but alcohols are applied in the ligand exchange reactions, therefore *CH*-activation is unlikely to occur (Scheme 58).

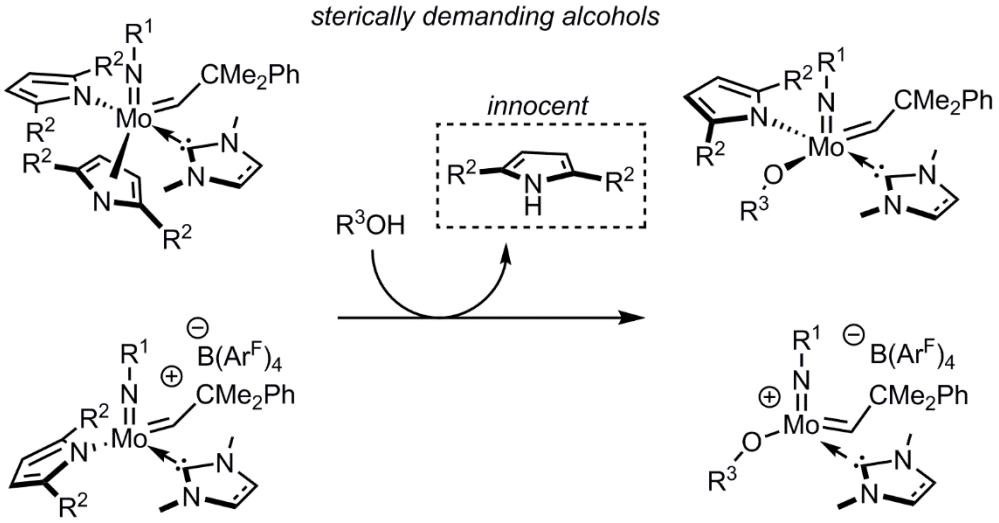

Scheme 58: Envisioned introduction of sterically demanding alcohols to molybdenum imido alkylidene bispyrrolide NHC complexes. No *CH*-activation expected, since no sterically demanding bases are present.

Consequently, several bispyrrolide complexes (**Mo-P6** - **Mo-P9**) were synthesized *via* conversion of bistriflate complexes (Mo(*N*-2,6-iPr$_2$-C$_6$H$_3$)(CHCMe$_2$Ph)(OTf)$_2$(DME) **Mo-P10**, **Mo-P1** - **Mo-P3**) with lithium 2,5-dimethylpyrrolide in accordance with literature.[22a]

Mo-P6: R^1 = 2,6-iPr$_2$-C$_6$H$_3$
Mo-P7: R^1 = 2-*t*Bu-C$_6$H$_4$
Mo-P8: R^1 = *t*Bu
Mo-P9: R^1 = 2,6-Me$_2$-C$_6$H$_3$

Mo-58: R^1 = 2,6-iPr$_2$-C$_6$H$_3$, R^2 = iPr
Mo-59: R^1 = 2-*t*Bu-C$_6$H$_4$, R^2 = iPr
Mo-60: R^1 = *t*Bu, R^2 = iPr
Mo-61: R^1 = 2,6-Me$_2$-C$_6$H$_3$, R^2 = iPr

Mo-62: R^1 = 2,6-iPr$_2$-C$_6$H$_3$, R^2 = Mes
Mo-63: R^1 = 2-*t*Bu-C$_6$H$_4$, R^2 = Mes
Mo-64: R^1 = *t*Bu, R^2 = Mes
Mo-65: R^1 = 2,6-Me$_2$-C$_6$H$_3$, R^2 = Mes

Scheme 59: Attempted conversion of bis(2,5-dimethylpyrrolide) molybdenum imido alkylidene complexes **Mo-P6** - **Mo-P9**, containing varying imido ligands, with NHCs.

However, when those bispyrrolide complexes were reacted with NHCs in benzene or diethyl ether, either no conversion (for IMes) or deprotonation at the alkylidene moiety (for IiPr) was observed by ^{1}H NMR spectroscopy of the reaction mixtures (Scheme 59). In the following, bispyrrolide complexes with the parent pyrrolide instead of the 2,5-dimethylpyrrolide ligand were synthesized. Since bispyrrolide complexes containing the less bulky pyrrolide ligand exhibit a dimeric structure in solution,[22b] the hypothesis was that they would be more likely to coordinate an additional donor ligand (NHC). In fact, *Schrock et al.* showed, that dimeric $[Mo(NAd)(CHCMe_2Ph)(NC_4H_4)_2]_2$ (**Mo-66**) forms a phosphine adduct $Mo(NAd)(CHCMe_2Ph)(NC_4H_4)_2(PMe_3)$ (**Mo-67**) upon addition of two equivalents of PMe_3 (Figure 60).[198]

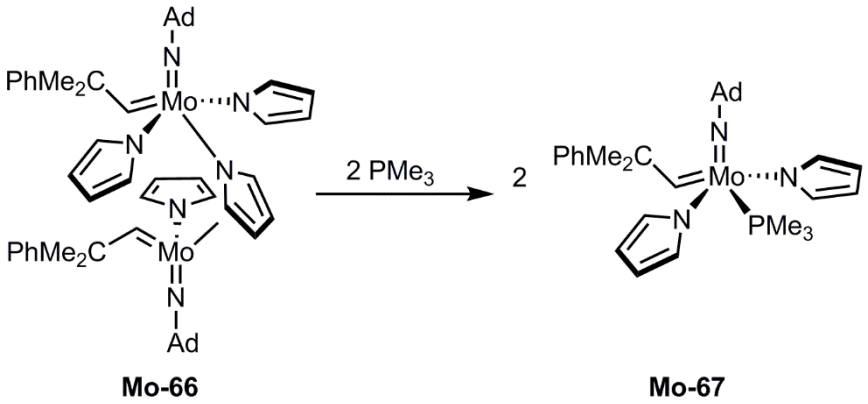

Figure 60: Addition of PMe_3 to a dimeric parent pyrrolide complex under formation of a phosphine adduct.[198]

To verify this hypothesis, a bispyrrolide complex with the 2-*tert*-butylphenylimido ligand Mo(*N*-2-*t*Bu-C_6H_4)$(CHCMe_2Ph)(NC_4H_4)_2$ (**Mo-68**) was synthesized. The conversion of **Mo-68** with IMes lead to the immediate precipitation of a light yellow solid from the diethyl ether solution. In case the solid was dissolved in CH_2Cl_2 or THF, the solution immediately turned red and in the ^{1}H NMR spectrum no residual alkylidene protons were visible. It is likely that the desired NHC adduct **Mo-69** forms but is highly unstable in solution and decomposes to afford the alkylidyne complex **Mo-70** (Scheme 60).

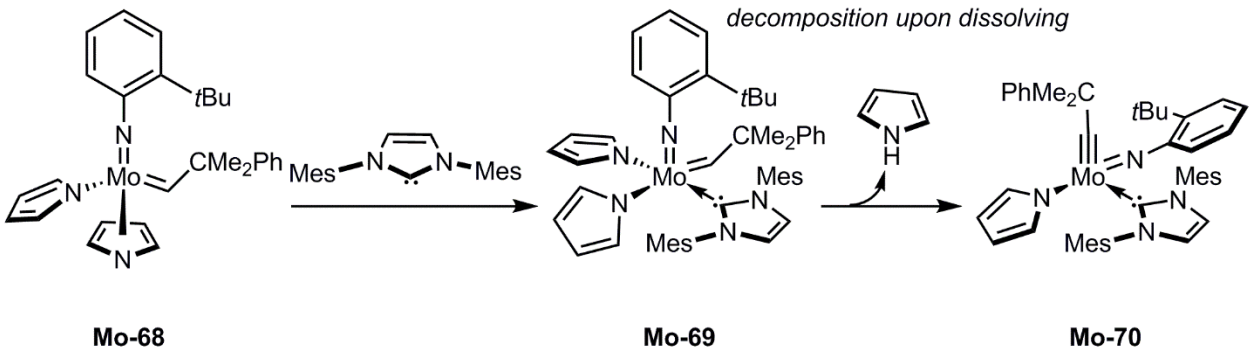

Scheme 60: Proposed decomposition of the obtained solid from reaction of **Mo-68** with IMes upon dissolving under α-hydrogen-abstraction by pyrrole elimination and alkylidyne formation.

Most probably, the deprotonation of the alkylidene moiety occurs after dissociation of one pyrrolide ligand because of electronic saturation and steric constraint at the molybdenum center (**Mo-69**, Scheme 60). To prevent deprotonation of the alkylidene moiety, a solution of *N,N*-dimethyl anilinium $B(Ar^F)_4$ in diethyl ether was added *in situ* to the yellow precipitate, to offer a proton to the pyrrolide ligand and enable direct access to the hypothetical cationic molybdenum imido monopyrrolide NHC complex. No desired product could be observed by ^1H NMR spectroscopy. However, upon reaction of **Mo-68** with 1,3-diisopropylimidazol-2-ylidene the pure desired product Mo(*N*-2-*t*Bu-C_6H_4)(CHCMe$_2$Ph)(NC_4H_4)$_2$(1,3-diisopropylimidazol-2-ylidene) (**Mo-71**) was successfully isolated from the reaction mixture in diethyl ether after three hours in 93% yield (Scheme 61).

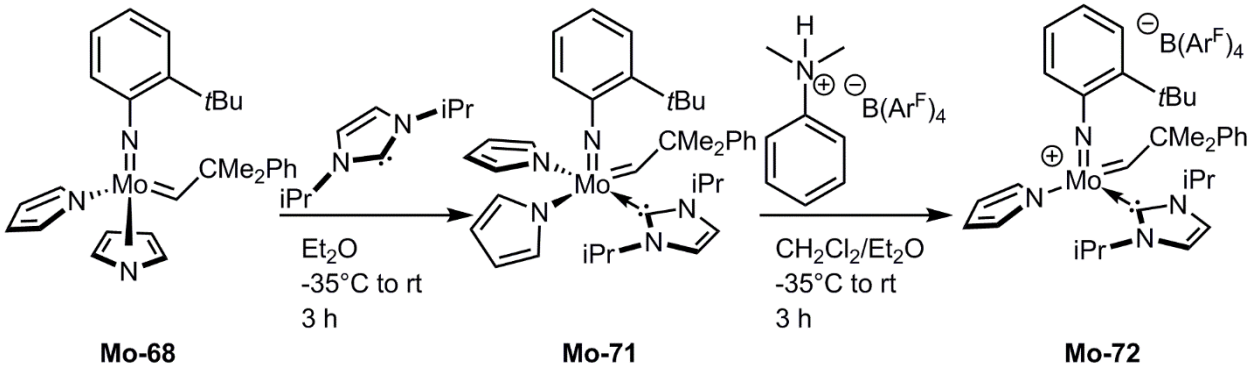

Scheme 61: Synthesis of the first molybdenum imido alkylidene NHC bispyrrolide complex **Mo-71** and the cationic derivative **Mo-72** (93 % and quantitative yield, respectively).

The ^1H NMR spectrum of Mo(*N*-2-*t*Bu-C_6H_3)(CHCMe$_2$Ph)(1,3-diisopropylimidazol-2-ylidene)(NC_4H_4)$_2$ (**Mo-71**) does not allow for the clarification whether the pyrrolide ligands bind η^1 or η^5 to the molybdenum center. All pyrrolide based aromatic signals appear with an integral of two protons (δ = 7.29, 6.85, 6.39 and 6.18 ppm). This could hint to a structure in which the pyrrolide ligands exhibit different coordination modes for example η^1 and η^5 or take different coordination sites in a trigonal bipyramidal or square pyramidal structure. Mo(*N*-2-*t*Bu-C_6H_4)(CHCMe$_2$Ph)(1,3-diisopropylimidazol-2-ylidene)(NC_4H_4)$_2$ (**Mo-71**) was protonated with *N,N*-dimethylanilinium $B(Ar^F)_4$ in CH_2Cl_2 and diethyl ether to yield the corresponding cationic mono pyrrolide NHC complex **Mo-72** in quantitative yield after washing with pentane to remove the resulting aniline and pyrrole (Scheme 61).

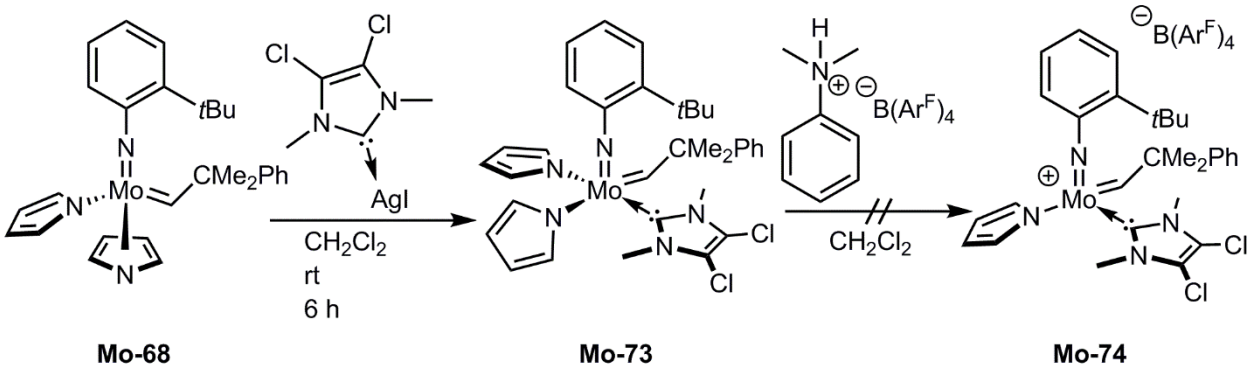

Scheme 62: Synthesis of the bispyrrolide NHC complex **Mo-73** with the sterically less demanding 4,5-dichloro-1,3-dimethyl imidazol-2-ylidene in 57% yield and attempted synthesis of the corresponding cationic complex **Mo-74**.

In view of the fact, that the 1,3-dimesitylimidazolin-2-ylidene as well as the 1,3-diisopropylimidazol-2-ylidene ligand can easily be *CH*-activated under formation of 5- or 6- ring chelates, 4,5-dichloro-1,3-dimethylimidazol-2-ylidene was investigated in the reaction with the bispyrrolide complex **Mo-68**. 4,5-Dichloro-1,3-dimethylimidazol-2-ylidene should not easily be *CH*-activated since *CH*-activation would result in the formation of a four-membered chelate. In fact, Mo(*N*-2-*t*Bu-C_6H_3)(CHCMe$_2$Ph)(NC_4H_4)$_2$(4,5-dichloro-1,3-dimethylimidazol-2-ylidene) **Mo-73** was obtained in 57% yield *via* reaction of **Mo-68** with the silver iodide salt of 4,5-dichloro-1,3-dimethylimidazol-2-ylidene in CH_2Cl_2 at room temperature and subsequent crystallization from a mixture of CH_2Cl_2, diethyl ether and pentane (Scheme 62). The pyrrolide ligands in **Mo-73**, comparable to those in **Mo-71**, seemingly also either exhibit different binding modes (η^1 or η^5) or take different coordination sites in a trigonal bipyramidal or square pyramidal ligand sphere. In addition, **Mo-74** was not accessible by protonation of one of the pyrrolide ligands in **Mo-73** with *N,N*-dimethylanilinium B(Ar^F)$_4$ in CH_2Cl_2. It is probable that **Mo-74** is prone to bimolecular decomposition due to the small ligands.

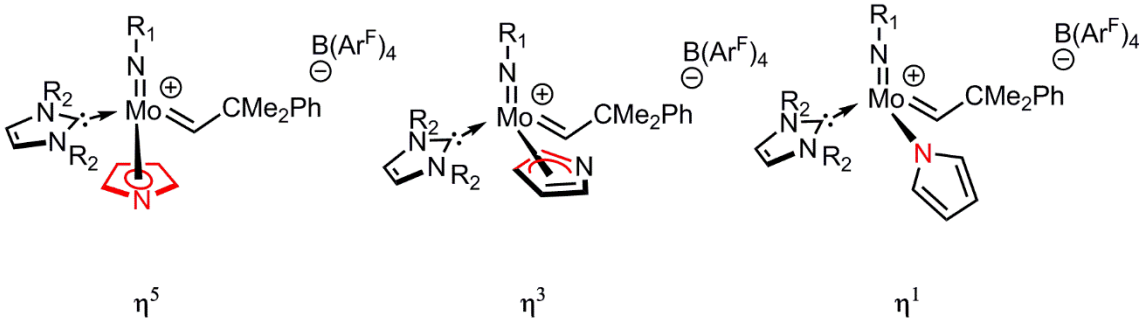

Figure 61: Different coordination modes (η^1, η^3 or η^5) of pyrrolide ligand provide flexibility to the catalyst system.

In molybdenum imido alkylidene bistriflate NHC complexes formation of the metathesis-active species requires formation of a complex with a weakly coordinated triflate and a positive partial charge on the metal center.[167,168e] A correlation between the σ-donor strength (usually described by TEP) and ease of triflate dissociation has been observed. To enable a similar

correlation between reactivity, structure and TEP (NHC) in newly synthesized cationic NHC pyrrolide imido alkylidene complexes, the introduction of a medium donor was of interest, in addition to good σ-donor 1,3-diisopropylimidazol-2-ylidene (TEP = 2051.5[24]) and weak σ-donor 4,5-dichloro-1,3-dimethylimidazol-2-ylidene (TEP = 2059.0[24]), It was expected, that the donor strength of the NHC would influence the binding mode of the pyrrolide ligand. Pyrrolide can coordinate η^1, η^3 or η^5, thereby providing either two, four or six electrons to the metal center (Figure 61). The electron count in turn severely influences catalyst activity. It was suspected, that a weak donor would result in η^5 coordination and a strong donor in η^1 coordination. It was also of interest, whether the binding mode of the pyrrolide ligand could be changed by applying heat.

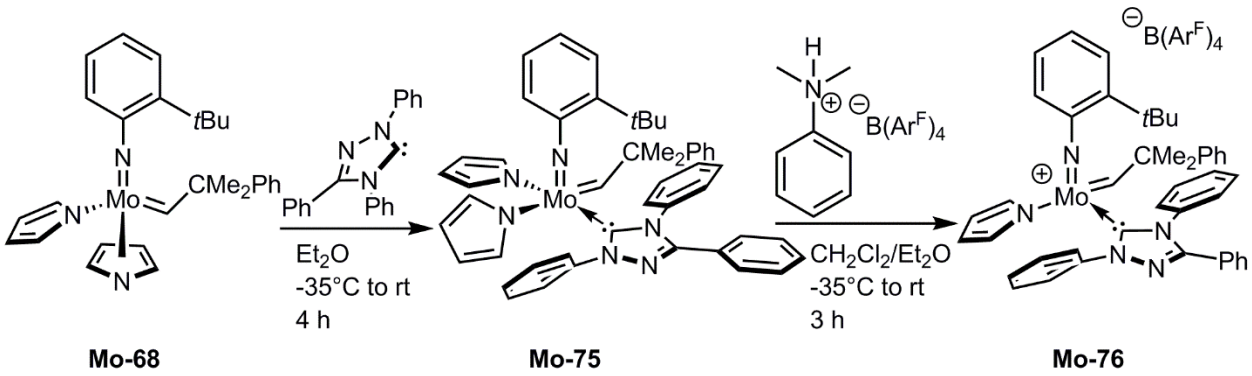

Scheme 63: Synthesis of the bispyrrolide triazolyl-5-ylidene complex **Mo-75** in 62% yield and preparation of the corresponding cationic complex **Mo-76** in 87% yield.

Therefore, additional complex **Mo-75** based on a medium σ-donor (1,3,4-triphenyl-1,2,4-triazol-5-ylidene, TEP = 2057.3[199]) was synthesized by conversion of **Mo-68** with the respective NHC in diethyl ether in 62% yield. Furthermore, **Mo-76** was synthesized by protonation of **Mo-75** with *N*,*N*-dimethyl anilinium $B(Ar^F)_4$ in CH_2Cl_2 and diethyl ether in 87% yield.

Activity investigations at room temperature and at 80°C showed high activity of **Mo-72** in RCM of 1,7-octadiene. **Mo-72** and **Mo-76** also showed good activity in the RCM of diallyl diphenyl silane, and allyl trimethyl silane as well as in the HM of 1-octene and allyl benzene. However, when functional groups were present (diallylsulfide and diethyl diallyl malonate), activity dropped, most probable due to coordination of the functional group (Table 9). Also, heating to 80°C did not lead to a substantial increase in activity, in some cases TON even dropped. The differences in activity between complexes **Mo-72** and **Mo-76** are not as pronounced as might have been expected due to the differences in the donor properties of their NHC ligands. It is likely that the pyrrolide ligand is already bound in a η^1 fashion in both complexes at room temperature. However, so far, this could not be verified by single crystal X-ray analysis of the respective complexes.

Table 9: Productivities in TON for catalysts **W-4**, **Mo-72** and **Mo-76** in 1,2-dichloroethane at room temperature and 80 °C.

Substrate	**W-4**[a]		**Mo-72**		**Mo-76**	
	rt	**80°C**	**rt**	**80°C**	**rt**	**80°C**
1,7-octadiene	0	1000	1000	1000	590	810
diallyl diphenylsilane	0	340	620	830	710	890
diallyl ether	0	0	730	560	230	0
diethyl diallylmalonate	0	0	40	40	140	60
diallylsulfide	0	0	100	130	0	50
allyl trimethylsilane	-	-	510	510	800	400
1-octene	0/600	600	500	530	490	620
allyl benzene	-	-	430	630	470	620

Reaction conditions: cat:substrate 1:1000, internal standard for GC analysis: dodecane, 3 hours.[a] Repeated for convenience: ***W-4*** *= [W(N-2,6-iPr$_2$-C$_6$H$_3$)(CHCMe$_2$Ph)(2,5-Me$_2$-NC$_4$H$_2$)(1,3-iPr$_2$-imidazol-2-ylidene)][B(Ar^F)$_4$].*

For a comparison of molybdenum- and tungsten-based complexes, **W-4** ([W(*N*-2,6-iPr$_2$-C$_6$H$_3$)(CHCMe$_2$Ph)(2,5-Me$_2$-NC$_4$H$_2$)(1,3-iPr$_2$-imidazol-2-ylidene)][B(Ar^F)$_4$]) was investigated in the same set of reactions and under the same conditions. It seems that the molybdenum complexes are much more reactive than the comparable tungsten complex **W-4**, which does not show any activity at room temperature. However, this might also result from the increased steric bulk of the ligands in the tungsten complex **W-4** compared to the molybdenum complexes: **W-4** contains the 2,5-dimethylpyrrolide instead of the pyrrolide ligand and the *N*-2,6-diisopropylphenylimido *vs.* the *N*-2-*tert*-butylphenylimido ligand.

6.4.7 Introduction of bulky (chiral) ligands to molybdenum imido alkylidene bispyrrolide *N*-heterocyclic carbene complexes - Proof of concept

To proof that molybdenum imido bispyrrolide NHC complexes and the respective cationic molybdenum imido alkylidene pyrrolide B(Ar^F)$_4$ complexes are suitable precursors to complexes with sterically demanding and basic ligands, HMTOH and **13** were introduced to **Mo-72** and **Mo-73**, respectively. MAP-type complexes bearing the OHMT ligand have been shown to be excellent catalysts for (*Z*)-selective metathesis.[61c,75,80,83a,178] Here, selectivity stems from unfavorable steric interactions of the bulky terphenoxide with the metallacyclobutane substituents, ultimately leading to a *cis*-orientation in the olefinic product. To transfer the catalyst design to cationic molybdenum imido alkylidene NHC complexes, which would be expected to be more reactive than the MAP-type catalysts due to increased *Lewis* acidity on the metal center, the synthesis of a cationic complex, bearing the OHMT ligand was pursued.

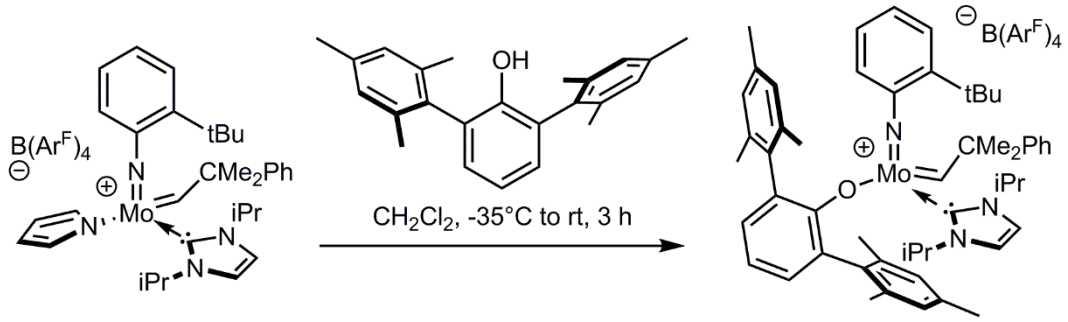

Mo-72 **Mo-77**

Scheme 64: Synthesis of the molybdenum imido alkylidene NHC complex **Mo-77** with the sterically demanding OHMT ligand as cationic mimic of (*Z*)-selective MAP-type complexes (quantitative yield).

HMTOH was reacted with **Mo-72** in CH_2Cl_2 to yield **Mo-77** in quantitative yield after simple washing of the crude reaction mixture with pentane. For further purification **Mo-77** can be crystallized from a mixture of CH_2Cl_2, diethyl ether and pentane. It should be noted that washing with pentane before crystallization is crucial, since the by-product pyrrole seems to interfere with crystallization. When acetonitrile was added to the reaction mixture, **Mo-77** was isolated with an additional acetonitrile ligand. The ^{1}H NMR spectrum of **Mo-77** shows one alkylidene signal at δ = 12.33 ppm in CD_2Cl_2. Also, the signals for the iPr-groups show up as only one heptet (δ = 3.92 ppm, hept, $^3J_{HH}$ = 6.62 Hz) and one doublet (δ =1.26 ppm, d, $^3J_{HH}$ = 6.62 Hz) and are perfectly resolved, indicating only low steric constraint resulting in free rotation of all groups.

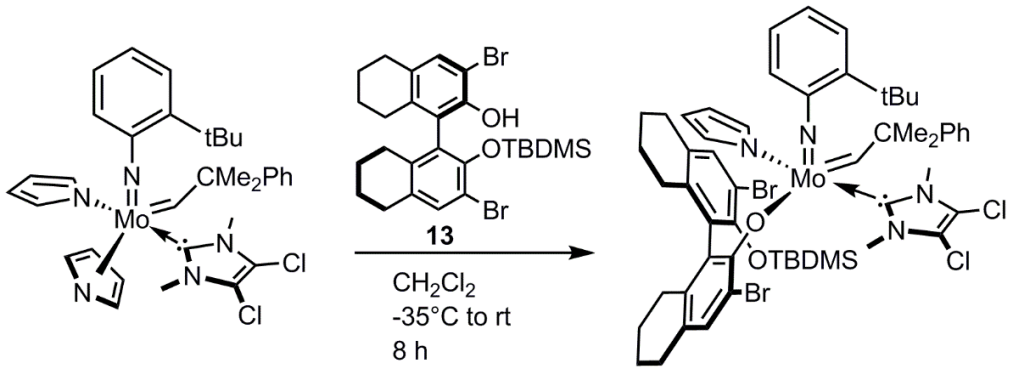

Mo-73 **Mo-78**

Scheme 65: Synthesis of molybdenum imido alkylidene NHC complex **Mo-78** with chiral ligand **13** (quantitative yield).

As outlined above, introduction of chiral monoprotected alkoxides like **13** to molybdenum imido alkylidene NHC complexes was envisioned to result in a new type of chiral metathesis-active complexes with eventual new reactivities. Consequently, **Mo-78** was synthesized from **Mo-73** and **13** in CH_2Cl_2 (Scheme 65). After eight hours, **Mo-78** can be isolated after simple washing as a sticky foam. The ^{1}H NMR spectrum of **Mo-78** in CD_2Cl_2 shows one alkylidene signal at δ = 13.14 ppm and one broad resonance for the methyl substituents at the imidazole-2-ylidene

at δ = 3.12 ppm. The residual pyrrole ligand resonances appear as multiplets at δ = 5.84 ppm and δ = 6.62 ppm.

The isolation of **Mo-77** and **Mo-78** clearly highlights the advantages of the “bispyrrolide-route”, since conversions are quantitative and the only by-products- pyrrole and *N*,*N*-dimethylaniline- can easily be removed. Beneficially, *CH*-activation and alkylidene proton abstraction were avoided by usage of alcohols instead of lithium or potassium alkoxides to introduce the X-type ligand.

6.4.8 *OUTLOOK*

Molybdenum imido alkylidene bispyrrolide NHC complexes offer the possibility to introduce bulky (chiral) ligands under circumvention of *CH*-activation. Furthermore, comparable to the synthesis of MAP-type complexes, coordination of a chiral bulky ligand to a cationic mono pyrrolide NHC complex leads to the formation of the desired complex and pyrrole. As already outlined by the *Schrock* group[22b] and underlined by the finding that pyrrole is a suitable solvent for biphasic metathesis reactions (*vide supra*, 6.1.4), pyrrole does not interfere with olefin metathesis. This severely facilitates catalyst screening. Obviously, the derived complexes must be tested in asymmetric and (*Z*)-selective reactions to investigate their performance in terms of activity and selectivity.

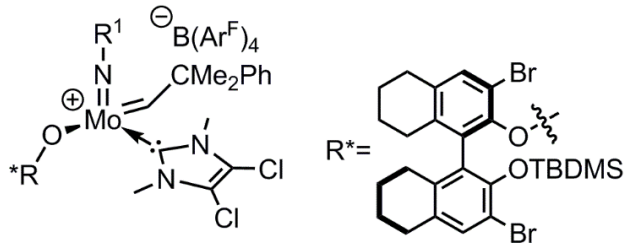

Mo-79: R^1 = 2-*t*Bu-C_6H_4
Mo-80: R^1 = *t*Bu

Figure 62: Cationic target complex **Mo-79** with a small NHC and a chiral ligand.

Also, it would be advantageous to convert **Mo-78** to its cationic counterpart **Mo-79** by protonation with *N*,*N*-dimethylanilinium $B(Ar^F)_4$ (Figure 62) to render the complex more active and more fluxionally stable (*vide infra*, optical isomers in pentacoordinated complexes, Figure 50). Furthermore, variations in the imido ligand to the less bulky *tert*-butylimido ligand should be tested in their impact on stereoselectivity (**Mo-80**, Figure 62). Additionally, the cationic imido alkylidene mono pyrrolide NHC complexes themselves are interesting targets. Since the pyrrolide ligand can coordinate either η^1, η^3 or η^5, additional stabilization of the cationic species might occur (Figure 61). Increased stability usually results in higher TON.

6.5 Investigations of structure- reactivity relations in molybdenum alkylidyne *N*-heterocyclic carbene complexes

Parts of the following chapter have already been published. Reprinted (adapted) with permission from (M. Koy, I. Elser, J. Meisner, W. Frey, K. Wurst, J. Kästner, M. R. Buchmeiser, *Chem. Eur. J.* **2017**, *23*, 15484-15490). Copyright (2017) John Wiley and Sons.

6.5.1 Preliminary Results and Working Hypothesis

The concept of NHC coordination to molybdenum or tungsten high oxidation state complexes to enable the synthesis of cationic active species or cationic complexes has been transferred from molybdenum imido alkylidene to molybdenum alkylidyne complexes by *M. Koy* during his master thesis.[10] He synthesized and characterized a variety of molybdenum (and tungsten) NHC complexes with monodentate and tridentate NHC ligands and tested them in the homo metathesis of 1-phenyl-1-propyne (Figure 63). Activity decreased in the order: **Mo-81** ≈ **Mo-82** ≈ **Mo-83** > **Mo-84** ≈ **Mo-86** ≈ **Mo-87** > **Mo-85**.

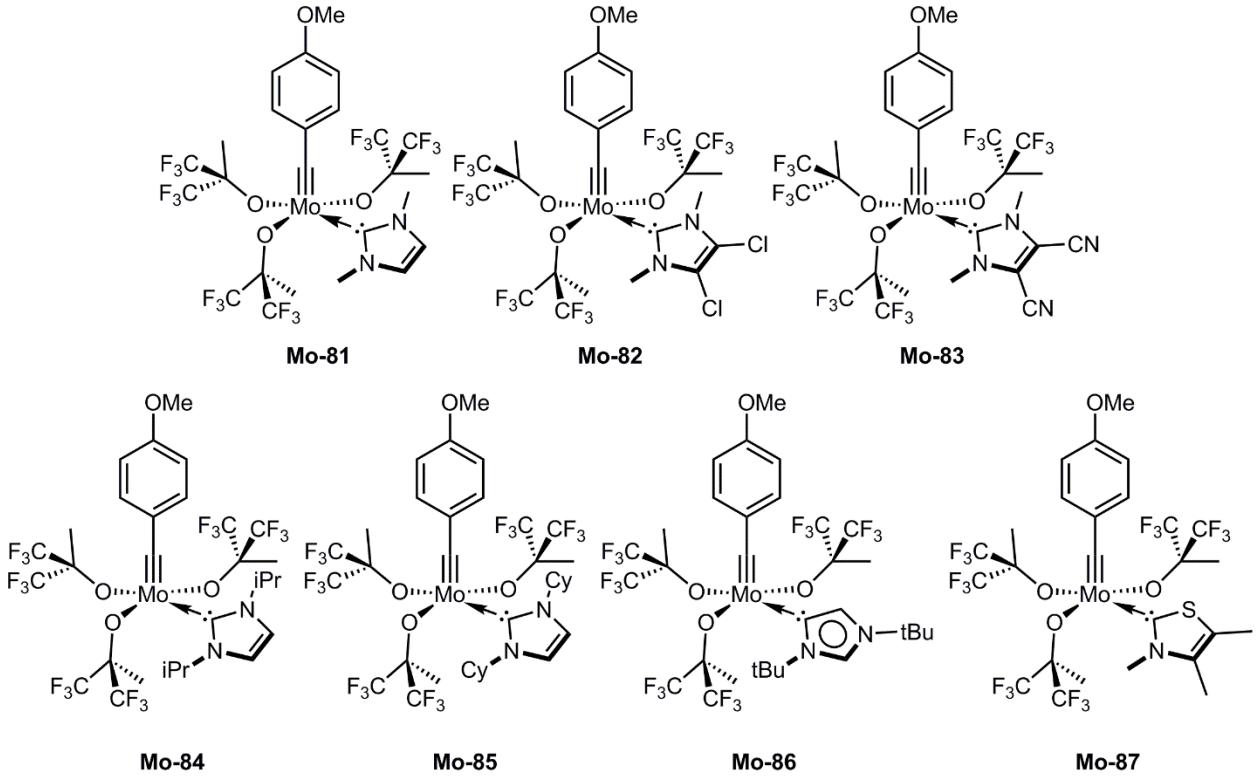

Figure 63: Molybdenum alkylidyne NHC complexes **Mo-81**-**Mo-87** synthesized by *M. Koy*.[10]

However, the mechanism and the active species had not yet been elucidated. Three possible active species can be envisioned. One possibility is that the neutral pentacoordinated $Mo(NHC)(OR)_3$ alkyne complexes are the active species (Figure 64). This, however, would make the described complexes the first pentacoordinated active species observed in alkyne metathesis. The pentacoordinated silanolate-based alkylidyne complexes developed in the

Fürstner group dissociate one ligand *prior* to olefin metathesis.[140,154] Dissociation of one of the ligands before substrate coordination presents an alternate possibility. Here, either the NHC or one of the alkoxide ligands can dissociate, forming a neutral tetracoordinated $Mo(OR)_3$ alkylidyne or a cationic tetracoordinated $Mo(OR)_2$(NHC) alkyne complex, respectively (Figure 64, **A** and **B**). The depiction of the active species as a fully dissociated ion pair (left, Figure 64) does most likely not represent reality. It is more probable that the fluorinated *tert*-butoxide is still coordinated, however with a long Mo-O bond length, therefore best described as a WCA.

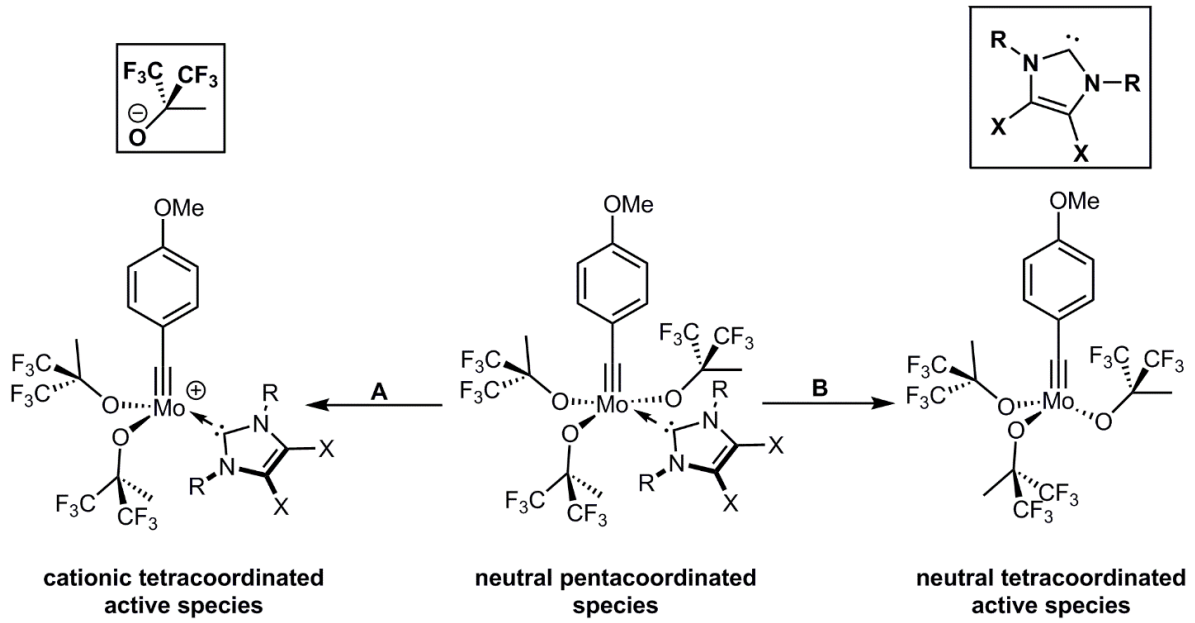

Figure 64: Hypothesized active species for molybdenum NHC alkylidyne complexes. *Left:* Activation *via* pathway **A**: Cationic molybdenum complex with a hexafluoro-*tert*-butoxide anion. Obviously, this is an extreme representation of the real circumstances, most probably the fluorinated *tert*-butoxide is still coordinated to the complex, however with a rather long Mo-$O_{alkoxide}$ bond, serving as a WCA. *Middle:* Neutral pentacoordinated species. *Right:* Activation *via* pathway **B**: Neutral tetracoordinated species.

6.5.2 *Results*

Complexes **Mo-84** - **Mo-87** were synthesized according to the procedures developed by *M. Koy*[10] by conversion of the NHC or the NHC silver salt with $Mo(OC((CF_3)_2Me))_3(\equiv C\text{-}p\text{-}OMe\text{-}C_6H_4)(DME)$ (**Mo-P11**) in toluene. In addition, mechanistic experiments were designed to provide evidence for any of the possible active species. Due to the high basicity of NHCs, it was expected that a dissociated NHC would react irreversibly with a proton source to form the neutral tetracoordinated complex and the corresponding imidazolium salt, which should conveniently be detectable by ^{1}H NMR spectroscopy. Hexafluoro-*tert*-butanol was chosen as the acidic compound, because any ligand exchange reaction with hexafluoro-*tert*-butanolate would not affect the experiment as such. As anticipated, free NHCs (1,3-diisopropyl- and 1,3-dicyclohexylimidazol-2-ylidene) react smoothly with hexafluoro-*tert*-butanol in benzene to form the corresponding imidazolium salts. In the same sequence of experiments, the formation of a species containing only weakly coordinated hexafluoro-*tert*-butoxide can be followed by monitoring the signals of the alkoxides *via* ^{19}F NMR spectroscopy.

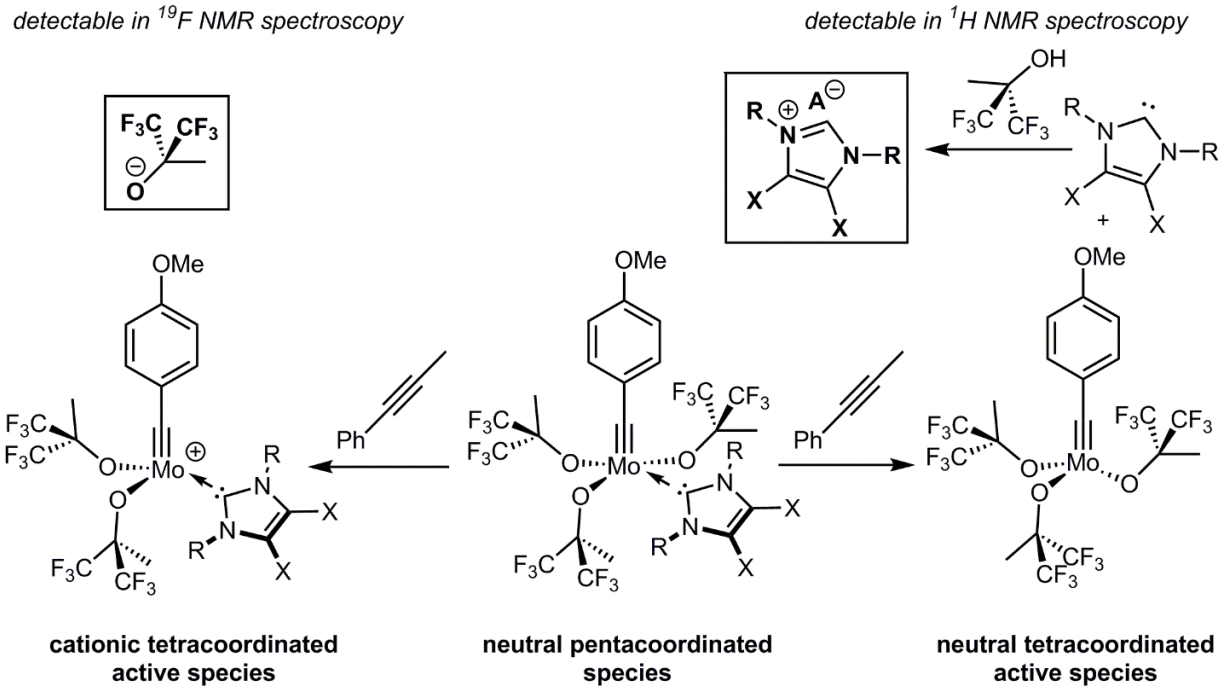

Scheme 66: Design of experiment for determination of active species. Addition of hexafluoro-*tert*-butanol to protonate any dissociated NHC. Detection of imidazolium salt by ^{1}H NMR spectroscopy. Detection of WCA hexafluoro-*tert*-butoxide in ^{19}F NMR spectroscopy.

In a typical experiment, first, the complex was spectroscopically investigated by ^{1}H and ^{19}F NMR spectroscopy in the presence of an internal standard, CH_2Cl_2. Then, hexafluoro-*tert*-butanol was added to the respective complex in C_6D_6 and the potential formation of the imidazolium salt was monitored by ^{1}H NMR spectroscopy. To the same reaction mixture was added 1-phenyl-1-propyne inside a Glove Box. The formation of the imidazolium salt was checked by ^{1}H NMR spectroscopy again. Finally, product formation was proven by GC-MS

analysis of the reaction mixture. On the one hand, **Mo-81**, **Mo-84**, **Mo-85**, **Mo-86** and **Mo-87** showed no dissociation of the NHC by ^{1}H NMR spectroscopy, while very minor but detectable amounts of imidazolium salt were observed for **Mo-82** after addition of substrate and for **Mo-83** after addition of the proton source (<1 % NHC dissociation for both complexes). This hints towards the formation of a neutral tetracoordinated active species.

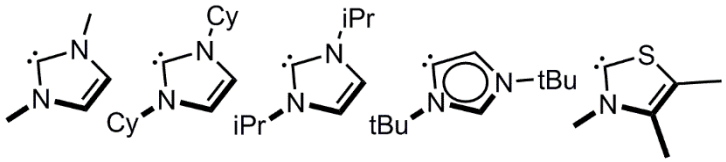

Figure 65: NHCs that did not dissociate during the reaction with 1-phenyl-1-propyne according to ^{1}H NMR spectroscopy.

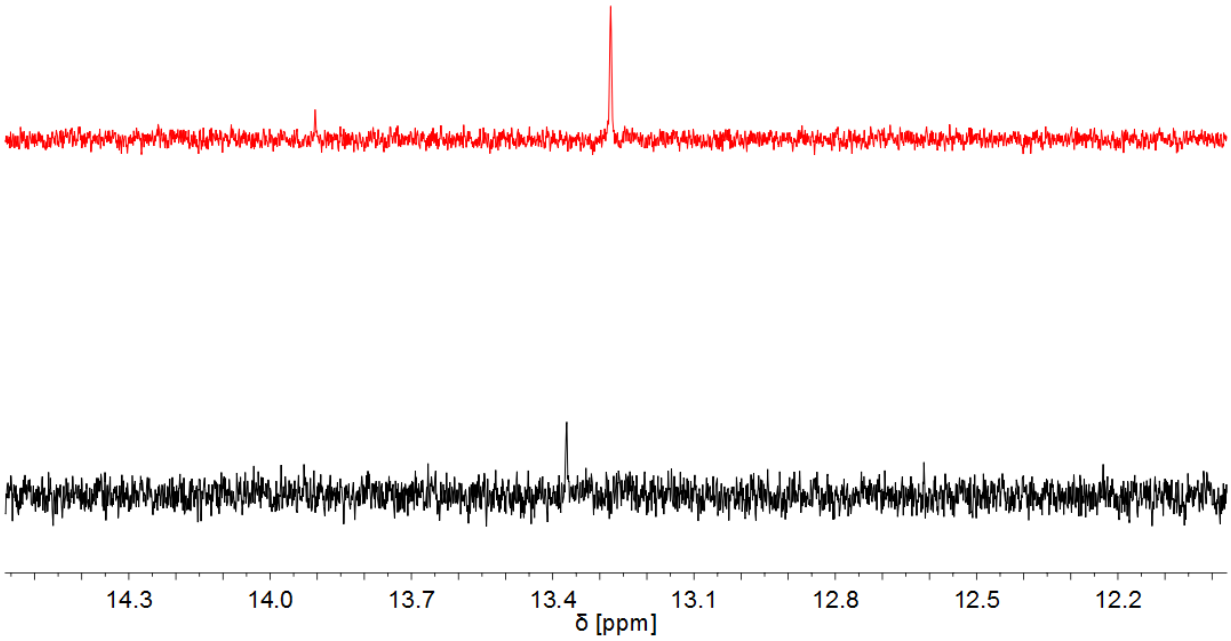

Figure 66: Zoom into the imidazolium region of the ^{1}H NMR spectra of **Mo-82** (black, bottom) after addition of substrate and **Mo-83** (red, top) after addition of hexafluoro-*tert*-butanol in C_6D_6.

On the other hand, upon addition of 1-phenyl-1-propyne to **Mo-84**, **Mo-85** and **Mo-86** a new signal was observed by ^{19}F NMR (δ = -78.58, -78.69 and -78.87 ppm; Figure 67). Those signals were tentatively assigned to weakly coordinated hexafluoro-*tert*-butoxide, resulting from formation of a quasi-cationic active species.

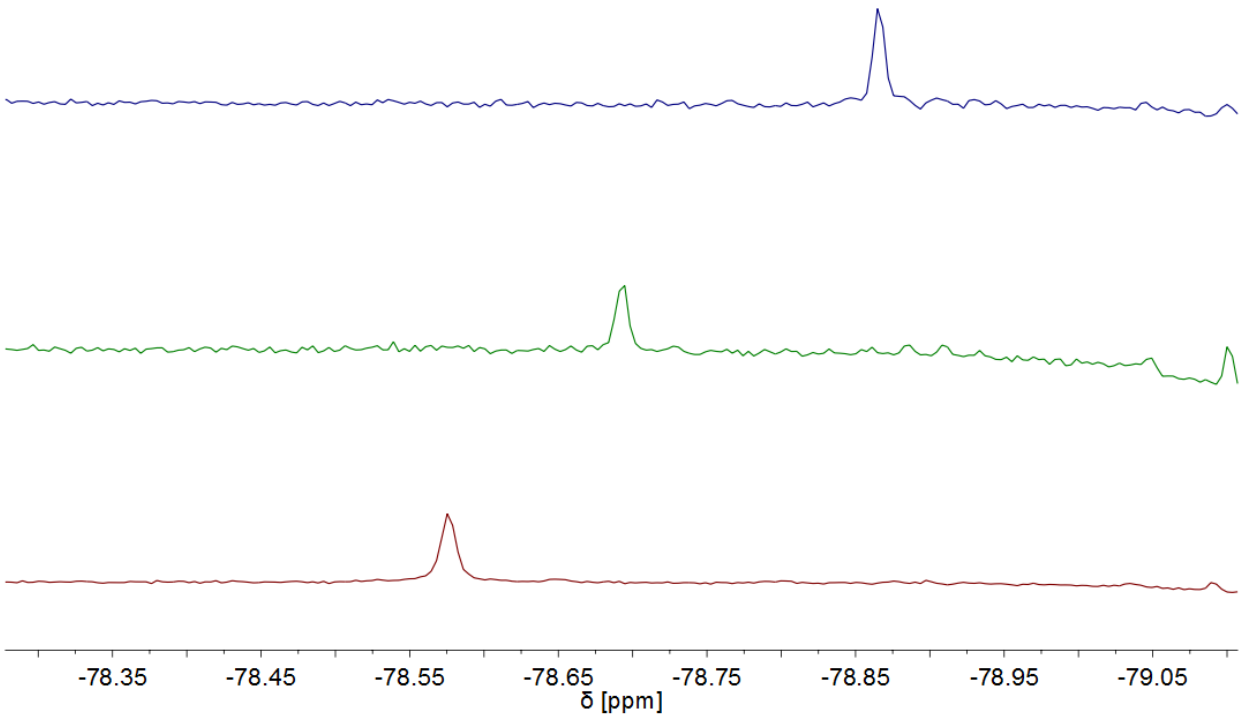

Figure 67: Stacking of ^{19}F NMR spectra of **Mo-84** (red), **Mo-85** (green) and **Mo-86** (blue) after addition of CH_2Cl_2 (internal standard), 1,1,1,3,3,3-hexafluoro-2-methyl-2-propanol and 1-phenyl-1-propyne in C_6D_6. Highlighted resonances: tentatively assigned to weakly coordinated 1,1,1,3,3,3-hexafluoro-2-methyl-2-propanoat.

Additionally, ^{1}H and ^{19}F NMR spectra of **Mo-81** – **Mo-87** were measured in CD_3CN to investigate whether the addition of a coordinating solvent would encourage alkoxide dissociation and the formation of a cationic species. In line with the results outlined above, some minor replacement of the NHC by CD_3CN was observed by ^{19}F NMR spectroscopy for **Mo-82**, **Mo-83** and **Mo-87**(~1 % dissociation). This finding was confirmed by comparison of the corresponding ^{19}F NMR spectra with the ^{19}F NMR spectrum of Mo(OC((CF$_3$)$_2$Me))$_3$(≡C-*p*-OMe-C$_6$H$_4$)(DME) (**Mo-P11**) in CD_3CN. By contrast, for **Mo-81** in CD_3CN two new signals at δ = –78.9 and –76.7 ppm (2:1 ratio) were observed in the ^{19}F NMR spectrum. This is in accordance with the formation of a species, with two chemically and magnetically equivalent hexafluoro-*tert*-butoxides and one hexafluoro-*tert*-butoxide, serving as WCA. Integration revealed ~3 % alkoxide dissociation. **Mo-84** containing the sterically more demanding diisopropylimidazol-2-ylidene, however, showed significant formation of a new species in CD_3CN. In the ^{1}H NMR spectrum, the most prominent new signal was the resonance of the protons adjacent to the nitrogen atoms of the imidazol-2-ylidene at δ = 4.55 ppm (hept, $^3J_{HH}$ = 6.54 Hz) (red, Figure 68).

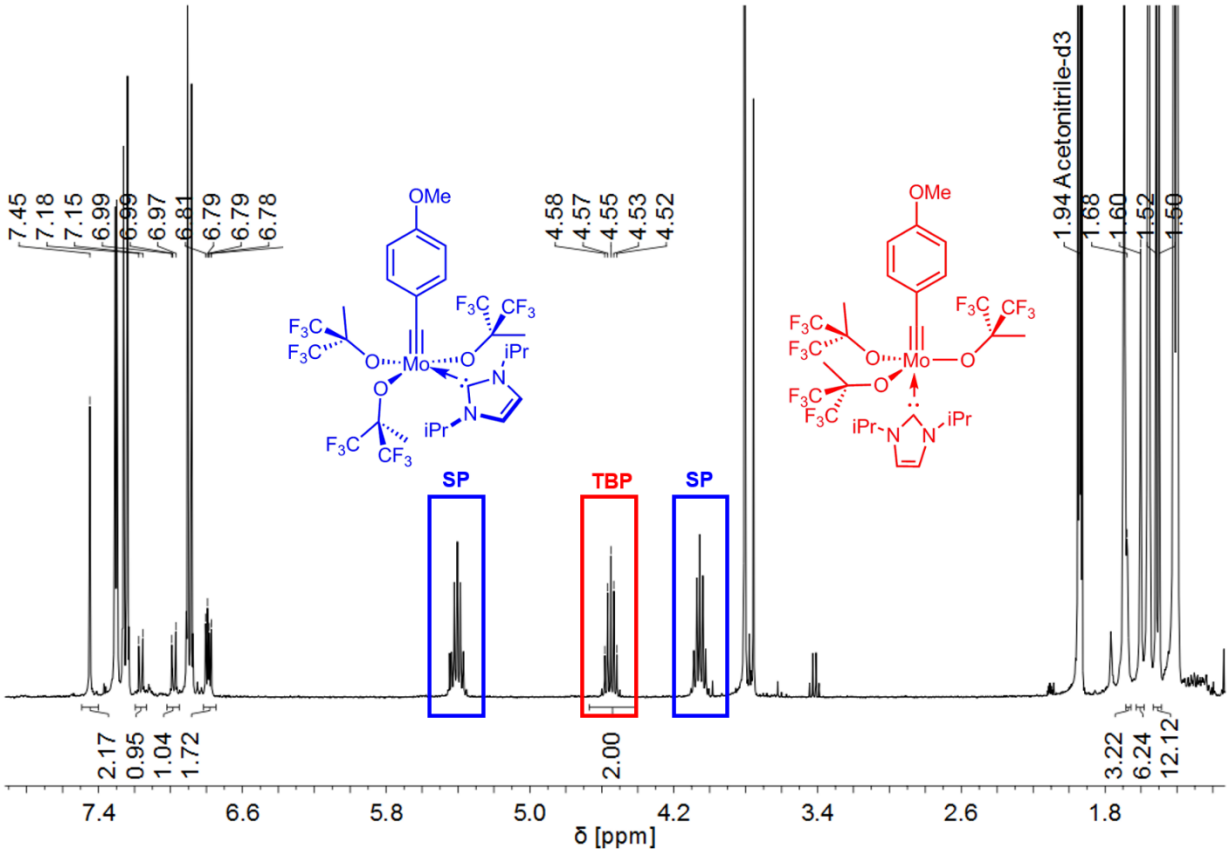

Figure 68: ^{1}H NMR spectrum of **Mo-84** in CD_3CN, 12 hours after dissolving. Resonances of C*H*Me$_2$ of **SP** (blue) and **TBP** (red) structure are highlighted. Only integrals and chemical shifts of TBP structure are displayed for convenience.

By contrast, in the parent complex the signals are split into two pseudo-heptets at δ = 5.40 ppm (hept., $^{3}J_{HH}$ = 6.53 Hz) and δ = 4.05 ppm (hept, $^{3}J_{HH}$ = 6.53 Hz), respectively (blue, Figure 68). This finding can be rationalized by a change of the complex geometry from square pyramidal (SP) in the parent complex to trigonal bipyramidal (TBP) with the NHC in an apical position. Compared to the basal position in the SP configuration, the apex in the TBP would allow for a free rotation of the substituents at the nitrogen atoms of the NHC. This hypothesis is supported by the ^{19}F NMR spectrum of **Mo-84**, in which only *one* new signal can be observed at δ = -76.7 ppm, in line with three magnetically equivalent hexafluoro-*tert*-butoxides in the plane of the TBP complex (red, Figure 69). In contrast, a quasi-cationic complex with one hexa-fluoro-*tert*-butoxide serving as WCA, should show two resonances in the ^{19}F NMR spectrum: One resonance with an integral of twelve (tightly bound hexa-fluoro-*tert*-butoxide) and one resonance with an integral of six (WCA).

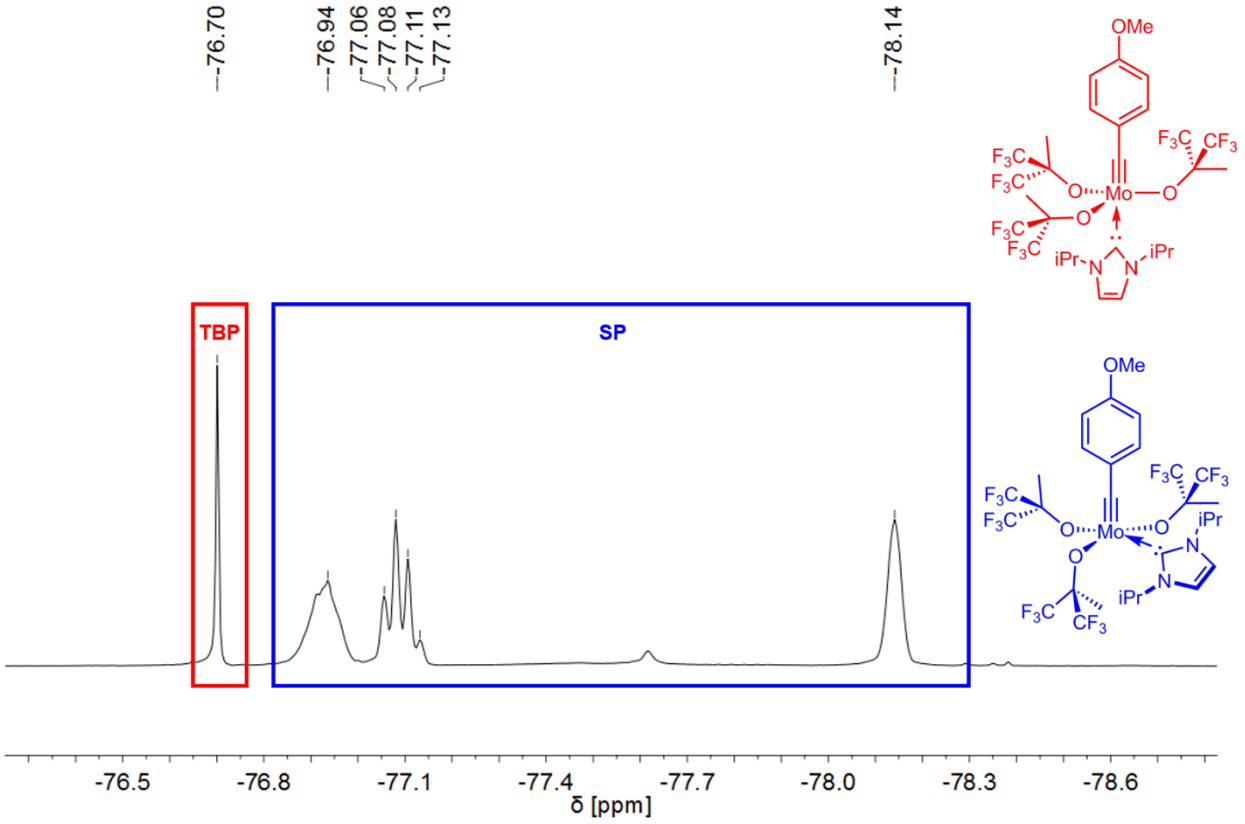

Figure 69: ^{19}F NMR spectrum of **Mo-84** in CD_3CN, 12 hours after dissolving. Resonances of **TBP** structure are highlighted in red, resonances of **SP** structure are highlighted in blue.

According to both ^{1}H and ^{19}F NMR spectroscopy, approximately 12 % of the **Mo-84** reorganized into the TBP geometry after twelve hours in CD_3CN. A comparison of the ^{1}H NMR spectra of free NHC 1,3-diisopropylimidazol-2-ylidene and **Mo-84** in CD_3CN ensured that the new imidazol-2-ylidene signals did *not* stem from dissociated NHC. Whether this reorganization proceeds *via* a cationic species remains speculative. For **Mo-85** a similar reorganization process was observed (Figure A 162, Figure A 163, appendix). A new resonance for the protons on the carbon atoms adjacent to the nitrogen atoms can be observed as a multiplet at δ = 4.22-4.14 ppm. After ten hours in deuterated acetonitrile 30 % of **Mo-85** reorganized into the TBP structure. As observed for **Mo-84**, the ^{19}F NMR spectrum of **Mo-85** in CD_3CN shows only one new resonance at δ = -76.7 ppm. Both, 1,3-diisopropylimidazol-2-ylidene and 1,3-dicyclohexylimidazol-2-ylidene are sterically demanding in comparison to the 1,3-dimethyl substituted imidazol-2-ylidenes, indicating that the observed rearrangement is a result of steric constraint.

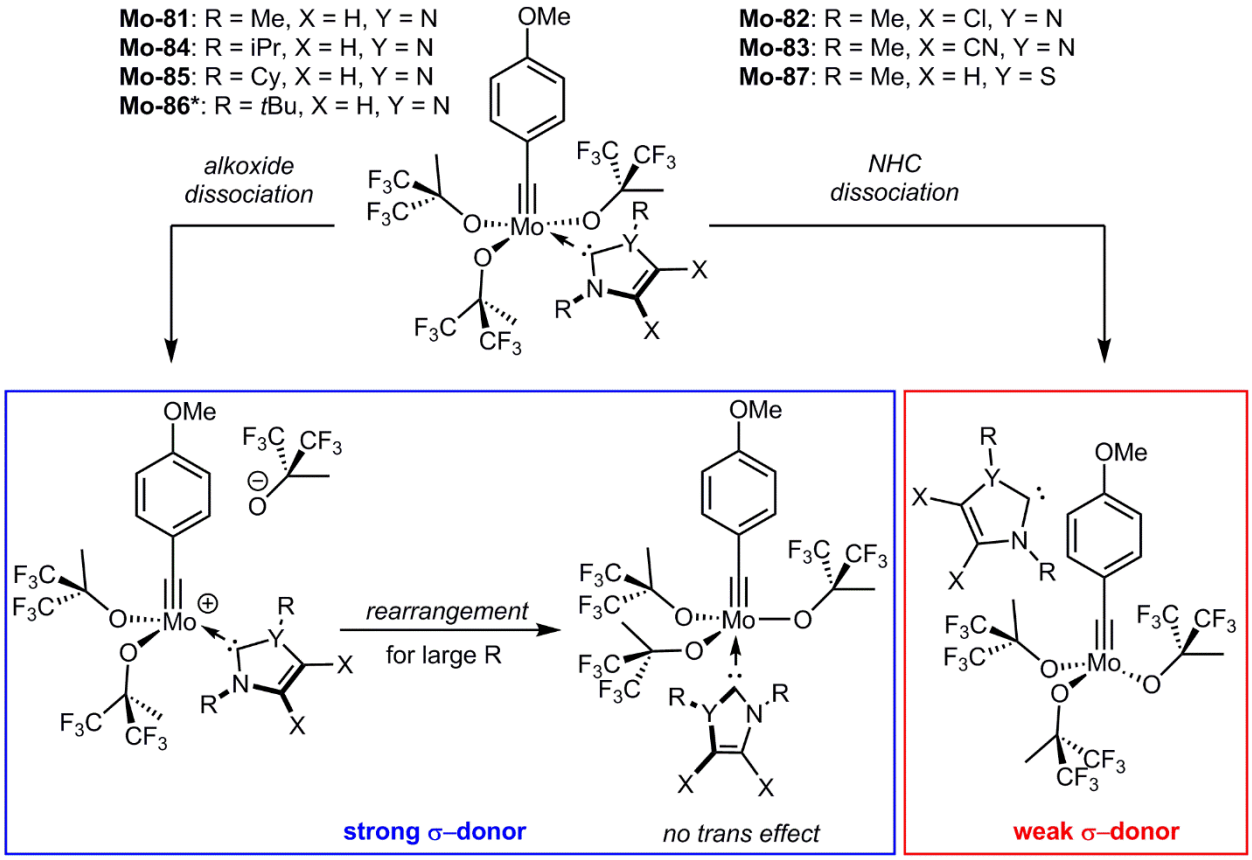

Scheme 67: Proposed active species in alkyne metathesis for molybdenum NHC alkylidyne complexes, depending on the donor strength of the respective NHC. *1,3-di-*tert*-butylimidazol-2-ylidene binds abnormal.

All the above-mentioned results hint to an NHC-dependant formation of the active species. In case of strong σ-donor NHCs with minor steric constraint (1,3-dimethylimidazol-2-ylidene, **Mo-81**, TEP = 2054.1)[24] partial dissociation of the fluorinated alkoxide under formation of a quasi-cationic intermediate seems most likely. Whether the formation of the cationic species is associative (first coordination of substrate, then formation of the cationic species) or dissociative (first formation of the cationic complex, then substrate coordination) remains speculative at this point. When strong σ-donors with high steric constraint like 1,3-diisopropy-imidazol-2-ylidene, 1,3-dicyclohexylimidazol-2-ylidene and the abnormal carbene are present (**Mo-84**, **Mo-85**; TEP = 2051.5, 2049.6;[24] no literature value for TEP of the abnormal carbene (**Mo-86)** could be found, however, abnormal carbenes are considered good donors[36]), formation of a cationic species seems to be possible. However, the competitive formation of the TBP structure (induced by steric bulk, eventually through a cationic intermediate), which itself is not able to form a cationic structure due to the missing *trans*-effect of the NHC, might result in the observed, somewhat unexpected reduced activity compared to **Mo-81**. For compounds **Mo-82** and **Mo-83**, dissociation of the *N*-heterocyclic carbene to form the active neutral tetracoordinated species can be observed. This is in accordance with the reduced σ-donor strength of both, 1,3-dimethyl-4,5-dichloro- and 1,3-dimethyl-4,5-dicyano-imidazol-2-ylidene (**Mo-82** and **Mo-83**, TEP of respective NHCs: 2059.0 and 2066.2)[24] and the

associated decrease in bond strength. The 1,3-thiazol-2-ylidene-based catalyst **Mo-87** showed no dissociation of NHC despite the rather low nucleophilicity (TEP = 2061.5) and the expected weak NHC-metal bond. The higher stability of the NHC-metal bond in **Mo-87** compared to **Mo-82** and **Mo-83** can be explained by the shorter molybdenum-NHC bond in **Mo-87** (Mo-C_{NHC} = 224.4 *vs*. 225.21 and 226.23 pm in **Mo-82** and **Mo-83**)[10] due to the decrease in steric bulk (one *vs.* two methyl groups). For **Mo-87**, either the pentacoordinated neutral species or the NHC dissociated neutral species are most likely to be the active species. Since all proposed active species only form to a minor extent, the complexes show small differences in activity. Of course, the neutral pentacoordinated species cannot fully be ruled out as active species in all cases.

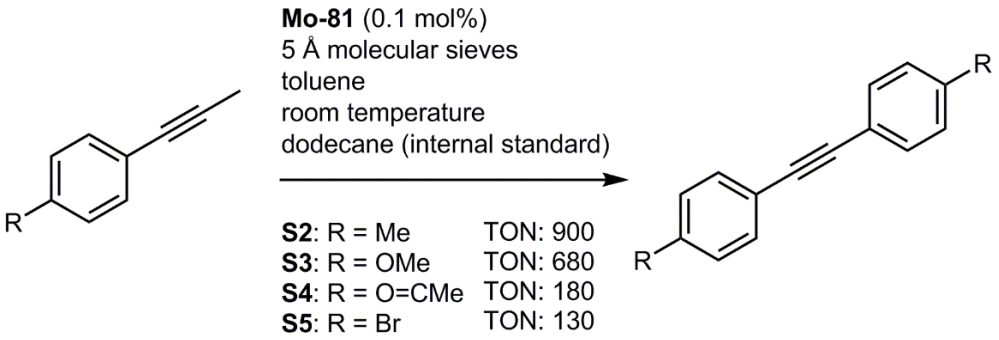

Figure 70: Homometathesis reactions of *p*-substituted 1-phenyl-1-propynes **S2-5** with **Mo-81** in toluene at room temperature. Catalyst: substrate 1:1000, molecular sieves 5Å, internal standard for GC-MS dodecane.

Finally, reactivity of **Mo-81** towards several p-substituted 1-phenyl-1-propynes **S2** - **S5** in the presence of molecular sieves (5 Å) was investigated. Substrates **S2** - **S5** were synthesized by literature-known decarboxylative *Sonogashira* coupling of 2-butynoic acid with the corresponding substituted 4-bromo-aryls, or, for **S5**, the corresponding 4-iodo-aryl. [200] **Mo-81** was the catalyst of choice, due to its higher reactivity compared to the other complexes that did not display NHC-dissociated active species. Productivity of **Mo-81** in the HM of *p*-substituted 1-phenyl-1-propynes **S2** - **S5** at room temperature increases with the electron-donating character of the *p*-substituents. The presence of electron-withdrawing bromo- and aceto- group (**S4** and **S5**) resulted in rather low TONs of 130 and 180, respectively, whereas with the methoxy- and the methyl- substituent high TONs of 680 and 900 were reached after only three hours reaction time at room temperature.

To receive complexes with higher activity and to provide evidence for the postulated formation of cationic species during a metathesis event, the synthesis of cationic molybdenum alkylidyne complexes bearing a monodentate NHC was further pursued. First attempts by *M. Koy* had been unsuccessful.[10]

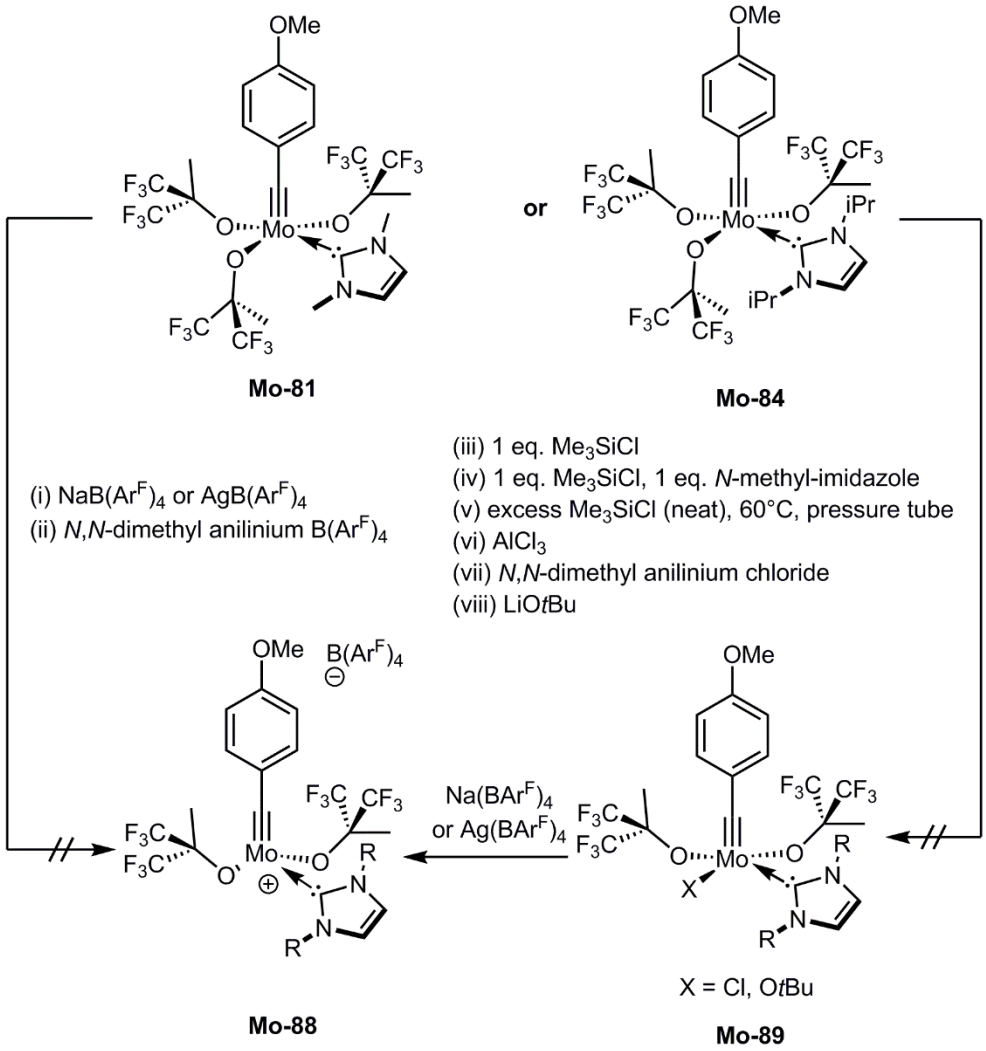

Scheme 68: Synthetic protocols for the attempted preparation of cationic alkylidyne complexes.

Mo-81 and **Mo-84** were chosen as candidates because they are accessible in good yields and bear good donors that should enable the stabilization of a cationic center. First, attempts to abstract one hexafluoro-*tert*-butoxide ligand with sodium B(Ar^F)$_4$ and silver B(Ar^F)$_4$ in three different solvents were made. Unfortunately, no conversion was observed in diethyl ether, acetonitrile and toluene at room temperature ((i), Scheme 68). This is most likely due to the good solubility of hexafluoro-*tert*-butoxide salts, since usually salt precipitation is the driving force for those kinds of reactions. Therefore, another route was investigated. The replacement of one hexafluoro-*tert*-butoxide by a chloride ligand that could then be abstracted under formation of sodium chloride with sodium B(Ar^F)$_4$ was attempted. As previously observed for *N*,*N*-dimethylanilinium B(Ar^F)$_4$ by *M. Koy*[10] ((ii), Scheme 68), conversion of **Mo-81** and **Mo-84**

with *N*,*N*-dimethylanilinium chloride lead to random protonation of NHC and alkoxide and resulted in decomposition and product mixtures ((vii), Scheme 68). Furthermore, to exploit the high affinity of silicon for oxygen, **Mo-81** and **Mo-84** were reacted with one equivalent of Me_3SiCl in toluene at room temperature, as well as in neat chlorotrimethyl silane at 60°C in a pressure tube ((iii), Scheme 68). Again, no reaction was observed. Addition of *N*-methylimidazol which is known to promote TMS protection of fluorinated alkoxides also did not lead to consumption of the educts ((iv), Scheme 68).[201] Last, **Mo-81** and **Mo-84** were reacted with one as well as 0.33 equivalents of aluminum trichloride in toluene at -35°C, which lead to complete decomposition of the complexes. Attempts to replace one hexafluoro-*tert*-butoxide with lithium *tert*-butoxide in toluene and diethyl ether were unsuccessful as well ((viii), Scheme 68). Most likely, ligand scrambling prevented the isolation of pure compounds.

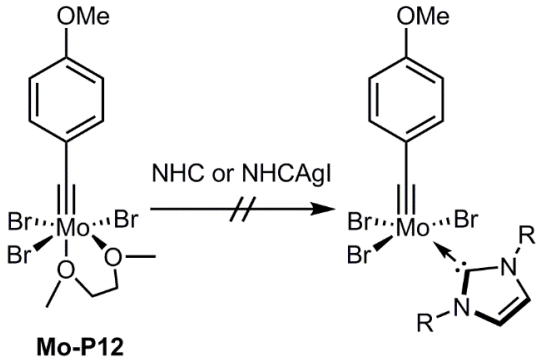

Mo-P12

Scheme 69: Attempted introduction of NHC to **Mo-P12**. Applied NHC/NHCAgI: 1,3-diisopropylimidazol-2-ylidene and 1,3-dimethylimidazol-2-ylidene AgI.

Since removal of one hexafluoro-*tert*-butoxide seemed impossible, several attempts to attach NHCs directly to $Mo(C(4\text{-}OMe\text{-}C_6H_4))Br_3(DME)$ (**Mo-P12**) were made (Scheme 69). Removal of one bromide ligand was thought to be more convenient. However, reactions with $Mo(C(4\text{-}OMe\text{-}C_6H_4))Br_3(DME)$ and 1,3-dimethylimidazol-2-ylidene AgI or 1,3-diisopropyl imidazol-2-ylidene in THF as well as toluene at room temperature and at 50°C, respectively, did not lead to any reaction.

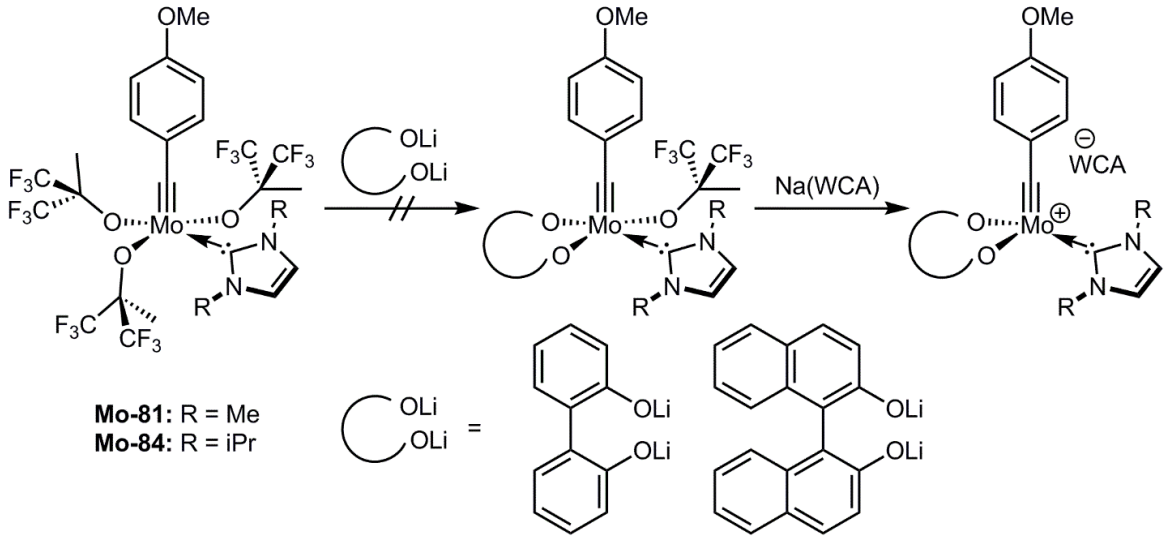

Scheme 70: Attempted introduction of chelating alkoxides (binaphtholate and biphenolate) to molybdenum alkylidyne NHC complexes.

Another approach entailed the replacement of two hexafluoro-*tert*-butoxides with a chelating ligand, since one cationic alkylidyne complex bearing a tridentate NHC had already been prepared by *M. Koy*.[10] The chelate effect was envisioned to stabilize the cationic species. However, introduction of biphenoxide and binaphtholate by conversion of **Mo-81** and **Mo-84** with the corresponding lithium salts in diethyl ether as well as in toluene was unsuccessful, most probably due to poor solubility of the lithium salts (Scheme 70).

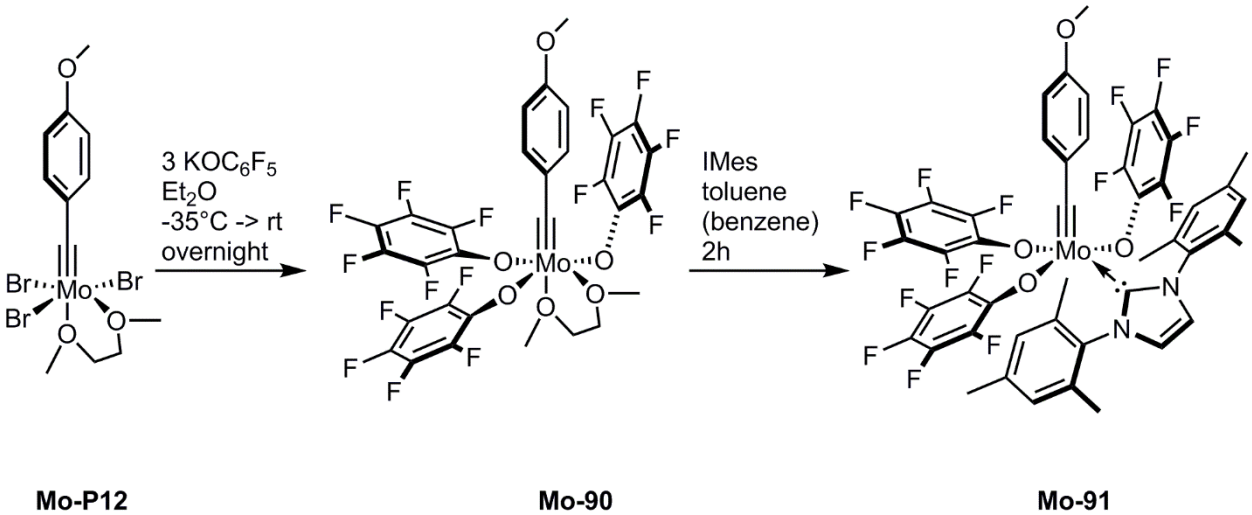

Mo-P12 **Mo-90** **Mo-91**

Figure 71: Synthesis of the tris(pentafluorophenoxy)(4-methoxy-benzylidyne) molybdenum complex **Mo-90** from the trisbromo(4-methoxy-benzylidyne)(DME) molybdenum complex **Mo-P12**. And synthesis of trispentafluorophenoxide (IMes)(4-methoxy-benzylidyne) molybdenum complex **Mo-91** by conversion of **Mo-90** with IMes. (Yield: **Mo-90**: 60%; **Mo-91**: 89%)

Alternatively, reaction of **Mo-P12** with three equivalents potassium pentafluorophenoxide in diethyl ether at room temperature yielded Mo(C(4-OMe-C_6H_4))(OC_6F_5)$_3$(DME) (**Mo-90**) in 60% yield. The aim was to then replace DME by an NHC and replace one pentafluorophenoxide with a WCA by conversion with the corresponding sodium-, lithium- or silver-WCA salt. The

salts of pentafluorophenoxide are less soluble then their hexafluoro-*tert*-butoxide analogues, their formation and precipitation should therefore be a better driving force. In addition, increased σ-donor propensity should render an IMes complex more prone to dissociation of an alkoxide ligand and should therefore promote alkoxide dissociation as well as alkoxide abstraction. However, introduction of IMes had been unsuccessful for the trishexafluoro-*tert*-butoxide complexes, most probably due to steric constraint in the target complex. IMes was reacted with **Mo-90** in benzene or toluene at -35°C and was stirred at room temperature for two hours. $Mo(OC_6F_5)_3(\equiv C(p\text{-}OME\text{-}C_6H_4))(IMes)$ **Mo-91** was isolated after simple trituration with diethyl ether in 89% yield. Interestingly, the ^{19}F NMR spectrum of **Mo-91** in $CDCl_3$ shows three pentafluorophenoxide ligands of which two are equivalent (Figure A 137, appendix). This could hint either to a square pyramidal structure with the alkylidyne in the apex and two pentafluorophenoxides *cis* to the NHC and one *trans* to the NHC or to a trigonal bipyramidal structure with the alkylidyne and one pentafluorophenoxide in the apex and the residual ligands in the plane.

6.5.3 *Outlook*

The synthesis of an alkylidyne complex bearing two hexafluoro-*tert*-butoxides and one chloride ligand has been described by *Schrock et al.* (Figure 72, left).[202] Since the complex also contains DME, it is highly likely that introduction of an NHC would be possible.[10,23] Subsequent replacement of the chloride with $NaB(Ar^F)_4$ would lead to the desired cationic complex. Since cationic species have been shown to be highly instable,[10,203] the introduction of good leaving groups that enable formation of more stable "ion pairs" comparable to the molybdenum imido alkylidene NHC complexes,[168d] seems preferable. Such leaving groups are triflate, tosylate and equivalent groups. Triflate could be introduced by reaction of for example **Mo-P11** with triflic acid (Figure 72, right).

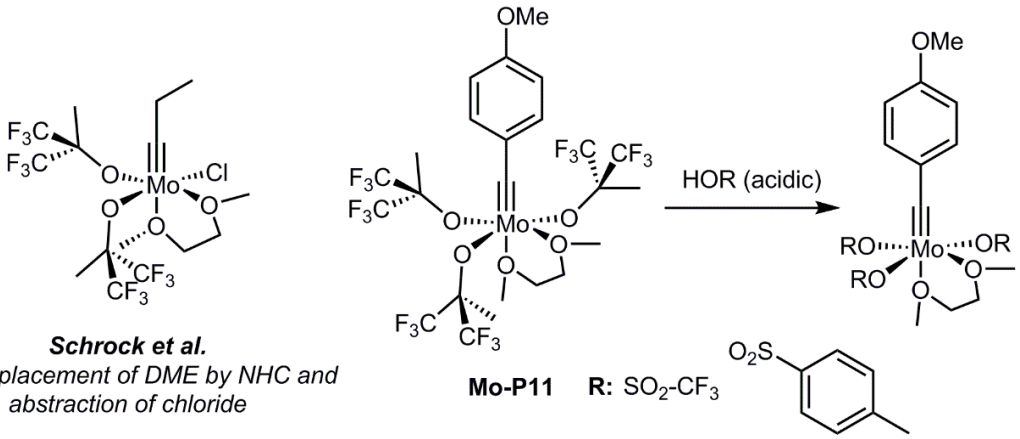

Figure 72: Left: Complex published by *Schrock et al.*, containing DME (easily replaceable by NHC) and a chloride (easily abstracted by $NaB(Ar^F)_4$). Right: Introduction of good leaving groups to molybdenum alkylidyne complexes by protonation of **Mo-P11** with acids.

7 EXPERIMENTAL

7.1 GENERAL

7.1.1 EQUIPMENT

The glove box used for reactions under inert conditions was an *MBraun Labmaster* with an *MBraun SPS-800* solvent purification system. NMR spectra were recorded on a *Bruker Avance III 400* spectrometer at a temperature of 298.15 K at 400 MHz (^{1}H), 376 MHz (^{19}F), 162 MHz (^{31}P) and 101 MHz (^{13}C). NMR spectra were internally calibrated to solvent signals.[204] Abbreviations for multiplicities: s (singlet), b s (broad signal), d (doublet), q (quartet), hept (heptet), m (multiplet). *Syn*- and *anti*-configuration of the alkylidene moiety are denoted by *syn* and *anti*. Coupling constants *J* are reported in Hz. GC-MS analyses were performed on an *Agilent Technologies 5975C inert MSD* device consisting of a triple-axis detector, a *7693 autosampler* and a *7890A GC* system equipped with an *SPB-5 fused silica column* (34.13 m×0.25 mm×0.25 µm film thickness). The column temperature ramped from 45 to 250°C within eight minutes and was then further held for five minutes. The injection temperature was set to 150°C and the column flow was 1.05 mL·min^{-1}. Elemental analyses were measured on a *Perkin Elmer 240* device at the Institute of Inorganic Chemistry, University of Stuttgart, Germany. Single crystal X-ray measurements were carried out on a *Nonius KappaCCD 4-circle diffractometer* equipped with graphite-monochromatized Mo-K irradiation, a *Micracol Fiber Optics collimator*, and a *Nonius FR590 generator* at the Institute of General, Inorganic and Theoretical Chemistry, University of Innsbruck, Austria (structure of **Mo-29**) and on a *Bruker Kappa APEXII Duo diffractometer* with Mo-K irradiation at the Institute of Organic Chemistry, University of Stuttgart, Germany (structures of **Mo-3**, **Mo-12**, **Mo-13**, **Mo-20**, **Mo-23**, **Mo-24**, **Mo-32**, **Mo-33**, **Mo-35**, **Mo-36**, **Mo-37**, **Mo-38**, **Mo-39**, **Mo-40**, **Mo-41**, **Mo-42**, **Mo-43** and **Mo-44**). GPC data were acquired at 35°C on an *Agilent Technologies 1200 Infinity Series* device with three consecutive *SDV PSS* (8mm x 300 mm) columns at a flow rate of 1.0 mL·min^{-1}. GPC samples were filtered over a 0.2 µm PTFE syringe filter *prior* to injection and had a concentration of 1-5 mg·mL^{-1}. IR spectra were measured on an ATR/FT-IR-spectrometer *IFS 128* (Bruker) and were edited with the *OPUS* software (version 7.2). Wavenumbers ν are reported in cm^{-1}, intensities of the signals are abbreviated as follows: s (strong), m (medium), w (weak). UV/Vis measurements were performed on an *UV-1800 Shimadzu* UV-spectrometer in either $CHCl_3$ or DMSO. Absorption wavelengths λ are reported in nm. DSC measurements were performed under nitrogen on a *Perkin Elmer DSC 4000* device and data were analyzed with the *Pyris*^{TM} software and plotted with *Microsoft Excel*. For centrifugation, a *Hettich R32 Universal* device was used.

7.1.2 METHODS

All reactions, unless stated otherwise, were performed under inert conditions, either in a nitrogen-filled glove box or under standard Schlenk techniques (nitrogen). Heating occurred either in an oil bath or in an aluminum block (for catalysis). Glass ware was cleaned by first storing it in a base bath (KOH, ethanol/ water) for at least three hours, and was then washed with water, transferred to a neutralization bath (HCl in water), followed by washing with water and, finally, demineralized water. Glass ware (flasks, pipets, vials etc.) for application in the glove box was dried for at least thirty minutes in an oven and cooled down under vacuum in the antechamber of the glove box.

7.2 CHEMICALS

If not explicitly stated otherwise, chemicals were purchased from common suppliers (*TCI*, *Sigma Aldrich*, *Alfa Aesar*, *ABCR*, *Fischer Scientific*) and used as received.

7.2.1 SOLVENTS AND MATERIALS

All solvents used for reactions with organometallic compounds were dried *prior* to use and degassed in three consecutive freeze-pump-thaw cycles. Toluene, CH_2Cl_2, diethyl ether and pentane were obtained from the solvent purification system of the glove box and stored over molecular sieves 4 Å. Tetrahydrofuran was obtained from the solvent purification system and additionally dried over Na/ benzophenone and distilled (to remove the contained stabilizer) to be stored over molecular sieves 4 Å. 1,2-Dimethoxyethane was dried over LiH for 12 hours and subsequently distilled from Na/benzophenone. 1,2-Dichloroethane, pyrrole, 2,5-dimethylpyrrole, triethylamine, pyridine, acetonitrile, dimethyl sulfoxide, 1,3-dichlorobenzene, 1,2,4-trichlorobenzene and heptane were dried over CaH_2 overnight and distilled. They were stored over molecular sieves 4 Å. Acetonitrile was stored over molecular sieves 3 Å. $CHCl_3$ was dried over LiH and distilled *prior* to use. Benzene was dried over Na/benzophenone and distilled. Ethylene glycol and methanol were purchased dry from *Sigma Aldrich* and stored under nitrogen in a sealed bottle. Deuterated solvents were purchased from *DeuChem GmBH* and *Euriso-top*, transferred into the glove box as received and dried over molecular sieves (3 or 4 Å) and dry activated neutral aluminum oxide, which were then filtered off, to be stored over molecular sieves (4 Å, except acetonitrile: 3 Å). Celite®, aluminum oxide, silica and molecular sieves (3, 4 and 5 Å) were dried under vacuum at 150°C for at least 12 hours before they were transferred to the glove box. 5 Å molecular sieves additionally were grinded before drying and the container was only opened after flushing of the glove box atmosphere to avoid adsorption of volatiles. Glass fiber filter paper for purposes of filtration in the glove box was stored in the oven over night and cooled in the antechamber of the glove box under vacuum.

7.2.2 *Purchased reagents with special purification prior to use*

Unless stated otherwise, all liquid substrates, for RCM, HM and CM were dried over CaH_2, distilled and degassed in three consecutive freeze-pump-thaw cycles before they were stored in a glove box with molecular sieves 4 Å. All solid substrates for RCM, HM and CM were dried under high vacuum overnight before they were transferred into the glove box. 1-Phenyl-1-propyne **S1** was purchased from *TCI*. **S1** was dried over CaH_2, distilled and degassed in three consecutive freeze-pump-thaw cycles *prior* to use. **S1** was stored in the fridge over molecular sieves (4 Å) under nitrogen. 3-Pyridinio-propanesulfonate **8** was purchased from *Sigma Aldrich*, transferred into the glove box, washed with dry THF and dried under vacuum *prior* to use. Nitron **9** was purchased from *Sigma Aldrich* and recrystallized from a mixture of CH_2Cl_2 and pentane *prior* to use. Dicyclopentadiene (DCPD) was purchased from *Acros Organics*, dried over CaH_2, distilled and degassed in three consecutive freeze-pump-thaw cycles *prior* to use (*endo*/*exo* = 95/5, determined by GC-MS). Ammonium molybdate ($(NH_4)_2Mo_2O_7$ and $(NH_4)_6Mo_7O_{24} \cdot 4\ H_2O$) for the precursor synthesis was dried at 50°C under high vacuum to remove water overnight.

7.3 Chemicals synthesized according to literature-known procedures

7.3.1 *Carbene precursors, derived carbenes and carbene silver salts*

1,3-dimethylimidazolium iodide,[205] 4,5-dichloro-1,3-dimethylimidazolium iodide,[205] 4,5-dicyano-1,3-dimethylimidazolium iodide,[205] 1,3-di-*tert*butylimidazolium tetrafluoroborate,[206] 1,3-dicyclohexylimidazolium tetrafluoroborate,[207] 1,3-dimesitylimidazolium tetrafluoroborate,[207] 1,3-dimesitylimidazolinium chloride,[207] 1,3-diisopropylimidazolium chloride,[208] *N*-mesityl-*N*-(2-picolyl)-imidazolium bromide **10**[52d], 4-[(dimethylamino)methyl]-4,5-dihydro-1,3-bis(2,4,6-trimethylphenyl)-imidazolium tetrafluoroborate **5**[127b] and 5-methoxy-1,3,4-triphenyl-4,5-dihydro-1H-1,2,4-triazoline (perchlorate salt was isolated)[209] were synthesized according to literature procedures. 1,3-diisopropylimidazolium chloride was additionally washed with boiling acetone, dried by azeotropic distillation with toluene and dried under vacuum overnight before it was transferred to the glove box.

The silver salts 1,3-dimethylimidazol-2-ylidene (AgI),[210] 4,5-dichloro-imidazol-2-ylidene (AgI)[205] and 4,5-dicyano-imidazol-2-ylidene (AgI)[205] were synthesized by deprotonation of the respective imidazolium iodides with silver(I)oxide according to literature procedures.

Carbenes were synthesized by deprotonation of the corresponding imidazolium salts with either KHMDS, KO*t*Bu, KH or a mixture of KO*t*Bu/KH in THF or toluene: 1,3-di-*tert*-butylimidazol-2-ylidene,[211] 1,3-dimesitylimidazol-2-ylidene,[212] 1,3-dimesitylimidazolin-2-ylidene,[213] 1,3-diisopropylimidazol-2-ylidene[208]. 1,3-Dicyclohexylimidazol-2-ylidene was

generated *in situ* by deprotonation of the imidazolium tetrafluoroborate in toluene with KHMDS. 1,3,4-Triphenyl-1,2,4-triazol-5-ylidene was generated by removal of methanol from the methanol adduct at 90°C for three days under dynamic vacuum.[209] [μ-[1,3-Bis[2,4,6-trimethylphenyl]-1,3-dihydro-2H-imidazol-4-yl-2-ylidene]][tris(2,3,4,5,6-pentafluorophenyl)boron]-lithium **6** was synthesized according to the literature.[181]

7.3.2 REAGENTS

$Na(BAr^F)_4$ was synthesized according to the literature.[214] *N,N*-Dimethylanilinium $B(Ar^F)_4$ was synthesized from *N,N*-dimethylanilinium chloride by conversion with $NaB(Ar^F)_4$ in a mixture of CH_2Cl_2 and diethyl ether and recrystallized from CH_2Cl_2, diethyl ether and pentane. *N,N*-Dimethylanilinium chloride was synthesized from commercially available *N,N*-dimethylaniline by protonation with HCl in diethyl ether.

7.3.3 LIGANDS

Hexamethylterphenoxide (**2a**) was synthesized according to a literature-known procedure from commercially available 1,3-dichlorobenzene.[179] Lithium and potassium salts of commercially available alcohols and amines (1,1,1-3,3,3-hexafluoro-*tert*-butoxide, *tert*-butanol, 2,6-diphenylphenol, pentafluorophenol, pyrrole, 2,5-dimethyl pyrrole, diisopropylamine) were prepared by deprotonation with one equivalent of lithium/potassium hydride or *n*-butyl lithium in THF or diethyl ether. Li_2(1,1´-binaphth-2,2´-olate) and Li_2(1,1´-biphen-2,2´-olate) were synthesized by deprotonation with *n*-BuLi (2 equiv.) in THF.. The ligands 3,3´-dibromo-2´-(*tert*-butyldimethylsilyloxy)-1,1´-binaphthalen-2-ol **12**[21e], 3,3´-dibromo-2´-(*tert*-butyldimethylsilyloxy)-5,5´,6,6´,7,7´,8,8´-octahydro-1,1´-binaphth-2-ol **13**[21e] and 2´-trimethylsilyloxy-3,3´-di(*tert*-butyl)-5,5´,6,6´-tetramethyl-1,1´-biphen-2-ol **14**[178], 3,3´-dibromo-2´-(methoxy)-5,5´,6,6´,7,7´,8,8´-octahydro-1,1´-binaphth-2-ol **25**[195] and **26**[196] were synthesized according to the literature starting from commercially available 1,1´-binapth-2,2´-ol, 5,5´,6,6´,7,7´,8,8´-octahydro-1,1´-binaphth-2,2´-ol and 3,3´-di-*tert*-butyl-5,5´,6,6´-tetramethyl-1,1´-biphen-2,2´-ol, respectively. However, for the synthesis of **12**, **13**, **14**, **25** and **26**, the SiR_3Cl compounds were used instead of the SiR_3OTf compounds in the protection step.

7.3.4 MONOMERS AND SUBSTRATES

M1[215] and **M2**[216] were synthesized according to literature-known procedures from commercially available **M3**. **M4**,[217] **M5**,[218] **M6**,[217], **M8**,[219] **M9**[220] were provided by *Dominik Imbrich* and synthesized according to literature-known procedures. **M7** was also provided by *Dominik Imbrich* and was synthesized in analogy to the procedure described in the literature for 3,5-dimethoxy-*N*-2-propen-1-yl-*N*-2-propyn-1-ylbenzene amine by using propargyl bromide instead of allyl bromide.[221] Substrates for asymmetric metathesis reactions **15**[96], **16**[177a], **17**[177b], **18**[177b] and **19**[194] were synthesized according to literature. Substrates **S2** - **S5** were synthesized according to literature or in a similar manner.[200]

7.3.5 *Organometallic compounds*

Mo-P1,[73b] **Mo-P2**,[73b] **Mo-P3**,[73b] **Mo-P4**,[73b] **Mo-P5**,[73b] **Mo-P6**,[73b], **Mo-P7**, [222] **Mo-P8**,[222] **Mo-P9**,[222] **Mo-P10**,[222] **Mo-P11**,[10,23] **Mo-P12**,[148] **Mo-1**,[167] **Mo-2**,[168a] **I1**,[168a] **Mo-21**[168a], **Mo-22**[190], **Mo-23**[168a], **Mo-49**,[222] **Mo-51**,[21e] **Mo-52**,[12a,21d,21e,80,82,98c] **Mo-53**,[12a,21d,21e,80,82,98c] **Mo-68**,[223] **W-1**,[224] **W-3**,[168f] were synthesized according to literature-known procedures from commercially available reagents in dry and degassed solvents under inert conditions. Compounds **Mo-7**,[15] **Mo-8**[15] and **Mo-9**[15] for biphasic catalysis were provided by *Roman Schowner*.

7.3.6 *Crystal data*

Crystal data for the determination of $\%V_{bur}$ of the imido ligands were provided by *Roman Schowner* (**Mo-23**,[168a] **Mo-32**,[168a] **Mo-38**,[15] **Mo-43**,[15] **Mo-44** (CCDC-1453116)[168e]), *Laura Stöhr* (**Mo-20**,[191] **Mo-39**,[191] **Mo-40**,[191] **Mo-42** (CCDC-1453115)[168e]), *Katharina Herz* (**Mo-24**,[169] **Mo-41**[169]), *Suman Sen* (**Mo-37**[167]) and *Christina Lienert* (**Mo-33** (CCDC-1453118),[168e] **Mo-35** (CCDC-1453120),[168e] **Mo-36** (CCDC-1453119)[168e]).

7.4 GROUP 6 METAL ALKYLIDENES BEARING IONIC LIGANDS

Parts of the following chapter have already been published. Reprinted (adapted) with permission from (I. Elser, R. Schowner, W. Frey, M. R. Buchmeiser, *Chem. Eur. J.* **2017**, *23*, 6398-6405). Copyright (2017) John Wiley and Sons. And reprinted (adapted) with permission from (D. A. Imbrich, I. Elser, W. Frey, M. R. Buchmeiser, *ChemCatChem* **2017**, *9*, 2996-3002). Copyright (2017) John Wiley and Sons.

7.4.1 SYNTHESIS OF LIGANDS

1 was prepared in a two-step synthesis from 4-bromo-2,6-di-*t*Bu-phenol **1a** in a procedure first developed by *Roman Schowner.*[14-15]

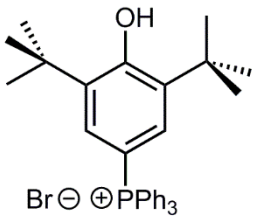

1b

Synthesis of 1b: **1a** (4.0 g, 14 mmol), triphenyl phosphine (5.52 g, 21 mmol) and $Pd_2(dba)_3$ (385 mg, 0.4 mmol) were dissolved in ethylene glycol (dry, degassed, 2 mL) and heated to 130 °C. After 20 hours, ethylene glycol was distilled from the reaction mixture. The resulting residue was dissolved in CH_2Cl_2 and filtered over Celite®. The filtrate was reduced and diethyl ether was added. The resulting colorless precipitate was purified by column chromatography (1/10, methanol/CH_2Cl_2, silica). [2,6-di-*t*Bu-1-hydroxyphen-4-yltriphenylphosphonium][Br] (**1b**) was isolated in 95 % yield as a colorless solid. ^{1}H NMR (400 MHz, CD_2Cl_2): δ = 7.93–7.89 (m, 3H), 7.82–7.87 (m, 6H), 7.26 (d, 2H, $^2J_{HP}$ = 13.6 Hz), 6.40 (s, 1H), 1.36 (s, 18H) ppm. ^{31}P NMR (162 MHz, $CDCl_3$): δ = 23.37 ppm. ^{13}C NMR (101 MHz, $CDCl_3$) δ = 160.6 (d, $^4J_{CP}$ = 3.1 Hz), 139.4 (d, $^2J_{CP}$ = 13.2 Hz), 135.7 (d, $^4J_{CP}$ = 2.9 Hz), 134.3 (d, $^3J_{CP}$ = 10.2 Hz), 131.6 (d, $^3J_{CP}$ = 12.5 Hz), 130.8 (d, $^2J_{CP}$ = 12.6 Hz), 118.62 (d, $^1J_{CP}$ = 89.6 Hz), 105.6 (d, $^1J_{CP}$ = 96.5 Hz), 35.0, 30.0 ppm. HRMS: *m/z* calc. for $C_{32}H_{36}OP^+$ 467.2498, found 467.2477, *m/z* calc. for Br^- 78.9189, found 78.9162.

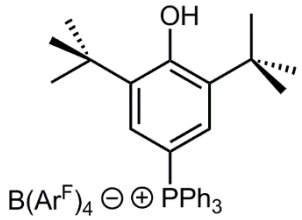

Synthesis of 1: **1b** (0.5 g, 0.9 mmol) was dissolved in CH_2Cl_2 and $NaB(Ar^F)_4$ (809 mg, 0.9 mmol) dissolved in CH_2Cl_2 and diethyl ether (2:1) was added. After eight hours the mixture

was filtered over Celite® and the filtrate was reduced and cooled to -35 °C for crystallization. **1** was isolated in 85 % yield as colorless crystals. ^{1}H NMR (400 MHz, CD_2Cl_2): δ = 7.86–7.83 (m, 3H), 7.73–7.67 (m, 14H), 7.61–7.55 (m, 10H), 7.31 (d, 2H, $^{2}J_{HP}$ = 13.7 Hz), 6.16 (s, 1H), 1.35 (s, 18H) ppm. ^{19}F NMR (376 MHz, CD_2Cl_2): δ = -62.87 ppm**.** ^{31}P NMR (162 MHz, $CDCl_3$): δ = 23.55 ppm. ^{13}C NMR (101 MHz, CD_2Cl_2) δ = 162.2 (q, $^{1}J_{CB}$ = 50.0 Hz, C_{ipso} $B(Ar^F)_4$), 160.8 (d, $^{4}J_{CP}$ = 3.2 Hz), 139.2 (d, $^{2}J_{CP}$ = 13.2 Hz), 135.8 (d, $^{4}J_{CP}$ = 3.0 Hz), 135.2 (br, s), 134.6 (d, $^{3}J_{CP}$ = 12.5 Hz), 132.1 (d, $^{3}J_{CP}$ = 12.5 Hz), 130.8 (d, $^{2}J_{CP}$ = 12.7 Hz), 129.3 (qq, $^{2}J_{CF}$ = 31.6 Hz, $^{3}J_{CB}$ = 2.8 Hz), 125.03 (q, $^{1}J_{CF}$ = 272.2 Hz, CF_3 $B(Ar^F)_4$), 119.1 (d, $^{1}J_{CP}$ = 89.8 Hz), 117.0 (hept, $^{3}J_{CF}$ = 3.9 Hz), 105.8 (d, $^{1}J_{CP}$ = 96.8 Hz), 35.1, 29.8 ppm. Elemental analysis calcd. (%). for $C_{64}H_{48}BF_{24}OP$: C 57.76, H 3.64; found: C 57.61, H 3.868.

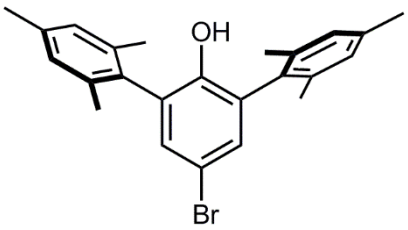

2b

Synthesis of 2b: *Reaction was run under ambient conditions.* **2a** (492 mg, 1.5 mmol) was dissolved in glacial acetic acid (20 mL). A solution of bromine (72 µL, 226 mg, 1.4 mmol) in glacial acetic acid (5 mL) was slowly dropped to this solution under vigorous stirring. After two hours, demineralized water was added and the resulting colorless residue was filtered off and washed with water. Then the solid was dissolved in diethyl ether and the organic phase was washed with water and brine and subsequently dried over Na_2SO_4. The solvent was evaporated. According to GC-MS, the crude product contains approximately 3 % of educt and a doubly brominated species. The crude product was used without further purification.

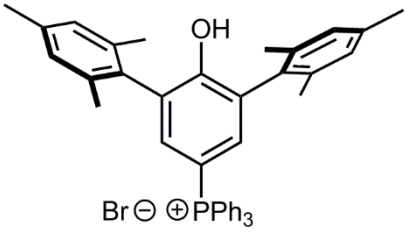

2c

Synthesis of 2c: **2b** (822 mg, 0.2 mmol), triphenylphosphine (789.5 mg, 0.3 mmol), tris(dibenzylideneacetone) dipalladium (55 mg, 3 mol%) were suspended in ethylene glycol (2 mL, dry) and heated to 130 °C. After 20 hours, the solvent was removed by distillation and the resulting residue was purified by column chromatography (silica, methanol/ CH_2Cl_2, 1/10). **2c** was isolated in 60 % yield as colorless foam. ^{1}H NMR (400 MHz, $CDCl_3$): δ = 7.93-7.89 (m,

3H), 7.82-7.77 (m, 6H), 7.68-7.63 (m, 6H), 7.23 (d, $^{3}J_{PH}$ = 12.7 Hz, 1H), 6.99 (s, 4H), 2.31 (s, 6H), 2.03 (s, 12H) ppm. ^{13}C NMR (101 MHz, CD_3CN): δ = 158.6 (d, $^{4}J_{PC}$ = 3.4 Hz), 139.1, 137.6, 137.4 (d, $^{3}J_{CP}$ = 11.1 Hz), 136.2 (d, $^{4}J_{CP}$ = 3.0 Hz), 135.5 (d, $^{3}J_{CP}$ = 10.4 Hz), 132.9, 131.5 (d, $^{2}J_{CP}$ = 14.6 Hz), 131.3 (d, $^{2}J_{CP}$ = 12.7 Hz), 129.3, 119.7 (d, $^{1}J_{CP}$ = 95.1 Hz), 108.3 (d, $^{1}J_{CP}$ = 95.1 Hz), 21.2, 20.6 ppm. HRMS-ESI *m/z* calcd. for $C_{42}H_{40}OP^{+}$: 591.2811; found 591.2819.

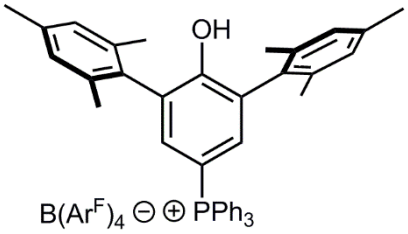

2

Synthesis of 2: **2c** (444 mg, 0.6 mmol) was dissolved in CH_2Cl_2 and $NaB(Ar^F)_4$ (584 mg, 0.6 mmol) in a mixture of CH_2Cl_2 and diethyl ether was added. After 14 hours the resulting suspension was filtered over silica and the solvent was removed under reduced pressure. **2** was isolated in 78% yield as a colorless foam. ^{1}H NMR (400 MHz, C_6D_6): δ = 7.71-7.66 (m, 3H), 7.56-7.51 (m, 14 H), 7.47-7.41 (m, 6H), 7.39 (br s, 4H), 7.14 (s, 1H), 7.11 (s, 1H), 6.83 (s, 4H), 5.40 (s, 1H), 2.13 (s, 6H), 1.85 (s, 12H) ppm. ^{19}F NMR (376 MHz, C_6D_6): δ = -62.88 ppm. ^{13}C NMR (101 MHz, CD_3CN): δ = 162.6 (q, $^{1}J_{CB}$ = 49.9 Hz, C_{ipso} $B(Ar^F)_4$), 158.5 (d, $^{4}J_{PC}$ = 3.4 Hz), 139.2, 137.7, 137.4 (d, $^{3}J_{CP}$ = 11.1 Hz), 136.2 (d, $^{4}J_{CP}$ = 2.9 Hz), 135.7 (m), 135.5 (d, $^{3}J_{PC}$ = 10.5 Hz), 132.7, 131.4*, 131.2 (d, $^{2}J_{PC}$ = 13.0 Hz), 129.94 (qq, $^{2}J_{CB}$ = 31.6 Hz, $^{3}J_{CF}$ = 2.8 Hz), 129.3, 125.5 (q, $^{1}J_{CF}$ = 271.7 Hz, CF_3 $B(Ar^F)_4$), 119.78 (d, $^{1}J_{CP}$ = 89.9 Hz), 118.7 (m), 108.4 (d, $^{1}J_{CP}$ = 95.0 Hz), 21.1, 20.5 ppm. Elemental analysis calcd. (%) for $C_{74}H_{52}BF_{24}OP$: C 61.09, H 4.03; found: C 61.47, H 4.03. *Expected: d, only one of the signals visible due to overlapping with d at δ = 131.2 ppm.

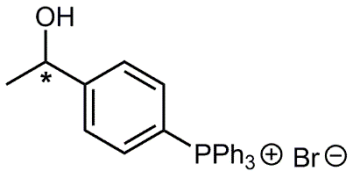

3b

Synthesis of 3b: **3a** (1 g, 5 mmol), triphenylphosphine (1.96 g, 7.5 mmol) and $Pd_2(dba)_3$ (137 mg, 0.1 mmol, 3 mol%) were dissolved in ethylene glycol and heated to 120 °C. After three days the mixture was cooled to room temperature and $CHCl_3$ and water were added. The water phase was extracted with $CHCl_3$ and the combined organic phases were washed with water and brine and dried over Na_2SO_4. The solvent was evaporated, and the resulting

residue was purified by column chromatography (silica, gradient: MeOH/CH_2Cl_2, 1/10, V/V to MeOH, change of solvent after elution of the first three fractions). **3b** was isolated as colorless foam in 83% yield. ^{1}H NMR (400 MHz, $CDCl_3$): δ= 7.93- 7.87 (m, 5H), 7.78- 7.73 (m, 6H), 7.63- 7.58 (m, 6H), 7.50- 7.44 (m, 2H), 5.15 (q, 1H), 1.54 (d, 3H) ppm. ^{13}C NMR (101 MHz, DMF-d7): δ= 157.0 (d, $^4J_{CP}$ = 3.1 Hz, $C_{para,aryl}$), 136.3 (d, $^4J_{CP}$ = 2.9 Hz, C_{para} PPh_3), 135.7 (d, $^3J_{CP}$ = 10.4 Hz, C_{meta} PPh_3), 135.7 (d, $^3J_{CP}$ = 10.9 Hz, $C_{meta,aryl}$), 131.4 (d, $^2J_{CP}$ = 13.0 Hz, C_{ortho} PPh_3), 128.4 (d, $^2J_{CP}$ = 13.2 Hz, $C_{ortho,aryl}$), 119.3 (d, $^1J_{CP}$ = 89.4 Hz, C_{ipso} PPh_3), 116.4 (d, $^1J_{CP}$ = 91.0 Hz, $C_{ipso,aryl}$), 68.8 (s, C-OH), 26.3 ppm. HRMS-ESI *m/z* calcd. for $C_{26}H_{24}OP^+$: 383.1559; found 383.1539.

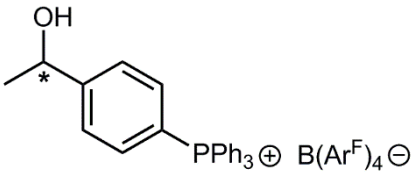

3

Synthesis of 3: **3b** (100 mg, 0.2 mmol) and $NaB(Ar^F)_4$ (191.3 mg, 0.2 mmol) were dissolved in a mixture of CH_2Cl_2 and acetonitrile and stirred at room temperature for three days. Subsequently the solvent was removed, and the residue was dissolved in CH_2Cl_2 and filtered over Celite®. Again, the solvent was evaporated to yield **3** in 94% yield. ^{1}H NMR (400 MHz, $CDCl_3$): δ= 7.81- 7.77 (m, 3H), 7.72- 7.61 (m, 16H), 7.55- 7.48 (m, 12H), 5.05- 5.00 (m, 1H), 1.93-1.92 (m, 1H), 1.52- 1,50 (m, 3H) ppm. ^{19}F NMR (376 MHz, CD_2Cl_2): δ= -62.41 ppm.^{13}C NMR (101 MHz, $CDCl_3$): δ= 161.9 (q, $^1J_{CB}$ = 49.9 Hz, C_{ipso} $B(Ar^F)_4$), 154.8 (d, $^4J_{CP}$ = 3.0 Hz, $C_{para,aryl}$),136.0 (d, $^4J_{CP}$ = 2.9 Hz, C_{para} PPh_3), 134.9 (br s, $B(Ar^F)_4$), 134.6 (d, $^3J_{CP}$ = 10.6 Hz, $C_{meta,aryl}$), 134.3 (d, $^3J_{CP}$ = 10.3 Hz, C_{meta} PPh_3), 130.8 (d, $^2J_{CP}$ = 13.0 Hz, C_{ortho} PPh_3), 127.77 (d, $^2J_{CP}$ = 13.43, $C_{ortho,aryl}$), 124.7 (q, $^1J_{CF}$ = 272.2 Hz, CF_3 $B(Ar^F)_4$), 117.7 (d, $^1J_{CP}$ = 89.7 Hz, C_{ipso} PPh_3), 117.73-117.46 (m, $B(Ar^F)_4$), 115.7 (d, $^1J_{CP}$ = 91.2 Hz, $C_{ipso,aryl}$), 69.39, 25.68 ppm. HRMS-ESI *m/z* calcd. for $C_{26}H_{24}OP^+$: 383.1559; found 383.1577.

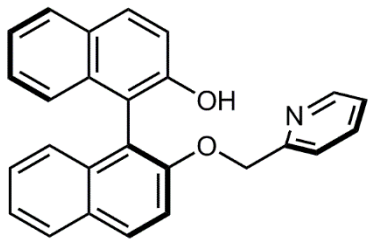

4b

Synthesis of 4b: *Reaction was run under ambient conditions.* **4a** (4 g, 14 mmol) was dissolved in acetone and a solution of potassium carbonate (5.79 g, 42 mmol) in water was added. Then,

picolyl hydrobromide (3.53 g, 14 mmol) was added. The mixture was stirred at 65°C for twenty hours. Subsequently all volatiles were removed and the water phase was twice extracted with CH_2Cl_2. The combined organic phases were dried over Na_2SO_4 and the solvent was evaporated. The resulting residue was purified by column chromatography (silica, diethyl ether) to provide **4b** in 74% yield as a colorless sticky foam. NMR data were in accordance with the literature and are repeated for convenience.[180] ^{1}H NMR (400 MHz, $CDCl_3$): δ= 8.41 (d, $^3J_{HH}$ = 4.5 Hz, 1H), 7.92- 7.83 (m, 4H), 7.57-7.53 (m, 1H), 7.41-7.30 (m, 4H), 7.25-7.18 (m, 2H), 7.14-7.11 (m, 1H), 7.07 (d, $^3J_{HH}$ = 8.4 Hz, 1H), 7.01 (d, $^3J_{HH}$ = 7.9 Hz, 1H), 5.41 (d, 1H), 5.30 (d, 1H) ppm. ^{13}C NMR (101 MHz, $CDCl_3$): δ= 153.8, 152.0, 183.3, 134.0, 133.9, 130.7, 129.9, 129.7, 129.1, 128.2, 128.1, 127.3, 126.5, 125.3, 124.9, 124.6, 123.4, 123.3, 122.5, 122.4, 119.7, 118.7, 119.7, 118.7, 118.1, 115.5, 115.3, 68.8 ppm.

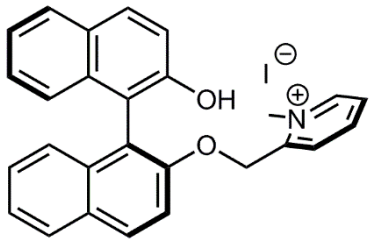

4c

Synthesis of 4c: *Reaction was run under ambient conditions.* **4b** (2.25 g, 6 mmol) was dissolved in acetone and CH_3I (1.49 mL, 3.38 g, 23.8 mmol) was added. The mixture was refluxed under stirring for four days. Next, the resulting colorless precipitate was filtered off and washed with diethyl ether to afford analytically pure **4c** in 61% yield. ^{1}H NMR (400 MHz, $CDCl_3$/MeOD): δ= 8.49 (d, $^3J_{HH}$ = 6.1 Hz, 1H), 7.92-7.87 (m, 2H), 7.77 (d, $^3J_{HH}$ = 8.2 Hz, 1H), 7.67-7.66 (m, 2H), 7.59 (t, $^3J_{HH}$ = 6.9 Hz, 1H), 7.50 (d, $^3J_{HH}$ = 8.9 Hz, 1H), 7.39 (d, $^3J_{HH}$ = 7.9 Hz, 1H), 7.29-7.25 (m, 1H), 7.15-7.07 (m, 4H), 6.99 (t, $^3J_{HH}$ = 7.6 Hz, 1H), 6.74 (d, $^3J_{HH}$ = 8.4 Hz,1H), 5.33 (d, $^3J_{HH}$ = 15 Hz, 1H), 5.25 (d, $^3J_{HH}$ = 15 Hz, 1H), 3.74 (s, 3H) ppm. ^{13}C NMR (101 MHz, $CDCl_3$/MeOD): δ= 153.7, 153.3, 153.1, 147.2, 145.8, 134.7, 134.4, 131.4, 131.0, 130.4, 129.1, 128.6, 128.3, 127.5, 127.4, 127.3, 126.2, 125.6, 124.9, 123.7, 122.7, 118.5, 118.1, 115.5, 68.9, 45.4 ppm. HRMS-ESI *m/z* calcd. for $C_{27}H_{22}NO_2^+$: 392.1645; found 392.1610.

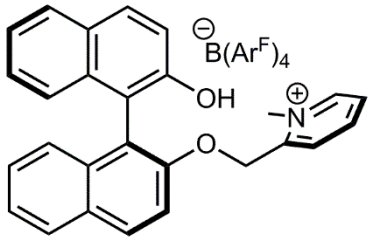

4

Synthesis of 4: **4c** (200 mg, 0.4 mmol) was dissolved in a mixture of acetonitrile and CH_2Cl_2 and a solution of $Na(BAr^F)_4$ (341 mg, 0.4 mmol) in a mixture of acetonitrile and CH_2Cl_2 was added. The mixture was stirred at room temperature for 12 hours. The solvent was removed, and the remaining residue was dissolved in CH_2Cl_2. The resulting suspension was filtered over Celite®. The slightly yellow filtrate was evaporated to dryness and **4** was isolated in 89% yield as slightly yellow solid foam. ^{1}H NMR (400 MHz, CD_2Cl_2): δ= 8.19 (d, $^3J_{HH}$ = 9.0 Hz, 1H), 8.07 (t, $^3J_{HH}$ = 7.3 Hz, 1H), 8.02 (d, $^3J_{HH}$ = 8.3 Hz, 1H), 7.96 – 7.82 (m, 3H), 7.76 – 7.69 (m, 8H), 7.65 – 7.58 (m, 2H), 7.55 (s, 4H), 7.54 – 7.49 (m, 2H), 7.35 (d, $^3J_{HH}$ = 2H), 7.27 (d, $^3J_{HH}$ = 8.9 Hz, 1H), 7.20 (m, 1H), 7.14 (m, 1H), 6.78 (m, 1H), 5.36-5.32 (m*, 1H), 5.24 (d, $^3J_{HH}$ = 14.6 Hz, 1H), 3.66 (s, 3H) ppm. ^{19}F NMR (376 MHz, CD_2Cl_2): δ= -62.85 ppm. ^{13}C NMR (101 MHz, CD_2Cl_2): δ= 161.85 (q, $^1J_{CB}$ = 49.8 Hz, C_{ipso} $B(Ar^F)_4$), 153.4, 151.7, 151.6, 145,8, 145.1, 134.9, 133.5, 133.4, 132.7, 131.7, 130.8, 129.2 (m, $B(Ar^F)_4$), 128.7, 128.5, 128.5, 127.7, 127.3, 126.8, 125.5, 124,6 (q, $^1J_{CF}$ = 272.5 Hz, CF_3 $B(Ar^F)_4$), 14.3, 124.1, 120.1, 118.1, 117.9, 117.7 (m, $B(Ar^F)_4$), 114.1, 69.3, 45.02 ppm. HRMS-ESI *m/z* calcd. for $C_{27}H_{22}NO_2^+$: 392.1645; found 392.1622. * Should be a doublet, second signal overlaps with CD_2Cl_2 solvent residual signal.

7.4.2 SYNTHESIS OF METAL COMPLEXES

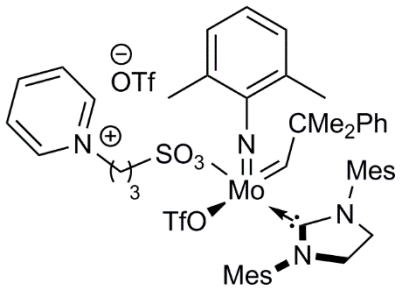

Mo-3

Synthesis of Mo-3**: Mo-1** (189 mg, 0.2 mmol) was dissolved in CH_2Cl_2 and the sulfobetaine **8** (40 mg, 0.2 mmol) was added as a solid. After three days the reaction mixture was filtered over Celite® and the solvent was removed *in vacuo*. The residue was crystallized from a mixture of CH_2Cl_2 and pentane. The obtained yellow crystals were rinsed with cold CH_2Cl_2 and **Mo-3** was isolated in 82 % yield as a bright yellow solid. ^{1}H NMR (400 MHz, CD_2Cl_2): δ = 12.94 (br, s,

1H)*, 9.05 (br, s, 2H), 8.44 (t, $^{3}J_{HH}$ = 7.8 Hz, 1H), 8.02 (t, $^{3}J_{HH}$ = 6.9 Hz, 2H), 7.14–7.11 (m, 3H), 7.04–6.99 (m, 7H), 6.78 (br, s, 2H), 4.75 (br, s, 2H), 4.12 (br, s, 4H), 2.90 (d, *J* = 42.8 Hz, 2H), 2.38–2.33 (m, 11H), 2.28 (br s, 6H), 2.19 (br, s, 6H), 1.82 (br, s, 3H), 1.50 (br, s, 3H), 0.92 (br, s, 3H) ppm. ^{19}F NMR (376 MHz, CD_2Cl_2): δ = -78.52 ppm. ^{13}C NMR (101 MHz, CD_2Cl_2): δ = 316.1, 205.1, 154.2, 147.1, 146.0, 145.5, 140.9, 137.1, 136.8, 135.5, 133.7, 130.9, 130.6, 130.3, 129.1, 128.6, 128.4, 127.0, 126.5, 121.1 (q, $^{1}J_{CF}$ = 313.5 Hz, CF_3 OTf), 59.6, 57.2, 52.7, 47.1, 28.9, 28.5, 26.2, 21.1, 20.1, 18.7, 18.3 ppm. Elemental analysis calcd. (%) for $C_{49}H_{58}F_6MoN_4O_9S_3$: C 51.04, H 5.07, N 4.86; found: C 51.07, H 5.269, N 4.75. Crystallographic data of **Mo-3** can be found under CCDC-1484327 at the Cambridge Crystallographic Data Centre. *The configuration of the alkylidene ligand in solution (*syn*- or *anti*-isomer) could not be determined from the ^{1}H NMR spectrum because the alkylidene signal was too broad due to the triflate exchange.

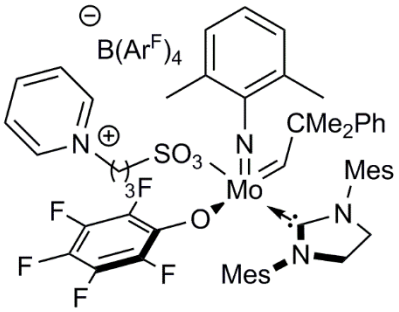

Mo-5

Synthesis of Mo-5: Sulfobetaine **8** (0.05 mmol, 9.4 mg) and $NaB(Ar^F)_4$ (0.05 mmol, 41 mg) were suspended in CH_2Cl_2 containing two drops of diethyl ether. A solution of **Mo-4** (0.05 mmol, 45.9 mg) in CH_2Cl_2 was added dropwise. The solution immediately turned red-orange. The solution was stirred for 12 hours during which the solution turned light yellow again. The reaction mixture was filtered and the solvent was removed from the filtrate. The resulting yellow residue was recrystallized from a mixture of CH_2Cl_2 and pentane to yield yellow crystals (Yield: 87%). ^{1}H NMR (400 MHz, CD_2Cl_2): δ = 14.7 (s, 0.43 H, $^{1}J_{CH}$ = 150.0 Hz, *anti*), 13.57 (s, 0.57 H), 8.42 (t, $^{3}J_{HH}$ = 7.0 Hz, 2H), 8.36–8.30 (m, 1H), 7.81 (t, $^{3}J_{HH}$ = 7.4 Hz, 2H), 7.64 (br, s, 8H), 7.48 (br, s, 4H), 7.31-7.23 (m, 5H), 7.10–6.76 (m, 4H), 4.47–4.35 (m, 2H), 3.93–3.67 (m, 4H), 2.58 (s, 1H), 2.30–2.26 (m, 3H), 2.21–2.11 (m, 4H), 2.03–1.95 (m, 17 H), 1.89–1.86 (m, 3H), 1.82–1.76 (m, 5H), 1.45 (s, 1H) ppm. ^{19}F NMR (376 MHz, CD_2Cl_2): δ = -62.87 (s, 24F), -159.58 – -161.02 (m, 2F), -168.43 – -168.55 (m, 2F), -174.39 – -175.01 (m, 1F) ppm. ^{13}C NMR (101 MHz, CD_2Cl_2): δ = 339.6, 318.7, 211.9, 211.6, 162.4 (q, $^{1}J_{BC}$ = 50 Hz, C_{ipso} $B(Ar^F)_4$), 156.5, 154. 3, 151.1, 150.7, 146.6, 144.8, 141.0, 139.9, 139.5, 138.6, 137.4, 136.7, 136.2, 136.0, 135.4, 135.2, 134.5, 130.2, 129.8, 129.6, 129.3, 129.0, 128.8, 128.8, 128.6, 128.4, 127.9, 127.5, 126.8, 126.5, 126.3, 126.1, 123.8 (q, $^{1}J_{CF}$ = 272.4 Hz, CF_3 $B(Ar^F)_4$),

121.1, 118.1, 60.1, 59.9, 55.7, 52.8, 52.0, 46.1, 45.7, 36.7, 34.1, 30.6, 29.8, 26.9, 26.8, 21.3, 21.2, 20.9, 20.5, 20.2, 18.9, 18.8, 18.5, 18.4 ppm. Elemental analysis calcd. (%) for $C_{85}H_{70}BF_{29}MoN_4O_4S$: C 53.70, H 3.71, N 2.95; found: C 53.85, H 3.718, N 2.98.

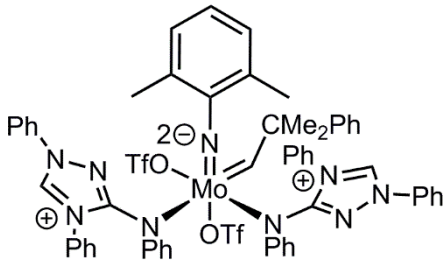

Mo-6

Synthesis of Mo-6: A solution of **Mo-P1** (100 mg, 0.14 mmol) in toluene was cooled to -35 °C. A suspension of nitron **9** (84.9 mg, 0.27 mmol) in toluene at -35 °C was slowly added to the precursor solution. After approximately 30 minutes the suspension turned into a bright orange solution and after one hour a yellow precipitate was observed. After two hours the suspension was filtered and the filtrate was washed with small amounts of toluene and diethyl ether. **Mo-6** was isolated in quantitative yield as a yellow solid. ^{1}H NMR (400 MHz, C_6D_6): δ = 14.74 (s, 1H, $^1J_{CH}$ = 126.1 Hz, *syn*), 8.95 (s, 2H), 7.74 (d, $^3J_{HH}$ = 6.3 Hz, 4H), 7.45 (d, $^3J_{HH}$ = 4.8 Hz, 4H), 7.08 (t, $^3J_{HH}$ = 7.2 Hz, 3H), 6,97 (t, $^3J_{HH}$ = 7.53 Hz, 4H), 6.90–6.81 (m, 9H), 6.77–6.66 (m, 9H), 6.60–6.57 (m, 4H), 2.45 (s, 6H), 0.94 (s, 6H) ppm. ^{19}F NMR (376 MHz, C_6D_6): δ = -77.75 (s, 3F), -77.93 (s, 3F) ppm. ^{13}C NMR (101 MHz, C_6D_6): δ = 322.2, 156.9, 154.7, 150.9, 148.4, 139.0, 137.2, 135.0, 132.9, 130.5, 129.7, 129.5, 129.3, 127.2, 126.8, 126.0, 125.7, 123.8, 121.1, 56.8, 29.4, 19.6 ppm. Elemental analysis calcd. (%) for $C_{60}H_{53}F_6MoN_9O_6S_2$: C 56.74, H 4.21, N 9.92; found: C 57.04, H 4.514, N 9.85.

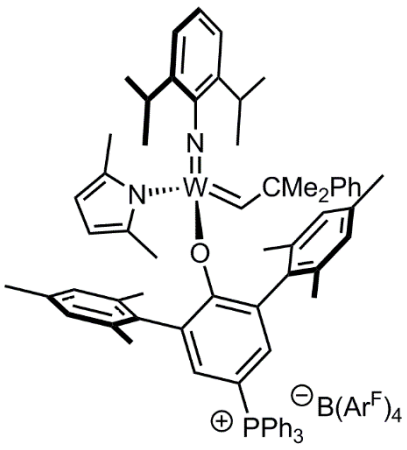

W-2

Synthesis of W-2. W-1 (50 mg, 0.10 mmol) was dissolved in benzene and **2** (99 mg, 0.10 mmol) was added as a solid. The suspension was heated to 70 °C for 12 hours. The

solvent was evaporated from the yellow solution and the resulting residue was washed with a mixture of pentane and diethyl ether to afford **W-2** in quantitative yield as yellow foam. ^{1}H NMR (400 MHz, $CDCl_3$): δ = 8.70 (s, 1H), 8.38 (br s, 8H, *o*-H, $B(Ar^F)_4$), 7.57 (s, 4H, *p*-H, $B(Ar^F)_4$), 7.26-7.24 (m, 2H), 7.17-7.13 (m, 2H), 7.07-6.91 (m, 18H), 6.83-6.78 (m, 6H), 6.73-6.70 (m, 5H), 6.01 (s, 1H), 5.79 (s, 1H), 3.10-2.99 (m*, 2H, H_3C-C*H*-CH_3, *i*Pr), 2.27 (s, 3H), 2.09 (s, 6H, H_3C, OHMT), 1.94 (s, 6H, H_3C, OHMT), 1.84 (s, 6H, H_3C, OHMT), 1.77 (s, 3H), 1.55 (s, 3H), 1.32 (s, 3H), 1.12 (br s, 3H, H_3C, *i*Pr)**, 1.06 (br s, 3H, H_3C, *i*Pr)**, 0.95 (br s, 3H, H_3C, *i*Pr)**, 0.66 (br s, 3H, H_3C, *i*Pr)** ppm. ^{19}F NMR (376 MHz, $CDCl_3$): δ = -62.2 ppm. ^{13}C NMR ($CDCl_3$): δ = 267.2 (alkylidene), 165.4 (d, $^{4}J_{CP}$ = 3.3 Hz, *ipso*-C, OHMT), 162.8 (q, $^{1}J_{CB}$ = 50 Hz, C_{ipso} $B(Ar^F)_4$), 151.8, 151.1, 149.1, 144.7,139.0, 137.5, 137.3, 136.2 (d, $^{2}J_{CP}$ = 19.1 Hz, *m*-C, OHMT), 135.7 (d, $^{3}J_{CP}$ = 14.2 Hz, *o*-C, OHMT), 135.42 ($B(Ar^F)_4$),133.7 (d, $^{3}J_{CP}$ = 10.5 Hz, *m*-C, PPh_3), 132.7, 132.7, 130.3 (d, $^{2}J_{CP}$ = 12.5 Hz, *o*-C, PPh_3), 130.0 (m, $B(Ar^F)_4$), 129.3, 128.5, 126.5, 126.4, 125.2 (q, $^{1}J_{CF}$ = 272.8 Hz, CF_3 $B(Ar^F)_4$), 123.1 (d, $^{1}J_{CP}$ = 71.1 Hz, *p*-C, OHMT), 118.3, 118.1 (m), 117.4, 111.3 (d, $^{1}J_{CP}$ = 39.5 Hz, *ipso*-C, PPh_3), 109.1, 108.2, 106.5, 54.47, 33.6, 30.9, 28.8, 28.1, 23.5, 23.1, 21.1, 20.8, 19.0, 15.2 ppm.*Expected: two heptets, not resolved due to fast rotation.** Expected: doublets, not resolved due to fast rotation. Elemental analysis calcd. (%) for $C_{102}H_{88}BF_{24}N_2OPW$: C 60.07, H 4.35, N 1.37; found: C 59.69, H 4.687, N 1.72.

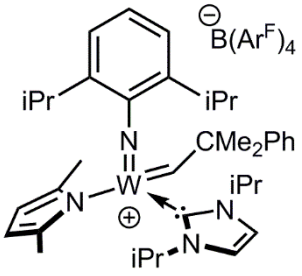

W-4

Synthesis of W-4: Compound **W-3** (50 mg, 0.006 mmol) was suspended in CH_2Cl_2 and a solution of *N*,*N*-dimethylanilinium $B(Ar^F)_4$ (62.6 mg, 0.006 mmol) in diethyl ether was added. The suspension immediately turned into a yellow orange solution. The reaction mixture was stirred for one hour at room temperature. Subsequently the solvent was removed, and the resulting residue was twice extracted with pentane to remove dimethylaniline and pyrrole. The remaining solid was crystallized from a mixture of CH_2Cl_2, diethyl ether and pentane. Complex **W-4** was obtained in 92% yield as light-yellow crystals. ^{1}H NMR (400 MHz, CD_2Cl_2): *δ*= 12.11 (s, 1H, $^{1}J_{CH}$ = 124.5 Hz, *syn*), 7.74 (br s, 8H), 7.58 (s, 4H), 7.46- 7.35 (m, 6H), 7.26- 7.17 (m, 4H), 6,19 (s, 1H), 5,97 (s, 1H), 4.32 (hept, 2H, $^{3}J_{HH}$ = 6.6 Hz), 3.29 (hept, 2H, $^{3}J_{HH}$= 6.8 Hz), 2.45 (s, 3H), 2.00 (s, 3H), 1.77 (s, 3H), 1.69 (s, 3H), 1,36 -1.20 (m, 18 H), 0.89 (s, 3H), 0.87

(s, 3H) ppm. ^{19}F NMR (376 MHz, CD_2Cl_2): δ= -62.81 ppm. ^{13}C NMR (101 MHz, CD_2Cl_2): δ= 298.4, 172.0, 162.4 (q, $^1J_{CB}$ = 50 Hz, C_{ipso} B(Ar^F)$_4$), 150.4, 149.4, 144.8, 135.4, 129.5 (m, B(Ar^F)$_4$), 129.3, 128.8, 127.3, 126.6, 125.2 (q*, $^1J_{CF}$ = 272.0 Hz, CF_3 B(Ar^F)$_4$), 123.9, 122.7, 118.1 (m, B(Ar^F)$_4$), 103.5, 100.3, 57.7, 56.0, 32.5, 31.1, 29.0, 24.3, 24.1, 23.6, 23.2, 18.6, 15.8 ppm. Elemental analysis calcd (%) for $C_{69}H_{65}BF_{24}N_4W$: C 51.77, H 4.09, N 3.50; found: C 51.61, H 4.133, N 3.47. * Only three of the four expected resonances of the quartet can be unambiguously assigned since the fourth signal overlaps with a set of other signals.

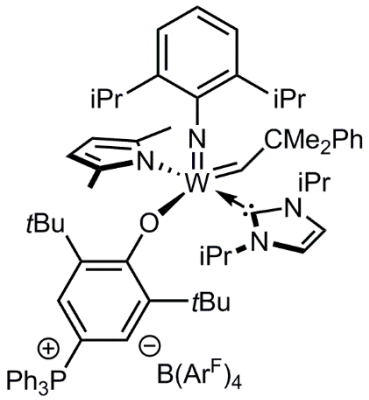

W-5

Synthesis of W-5. W(*N*-2,6-iPr-C_6H_3)(CHCMe$_2$Ph)(2,5-Me$_2$-C_4H_2)$_2$(IPr) **W-3** (100 mg, 0.1 mmol) was suspended in CH_2Cl_2 and a solution of [HO(2,6-*t*Bu-4-PPh$_3$-C_6H_3)][B(Ar^F)$_4$] **1** (157.1 mg, 0.1 mmol) was added at -35 °C. After eight hours, the solvent was removed, and the resulting residue was washed with mixture of pentane and diethyl ether (1/1, V/V) to remove residual 2,5-dimethylpyrrole. The remaining residue was crystallized from a mixture of CH_2Cl_2, diethyl ether and pentane to afford **W-5** as yellow crystals in 79 % yield. ^{1}H NMR (400 MHz, C_6D_6): δ = 11.66 (s, 1H, $^1J_{CH}$ = 124.71 Hz, *syn*), 7.29–7.26 (m, 12H), 7.21–7.17 (m, 6H), 7.15–7.14 (m, 5H), 7.08 (s, 4H), 6.98–6.92 (m, 4H), 6.90 (s, 2H), 6.83–6.78 (m, 2H), 6.73 (s, 1H), 6.71 (s, 1H), 6.41 (d, 2H, $^2J_{HP}$ = 13.0 Hz), 5.68 (s, 1H), 5.47 (s, 1H), 3.87–3.81 (m, 2H), 2.85–2.78 (m, 2H), 2.00 (s, 3H), 1.50 (s, 3H), 1.32 (s, 3H), 1.23 (s, 3H), 0.99–0.88 (br, s, 33H), 0.81 (s, 3H), 0.80 (s, 3H), 0.45–0.42 (m, 6H) ppm. ^{19}F NMR (376 MHz, C_6D_6): δ = -62.4 ppm. ^{31}P NMR (162 MHz, $CDCl_3$): δ = 21.34 ppm. ^{13}C NMR (101 MHz, CD_2Cl_2): δ = 298.3, 177.0, 171.9, 162.4 (q, $^1J_{CB}$ = 50 Hz, C_{ipso} B(Ar^F)$_4$), 149.9 (d, $^1J_{CP}$ = 96.7 Hz), 144.8, 140.8 (d, $^2J_{CP}$ = 14.1 Hz), 135.4, 134.7 (d, $^3J_{CP}$ = 9.9 Hz), 134.3 (d, $^4J_{CP}$ = 2.4 Hz), 130.1 (d, $^3J_{CP}$ = 13.3 Hz), 130.0 (d, $^2J_{CP}$ = 12.6 Hz), 129.5 (qq, $^3J_{CB}$ = 3.1 Hz, $^2J_{CF}$ = 32.9 Hz), 128.8, 127.3, 125.2 (q, $^1J_{CF}$ = 271.8 Hz, CF_3 B(Ar^F)$_4$), 124.6, 123.6 (d, $^1J_{CP}$ = 89.2 Hz), 122.9 (br, s), 118.1 (hept, $^2J_{CF}$ = 3.9 Hz), 106.2, 103.4, 100.3, 79.2, 78.1, 57.7, 55.9, 35.7, 32.5, 31.1, 29.6, 28.9, 24.3, 24.1, 23.6, 18.6, 15.8 ppm. Elemental analysis calcd. (%) for $C_{101}H_{100}BF_{24}N_4OPW$: C 58.67, H 4.88, N 2.71; found: C 58.95, H 4.965, N 2.77.

7.4.3 CATALYSIS

Biphasic RCM and HM with catalysts Mo-3, Mo-5, Mo-6, Mo-7, Mo-8, Mo-9 and W-2: Substrate (1000 equiv. with respect to catalyst) and dodecane (two drops, internal standard) were dissolved in heptane (0.3 mL) and filtered over aluminum oxide. A sample for GC-MS was withdrawn. Next, a stock solution of catalyst **Mo-3**, **Mo-5**, **Mo-6**, **Mo-7**, **Mo-8**, **Mo-9** or **W-2** (0.2 mL, 1 mg/mL in pyrrole) was added. The reaction mixture was stirred for six hours at the indicated temperature (80 °C, 60 °C or room temperature). Subsequently, the sample was cooled to room temperature and acetone was added to homogenize the mixture. A sample for GC-MS was withdrawn.

RCM and HM with catalysts Mo-3, Mo-5, Mo-6, Mo-7, Mo-8, Mo-9, W-2 and W-5: Substrate (1000 equiv. with respect to catalyst) and dodecane (two drops) were dissolved in the indicated solvent (0.3 mL, toluene or 1,2-dichloroethane) and filtered over aluminum oxide. A sample for GC-MS was taken. Subsequently, a stock solution of catalysts **Mo-3**, **Mo-5**, **Mo-6**, **Mo-7**, **Mo-8**, **Mo-9**, **W-2** or **W-5** (0.2 mL, 1 mg/mL in toluene or 1,2-dichloroethane) was added. The reaction mixture was stirred for six hours at the indicated temperature (80 °C, 60 °C or room temperature). Then the sample was cooled to room temperature and acetone was added. A sample for GC-MS was withdrawn.

Recycling of catalysts Mo-3 and Mo-5: Substrate (1000 equivalents with respect to catalyst) and dodecane (two drops) were dissolved in heptane (0.3 mL) and filtered over aluminum oxide. Subsequently, a stock solution of catalyst **Mo-3** or **Mo-5** (0.2 mL, 1 mg/mL in pyrrole) was added. The reaction mixture was stirred for six hours at the indicated temperature (80 °C or room temperature). Then the sample was cooled to room temperature and the nonpolar heptane phase was removed with a syringe. Again, a mixture of substrate (1000 equivalents) and dodecane (two drops) in heptane (0.3 mL) that had been passed over aluminum oxide was added. Once more the reaction mixture was stirred for six hours at the indicated temperature (80 °C or room temperature). Then the sample was cooled to room temperature and acetone was added to homogenize the mixture. A sample for GC-MS was withdrawn.

Determination of the Mo-content in the heptane phase by ICP-OES: Once the corresponding olefin metathesis reaction was finished (indicated reaction temperature, reaction time), additional 0.3 mL of heptane were added. The sample was stored in the fridge (-35 °C) for 10 minutes. Then the upper part of the heptane layer (0.3 mL) was carefully removed with a syringe and transferred into a microwave vessel. The solvent was removed *in vacuo*. Freshly prepared *aqua regia* (HCl : HNO_3 = 3:1, approximately 1.5 g) was added. The mixture was exposed to microwave irradiation (Table 10). The resulting residue was diluted with demineralized water (25 mL) and filtered over glass fiber filter paper. The resulting clear

solution was subjected to ICP-OES. For calibration, Mo-containing standard solutions (5 % HNO_3, Chem-Lab, Zedelgem, Belgium) containing 0.00, 0.10, 1.00, and 5.00 mg Mo per kg were used. Mo was measured at λ = 202.095 nm, the background was measured at λ = 430.01 nm. The detection range was from 0.00205 to 6 $mg \cdot L^{-1}$. The standard error was 0.0636 $mg \cdot L^{-1}$.

Table 10: Microwave program for ICP-OES samples.

t [min]	Power [W]	T [°C]
20	0	r.t.
10	600	r.t. → 160°C
60	600	160°C
30	0	160°C → r.t.

NMR experiments with Mo-1 and Mo-3: The respective catalyst (approx. 5 mg, 1 equiv.) was dissolved in $CDCl_3$ (0.3 mL) and a solution of 5,6-bis(pentyloxymethyl)bicyclo[2.2.1]hept-2-ene **M1** (approx. 5 equiv.) in $CDCl_3$ (0.3 mL) was added quickly. After 5 minutes ^{1}H NMR spectra of the samples were taken to compare the resonances of the propagating species.

Polymerization of M1 with Mo-3: A solution of catalyst **3** (8 mg, 1 equiv.) in 1,2-dichloroethane (0.5 mL) was added to a solution of 5,6-bis((pentyloxy)methyl)bicyclo[2.2.1]hept-2-ene **M1** (50 eq) in 1,2-dichloroethane (0.5 mL). The reaction mixture was stirred at 80 °C for 3 hours and then poured into methanol. The precipitated polymer was isolated by centrifugation, washed with pentane and dried. For GPC analysis a solution of the polymer in dry $CHCl_3$ with a concentration of 5 mg·mL was prepared. An off-white gum was precipitated from methanol. Yield: Quantitative. ^{1}H NMR (400 MHz, $CDCl_3$) δ = 5.27- 5.17 (br s, 2H), 3.42- 3.31 (m, 8H), 2.32 (br s, 2H), 1.93- 1.88 (m, 4H); 1.56- 1.53 (m, 4H), 1.33- 1.30 (m, 8H); 0.91- 0.88 (m, 6H) ppm. ^{13}C NMR (101 MHz, $CDCl_3$) δ = 133.7, 71.22- 70.23 (m), 50.7- 39.9 (m), 29.6, 28.6, 22.6, 14.2 ppm. FT- IR (ATR, cm^{-1}):v = 2926 (s), 2855 (s), 1460 (m), 1368 (m), 1103 (s), 1009 (m), 969 (m), 737 (w). GPC Data ($CHCl_3$): M_n = 21,900 $g \cdot mol^{-1}$ ($M_{n,theor}$ = 14,700 $g \cdot mol^{-1}$); PDI = 3.

Polymerizations with W-4: Catalyst **W-4** (1 equiv., approximately 8 mg) was dissolved in 1,2-dichloroethane (0.5 mL) and a solution of the corresponding monomer **M1**-**M9** for cyclopolymerization or ROMP (50 equiv.) in 1,2-dichloroethane (0.5 mL) was added. The resulting mixture was heated to 80 °C and stirred for six hours. Next, the reaction mixture was cooled to room temperature and precipitated in methanol or pentane. The resulting precipitate was isolated by centrifugation and dried *in vacuo* to yield the ROMP or cyclopolymerization derived polymer.

*ROMP of 5,6-bis((pentyloxy)methyl)bicyclo[2.2.1]hept-2-ene **M1** with **W-4**:* An off-white gum was precipitated from methanol. Yield: Quantitative. ^{1}H NMR (400 MHz, $CDCl_3$): δ = 5.26 (m, 2H), 3.47- 3.29 (m, 8H), 2.31 (br s, 2H), 1,92 (br s, 2H), 1.56- 1.52 (m, 4H), 1.33- 1.29 (m, 8H); 0.91- 0.87 (m, 6H) ppm. ^{13}C NMR (101 MHz, $CDCl_3$): δ = 133.7, 71.1, 70.6, 50.6, 46.8, 45.1, 43.5, 40.9, 29.5, 28.6, 22.6, 14.1 ppm. FT- IR (ATR, cm^{-1}): v = 2915 (s), 2856 (s), 1461 (m), 1368 (m), 1103 (s). GPC Data ($CHCl_3$): M_n = 23,000 g/mol ($M_{n,theor}$ = 14,700 g/mol); PDI = 7.6.

*ROMP of (7-oxabicyclo[2.2.1]hept-5-ene-2,3-diyl)bis(methylene) diacetate **M2** with **W-4**:* An off-white gum was precipitated from methanol. Yield: 48 mg (64 %). ^{1}H NMR (400 MHz, $CDCl_3$): δ = 5.73- 5.55 (m, 2H), 4.51 (br s, 1H), 4.18- 4.14 (m, 5H), 2.41 (br s, 2H), 2.04- 2.03 (m, 6H) ppm. ^{13}C NMR (101 MHz, $CDCl_3$): δ = 170.7, 133.1- 132.1 (m), 81.4, 62.0, 46.4- 43.5 (m), 20.8 ppm. FT-IR (ATR, cm^{-1}): v = 3206 (s), 2951, 2259, 1732 (s), 1222 (s). GPC ($CHCl_3$): M_n = 23,000 g·mol^{-1} ($M_{n,theor}$ = 12,000 g·mol^{-1}); PDI = 2.4.

*ROMP of norborn-5-ene-2,3-dimethanol **M3** with **W-4**:* An off-white powder was precipitated from methanol. Yield: 9 mg (18 %). ^{1}H NMR (400 MHz, C_6D_6): δ = 5.31- 5.18 (m, 2H), 4.79 (br s, 2H), 3.51- 3.40 (m, 4H), 2.56 (br s, 2H), 2.14 (br s, 1H), 1.84 (br s, 1H) ppm. FT-IR (ATR, cm^{-1}): v = 3276 (b, OH), 2914 (m), 988 (b).

*Cyclopolymerization of 4-carboxy-1,6-heptadiyne **M4** with **W-4**:* Precipitated from methanol. Yield:12 mg (23 %). FT-IR (ATR, cm^{-1}): v = 3419 (b, OH), 2978 (w), 2889 (w), 1716 (s, C=O), 1593 (s), 1449 (s). Due to poor solubility in common solvents no NMR spectroscopy and GPC data could be obtained.

*Cyclopolymerization of dipropargylmalodinitrile **M5** with **W-4**:* A violett powder was precipitated from methanol. Yield: Quantitative. Due to poor solubility in common solvents no NMR spectra and GPC data could be obtained. FT-IR (ATR, cm^{-1}): v = 3417 (w), 2919 (s), 2854 (s), 2250 (w, CN), 1017 (s), 954 (s).

*Cyclopolymerization of 2,2-dipropargyl-1,3-propanediol **M6** with **W-4**:* Violet powder, precipitated from methanol. Yield: 8 mg (16 %). FT-IR (ATR, cm^{-1}): v = 3302 (b, OH), 2912 (s), 2846 (s), 1010 (s), 946. Due to poor solubility in common solvents no NMR spectroscopy and GPC data could be obtained.

*Cyclopolymerization of 3,5-dimethoxy- N,N- dipropargylaniline **M7** with **W-4**:* A dark violett to black powder was precipitated from methanol. Yield: 28 mg (38 %). Due to poor solubility in common solvents no NMR spectra and GPC data could be obtained. FT-IR (ATR, cm^{-1}): v = 2930 (b), 2830 (b), 1670 (s), 1446 (s), 1140 (s).

*Cyclopolymerization of dipropargyl sulfide **M8** with **W-4***: A dark violet powder was precipitated from methanol. Yield:10 mg (28 %). Due to poor solubility in common solvents no NMR spectroscopy and GPC data could be obtained. FT-IR (ATR, cm^{-1}): v = 3419 (b, OH), 2978 (w), 2889 (w), 1716 (s, C=O), 1593 (s), 1449 (s).

*Cyclopolymerization of 3,5-diethoxy-1,1'-(2,2-di-2-propyn-1-yl-1,3-propanediyl) benzoic acid ester **M9** with **W-4**:* A violett powder was precipitated from pentane. Yield: Quantitative. ^{1}H NMR (400 MHz, C_6D_6): δ = 7.04 (br s, 4H), 6.53 (br s, 2H), 4.27 (br s, 4H), 3.94 (br s, 8H), 1.34 (br s, 12H) ppm. ^{13}C NMR (101 MHz, C_6D_6): δ = 166.0, 160.1, 107.8, 106.4, 63.8, 14.8 ppm. FT-IR (ATR, cm^{-1}): v = 2977, 2888, 1716 (s), 1592 (s), 1159. UV- Vis: Absorption maximum: λ_{max}= 309 nm.

General procedure for RCM, HM and SM reactions with W-4: Reactions were carried out in closed cap vials in 1,2-dichloroethane (2 mL). Substrates (1000 equiv.) and solvent were passed over freshly dried neutral alumina oxide *prior* to catalyst (1 equiv.) addition. Reactions were run at 80 °C for three hours. TONs were determined by GC-MS with *n*-dodecane as internal standard.

Table 11: Additional attempted syntheses of olefin metathesis catalysts bearing alkoxide-based betaine ligands.

precursor complex	equiv. precursor complex/ligand	ionic ligand	base	solvent deprotonation	solvent reaction
Mo-P1 – **Mo-P5**	1/2	**1**	KH, KHMDS, *n*-BuLi	diethyl ether, THF, toluene	diethyl ether, THF, DMSO, toluene
Mo-P1 – **Mo-P5**	1/2	**2**	KH, KHMDS, *n*-BuLi	diethyl ether, THF, toluene	diethyl ether, THF, DMSO, toluene
Mo-P1 – **Mo-P5**	1/2	**3**	KH, KHMDS, *n*-BuLi	diethyl ether, THF, toluene	diethyl ether, THF, DMSO, toluene
Mo-P1 – **Mo-P5**	1/2	**4**	KH, KHMDS, *n*-BuLi	diethyl ether, THF, toluene	diethyl ether, THF, DMSO, toluene
Mo-1	1/1	**1**	KH, KHMDS, *n*-BuLi	diethyl ether, THF, toluene	CH_2Cl_2, THF, diethyl ether, toluene
Mo-1	1/1	**2**	KH, KHMDS, *n*-BuLi	diethyl ether, THF, toluene	CH_2Cl_2, THF, diethyl ether, toluene
Mo-1	1/1	**3**	KH, KHMDS, *n*-BuLi	diethyl ether, THF, toluene	CH_2Cl_2, THF, diethyl ether, toluene
Mo-1	1/1	**4**	KH, KHMDS, *n*-BuLi	diethyl ether, THF, toluene	CH_2Cl_2, THF, diethyl ether, toluene

The respective ligand was dissolved/suspended in the indicated solvent for deprotonation and the base (1 equiv. in respect to ligand) was added. The mixture was stirred until deprotonation was complete. Then, the mixture was filtered, dissolved in the indicated solvent for the reaction and cooled to -35°C. The respective precursor complex (0.5 or 1 equiv. respective to ligand) was dissolved in the reaction solvent and cooled to -35°C. The solution of the deprotonated ligand was slowly added to the solution of the precursor complex. Reaction mixtures were stirred 3-12 hours. Then, if necessary, the mixtures were filtered over Celite® and evaporated to dryness. The outcome of the reactions was checked by ^{1}H, ^{19}F and ^{31}P (if necessary) NMR spectroscopy.

7.5 *Molybdenum imido alkylidene complexes with chelating N-heterocyclic carbenes*

Parts of the following chapter have already been published. Reprinted (adapted) with permission from (I. Elser, W. Frey, K. Wurst, M. R. Buchmeiser, *Organometallics* **2016**, *35*, 4106-4111). Copyright (2016) American Chemical Society.

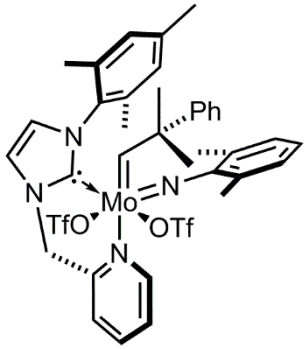

Mo-12

Synthesis of Mo-12: Imidazolium salt **10** (429 mg, 1.2 mmol) was suspended in benzene (5 mL) and a solution of KHMDS (239 mg, 1.2 mmol) in benzene (2 mL) was added. After one hour the brown-red suspension was filtered over Celite®. The filtrate was slowly added to a solution of **Mo-P1** (880 mg, 1.20 mmol) in benzene (20 mL). After a few minutes, precipitation of a yellow solid was observed. After two hours the product was filtered off as yellow solid and recrystallized from CH_2Cl_2 (6 mL) and pentane (0.5 mL) in 52 % yield. ^{1}H NMR (400 MHz, CD_2Cl_2): δ= 14.36 (s, 1H)*, 9.12 (d, 1H, $^3J_{HH}$ = 5.4 Hz), 8.00 (t, 2H, $^3J_{HH}$ = 8.35 Hz), 7.62 – 7.58 (m, 3H), 7.35 -7.31 (m, 3H), 7.21- 7.17 (m, 2H), 7.14- 7.12 (m, 1H), 7.03 – 6.99 (m, 1H), 6.92-6.89 (m, 3H), 6.49 (d, 2H), 5.58- 5.36 (m, 2H), 2.21 (s, 3H), 1.98 (br s, 6H), 1.75 (s, 3H), 1.62 (s, 6H), 1.41 (s, 3H) ppm. ^{19}F NMR (376 MHz, CD_2Cl_2): δ = -77.26 (s, 3F), -77.59 (s, 3F) ppm. ^{13}C NMR (101 MHz, CD_2Cl_2): δ = 330.6, 327.5, 183.4, 182.4, 158.4, 153.6, 153.4 152.8, 151.9, 149.5, 148.8, 146.7, 144.3, 140.9, 140.6, 140.4, 139.5, 136.5, 135.8, 135.1, 134.7, 134.1, 134.0, 131.2, 131.0, 130.4, 130.0, 129.7, 129.3, 129.0, 128.9, 128.8, 128.7, 128.4, 128.2, 127.4, 126.6, 126.2, 126.1, 126.1, 126.0, 125.5, 125.2, 125.2, 124.9, 120.3 (q, $^1J_{CF}$ = 318.7 Hz, CF_3 OTf), 119.9 (q, $^1J_{CF}$ = 319.7 Hz, CF_3 OTf), 57.9, 57.6, 55.5, 51.8, 33.8, 31.9, 29.0, 28.5, 21.1, 20.6, 19.2, 18.9, 18.7, 18.7, 18.0 ppm. Despite numerous efforts, inconsistent elemental analysis data were obtained. Crystallographic data of **Mo-12** can be found under CCDC-1504350 at the Cambridge Crystallographic Data Centre. *Assignment of *syn*- or *anti*-configuration was impossible due to the broad alkylidene signal.

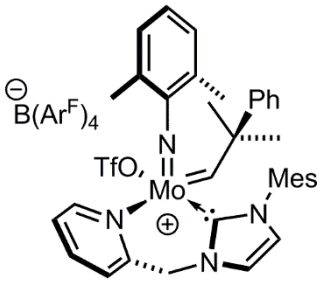

Mo-13

Synthesis of Mo-13: **Mo-12** (100 mg, 0.11 mmol) was dissolved in CH_2Cl_2 (3 mL) and a solution of $NaB(Ar^F)_4$ (96 mg, 0.11 mmol) in diethyl ether (1 mL) was added. After three hours the suspension was filtered over Celite® and the solvent was removed. The crude product was recrystallized from a mixture of CH_2Cl_2 (1 mL) and pentane (0.3 mL). **Mo-13** was isolated in 91 % yield in form of yellow crystals. ^{1}H NMR (400 MHz, CD_2Cl_2): δ = 14.73 (s, 1H, $^1J_{CH}$= 147.5 Hz, *anti*), 8.90 (d, 1H, $^3J_{HH}$ = 7.2 Hz), 8.16 (t, 1H, $^3J_{HH}$ = 8.5 Hz), 7.79 (m, 1H), 7.71 (m, 11H), 7.55 (s, 4H), 7.49 (d, 1H, $^3J_{HH}$ = 7.8 Hz), 7.27 (d, 1H, $^3J_{HH}$ = 1.9 Hz), 7.21- 7.11 (m, 4H), 7.00- 6.98 (m, 3H), 6.92 (s, 1H), 6.04 (s, 1H), 4.61 (d, 1H, $^3J_{HH}$ = 16.1 Hz), 3.10 (d, 1H, $^3J_{HH}$ = 16.1 Hz), 2.37 (s, 6H), 2.05 (s, 3H), 2.03 (s, 3H), 1.47 (s, 3H), 1.46 (s, 3H), 1.36 (s, 3H) ppm. ^{19}F NMR (376 MHz, CD_2Cl_2): δ = -62.86 (s, 24F), -77.81 (s, 3F) ppm. ^{13}C NMR (101 MHz, CD_2Cl_2): δ = 331.7, 184.2, 162.2 (q, $^1J_{CB}$ =49.5 Hz, C_{ipso} $B(Ar^F)_4$), 158.9, 152.5, 150.2, 146.7, 144.5, 140.9, 140.6, 135.3, 134.8, 134.3, 134.0, 131.6, 130.3, 129.8, 129.6, 129.5, 129.1, 128.9, 128.3, 126.9, 126.7, 126.4, 126.1, 125.19 (q, $^1J_{CF}$ = 272.7 Hz, CF_3 $B(Ar^F)_4$), 124.0, 117.9, 58.3, 52.5, 32.2, 28.5, 21.1, 20.6, 18.8, 17.8 ppm. Elemental analysis calcd. (%) for $C_{69}H_{52}BF_{27}MoN_4O_3S$: C 50.63, H 3.20, N 3.42; found: C 50.45, H 3.282, N 3.36. Crystallographic data of **Mo-13** can be found under CCDC-1504252 at the Cambridge Crystallographic Data Centre.

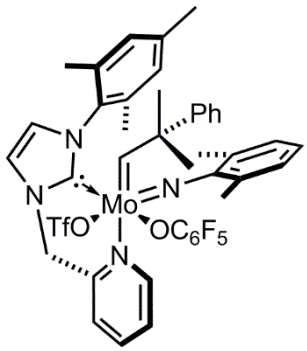

Mo-14

Synthesis of Mo-14: **Mo-12** (100 mg, 0.11 mmol) was dissolved in CH_2Cl_2 (3 mL) and cooled to -35 °C. A solution of lithium pentafluorophenoxide (20.6 mg, 0.11 mmol) in CH_2Cl_2 (1 mL)

was added dropwise. After 20 minutes, precipitation of a yellow solid was observed. After three hours, all solids (including the desired catalyst and lithium triflate) were removed by filtration. The solids were washed with acetonitrile (approx. 3 mL) to dilute the catalyst. The solvent was removed from the filtrate and the resulting solid was again dissolved in CH_2Cl_2 (8 mL) and filtered to remove residual lithium triflate. Removal of solvent afforded **Mo-14** as analytically pure solid in 96 % yield. ^{1}H NMR (400 MHz, CD_3CN): δ = 13.92 (s, 1H, $^1J_{CH}$= 126.2 Hz, *syn*), 8.26 (d, 1H, $^3J_{HH}$ = 4.7 Hz), 7.98 (td, 1H, $^3J_{HH}$ = 7.7 Hz, J = 1.7 Hz), 7.71 (d, 1H, $^3J_{HH}$ = 1.9 Hz), 7.66 (d, 1H, $^3J_{HH}$ = 7.7 Hz), 7.37- 7.18 (m, 7H), 7.11- 7.05 (m, 2H), 7.00 (s, 1H), 6.97 (s, 1H), 6.92 (s, 1H), 5.39 (d, 1H, $^3J_{HH}$ = 15.3 Hz), 5.19 (d, 1H, J = 15.3 Hz), 2.35 (s, 3H), 2.27 (s, 3H), 2.09 (s, 3H), 1.99 (s, 6H), 1.77 (s, 3H), 1.77 (s, 3H), 1.23 (s, 3H) ppm. ^{19}F NMR (376 MHz, CD_3CN): δ = -79.36 (s, 3F), -163.34- -163.42 (m, 2F), -169.18- -169. 30 (m, 2F), -177.82- -177.99 (m, 1F) ppm. ^{13}C NMR (101 MHz, CD_3CN): δ = 338.7 (Mo=C), 186.3, 153.6, 153.3, 151.1, 147.4, 141.1, 140.3, 140.1, 137.4, 136.7, 135.9, 135.5, 130.5, 129.2, 128.3, 127.4, 127.0, 126.3, 125.6, 125.3, 124.1, 121.8 (q, $^1J_{CF}$ = 319.6 Hz, CF_3 OTf), 75.3, 55.6, 30.0, 29.5, 21.1, 20.4, 19.1, 19.0, 7.4 ppm. Elemental analysis calcd. (%) for $C_{43}H_{40}F_8MoN_4O_4 \cdot CH_3CN$: C 54.16, H 4.34, N 7.02; found C 54.52, H 4.493, N 7.02.

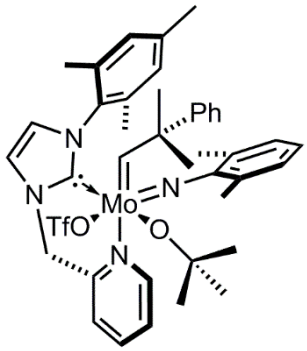

Mo-15

Synthesis of Mo-15: **Mo-12** (80 mg, 0.09 mmol) was dissolved in CH_2Cl_2 (2 mL) and cooled to -35°C. A solution of lithium *tert*-butoxide (6.9 mg, 0.09 mmol) in CH_2Cl_2 and diethyl ether (1 mL, V/V 1/1) was cooled to -35°C and added to the solution of **Mo-12**. After three hours, lithium triflate was removed by filtration over Celite®. The filtrate was concentrated, and pentane was added until the solution turned cloudy. **Mo-15** was obtained by storing the solution at -35°C as yellow crystals in 57 % yield. ^{1}H NMR (400 MHz, CD_2Cl_2): δ = 11.87 (s, 1H, $^1J_{CH}$= 119.7 Hz, *syn*), 9.23 (d, 1H, $^3J_{HH}$ = 5.4 Hz), 7.98 (d, 1H, $^3J_{HH}$ = 1.7 Hz), 7.80 (t, 1H, $^3J_{HH}$ = 7.6 Hz), 7.69 (d, 1H, $^3J_{HH}$ = 7.6 Hz), 7.41-7.38 (m, 1H), 7.09 (d, 1H, $^3J_{HH}$ = 1.7 Hz), 7.06-7.02 (m, 4H), 6.99-6.92 (m, 7H), 5.68 (d, 1H, $^3J_{HH}$ = 14.9 Hz), 5.35 (d, 1H, $^3J_{HH}$ = 14.9 Hz), 2.37 (s, 3H), 2.19 (s, 6H), 1.95 (s, 3H), 1.74 (s, 3H), 1.47 (s, 3H), 1.17 (s, 3H), 1.08 (s, 9H) ppm. ^{19}F NMR (376 MHz, CD_2Cl_2): δ = -78.93 ppm. ^{13}C NMR (101 MHz, CD_2Cl_2): δ = 303.2, 183.8,

155.4, 153.0, 149.6, 148.3, 141.2, 140.1, 135.9, 135.6, 134.9, 130.8, 130.46, 128.7, 128.5, 128.5, 126.6, 126.5, 126.5, 125.7, 125.6, 124.7, 124.7, 121.5 (q, $^{1}J_{CF}$ = 320.6 Hz, CF_3 OTf), 81.5, 55.7, 55.0, 34.7, 32.2, 31.7, 31.4, 22.9, 21.5, 19.6, 19.2, 18.9, 14.4 ppm. Despite numerous efforts, inconsistent elemental analysis data were obtained.

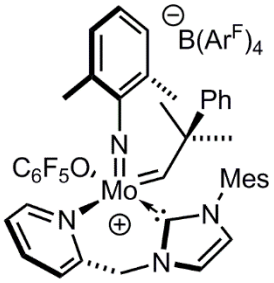

Mo-16

Synthesis of Mo-16: **Mo-14** (30 mg, 0.03 mmol) was dissolved in CH_2Cl_2 (1 mL) and a solution of $NaB(Ar^F)_4$ (27.8 mg, 0.03 mmol) in diethyl ether (0.5 mL) was added dropwise. After two hours, the solvent was removed, and the residue was dissolved in CH_2Cl_2. The suspension was filtered over Celite® and the filtrate was evaporated to dryness. **Mo-16** was obtained by crystallization from CH_2Cl_2 (0.5 mL) and pentane (0.1 mL) in 77 % yield. ^{1}H NMR (400 MHz, CD_2Cl_2): δ = 13.90 (s, 1H, $^{1}J_{CH}$ = 125.6 Hz, *syn*), 8.22 (d, 2H, $^{3}J_{HH}$ = 6.0 Hz), 7.95 (td, 1H, $^{3}J_{HH}$ = 7.7 Hz, $^{3}J_{HH}$ = 1.7 Hz), 7.70 (br s, 8H), 7.67 (br s, 4H), 7.65 (d, 1H, $^{3}J_{HH}$ = 1.9 Hz) 7.62 (d, 1H, $^{3}J_{HH}$ = 7.7 Hz), 7.33- 7.22 (m, 6H), 7.19- 7.15 (m, 1H), 7.08- 7.00 (m, 2H), 6.95 (br s, 2H), 6.89 (br s, 1H), 5.34 (d, 1H, $^{3}J_{HH}$ = 15.3 Hz), 5.16 (d, 1H, $^{3}J_{HH}$ = 15.3 Hz), 2.32 (s, 3H), 2.24 (s, 3H), 2.05 (s, 3H), 1.97 (s, 3H), 1.75 (s, 3H), 1.74 (s, 3H), 1.20 (s, 3H) ppm. ^{19}F NMR (376 MHz, CD_2Cl_2): δ = -62.42 (s, 24F), -162.74 (s, 2F)*, -165.95 (s, 2F)*, -173.21 (s, 1F)* ppm. ^{13}C NMR (101 MHz, CD_2Cl_2): δ = 339.7, 186.3, 162.2 (q, $^{1}J_{CB}$ = 50.0 Hz, C_{ipso} $B(Ar^F)_4$), 152.6, 149.5, 146.2, 140.7, 139.7, 139.2, 137.4, 136.9, 135.3, 134.5, 130.3, 130.0, 129.4 (qq, $^{2}J_{CF}$ = 31.7 Hz, $^{3}J_{CB}$ = 2.8 Hz), 128.0, 127.2, 126.6, 126.4, 125.8, 125.2, 123.7, 123.0, 121.0, 118.0, 57.1, 56.1, 30.3, 28.7, 21.2, 20.4, 19.0, 18.8, 17.4 ppm. Elemental analysis calcd. (%) for $C_{74}H_{52}BF_{29}MoN_4O \cdot MeCN$: C 53.32, H 3.24, N 4.09; found: C 53.57, H 3.571, N 4.10. * Expected: d, dd, t. Not resolved.

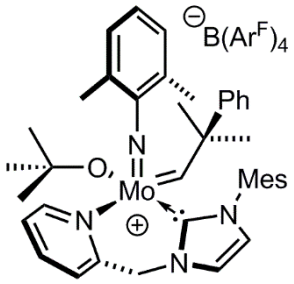

Mo-17

Synthesis of Mo-17: **Mo-15** (30 mg, 0.03 mmol) was dissolved in CH_2Cl_2 (1 mL) and a solution of $NaB(Ar^F)_4$ (31.4 mg, 0.03 mmol) in diethyl ether (0.5 mL) was added dropwise. After two hours, the solvent was removed, and the residue was dissolved in CH_2Cl_2 (2 mL). The suspension was filtered over Celite® and the filtrate was evaporated to dryness. **Mo-17** was obtained by crystallization from CH_2Cl_2 (0.5 mL) and pentane (0.1 mL) in 81 % yield. ^{1}H NMR (400 MHz, CD_2Cl_2): δ = 12.00 (s, 1H, $^1J_{CH}$= 119.5 Hz, *syn*), 9.34 (d, 1H, $^3J_{HH}$ = 6.2 Hz), 7.85-7.81 (m, 1H), 7.72 (br s, 8H), 7.56 (s, 4H), 7.52-7.49 (m, 1H), 7.46 (d, 1H, $^3J_{HH}$ = 1.8 Hz), 7.43 (d, 1H, $^3J_{HH}$ = 7.6 Hz), 7.19 (d, 1H, $^3J_{HH}$ = 1.8 Hz), 7.13-7.10 (m, 3H), 7.06-7.04 (m, 3H), 7.04 (br s, 4H), 5.56 (d, 1H, $^3J_{HH}$ = 14.9 Hz), 5.14 (d, 1H, $^3J_{HH}$ = 14.9 Hz), 2.45 (s, 3H), 2.24 (br s, 6H), 2.01 (s, 3H), 1.81 (s, 3H), 1.55 (s, 3H), 1.26 (s, 3H), 1.18 (s, 9H) ppm. ^{19}F NMR (376 MHz, CD_2Cl_2): δ = -62.84 ppm. ^{13}C NMR (CD_2Cl_2): δ = 304.2, 184,92, 162.4 (q, $^1J_{CB}$ = 50.0 Hz, C_{ipso} $B(Ar^F)_4$), 155.34, 151.8, 149.3, 149.0, 141.8, 140.1, 135.6, 135.4, 134.7, 131.0, 130.7, 129.5 (qq, $^2J_{CF}$ = 31.7 Hz, $^3J_{CB}$ = 2.8 Hz), 128.8, 128.7, 128.6, 126.7, 125.2 (q, $^1J_{CF}$ = 273.1 Hz, CF_3 $B(Ar^F)_4$), 124.6, 124.2, 118.1, 82.0, 56.7, 55.2, 32.2, 31.7, 31.4, 31.0, 21.5, 19.6, 19.1, 18.8 ppm. Despite numerous efforts, inconsistent elemental analysis data were obtained.

Synthesis of Mo-18·RCN: **Mo-13** (1 equiv.) was dissolved in CH_2Cl_2 and the respective nitrile (2 drops) was added. Then, a solution of $NaB(Ar^F)_4$ (1 equiv.) in CH_2Cl_2 was added. The mixture was stirred for 3 hours, evaporated to dryness, and the resulting residue was redissolved in CH_2Cl_2. The suspension was filtered over Celite® and the solvent was again evaporated. **Mo-18·RCN** *could not be isolated in pure form*. Nevertheless, resonances belonging to the product could be assigned in ^{1}H and ^{19}F NMR spectroscopy and are provided for convenience. For R = MeCN: ^{1}H NMR (400 MHz, CD_2Cl_2): δ = 13.66, 8.44 (d, $^3J_{HH}$ = 5.5 Hz, 1H), 7.92-7.87 (m, 1H), 7.73 (br s, 16H), 7.60-7.57 (m, 1H), 7.56 (br s, 8H), 7.53-7.48 (m, 3H), 7.36-7.31 (m, 3H), 7.26-7.24 (m, 3H), 7.18-7.15 (m, 3H), 7.19 (br s, 1H), 7.04-7.03 (m, 3H), 5.26 (d, $^3J_{HH}$ = 15 Hz, 1H), 5.16 (d, $^3J_{HH}$ = 15 Hz, 1H), 2.41 (s, 3H), 2.06 (br s, 9H), 2.00 (s, 3H), 2.06 (s, 6H), 2.00 (s, 3H), 1.78 (s, 3H), 1.77 (s, 3H), 1.28 (s, 6H) ppm. ^{19}F NMR (376 MHz, CD_2Cl_2): δ = -62.78 ppm.

7.6 (PRE-)CATALYSTS FOR LATENT RING-OPENING METATHESIS POLYMERIZATION OF DICYCLOPENTADIENE

Parts of the following chapter are incorporated in a publication: I. Elser, B. R. Kordes, W. Frey, K. Herz, R. Schowner, L. Stöhr, H. J. Altmann, M. R. Buchmeiser, *Chem. Eur. J.*, Latent and Air Stable Pre-Catalysts for the Polymerization of Dicyclopentadiene: From Penta- to Hexacoordination in Molybdenum Imido Alkylidene N-Heterocyclic Carbene Complexes, *accepted paper*.

7.6.1 SYNTHESIS OF CATALYSTS AND REAGENTS

Synthesis of 11: **11** was synthesized according to a literature-known procedure starting from commercially available salicylaldehyde.[225] **11** was dried over CaH_2, distilled and degassed in three consecutive freeze-pump-thaw cycles *prior* to use. **11** was stored in the fridge under nitrogen over molecular sieves 4 Å.

Synthesis of Mo-21 - Mo-23: **Mo-21**[168a], **Mo-22**[190]and **Mo-23**[168a] were synthesized according to previously published procedures, by conversion of the respective precursor complexes **Mo-P1**, **Mo-P4** and **Mo-P5** with IMes in toluene or benzene and subsequent crystallization from a mixture of CH_2Cl_2, diethyl ether and pentane.

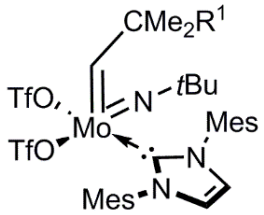

Mo-19

Synthesis of Mo-19: *This catalyst was first isolated by Roman Schowner*.[15] Mo(*N*-*t*Bu)(CHCMe$_2$Ph)(OTf)$_2$(DME) **Mo-P2** (130 mg, 0.19 mmol) was dissolved in toluene (4 mL) and a solution of 1,3-dimesitylimidazol-2-ylidene (57.7 mg, 0.19 mmol) in toluene (1 mL) was added. The reaction mixture was stirred for twelve hours at room temperature. Next, the solvent was removed, and the residue was dissolved in CH_2Cl_2 and filtered over Celite® to remove any imidazolium salt impurities. The filtrate was evaporated to dryness and the remaining solid was crystallized from a mixture of CH_2Cl_2, diethyl ether and pentane. **Mo-19** was isolated in 68 % yield in form of light yellow crystals. Two *syn*-isomers were observable by NMR spectroscopy. The sum of the integrals of both alkylidene signals was set to one. ^{1}H NMR ($CDCl_3$, 400 MHz): δ = 13.62 (s, 0.55H, Mo=CH, $^1J_{CH}$ = 122.7 Hz, *syn*), 11.35 (s, 0.45H, Mo=CH, $^1J_{CH}$ = 116.31 Hz, *syn*), 7.30-7.28 (m, 1H), 7.23-7.15 (m, 5H), 7.12-7.08 (m, 2H), 7.04 (s, 1H), 6.96 (s, 1H), 6.94 (s, 1H), 2.39-2.30 (m, 6H, IMes), 2.18-2.07 (m, 12H, IMes), 1.68-1.61 (m, 6H, C(CH$_3$)$_2$Ph), 1.24-1.14 (m, 9H, *t*Bu) ppm. ^{19}F NMR ($CDCl_3$, 376 MHz): δ = -76.12

(s,3F), -76.70 (s, 3F) ppm. ^{13}C NMR (101 MHz, $CDCl_3$): δ = 323.2 (Mo=C), 317.1, 190.1, 184.1, 150.1, 150.0, 148.8, 146.6, 141.1, 140.9, 140.8, 140.0, 136.7, 136.2, 135.8, 134.3, 134.0, 133.9, 130.3, 129.9, 129.8, 129.7, 128.3, 128.1, 127.8, 126.6, 126.5, 126.1, 125.9, 125.8, 125.6, 123.7, 123.2, 119.4 (q, $^1J_{CF}$ = 319 Hz), 119.1 (q, $^1J_{CF}$ = 318 Hz, CF_3 OTf), 119.1 (q, $^1J_{CF}$ = 318 Hz, CF_3 OTf), 118.6 (q, $^1J_{CF}$ = 318 Hz, CF_3 OTf), 79.9, 78.2, 55.0, 54.5, 54.4, 53.5, 34.8, 34.3, 30.4, 30.2, 29.7, 38.3, 22.5, 21.1, 18.6, 18.0 ppm. Elemental analysis (%) calcd. for $C_{37}H_{45}F_6MoN_3O_6S_2$: C 49.28, H 5.03, N 4.66, found: C 48.92, H 4.951, N 4.87.

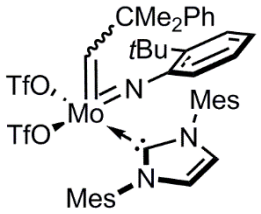

Mo-20

Synthesis of Mo-20. *This catalyst was first isolated by Laura Stöhr*.[191] Mo(*N*-2-*t*Bu-C_6H_4)(CHCMe$_2$Ph)(OTf)$_2$(DME) **Mo-P3** (130 mg, 0.17 mmol) was dissolved in toluene (5 mL) and the solution was cooled to -35°C. A chilled (-35°C) solution of IMes (51.9 mg, 0.17 mmol) was added. After five hours at room temperature the solvent was removed, and the remaining residue was crystallized from a mixture of CH_2Cl_2, diethyl ether and pentane. **Mo-20** was isolated in 72% yield in form of yellow crystals. Two isomers were observable in NMR spectroscopy. Only the signals of the major isomer (*syn*) are reported. ^{1}H NMR (400 MHz, $CDCl_3$): δ = 14.30 (s, 1H, Mo=CH, $^1J_{CH}$ = 121.8 Hz, *syn*), 7.31-7.29 (m, 1H), 7.23-7.10 (m, 8H), 6.99-6.95 (m, 3H), 6.87-6.85 (m, 2H), 6.55 (s, 2H), 2.28 (s, 6H, IMes), 2.19 (s, 6H, IMes), 1.89 (s, 6H, IMes), 1.41 (s, 3H, C(CH$_3$)$_2$Ph), 1.35 (s, 3H, C(CH$_3$)$_2$Ph), 1.34 (s, 9H, 2-*t*Bu) ppm. ^{19}F NMR (376 MHz, $CDCl_3$, 376 MHz): δ = -74.36 (s, 3F), -76.31 (s, 3F) ppm. ^{13}C NMR (101 MHz, $CDCl_3$): δ = 317.84 (Mo=C), 182.5, 153.6, 148.3, 147.2, 140.7, 137.3, 135.7, 133.7, 130.5, 130.1, 129.6, 128.2, 126.6, 126.6, 126.0, 126.0, 125.6, 119.4 (q, $^1J_{CF}$ = 318 Hz, CF_3 OTf), 59.1, 36.2, 33.9, 31.1, 29.3, 21.1, 19.0, 18.9 ppm. Elemental analysis (%) calcd. for $C_{44}H_{51}Cl_2F_6MoN_3O_6S_2$: C 49.72, H 4.84, N 3.95 found: C 50.07, H 5.02, N 4.05.

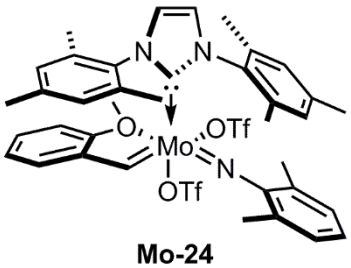

Mo-24

Synthesis of Mo-24**:** *This catalyst was first isolated by Katharina Herz*.[169] Mo(*N*-2,6-Me_2-C_6H_3)(CHCMe_2Ph)$(OTf)_2$(IMes) **Mo-21** (100 mg, 0.1 mmol) was dissolved in CH_2Cl_2 and 2-methoxystyrene **11** (42.4 mg, 0.3 mmol) in CH_2Cl_2 was added. The orange solution was stirred for three hours at room temperature. Then, all volatiles were removed *in vacuo* and the resulting residue was washed with pentane until it solidified. The solid was isolated by filtration and crystallized at -35°C from a mixture of CH_2Cl_2 and diethyl ether to afford **Mo-24** in 95% yield. ^{1}H NMR (CD_2Cl_2, 400 MHz): δ = 13.97 (s, 1H, Mo=CH, $^1J_{CH}$ = 150.1 Hz, *anti*), 7.16-6.99 (m, 5H, Ar*H*), 6.96-6.82 (m, 2H, Ar*H*), 6.71-6.55 (m, 4H, Ar*H*), 6.43 (s, 2H, C*H*NC), 4.05 (s, 3H, OCH_3), 3.16-2.27 (m, 6H, CH_3), 2.17-2.03 (m, 12H, CH_3), 1.91 (s, 6H, CH_3) ppm; ^{19}F NMR (376 MHz, CD_2Cl_2): δ = -77.14 (m, 3F), -78.44 (m, 3F) ppm; ^{13}C NMR (100 MHz, CD_2Cl_2): δ = 300.7 (Mo=C), 186.3, 160.6, 156.0, 141.9, 140.3, 135.7, 135.3, 135.2, 134.7, 131.7, 129.5, 128.8, 127.8, 126.2, 123.2, 120.9, 119.9 (q, $^1J_{CF}$ = 318.0 Hz, CF_3 OTf), 119.3 (q, $^1J_{CF}$ = 318.0 Hz, CF_3 OTf), 110.8, 60.0, 21.2, 18.9, 18.6 ppm. Elemental analysis (%) calcd. for $C_{39}H_{41}F_6MoN_3O_7S_2$: C 49.95, H 4.41, N 4.48; found: C 49.91, H 4.53, N 4.48.

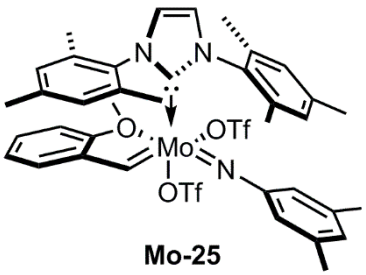

Mo-25

Synthesis of Mo-25**:** *This catalyst was first isolated by Benjamin Kordes*.[17a] Mo(*N*-3,5-Me_2-C_6H_3)(CHCMe_2Ph)$(OTf)_2$(IMes) **Mo-22** (300 mg, 0.316 mmol) was dissolved in CH_2Cl_2 and 2-methoxystyrene **11** (132 µL, 0.947 mmol) was added via an Eppendorf pipette. The orange solution was stirred for one hour at room temperature. Subsequently, all volatiles were removed *in vacuo* and the resulting residue was washed with pentane until it solidified. The solid was isolated by filtration and crystallized at -35°C from a mixture of CH_2Cl_2, diethyl ether and pentane to provide **Mo-25** in 61% yield. ^{1}H NMR ($CDCl_3$, 400 MHz): δ = 13.88 (s, 1H, Mo=CH), 7.11 (s, 2H), 7.09-7.04 (m, 2H), 6.98 (s, 2H), 6.82 (s, 1H), 6.77 (s, 2H), 6.62-6.55 (m, 2H), 6.45 (s, 2H), 3.79 (s, 3H), 2.25 (s, 6H), 2.18 (s, 6H), 2.11 (s, 6H), 1.80 (s, 6H) ppm. ^{19}F NMR ($CDCl_3$, 376 MHz): δ = -76.94 (s, 3F), -77.89 (s, 3F) ppm. ^{13}C NMR ($CDCl_3$, 100 MHz): δ

= 296.3 (Mo=C), 187.75 (*C*N*carbene*), 160.0, 154.7, 139.6, 136.7, 135.7, 135.5, 135.1, 134.6, 131.6, 131.1, 129.4, 129.1, 125.6, 124.6, 124.4, 123.7, 123.3, 123.0, 119.6 (q, $^1J_{CF}$ = 320 Hz, CF_3 OTf), 117.4 (q, $^1J_{CF}$ = 320 Hz, CF_3 OTf), 110.9, 59.2, 53.6, 21.2, 21.0, 18.1, 17.8 ppm. Elemental analysis (%) calcd. for $C_{39}H_{41}F_6MoN_3O_7S_2$: C 49.89, H 4.51, N 4.48; found: C 50.21, H 4.57, N 4.41.

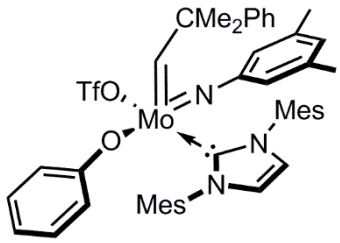

Mo-26

***Synthesis of Mo-26*:** Mo(*N*-3,5-Me_2-C_6H_3)(CHCMe_2Ph)(OTf)$_2$(IMes) **Mo-22** (200 mg, 0.21 mmol) was dissolved in CH_2Cl_2 and the solution was cooled to -35 °C. A suspension of lithium phenoxide (21.1 mg, 0.21 mmol) in CH_2Cl_2 was added dropwise. The reaction mixture was stirred for two hours at room temperature. The suspension was filtered over Celite® and all volatiles were removed *in vacuo*. Crystallization from a mixture of CH_2Cl_2, diethyl ether and pentane afforded the target compound **Mo-26** in 68 % yield in form of yellow crystals. ^{1}H NMR (400 MHz, $CDCl_3$): δ = 13.95 (s, 1H, Mo=CH, $^1J_{CH}$ = 125.9 Hz, *syn*), 7.33 – 7.22 (m, 4H), 7.19 – 7.15 (m, 2H), 7.02 (s, 2H), 6.81 – 6.78 (m, 1H), 6.71 (s, 1H), 6.62 (s, 4H), 6.58 – 6.56 (m, 2H), 6.45 (s, 2H), 2.23 (s, 6H), 2.13 (s, 6H), 2.12 (s, 3H), 1.98 (s, 6H), 1.79 (s, 6H), 1.53 (s, 3H) ppm. ^{19}F NMR (376 MHz, $CDCl_3$): δ = -77.77 ppm. ^{13}C NMR (100 MHz, $CDCl_3$): δ = 321.1 (Mo=C), 186.7 (*C*N*carbene*), 164.2, 153.9, 149.7, 139.4, 136.5, 135.5, 135.5, 133.9, 129.4, 129.4, 129.2, 128.6, 128.2, 126.1, 126.0, 125.4, 124.2, 119.9, 119.3 (q, $^1J_{CF}$ = 319.6 Hz, CF_3 OTf), 119.2, 54.5, 53.6, 34.9, 30.5, 21.3, 21.2, 18.2 ppm. Elemental analysis (%) calcd. for $C_{46}H_{50}F_3MoN_3O_4S$: C 61.81, H 5.64, N 4.70; found: C 61.50, H 5.879, N 4.83.

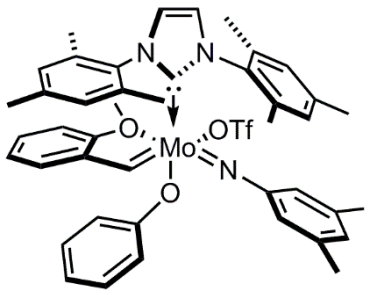

Mo-27

Synthesis of Mo-27: Mo(*N*-3,5-Me_2-C_6H_3)(CHCMe_2Ph)(OTf)(OPh)(IMes) **Mo-26** (60.8 mg, 0.07 mmol) was dissolved in CH_2Cl_2 and a solution of 2-methoxystyrene **11** (9.1 mg,

0.07 mmol) in CH_2Cl_2 was added dropwise. After two hours, the red solution was evaporated to dryness and the resulting residue was washed with pentane. The remaining red solid was crystallized from a mixture of CH_2Cl_2 and diethyl ether to afford **Mo-27** in the form of red crystals in 66 % yield. ^{1}H NMR (400 MHz, $CDCl_3$): δ = 13.88 (s, 1H)*, 7.10 (t, 3H, $^3J_{HH}$ = 7.6 Hz), 6.96 – 6.86 (m, 6H), 6.79 (s, 1H), 6.75 – 6.73 (br s, 2H), 6.66 – 6.61 (m, 3H), 6.51 – 6.49 (m, 2H), 6.42 (s, 2H), 3.90 (s, 3H), 2.26 (s, 6H), 2.22 (s, 6H), 2.11 (s, 6H), 1.69 (s, 6H) ppm. ^{19}F NMR ($CDCl_3$, 376 MHz): δ = -77.84 (s, 3F) ppm. ^{13}C NMR (100 MHz, $CDCl_3$): δ = 286.6 (Mo=C), 189.2 ($CN_{carbene}$), 165.6, 160.1, 155.6, 139.4, 136.7, 135.3, 135.2, 130.3, 128.7, 128.6, 124.5, 124.2, 122.1, 121.9, 119.9, 119.4 (q, $^1J_{CF}$ = 319.1 Hz, CF_3 OTf), 116.6, 109.9, 57.3, 53.6, 21.4, 21.2, 18.4, 17.5 ppm. Elemental analysis (%) calcd. for $C_{44}H_{46}F_3MoN_3O_5S$: C 59.93, H 5.26, N 4.76; found: C 60.07, H 5.497, N 4.98. *Determination of $^1J_{CH}$ coupling constant (*syn*- or *anti*-isomer) was impossible due to the broad resonance.

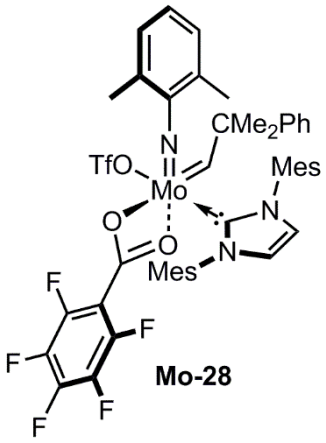

Mo-28

Synthesis of Mo-28: Mo(*N*-2,6-Me_2-C_6H_3)(CHCMe_2Ph)$(OTf)_2$(IMes) **Mo-21** (162 mg, 0.1 mmol) was dissolved in CH_2Cl_2; cooled to -35°C, and a solution of lithium pentafluorobenzoate (37.2 mg, 0.18 mmol) in diethyl ether was added. The reaction mixture was stirred overnight and the volatiles were removed. The resulting residue was dissolved in CH_2Cl_2 and filtered over a pad of Celite®. After removal of CH_2Cl_2 in vacuo, the resulting foam was crystallized from CH_2Cl_2, diethyl ether and pentane to yield **Mo-28** with varying amounts of *anti*-isomer in 67% yield. ^{1}H NMR (400 MHz, $CDCl_3$)*: δ 14.24 (s, 1H, $^1J_{CH}$ = 133.3 Hz, *anti*), 7.35-7.28 (m, 4H), 7.23-7.19 (m, 1H), 7.01- 6.94 (m, 4H), 6.85 (m, 1H), 6.58-6.53 (m, 4H), 2,6 (s, 3H), 2.17 (s, 3H), 2.07 (s, 3H), 2.06 (s, 6H), 1.88 (s, 6H), 1.65 (br s, 6H), 1.59 (s, 3H) ppm. ^{19}F NMR (376 MHz, $CDCl_3$): δ -78.26 (s, 3F), -135.00- -135.07 (m, 2F), -148.4- -148.58 (m, 1F), -162.95- -163.09 (m, 2F) ppm. ^{13}C NMR (101 MHz, $CDCl_3$): δ = 333.1 (Mo=C), 185.2 ($CN_{Carbene}$), 175.0 (CO_2), 155.9, 153.8, 152.3, 149.3, 148.2, 146.6, 141.6, 141.5, 140.0, 139.3, 138.6, 136.2, 136.0, 135.7, 129.8, 129.6, 129.0, 128.8, 128.1, 127.7, 127.4, 127.4, 126.6, 126.3, 125.8, 125.5, 119.3 (q, $^1J_{CF}$ = 319.2 Hz, CF_3 OTf), 106.7, 56.5, 32.1, 27.5, 20.8, 20.0,

19.8, 18.1, 17.9 ppm. * *Syn*-isomer resonances are neglected due to low amount of *syn*-isomer in the measured sample.

7.6.2 Air Stability Tests

Sample treatment: The pre-catalyst was transferred out of the glove box and stored for one day in a fume hood on a glass plate. Next, the sample was transferred back into the glove box and an NMR sample in dry solvent was prepared.

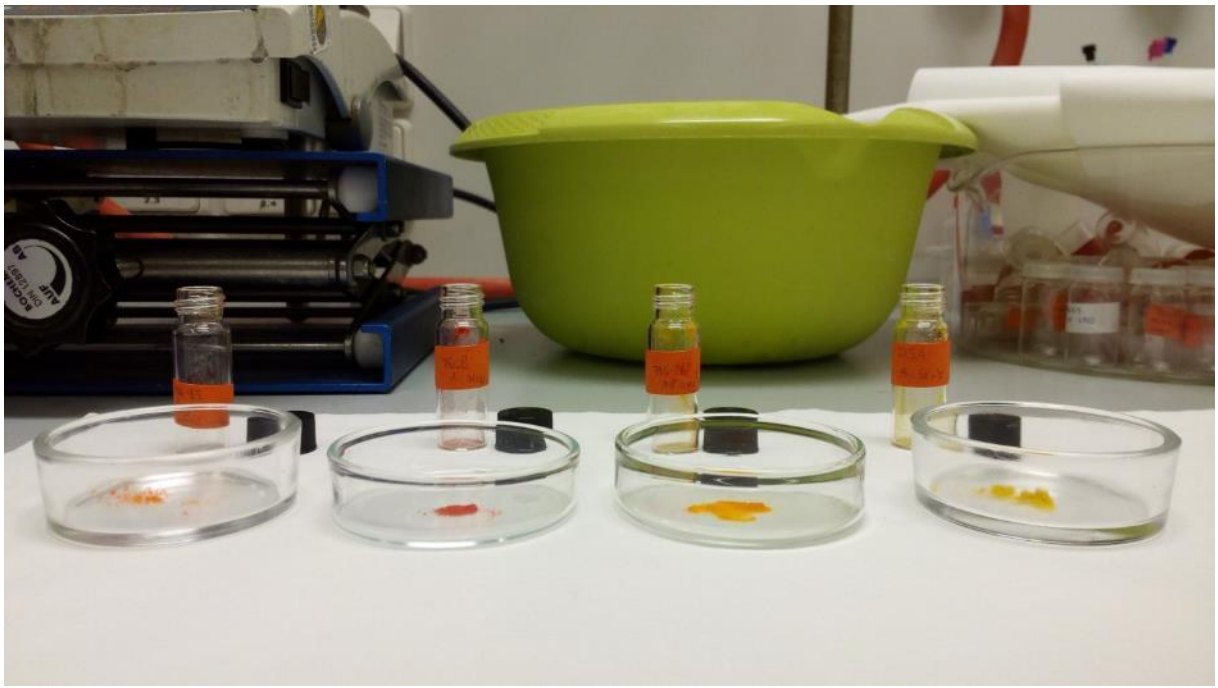

Figure 73: Air stability test. Pre-catalysts were stored on a glass plate in a fume hood for one day.

.

7.6.3 DSC MEASUREMENTS

Determination of $T_{onset,TScan}$ and $T_{exo,max}$ for pre-catalysts Mo-19 - Mo-23: The pre-catalyst (1 equiv., approx. 2-4 mg) was suspended in CH_2Cl_2 (10 µL) and DCPD (500 eq) was added. The mixture was stirred at room temperature for five minutes and a sample for DSC measurements was withdrawn. The DSC pans were pressed inside a glove box and the sample was subjected to temperature scan DSC measurements. $T_{onset,TScan}$ was defined as the temperature were polymerization started to occur and $T_{exo,max}$ was defined as the minimum of the DSC curve.

Heating program TScan: 0°C for 1 minute

0°C to 200°C; 10 K·min^{-1}

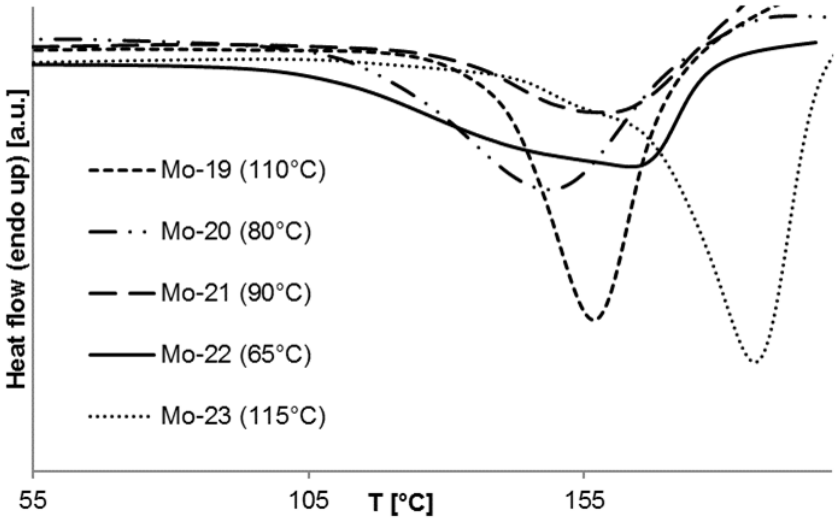

Figure 74: DSC curves of the temperature scan DSC measurements of bistriflate NHC alkylidene complexes **Mo-19** - **Mo-23**. Pre-catalyst/ CH_2Cl_2/DCPD 1 equiv./10 µL/500 equiv. *Heating program:* 0°C for one minute, 0°C → 200°C (10 K·min^{-1}).

Table 12: $T_{exo,max}$ and reaction enthalpies for pre-catalysts **Mo-19** - **Mo-23**.

pre-catalyst	T_{exo} [°C][(i)]	ΔH [J·g^{-1}][(ii)]	$T_{onset,TScan}$ [°C][(iii)]
Mo-19	157	-340	110
Mo-20	149	-300	80
Mo-21	160	-210	90
Mo-22	164	-320	65
Mo-23	186	-350	115

Pre-catalyst/ CH_2Cl_2/DCPD 1 equiv./10 µL/500 equiv. Heating program: 0°C for one minute, 0°C → 200°C (10 K·min^{-1}). (i) Minimum of the DSC temperature scan curve; (ii) derived from integration of the area under the curve by Pyris Manager (Perkin Elmer); (iii) temperature at which the heat flow begins to drop.

Determination of $T_{onset,TScan}$ and $T_{exo,max}$ for pre-catalysts Mo-12, Mo-15, Mo-24, Mo-25, Mo-27: The pre-catalyst (1 equiv., approx. 4-7 mg) was suspended in 1,2,4-trichlorobenzene (10 equiv., approx. 3-7 µL) and DCPD (100 equiv.) was added. The mixture was stirred at room temperature for five minutes and a sample for DSC measurements was withdrawn. The DSC pans were pressed inside a glove box and the sample was subjected to temperature scan DSC measurements. $T_{onset,TScan}$ was defined as the temperature were polymerization started and $T_{exo,max}$ was defined as the minimum of the DSC curve. Additionally, all samples were subjected to a second temperature scan measurement to ensure complete curing.

Heating program TScan: 0°C for 1 min

0°C to 200°C (220°C); 5 $K \cdot min^{-1}$

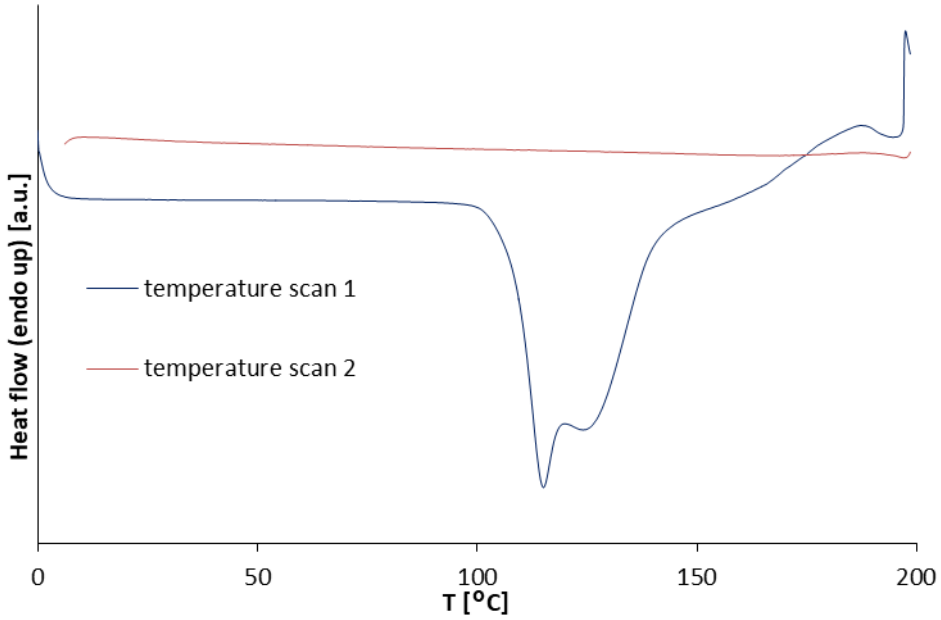

Figure 75: DSC curve of the first and the second temperature scan of a sample of **Mo-12**/TCB/DCPD 1/10/100. *Heating program*: 0°C for one minute, 0°C → 200°C (5 $K \cdot min^{-1}$). At the end of temperature scan 1, cracking of DCPD (exothermal) is observable. This indicates that Mo-12 decomposes before full monomer conversion is achieved. ΔH = -140 $J \cdot g^{-1}$. $T_{exo,max}$ = 115°C. $T_{onset,TScan}$ = 80°C.

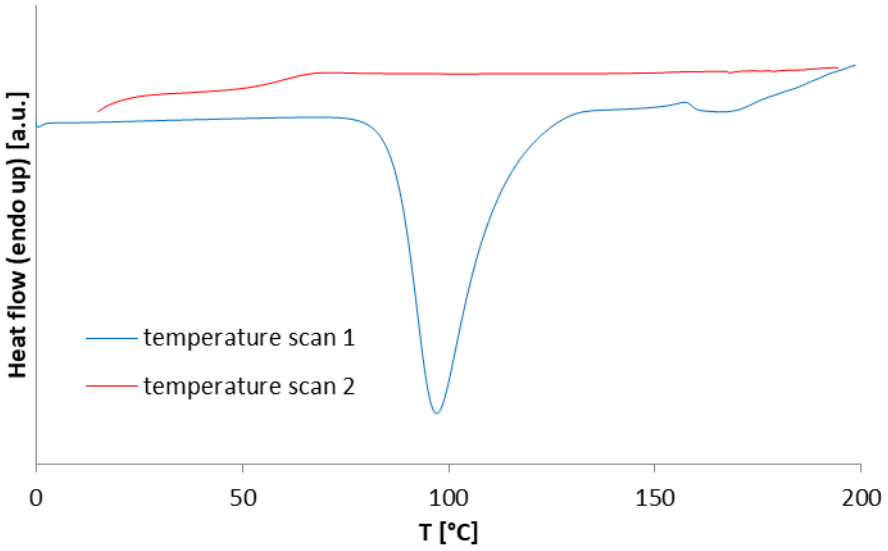

Figure 76: DSC curve of the first and the second temperature scan of a sample of **Mo-15**/TCB/DCPD 1/10/100. Heating program: 0°C for one minute, 0°C → 200°C (5 K·min^{-1}). ΔH= -260 J·g^{-1}. $T_{exo,max}$ = 98°C. $T_{onset,TScan}$ = 70°C.

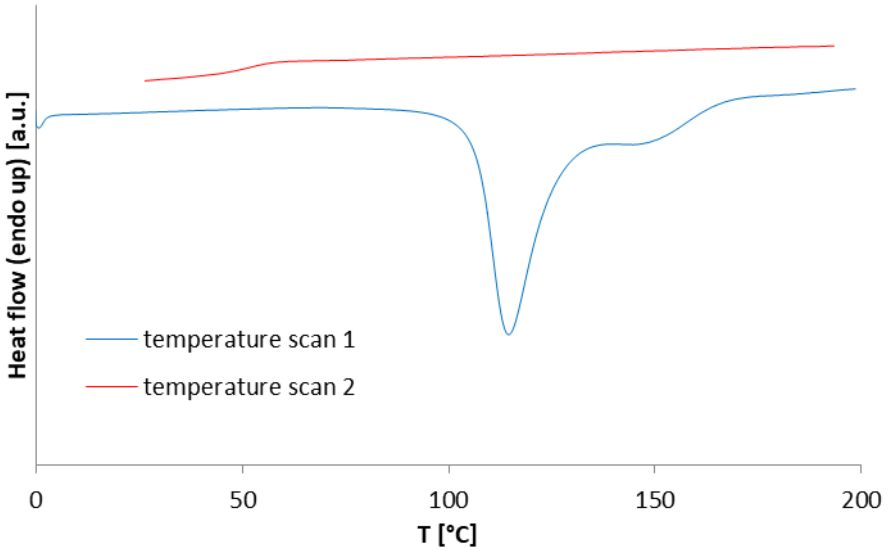

Figure 77: DSC curve of the first and the second temperature scan of a sample of **Mo-21**/TCB/DCPD 1/10/100. Heating program: 0°C for one minute, 0°C → 200°C (5 K·min^{-1}). ΔH= -220 J·g^{-1}. $T_{exo,max}$ = 115°C. $T_{onset,TScan}$ = 90°C.

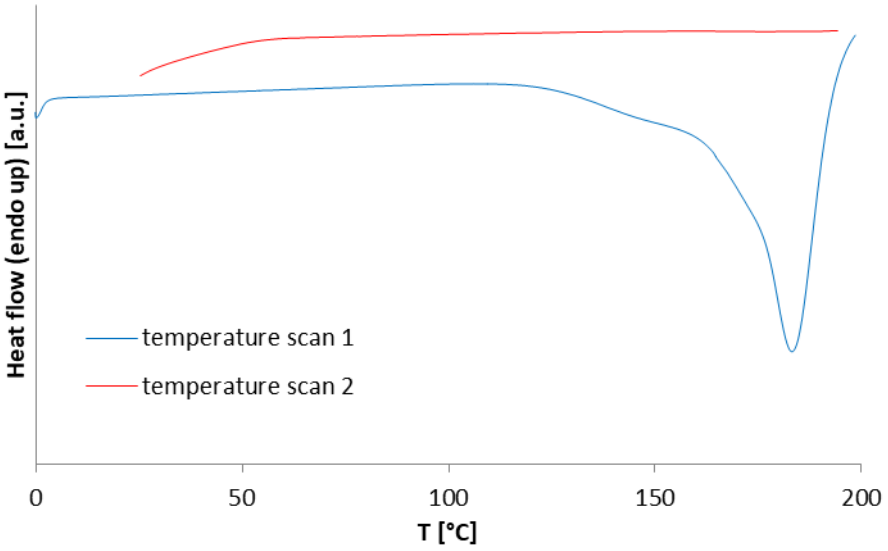

Figure 78: DSC curve of the first and the second temperature scan of a sample of **Mo-24**/TCB/DCPD 1/10/100. Heating program: 0°C for one minute, 0°C → 200°C (5 K·min^{-1}). ΔH= -250 J·g^{-1}. $T_{exo,max}$ = 183°C. $T_{onset,TScan}$ = 120°C.

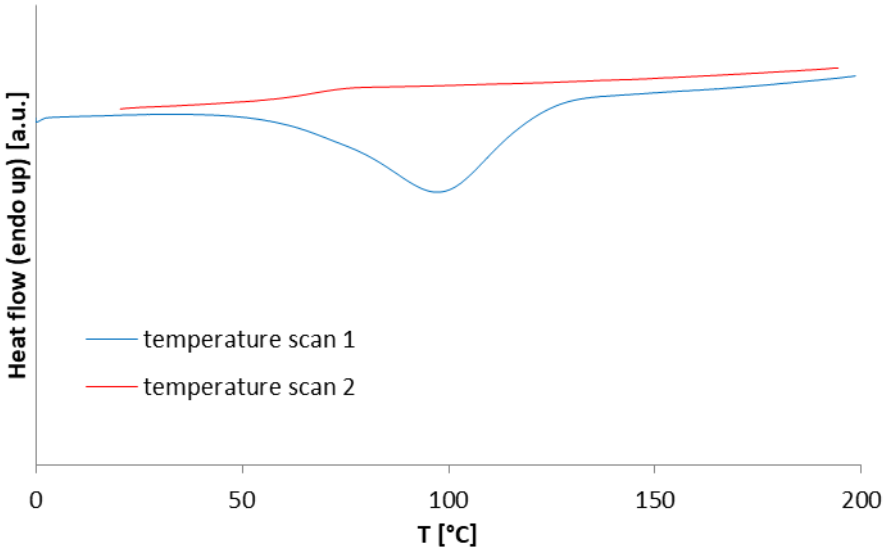

Figure 79: DSC curve of the first and the second temperature scan of a sample of **Mo-22**/TCB/DCPD 1/10/100. Heating program: 0°C for one minute, 0°C → 200°C (5 K·min^{-1}). ΔH= -250 J·g^{-1}. $T_{exo,max}$ = 98°C. $T_{onset,TScan}$ = 40°C.

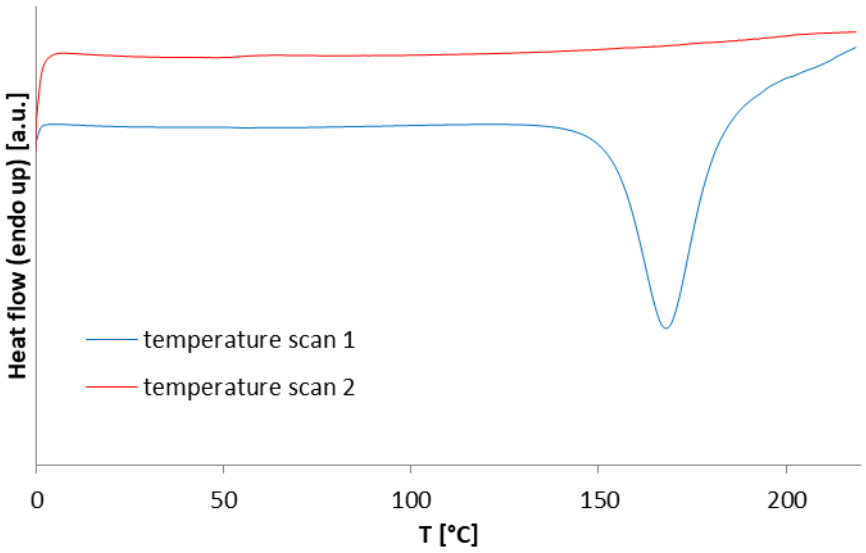

Figure 80: DSC curve of the first and the second temperature scan of a sample of **Mo-25**/TCB/DCPD 1/10/100. Heating program: 0°C for one minute, 0°C → 220°C (5 K·min^{-1}). ΔH= -260 J·g^{-1}. $T_{exo,max}$ = 168°C. $T_{onset,TScan}$ = 130°C.

Determination of $T_{onset,isothermal}$ for pre-catalysts Mo-21, Mo-22, Mo-24 and Mo-25: The pre-catalyst (1 equiv., approx. 4-7 mg) was suspended in 1,2,4-trichlorobenzene (10 equiv., approx. 3-7 µL) and DCPD (100 equiv.) was added. The mixture was stirred at room temperature for five minutes and the samples for DSC measurements were withdrawn. The DSC pans were pressed inside a glove box . The samples were submitted to isothermal measurements and subsequent temperature scans to check for complete curing. $T_{onset,isothermal}$ was defined as the highest temperature a sample could be heated at for thirty minutes without polymerization. For that purpose the reaction enthalpy of the temperature scan of the preheated sample was compared to the reaction enthalpy measured for the reference.

Heating program for isothermal measurements: Hold at temperature for 30 minutes

Cool to 0°C

0°C for 1 minute

0°C to 200°C; 10 K·min^{-1}

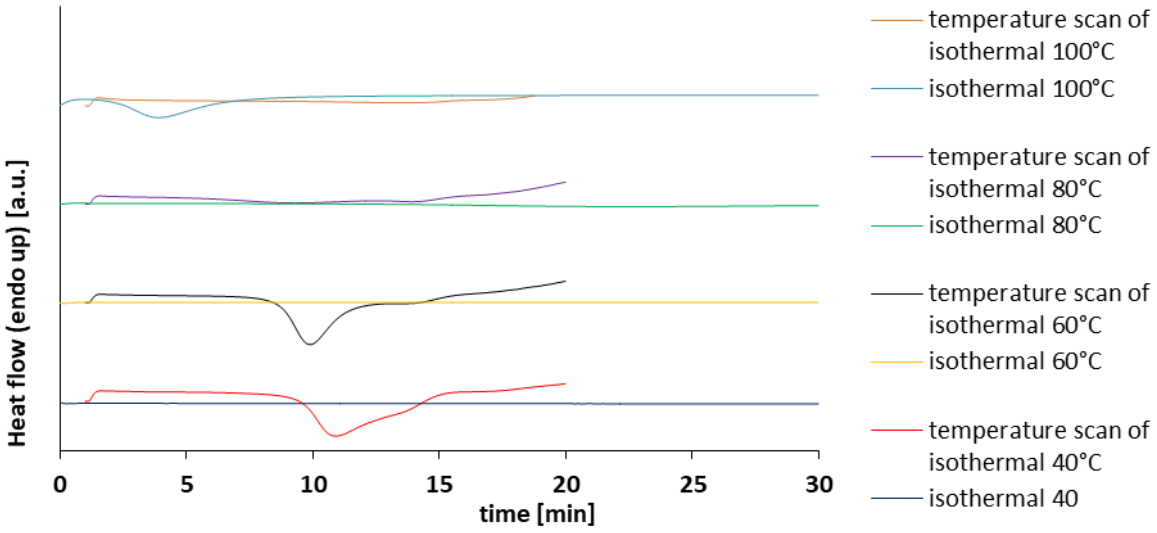

Figure 81: DSC curves of isothermal DSC measurements and subsequent temperature scans of the preheated samples. **Mo-21**/TCB/DCPD 1/10/100. Pre-catalyst decomposes during thermal treatment for 30 minutes at 80°C. $T_{onset,isothermal}$ = 100°C. *Heating program*: Hold at indicated temperature for 30 minutes. Cool to 0°C. Then hold for 1 minute and heat from 0°C to 200°C (10 K·min^{-1}).

Table 13: Reaction enthalpies for isothermal measurements with **Mo-21**.

T [°C]	ΔH [J·g^{-1}][(i)]
40	-240
60	-250

Pre-catalyst/TCB/DCPD 1/10/100. Heating program: 0°C for one minute, 0°C → 200°C (10 K·min^{-1}). (i) derived from integration of the area under the curve by Pyris Manager (Perkin Elmer).

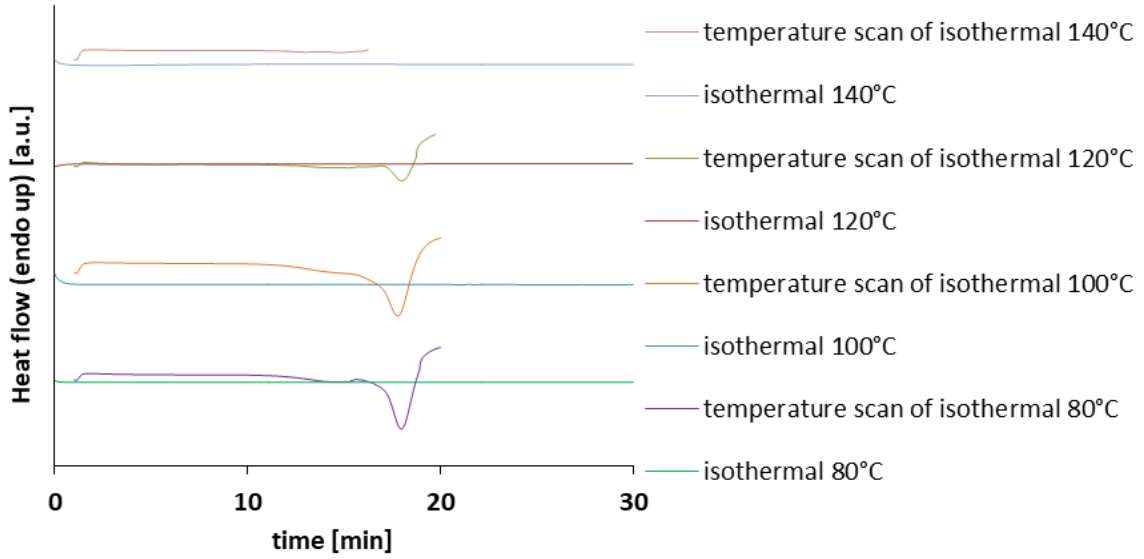

Figure 82: DSC curves of isothermal DSC measurements and subsequent temperature scans of the preheated samples. **Mo-24**/TCB/DCPD 1/10/100. Pre-catalyst decomposes during thermal treatment for 30 minutes at 140°C. $T_{onset,isothermal}$ > 140°C. *Heating program*: Hold at indicated temperature for 30 minutes. Cool to 0°C. Then hold for 1 minute and heat from 0°C to 200°C (10 K·min^{-1}).

Table 14: Reaction enthalpies for isothermal measurements with **Mo-24**.

T [°C]	ΔH [J·g^{-1}][(i)]
80	-250
100	-240
120	-240
140	0

Pre-catalyst/TCB/DCPD 1/10/100. Heating program: 0°C for one minute, 0°C → 200°C (10 K·min^{-1}). (i) derived from integration of the area under the curve by Pyris Manager (Perkin Elmer).

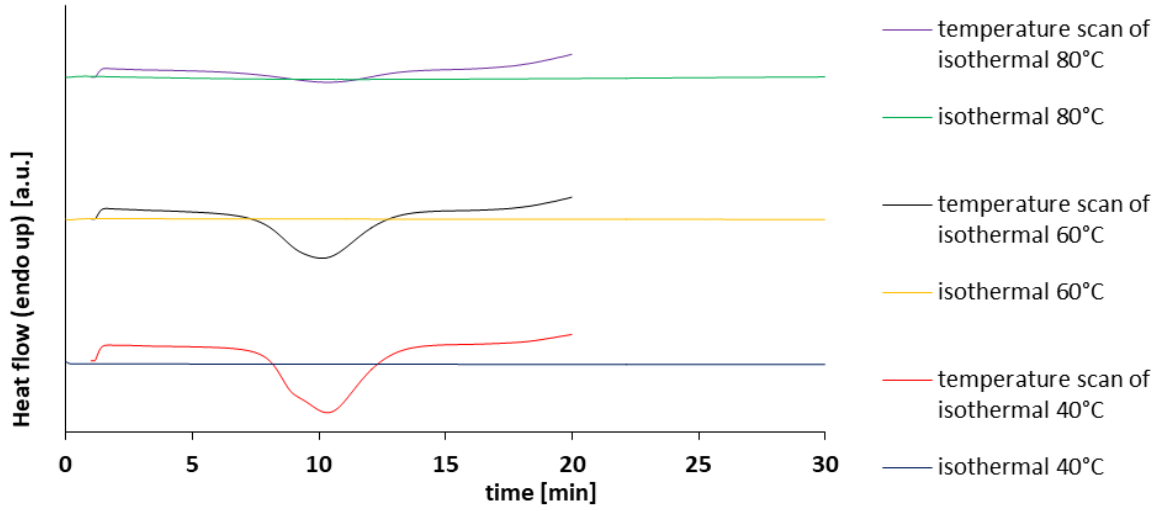

Figure 83: DSC curves of isothermal DSC measurements and subsequent temperature scans of the preheated samples. Mo-22/TCB/DCPD 1/10/100. $T_{onset,isothermal}$ = 60°C. *Heating program*: Hold at indicated temperature for 30 minutes. Cool to 0°C. Then hold for 1 minute and heat from 0°C to 200°C (10 K·min^{-1}).

Table 15: Reaction enthalpies for isothermal measurements with **Mo-22**.

T [°C]	ΔH [J·g^{-1}][(i)]
40	-240
60	-260
80	-140

Pre-catalyst/TCB/DCPD 1/10/100. Heating program: 0°C for one minute, 0°C → 200°C (10 K·min^{-1}). (i) derived from integration of the area under the curve by Pyris Manager (Perkin Elmer).

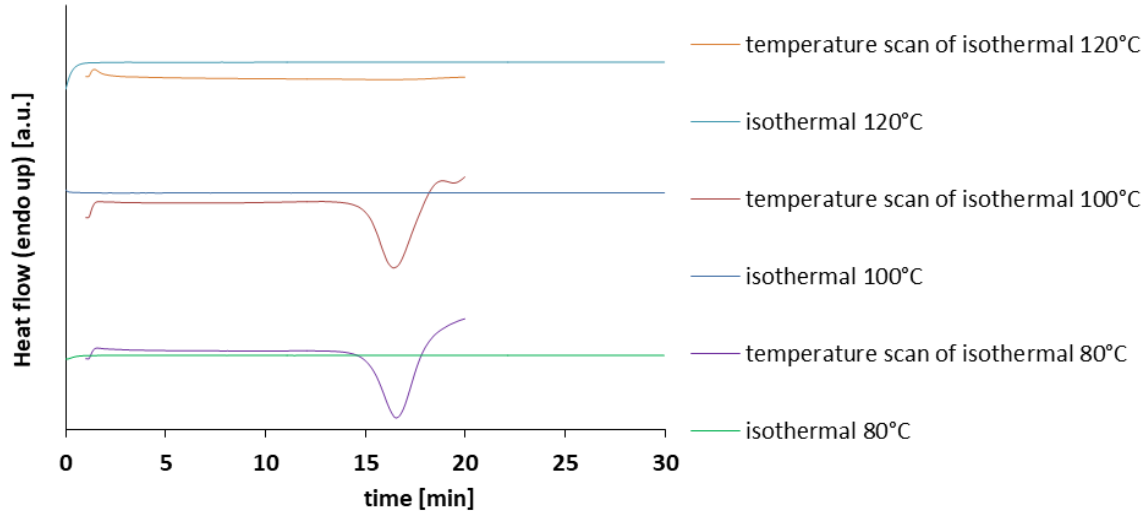

Figure 84: DSC curves of isothermal DSC measurements and subsequent temperature scans of the preheated samples. **Mo-25**/TCB/DCPD 1/10/100. $T_{onset,isothermal}$ = 100°C. *Heating program*: Hold at indicated temperature for 30 minutes. Cool to 0°C. Then hold for 1 minute and heat from 0°C to 200°C (10 K·min^{-1}).

Table 16: Reaction enthalpies for isothermal measurements with **Mo-25**.

T [°C]	ΔH [J·g^{-1}][(i)]
80	-250
100	-220
120	0

Pre-catalyst/TCB/DCPD 1/10/100. Heating program: 0°C for one minute, 0°C → 200°C (10 K·min^{-1}). (i) derived from integration of the area under the curve by Pyris Manager (Perkin Elmer).

Determination of latency of pre-catalysts Mo-12, Mo-15, Mo-19 - Mo-25: The pre-catalyst (1 equiv., approx. 4-7 mg) was suspended in 1,2,4-trichlorobenzene (10 equiv., approx. 3-7 µL) and DCPD (100 equiv.) was added. The mixture was stirred at room temperature and a sample for DSC measurements was withdrawn. Then, the mixture was stirred for the indicated time at room temperature and samples for DSC measurements were withdrawn. All samples were subjected to temperature scan DSC measurement. A pre-catalyst was declared latent for the indicated time when the reaction enthalpy of the aged sample was similar to the one observed for the reference.

Heating program TScan: 0°C for 1 minute

0°C to 200°C; 10 K·min^{-1}

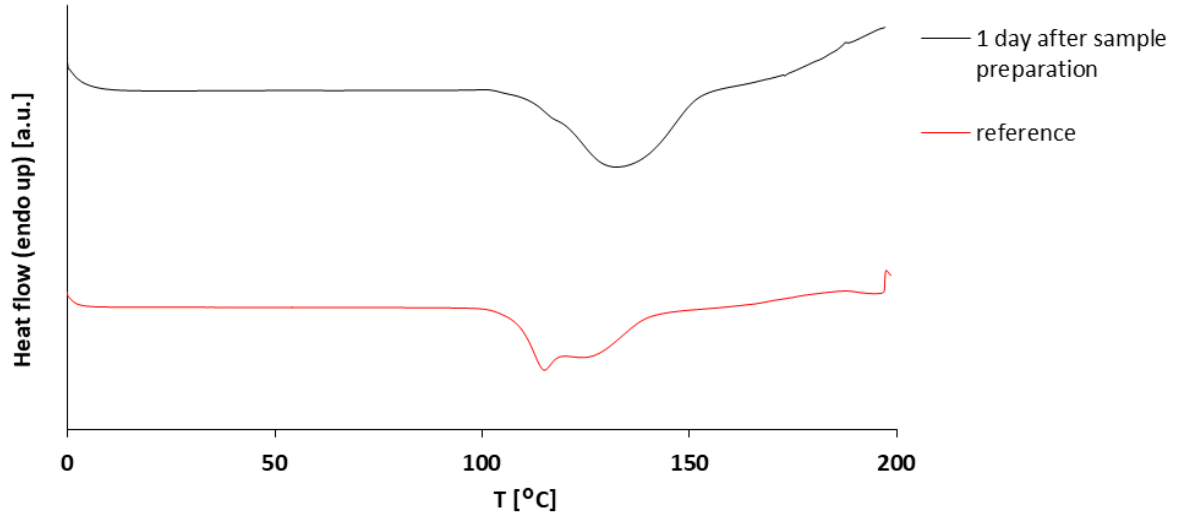

Figure 85: DSC curves of temperature scans of the reference sample and the aged sample, 1 day after sample preparation. **Mo-12**/TCB/DCPD 1/10/100. *Heating program* for reference: 0°C for one minute, 0°C → 200°C (5 K·min^{-1}). *Heating program* for aged sample: 0°C for one minute, 0°C → 200°C (10 K·min^{-1}).

Table 17: Reaction enthalpies for temperature scan DSC measurements with **Mo-12**.

time	ΔH [J·g^{-1}][(i)]
0	-140
1 day	-200

Pre-catalyst/TCB/DCPD 1/10/100. Heating program: 0°C for one minute, 0°C → 200°C (10 K·min^{-1}). (i) derived from integration of the area under the curve by Pyris Manager (Perkin Elmer).

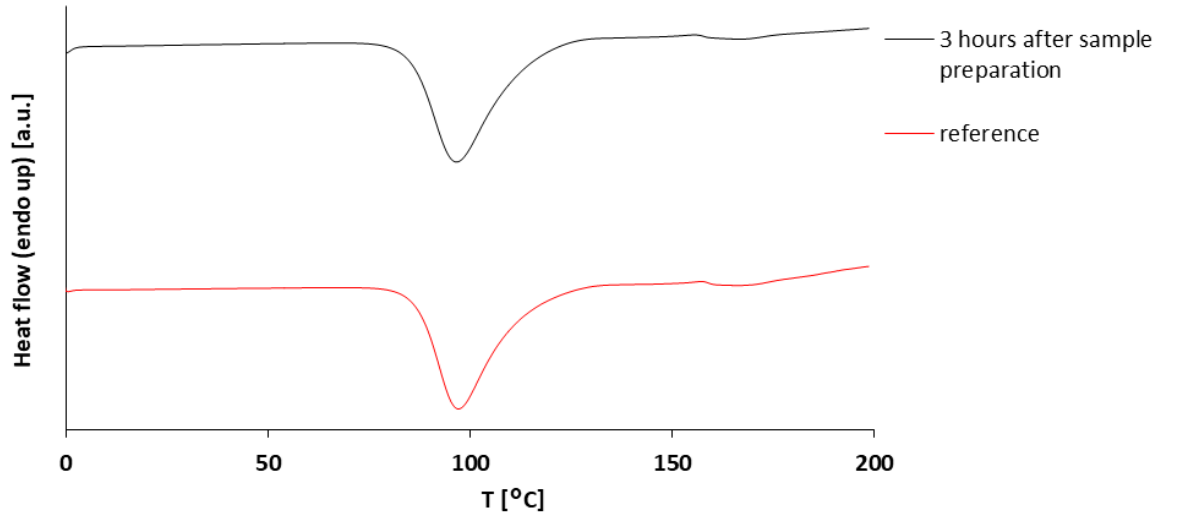

Figure 86: DSC curves of temperature scans of the reference sample and the aged sample, 3 hours after sample preparation. **Mo-15**/TCB/DCPD 1/10/100. *Heating program*: 0°C for one minute, 0°C → 200°C (5 K·min^{-1}).

Table 18: Reaction enthalpies for temperature scan DSC measurements with **Mo-15**.

time	ΔH [J·g^{-1}][(i)]
0	-240
3 hours	-260

Pre-catalyst/TCB/DCPD 1/10/100. Heating program: 0°C for one minute, 0°C → 200°C (10 K·min^{-1}). (i) derived from integration of the area under the curve by Pyris Manager (Perkin Elmer).

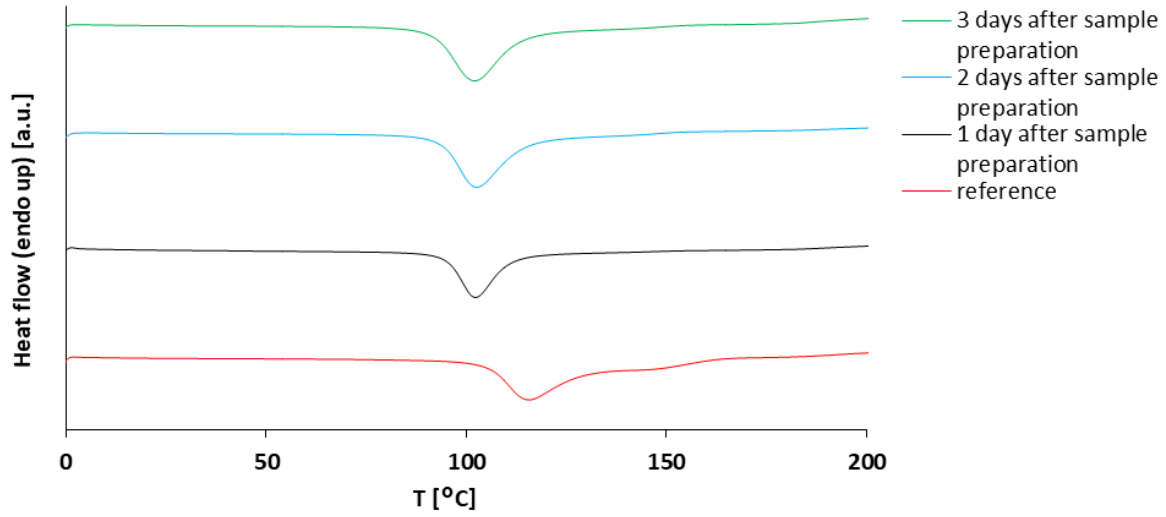

Figure 87: DSC curves of temperature scans of the reference sample and the aged sample, 1, 2 and 3 days after sample preparation. **Mo-21**/TCB/DCPD 1/10/100. *Heating program* for aged samples: 0°C for one minute, 0°C → 200°C (10 K·min^{-1}). *Heating program* for reference: 0°C for one minute, 0°C → 200°C (5 K·min^{-1}).

Table 19: Reaction enthalpies for temperature scan DSC measurements with **Mo-21**.

time	ΔH [J·g^{-1}][(i)]
0	-250
1 day	-250
2 days	-250
3 days	-270

Pre-catalyst/TCB/DCPD 1/10/100. Heating program: 0°C for one minute, 0°C → 200°C (10 K·min^{-1}). (i) derived from integration of the area under the curve by Pyris Manager (Perkin Elmer).

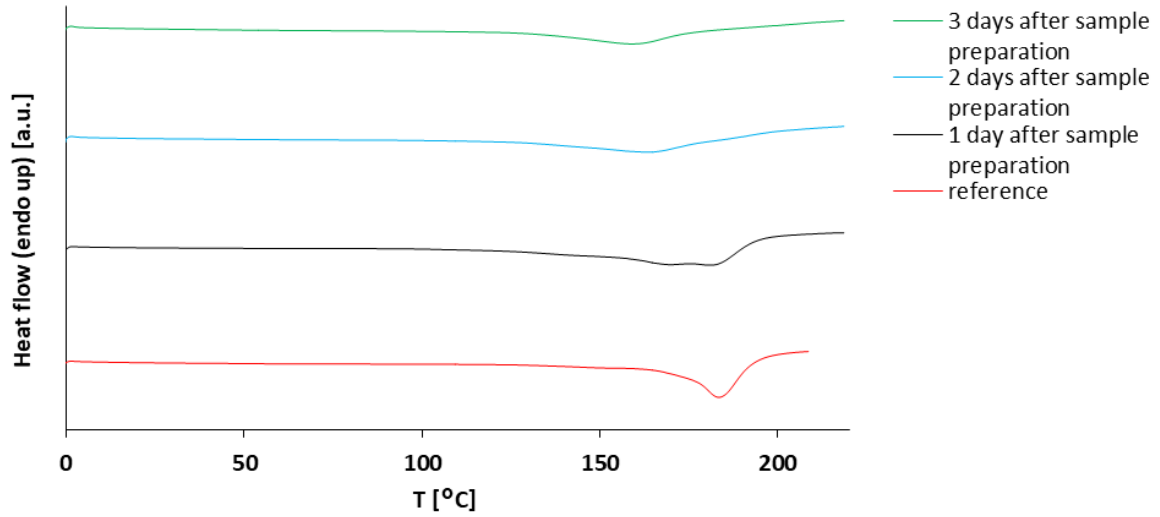

Figure 88: DSC curves of temperature scans of the reference sample and the aged samples, 1, 2 and 3 days after sample preparation. **Mo-24**/TCB/DCPD 1/10/100. *Heating program* for aged samples: 0°C for one minute, 0°C → 220°C (10 K·min^{-1}). *Heating program* for reference: 0°C for one minute, 0°C → 200°C (5 K·min^{-1}).

Table 20: Reaction enthalpies for temperature scan DSC measurements with **Mo-24**.

time	ΔH [J·g^{-1}][(i)]
0	-240
1 day	-270
2 days	-260
3 days	-230

Pre-catalyst/TCB/DCPD 1/10/100. Heating program: 0°C for one minute, 0°C →200°C (10 K·min^{-1}). (i) derived from integration of the area under the curve by Pyris Manager (Perkin Elmer).

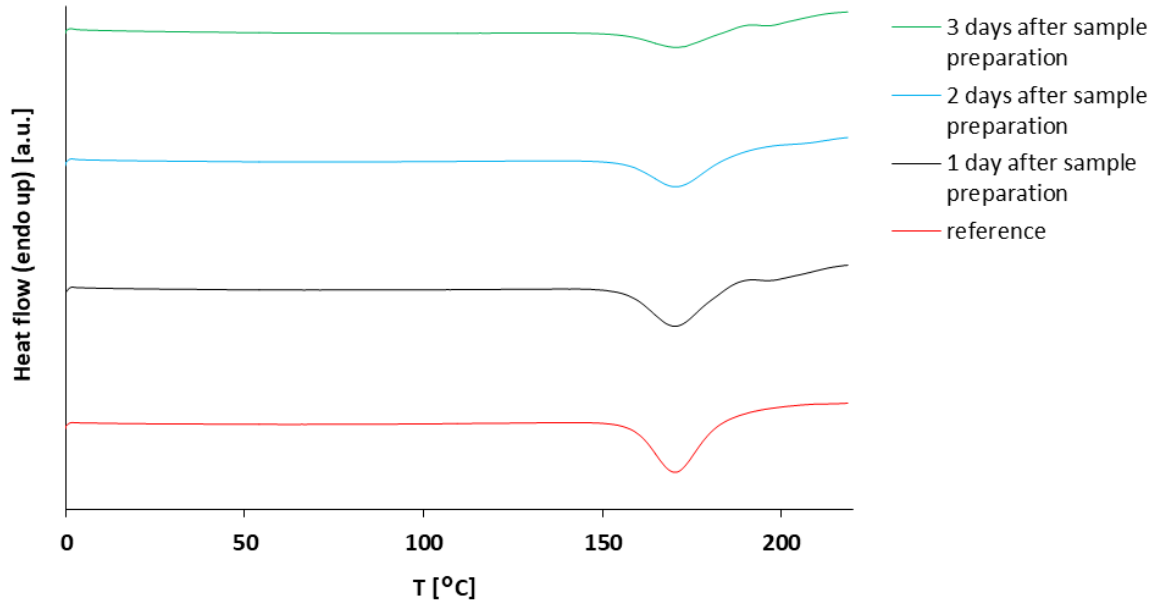

Figure 89: DSC curves of temperature scans of the reference sample and the aged samples, 1, 2 and 3 days after sample preparation. **Mo-25**/TCB/DCPD 1/10/100. *Heating program*: 0°C for one minute, 0°C → 220°C (10 K·min^{-1}).

Table 21: Reaction enthalpies for temperature scan DSC measurements with **Mo-25**.

time	ΔH [J·g^{-1}][(i)]
0	-240
1 day	-210
2 days	-240
3 days	-250

Pre-catalyst/TCB/DCPD 1/10/100. Heating program: 0°C for one minute, 0°C → 200°C (10 K·min^{-1}). (i) derived from integration of the area under the curve by Pyris Manager (Perkin Elmer).

Measurement of different pre-catalyst/monomer ratios with pre-catalysts Mo-24 and Mo-25: Pre-catalyst (1 equiv., approx. 3-7 mg) was suspended in 1,2,4-trichlorobenzene (10 equiv.) and DCPD (100, 175 or 200 equiv.) was added. The mixture was stirred for five minutes and a sample for the DSC temperature scan measurement was withdrawn. The DSC pans were pressed inside a glove box.

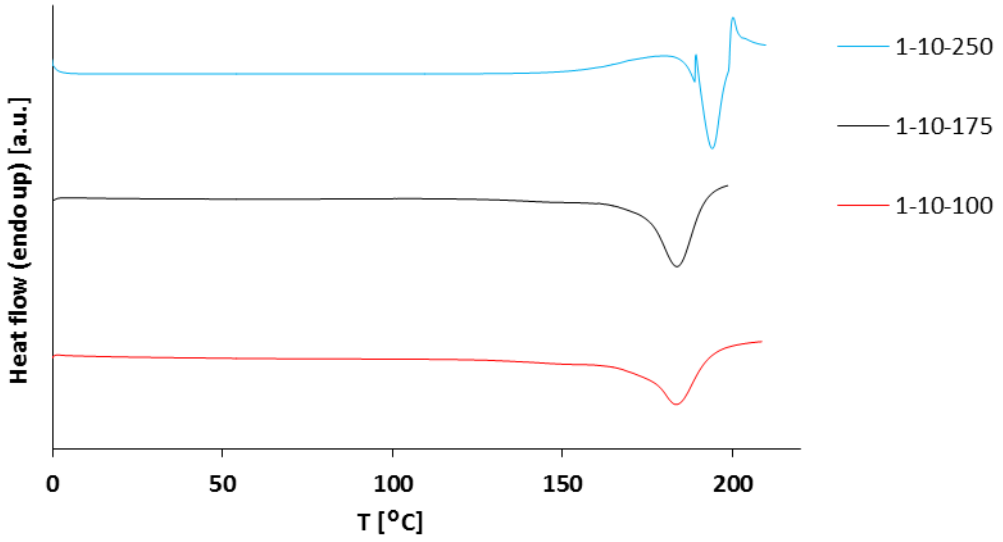

Figure 90: DSC curves of the temperature scan DSC measurements of different pre-catalyst/solvent/monomer ratios 1/10/100,175,250 with **3**. *Heating program*: 0°C for one minute, 0°C → 200°C (220°C) (10 K·min^{-1}). *Heating program* for 1-10-250: 0°C → 220°C (5 K·min^{-1}).

Table 22: Reaction enthalpies for temperature scan DSC measurements with **Mo-24**.

Pre-catalyst-solvent-DCPD	ΔH [J·g^{-1}][(i)]
1-10-100	-240
1-10-175	-260
1-10-250	-290

Pre-catalyst/TCB/DCPD 1/10/100,175,250. Heating program: 0°C for one minute, 0°C → 200°C (220°C) (10 K·min^{-1}). (i) derived from integration of the area under the curve by Pyris Manager (Perkin Elmer).

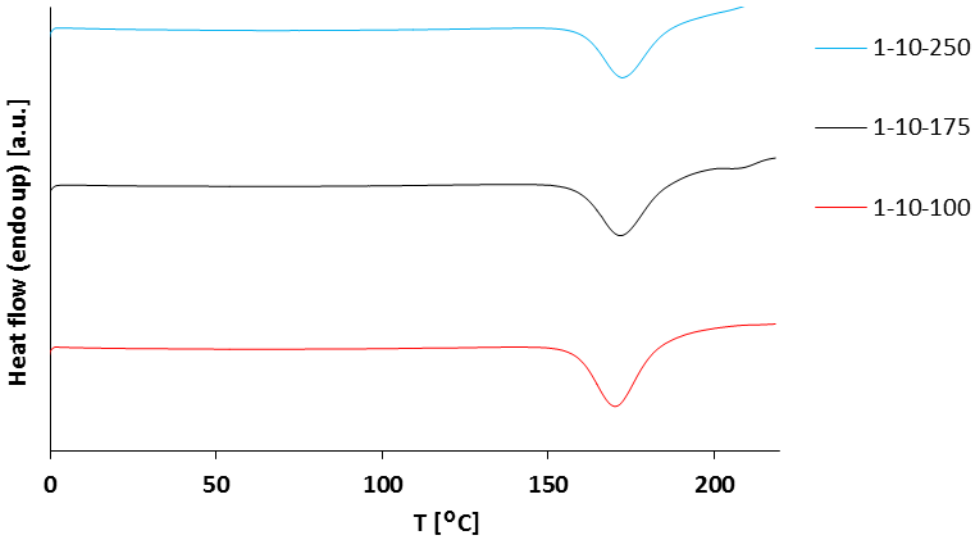

Figure 91: DSC curves of the temperature scan DSC measurements of different pre-catalyst/solvent/monomer ratios 1/10/100,175,250 with **Mo-25**. *Heating program*: 0°C for one minute, 0°C → 220 (220°C) (10 K·min^{-1}).

Table 23: Reaction enthalpies for temperature scan DSC measurements with **Mo-25**.

Pre-catalyst-solvent-DCPD	ΔH [J·g^{-1}][(i)]
1-10-100	-250
1-10-175	-260
1-10-250	-300

Pre-catalyst/TCB/DCPD 1/10/100,175,250. Heating program: 0°C for one minute, 0°C → 220°C (10 K·min^{-1}). (i) derived from integration of the area under the curve by Pyris Manager (Perkin Elmer).

7.6.4 *Swelling Propensity*

Determination of swelling propensity for catalysts Mo-19, Mo-20, Mo-23: The reaction was carried out in a cylindric mold 12 mm in diameter. The catalyst (1 equiv., approx. 5-7 mg) was suspended in CH_2Cl_2 (10 µL) and DCPD (250 equiv.) was added. The mixture was stirred at the indicated temperature until polymerization was complete (as indicated by viscosity, approx. 30-90 min). The polymer was dried under reduced pressure for twelve hours in the cylindric mold. Subsequently, toluene (3 mL) was added. The mixture was stored at room temperature for two days. Then, toluene was decanted and the mass of the swollen polymer was determined.

Determination of swelling propensity for catalysts Mo-12, Mo-15, Mo-21, Mo-22, Mo-24 and Mo-25: The reaction was done in a cylindric mold 12 mm in diameter. The catalyst (1 equiv., approx. 5-7 mg) was suspended in 1,2,4-trichlorobenzene (10 equiv., approx. 5-10 µL) and DCPD (250 equiv.) was added. The mixture was stirred at the indicated temperature until polymerization was complete (as indicated by viscosity, approx. 30-90 min). The polymer was dried under reduced pressure for twelve hours in the cylindric mold. The mass was noted (m_0). Subsequently, toluene (3 mL) was added. The mixture was stored at room temperature for two days. Then, toluene was decanted, the cylindric mold was placed upside down on a tissue for 15 minutes and the mass of the swollen polymer (m_q) was determined.

Table 24: Swelling propensities *Q* of poly-DCPD derived from the polymerization of DCPD with pre-catalysts **Mo-12**, **Mo-15** and **Mo-19**-**Mo-25**.

pre-catalyst	*T* [°C][(i)]	*Q*[(ii)] [%]
Mo-19[(iii)]	110	25
Mo-20[(iii)]	80	no swelling detected
Mo-21[(iv)]	110	45
Mo-22[(iv)]	80	50
Mo-23[(iii)]	140	no swelling detected
Mo-12[(iv)]	110	8[(v)]
Mo-15[(iv)]	80	34
Mo-24[(iv)]	140	no swelling detected
Mo-25[(iv)]	130	no swelling detected
Mo-25[(iv)]	155	no swelling detected

(i) Reaction temperature; (ii) Swelling propensity $Q = \frac{(m_q - m_0)}{m_0}$ *with* m_q *= mass of swollen polymer and* m_0 *= mass of polymer before swelling; (iii) pre-catalyst/DCM/DCPD 1 equiv./10 µL/250 equiv.; (iv) pre-catalyst/TCB/DCPD 1/10/250 equiv.; (v) Poly-DCPD derived from polymerization of DCPD with* ***Mo-12*** *also contained soluble (non-cross-linked) poly-DCPD.*

7.6.5 Glass Transition Temperatures

Determination of the glass transition temperature: Poly(DCPD) was prepared by heating the catalyst/CH_2Cl_2/DCPD mixture (approx. 2 mg, 1 equiv./10 µL/ appr. 150-200 µL, 500 equiv.) to the indicated, catalyst-specific temperature for 30 minutes in a cylindric mold. The polymer was then dried *in vacuo* at room temperature and samples for DSC were prepared and subjected to DSC temperature scan measurements with heating rates of 20, 40 and 60 K min^{-1}, respectively, to determine T_g.

Heating program TScan: *-30°C for 3 min*

-30°C to 220°C; 20,40 and 60°K·min^{-1}

Table 25: Glass transition temperatures T_g of poly-DCPD derived from the polymerization of DCPD with pre-catalysts **Mo-19** - **Mo-23** and **Mo-12**, **Mo-15**, **Mo-24** and **Mo-25**.

pre-catalyst	polymerization temperature [°C]	Heating rate [K·min^{-1}]	T_g [°C]
Mo-19	100		169*
Mo-20	100	60	168
Mo-21	100	-	not observed
Mo-22	100	60	167
Mo-23	140	80	139
Mo-12	100	60	167
Mo-15	100	80	126
Mo-24	140		164*
Mo-25	140	-	not observed

Pre-catalyst/ CH_2Cl_2/DCPD 1 equiv./10µL/500 equiv. determined from cooling curve at 40 K min^{-1}.*

7.7 SYNTHETIC ROUTES TO CHIRAL MOLYBDENUM IMIDO ALKYLIDENE *N*-HETEROCYCLIC CARBENE COMPLEXES

Parts of the following chapter have already been published. Reprinted (adapted) with permission from (I. Elser, W. Frey, K. Wurst, M. R. Buchmeiser, *Organometallics* **2016**, *35*, 4106-4111). Copyright (2016) American Chemical Society.

Synthesis of an authentic, racemic sample of 20 - 24 for the development of a suitable GC-MS-method or HPLC-method: The respective substrate **15**-**19** (100 equiv.) was dissolved in benzene (1 mL) and a solution of the catalyst (1 equiv., Mo(*N*-2,6-iPr_2-C_6H_3)(CHCMe_2Ph)(OC($(CF_3)_2Me)_2$ for **15**, **16**, **19**; Ru(Cl_2)(PCy_3)(CHPh)(sIMes) for **17**, **18**) in benzene (1 mL) was added. After completion of the reaction (verified by GC-MS) the reaction mixtures were filtered over silica to remove the catalyst to afford samples of the racemic products. All products **20**,[96] **21**,[177a] **22**,[177b] **23**,[177b] **24**[194] are literature-known.

Table 26: Parameters for separation of enantiomers of **20**, **21** and **24** on GC-MS.

substrate/product	inj. initial temp. [°C]	flow rate [mLmin^{-1}]	heating program
15/20	150	3	90°C → 100°C heating rate: 1 K/min hold for 1 min
16/21	150	3	90 → 180°C heating rate: 5 K/min hold for 1 min
19/24	150	3	90°C →130°C heating rate: 2 K/min hold for 1 min

Column: Beta Dex^{TM}-120, Supelco, 30m x 0.25 mm x 0.25 µm.

Table 27: Parameters for separation of enantiomers of **22** and **23** on HPLC.

substrate/product	solvent	inj. volume. [µL]	flow rate [mLmin^{-1}]	temperature
17/22	hexane/iPrOH 99.9/0.1	5	1.0	0°C (ice bath)
18/23	hexane/iPrOH 99.9/0.1	5	0.35	0°C (ice bath)

Column: AD-H, Chiral Technologies Europe, 250 x 4.6 mm ID.

7.7.1 *Reactions with molybdenum imido alkylidene N-heterocyclic carbene bistriflate complexes - CH-activation issue*

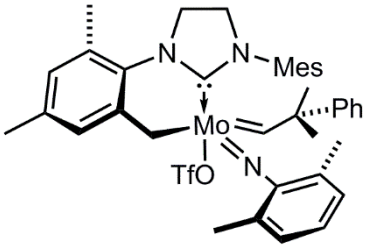

Mo-29

Synthesis of Mo-29: **Mo-1** (87 mg, 0.1 mmol) was suspended in toluene (5 mL) and cooled to -35°C. K(O(2,6-$Ph_2(C_6H_3)$)) (26 mg, 0.1 mmol) was suspended in toluene (2 mL) and cooled to -35°C. The two suspensions were mixed and stirred at room temperature for two hours. The resulting brownish suspension was filtered over Celite® to remove all potassium triflate. The filtrate was evaporated to dryness and the residue was crystallized from a mixture of CH_2Cl_2 (0.5 mL), diethyl ether (2 mL) and pentane (3 mL) to yield **Mo-29** in 76 % yield. K(O(2,6-$Ph_2(C_6H_3)$) can be replaced by **13-K**. ^{1}H NMR (400 MHz, C_6D_6): δ = 12.09 (s, 1H, $^1J_{CH}$= 120.3 Hz, *syn*), 7,48 (s, 1H), 7,23- 7,17 (m, 4H), 7.10- 7.06 (m, 1H), 6.76 – 6.70 (m, 1H), 6.67 (s, 1H), 6.61 (t, 1H, $^3J_{HH}$ = 7.5 Hz), 6.46 (d, 1H, $^3J_{HH}$ = 7.2 Hz), 6.28 (s, 1H), 5.89 (s, 1H), 3.55-3.50 (m, 1H), 3.22 (d, 1H, $^2J_{HH}$ = 8.6 Hz), 3,09 (d, 1H, $^2J_{HH}$ = 8.6 Hz), 3.04- 2.90 (sm, 3H), 2.41 (s, 3H), 2.17 (s, 6H), 2.02 (s, 3H), 1.94 (s, 3H), 1.79 (s, 3H), 1.76 (s, 3H), 1.61 (s, 3H), 1.55 (s, 3H) ppm. ^{19}F NMR (376 MHz, C_6D_6): δ = -77.37 ppm. ^{13}C NMR (101 MHz, C_6D_6): δ = 310.5, 222.19, 155.56, 150.07, 139.4, 138.1, 138.0, 137.9, 137.1, 134.7, 134.3, 134.0, 131.7, 131.6, 129.7, 129.1, 128.9, 126.7, 126.3, 125.7, 125.0, 120.5 (q, $^1J_{CF}$ = 318.4 Hz, CF_3 OTf), 59.1, 53.5, 53.2, 50.6, 32.0, 31.6, 22.9, 20.9, 20.8, 18.8, 18.1, 17.7 ppm. Despite numerous efforts, inconsistent elemental analysis data were obtained. Crystallographic data of **Mo-29** can be found under CCDC-1504351 at the Cambridge Crystallographic Data Centre.

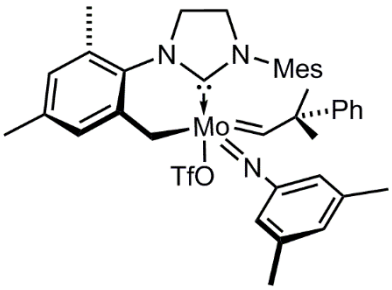

Mo-31

Synthesis of Mo-31: **Mo-22** (108.8 mg, 0.1 mmol) was suspended in toluene (2 mL) and cooled to -35°C. K(O(2,6-$Ph_2(C_6H_3)$)) (32.5 mg, 0.1 mmol) was suspended in toluene (3 mL) and cooled to -35°C. The alkoxide suspension was added to the suspension of **Mo-22** and stirred at room temperature for two hours. The resulting brownish suspension was filtered over Celite® to remove all potassium triflate. The filtrate was evaporated to dryness and the residue was crystallized from a mixture of CH_2Cl_2, diethyl ether and pentane to yield **Mo-31** in 30% yield as red crystals. ***Mo-31*** *was only characterized by* ^{1}H *and* ^{19}F *NMR spectroscopy.* ^{1}H NMR (400 MHz, CD_2Cl_2): δ = 11.51 (s, 1H), 7.22-7.18 (m, 2H), 7.15-7.13 (m, 3H), 7.05 (s, 1H), 7.02 (s, 1H), 6.95 (s, 1H), 6.65 (s, 1H), 6.60 (s, 1H), 6.33 (s, 2H), 6.23 (s, 1H), 4.37-4.34 (m, 1H), 3.98-3.88 (m, 3H), 3.09 (d, $^{3}J_{HH}$ = 8.2 Hz, 1H), 2.65 (d, $^{3}J_{HH}$ = 8.2 Hz, 1H), 2.25 (s, 3H), 2.22 (s, 3H), 2.18 (s, 6H), 2.16 (s, 3H), 1.96 (s, 3H), 1.91 (s, 3H), 1.67 (s, 3H), 1.36 (s, 3H) ppm. ^{19}F NMR (376 MHz, C_6D_6): δ = -77.98 ppm.

Calculation of Buried Volume: *%*V_{bur} was calculated with the *Sambvca2* online tool.[41a] Geometries of the ligands were taken from crystal data. Unless stated otherwise, all default settings were used (exception: distance from the metal center). H atoms were omitted from the calculation as suggested by the *Sambvca 2* user manual.

Default Settings: Bondii Radii: scaled by 1.17. Sphere radius: 3.5 Å. Mesh spacing value *s* = 0.10 Å.

7.7.2 *Molybdenum imido alkylidene bispyrrolide N-heterocyclic carbene complexes*

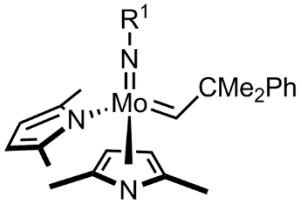

Mo-P6: R^1 = 2,6-iPr_2-C_6H_3
Mo-P7: R^1 = 2-*t*Bu-C_6H_4
Mo-P8: R^1 = *t*Bu
Mo-P9: R^1 = 2,6-Me_2-C_6H_3

Synthesis of Mo(NR¹)(CHCMe₂Ph)(2,5-Me₂-NC₄H₂)₂ complexes Mo-P6-Mo-P9: 2,5-dimethyl pyrrolide complexes are literature-known and were prepared according to a slightly changed procedure.[222] The corresponding bistriflate complex (1 equiv.) was suspended in diethyl ether and Li(2,5-Me_2-NC_4H_2) (2 equiv.) was added as a solid in one portion. After three hours the solvent was removed under reduced pressure and the residue was taken up in toluene and filtered over Celite®. The filtrate was dried under reduced pressure and the resulting residue was triturated with diethyl ether until a yellow solid precipitated. The solid was filtered off and recrystallized from diethyl ether and pentane to afford the Mo(NR^1)($CHCMe_2Ph$)(2,5-Me_2-NC_4H_4)$_2$ complexes.

Synthesis of chiral MAP-type complexes Mo-48 – Mo-50: The chiral MAP-type complexes were prepared in accordance to the literature.[21d,21e,98b]

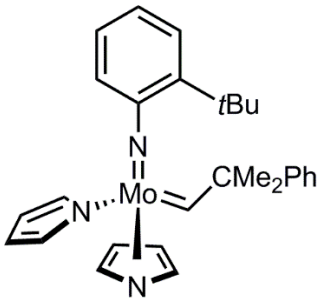

Mo-68

Synthesis of Mo-68: Bispyrrolide complex **Mo-68** is literature-known and was prepared according to a slightly changed procedure.[223] The corresponding bistriflate complex (1 equiv.) was suspended in diethyl ether and Li(NC_4H_2) (2 equiv.) was added as a solid in one portion. After three hours the solvent was removed under reduced pressure and the residue was taken up in toluene and filtered over Celite®. The filtrate was dried under reduced pressure and the

resulting residue was triturated with pentane until a yellow solid precipitated. The solid was filtered off and recrystallized from diethyl ether and pentane to afford **Mo-68**.

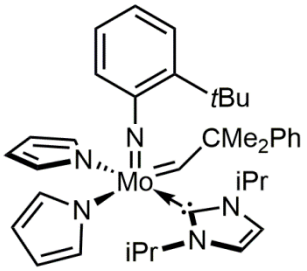

Mo-71

Synthesis of Mo-71: **Mo-68** (467.2 mg, 0.9 mmol) was dissolved in diethyl ether and cooled to -35°C. A solution of 1,3-diisopropylimidazol-2-ylidene (140 mg, 0.9 mmol) in diethyl ether at -35°C was added to the solution of **Mo-71**. After 30 minutes a yellow precipitate formed. After two hours the solid was filtered off and recrystallized from a mixture of CH_2Cl_2, diethyl ether and pentane. **15** was isolated in the form of yellow crystals in 93% yield. **Mo-71** can also be used as received from the reaction mixture without recrystallization. ^{1}H NMR (400 MHz, $CDCl_3$): δ = 13.87 (s, 1H, $^1J_{CH}$ = 123.7 Hz, *syn*), 7.40 (br s, 2H), 7.24 (s, 1H), 7.12-7.05 (m, 5H), 6.96 (br s, 2H), 6.87 (t, $^3J_{HH}$= 7.2 Hz, 1H), 6.79 (t, $^3J_{HH}$= 7.5 Hz, 1H), 6.52-6.50 (m, 3H), 6.41 (s, 2H), 6.29 (br s, 2H),4.40-4.34 (m, 2H), 2.04 (s, 3H), 1.62 (s, 3H), 1.52 (s, 9H), 0.89 (d, $^3J_{HH}$= 6.7 Hz, 6H), 0.67 (d, $^3J_{HH}$= 6.6 Hz, 6H) ppm. ^{13}C NMR (101 MHz, C_6D_6): δ = 299.72, 185.9, 153.5, 147.7, 145.8, 131.0, 131.0, 128.7, 126.5, 126.2, 125.8, 118.1, 107.1, 107.2, 56.3, 53.9, 35.2, 32.9, 30.4, 29.5, 23.1, 23.0 ppm.

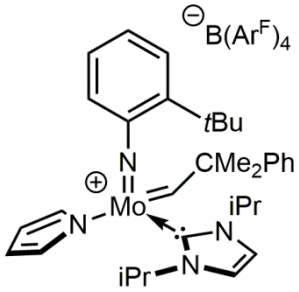

Mo-72

Synthesis of Mo-72: **Mo-71** (20 mg, 0.03 mmol) was dissolved in CH_2Cl_2 and cooled to -35°C. A solution of *N,N*-dimethyl anilinium $B(Ar^F)_4$ (31 mg, 0.03 mmol) in diethyl ether at -35°C was added dropwise. After three hours the solvent was removed and the resulting residue was washed with pentane to remove the aniline and the pyrrole side products. **Mo-72** was isolated

as yellow solid foam in quantitative yield. **Mo-72** can also be crystallized from a mixture of CH_2Cl_2, diethyl ether and pentane to yield light yellow crystals. ^{1}H NMR (400 MHz, CD_2Cl_2): δ = 14.05 (s, 1H, $^1J_{CH}$ = 127.3 Hz, *syn*), 7.74 (br s, 8H), 7.58 (br s, 4H), 7.41- 7.31 (m, 9H), 7.26-7.22 (m, 2H), 7.11- 7.07 (m, 1H), 6.95- 6.93 (m, 1H), 6.59 (s, 2H), 4.18 (s, 4H), 1.72 (s, 3H), 1.70 (s, 3H), 1.25 (d, $^3J_{HH}$ = 6.4 Hz, 6H), 1.1 (d, $^3J_{HH}$ = 6.4 Hz, 6H) ppm. ^{13}C NMR (101 MHz, C_6D_6): δ = 328.8, 328.56, 169.2, 162.3 (q, $^1J_{CB}$ = 49.8 Hz, C_{ipso}, $B(Ar^F)_4$), 153.7, 147.3, 145.5, 135.4 ($B(Ar^F)_4$), 129.8, 129.5 (m*, $B(Ar^F)_4$), 129.5, 128.9, 127.6, 127.4, 127.3, 126.5, 126.3, 123.8, 122.0, 121.1, 118.1 (m, $B(Ar^F)_4$), 116.9, 113.1, 61.8, 40.9, 36.4, 32.6, 30.3, 30.2, 23.9 ppm. * Expected: qq, not resolved.

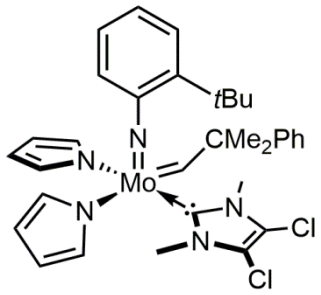

Mo-73

Synthesis of Mo-73: **Mo-68** (400 mg, 0.8 mmol) was dissolved in CH_2Cl_2 and 4,5-Cl_2-1,3-Me_2-imidazol-2-ylidene AgI (315 mg, 0.8 mmol) was added as a solid under exclusion of light. The resulting suspension was stirred for six hours and then filtered over Celite® to remove AgI. All volatiles were removed and the resulting brownish residue was treated with pentane and diethyl ether until a yellow solid was obtained. This solid was recrystallized from a mixture of CH_2Cl_2, diethyl ether and pentane to yield **17** in 57% yield as yellow crystals. ^{1}H NMR (400 MHz, CDCl3): δ = 13.62 (s, 1H, $^1J_{CH}$ = 120.7 Hz, *syn*), 7.44- 7.41 (m, 2H), 7.37-7.35 (m, 1H), 7.31-7.27 (m, 2H), 7.23-7.21 (m, 1H), 7.16-7.07 (m, 3H), 6.79-6.76 (m, 1H), 6.59 (br s, 2H), 6.05 (br s, 2H), 5.99 (br s, 2H), 5,90 (br s, 2H), 3.10 (s, 6H), 1.95 (s, 3H), 1.78 (s, 3H), 1.24 (s, 9H) ppm. ^{13}C NMR (101 MHz, C_6D_6): δ = 306.1, 306.0, 189.9, 154.6, 147.6, 146.0, 131.9, 131.5, 131.2, 129.5, 129.3, 129.2, 127.2, 127.2, 127.0, 126.8, 126.7, 126.6, 119.0, 108.3, 107.6, 57.03, 36.8, 35.6, 31.1, 30.8, 30.5, 30.4 ppm.

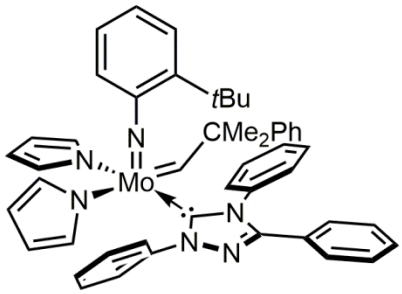

Mo-75

Synthesis of Mo-75: **Mo-68** (195 mg, 0.4 mmol) was dissolved in diethyl ether and a solution of 1,3,4-triphenyl-1,2,4-triazol-5-ylidene (174.7 mg, 0.4 mmol) in diethyl ether was added at -35°C. The solution was stirred for four hours and reduced until a saturated solution was reached. Then, the solution was layered with pentane and crystallized at -35°C to give **Mo-75** in 62 % yield. **Mo-75** co-crystallizes with one molecule of diethyl ether. ^{1}H NMR (400 MHz, $CDCl_3$): δ = 13.87 (br s, 0.5H)*, 13.41 (br s, 0.5H)*, 7.80 (br s, 1H), 7.44-7.41 (m, 1H), 7.34-7.27 (m, 6H), 7.24-7.12 (m, 7H), 7.07-6.99 (m, 6H), 6.54-6.26 (br s, 5H), 6.18-6.14 (m, 3H), 6.05-5.97 (m, 3H), 1.59 (s, 3H), 0.93-0.77 (br s, 12H) ppm. ^{13}C NMR (101 MHzC_6D_6): δ = 310.12, 309.15, 192.8, 191.5, 155.9, 153.8, 148.3, 146.5, 140.6, 140.0, 136.6, 135.9, 132.0 (br s), 131.8 (br s), 131.6 (br s), 131.4 (br s), 130.6 (br s), 130.2 (br s), 130.0 (br s), 129.7, 129.3, 128.7, 126.7 (br s), 126.4, 126.0 , 125.0 (br s), 122.9, 109.2, 108.4, 107.0, 66.2 (Et_2O), 56.6 (br s), 35.2, 32.1, 31.9, 30.9, 15.7 (Et_2O) ppm. Elemental analysis (%) calcd. for $C_{49}H_{51}MoN_6$ Et_2O: C 71.2, H 6.821, N 9.40; found: C 70.77, H 6.821, N 9.58. * **Mo-75** was isolated as mixture of two isomers (1/1), however, determination of *syn*- or *anti*-configuration was impossible due to the broad resonances. The sum of the integrals of both isomers was set to one in the ^{1}H NMR spectrum. Most probably the isomers differ in the coordination mode of the pyrrolide ligands and constantly interchange, thereby explaining the broad signals (in both, the ^{1}H and ^{13}C NMR spectrum).

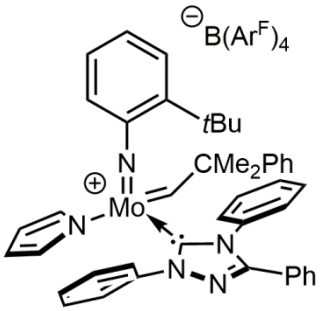

Mo-76

Synthesis of Mo-76: **Mo-68** (135.2 mg, 0.2 mmol) was dissolved in CH_2Cl_2 and cooled to -35°C. *N*,*N*-Dimethyl anilinium $B(Ar^F)_4$ (174.7 mg, 0.2 mmol) was dissolved in diethyl ether and cooled to -35°C. The *N*,*N*-dimethyl anilinium $B(Ar^F)_4$ solution was slowly dropped to the solution of the precursor complex and the resulting mixture was stirred at room temperature for three hours. The solvent was removed, the resulting residue was washed with pentane to remove *N*,*N*-dimethyl aniline and pyrrole, again dried and then crystallized from a mixture of CH_2Cl_2, diethyl ether and pentane to yield light yellow crystals of **Mo-76** in 87 % yield. ^{1}H NMR (400 MHz, $CDCl_3$): δ = 13.67 (br s, 1H, Mo=CH)*, 7.71-7.67 (m, 12H), 7.52-7.51 (m, 5H), 7.46-7.40 (m, 7H), 7.31-7.27 (m, 2H), 7.23-7.17 (m, 5H), 7.11-7.08 (m, 2H), 7.02-7.00 (m, 3H), 6.96-6.94 (m, 2H), 5.79 (br s, 2H), 1.51 (s, 3H), 1.11 (s, 9H), 0.82 (s, 3H) ppm. ^{13}C NMR (101 MHz, C_6D_6): δ = 338.1, 180.3, 162.3 (q, $^1J_{CB}$ = 49.8 Hz, C_{ipso} $B(Ar^F)_4$), 157.4, 153.9, 147.9, 145.8, 139.3, 135.6, 135.4, 132.6, 130.8, 130.0, 129.6, 129.5, 129.2, 129.0, 128.4, 127.6, 127.4, 127.1, 126.2, 125.2 (q, $^1J_{CF}$ = 272.4 Hz, CF_3 $B(Ar^F)_4$), 123.6, 118.1 ($B(Ar^F)_4$), 112.0, 61.7, 36.1, 32.1, 30.2, 29.1 ppm. * Determination of *syn*- or *anti*-configuration was impossible due to the broad resonance.

7.7.3 *INTRODUCTION OF BULKY (CHIRAL) LIGANDS*

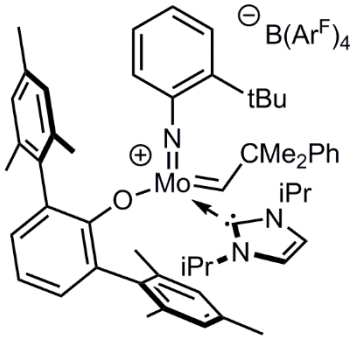

Mo-77

Synthesis of Mo-77: **Mo-72** (64.4 mg, 0.04 mmol) was dissolved in CH_2Cl_2 and a solution of HMTOH (14.5mg, 0.04 mmol) in CH_2Cl_2 was added at -35°C. The solution was stirred for three hours and the solvent was removed. The resulting yellow foam was twice co-evaporated with pentane and then stirred with pentane until a solid formed. Pentane was decanted (removal of pyrrole) and the remaining yellow solid was crystallized from CH_2Cl_2, diethyl ether and pentane to afford **Mo-77** in quantitative yield. If acetonitrile was used in the synthesis or during purification, **Mo-77** contains 1 equiv. of acetonitrile. NMR spectra were measured for **Mo-77**·MeCN, whereas elemental analysis is for **Mo-77**. ^{1}H NMR (400 MHz, CD_2Cl_2): δ = 12.48 (s, 1H, $^1J_{CH}$ = 122.5 Hz, *syn*), 7.74 (br s, 8H, B(ArF)$_4$), 7.57 (br s, 4H, B(Ar^F)$_4$), 7.37-7.28 (m, 5H), 7.26-7.22 (m, 1H), 7.15 (s, 2H), 7.09-6.96 (m, 6H), 6.91-6.66 (m, 3H), 5.97 (d, $^3J_{HH}$ = 7.84 Hz, 1H), 3.93 (hept, 2H, $^3J_{HH}$ = 6.5 Hz), 2.31 (s, 6H), 2.00 (s, 12H), 1.76 (s, 3H), 1.68 (s, 3H), 1.46 (s, 3H); 1.28 (s, 9H), 1.26 (d, 6H, $^3J_{HH}$ = 6.5 Hz), 0.77 (d, 6H, $^3J_{HH}$ = 6.5 Hz) ppm. ^{13}C NMR (101 MHz, C_6D_6)*: δ = 177.6, 162.3 (q, $^1J_{CB}$ = 49.8 Hz, C_{ipso}, B(Ar^F)$_4$), 160.9, 154.9, 145.1, 144.6, 138.0, 137.6, 137.2, 137.1, 137.0, 135.4, 132.1, 131.9, 131.5, 130.1, 129.8, 129.6, 129.2, 129.1, 128.9, 127.5, 127.3, 127.2, 127.0, 125.16 (q, $^1J_{CF}$ = 272.4 Hz, CF_3 B(Ar^F)$_4$)**, 121.8, 119.72, 118.0, 58.7, 36.0, 31.2, 31.0, 30.2, 29.3, 24.5, 24.2, 21.9, 21.3, 20.6, 3.41 (CH_3, MeCN)*** ppm. Elemental analysis (%) calcd. for $C_{85}H_{78}BF_{24}MoN_3O$: C 59.35, H 4.57, N 2.44; found: C 59.08, H 4.662, N 2.62. * The alkylidene carbon signal was not clearly visible in the ^{13}C NMR spectrum, even though 80 mg of catalyst were used and the spectrum was measured from 0 to 400 ppm. However, a tiny peak at 324.9 ppm was observed. ** The fourth signal of the quartet is not observable due to overlapping with other aromatic signals. *** The signal of the nitrile carbon most probably overlaps with the broad signal at 118.0 ppm.

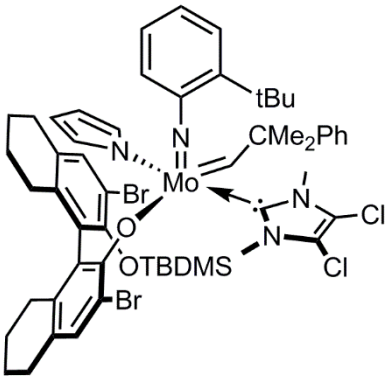

Mo-78

Synthesis of Mo(N-2-tBu-C_6H_4)(CHCMe$_2$Ph)(NC_4H_4)(HOBitet)(4,5-Cl_2-1,3-Me_2-imidazol-2-ylidene) Mo-78: **Mo-73** (75.4 mg, 0.1 mmol) was dissolved in CH_2Cl_2 and a solution of **13** (63.5 mg, 0.1 mmol) in CH_2Cl_2 was added at -35°C. The solution was stirred at room temperature for eight hours. The volatiles were removed under reduced pressure and the resulting residue was washed with *3M™ Novec™ 7300 Engineered Fluid* to remove pyrrole. The resulting solid was dried. **Mo-78** was isolated as yellow solid foam in quantitative yield. ^{1}H NMR (400 MHz, CD_2Cl_2): δ =13.14 (s, 1H, $^1J_{CH}$ = 124.9 Hz, *syn*), 7.39- 7.34 (m, 3H), 7.30- 7.28 (m, 3H), 7.25- 7.21 (m, 1H), 7.10- 7.00 (m, 3H), 6.64- 6.61 (m, 3H), 5.84 (m, 2H), 3.12 (s, 6H), 2.73- 2.55 (m, 5H), 2.11- 1.99 (m, 3H), 1.84 (s, 3H), 1.67- 1.64 (m, 8H), 1.53 (s, 3H), 1,14 (s, 9H), 0.46 (s, 9H), 0.23 (s, 3H), -0.18 (s, 3H) ppm. ^{13}C NMR (101 MHz, C_6D_6): δ = 309.5, 188.2, 158.1, 154.6, 148.2, 147.9, 147.0, 139.2, 135.9, 133.2, 133.0, 132.1, 131.4, 131.1, 129.4, 128.2, 127.3, 126.7, 126.6(9), 126.6, 126.4, 117.6, 112.8, 110.9, 106.3, 65.5, 37.6, 35.3, 34.7, 31.1, 30.4, 30.2, 29.5, 28.1, 26.0, 25.9, 24.4, 23.5, 23.4, 22.9, 19.0, 14.4, -1.2, -3.64 ppm.

7.7.4 ADDITIONAL REACTIONS

Table 28: Additional attempted syntheses of chiral molybdenum imido alkylidene NHC complexes.

metal complex	chiral ligand	base	solvent deprotonation	solvent reaction	reaction time [h]
Mo(*N*-*t*Bu)(CHCMe$_2$Ph)(OTf)$_2$(4,5-Cl$_2$-1,3-Me$_2$-imidazol-2-ylidene)[14]	**13-K**	KH	toluene	toluene	1
Mo(*N*-*t*Bu)(CHCMe$_2$Ph)(OTf)$_2$(4,5-Cl$_2$-1,3-Me$_2$-imidazol-2-ylidene)[14]	**13-Na**	KH	toluene	toluene	1
Mo(*N*-*t*Bu)(CHCMe$_2$Ph)(OTf)$_2$(4,5-Cl$_2$-1,3-Me$_2$-imidazol-2-ylidene)[14]	**13-K**	KH	diethyl ether	CH_2Cl_2	3
Mo(*N*-*t*Bu)(CHCMe$_2$Ph)(OTf)$_2$(4,5-Cl$_2$-1,3-Me$_2$-imidazol-2-ylidene)[14]	**12-K**	KH	toluene	toluene	3
Mo(*N*-*t*Bu)(CHCMe$_2$Ph)(OTf)$_2$(4,5-Cl$_2$-1,3-Me$_2$-imidazol-2-ylidene)[14]	**12-K**	KH	diethyl ether	CH_2Cl_2	3
Mo(*N*-3,5-Me$_2$-C$_6$H$_3$)(CHCMe$_2$Ph)(OTf)$_2$(sIMes)[169]	**12-K**	KH	toluene	toluene	2
Mo(*N*-3,5-Me$_2$-C$_6$H$_3$)(CHCMe$_2$Ph)(OTf)$_2$(sIMes)[169]	**12-K**	KH	diethyl ether	CH_2Cl_2	2
Mo(*N*-2,6-Me$_2$-C$_6$H$_3$)(CHCMe$_2$Ph)(OC$_6$F$_5$)(OTf)(sIMes)[168a]	**12-Na**	NaH	benzene	benzene	2
Mo(*N*-3,5-Me$_2$-C$_6$H$_3$)(CHCMe$_2$Ph)(OTf)$_2$(sIMes)[169]	**13-K**	KH	diethyl ether	CH_2Cl_2	2
Mo(*N*-3,5-Me$_2$-C$_6$H$_3$)(CHCMe$_2$Ph)(OTf)$_2$(sIMes)[169]	**13-Na**	NaH	diethyl ether	CH_2Cl_2	2
Mo(*N*-2,6-Me$_2$-C$_6$H$_3$)(CHCMe$_2$Ph)(OTf)$_2$(sIMes)[168a]	**13-K**	KH	THF	THF	0.5
Mo(*N*-2,6-Me$_2$-C$_6$H$_3$)(CHCMe$_2$Ph)(OTf)$_2$(sIMes)[168a]	**13-Na**	NaH	diethyl ether	CH_2Cl_2	3
Mo(*N*-2,6-Me$_2$-C$_6$H$_3$)(CHCMe$_2$Ph)(OTf)$_2$(sIMes)[168a]	**13-Li**	*n*BuLi	diethyl ether	CH_2Cl_2	3
Mo(*N*-2,6-Me$_2$-C$_6$H$_3$)(CHCMe$_2$Ph)(OTf)$_2$(sIMes)[168a]	**25-Li**	*n*BuLi	THF	CH_2Cl_2	3
Mo(*N*-2,6-Me$_2$-C$_6$H$_3$)(CHCMe$_2$Ph)(OTf)$_2$(sIMes)[168a]	**25-K**	KH	THF	CH_2Cl_2	3
Mo(*N*-2,6-Me$_2$-C$_6$H$_3$)(CHCMe$_2$Ph)(OTf)$_2$(sIMes)[168a]	**26-K**	KH	THF	CH_2Cl_2	3
Mo(*N*-2,6-Me$_2$-C$_6$H$_3$)(CHCMe$_2$Ph)(OTf)$_2$(sIMes)[168a]	**25-Na**	NaH	THF	CH_2Cl_2	3
Mo(*N*-2,6-Me$_2$-C$_6$H$_3$)(CHCMe$_2$Ph)(OTf)$_2$(sIMes)[168a]	**26-Na**	NaH	THF	CH_2Cl_2	3
Mo(*N*-*t*Bu)(CHCMe$_2$Ph)(OC$_6$F$_5$)$_2$(4,5-Cl$_2$-1,3-Me$_2$-imidazol-2-ylidene)[168e]	**13-K**	KH	toluene	toluene	3
Mo(*N*-*t*Bu)(CHCMe$_2$Ph)(OC$_6$F$_5$)$_2$(4,5-Cl$_2$-1,3-Me$_2$-imidazol-2-ylidene)[168e]	**13-Na**	NaH	toluene	toluene	3
Mo(*N*-*t*Bu)(CHCMe$_2$Ph)(OC$_6$F$_5$)$_2$(4,5-Cl$_2$-1,3-Me$_2$-imidazol-2-ylidene)[168e]	**13-K**	KH	diethyl ether	CH_2Cl_2	3
Mo(*N*-*t*Bu)(CHCMe$_2$Ph)(OTf)$_2$(sIMes)[15]	**13-K**	KH	diethyl ether	toluene	3
Mo(*N*-*t*Bu)(CHCMe$_2$Ph)(OTf)$_2$(sIMes)[15]	**13-K**	KH	diethyl ether	CH_2Cl_2	3
Mo(*N*-Ad)(CHCMe$_2$Ph)(OTf)$_2$(1,3-Cy$_2$-imidazol-2-ylidene)[191]	**13-K**	KH	diethyl ether	diethyl ether	3
Mo(*N*-Ad)(CHCMe$_2$Ph)(OTf)$_2$(1,3-Cy$_2$-imidazol-2-ylidene)[191]	**13-K**	KH	diethyl ether	CH_2Cl_2	3

Reaction procedure: Metal complex (1 equiv.) was dissolved in the indicated solvent and a solution of the respective ligand (1 equiv.) in the indicated solvent at -35°C was added. The reaction mixture was stirred at room temperature for the indicated time and the solvent was removed. The residue was dissolved in CD_2Cl_2, filtered over Celite® and analyzed by ^1H and ^{19}F NMR spectroscopy. Lithium, sodium and potassium salts were prepared beforehand by deprotonation of the ligand (1 equiv.) with the indicated bases (1 equiv.) in the indicated solvent. The metal precursor complexes were synthesized according to the literature.

7.8 INVESTIGATIONS OF STRUCTURE-REACTIVITY RELATIONS IN MOLYBDENUM ALKYLIDYNE *N*-HETEROCYCLIC CARBENE COMPLEXES

Parts of the following chapter have already been published. Reprinted (adapted) with permission from (M. Koy, I. Elser, J. Meisner, W. Frey, K. Wurst, J. Kästner, M. R. Buchmeiser, *Chem. Eur. J.* **2017**, *23*, 15484-15490). Copyright (2017) John Wiley and Sons.

7.8.1 SYNTHESIS OF SUBSTRATES AND METAL COMPLEXES

Synthesis of Substrates S2 - S5: Substrates **S2** - **S5** were synthesized according to literature or in a similar manner. NMR data were in accordance to the literature. Procedures are repeated for convenience.[200]

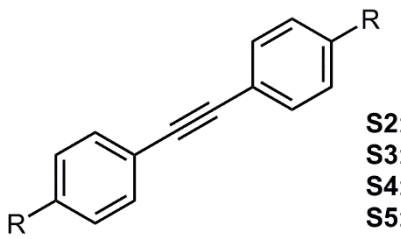

S2: R = Me
S3: R = OMe
S4: R = O=CMe
S5: R = Br

Synthesis of 4-(prop-1-yn-1-yl)toluene S2: 4-Bromotoluene (2.0 g, 11.7 mmol), $Pd_2(PPh_3)_2Cl_2$ (41.0 mg, 0.06 mmol), 1,3-bis(diphenylphosphino)propane (48.2 mg, 0.12 mmol) and DBU (3.23 g, 23.4 mmol) and 2-butynoic acid (933 mg, 11.7 mmol) were dissolved in dimethyl sulfoxide (5 mL, dry, degassed) and stirred at 110 °C for 36 hours. Subsequently the reaction mixture was poured into saturated NH_4Cl solution. The water phase was extracted with CH_2Cl_2 and the combined organic layers were extracted with water and saturated NaCl solution and were dried over Na_2SO_4. The volatiles were removed, and the resulting residue was dissolved in diethyl ether and filtered. The filtrate was evaporated to dryness and the resulting oil was purified via column chromatography (silica, hexane). 4-(Prop-1-yn-1-yl)toluene was isolated in form of a colorless oil (1.14 g, 75 % yield). ^{1}H NMR (400 MHz, $CDCl_3$): δ = 7.29 (d, $^3J_{HH}$ = 8.22 Hz), 7.09 (d, $^3J_{HH}$ = 8.22 Hz, 2H), 2.34 (s, 3H), 2.05 (s, 3H) ppm. ^{13}C NMR (100 MHz, $CDCl_3$): δ = 137.6, 131.5, 129.1, 121.1, 85.1, 79.9, 22.5, 4.44 ppm. NMR data were in accordance to the literature.[200a]

Synthesis of 4-(prop-1-yn-1-yl)anisole S3: 4-Bromoanisole (2.0 g, 10.7 mmol), $Pd_2(PPh_3)_2Cl_2$ (37.5 mg, 0.05 mmol), 1,3-bis(diphenylphosphino)propane (44.1 mg, 0.1 mmol) and DBU (2.95 g, 21.4 mmol) and 2-butynoic acid (854 mg, 10.7 mmol) were dissolved in dimethyl sulfoxide (5 mL, dry, degassed) and stirred at 110 °C for 12 hours. Subsequently the reaction mixture was poured into saturated NH_4Cl solution. The water phase was extracted with CH_2Cl_2 and the combined organic layers were washed with water and saturated NaCl solution and were dried over Na_2SO_4. The volatiles were removed, and the resulting residue

was dissolved in diethyl ether and filtered. The filtrate was evaporated to dryness and the resulting oil was purified via column chromatography (silica, hexane). 4-(prop-1-yn-1-yl)anisole was isolated in form of a colorless oil (856 mg, 55 % yield). ^{1}H NMR (400 MHz, $CDCl_3$): δ = 7.34 (d, $^{3}J_{HH}$ = 8.7 Hz, 2H), 6.82 (d, $^{3}J_{HH}$ = 8.6 Hz, 2H), 3,79 (s, 3H), 2.04 (s, 3H) ppm. ^{13}C NMR (101 MHz, $CDCl_3$): δ = 159.0, 132.8, 116.2, 113.8, 84.1, 79.5, 55.2, 4.3 ppm. NMR data were in accordance with the literature.[200a]

Synthesis of 4-(prop-1-yn-1-yl)acetophenone S4: 4-Bromoacetophenone (1.0 g, 5.5 mmol), $Pd_2(PPh_3)_2Cl_2$ (38.6 mg, 0.05 mmol), 1,3-bis(diphenylphosphino)propane (45.3 mg, 0.1 mmol) and TBAF (1 M solution in THF, 11.0 mL, 11.0 mmol) and 2-butynoic acid (453 mg, 5.4 mmol) were dissolved in dimethyl sulfoxide (5 mL, dry, degassed) and stirred at 110°C for 3 hours. Subsequently the reaction mixture was poured into saturated NH_4Cl solution. The water phase was extracted with diethyl ether and the combined organic layers were washed with water and saturated NaCl solution and were dried over Na_2SO_4. The volatiles were removed and the resulting oil was purified via column chromatography (silica, hexane/ethyl acetate, 2/1). 4-(prop-1-yn-1-yl)acetophenone was isolated in form of a colorless oil (0.651 g, 74 % yield). ^{1}H NMR (400 MHz, $CDCl_3$): δ = 7.85 (d, $^{3}J_{HH}$ = 8.38 Hz, 2H), 7.44 (d, $^{3}J_{HH}$ = 8.38 Hz, 2H), 2.56 (s, 3H), 2.06 (s, 3H) ppm. ^{13}C NMR (101 MHz, $CDCl_3$): δ = 197.5, 135.8, 131.7, 129.2, 128.3, 89.9, 79.4, 26.7, 4.6 ppm. NMR data were in accordance with the literature.[200b]

***Synthesis of 4-(prop-1-yn-1-yl)bromobenzene S5*:** 4-Bromo-1-iodobenzene (1.0 g, 3.5 mmol), $Pd_2(PPh_3)_2Cl_2$ (24.8 mg, 0.04 mmol), 1,3-bis(diphenylphosphino)propane (29.2 mg, 0.07 mmol) and TBAF (1 M solution in THF, 7.1 mL, 7.1 mmol) and 2-butynoic acid (291 mg, 3.5 mmol) were dissolved in dimethyl sulfoxide (5 mL, dry, degassed) and stirred at 110°C for 3 hours. Subsequently the reaction mixture was poured into saturated NH_4Cl solution. The water phase was extracted with diethyl ether and the combined organic layers were washed with water and saturated NaCl solution and were dried over Na_2SO_4. The volatiles were removed and the resulting oil was purified via column chromatography (silica, hexane/ethyl acetate, 2/1). 4-(prop-1-yn-1-yl)bromobenzene was isolated in form of a light yellow oil (0.468 g, 68 % yield). ^{1}H NMR (400 MHz, $CDCl_3$): δ = 7.37 (d, $^{3}J_{HH}$ = 8.59 Hz, 2H), 7.21 (d, $^{3}J_{HH}$ = 8.59 Hz, 2H), 2.00 (s, 3H) ppm. ^{13}C NMR (100 MHz, $CDCl_3$): δ = 133.1, 131.6, 123.1, 121.7, 87.3, 78.9, 4.5 ppm. NMR data were in accordance with the literature.[200b]

Synthesis of Mo-P11 and Mo-P12: **Mo-P11**[140,154] and **Mo-P12**[10,23] were synthesized in accordance to the literature.

Synthesis of Mo-81- Mo-87: **Mo-81**-**Mo-84** were synthesized according to the literature.[10,23] **Mo-85** - **Mo-87** were synthesized according to procedures developed by *M. Koy* during his master thesis and are reported for convenience.[10]

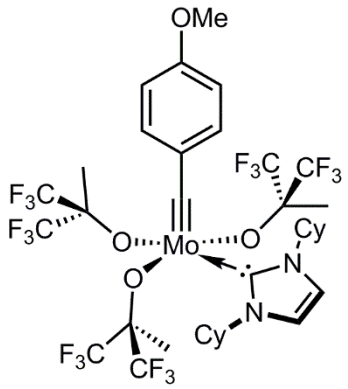

Mo-85

Synthesis of Mo-85: *This catalyst was first isolated by M. Koy.*[10] 1,3-Dicyclohexylimidazolium tetrafluoroborate (35 mg, 0.11 mmol) was suspended in toluene and KHMDS (22 mg, 0.11 mmol) was dissolved in toluene in 10 mL glass vials. Both mixtures were cooled to -35°C. The solution of KHMDS was slowly added to the solution of the imidazolium salt under stirring. The reaction mixture stirred for 1 h at room temperature, then filtered, again cooled to -35°C and then added to a cold solution of **Mo-P11** (100 mg, 0.12 mmol) in a Schlenk tube equipped with a magnetic stir bar. The reaction mixture was removed from the glove box and stirred for 20 min at room temperature and then for 3 h at 40°C. In course of the reaction a color change from brown to red was observed. The reaction mixture was concentrated *in vacuo* and brought back into the glove box. The remaining solid was crystalized form diethyl ether/pentane to give the product as a red solid (79 mg, 0.080 mmol, 67%). ^{1}H NMR (400 MHz, C_6D_6): δ = 7.42-7.40 (m, 2H), 6.56-6.54 (m, 2H), 6.37-6.36 (m, 2H), 5.01-4.95 (m, 1H), 3.86-3.81 (m, 1H), 3.17 (s, 3H), 2.29 (d, $^{3}J_{HH}$ = 11.80 Hz, 2H), 2.08 (d, $^{3}J_{HH}$ = 11.60 Hz, 2H), 1.88 (s, 3H), 1.73 (s, 6H), 1.68 (s, 2H), 1.51-1-13 (m, 14H) ppm. ^{19}F NMR (377 MHz, C_6D_6): δ = -76.19 - -76.27 (m, 6F), -76.41 (s, 6F), -77.22 (s, 6F) ppm. ^{13}C NMR (100 MHz, CD_2Cl_2): δ = 297.6, 186.2, 160.5, 138.1, 132.7, 124.68 (q, $^{1}J_{CF}$ = 288.95 Hz), 124.59 (q, $^{1}J_{CF}$ = 289.98 Hz), 124.40 (q, $^{1}J_{CF}$ = 290.25 Hz), 117.6, 117.2, 113.5, 83.5 (hept., $^{1}J_{CF}$ = 28.39 Hz), 82.79 (hept., $^{1}J_{CF}$ = 28.83 Hz)*, 61.2, 60.4, 55.8, 34.7, 33.7, 25.8, 25.7, 25.6, 19.8 ppm. Elemental analysis (%) calcd. for $C_{35}H_{40}F_{18}MoN_2O_4$: C, 42.44; H, 4.07; N, 2.83. found: C, 42.12; H, 4.16; N, 2.83. *Terminal signals of the heptet are not observable. Red crystals suitable for single crystal X-ray diffraction were obtained by over layering an almost saturated solution of **Mo-85** in CH_2Cl_2 with pentane and allowing the solution to stand at -40°C for several days.

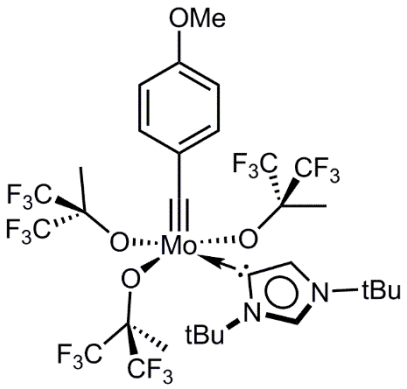

Mo-86

Synthesis of Mo-86: *This catalyst was first isolated by M. Koy.*[10] **Mo-P11** (200 mg, 0.24 mmol) and 1,3-di-*tert*-butylimidazol-2-ylidene (43 mg, 0.24 mmol) were separately dissolved in toluene (2 mL). Both solutions were cooled to -35°C. The solution of the imidazol-2-ylidene was slowly added to the solution of **Mo-P11**. The reaction mixture was stirred at 40°C for 3 h. The reaction mixture was concentrated *in vacuo* and brought back into the glove box. The remaining solid was crystalized form diethyl ether/pentane to give the product as a red solid (98 mg, 0.104 mmol, 44%). ^{1}H NMR (400 MHz, $CDCl_3$): δ = 7.86 (d, $^{3}J_{HH}$ = 1.80 Hz, 1H), 7.19-7.16 (m, 2H), 7.09 (b s, 1H), 6.84-6.80 (m, 2H), 3.81 (s, 3H), 1.65 und 1.64 (2xs, 18H), 1.62 (s, 9H) ppm. ^{19}F NMR (377 MHz, $CDCl_3$): δ = -75.33 - -75.41 (m, 6F), -77.64 - -77.68 (m, 6F), -77.92 (s, 6F) ppm. ^{13}C NMR (100 MHz, CD_2Cl_2): δ = 292.2, 170.2, 159.8, 138.5, 131.6, 127.3, 126.1, 124.9 (q, $^{1}J_{CF}$ = 289.73 Hz), 124.4 (q, $^{1}J_{CF}$ = 290.98 Hz), 113.7, 83.37 (hept., $^{1}J_{CF}$ = 28.03 Hz)*, 81.7 (hept., $^{1}J_{CF}$ = 28.41 Hz)*, 60.2, 57.8, 55.7, 30.8, 30.2, 19.5, 19.3 ppm. Elemental analysis (%) calcd. for $C_{31}H_{36}F_{18}MoN_2O_4$: C, 39.65; H, 3.87; N, 2.98 found: C, 39.66; H, 3.85; N, 3.07. Red crystals suitable for single crystal X-ray diffraction were obtained by over layering an almost saturated solution of **Mo-86** in diethyl ether with pentane and allowing the solution to stand at -40°C overnight. *Terminal signals of the heptet are not observable.

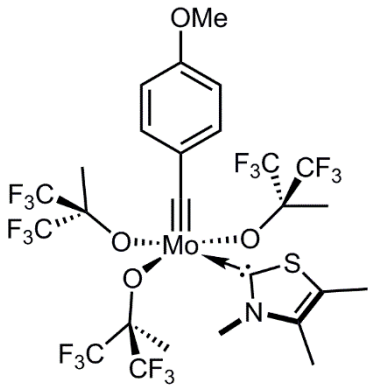

Mo-87

Synthesis of Mo-87: *This catalyst was first isolated by M. Koy*.[10] In the glove box under exclusion of light, 3,4,5-trimethylthiazolium iodide (100 mg, 0.118 mmol), 4 Å molecular sieve (100 mg), Ag_2O (55 mg, 0.236 mmol) and DCM (4 mL) were added to a Schlenk tube equipped with a magnetic stir bar. The reaction mixture was stirred at room temperature for 1 h under exclusion of light. Volatile components were removed under reduced pressure. Toluene (2 mL) and **Mo-P11** (333 mg, 0.393 mmol) in toluene (2mL) were added to the reaction mixture. The reaction mixture was removed from the glove box, sonicated for 3 h at 40°C under the exclusion of light, concentrated *in vacuo* and brought back into the glove box. The brownish green solid was extracted with diethyl ether, filtered and concentrated in *vacuo* to give a dark red solid. Crystallization from diethyl ether/pentane at -40°C gave the product as a red solid (175 mg, 0.198 mmol, 50%). ^{1}H NMR (400 MHz, C_6D_6): δ = 7.45-7.41 (m, 2H), 6.60-6.56 (m, 2H), 3.20 (s, 3H), 2.96 (s, 3H), 1.98 (s, 3H), 1.80 (s, 6H), 1.36 (s, 3H), 1.17 (s, 3H) ppm. ^{19}F NMR (376 MHz, C_6D_6): δ = -76.66 - -76.78 (m, 12F), -77.14 - -77.22 (m, 6F) ppm.^{13}C NMR (101 MHz, CD_2Cl_2): δ = 300.7, 209.0, 160.6, 140.2, 138.4, 133.0, 132.5, 124.65 (q, *J* = 289.70 Hz), 124.28 (q, *J* = 289.97 Hz), 124.08 (q, *J* = 289.83 Hz), 113.7, 83.8-82.7 (m)*, 55.8, 40.6, 20.0, 19.7, 12.2, 12.0 ppm. Elemental analysis (%) calcd. for $C_{26}H_{25}F_{18}MoNO_4S$: C, 35.27; H, 2.85; N, 1.58 found: C, 35.08; H, 3.09; N, 1.59. Red crystals suitable for single crystal X-ray diffraction were obtained by over layering a saturated solution of **Mo-87** in diethyl ether with pentane and allowing the solution to stand at -40°C overnight. *the expected heptets are reported as a multiplet due to strong overlapping.

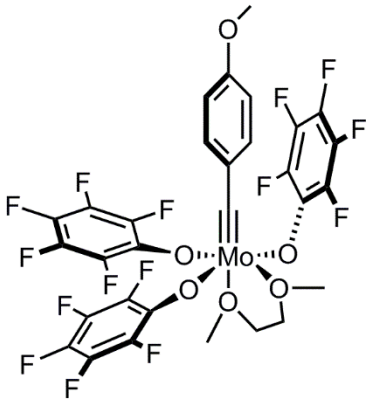

Mo-90

Synthesis of Mo-90: *This synthesis route has already been reported by J. Groos*.[203] **Mo-P12** (813 mg, 1.5 mmol) was dissolved in diethyl ether and cooled to -35°C. A suspension of potassium pentafluorophenoxide (995 mg, 4.5 mmol) in diethyl ether was added and the mixture was stirred overnight. Subsequently solvent was removed and the resulting residue was dissolved in CH_2Cl_2 and filtered over Celite®. Again, the volatiles were removed and the resulting residue was crystallized from a mixture of diethyl ether and pentane to afford **Mo-90** in 60% yield. ^{1}H NMR (400 MHz, CD_2Cl_2): δ = 6.63 (d, $^{3}J_{HH}$ = 8.8 Hz, 2H, H_{Ar}), 6.20 (d, $^{3}J_{HH}$ = 8.7 Hz, 2H, H_{Ar}), 3.64 (s, 3H, Me), 3.42 (s, 4H), 3.23 (s, 6H) ppm. ^{19}F NMR (376 MHz, CD_2Cl_2): δ = -161.51 (d, $^{3}J_{FF}$ = 24.4 Hz, 2F), -166.90 (t, $^{3}J_{FF}$ = 22.3 Hz, 2F), -171.52 (s, 1F) ppm. ^{13}C NMR (101 MHz, CD_2Cl_2): δ = 302.2 (Mo≡*C*), 161.5 (N-*C*-N), 145.4 (t, $^{2}J_{CF}$ = 13.0 Hz), 139.8 (dd, $^{1}J_{C\text{-}F}$ = 243.3 Hz, $^{2}J_{C\text{-}F}$ = 11.2 Hz, C_6F_5), 138.6 (dt, $^{1}J_{C\text{-}F}$ = 247.3 Hz, $^{2}J_{CF}$ = 13.6 Hz, C_6F_5), 136.2, 135.2 (dt, $^{1}J_{CF}$ = 243.5 Hz, $^{2}J_{CF}$ = 13.9 Hz, C_6F_5), 132.0 (C_{Ar}), 113.6 (C_{Ar}), 55.9 (Me) ppm. Elemental Anal. Calcd. (%) for $C_{29}H_{17}O_6F_{15}Mo$: C 42.17, H 2.01; found: C 42.34, H 2.195.

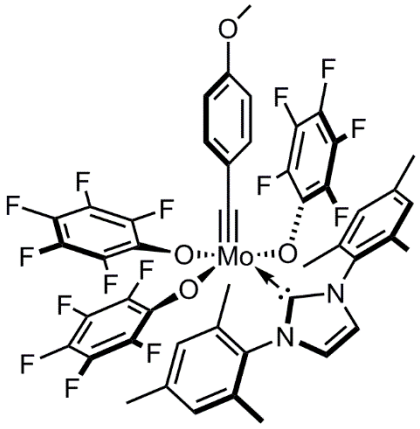

Mo-91

Synthesis of Mo-91: **Mo-90** (226 mg, 0.3 mmol) was dissolved in toluene (approx. 15 mL) and cooled to -35°C. IMes (81 mg, 0.3 mmol) was dissolved in toluene (approx. 5 mL) and

slowly dropped to the complex solution. The mixture was stirred for three hours at room temperature and the solvent was removed. The resulting greenish residue was washed with diethyl ether to afford **Mo-91** in 89 % yield. ^{1}H NMR (400 MHz, $CDCl_3$): δ = 7.16 (s, 2H), 6.65 (s, 4H), 6.48 (s, 4H), 3.75 (s, 3H), 2.15 (s, 6H), 1.99 (s, 12H) ppm. ^{19}F NMR (376 MHz, $CDCl_3$): δ = -160.3 (m, 4F), -162.4 (m, 2F), -166.2 (m, 4F), -168.0 (m, 2F), -171.1 (m, 2F), -174.0 (m, 1F) ppm. ^{13}C NMR (101 MHz, CD_2Cl_2): δ = 310.2, 189.9, 160.8, 143.3-136.1 (m, OC_6F_5), 135.5, 133.0, 129.1, 124.1, 111.8, 55.4, 21.0, 17.5 ppm.

7.8.2 NMR EXPERIMENTS

General procedure for the determination of the active species: A solution of catalyst (approx. 10 mg, 1 equiv.) and CH_2Cl_2 (5 µL) as internal standard in C_6D_6 was prepared and ^{1}H and ^{19}F NMR spectra were acquired. The NMR sample was transferred back into the glove box and 1,1,1,3,3,3-hexafluoro-2-methyl-2-propanol (1 equiv.) was added and ^{1}H and ^{19}F NMR spectra were acquired. Again, the NMR sample was transferred into the glove box and 1-phenyl-1-propyne (5 equiv.) was added to the mixture. Subsequently ^{1}H and ^{19}F NMR spectra were acquired after indicated time spans. Then, an aliquot of the reaction mixture was subjected to GC-MS analysis to confirm product formation.

7.8.3 CATALYSIS

General procedure for HM reactions with Mo-81: A stock solution of **Mo-81** in toluene (40 µL, 5 mg/mL, at least 15 mg of catalyst were used for the preparation of the stock solution, 0.2 mg, 1 equiv.) was added to a suspension of the corresponding substrate (1000 equiv.), dodecane (2 drops) and 5 Å molecular sieves (250 mg, dried, powdered) in toluene (1 mL) from which an aliquot for GC-MS analysis had been withdrawn before. The reaction mixture was stirred for three hours at room temperature. Then, an aliquot for GC-MS analysis was withdrawn. Both aliquots were diluted with HPLC grade acetone, filtered over glass fiber filter paper and analyzed via GC-MS to determine TON.

8 LITERATURE

[1] a) A. Suzuki, *J. Organomet. Chem.* **1999**, *576*, 147-168; b) J. F. Hartwig, *Nature* **2008**, *455*, 314-322; c) E. Negishi, *Acc. Chem. Res.* **2002**, *15*, 340-348.

[2] a) R. G. Bergman, *Nature* **2007**, *446*, 391-393; b) J. A. Labinger, J. E. Bercaw, *Nature* **2002**, *417*, 507-514.

[3] a) X. Chen, K. M. Engle, D. H. Wang, J. Q. Yu, *Angew. Chem. Int. Ed. Engl.* **2009**, *48*, 5094-5115; b) R. Giri, S. Thapa, A. Kafle, *Adv. Synth. Catal.* **2014**, *356*, 1395-1411; c) M. M. Heravi, Z. Kheilkordi, V. Zadsirjan, M. Heydari, M. Malmir, *J. Organomet. Chem.* **2018**, *861*, 17-104.

[4] a) G. W. Parshall, *Organometallics* **1987**, *6*, 687-692; b) J. Mol, *J. Mol. Catal. A: Chem.* **2004**, *213*, 39-45; c) C. Slugovc, in *Olefin Metathesis: Theory and Practice* (Ed.: K. Grela), **2014**.

[5] a) R. H. Grubbs, *Nobel Lecture* **2005**; b) R. R. Schrock, *Nobel Lecture* **2005**; c) E.-I. Negishi, *Nobel Lecture* **2010**; d) Y. Chauvin, *Nobel Lecture* **2006**; e) E. O. Fischer, *Nobel Lecture* **1973**; f) W. S. Knowles, *Nobel Lecture* **2001**; g) G. Natta, *Nobel Lecture* **1963**; h) R. Noyori, *Nobel Lecture* **2001**; i) K. B. Sharpless, *Nobel Lecture* **2001**; j) A. Suzuki, *Nobel Lecture* **2010**; k) G. Wilkinson, *Nobel Lecture* **1973**; l) K. Ziegler, *Nobel Lecture* **1963**.

[6] a) A. H. Hoveyda, A. R. Zhugralin, *Nature* **2007**, *450*, 243-251; b) A. Fürstner, P. W. Davies, *Chem. Commun.* **2005**, 2307-2320; c) R. R. Schrock, *Chem. Commun.* **2013**, *49*, 5529-5531; d) A. Fürstner, *Angew. Chem.* **2013**, *125*, 2860-2887; *Angew. Chem. Int. Ed.* **2013**, *52*, 2794-2819.

[7] G. Schwarzenbach, *Helv. Chim. Acta* **1952**, *35*, 2344-2359.

[8] T. Droge, F. Glorius, *Angew. Chem.* **2010**, *49*, 7094-7107; *Angew. Chem. Int. Ed.* **2010**, *39*, 6940-6952.

[9] a) A. Fürstner, *Science* **2013**, *341*, 1229713; b) A. H. Hoveyda, R. R. Schrock, in *Organic Synthesis Highlights V, Vol. 5* (Eds.: H.-G. Schmalz, T. Wirth), **2003**, 210-229.

[10] M. Koy, *N-Heterozyklische Carben-Metallalkylidinkomplexe der Gruppe 6*, Master thesis, University of Stuttgart **2017**.

[11] a) R. R. Schrock, *Science* **1983**, *219*, 13-18; b) R. R. Schrock, *Chem. Rev.* **2002**, *102*, 145-180; c) R. R. Schrock, *Acc. Chem. Res.* **2002**, *19*, 342-348; d) M. Schuster, S. Blechert, *Angew. Chem.* **1997**, *36*, 2037-2056; *Angew. Chem. Int. Edit.* **1997**, *19*, 2036-2056; e) X. Wu, M. Tamm, *Beilstein J. Org. Chem.* **2011**, *7*, 82-93; f) P. Schwab, M. B. France, J. W. Ziller, R. H. Grubbs, *Angew. Chem. Int. Ed.* **1995**, *34*; g) M. S. Sanford, J. A. Love, R. H. Grubbs, *J. Am. Chem. Soc.* **2001**, *123*, 6543-6554.

[12] a) R. R. Schrock, *Dalton Trans.* **2011**, *40*, 7484-7495; b) M. R. Buchmeiser, in *Mater. Sci. Technol.* (Eds.: R. W. Cahn, P. Haasen, E. J. Kramer), **2013**; c) A. Gradillas, J. Perez-Castells, *Angew. Chem.* **2006**, *118*, 6232-6247; *Angew. Chem. Int. Ed.* **2006**, *45*, 6086-6101.

[13] a) P. J. Dyson, D. J. Ellis, T. Welton, *Platinum Met. Rev.* **1998**, *42*, 135-140; b) W. Keim, *Green Chem.* **2003**, *5*, 105-111.

[14] I. Elser, R. Schowner, W. Frey, M. R. Buchmeiser, *Chem. Eur. J.* **2017**, *23*, 6398-6405.

[15] R. Schowner, Ph. D. thesis, University of Stuttgart **2018**.

[16] I. Elser, W. Frey, K. Wurst, M. R. Buchmeiser, *Organometallics* **2016**, *35*, 4106-4111.

[17] a) B. R. Kordes, *Latente Molybdän-Imidoalkyliden NHC Komplexe für die Metathesepolymerisation*, Bachelor thesis, University of Stuttgart **2017**; b) K. Herz, J. Unold, J. Hänle, R. Schowner, S. Sen, W. Frey, M. R. Buchmeiser, *Macromolecules* **2015**, *48*, 4768-4778.

[18] J. Beerhues, S. Sen, R. Schowner, G. Mate Nagy, D. Wang, M. R. Buchmeiser, *J. Polym. Sci., Part A: Polym. Chem.* **2017**, *55*, 3028-3033.

[19] J. Heppekausen, A. Fürstner, *Angew. Chem.* **2011**, *123*, 7975-7978; *Angew. Chem. Int. Ed.* **2011**, *50*, 7829-32.

[20] S. Kress, S. Blechert, *Chem. Soc. Rev.* **2012**, *41*, 4389-4408.
[21] a) X. Solans-Monfort, E. Clot, C. Coperet, O. Eisenstein, *J. Am. Chem. Soc.* **2005**, *127*, 14015-14025; b) A. Poater, X. Solans-Monfort, E. Clot, C. Coperet, O. Eisenstein, *J. Am. Chem. Soc.* **2007**, *129*, 8207-8216; c) X. Solans-Monfort, C. Copéret, O. Eisenstein, *Organometallics* **2015**, *34*, 1668-1680; d) E. S. Sattely, S. J. Meek, S. J. Malcolmson, R. R. Schrock, A. H. Hoveyda, *J. Am. Chem. Soc.* **2009**, *131*, 943-953; e) S. J. Malcolmson, S. J. Meek, E. S. Sattely, R. R. Schrock, A. H. Hoveyda, *Nature* **2008**, *456*, 933-937.
[22] a) S. C. Marinescu, R. Singh, A. S. Hock, K. M. Wampler, R. R. Schrock, P. Müller, *Organometallics* **2008**, *27*, 6570-6578; b) A. S. Hock, R. R. Schrock, A. H. Hoveyda, *J. Am. Chem. Soc.* **2006**, *128*, 16373-16375.
[23] M. Koy, I. Elser, J. Meisner, W. Frey, K. Wurst, J. Kästner, M. R. Buchmeiser, *Chem. Eur. J.* **2017**, *23*, 15484-15490.
[24] D. G. Gusev, *Organometallics* **2009**, *28*, 6458-6461.
[25] J. S. Kingsbury, J. P. A. Harrity, P. J. Bonitatebus, A. H. Hoveyda, *J. Am. Chem. Soc.* **1999**, *121*, 791-799.
[26] a) W. A. Herrmann, *Angew. Chem.* **2002**, *114*, 1342; *Angew. Chem. Int. Ed.* **2002**, *41*, 1290-1309; b) M. N. Hopkinson, C. Richter, M. Schedler, F. Glorius, *Nature* **2014**, *510*, 485-496; c) F. E. Hahn, M. C. Jahnke, *Angew. Chem.* **2008**, *120*, 3166-3216; *Angew. Chem. Int. Ed.* **2008**, *47*, 3122-3172; d) D. Bourissou, O. Guerret, F. P. Gabbaï, G. Bertrand, *Chem. Rev.* **2000**, *100*, 39-92.
[27] a) H.-W. Wanzlick, E. Schikora, *Angew. Chem.* **1960**, *72*, 494; b) H.-W. Wanzlick, E. Schikora, *Chem. Ber.* **1961**, *94*, 2389-2393.
[28] A. J. Arduengo, R. L. Harlow, M. Kline, *J. Am. Chem. Soc.* **1991**, *113*, 361-363.
[29] a) H.-J. Schönherr, H.-W. Wanzlick, *Chem. Ber.* **1970**, *103*, 1037-1046; b) H.-J. Schönherr, H.-W. Wanzlick, *Liebigs Ann. Chem.* **1970**, *731*, 176-179.
[30] K. Öfele, *J. Organomet. Chem.* **1968**, *12*, P42-P43.
[31] L. Benhamou, E. Chardon, G. Lavigne, S. Bellemin-Laponnaz, V. Cesar, *Chem. Rev.* **2011**, *111*, 2705-2733.
[32] a) H. Jacobsen, A. Correa, A. Poater, C. Costabile, L. Cavallo, *Coord. Chem. Rev.* **2009**, *253*, 687-703; b) J. Clayden, N. Greeves, S. Warren, P. Wothers, *Organic Chemistry*, Oxford University Press, **2001**.
[33] M. Soleilhavoup, G. Bertrand, *Acc. Chem. Res.* **2015**, *48*, 256-266.
[34] D. Martin, N. Lassauque, B. Donnadieu, G. Bertrand, *Angew. Chem.* **2012**, *124*, 6276-6279; *Angew. Chem. Int. Ed.* **2012**, *51*, 6172-6175.
[35] a) N. I. Korotkikh, G. F. Rayenko, O. P. Shvaika, T. M. Pekhtereva, A. H. Cowley, J. N. Jones, C. L. B. Macdonald, *J. Org. Chem.* **2003**, *68*, 5762-5765; b) K. F. Donnelly, A. Petronilho, M. Albrecht, *Chem. Commun.* **2013**, *49*, 1145-1159; c) E. Stander-Grobler, O. Schuster, C. E. Strasser, M. Albrecht, S. Cronje, H. G. Raubenheimer, *Polyhedron* **2011**, *30*, 2776-2782; d) A. J. Arduengo, J. R. Goerlich, W. J. Marshall, *Liebigs Ann. Chem.* **1997**, *1997*, 365-374.
[36] R. H. Crabtree, *Coord. Chem. Rev.* **2013**, *257*, 755-766.
[37] T. Weskamp, V. P. W. Böhm, W. A. Herrmann, *J. Organomet. Chem.* **2000**, *600*, 12-22.
[38] A. R. Chianese, L. Xingwei, M. C. Janzen, J. W. Faller, R. H. Crabtree, *Organometallics* **2003**, *22*, 1663-1667.
[39] a) S. Díez-González, S. P. Nolan, *Coord. Chem. Rev.* **2007**, *251*, 874-883; b) C. A. Tolman, *Chem. Rev.* **1977**, *77*, 313-348; c) D. J. Nelson, S. P. Nolan, *Chem. Soc. Rev.* **2013**, *42*, 6723-6753.
[40] T. L. Brown, K. J. Lee, *Coord. Chem. Rev.* **1993**, *128*, 89-116.
[41] a) L. Falivene, R. Credendino, A. Poater, A. Petta, L. Serra, R. Oliva, V. Scarano, L. Cavallo, *Organometallics* **2016**, *35*, 2286-2293; b) A. Poater, B. Cosenza, A. Correa, S. Giudice, F. Ragone, V. Scarano, L. Cavallo, *Eur. J. Inorg. Chem.* **2009**, *2009*, 1759-1766; c) A. C. Hillier, W. J. Sommer, B. S. Yong, J. L. Petersen, L. Cavallo, S. P. Nolan, *Organometallics* **2003**, *22*, 4322-4326; d) L. Cavallo, A. Correa, C. Costabile, H.

Jacobsen, *J. Organomet. Chem.* **2005**, *690*, 5407-5413; e) A. Poater, F. Ragone, S. Giudice, C. Costabile, R. Dorta, S. P. Nolan, L. Cavallo, *Organometallics* **2008**, *27*, 2679-2681; f) H. Clavier, S. P. Nolan, *Chem. Commun.* **2010**, *46*, 841-861.
[42] a) V. Cesar, S. Bellemin-Laponnaz, L. H. Gade, *Chem. Soc. Rev.* **2004**, *33*, 619-636; b) F. Wang, L.-j. Liu, W. Wang, S. Li, M. Shi, *Coord. Chem. Rev.* **2012**, *256*, 804-853.
[43] J. J. Van Veldhuizen, S. B. Garber, J. S. Kingsbury, A. H. Hoveyda, *J. Am. Chem. Soc.* **2002**, *124*, 4954-4955.
[44] U. Siemeling, *Eur. J. Inorg. Chem.* **2012**, *2012*, 3523-3536.
[45] T. J. Colacot, *Chem. Rev.* **2003**, *103*, 3101-3118.
[46] a) O. Kühl, *Chem. Soc. Rev.* **2007**, *36*, 592-607; b) S. T. Liddle, I. S. Edworthy, P. L. Arnold, *Chem. Soc. Rev.* **2007**, *36*, 1732; c) A. T. Normand, K. J. Cavell, *Eur. J. Inorg. Chem.* **2008**, *2008*, 2781-2800; d) E. Peris, R. H. Crabtree, *Coord. Chem. Rev.* **2004**, *248*, 2239-2246.
[47] a) H. Clavier, L. Coutable, L. Toupet, J.-C. Guillemin, M. Mauduit, *J. Organomet. Chem.* **2005**, *690*, 5237-5254; b) T. Uchida, T. Katsuki, *Tetrahedron Lett.* **2009**, *50*, 4741-4743; c) A. W. Waltman, R. H. Grubbs, *Organometallics* **2004**, *23*, 3105-3107.
[48] M. Bierenstiel, E. D. Cross, *Coord. Chem. Rev.* **2011**, *255*, 574-590.
[49] W. Wang, T. Zhang, F. Wang, M. Shi, *Tetrahedron* **2011**, *67*, 1523-1529.
[50] F. Godoy, C. Segarra, M. Poyatos, E. Peris, *Organometallics* **2011**, *30*, 684-688.
[51] X. Liu, P. Braunstein, *Inorg. Chem.* **2013**, *52*, 7367-7379.
[52] a) M. Hollering, M. Albrecht, F. E. Kühn, *Organometallics* **2016**, *35*, 2980-2986; b) M. V. Jiménez, J. Fernández-Tornos, J. J. Pérez-Torrente, F. J. Modrego, P. García-Orduña, L. A. Oro, *Organometallics* **2015**, *34*, 926-940; c) A. G. Nair, R. T. McBurney, D. B. Walker, M. J. Page, M. R. Gatus, M. Bhadbhade, B. A. Messerle, *Dalton Trans.* **2016**, *45*, 14335-14342; d) S. Warsink, C. M. S. van Aubel, J. J. Weigand, S.-T. Liu, C. J. Elsevier, *Eur. J. Inorg. Chem.* **2010**, *2010*, 5556-5562.
[53] W. Kosnik, K. Grela, *Dalton Trans.* **2013**, *42*, 7463-7467.
[54] a) P. Braunstein, F. Naud, *Angew. Chem.* **2001**, *113*, 702-722; *Angew. Chem. Int. Ed.* **2001**, *40*, 680-699; b) K. Riener, M. J. Bitzer, A. Pothig, A. Raba, M. Cokoja, W. A. Herrmann, F. E. Kuhn, *Inorg. Chem.* **2014**, *53*, 12767-12777.
[55] a) J. A. Mata, M. Poyatos, E. Peris, *Coord. Chem. Rev.* **2007**, *251*, 841-859; b) A. Huffer, B. Jeffery, B. J. Waller, A. A. Danopoulos, *C. R. Chim.* **2013**, *16*, 557-565.
[56] D. L. Hughes, *Org. Proc. Res. Dev.* **2016**, *20*, 1008-1015.
[57] C. Deraedt, M. d'Halluin, D. Astruc, *Eur. J. Inorg. Chem.* **2013**, n/a-n/a.
[58] R. R. Schrock, A. H. Hoveyda, *Angew. Chem.* **2003**, *115*, 4740-4782; *Angew. Chem. Int. Ed.* **2003**, *42*, 4592-4633.
[59] B. J. v. Lierop, J. A. M. Lummiss, D. E. Fogg, in *Olefin Metathesis* (Ed.: K. Grela), **2014**.
[60] P. Atallah, K. B. Wagener, M. D. Schulz, *Macromolecules* **2013**, *46*, 4735-4741.
[61] a) V. M. Marx, M. B. Herbert, B. K. Keitz, R. H. Grubbs, *J. Am. Chem. Soc.* **2013**, *135*, 94-97; b) A. W. Speed, T. J. Mann, R. V. O'Brien, R. R. Schrock, A. H. Hoveyda, *J. Am. Chem. Soc.* **2014**, *136*, 16136-16139; c) C. Wang, M. Yu, A. F. Kyle, P. Jakubec, D. J. Dixon, R. R. Schrock, A. H. Hoveyda, *Chem. Eur. J.* **2013**, *19*, 2726-2740; d) H. Zhang, E. C. Yu, S. Torker, R. R. Schrock, A. H. Hoveyda, *J. Am. Chem. Soc.* **2014**, *136*, 16493-16496.
[62] A. K. Chatterjee, T. L. Choi, D. P. Sanders, R. H. Grubbs, *J. Am. Chem. Soc.* **2003**, *125*, 11360-11370.
[63] a) C. W. Bielawski, R. H. Grubbs, *Prog. Polym. Sci.* **2007**, *32*, 1-29; b) R. R. Schrock, *Acc. Chem. Res.* **2002**, *23*, 158-165.
[64] J. Bidange, C. Fischmeister, C. Bruneau, *Chem. Eur. J.* **2016**, *22*, 12226-12244.
[65] W. L. Truett, D. R. Johnson, B. A. Montague, *J. Am. Chem. Soc.* **1960**, 23370-22340.
[66] G. Natta, G. Dall´Asta, G. Mazzanti, *Angew. Chem.* **1964**, *76*, 765-772; *Angew. Chem. Int. Ed.* **1964**, *3*, 723-729.
[67] R. L. Banks, G. C. Bailey, *Ind. Eng. Chem. Prod. Res. Dev.* **1964**, *3*, 170-173.
[68] P. Jean-Louis Hérisson, Y. Chauvin, *Die Makromolekulare Chemie* **1971**, *141*, 161-176.

[69] J. Feldman, W. M. Davis, R. R. Schrock, *Organometallics* **1989**, *8*, 2266-2268.
[70] C. P. Gordon, K. Yamamoto, W. C. Liao, F. Allouche, R. A. Andersen, C. Coperet, C. Raynaud, O. Eisenstein, *ACS Cent. Sci.* **2017**, *3*, 759-768.
[71] F. N. Tebbe, G. W. Parshall, G. S. Reddy, *J. Am. Chem. Soc.* **1978**, *100*, 3611-3613.
[72] C. Elschenbroich, *Organometallchemie*, Springer Vieweg, **2008**.
[73] a) K. Dreisch, C. Andersson, C. Stalhåndske, *Polyhedron* **1991**, *10*, 2417-2421; b) J. H. Oskam, H. H. Fox, K. B. Yap, D. H. McConville, R. O`Dell, B. J. Lichtenstein, R. R. Schrock, *J. Organomet. Chem.* **1993**, *459*, 185-198; c) H. Jeong, J. C. Axtell, B. Török, R. R. Schrock, P. Müller, *Organometallics* **2012**, *31*, 6522-6525; d) K. V. Bukhryakov, S. Venkat Ramani, C. Tsay, A. Hoveyda, R. R. Schrock, *Organometallics* **2017**, *36*, 4208-4214; e) J. C. Axtell, R. R. Schrock, P. Müller, S. J. Smith, A. H. Hoveyda, *Organometallics* **2014**, *33*, 5342-5348.
[74] J. C. Axtell, R. R. Schrock, P. Müller, A. H. Hoveyda, *Organometallics* **2015**, *34*, 2110-2113.
[75] H. Jeong, D. J. Kozera, R. R. Schrock, S. J. Smith, J. Zhang, N. Ren, M. A. Hillmyer, *Organometallics* **2013**, *32*, 4843-4850.
[76] a) R. Toreki, R. R. Schrock, W. M. Davis, *J. Am. Chem. Soc.* **1992**, *114*, 3367-3380; b) H. H. Fox, M. H. Schofield, R. R. Schrock, *Organometallics* **1994**, *13*, 2804-2815; c) R. R. Schrock, W. E. Crowe, G. C. Bazan, M. DiMare, M. B. O'Regan, M. H. Schofield, *Organometallics* **1991**, *10*, 1832-1843.
[77] a) J. H. Oskam, R. R. Schrock, *J. Am. Chem. Soc.* **1992**, *114*, 7588-7590; b) J. H. Oskam, R. R. Schrock, *J. Am. Chem. Soc.* **1993**, *115*, 11831-11845.
[78] C. Lienert, W. Frey, M. R. Buchmeiser, *Macromolecules* **2017**, *50*, 5701-5710.
[79] A. Sinha, R. R. Schrock, *Organometallics* **2004**, *23*, 1643-1645.
[80] S. C. Marinescu, R. R. Schrock, P. Müller, A. H. Hoveyda, *J. Am. Chem. Soc.* **2009**, *131*, 10840-10841.
[81] X. Solans-Monfort, C. Coperet, O. Eisenstein, *J. Am. Chem. Soc.* **2010**, *132*, 7750-7757.
[82] S. C. Marinescu, R. R. Schrock, B. Li, A. H. Hoveyda, *J. Am. Chem. Soc.* **2009**, *131*, 58-59.
[83] a) E. M. Townsend, R. R. Schrock, A. H. Hoveyda, *J. Am. Chem. Soc.* **2012**, *134*, 11334-11337; b) M. Yu, R. R. Schrock, A. H. Hoveyda, *Angew. Chem.* **2015**, *127*, 217-222; *Angew. Chem. Int. Ed.* **2015**, *54*, 215-220; c) C. Wang, F. Haeffner, R. R. Schrock, A. H. Hoveyda, *Angew. Chem.* **2013**, *125*, 1993-1997; *Angew. Chem. Int. Ed.* **2013**, *52*, 1939-1943.
[84] S. J. Meek, R. V. O'Brien, J. Llaveria, R. R. Schrock, A. H. Hoveyda, *Nature* **2011**, *471*, 461-466.
[85] a) J. C. Conrad, M. D. Eelman, J. A. Silva, S. Monfette, H. H. Parnas, J. L. Snelgrove, D. E. Fogg, *J. Am. Chem. Soc.* **2007**, *129*, 1024-1025; b) S. D. Kamau, P. Hodge, A. J. Hall, S. Dad, A. Ben-Haida, *Polymer* **2007**, *48*, 6808-6822.
[86] C. S. Higman, D. L. Nascimento, B. J. Ireland, S. Audorsch, G. A. Bailey, R. McDonald, D. E. Fogg, *J. Am. Chem. Soc.* **2018**, *140*, 1604-1607.
[87] A. H. Hoveyda, *J. Org. Chem.* **2014**, *79*, 4763-4792.
[88] a) D. H. McConville, J. R. Wolf, R. R. Schrock, *J. Am. Chem. Soc.* **1993**, *115*, 4413-4414; b) R. O'Dell, D. H. McConville, G. E. Hofmeister, R. R. Schrock, *J. Am. Chem. Soc.* **1994**, *116*, 3414-3423.
[89] O. Fujimura, R. H. Grubbs, *J. Am. Chem. Soc.* **1996**, *118*, 2499-2500.
[90] a) J. B. Alexander, D. S. La, D. R. Cefalo, A. H. Hoveyda, R. R. Schrock, *J. Am. Chem. Soc.* **1998**, *120*, 4041-4042; b) O. Fujimura, R. H. Grubbs, *J. Org. Chem.* **1998**, *63*, 824-832; c) S. S. Zhu, D. R. Cefalo, D. S. La, J. Y. Jamieson, W. M. Davis, A. H. Hoveyda, R. R. Schrock, *J. Am. Chem. Soc.* **1999**, *121*, 8251-8259; d) D. R. Cefalo, A. F. Kiely, M. Wuchrer, J. Y. Jamieson, R. R. Schrock, A. H. Hoveyda, *J. Am. Chem. Soc.* **2001**, *123*, 3139-3140; e) W. C. P. Tsang, R. R. Schrock, A. H. Hoveyda, *Organometallics* **2001**, *20*, 5658-5669; f) E. S. Sattely, G. A. Cortez, D. C. Moebius, R. R. Schrock, A. H. Hoveyda, *J. Am. Chem. Soc.* **2005**, *127*, 8526-8533; g) J. S. Harvey,

S. J. Malcolmson, K. S. Dunne, S. J. Meek, A. L. Thompson, R. R. Schrock, A. H. Hoveyda, V. Gouverneur, *Angew. Chem.* **2009**, *48*, 776-780; *Angew. Chem. Int. Ed.* **2009**, *4*, 762-766; h) T. S. Pilyugina, R. R. Schrock, P. Müller, A. H. Hoveyda, *Organometallics* **2007**, *26*, 831-837.

[91] a) G. S. Weatherhead, G. A. Cortez, R. R. Schrock, A. H. Hoveyda, *Proc. Natl. Acad. Sci. USA* **2004**, *101*, 5805-5809; b) A. H. Hoveyda, S. J. Malcolmson, S. J. Meek, A. R. Zhugralin, *Angew. Chem.* **2010**, *122*, 38-49; *Angew. Chem. Int. Ed.* **2010**, *49*, 34-44.

[92] O. Fujimura, R. H. Grubbs, *J. Org. Chem.* **1998**, *63*, 824-832.

[93] Y.-D. Wu, Z.-H. Peng, *J. Am. Chem. Soc.* **1997**, *119*, 8043-8049.

[94] A. L. Lee, S. J. Malcolmson, A. Puglisi, R. R. Schrock, A. H. Hoveyda, *J. Am. Chem. Soc.* **2006**, *128*, 5153-5157.

[95] W. C. Tsang, J. A. Jernelius, G. A. Cortez, G. S. Weatherhead, R. R. Schrock, A. H. Hoveyda, *J. Am. Chem. Soc.* **2003**, *125*, 2591-2596.

[96] S. S. Zhu, D. R. Cefalo, D. S. La, J. Y. Jamieson, W. M. Davis, A. H. Hoveyda, R. R. Schrock, *J. Am. Chem. Soc.* **1999**, *121*, 8251-8259.

[97] a) R. R. Schrock, J. Y. Jamieson, S. J. Dolman, S. A. Miller, P. J. Bonitatebus, A. H. Hoveyda, *Organometallics* **2002**, *21*, 409-417; b) S. L. Aeilts, D. R. Cefalo, J. Peter J. Bonitatebus, J. H. Houser, A. H. Hoveyda, R. R. Schrock, *Angew. Chem. Int. Ed.* **2001**, *40*, 1452-1456.

[98] a) Y. Zhao, A. H. Hoveyda, R. R. Schrock, *Org. Lett.* **2011**, *13*, 784-787; b) M. Yu, I. Ibrahem, M. Hasegawa, R. R. Schrock, A. H. Hoveyda, *J. Am. Chem. Soc.* **2012**, *134*, 2788-2799; c) I. Ibrahem, M. Yu, R. R. Schrock, A. H. Hoveyda, *J. Am. Chem. Soc.* **2009**, *131*, 3844-3845.

[99] M. M. Flook, J. Börner, S. M. Kilyanek, L. C. H. Gerber, R. R. Schrock, *Organometallics* **2012**, *31*, 6231-6243.

[100] T. T. Nguyen, M. J. Koh, X. Shen, F. Romiti, R. R. Schrock, A. H. Hoveyda, *Science* **2016**, *352*, 569-575.

[101] M. J. Koh, T. T. Nguyen, J. K. Lam, S. Torker, J. Hyvl, R. R. Schrock, A. H. Hoveyda, *Nature* **2017**, *542*, 80-85.

[102] a) J. C. Bryan, J. M. Mayer, *J. Am. Chem. Soc.* **1990**, *112*, 2298-2308; b) L. L. Blosch, K. Abboud, J. M. Boncella, *J. Am. Chem. Soc.* **1991**, *113*, 7066-7068; c) F. J. de la Mata, R. H. Grubbs, *Organometallics* **1996**, *15*, 577-584; d) T. W. Crane, P. S. White, J. L. Templeton, *Organometallics* **1999**, *18*, 1897-1903.

[103] D. V. Peryshkov, R. R. Schrock, *Organometallics* **2012**, *31*, 7278-7286.

[104] a) J. H. Wengrovius, R. R. Schrock, *Organometallics* **1982**, *1*, 148-155; b) M. R. Churchill, A. L. Rheingold, W. J. Youngs, R. R. Schrock, J. H. Wengrovius, *J. Organomet. Chem.* **1981**, *204*, C17-C20.

[105] a) D. V. Peryshkov, W. P. Forrest, R. R. Schrock, S. J. Smith, P. Müller, *Organometallics* **2013**, *32*, 5256-5259; b) D. V. Peryshkov, R. R. Schrock, M. K. Takase, P. Müller, A. H. Hoveyda, *J. Am. Chem. Soc.* **2011**, *133*, 20754-20757.

[106] M. B. O'Donoghue, R. R. Schrock, A. M. LaPointe, W. M. Davis, *Organometallics* **1996**, *15*, 1334-1336.

[107] T. Weskamp, W. C. Schattenmann, M. Spiegler, W. A. Herrmann, *Angew. Chem.* **1998**, *111*, 1360-1364; *Angew. Chem. Int. Ed.* **1998**, *18*, 2490-2493.

[108] a) M. Buchmeiser, E. Anderson, *Synlett* **2011**, *2012*, 185-207; b) M. R. Buchmeiser, I. Ahmad, V. Gurram, P. S. Kumar, *Macromolecules* **2011**, *44*, 4098-4106; c) J. C. Conrad, H. H. Parnas, J. L. Snelgrove, D. E. Fogg, *J. Am. Chem. Soc.* **2005**, *127*, 11882-11883.

[109] a) C. Samojlowicz, M. Bieniek, K. Grela, *Chem. Rev.* **2009**, *109*, 3708-3742; b) G. C. Vougioukalakis, R. H. Grubbs, *Chem. Rev.* **2010**, *110*, 1746-1787.

[110] a) V. M. Marx, A. H. Sullivan, M. Melaimi, S. C. Virgil, B. K. Keitz, D. S. Weinberger, G. Bertrand, R. H. Grubbs, *Angew. Chem.* **2015**, *127*, 1939-1943; *Angew. Chem. Int. Ed.* **2015**, *54*, 1919-1923; b) R. Gawin, A. Kozakiewicz, P. A. Gunka, P. Dabrowski, K.

Skowerski, *Angew. Chem.* **2017**, *129*, 1001-1006; *Angew. Chem. Int. Ed.* **2017**, *56*, 981-986.
[111] D. Martin, V. M. Marx, R. H. Grubbs, G. Bertrand, *Adv. Synth. Catal.* **2016**, *358*, 965-969.
[112] a) K. Endo, R. H. Grubbs, *J. Am. Chem. Soc.* **2011**, *133*, 8525-8527; b) J. Hartung, R. H. Grubbs, *J. Am. Chem. Soc.* **2013**, *135*, 10183-10185; c) M. B. Herbert, B. A. Suslick, P. Liu, L. Zou, P. K. Dornan, K. N. Houk, R. H. Grubbs, *Organometallics* **2015**, *34*, 2858-2869.
[113] L. E. Rosebrugh, V. M. Marx, B. K. Keitz, R. H. Grubbs, *J. Am. Chem. Soc.* **2013**, *135*, 10032-10035.
[114] B. K. Keitz, K. Endo, P. R. Patel, M. B. Herbert, R. H. Grubbs, *J. Am. Chem. Soc.* **2012**, *134*, 693-699.
[115] a) E. Tzur, A. Szadkowska, A. Ben-Asuly , A. Makal, I. Goldberg, K. Woźniak, K. Grela , N. G. Lemcoff, *Chem. Eur. J.* **2010**, *16*, 8726-8737; b) Y. Vidavsky, A. Anaby, G. N. Lemcoff, *Dalton Trans.* **2012**, *41*, 32-43.
[116] a) A. Kozlowska, M. Dranka, J. Zachara, E. Pump, C. Slugovc, K. Skowerski, K. Grela, *Chem. Eur. J.* **2014**, *20*, 14120-14125; b) R. Drozdzak, B. Allaert, N. Ledoux, I. Dragutan, V. Dragutan, F. Verpoort, *Coord. Chem. Rev.* **2005**, *249*, 3055-3074; c) S. Monfette, D. E. Fogg, *Organometallics* **2006**, *25*, 1940-1944; d) J. B. Binder, I. A. Guzei, R. T. Raines, *Adv. Synth. Catal.* **2007**, *349(3)*, 395-404; e) C. C. Brown, F. Rominger, M. Limbach, P. Hofmann, *Inorg. Chem.* **2015**, *54*, 10126-10140; f) M. S. Mikus, S. Torker, C. Xu, B. Li, A. H. Hoveyda, *Organometallics* **2016**, *35*, 3878-3892; g) J. S. Kingsbury, J. P. A. Harrity, J. P. J. Bonitatebus, A. H. Hoveyda, *J. Am. Chem. Soc.* **1999**, *121*, 791-799.
[117] a) H. Jeong, R. R. Schrock, P. Müller, *Organometallics* **2015**, *34*, 4408-4418; b) K. M. Engle, G. Lu, S.-X. Luo, L. M. Henling, M. K. Takase, P. Liu, K. N. Houk, R. H. Grubbs, *J. Am. Chem. Soc.* **2015**, *137*, 5782-5792; c) S. Monsaert, A. Lozano Vila, R. Drozdzak, P. Van Der Voort, F. Verpoort, *Chem. Soc. Rev.* **2009**, *38*, 3360-3372; d) Y. Xie, Y. Yuan, B. Mousavi, Y. Cai, C. Kai, Y. Lu, M. Yusubov, F. Verpoort, *Appl. Organometal. Chem.* **2015**, *29*, 573-579.
[118] H. H. Fox, J.-K. Lee, L. Y. Park, R. R. Schrock, *Organometallics* **1993**, *12*, 759-768.
[119] L. Piola, F. Nahra, S. P. Nolan, *Beilstein J. Org. Chem.* **2015**, *11*, 2038-2056.
[120] L. Ondi, G. M. Nagy, J. B. Czirok, A. Bucsai, G. E. Frater, *Org. Process. Res. Dev.* **2016**, *20*, 1709-1716.
[121] T. Ung, A. Hejl, R. H. Grubbs, Y. Schrodi, *Organometallics* **2004**, *23*, 5399-5401.
[122] R. Gawin, A. Makal, K. Woźniak, M. Mauduit, K. Grela, *Angew. Chem. Int. Ed.* **2007**, *46*, 7206-7209.
[123] R. Gavin, P. Czarnecka, K. Grela, *Tetrahedron* **2010**, *66*, 1051-1056.
[124] a) C. E. Diesendruck, O. Iliashevsky, A. Ben-Asuly, I. Goldberg, G. N. Lemcoff, *Macromol. Symp.* **2010**, *293*, 33-38; b) Y. Vidavsky, A. Anaby, G. N. Lemcoff, *Dalton Trans.* **2012**, *41*, 32-43.
[125] a) C. E. Diesendruck, O. Iliashevsky, A. Ben-Asuly, I. Goldberg, G. N. Lemcoff, *Macromol. Symp.* **2010**, *293*, 33-38; b) K. M. Engle, G. Lu, S.-X. Luo, L. M. Henling, M. K. Takase, P. Liu, K. N. Houk, R. H. Grubbs, *J. Am. Chem. Soc.* **2015**, *137*, 5782-5792.
[126] S. Monsaert, N. Ledoux, R. Drozdzak, F. Verpoort, *J. Polym. Sci., Part A: Polym. Chem.* **2010**, *48*, 302-310.
[127] a) P. Sledz, M. Mauduit, K. Grela, *Chem. Soc. Rev.* **2008**, *37*, 2433-2442; b) K. Skowerski, C. Wierzbicka, G. Szczepaniak, Ł. Gułajski, M. Bieniek, K. Grela, *Green Chem.* **2012**, *14*, 3264; c) B. Authenrieth, F. Willig, D. Pursley, S. Naumann, M. R. Buchmeiser, *ChemCatChem* **2013**, 3033-3040.
[128] a) W. M. Vaughan, K. A. Abboud, J. M. Boncella, *Organometallics* **1995**, *14*, 1567-1577; b) Z. J. Tonzetich, A. J. Jiang, R. R. Schrock, P. Müller, *Organometallics* **2006**, *25*, 4725-4727; c) A. J. Jiang, R. R. Schrock, P. Müller, *Organometallics* **2008**, *27*, 4428-4438.

[129] a) S. H. Hong, R. H. Grubbs, *J. Am. Chem. Soc.* **2006**, *128*, 3508-3509; b) J. Tomasek, J. Schatz, *Green Chem.* **2013**, *15*, 2317-2338; c) B. H. Lipshutz, S. Ghorai, in *Olefin Metathesis* (Ed.: K. Grela), **2014**.
[130] E. Borré, M. Rouen, I. Laurent, M. Magrez, F. Caijo, C. Crévisy, W. Solodenko, L. Toupet, R. Frankfurter, C. Vogt, A. Kirschning, M. Mauduit, *Chem. Eur. J.* **2012**, *18*, 16369-16382.
[131] a) B. Autenrieth, W. Frey, M. R. Buchmeiser, *Chem. Eur. J.* **2012**, *18*, 14069-14078; b) B. Autenrieth, E. B. Anderson, D. Wang, M. R. Buchmeiser, *Macromol. Chem. Phys.* **2013**, *214*, 33-40.
[132] a) C. Copéret, A. Comas-Vives, M. P. Conley, D. P. Estes, A. Fedorov, V. Mougel, H. Nagae, F. Nunez-Zarur, P. A. Zhizhko, *Chem. Rev.* **2016**, *116*, 323-421; b) M. R. Buchmeiser, *Chem. Rev.* **2009**, *109*, 303-321; c) M. R. Buchmeiser, in *Olefin Metathesis* (Ed.: K. Grela), **2014**.
[133] K. Skowerski, J. Bialecki, S. J. Czarnocki, K. Zukowska, K. Grela, *Beilstein J. Org. Chem.* **2016**, *12*, 5-15.
[134] D. Wang, R. Kröll, M. Mayr, K. Wurst, M. R. Buchmeiser, *Adv. Synth. Catal.* **2006**, *348*, 1567-1579.
[135] a) S. J. Dolman, K. C. Hultzsch, F. Pezet, X. Teng, A. H. Hoveyda, R. R. Schrock, *J. Am. Chem. Soc.* **2004**, *126*, 10945-10953; b) R. M. Kröll, N. Schuler, S. Lubbad, M. R. Buchmeiser, *Chem. Commun.* **2003**, 2742-2743; c) K. C. Hultzsch, J. A. Jernelius, A. H. Hoveyda, R. R. Schrock, *Angew. Chem. Int. Ed.* **2002**, *41*, 589-593.
[136] D. Bek, H. Balcar, N. Žilková, A. Zukal, M. Horáček, J. Čejka, *ACS Catalysis* **2011**, *1*, 709-718.
[137] a) S. C. Schürer, S. Gessler, N. Buschmann, S. Blechert, *Angew. Chem.* **2000**, *112*, 4062-4065; *Angew. Chem. Int. Ed.* **2000**, *39*, 3898-3901; b) A. Monge-Marcet, R. Pleixats, X. Cattoën, M. Wong Chi Man, *J. Mol. Catal. A: Chem.* **2012**, *357*, 59-66.
[138] Q. Yao, A. Rodriguez Motta, *Tetrahedron Lett.* **2004**, *45*, 2447-2451.
[139] J. Scholz, S. Loekman, N. Szesni, W. Hieringer, A. Görling, M. Haumann, P. Wasserscheid, *Adv. Synth. Catal.* **2011**, *353*, 2701-2707.
[140] J. Heppekausen, R. Stade, R. Goddard, A. Fürstner, *J. Am. Chem. Soc.* **2010**, *132*, 11045-11057.
[141] a) J. H. Freudenberger, R. R. Schrock, *Organometallics* **1986**, *5*, 1411-1417; b) A. Bray, A. Mortreux, F. Petit, M. Petit, T. Szymanska-Buzar, *J. Chem. Soc., Chem. Commun.* **1993**, 197.
[142] A. Mortreux, M. Blanchard, *J. Chem. Soc., Chem. Commun.* **1974**, 786-787.
[143] R. H. Crabtree, *The Organometallic Chemistry of the Transition Metals*, John Wiley & Sons, **2014**.
[144] a) F. Pennella, R. L. Banks, G. C. Bailey, *Chem. Comm.* **1968**, 1548; b) A. Mortreux, M. Blanchard, *Bull. Soc. Chim. Fr.* **1972**, *4*, 1641-1643.
[145] R. R. Schrock, D. N. Clark, J. Sancho, J. H. Wengrovius, S. M. Rocklage, S. F. Pedersen, *Organometallics* **1982**, *1*, 1645-1651.
[146] M. L. Listemann, R. R. Schrock, *Organometallics* **1985**, *4*, 74-83.
[147] R. L. Gdula, M. J. Johnson, *J. Am. Chem. Soc.* **2006**, *128*, 9614-9615.
[148] A. Mayr, G. A. McDermott, *J. Am. Chem. Soc.* **1986**, *108*, 548-549.
[149] M. A. Stevenson, M. D. Hopkins, *Organometallics* **1997**, *16*, 3572-3573.
[150] A. Fürstner, C. Mathes, C. W. Lehmann, *J. Am. Chem. Soc.* **1999**, *121*, 9453-9454.
[151] C. E. Laplaza, M. J. A. Johnson, J. C. Peters, A. L. Odom, E. Kim, C. C. Cummins, G. N. George, I. J. Pickering, *J. Am. Chem. Soc.* **1996**, *118*, 8623-8638.
[152] W. Zhang, S. Kraft, J. S. Moore, *J. Am. Chem. Soc.* **2004**, *126*, 329-335.
[153] a) K. Jyothish, Q. Wang, W. Zhang, *Adv. Synth. Catal.* **2012**, *354*, 2073-2078; b) Y.-C. Tsai, P. L. Diaconescu, C. C. Cummins, *Organometallics* **2000**, *19*, 5260-5262.
[154] J. Heppekausen, R. Stade, A. Kondoh, G. Seidel, R. Goddard, A. Fürstner, *Chem. Eur. J.* **2012**, *18*, 10281-10299.
[155] S. Beer, C. G. Hrib, P. G. Jones, K. Brandhorst, J. Grunenberg, M. Tamm, *Angew. Chem.* **2007**, *46*, 9047-9051; *Angew. Chem. Int. Ed.* **2007**, *46*, 8890-8894.

[156] S. Beer, K. Brandhorst, C. G. Hrib, X. Wu, B. Haberlag, J. r. Grunenberg, P. G. Jones, M. Tamm, *Organometallics* **2009**, *28*, 1534-1545.
[157] S. Beer, K. Brandhorst, J. Grunenberg, C. G. Hrib, P. G. Jones, M. Tamm, *Org. Lett.* **2008**, *10*, 981-984.
[158] S. Lysenko, B. Haberlag, X. Wu, M. Tamm, *Macromol. Symp.* **2010**, *293*, 20-23.
[159] B. Haberlag, M. Freytag, C. G. Daniliuc, P. G. Jones, M. Tamm, *Angew. Chem.* **2012**, *124*, 13195-13199; *Angew. Chem. Int. Ed.* **2012**, *51*, 13019-13022.
[160] C. Bittner, H. Ehrhorn, D. Bockfeld, K. Brandhorst, M. Tamm, *Organometallics* **2017**, *36*, 3398-3406.
[161] a) A. M. Geyer, R. L. Gdula, E. S. Wiedner, M. J. Johnson, *J. Am. Chem. Soc.* **2007**, *129*, 3800-3801; b) A. M. Geyer, E. S. Wiedner, J. B. Gary, R. L. Gdula, N. C. Kuhlmann, M. J. Johnson, B. D. Dunietz, J. W. Kampf, *J. Am. Chem. Soc.* **2008**, *130*, 8984-8999.
[162] A. Fürstner, O. Guth, A. Rumbo, G. Seidel, *J. Am. Chem. Soc.* **1999**, *121*, 11108-11113.
[163] a) A. R. Rossi, R. Hoffmann, *Inorg. Chem.* **2002**, *14*, 365-374; b) C. A. Tolman, *Chem. Soc. Rev.* **1972**, *1*, 337.
[164] A. W. Addison, T. N. Rao, J. Reedijk, J. van Rijn, G. C. Verschoor, *J. Chem. Soc., Dalton Trans.* **1984**, 1349-1356.
[165] I. Ugi, D. Marquarding, H. Klusacek, P. Gillespie, F. Ramirez, *Acc. Chem. Res.* **2002**, *4*, 288-296.
[166] A. Lennartson, M. Håkansson, *New J. Chem.* **2015**, *39*, 5936-5943.
[167] M. R. Buchmeiser, S. Sen, J. Unold, W. Frey, *Angew. Chem.* **2014**, *126*, 9538-9542; *Angew. Chem. Int. Ed.* **2014**, *53*, 9384-9388.
[168] a) S. Sen, R. Schowner, D. A. Imbrich, W. Frey, M. Hunger, M. R. Buchmeiser, *Chem. Eur. J.* **2015**, *21*, 13778-13787; b) R. Schowner, W. Frey, M. R. Buchmeiser, *J. Am. Chem. Soc.* **2015**, *137*, 6188-6191; c) S. Sen, R. Schowner, M. R. Buchmeiser, *Monatsh. Chem.* **2015**, *146*, 1037-1042; d) M. R. Buchmeiser, S. Sen, C. Lienert, L. Widmann, R. Schowner, K. Herz, P. Hauser, W. Frey, D. Wang, *ChemCatChem* **2016**, *8*, 2710-2723; e) M. R. Buchmeiser, S. Sen, C. Lienert, L. Widmann, R. Schowner, K. Herz, P. Hauser, W. Frey, D. Wang, *ChemCatChem* **2016**, *8*, 2710-2723; f) D. A. Imbrich, I. Elser, W. Frey, M. R. Buchmeiser, *ChemCatChem* **2017**, *9*, 2996-3002.
[169] K. Herz, *Mechanismus der Olefinmetathese mit neutralen und kationischen Molybdän-Imido-Alkyliden-N-heterozyklischen Carbenkomplexen*, Ph. D. thesis, University of Stuttgart **2018**.
[170] M. Pucino, V. Mougel, R. Schowner, A. Fedorov, M. R. Buchmeiser, C. Copéret, *Angew. Chem.* **2016**, *128*, 4372-4374; *Angew. Chem. Int. Ed.* **2016**, *55*, 4300-4302.
[171] G. C. Vougioukalakis, *Chem. Eur. J.* **2012**, *18*, 8868-8880.
[172] D. J. Cole-Hamilton, *Science* **2003**, *299*, 1702-1706.
[173] a) G. A. Cortez, C. A. Baxter, R. R. Schrock, A. H. Hoveyda, *Org. Lett.* **2007**, *9*, 2871-2874; b) M. F. Schneider, N. Lucas, J. Velder, S. Blechert, *Angew. Chem.* **1997**, *109*, 257-259; *Angew. Chem. Int. Ed.* **1997**, *36*, 257-259; c) A. Michrowska, M. Bieniek, M. Kim, R. Klajn, K. Grela, *Tetrahedron* **2003**, *59*, 4525-4531; d) P. E. Sues, K. V. Bukhryakov, R. R. Schrock, *Helv. Chim. Acta* **2017**, *100*, e1700181.
[174] I. Elser, *Synthese chiraler ionischer Liganden für Schrock Katalysatoren*, Master thesis, University of Stuttgart **2014**.
[175] R. R. Schrock, *Polyhedron* **1995**, *14*, 3177-3195.
[176] W. P. Forrest, J. G. Weis, J. M. John, J. C. Axtell, J. H. Simpson, T. M. Swager, R. R. Schrock, *J. Am. Chem. Soc.* **2014**, *136*, 10910-10913.
[177] a) D. S. La, J. B. Alexander, D. R. Cefalo, D. D. Graf, A. H. Hoveyda, R. R. Schrock, *J. Am. Chem. Soc.* **1998**, *120*, 9720-9721; b) S. J. Dolman, E. S. Sattely, A. H. Hoveyda, R. R. Schrock, *J. Am. Chem. Soc.* **2002**, *124*, 6991-6997.
[178] A. J. Jiang, Y. Zhao, R. R. Schrock, A. H. Hoveyda, *J. Am. Chem. Soc.* **2009**, *131*, 16630-16631.

[179] D. A. Dickie, I. S. MacIntosh, D. D. Ino, Q. He, O. A. Labeodan, M. C. Jennings, G. Schatte, C. J. Walsby, J. A. C. Clyburne, *Can. J. Chem.* **2008**, *86*, 20-31.
[180] K. N. Gavrilov, S. V. Zheglov, E. A. Rastorguev, N. N. Groshkin, M. G. Maksimova, E. B. Benetsky, V. A. Davankov, M. T. Reetz, *Adv. Synth. Catal.* **2010**, *352*, 2599-2610.
[181] E. L. Kolychev, S. Kronig, K. Brandhorst, M. Freytag, P. G. Jones, M. Tamm, *J. Am. Chem. Soc.* **2013**, *135*, 12448-12459.
[182] D. Imbrich, *Synthese von Wolfram-Imido-Alkyliden N-heterozyklischen-Carben und N-heterozyklischen-Olefin Komplexen*, Ph. D. thesis, University of Stuttgart **2018**.
[183] S. Sen, R. Schowner, D. A. Imbrich, W. Frey, M. Hunger, M. R. Buchmeiser, *Chem. Eur J.* **2015**, *21*, 13778-13787.
[184] a) C. Färber, M. Leibold, C. Bruhn, M. Maurer, U. Siemeling, *Chem. Commun.* **2012**, *48*, 227-229; b) S. Hitzel, C. Färber, C. Bruhn, U. Siemeling, *Organometallics* **2013**, *33*, 425-428.
[185] D. A. Imbrich, W. Frey, S. Naumann, M. R. Buchmeiser, *Chem. Commun.* **2016**, *52*, 6099-6102.
[186] I. Elser, R. Schowner, W. Frey, K. Wurst, M. R. Buchmeiser, *Chem. Eur. J.* **2017**, *23*, 6398-6405.
[187] J. Yuan, E. M. Townsend, R. R. Schrock, A. S. Goldman, P. Müller, M. K. Takase, *Adv. Synth. Catal.* **2011**, *353*, 1985-1992.
[188] A. G. Lichtscheidl, V. W. Ng, P. Muller, M. K. Takase, R. R. Schrock, S. J. Malcolmson, S. J. Meek, B. Li, E. T. Kiesewetter, A. H. Hoveyda, *Organometallics* **2012**, *31*, 4558-4564.
[189] Y. Vidavsky, A. Anaby, N. G. Lemcoff, *Dalton Trans.* **2012**, *41*, 32-43.
[190] M. R. Buchmeiser, S. Sen, C. Lienert, L. Widmann, R. Schowner, K. Herz, P. Hauser, W. Frey, D. Wang, *ChemCatChem* **2016**, *8*, 2710 – 2723.
[191] L. Stöhr, *Liganden-Variation in Molybdän-Imido-Alkyliden-N-Heterozyklischen Carbenkomplexen*, Ph. D. thesis, **2018**.
[192] I. Elser, W. Frey, K. Wurst, M. R. Buchmeiser, *Organometallics* **2016**, *35*, 4106-4111.
[193] a) K. M. Totland, T. J. Boyd, G. G. Lavoie, W. M. Davis, R. R. Schrock, *Macromolecules* **1996**, *29*, 6114-6125; b) J. B. Alexander, D. S. La, D. R. Cefalo, A. H. Hoveyda, R. R. Schrock, *J. Am. Chem. Soc.* **1998**, *120*, 4041-4042; *J. Am. Chem. Soc*; c) Y. Chen, S. Yekta, A. K. Yudin, *Chem. Rev.* **2003**, *103*, 3155-3212.
[194] T. W. Funk, J. M. Berlin, R. H. Grubbs, *J. Am. Chem. Soc.* **2006**, *128*, 1840-1846.
[195] N. T. McDougal, S. E. Schaus, *J. Am. Chem. Soc.* **2003**, *125*, 12094-12095.
[196] Y. Luan, S. E. Schaus, *J. Am. Chem. Soc.* **2012**, *134*, 19965-19968.
[197] A. C. Hans, *Stereoselektive Olefinmetathese mit chiralen Molybdän-Alkyliden-NHC-Komplexen*, Bachelor thesis, **2016**.
[198] S. C. Marinescu, R. Singh, A. S. Hock, K. M. Wampler, R. R. Schrock, P. Müller, *Organometallics* **2008**, *27*, 6570-6578.
[199] R. A. Kelly Iii, H. Clavier, S. Giudice, N. M. Scott, E. D. Stevens, J. Bordner, I. Samardjiev, C. D. Hoff, L. Cavallo, S. P. Nolan, *Organometallics* **2008**, *27*, 202-210.
[200] a) Y. Okuno, M. Yamashita, K. Nozaki, *Eur. J. Inorg. Chem.* **2011**, 3951-3958; b) J. Hyun, T. Song, Y. K. Chung, *Org. Lett.* **2017**, *19*, 1248- 1251.
[201] B. Lee, J. H. Kim, H. Lee, B. S. Ahn, M. Cheong, H. S. Kim, H. Kim, *J. Fluor. Chem.* **2007**, *128*, 110-113.
[202] L. G. McCullough, R. R. Schrock, C. D. Dewan, J. C. Murdzek, *J. Am. Chem. Soc.* **1985**, *107*, 5987-5998.
[203] J. Groos, *Chelatisierende N-Heterozyklische Carben Metallalkylidinkomplexe der Gruppe 6*, Master thesis, University of Stuttgart **2017**.
[204] G. R. Fulmer, A. J. M. Miller, N. H. Sherden, H. E. Gottlieb, A. Nudelman, B. M. Stoltz, J. E. Bercaw, K. I. Goldberg, *Organometallics* **2010**, *29*, 2176-2179.
[205] D. M. Khramov, V. M. Lynch, C. W. Bielawski, *Organometallics* **2007**, *26*, 6042-6049.
[206] W. A. Herrmann, V. P. W. Böhm, C. W. K. Gstöttmayr, M. Grosche, C.-P. Reisinger, T. Weskamp, *J. Organomet. Chem.* **2001**, *617-618*, 616-628.

[207] M. Hans, J. Lorkowski, A. Demonceau, L. Delaude, *Beilstein J. Org. Chem.* **2015**, *11*, 2318-2325.
[208] T. Schaub, U. Radius, *Chemistry* **2005**, *11*, 5024-5030.
[209] D. Enders, K. Breuer, U. Kallfass, T. Balensiefer, *Synthesis* **2003**, *2003*, 1292-1295.
[210] C. Cesari, S. Conti, S. Zacchini, V. Zanotti, M. C. Cassani, R. Mazzoni, *Dalton Trans.* **2014**, *43*, 17240-17243.
[211] J. J. Song, J. T. Reeves, D. R. Fandrick, Z. Tan, N. K. Yee, C. H. Senanayake, **2008**.
[212] A. J. Arduengo, R. Krafczyk, R. Schmutzler, H. A. Craig, J. R. Goerlich, W. J. Marshall, M. Unverzagt, *Tetrahedron* **1999**, *55*, 14523-14534.
[213] A. J. Arduengo, J. R. Goerlich, W. J. Marshall, *J. Am. Chem. Soc.* **1995**, *117*, 11027-11028.
[214] C. R. Smith, A. Zhang, D. J. Mahns, T. V. RajanBabu, *Org. Synth.* **2008**, *85*, 248.
[215] A. Carrillo, R. S. Kane, *J. Polym. Sci., Part A: Polym. Chem.* **2004**, *42*, 3352-3359.
[216] W. J. Bailey, W. B. Lawson, *J. Am. Chem. Soc.* **1955**, *77*, 1606-1608.
[217] S.-H. Kim, Y.-H. Kim, H.-N. Cho, S.-K. Kwon, H.-K. Kim, S.-K. Choi, *Macromolecules* **1996**, *29*, 5422-5426.
[218] A. S. Hashmi, T. Haffner, M. Rudolph, F. Rominger, *Chemistry* **2011**, *17*, 8195-8201.
[219] U. Anders, J. O. Krause, D. Wang, O. Nuyken, M. R. Buchmeiser, *Des. Monomers and Polym.* **2012**, *7*, 151-163.
[220] P. S. Kumar, K. Wurst, M. R. Buchmeiser, *J. Am. Chem. Soc.* **2009**, *131*, 387-395.
[221] H.-D. Xu, K. Xu, Z.-H. Jia, H. Zhou, P. Jiang, X.-L. Lu, Y.-P. Pan, H. Wu, Y. Ding, M.-H. Shen, X.-H. Pan, *Asian J. Org. Chem.* **2014**, *3*, 1154-1158.
[222] a) A. G. Lichtscheidl, V. W. L. Ng, P. Müller, T. M. K., R. R. Schrock, *Organometallics* **2012**, *31*, 2388- 2394; b) S. C. Marinescu, R. Singh, A. S. Hock, K. M. Wampler, R. R. Schrock, P. Müller, *Organometallics* **2008**, *27*, 6570- 6578.
[223] A. S. Hock, R. R. Schrock, A. H. Hoveyda, *J. Am. Chem. Soc.* **2006**, *128*, 16373-16375.
[224] T. Kreickmann, S. Arndt, R. R. Schrock, P. Müller, *Organometallics* **2007**, *26*, 6684-6684.
[225] S. J. J. Cho, N. H. Jensen, T. Kurome, S. Kadari, M. L. Manzano, J. E. Malberg, B. Caldarone, B. L. Roth, A. P. Kozikowski, *J. Med. Chem.* **2009**, *52*, 1885-1902.

9 APPENDIX

9.1 GROUP 6 METAL ALKYLIDENES BEARING IONIC LIGANDS

9.1.1 SPECTRA OF NOVEL COMPOUNDS

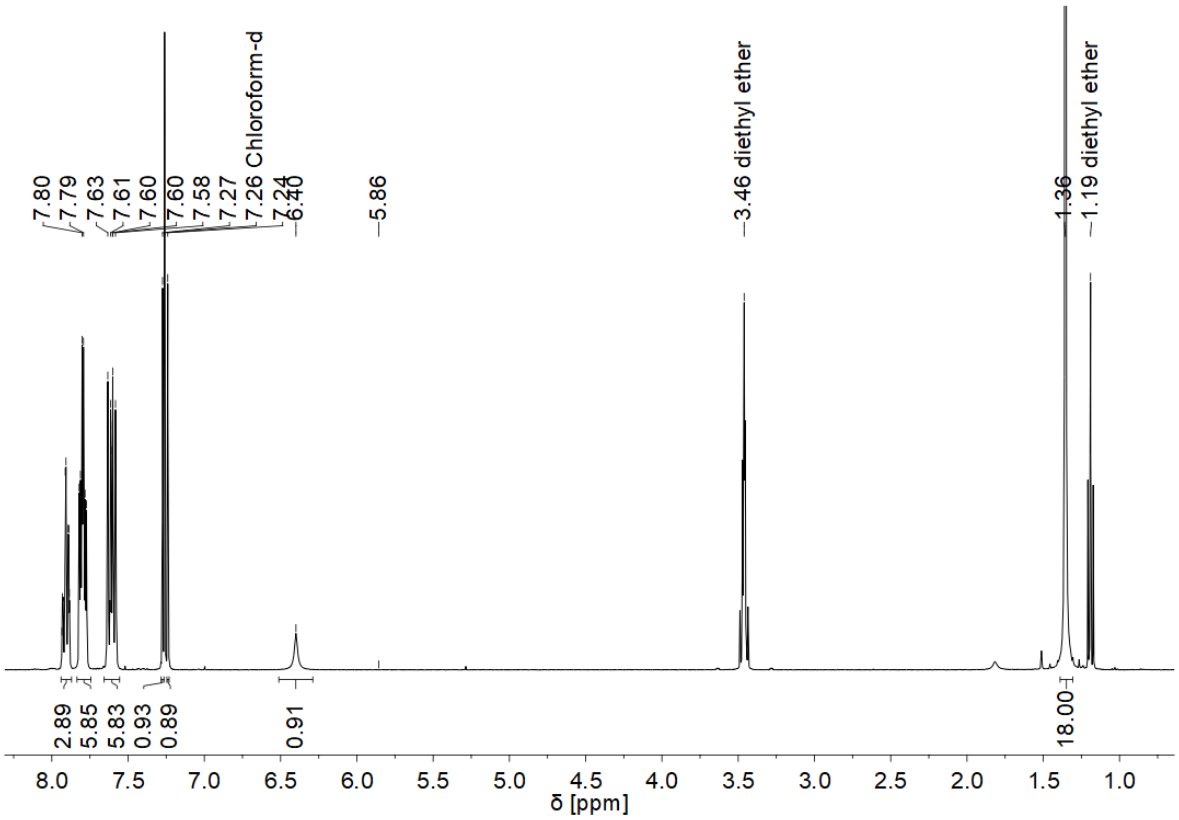

Figure A 1: ^{1}H NMR spectrum of **1b** (400 MHz, $CDCl_3$).

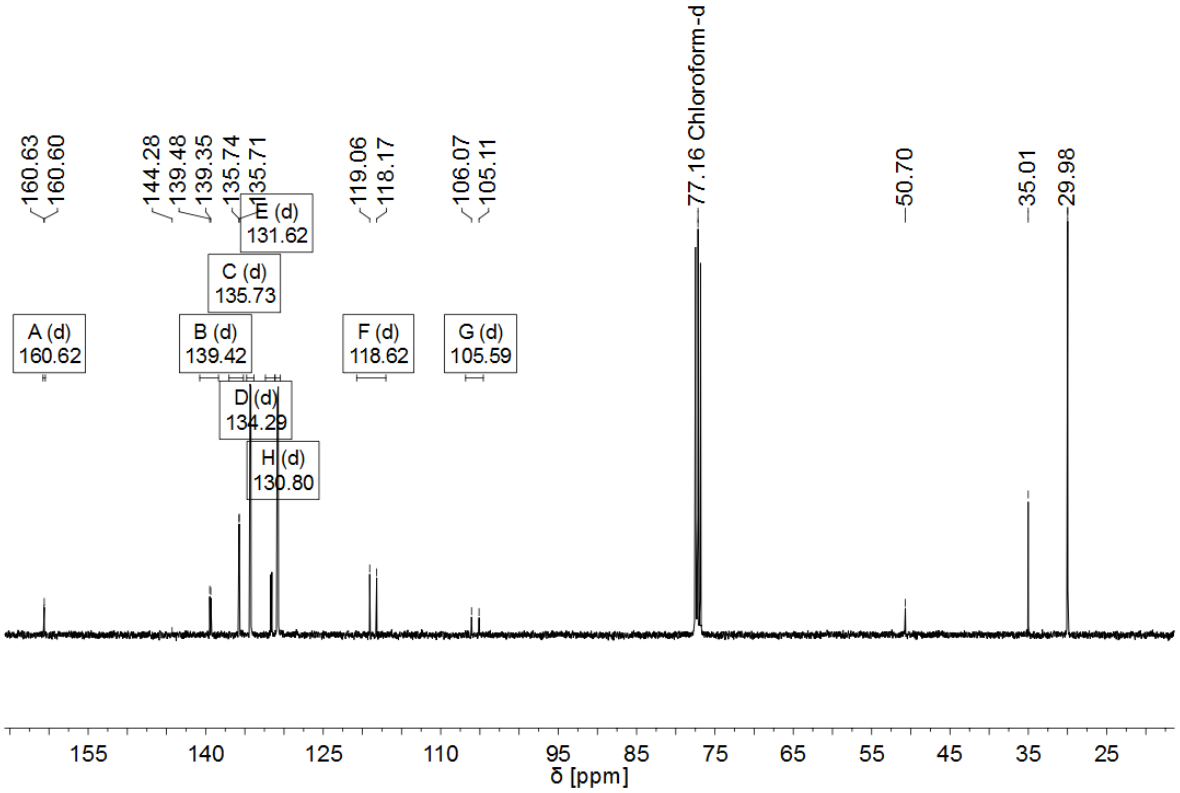

Figure A 2: ^{13}C NMR spectrum of **1b** (101 MHz, $CDCl_3$).

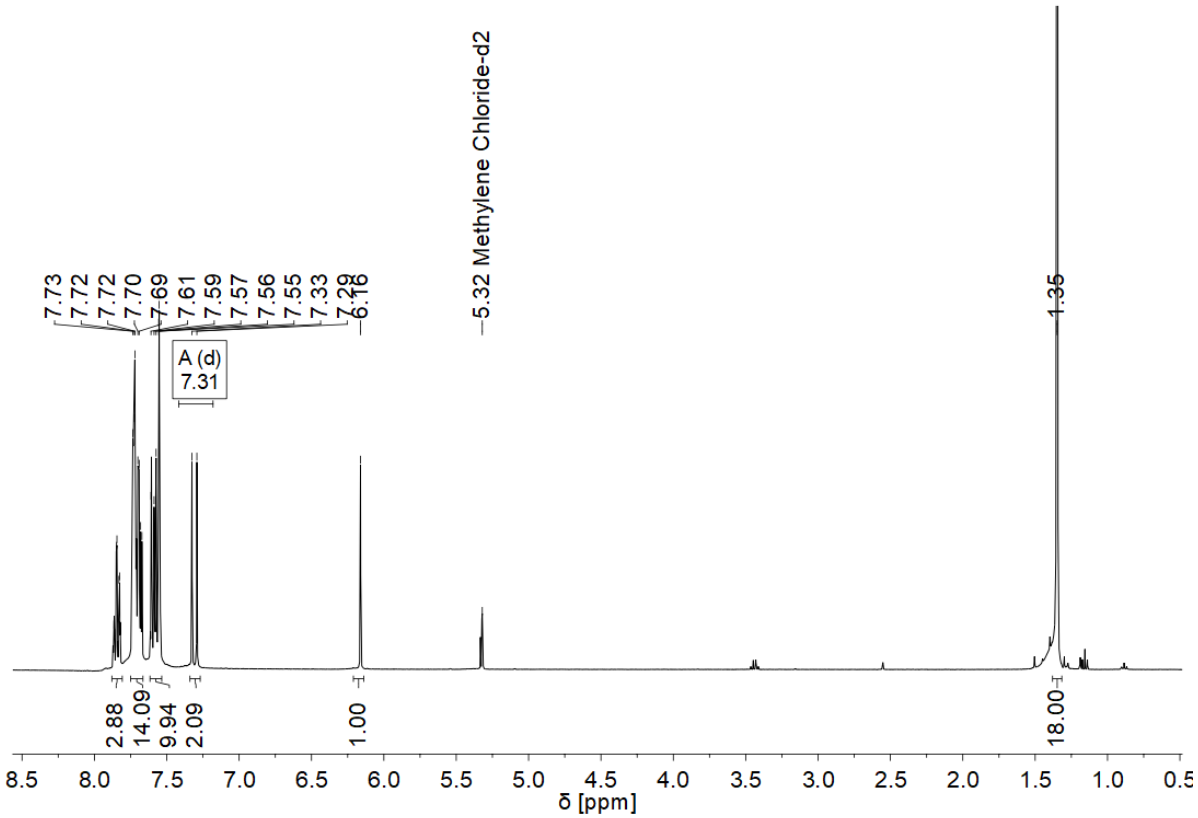

Figure A 3: ^{1}H NMR spectrum of **1** (400 MHz, $CDCl_3$).

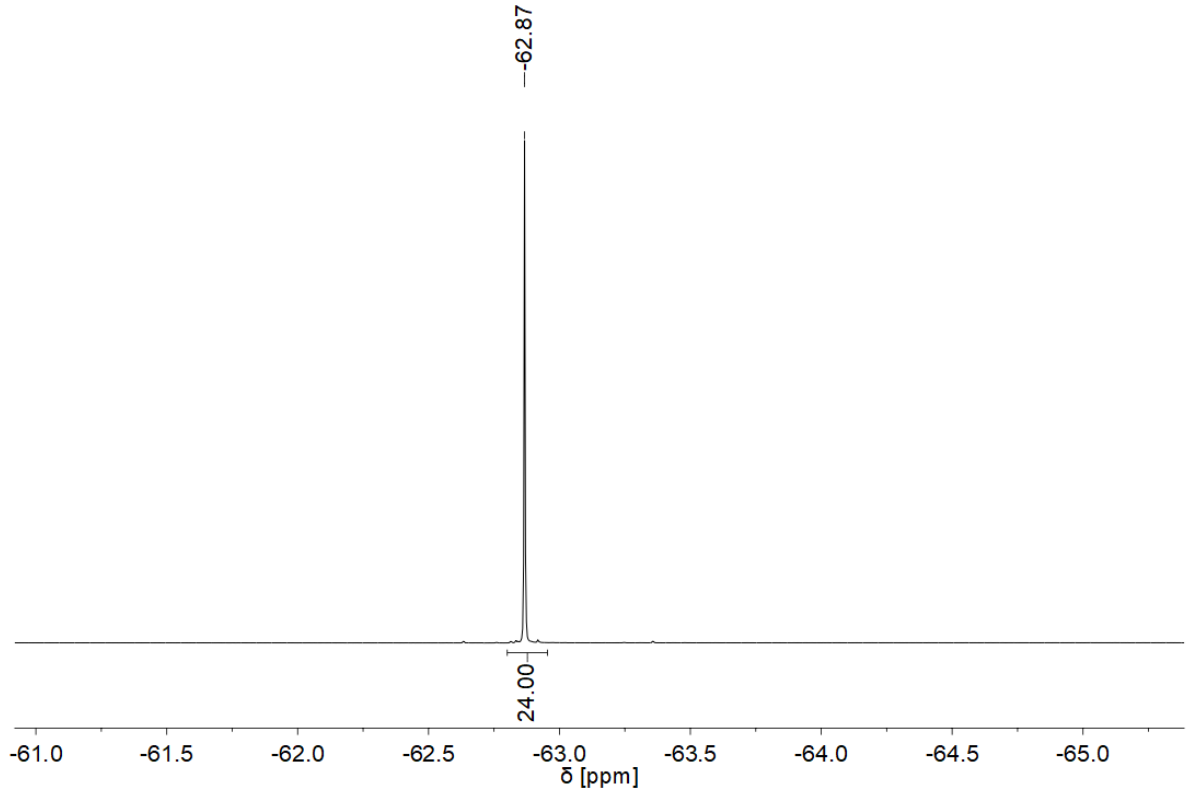

Figure A 4: ^{19}F NMR spectrum of **1** (376 MHz, $CDCl_3$).

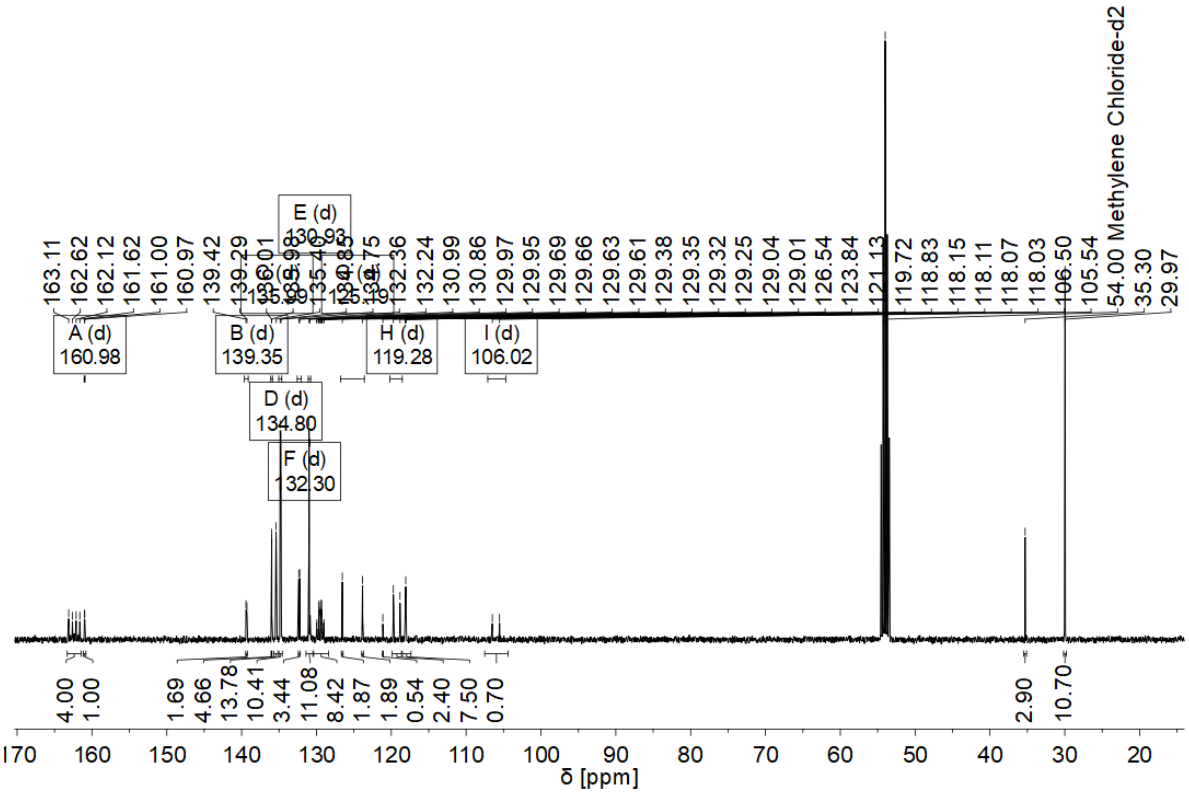

Figure A 5: ^{13}C NMR spectrum of **1** (101 MHz, $CDCl_3$).

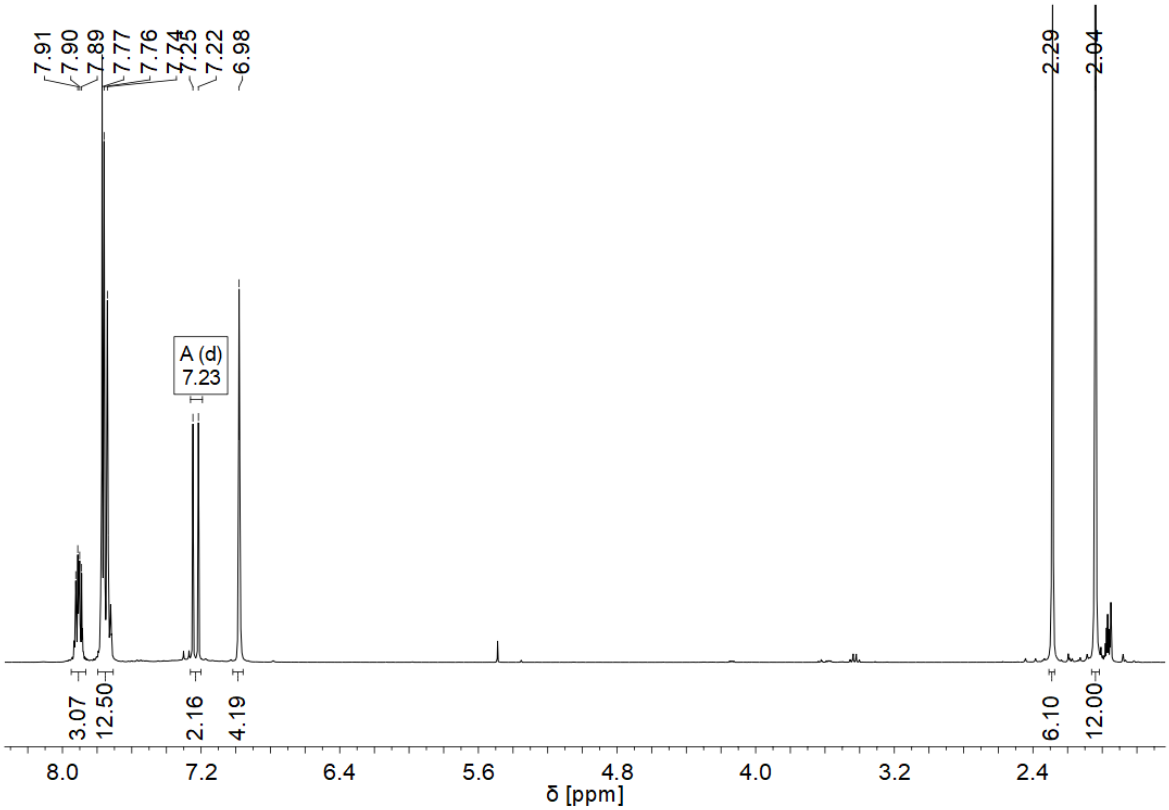

Figure A 6: ^{1}H NMR spectrum of **2c** (400 MHz, $CDCl_3$). Due to the high concentration of the analyte the solvent residual signal could not be assigned.

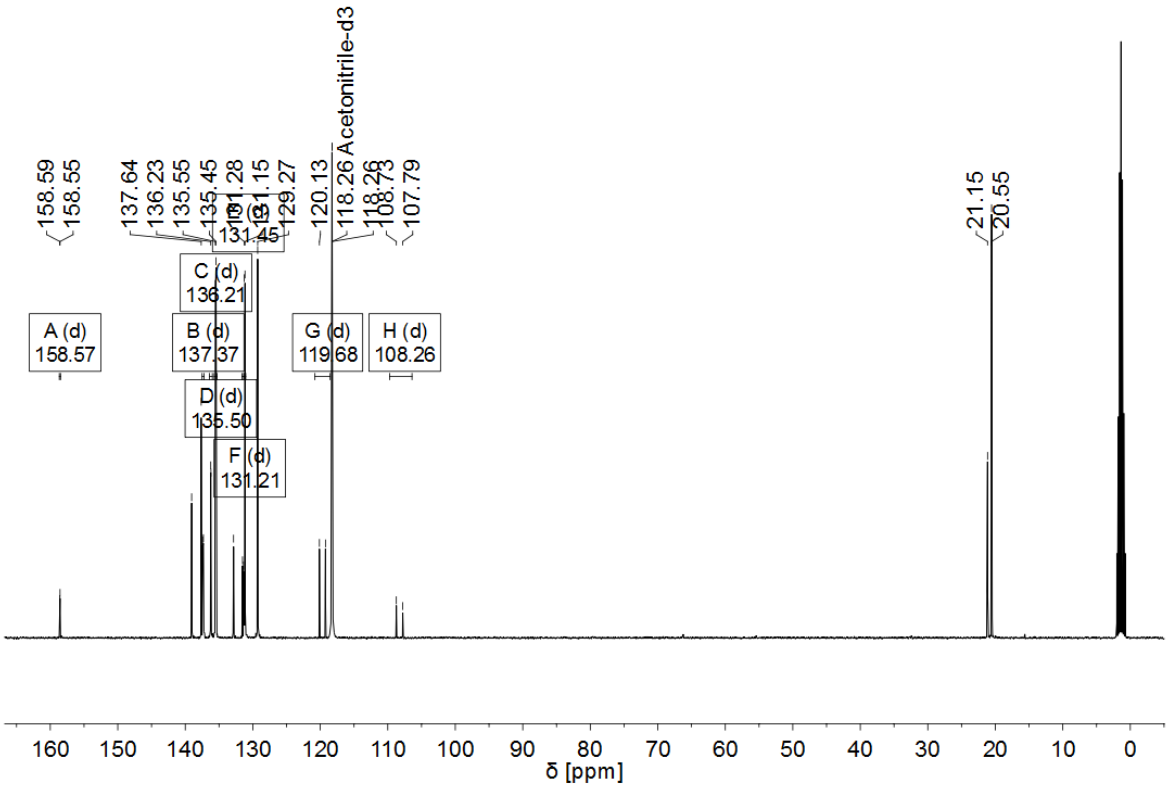

Figure A 7: ^{13}C NMR spectrum of **2c** (101 MHz, MeCN-d3).

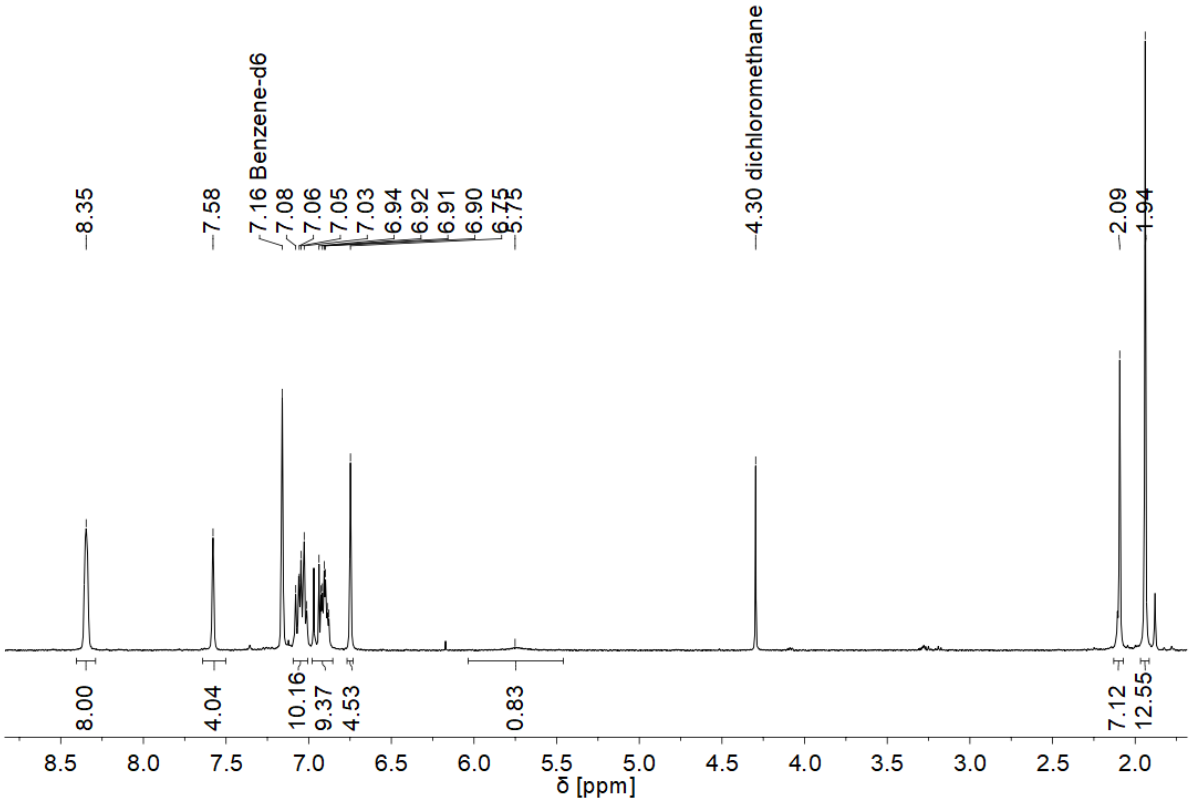

Figure A 8: ^{1}H NMR spectrum of **2** (400 MHz, C_6D_6).

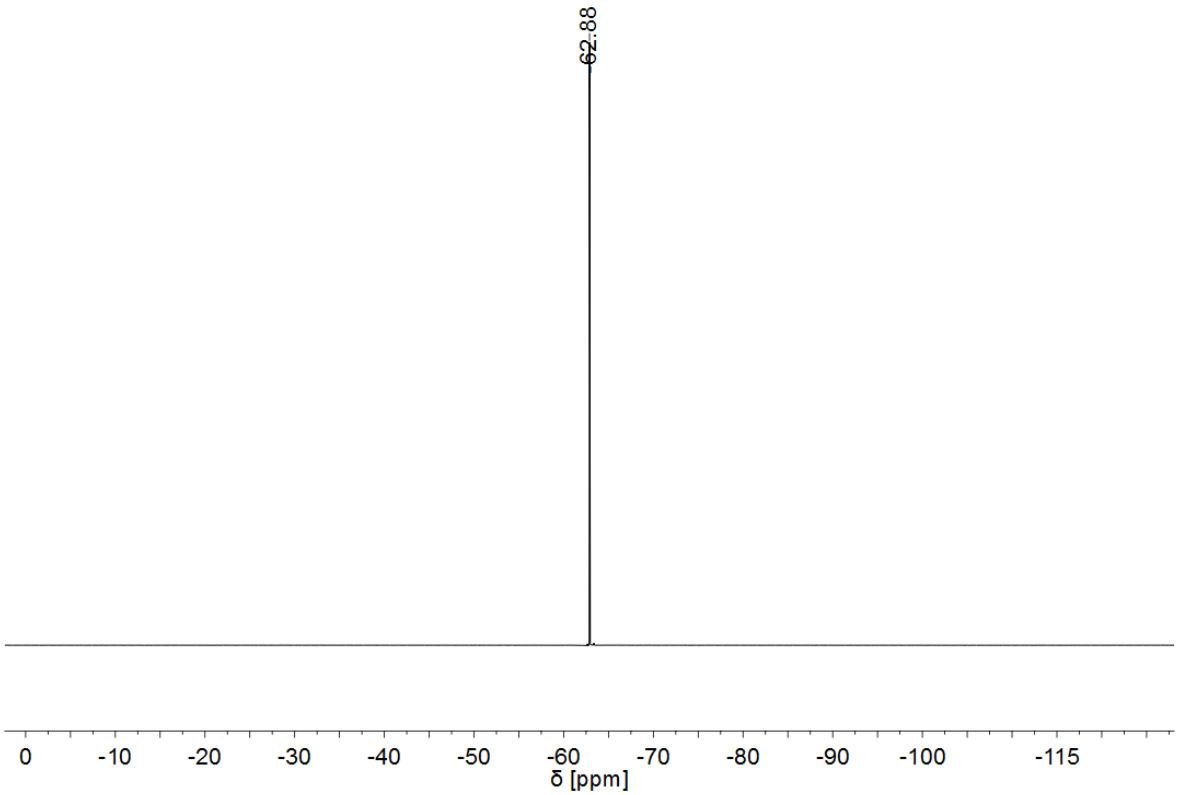

Figure A 9: ^{19}F NMR spectrum of **2** (376 MHz, C_6D_6).

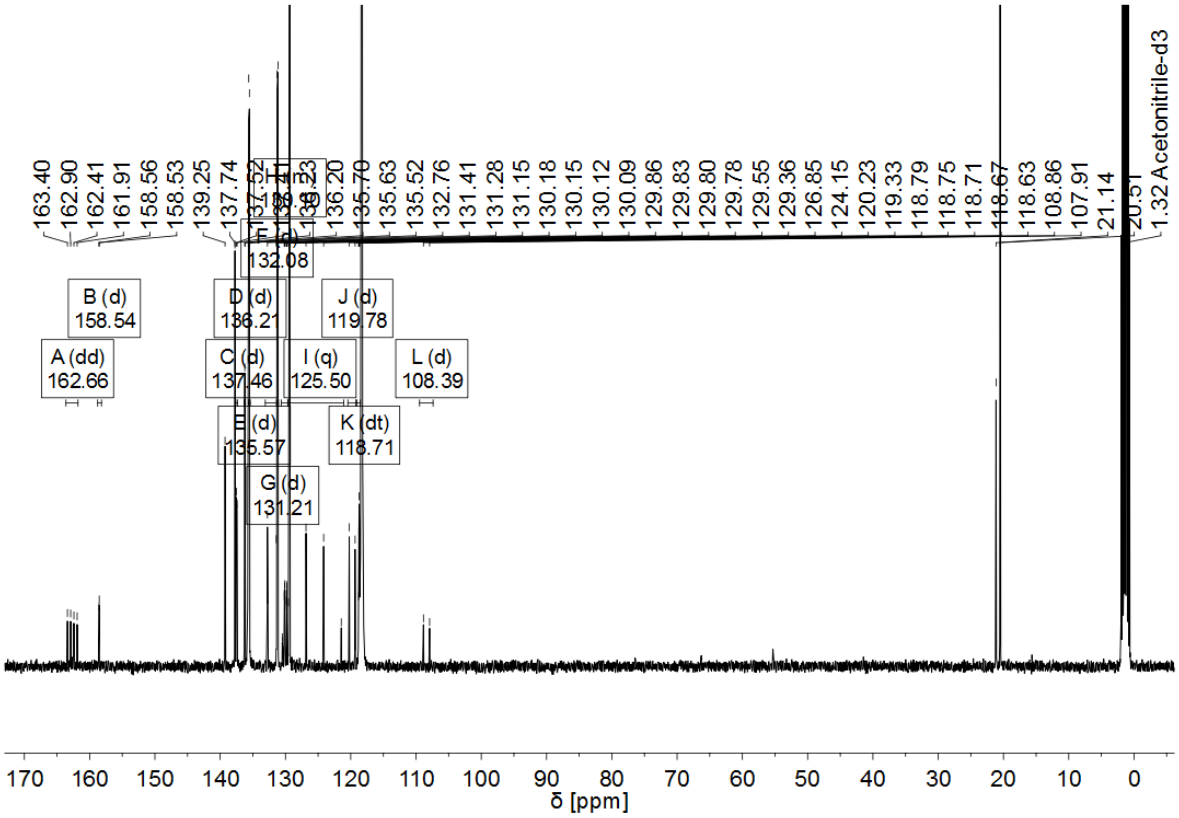

Figure A 10: ^{13}C NMR spectrum of **2** (101 MHz, MeCN-d3).

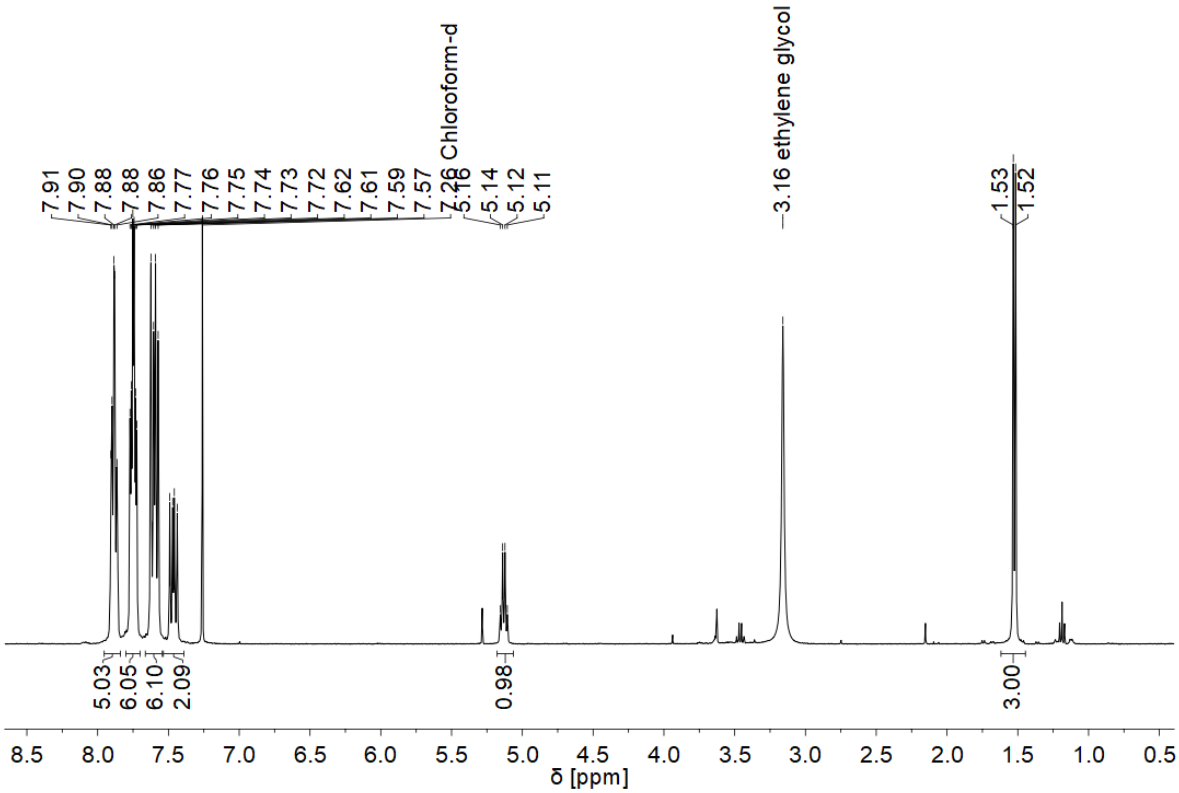

Figure A 11: ^{1}H NMR spectrum of **3b** (400 MHz, $CDCl_3$).

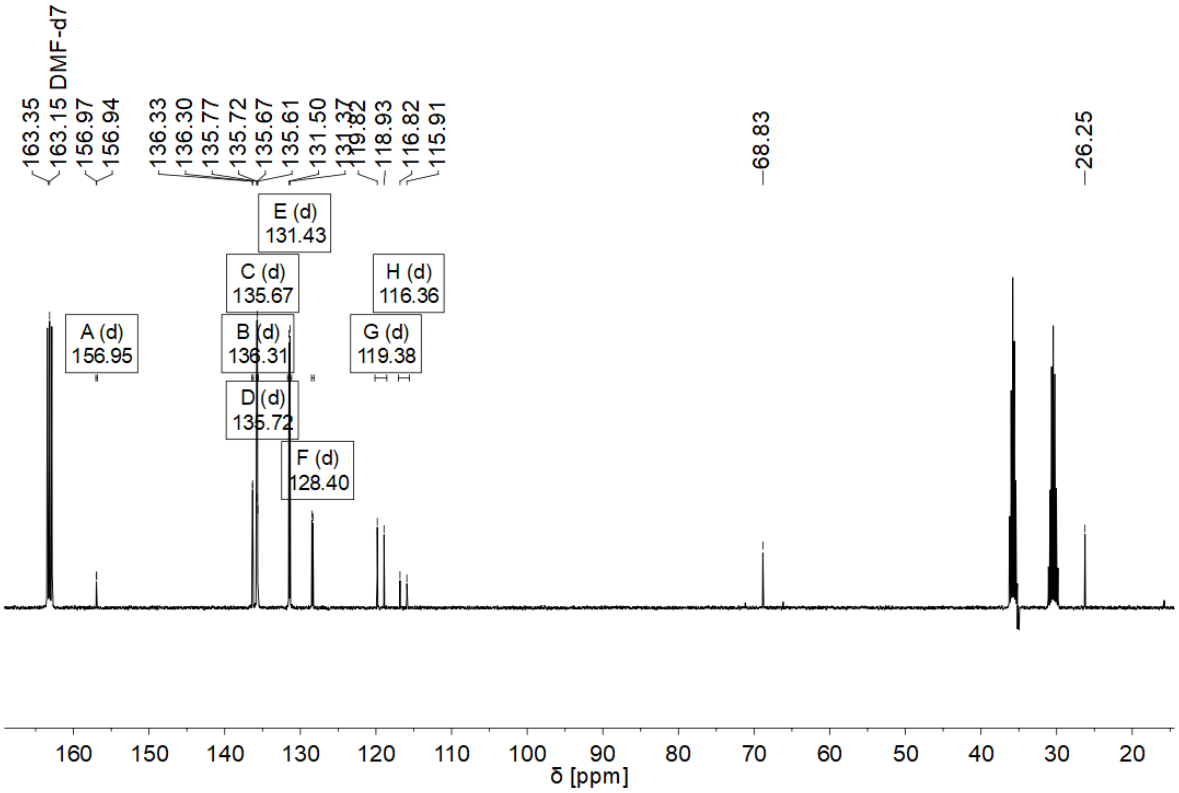

Figure A 12: ^{13}C NMR spectrum of **3b** (101 MHz, DMF-d7).

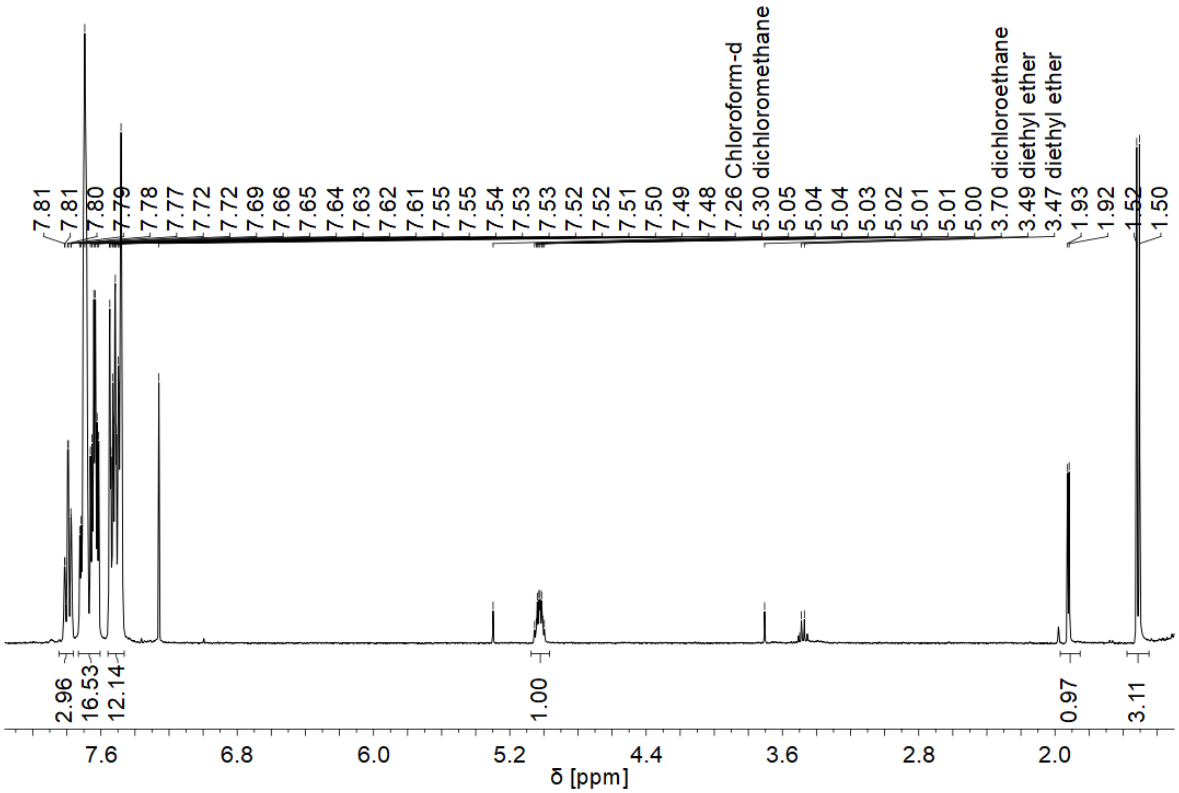

Figure A 13: ^{1}H NMR spectrum of **3** (400 MHz, $CDCl_3$).

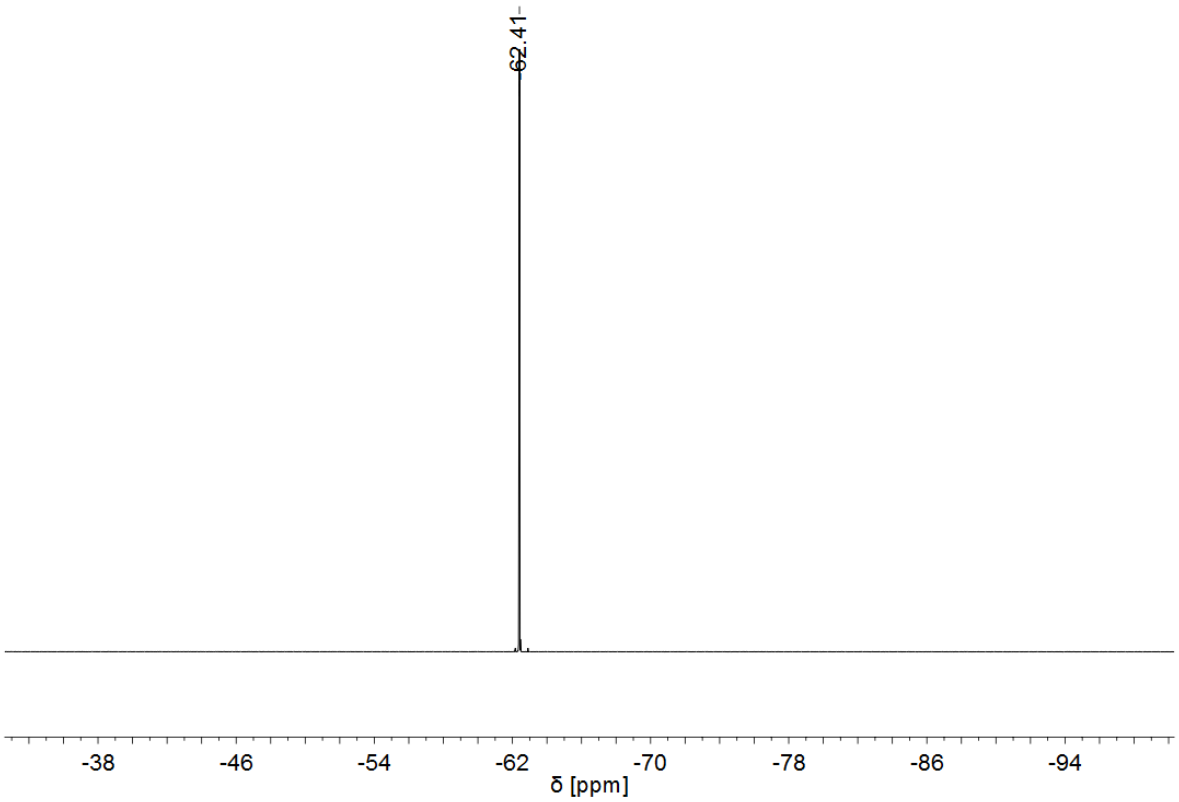

Figure A 14: ^{19}F NMR spectrum of **3** (376 MHz, $CDCl_3$).

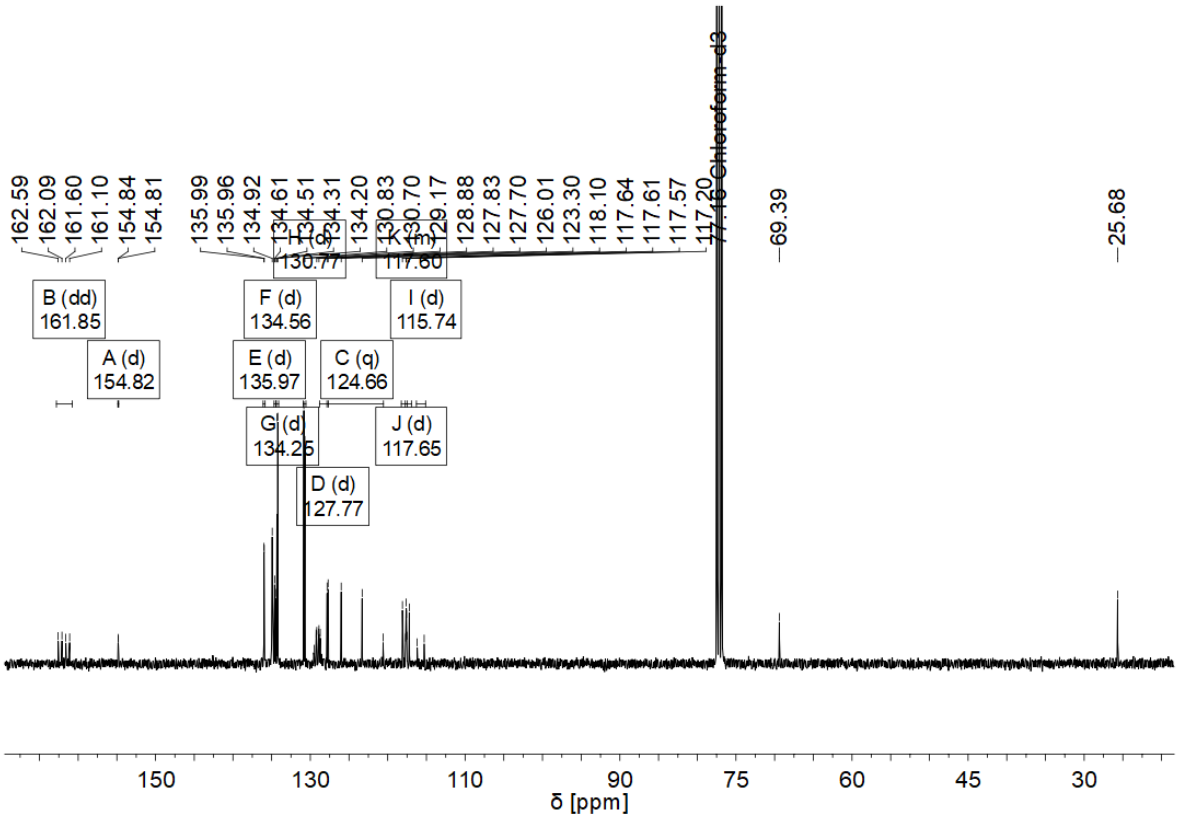

Figure A 15: ^{13}C NMR spectrum of **3** (101 MHz, $CDCl_3$).

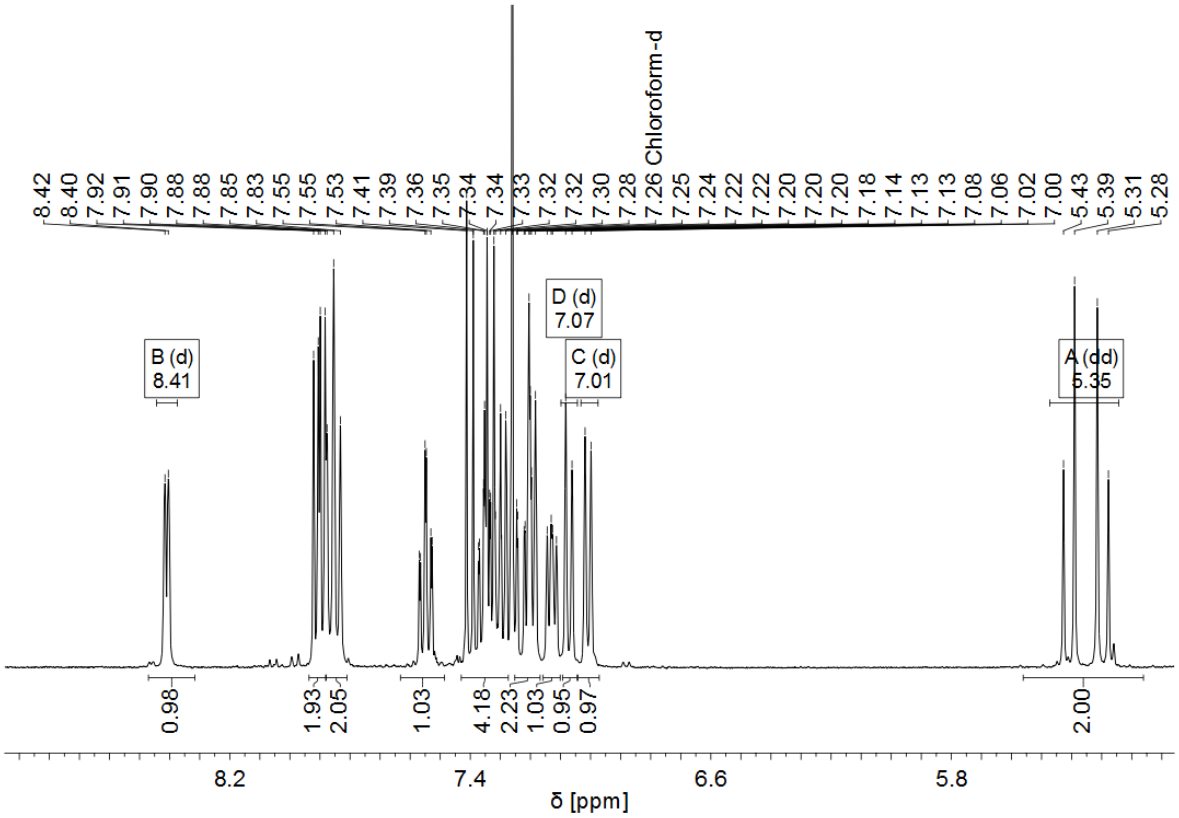

Figure A 16: ^{1}H NMR spectrum of **4b** (400 MHz, $CDCl_3$).

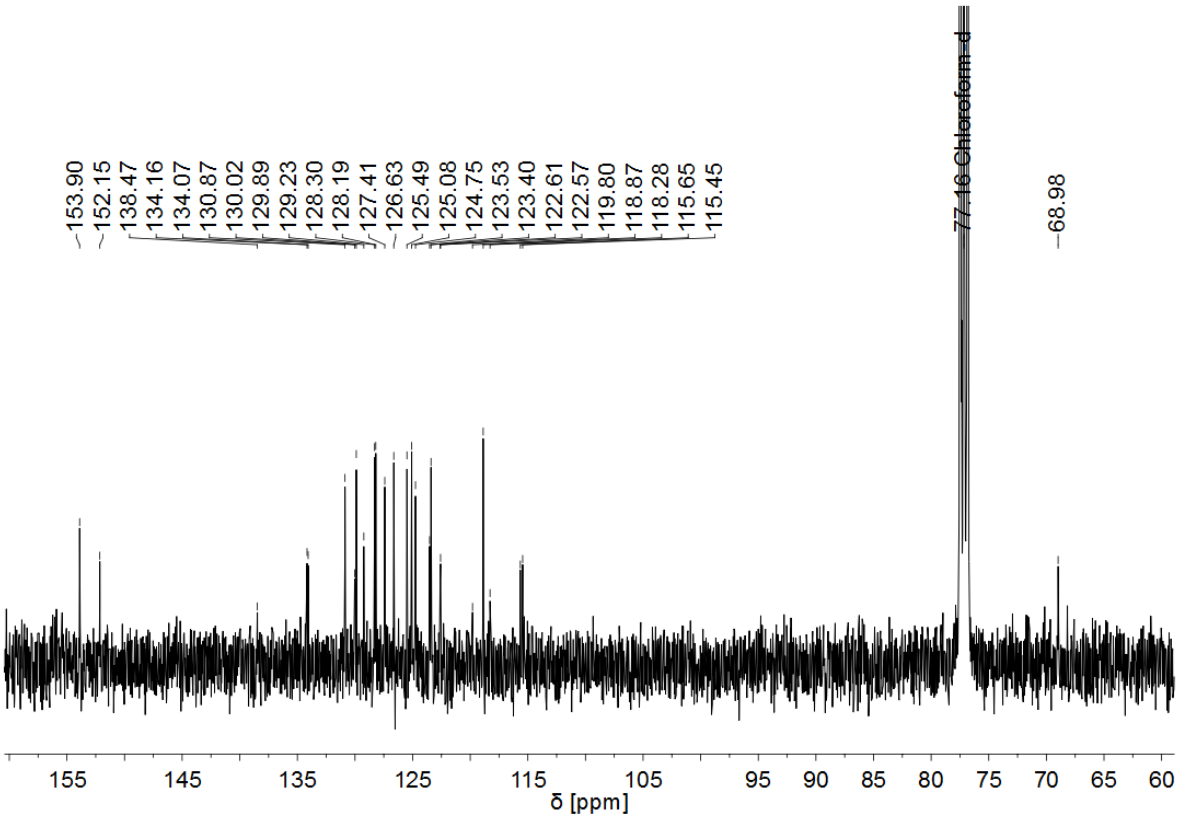

Figure A 17: ^{13}C NMR spectrum of **4b** (101 MHz, $CDCl_3$).

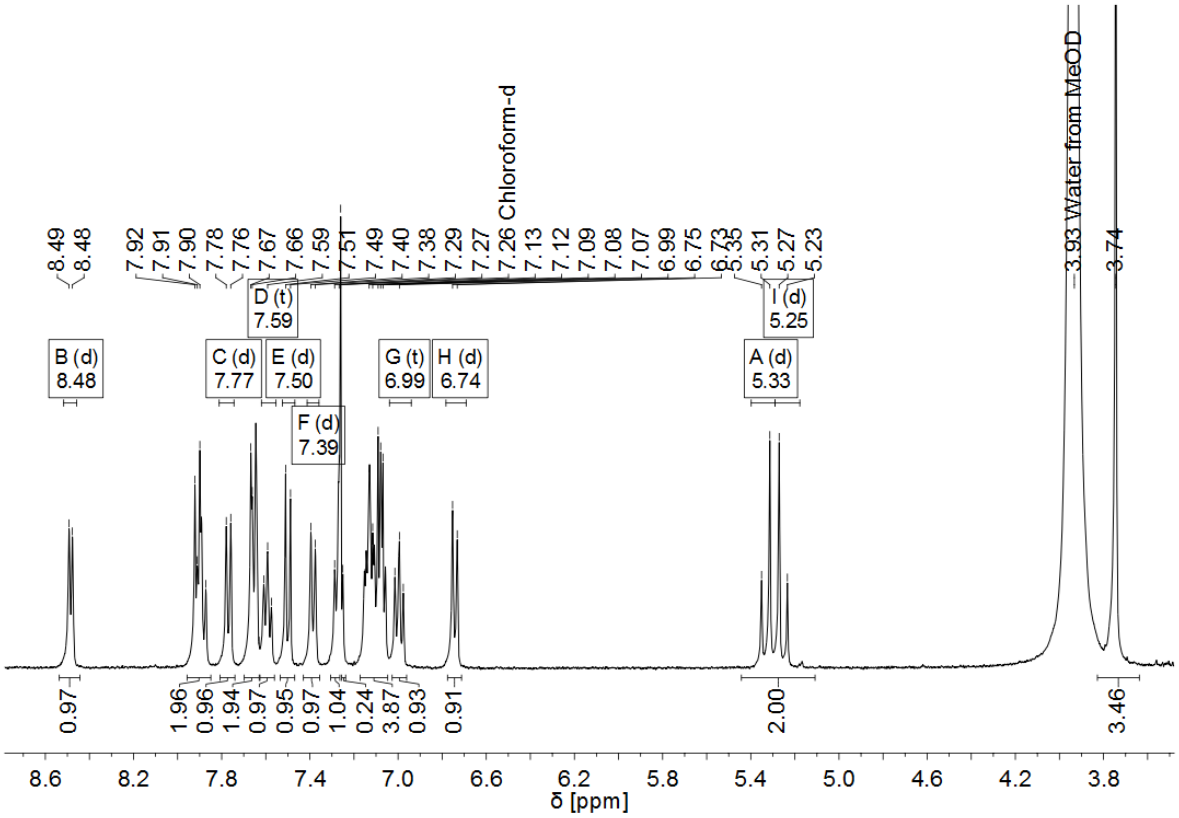

Figure A 18: ^{1}H NMR spectrum of **4c** (400 MHz, $CDCl_3$/MeOD).

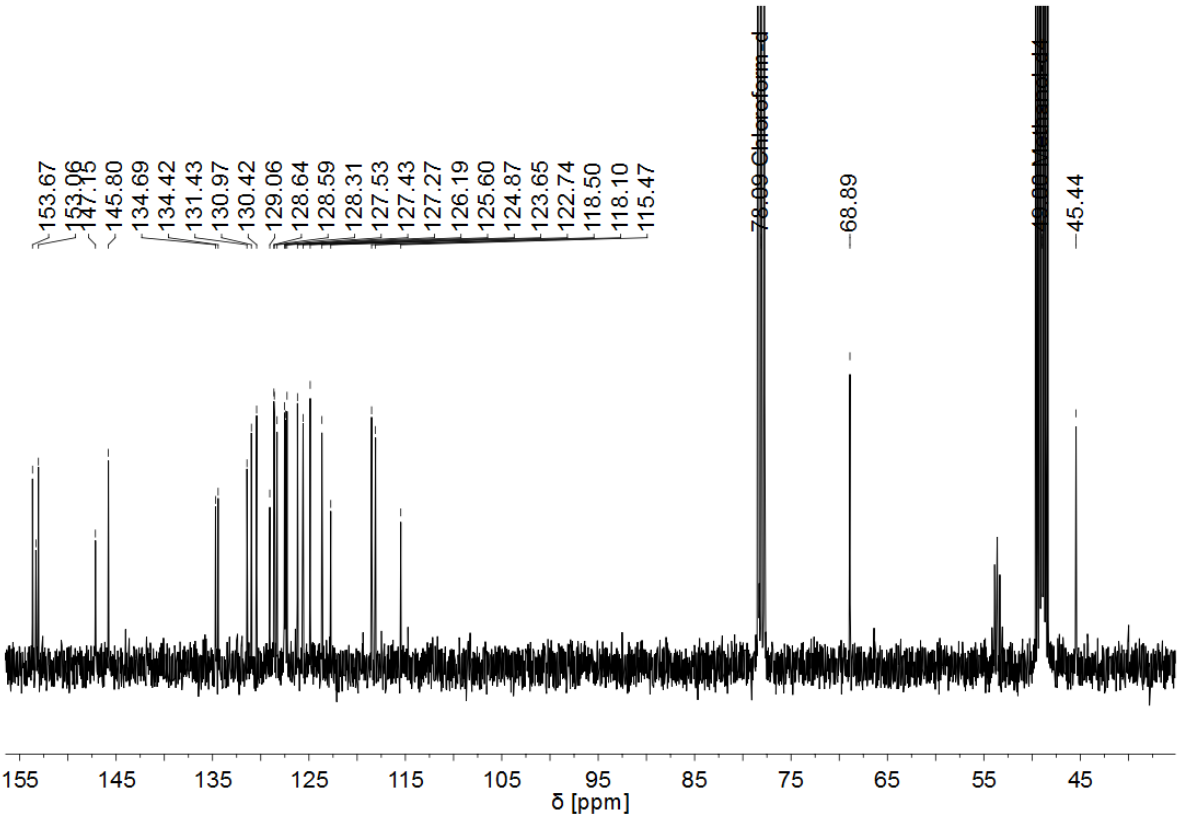

Figure A 19: ^{13}C NMR spectrum of **4c** (101 MHz, $CDCl_3$/MeOD).

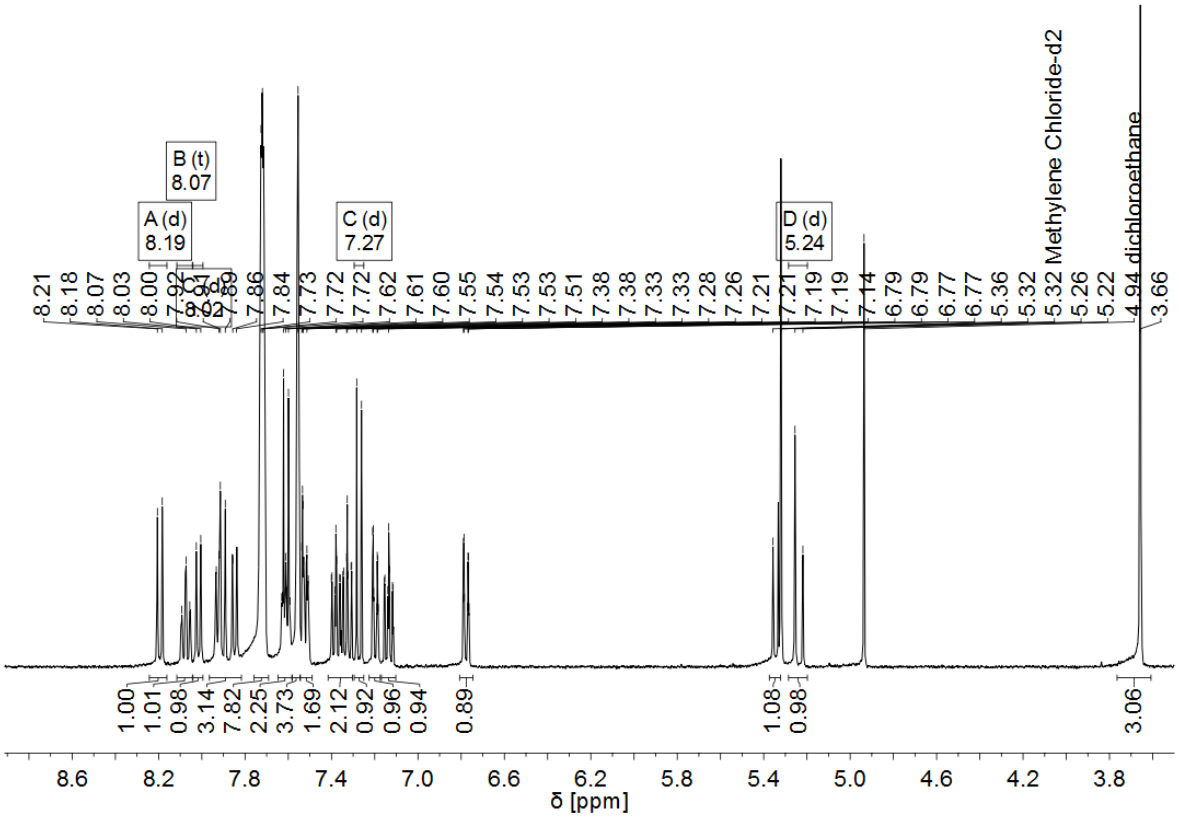

Figure A 20: ^{1}H NMR spectrum of **4** (400 MHz, CD_2Cl_2).

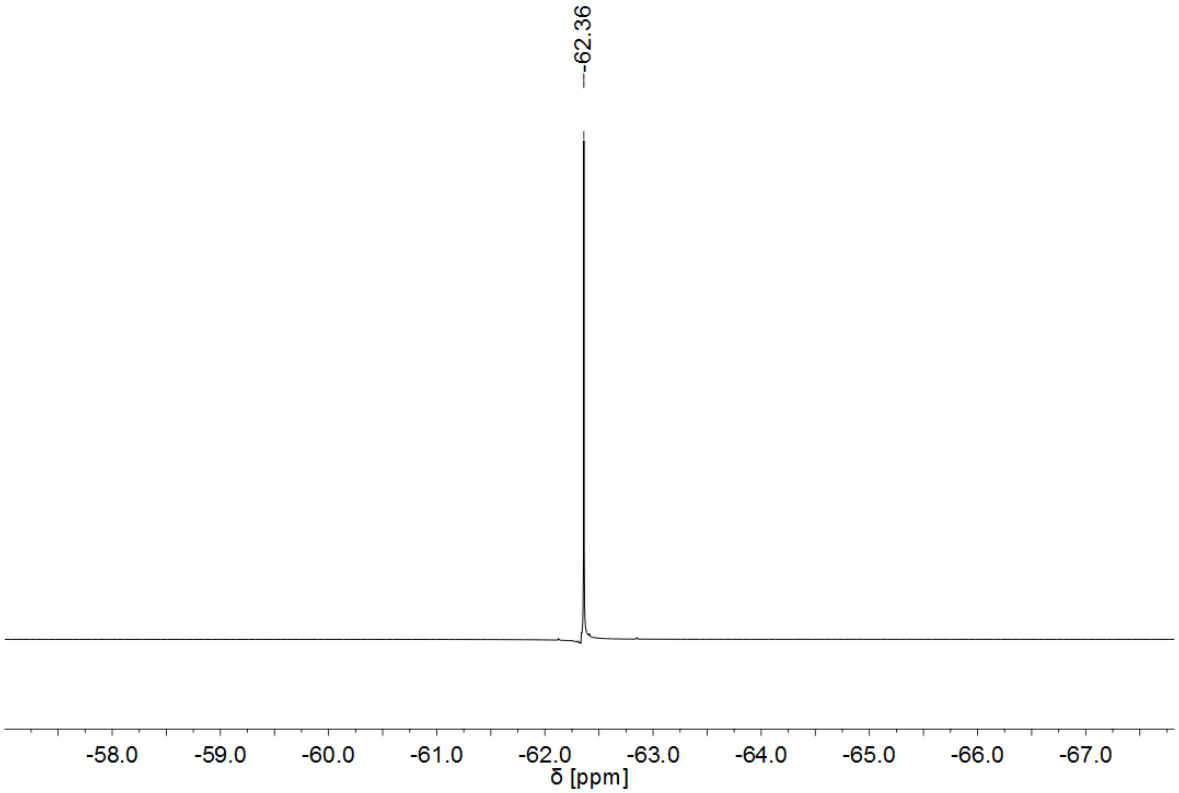

Figure A 21: ^{19}F NMR spectrum of **4** (376 MHz, $CDCl_3$).

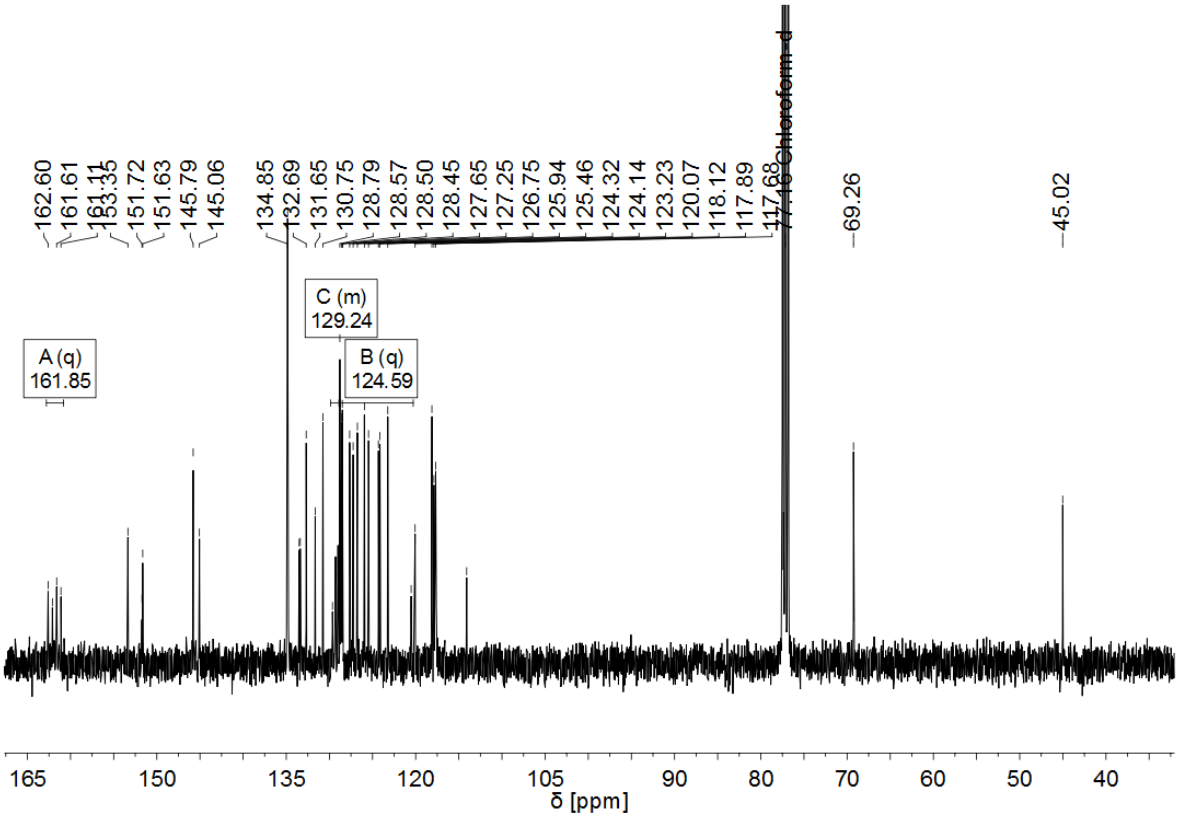

Figure A 22: ^{13}C NMR spectrum of **4** (101 MHz, $CDCl_3$).

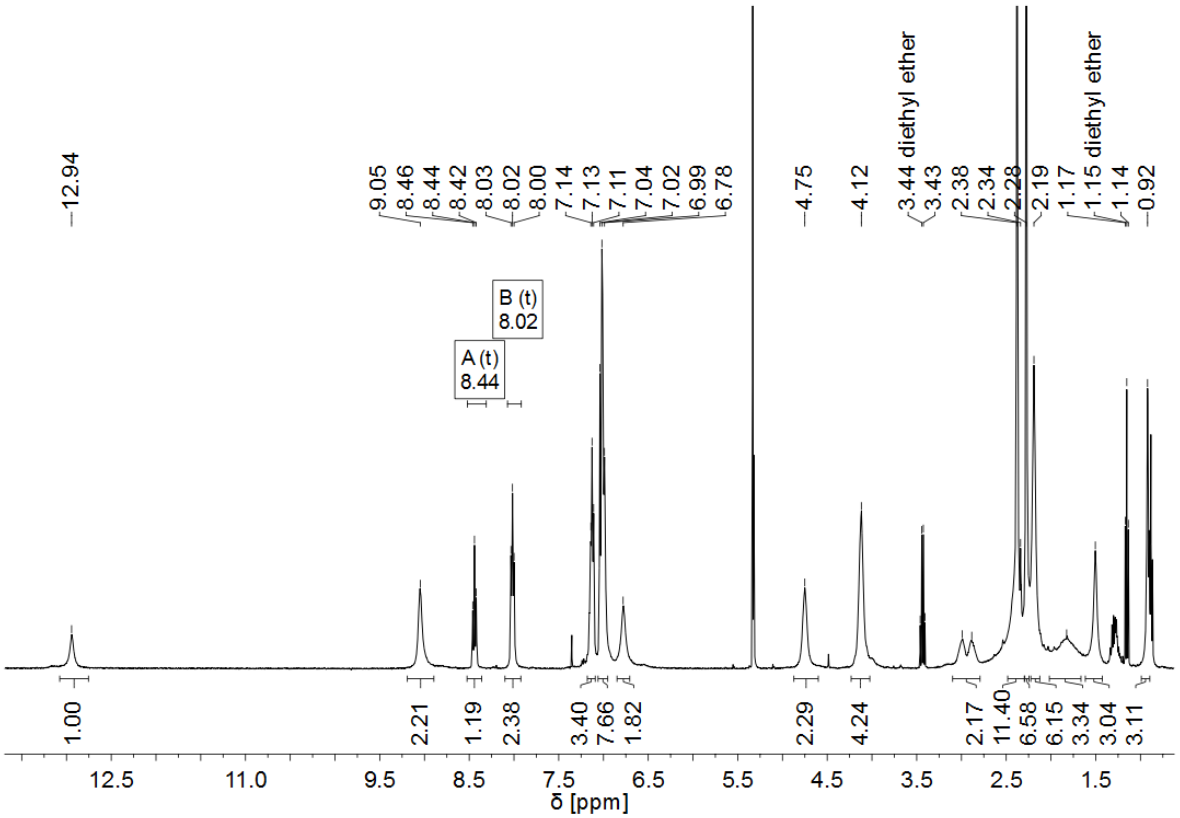

Figure A 23: ^{1}H NMR spectrum of **Mo-3** (400 MHz, CD_2Cl_2).

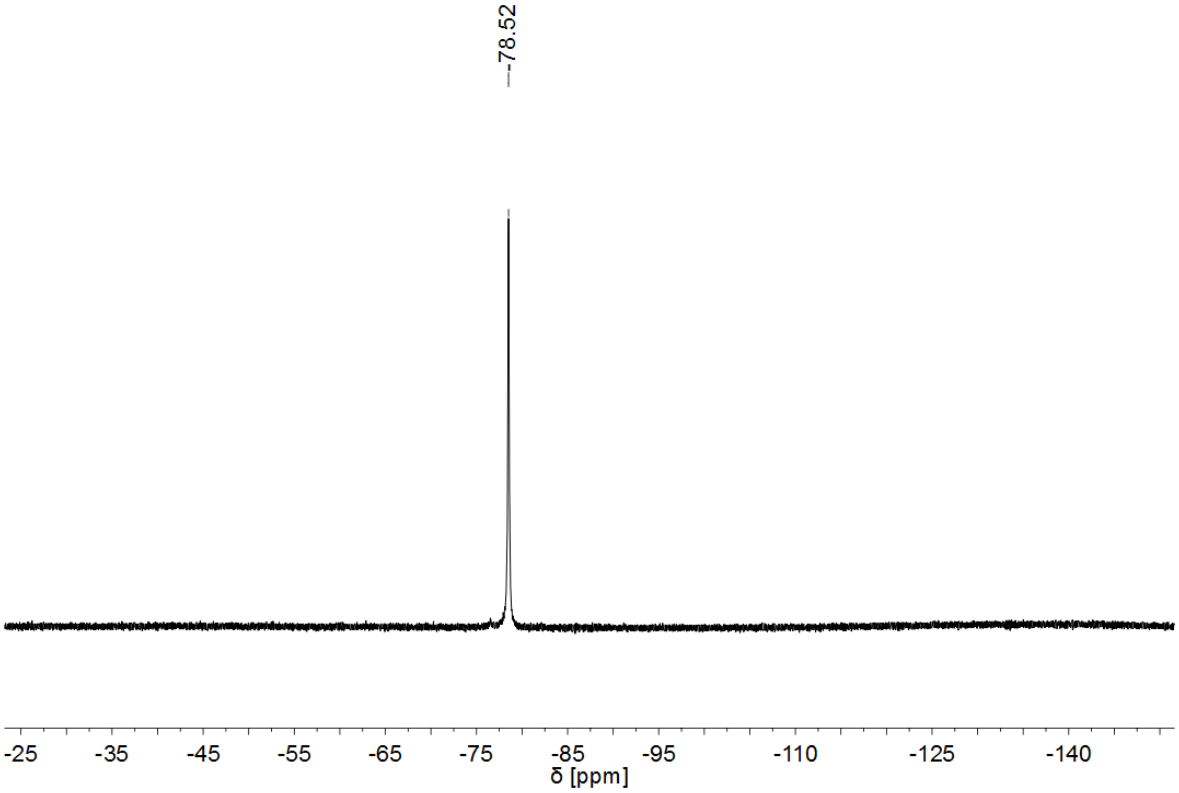

Figure A 24: ^{19}F NMR spectrum of **Mo-3** (376 MHz, CD_2Cl_2).

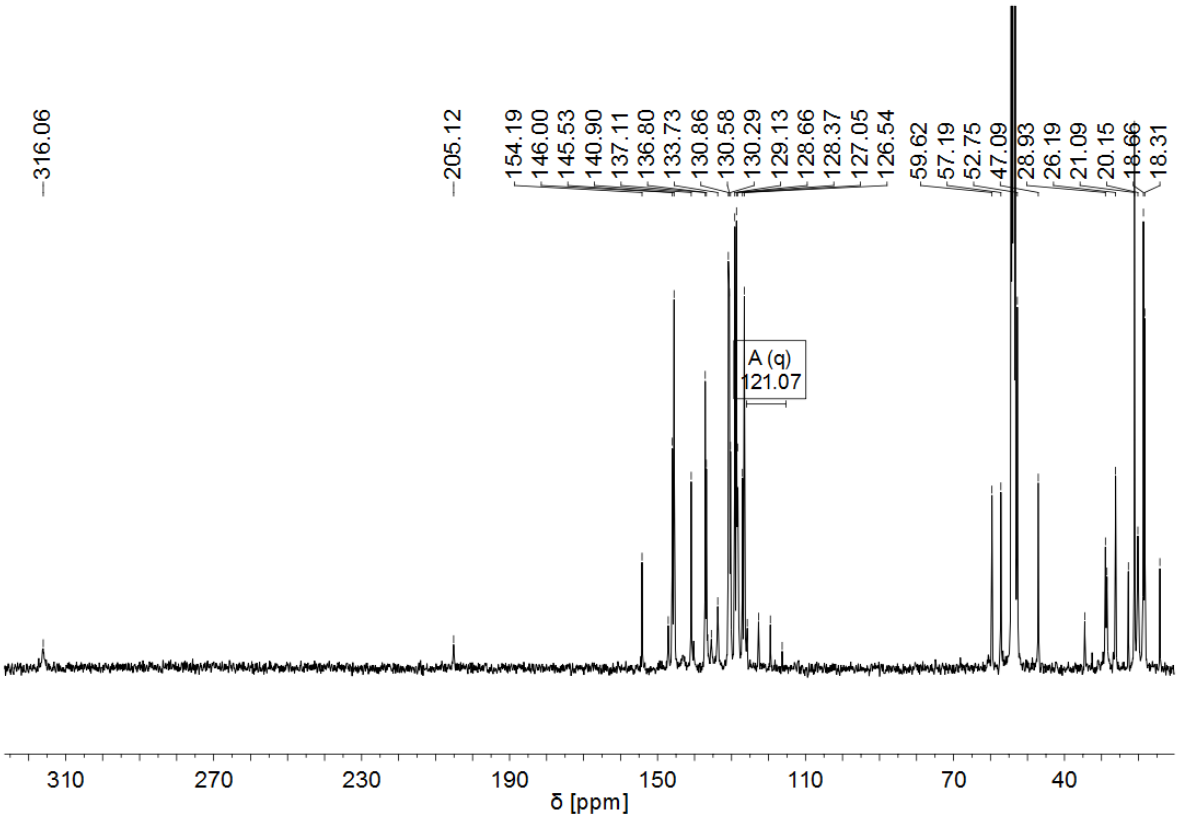

Figure A 25: ^{13}C NMR spectrum of **Mo-3** (101 MHz, CD_2Cl_2).

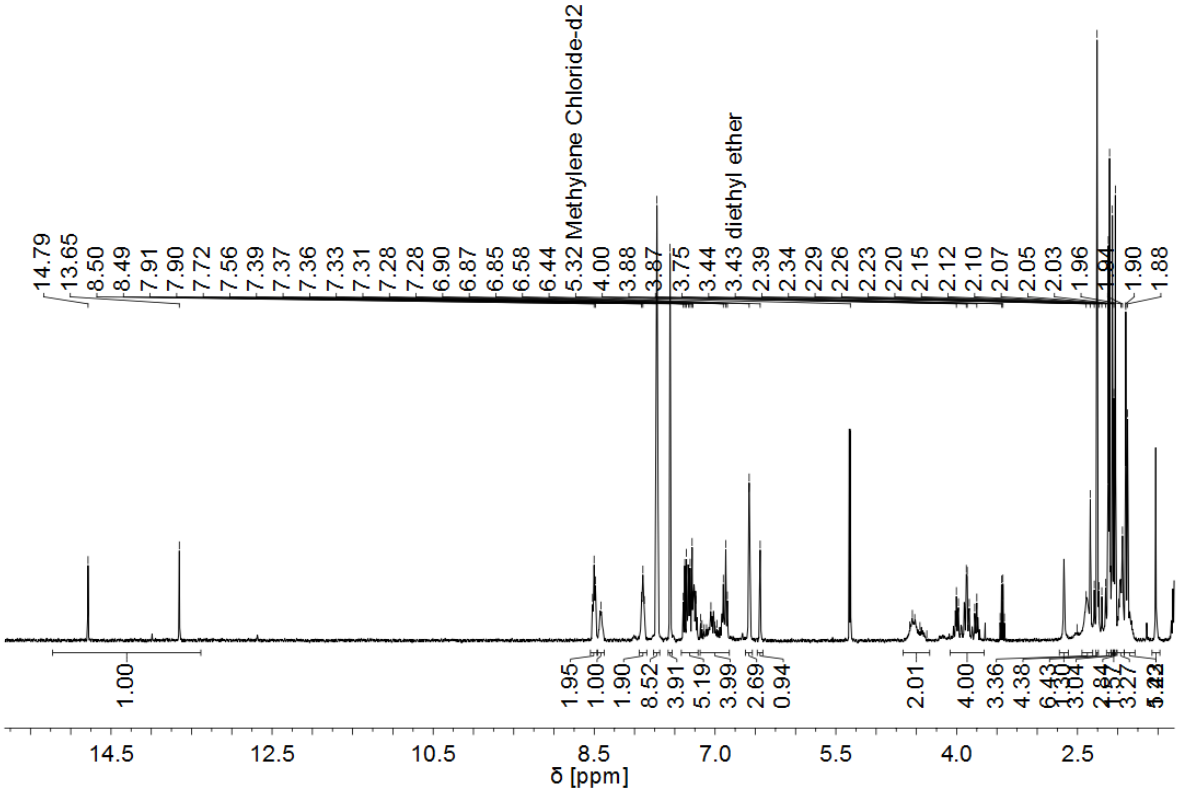

Figure A 26: ^{1}H NMR spectrum of **Mo-5** (400 MHz, CD_2Cl_2).

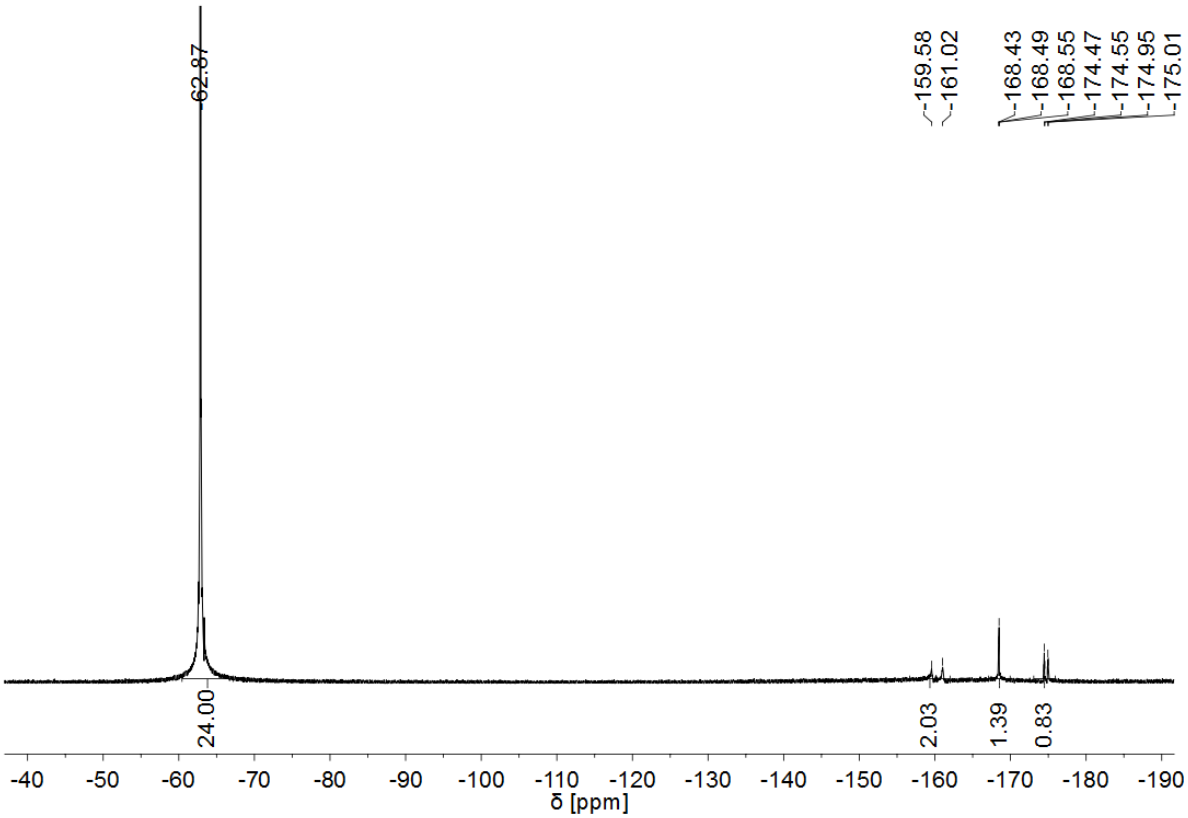

Figure A 27: ^{19}F NMR spectrum of **Mo-5** (376 MHz, $CDCl_3$).

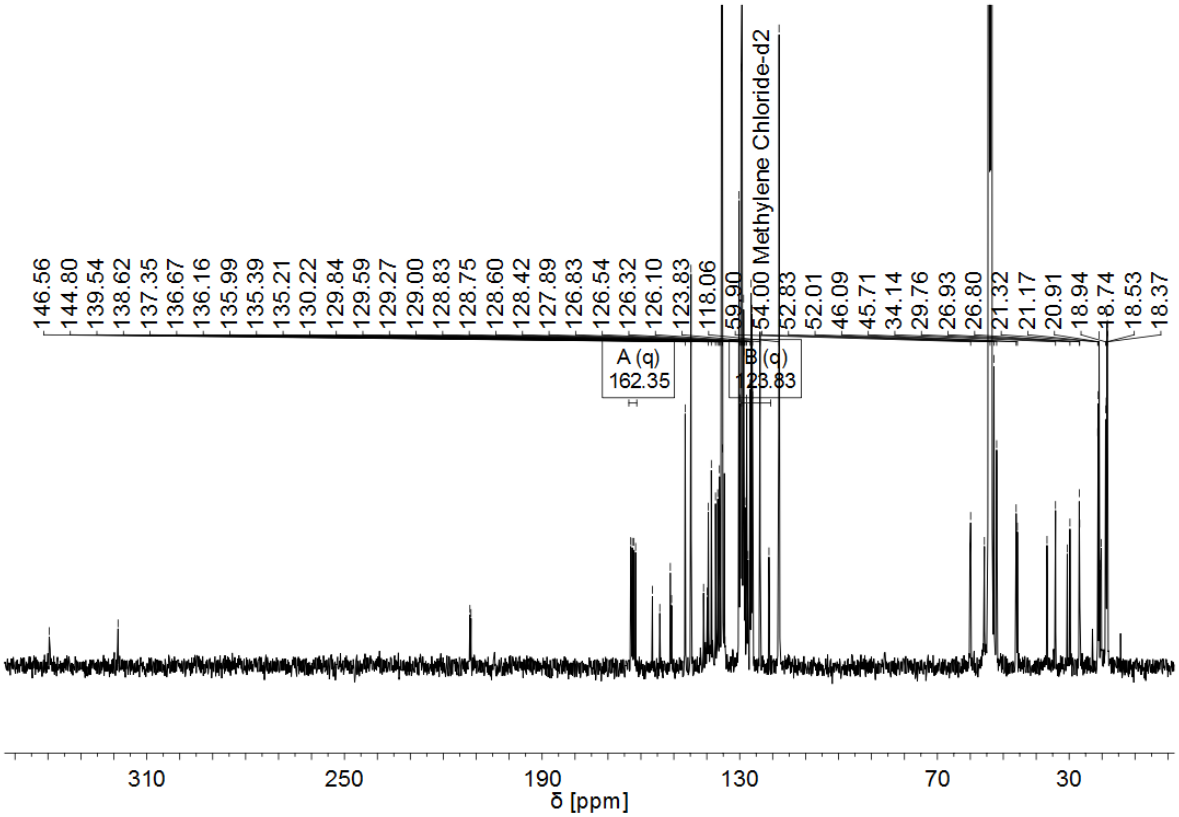

Figure A 28: ^{13}C NMR spectrum of **Mo-5** (101 MHz, CD_2Cl_2).

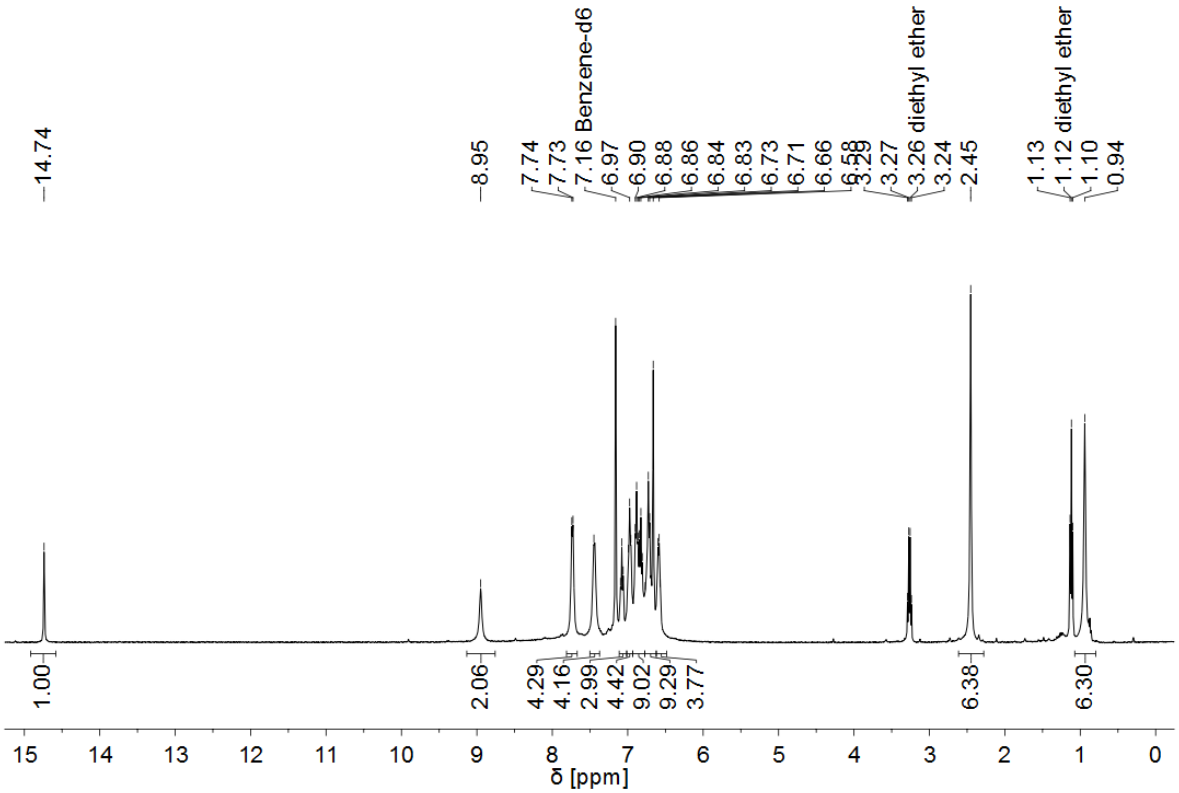

Figure A 29: ^{1}H NMR spectrum of **Mo-6b** (400 MHz, C_6D_6).

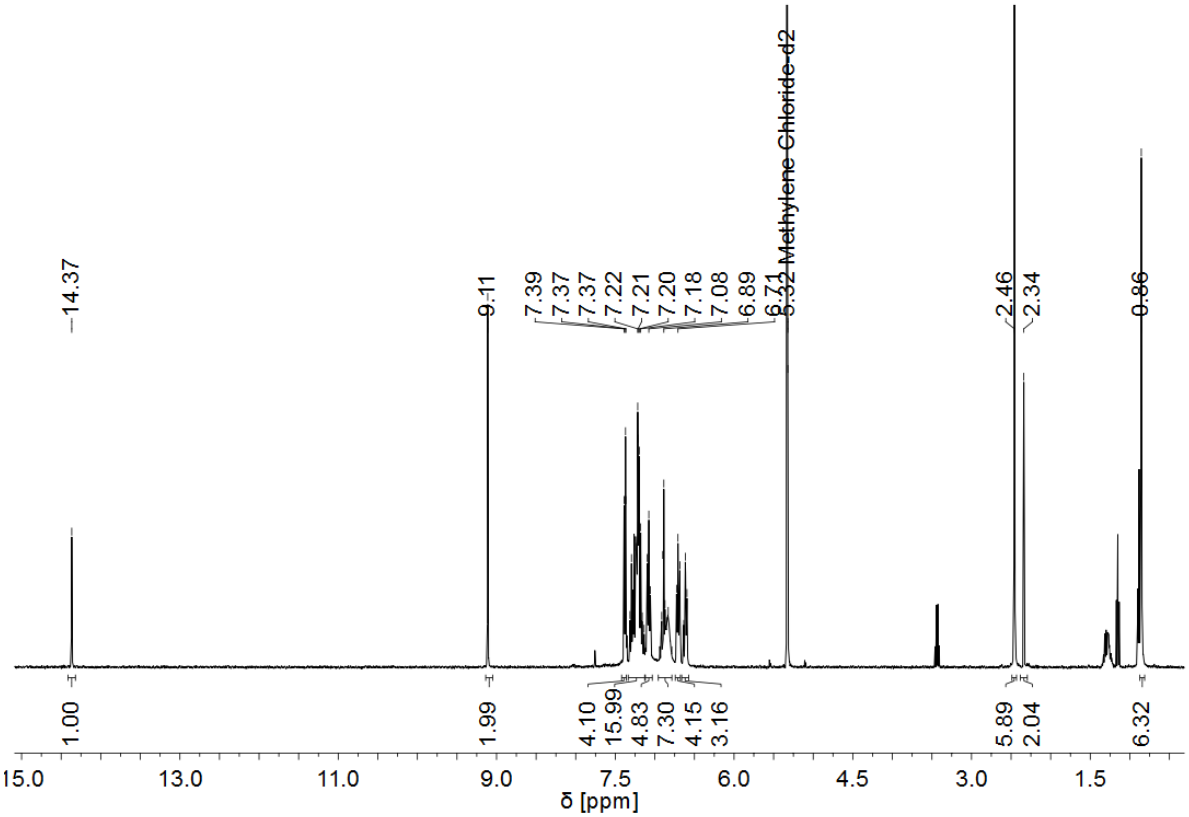

Figure A 30: ^{1}H NMR spectrum of **Mo-6a** (400 MHz, CD_2Cl_2).

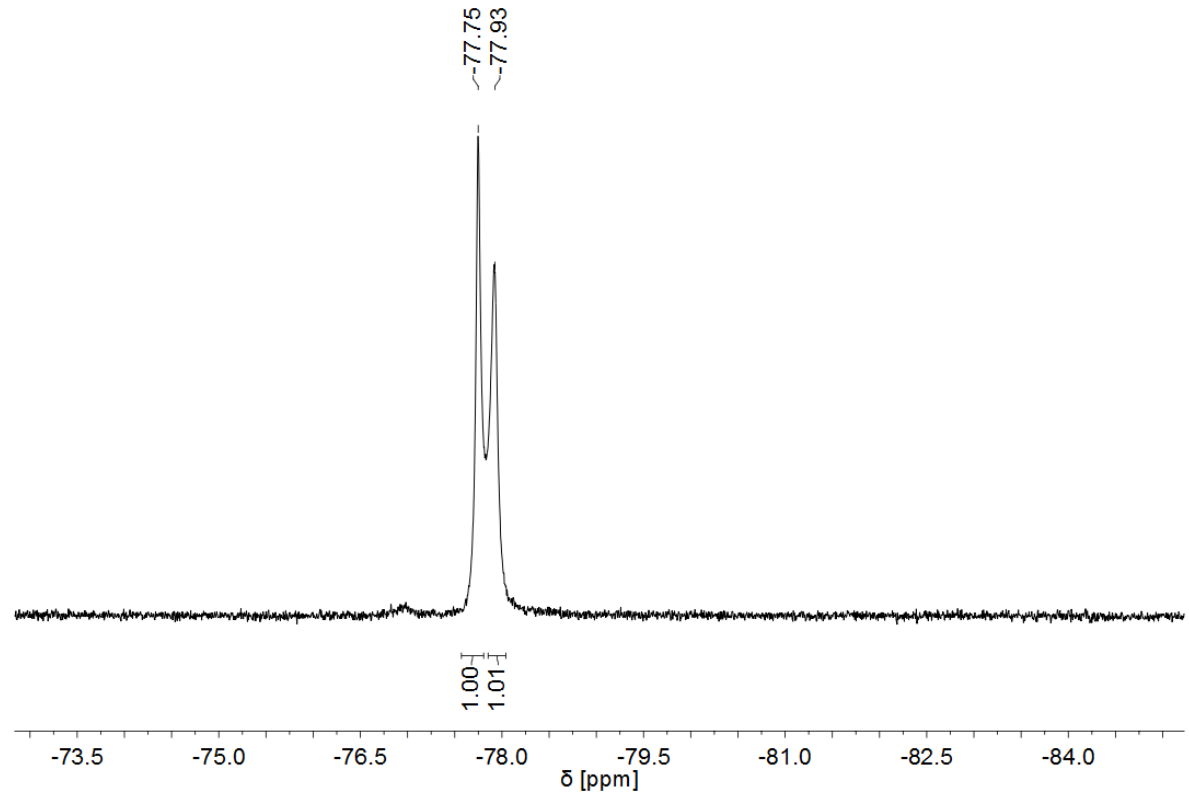

Figure A 31: ^{19}F NMR spectrum of **Mo-6b** (376 MHz, C_6D_6).

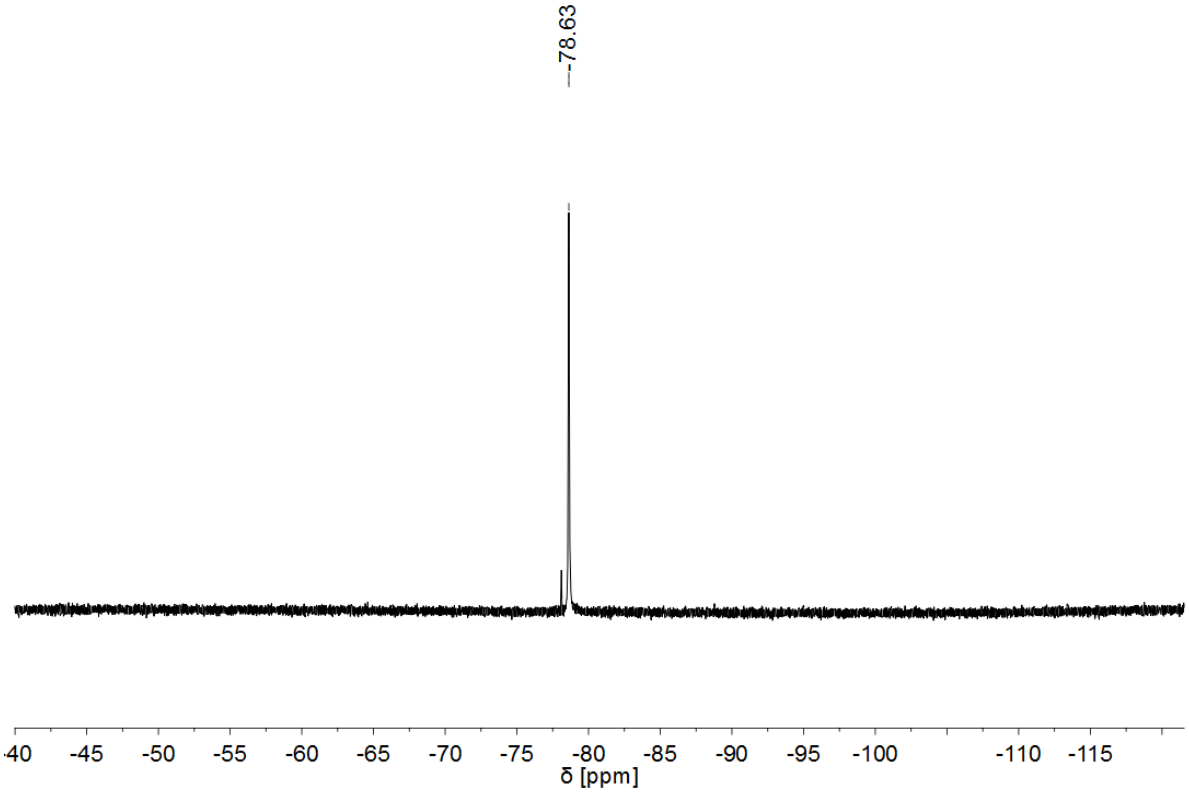

Figure A 32: ^{19}F NMR spectrum of **Mo-6a** (376 MHz, CD_2Cl_2).

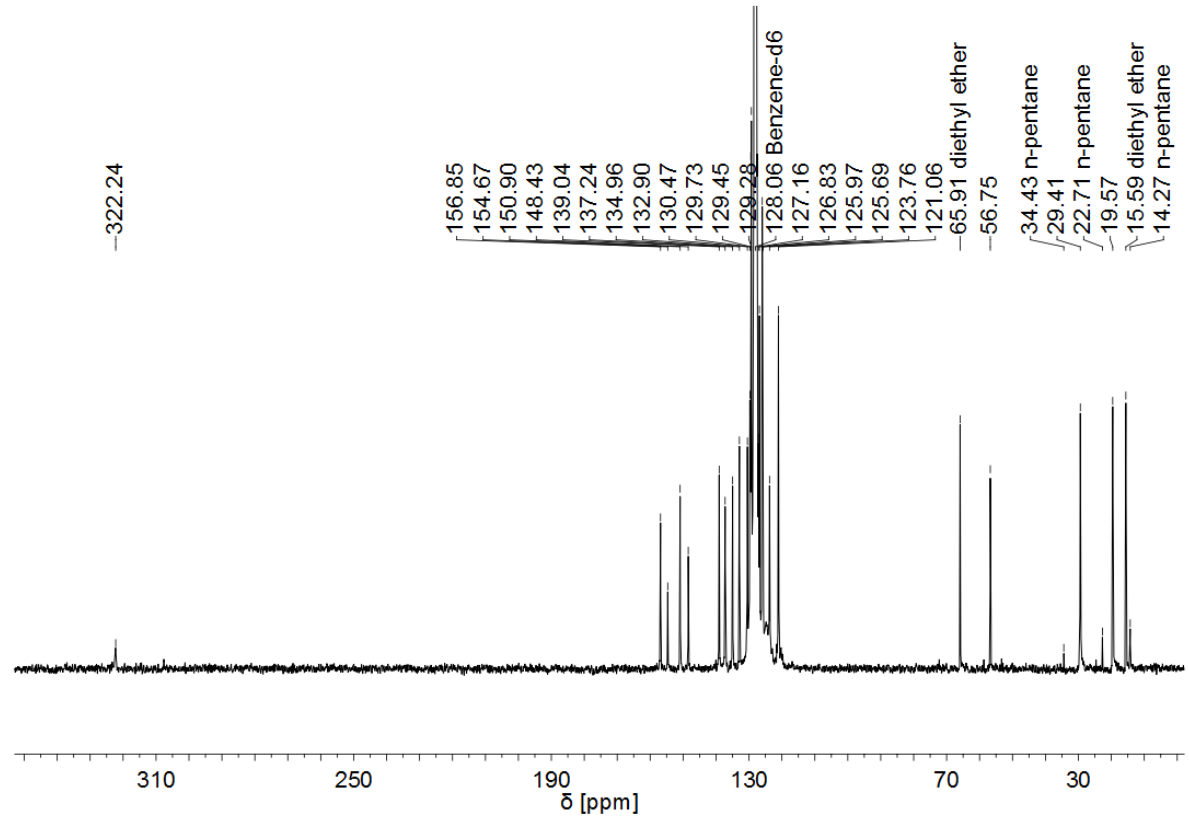

Figure A 33: ^{13}C NMR spectrum of **Mo-6** (101 MHz, C_6D_6).

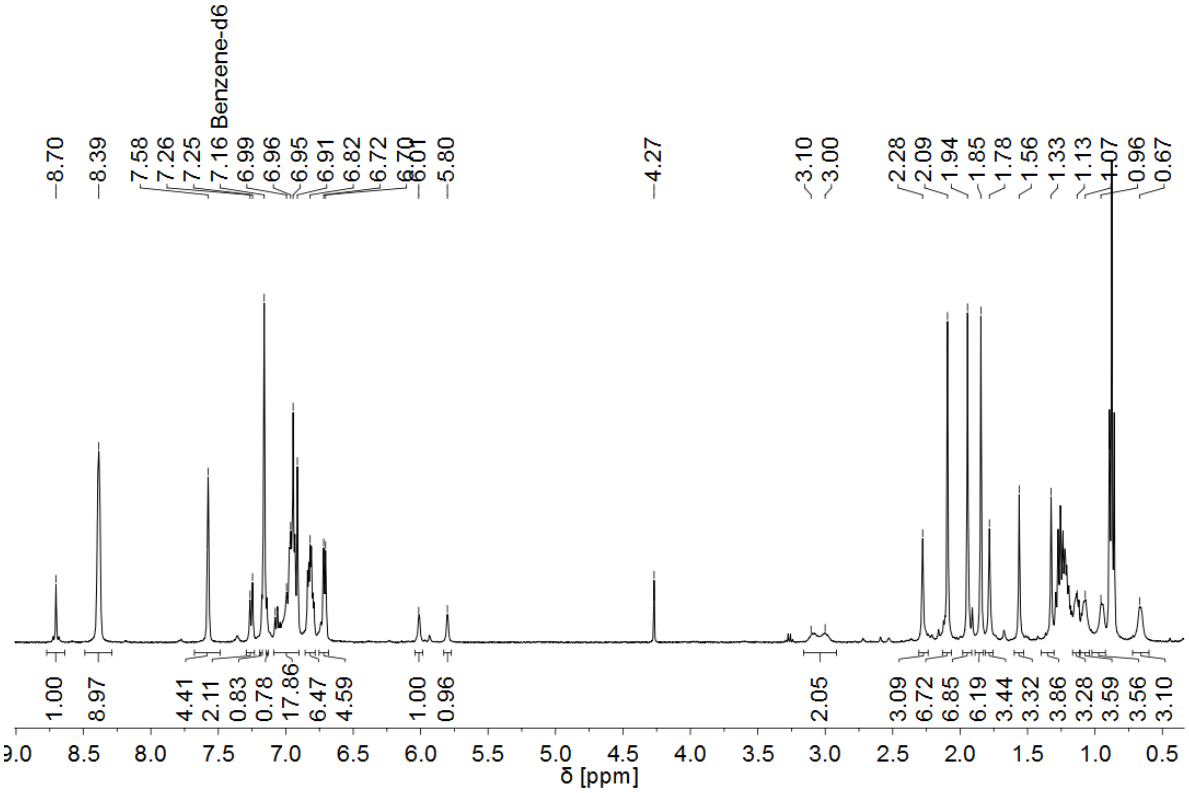

Figure A 34: ^{1}H NMR spectrum of **W-2** (400 MHz, C_6D_6).

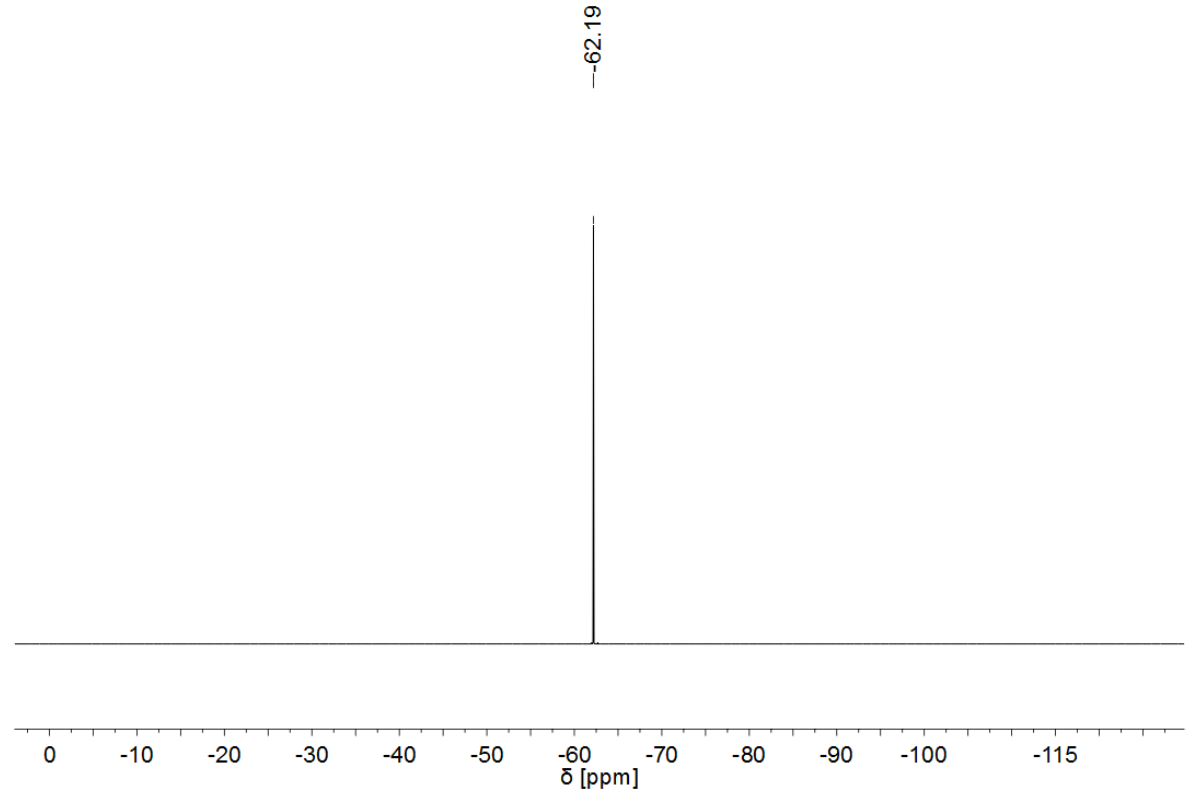

Figure A 35: ^{19}F NMR spectrum of **W-2** (376 MHz, C_6D_6).

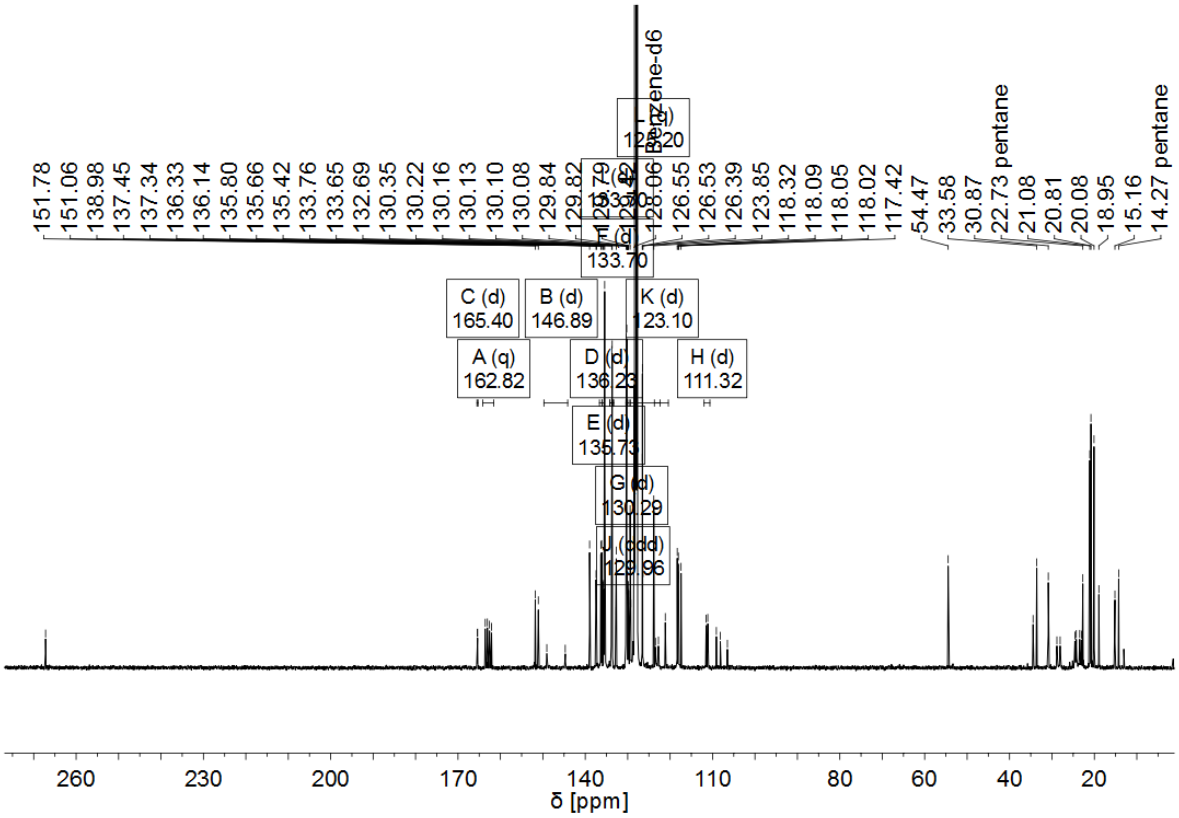

Figure A 36: ^{13}C NMR spectrum of **W-2** (101 MHz, C_6D_6).

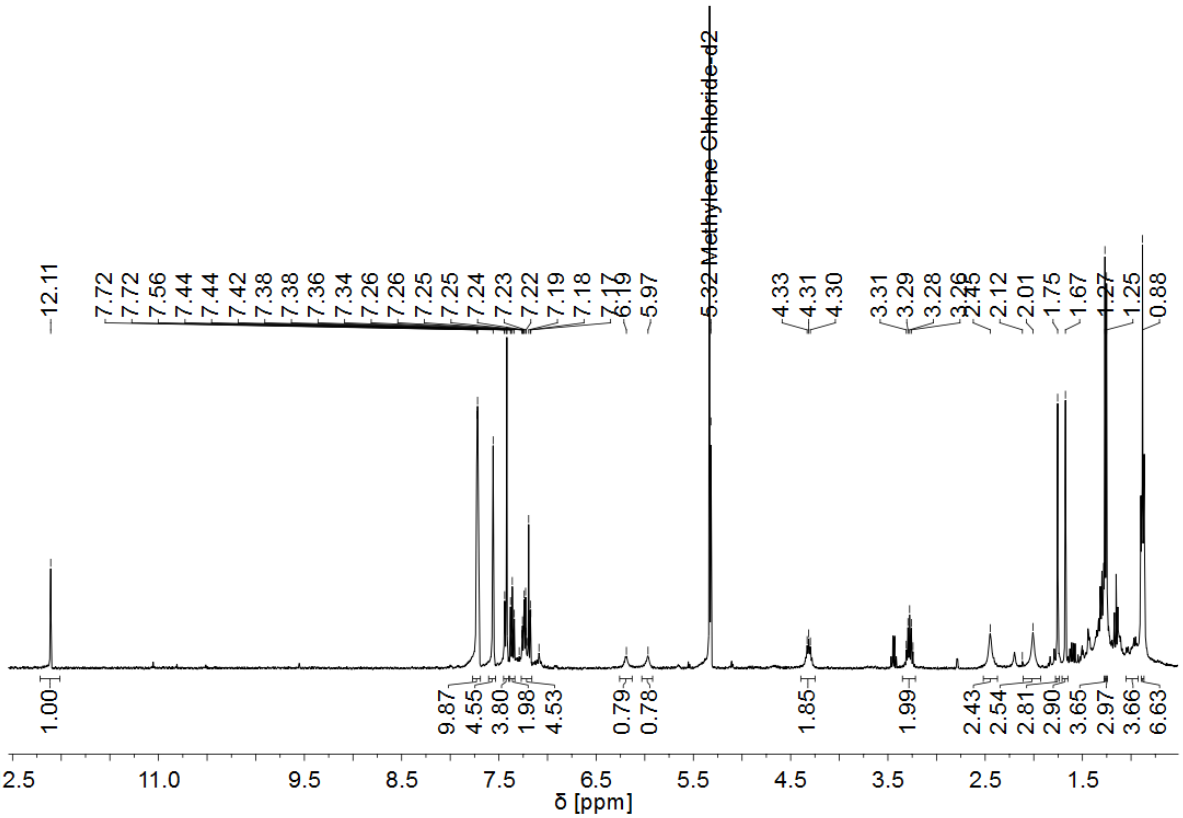

Figure A 37: ^{1}H NMR spectrum of **W-4** (400 MHz, CD_2Cl_2).

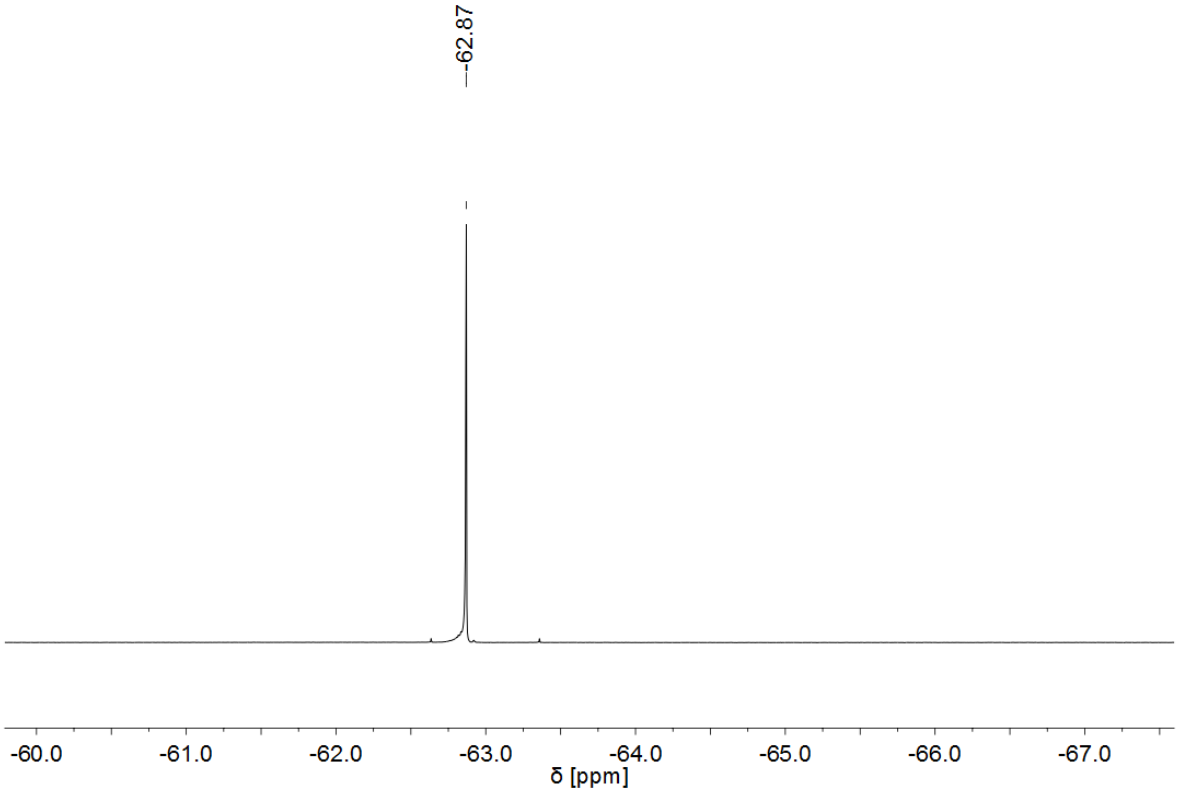

Figure A 38: ^{19}F NMR spectrum of **W-4** (376 MHz, CD_2Cl_2).

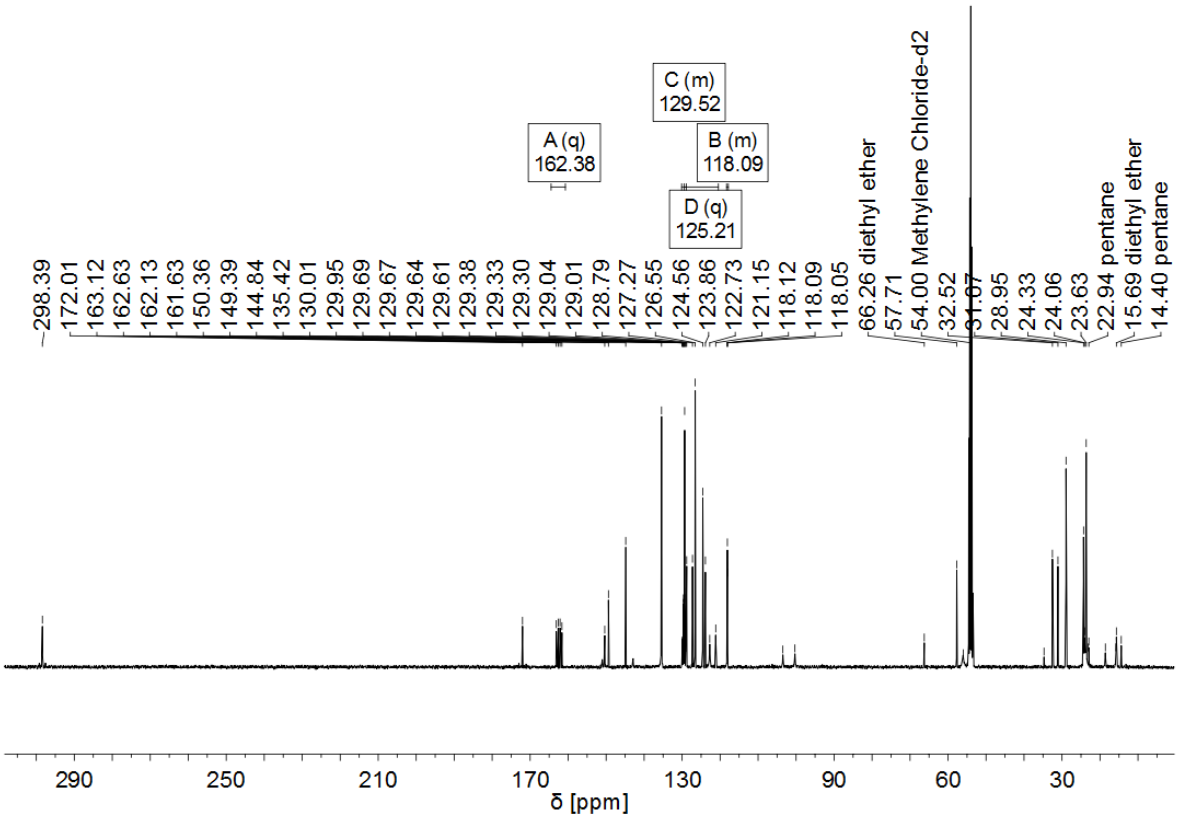

Figure A 39: ^{13}C NMR spectrum of **W-4** (101 MHz, CD_2Cl_2).

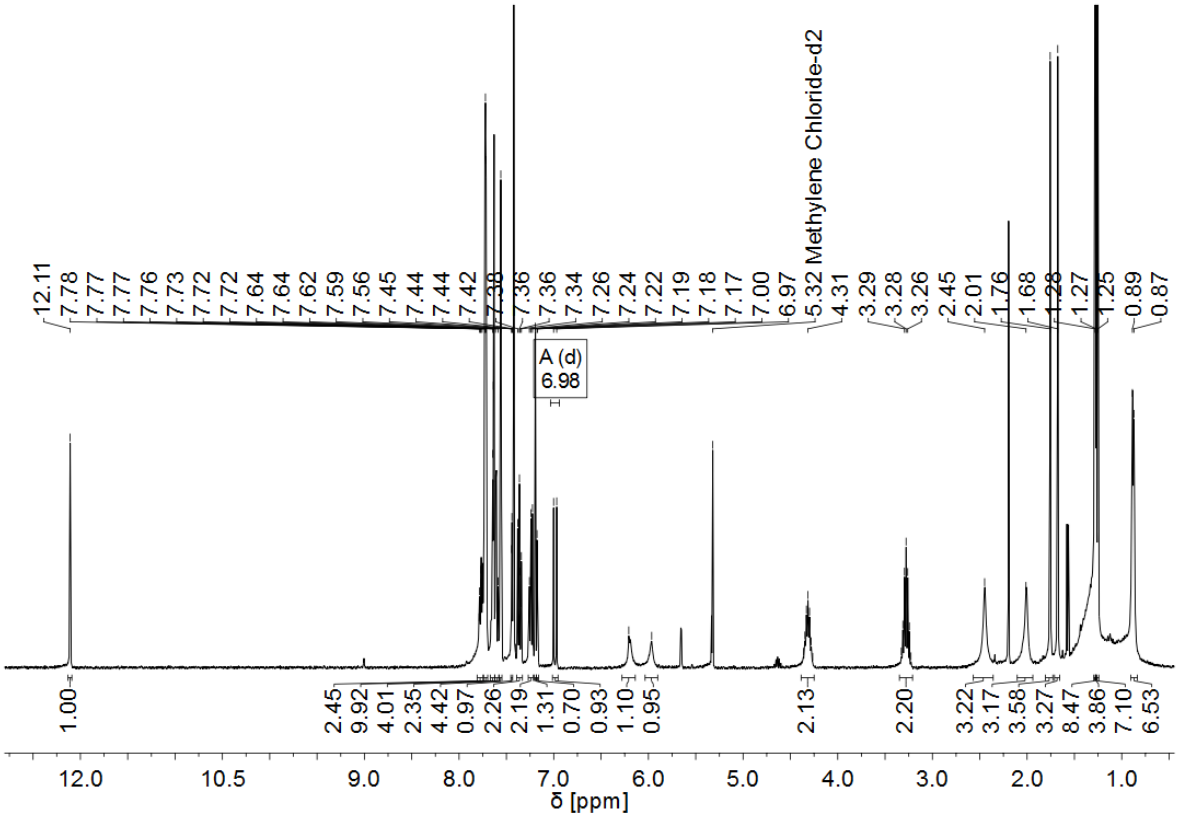

Figure A 40: ^{1}H NMR spectrum of **W-5** (400 MHz, CD_2Cl_2).

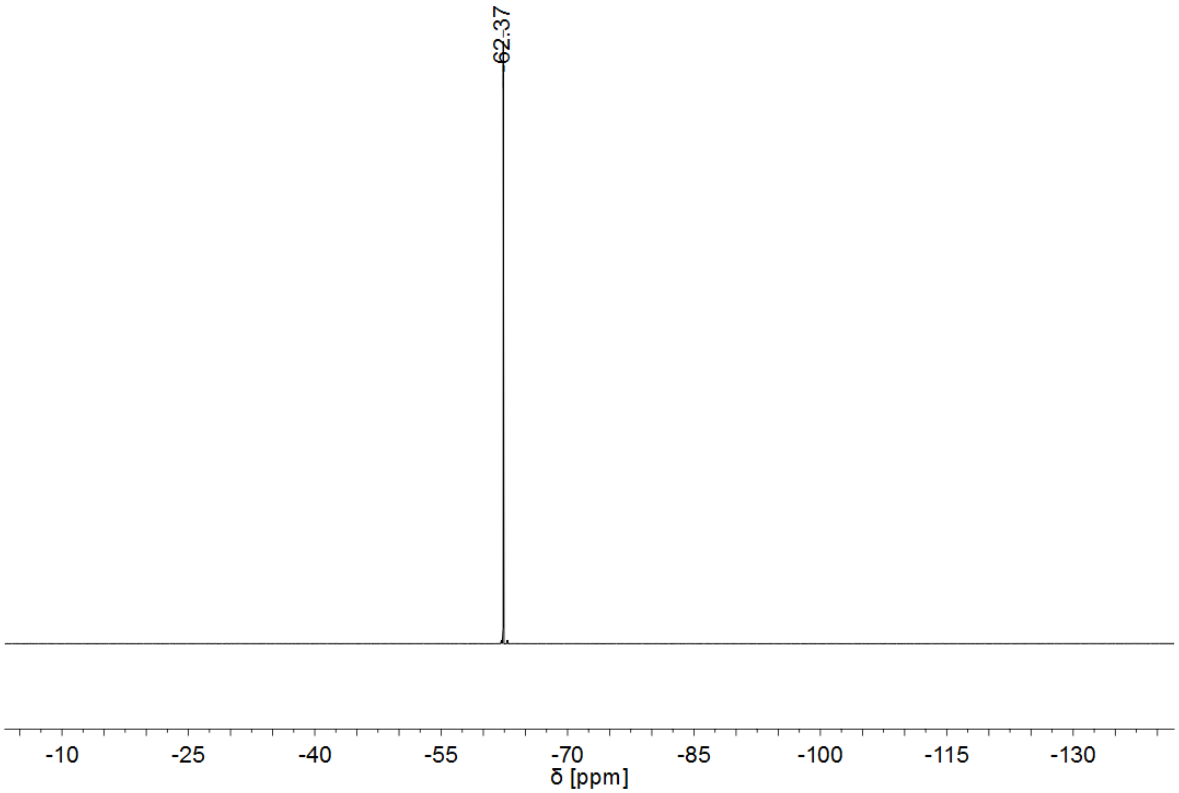

Figure A 41: ^{19}F NMR spectrum of **W-5** (376 MHz, CD_2Cl_2).

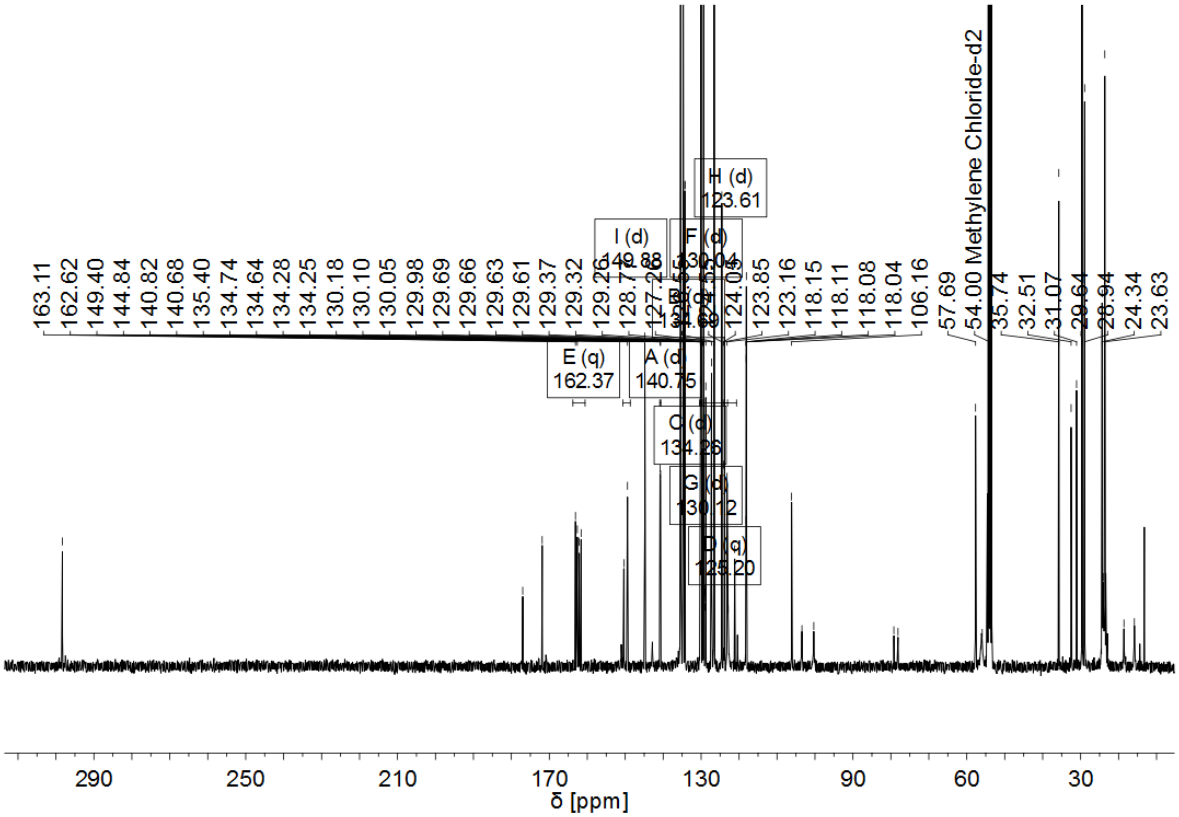

Figure A 42: ^{13}C NMR spectrum of **W-5** (101 MHz, CD_2Cl_2).

9.1.2 NMR EXPERIMENT WITH ***Mo-1*** AND ***Mo-3***

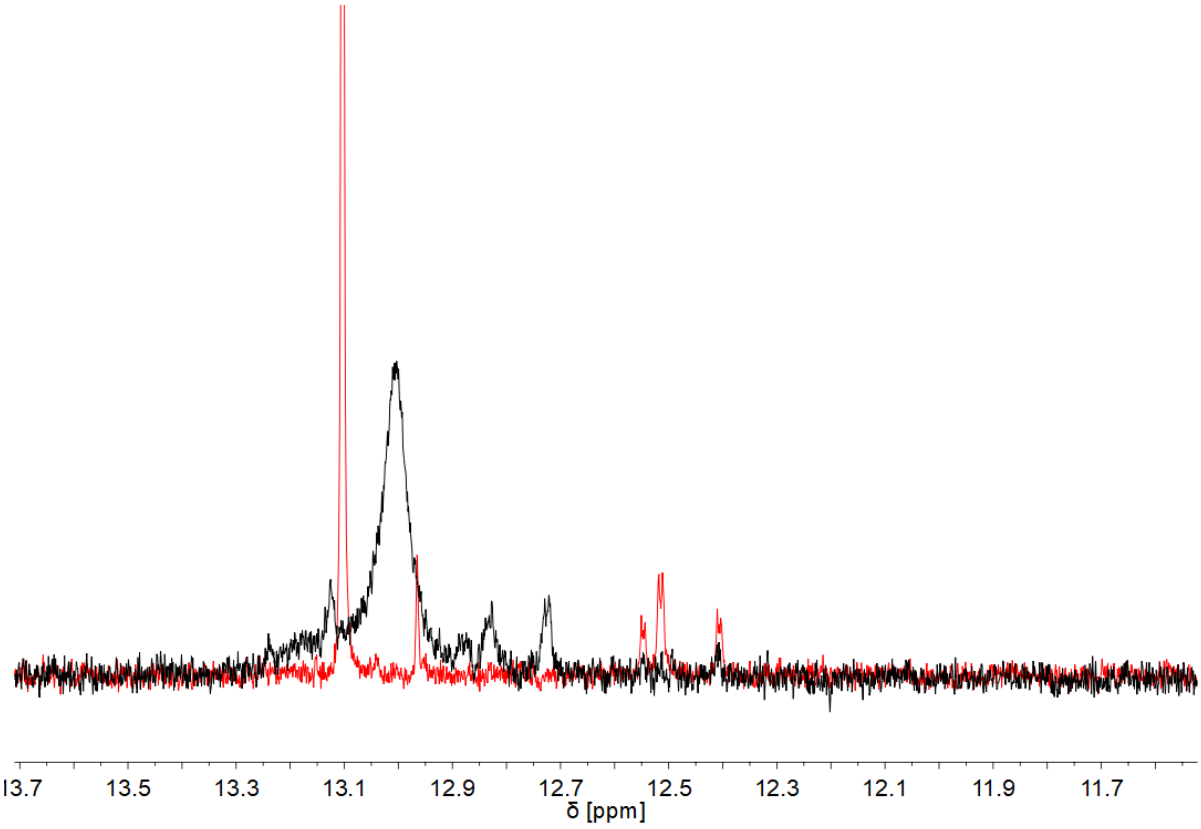

Figure A 43: Stacked ^{1}H NMR spectra in $CDCl_3$. Reaction of **Mo-1** (red) and **Mo-3** (black) with **M1**. Catalyst/substrate approximately 1/5.

9.1.3 *ANALYTICS OF POLYMERS*

Data for poly(**M1**) derived from the ROMP with Catalyst **Mo-1** have been published before.[167]

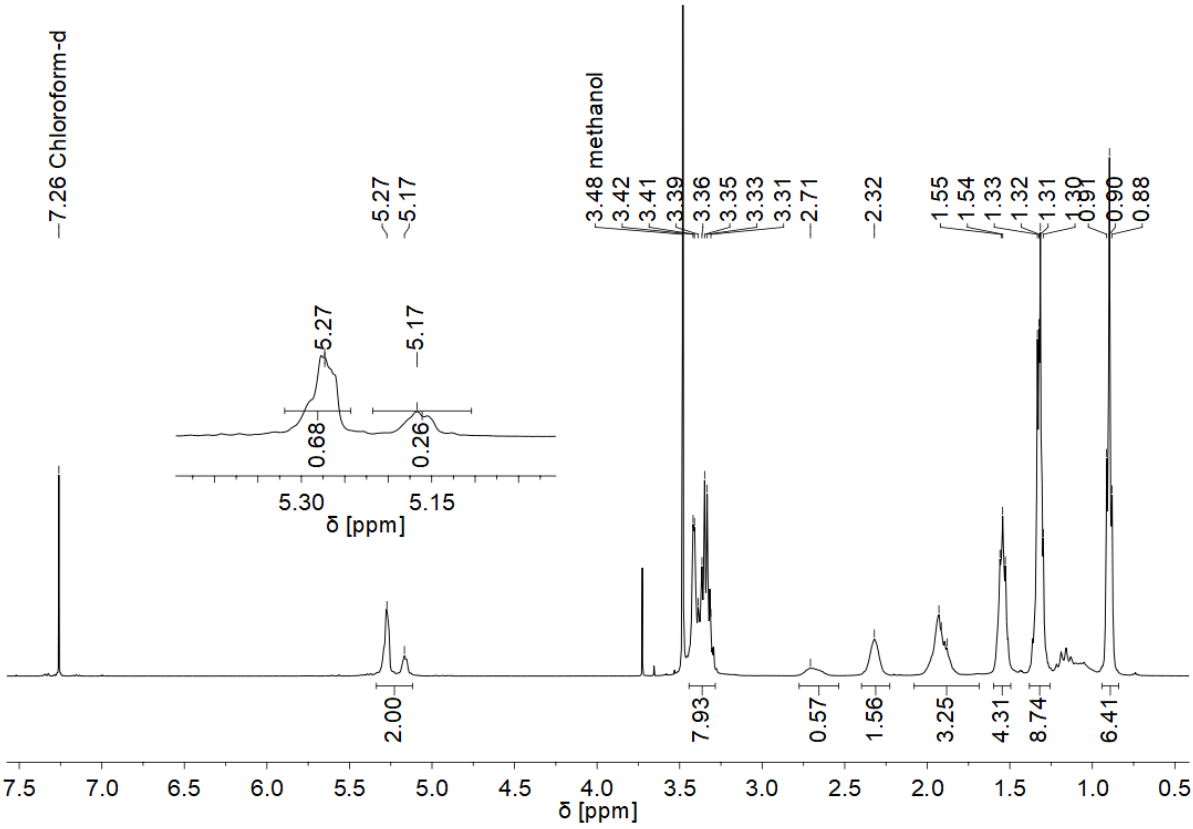

Figure A 44: ^{1}H NMR spectrum of poly(**M1**) derived from polymerization with **Mo-3** in $CDCl_3$. *Trans*-content: 70%.

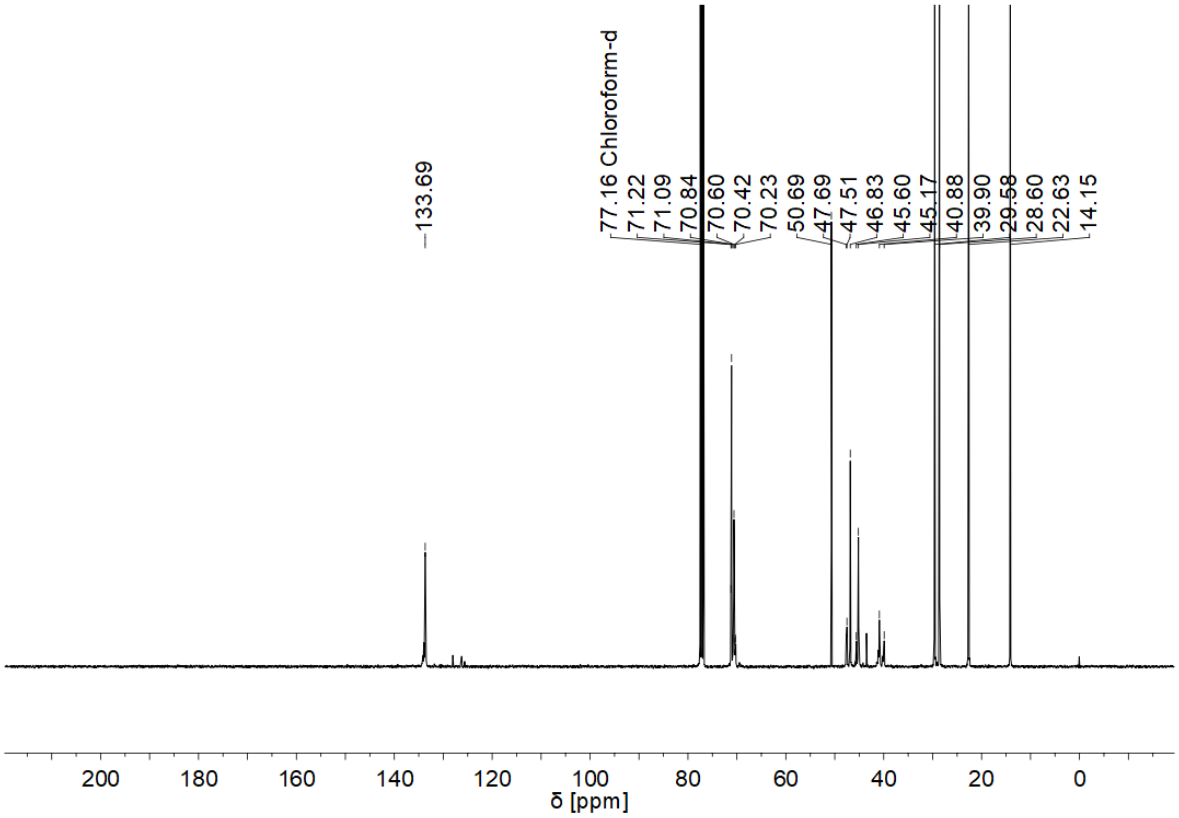

Figure A 45: ^{13}C NMR spectrum of poly(**M1**) derived from polymerization with **Mo-3** in $CDCl_3$.

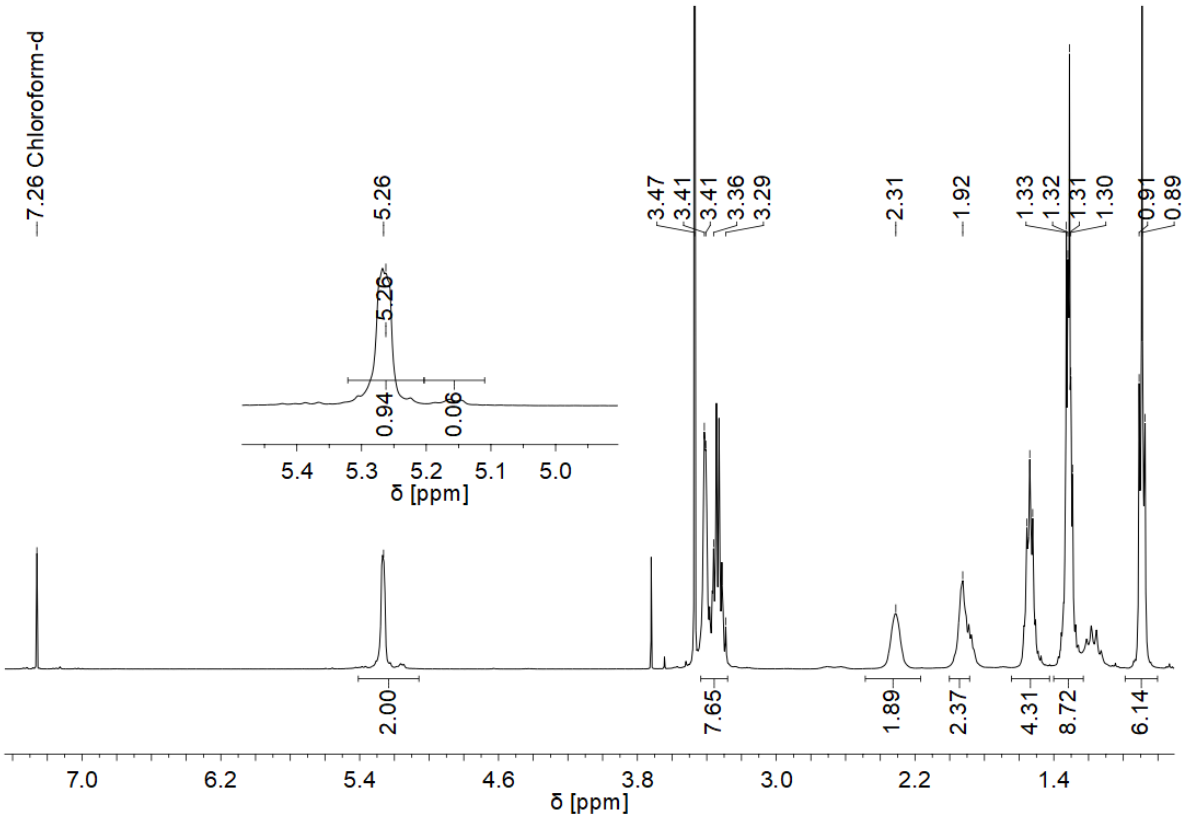

Figure A 46: ^{1}H NMR spectrum of poly(**M1**) derived from ROMP with **W-4** in $CDCl_3$. *Trans*-content: 94%.

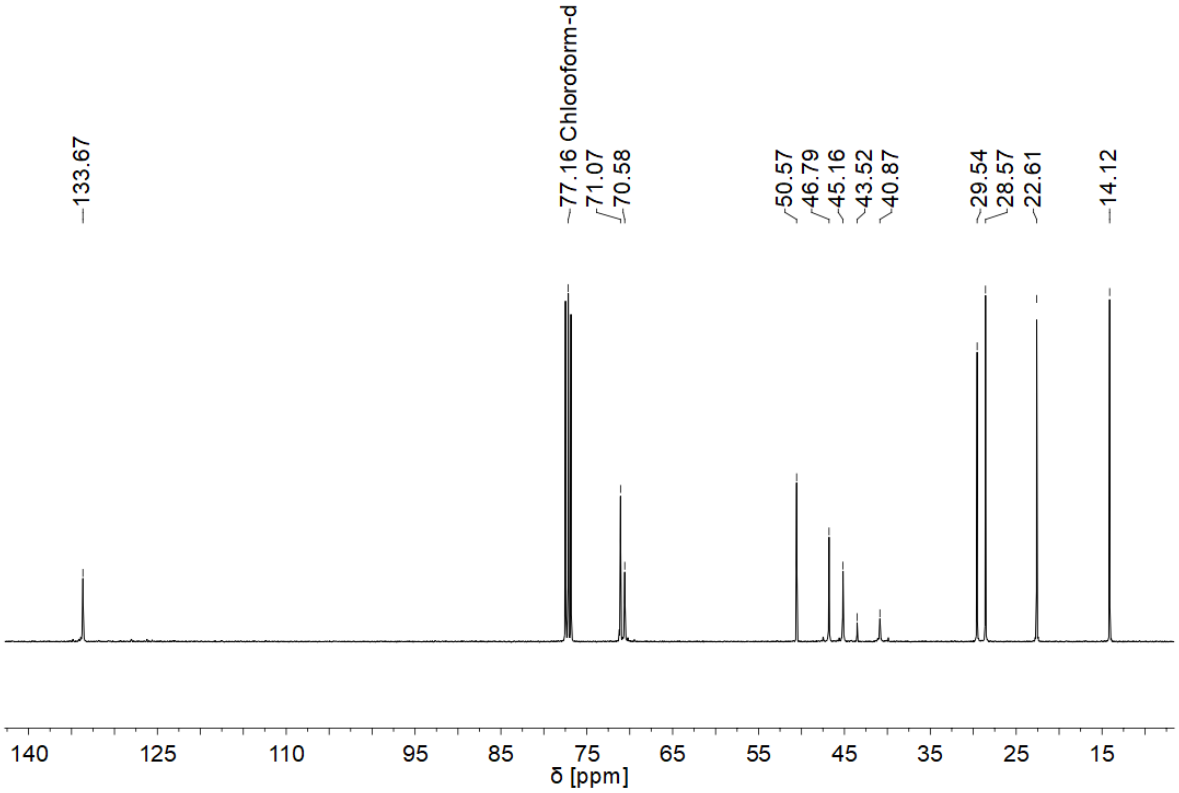

Figure A 47: ^{13}C NMR spectrum of poly(**M1**) derived from ROMP with **W-4** in $CDCl_3$.

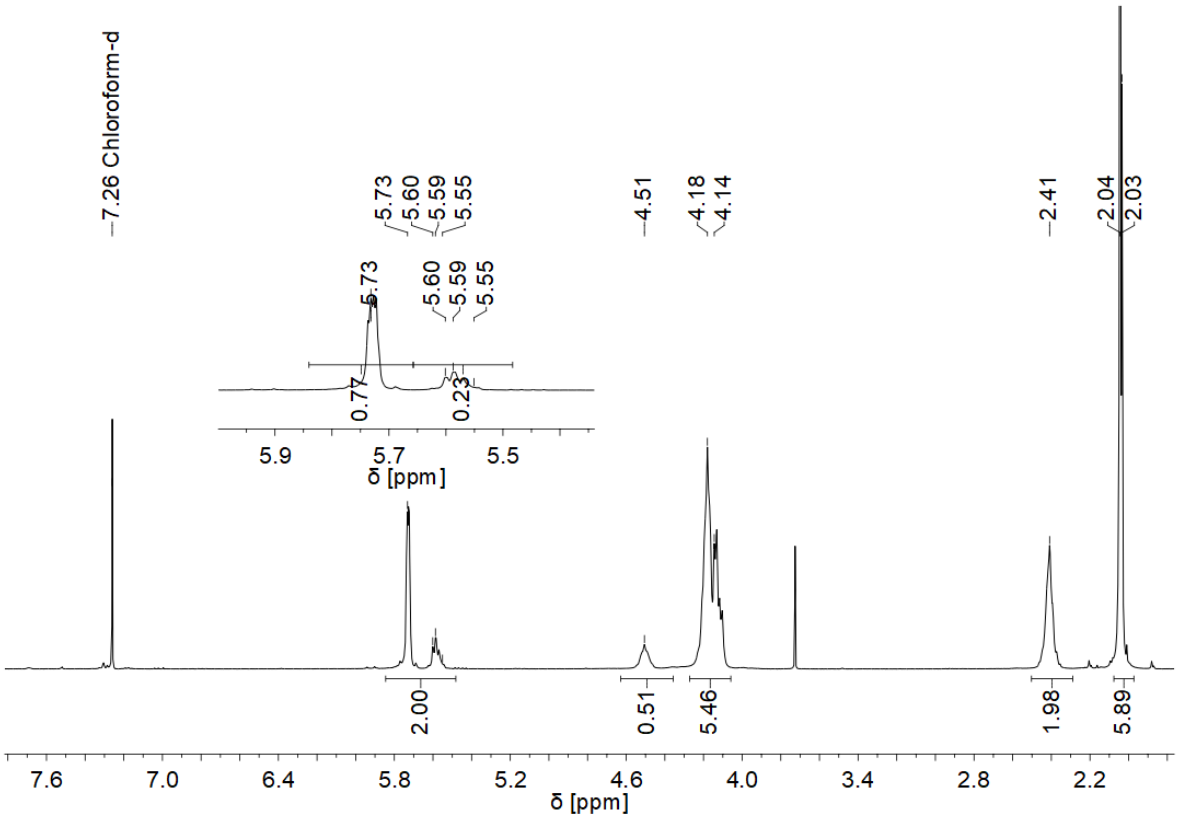

Figure A 48: ^{1}H NMR spectrum of poly(**M2**) derived from ROMP with **W-4** in $CDCl_3$. *Trans*-content: 77%.

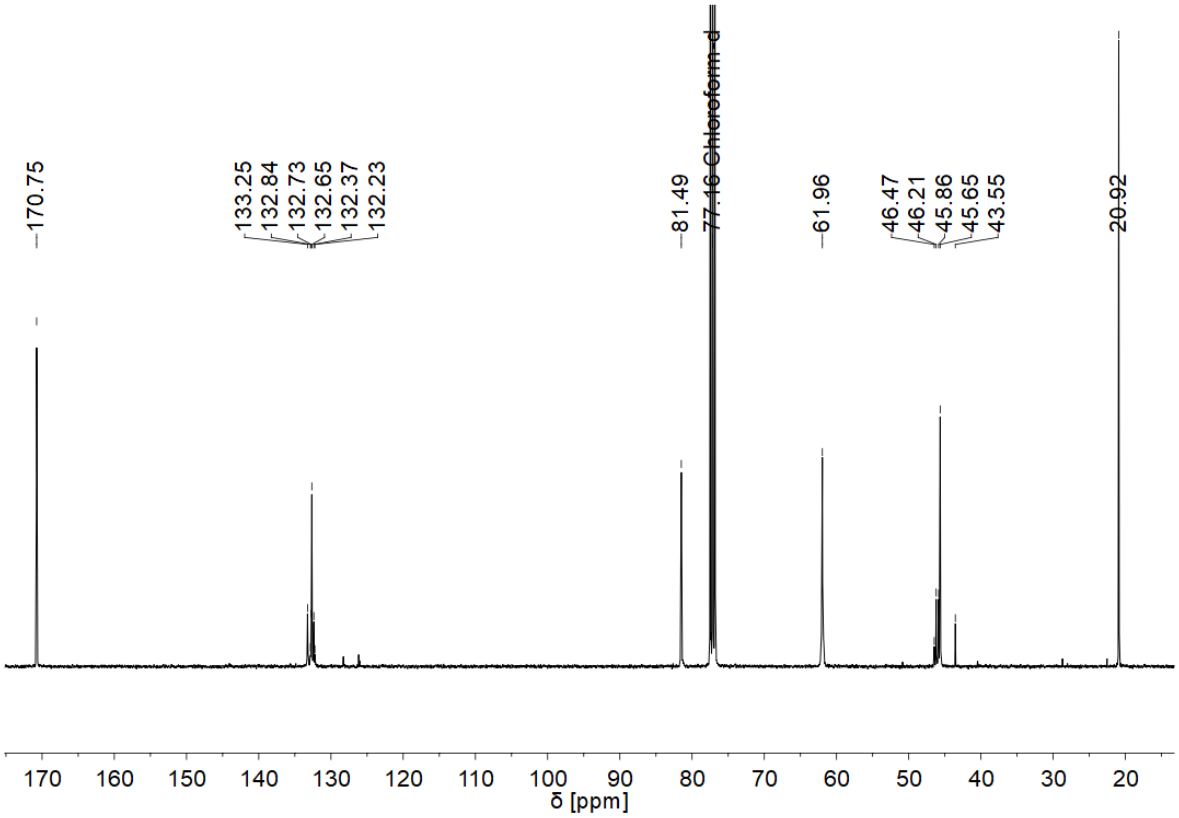

Figure A 49: ^{13}C NMR spectrum of poly(**M2**) derived from ROMP with **W-4** in $CDCl_3$.

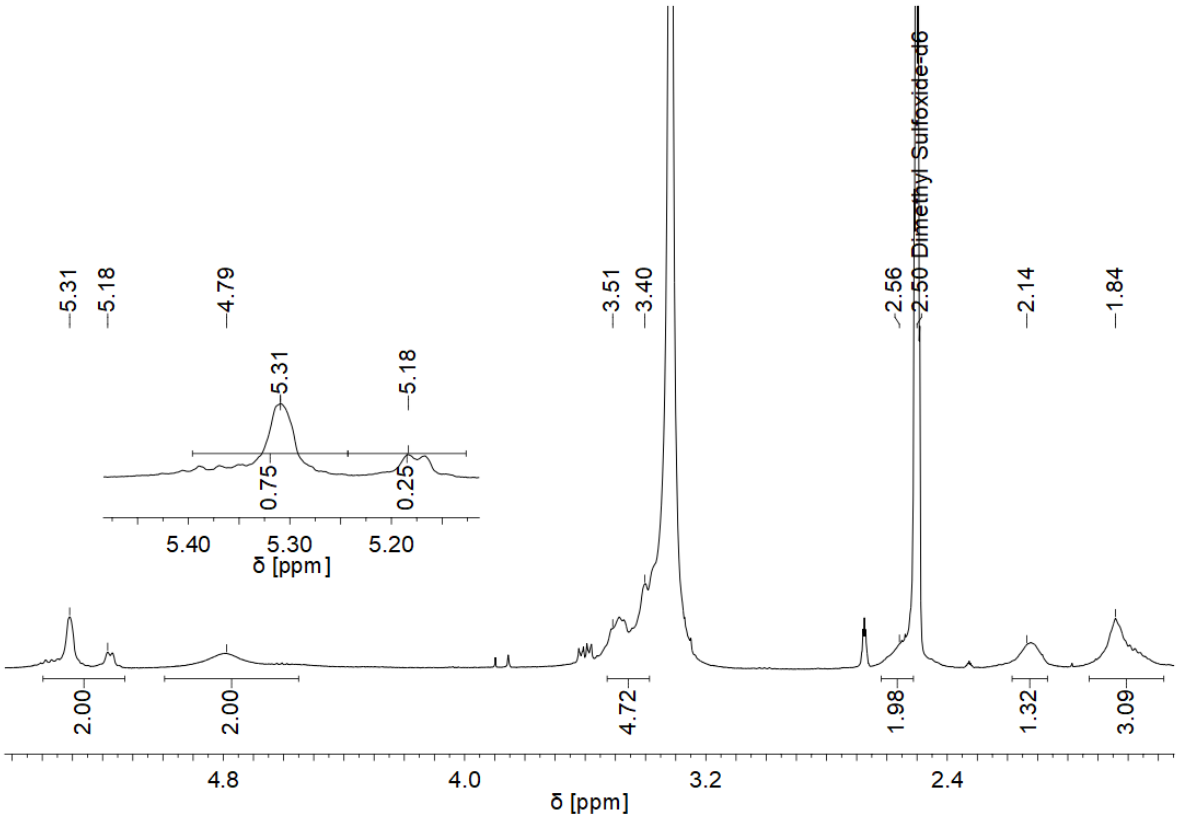

Figure A 50: ^{1}H NMR spectrum of poly(**M3**) derived from ROMP with **W-4** in DMSO-d6. *Trans*-content: 75%.

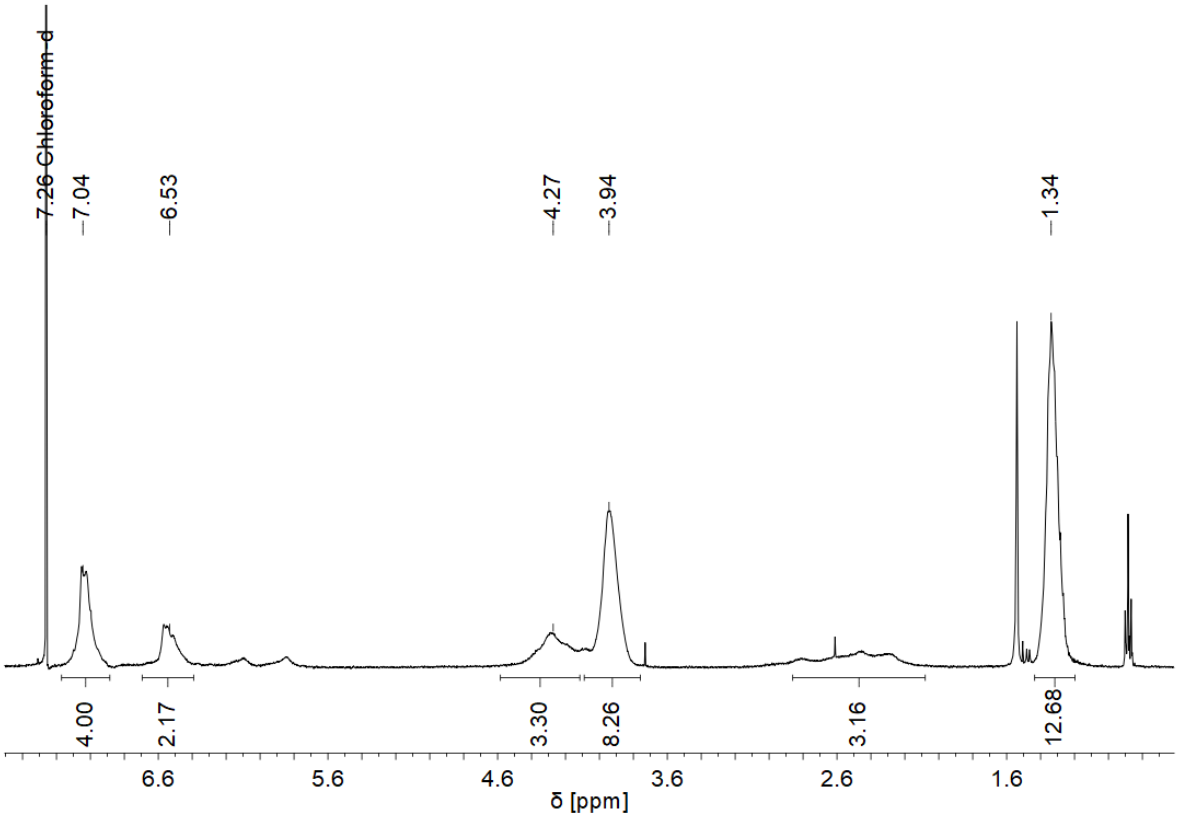

Figure A 51: ^{1}H NMR spectrum of poly(**M9**) derived from cyclopolymerization with **W-4** in $CDCl_3$.

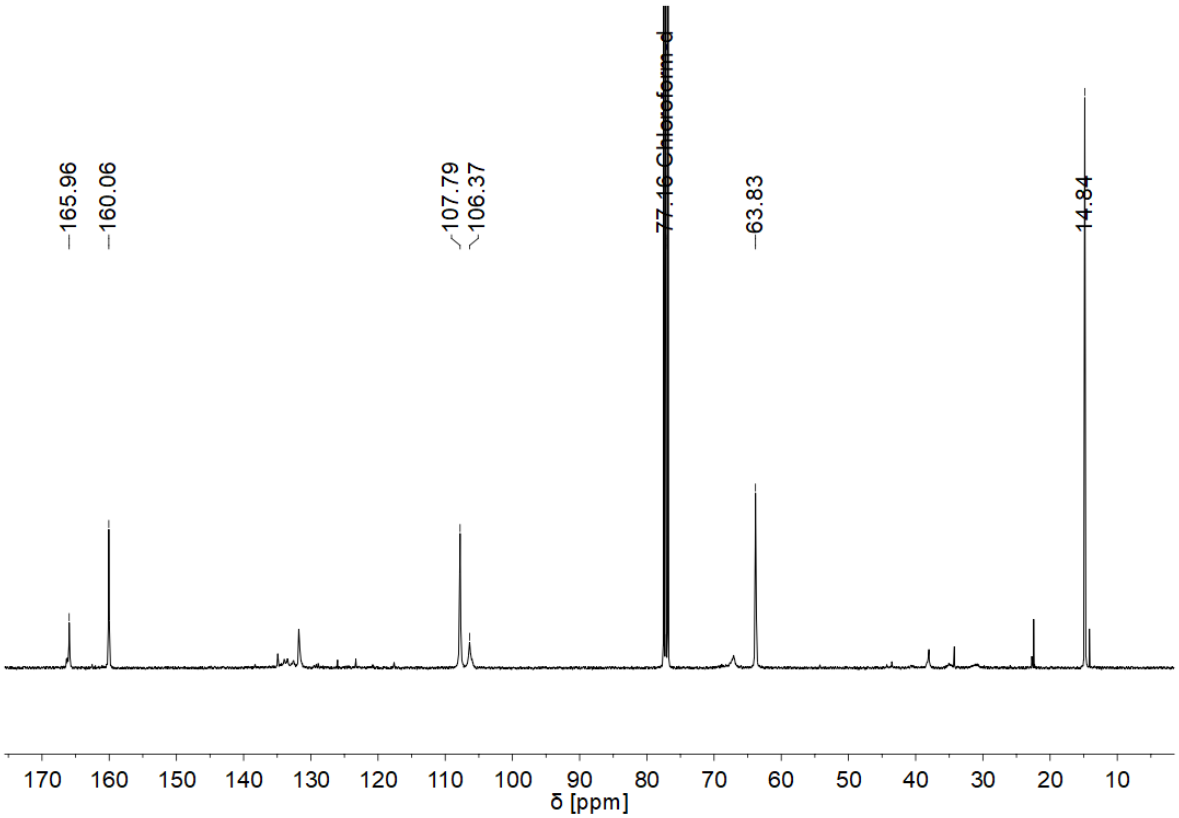

Figure A 52: ^{13}C NMR spectrum of poly(**M9**) derived from cyclopolymerization with **W-4** in $CDCl_3$.

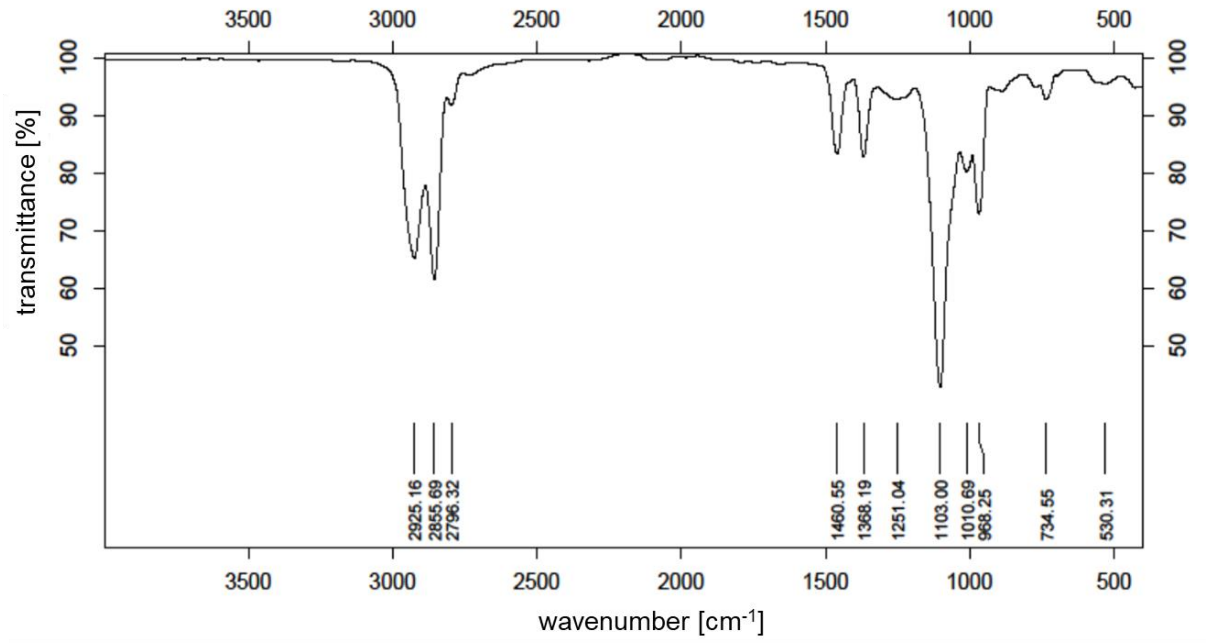

Figure A 53: IR spectrum of poly(**M1**) derived from polymerization with **W-4**.

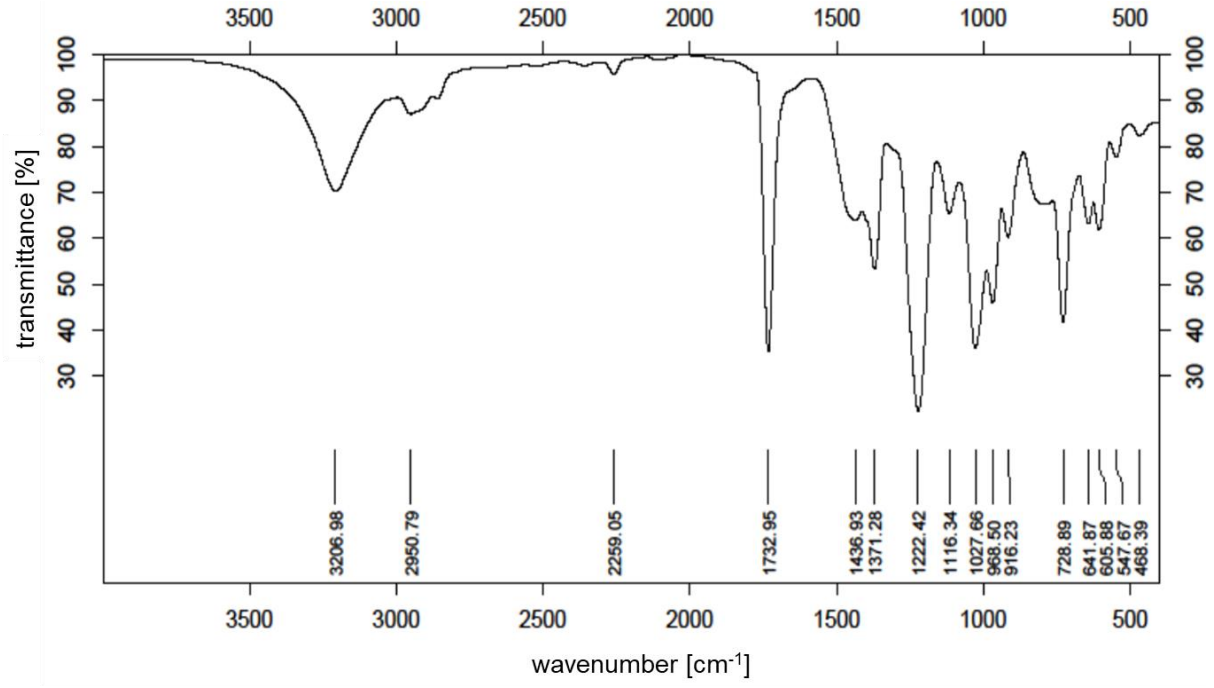

Figure A 54: IR spectrum of poly(**M2**) derived from polymerization with **W-4**.

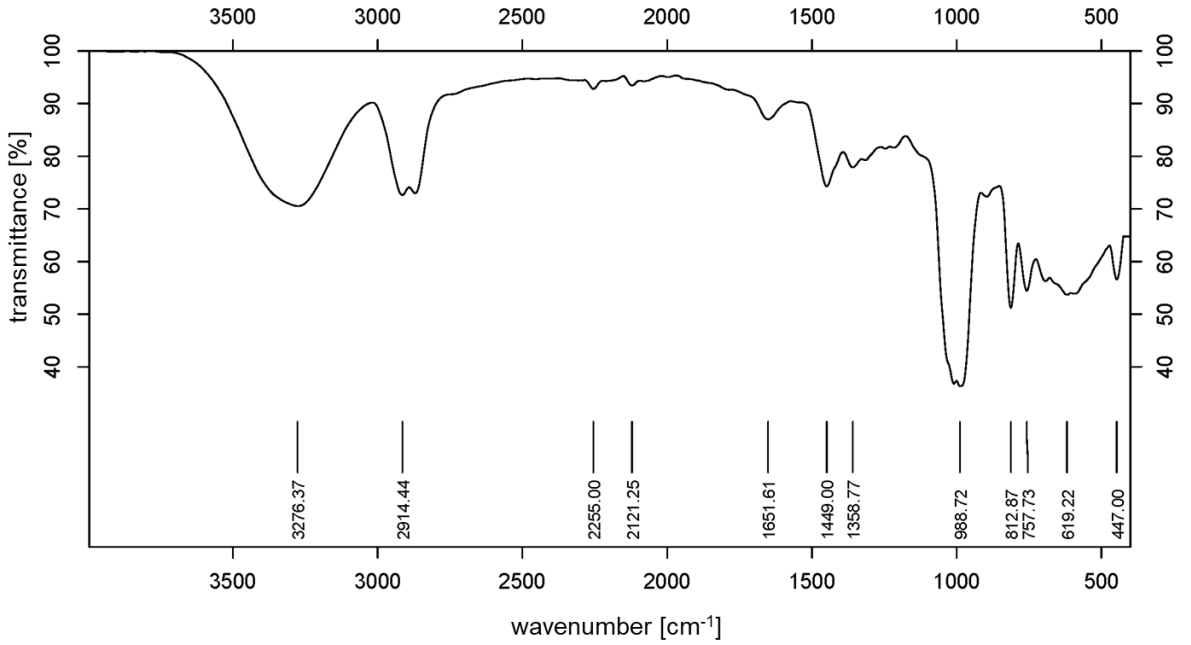

Figure A 55: IR spectrum of poly(**M3**) derived from polymerization with **W-4**.

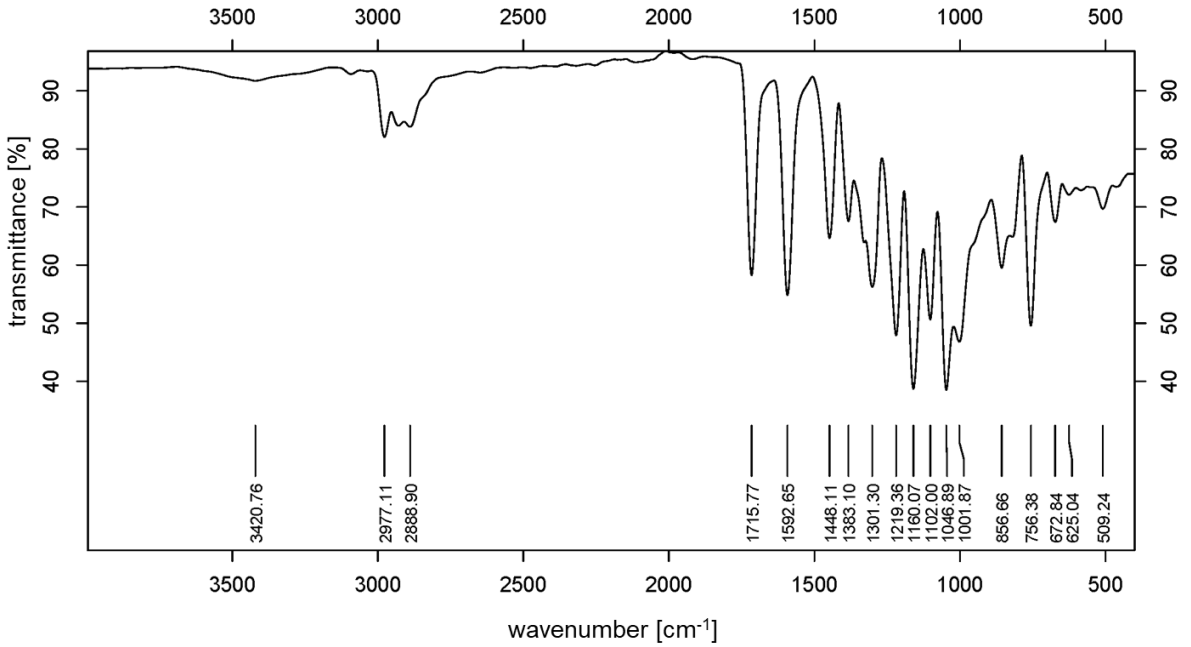

Figure A 56: IR spectrum of poly(**M4**) derived from polymerization with **W-4**.

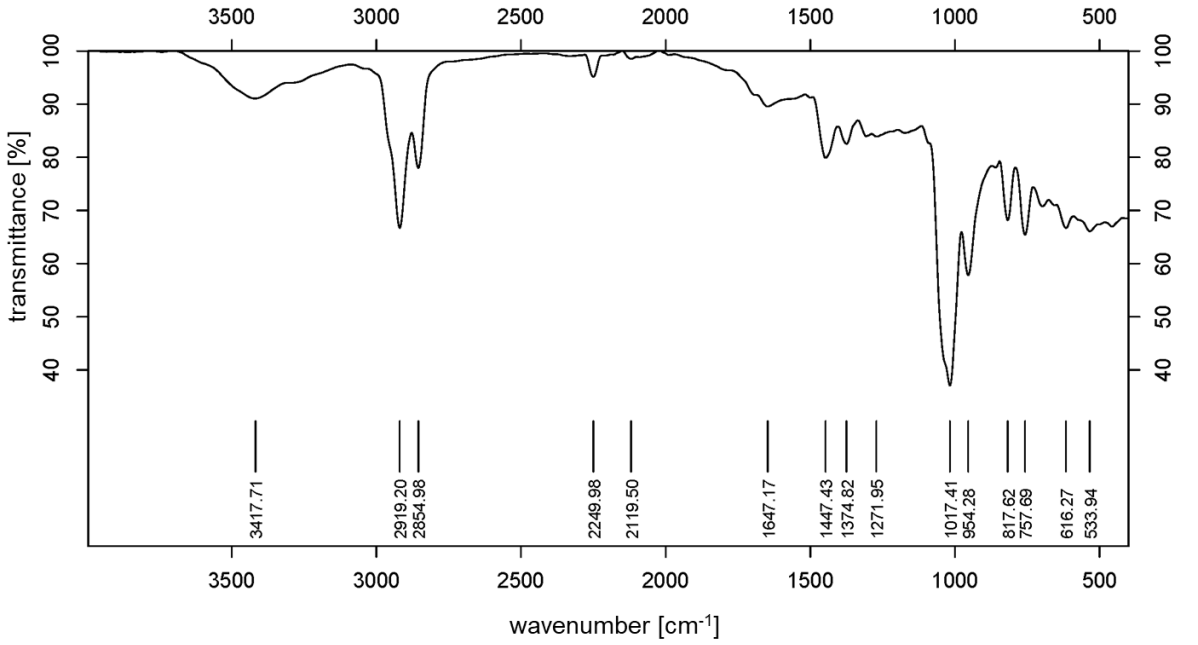

Figure A 57: IR spectrum of poly(**M5**) derived from polymerization with **W-4**.

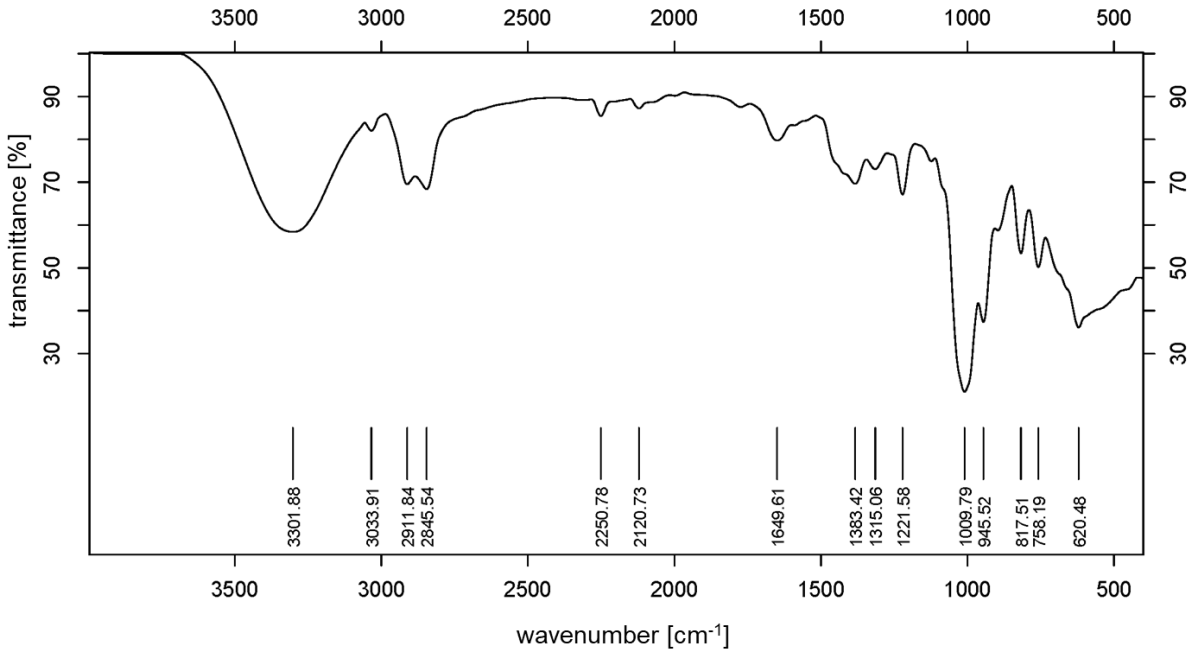

Figure A 58: IR spectrum of poly(**M6**) derived from polymerization with **W-4**.

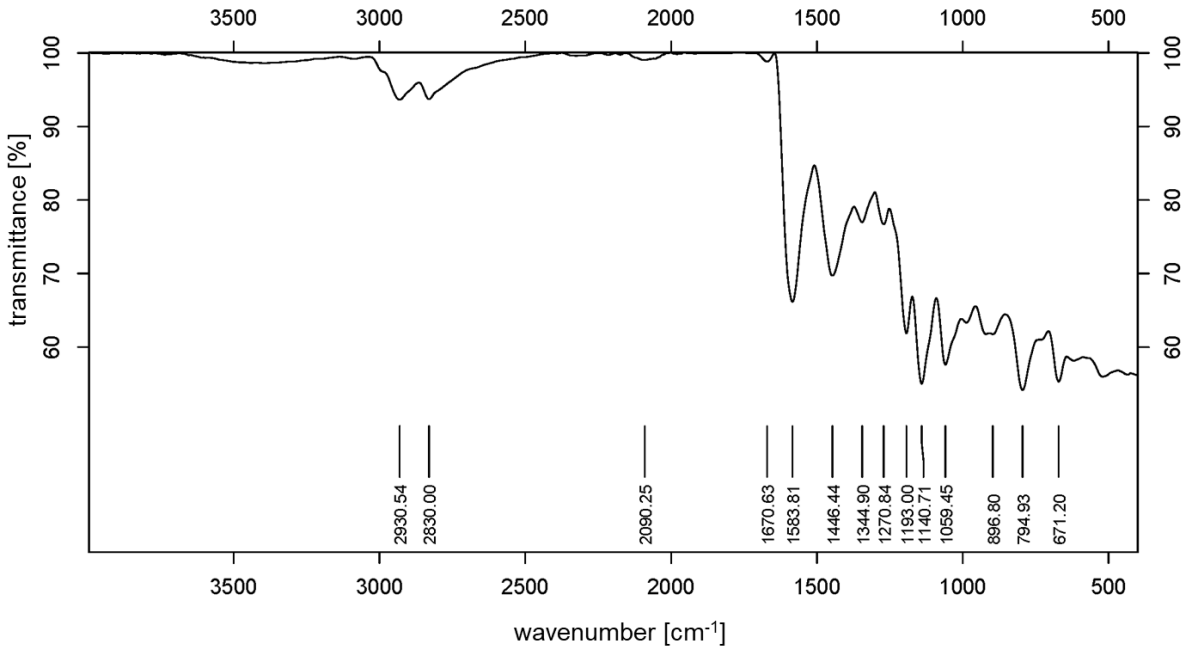

Figure A 59: IR spectrum of poly(**M7**) derived from polymerization with **W-4**.

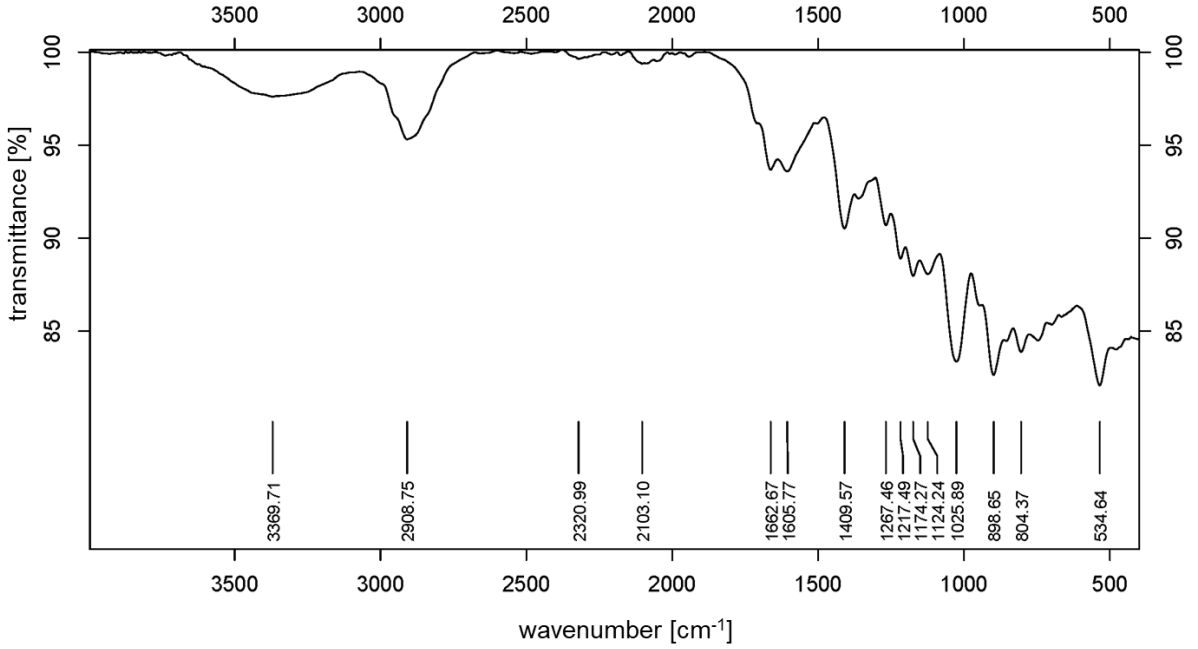

Figure A 60: IR spectrum of poly(**M8**) derived from polymerization with **W-4**.

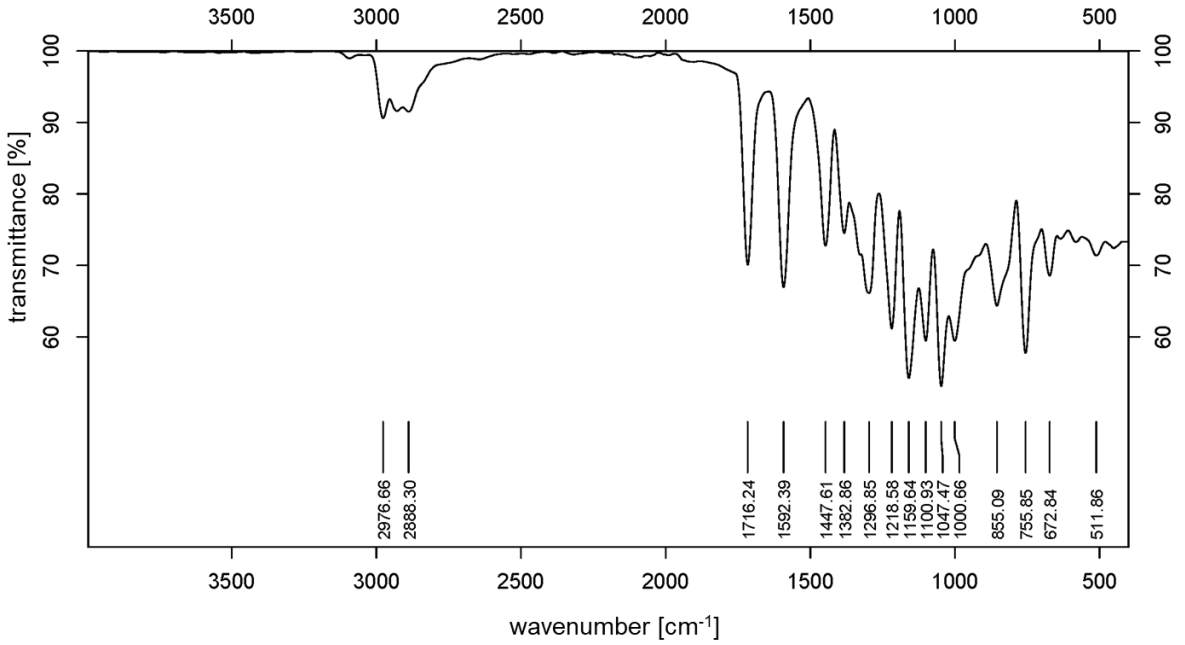

Figure A 61: IR spectrum of poly(**M9**) derived from polymerization with **W-4**.

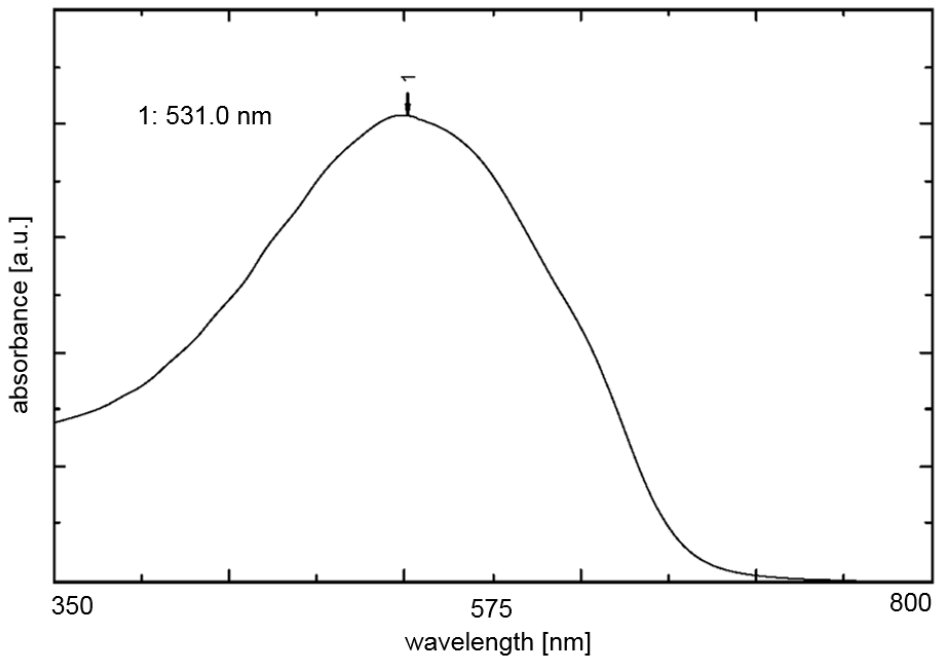

Figure A 62: UV/Vis spectrum of poly(**M5**) in DMSO.

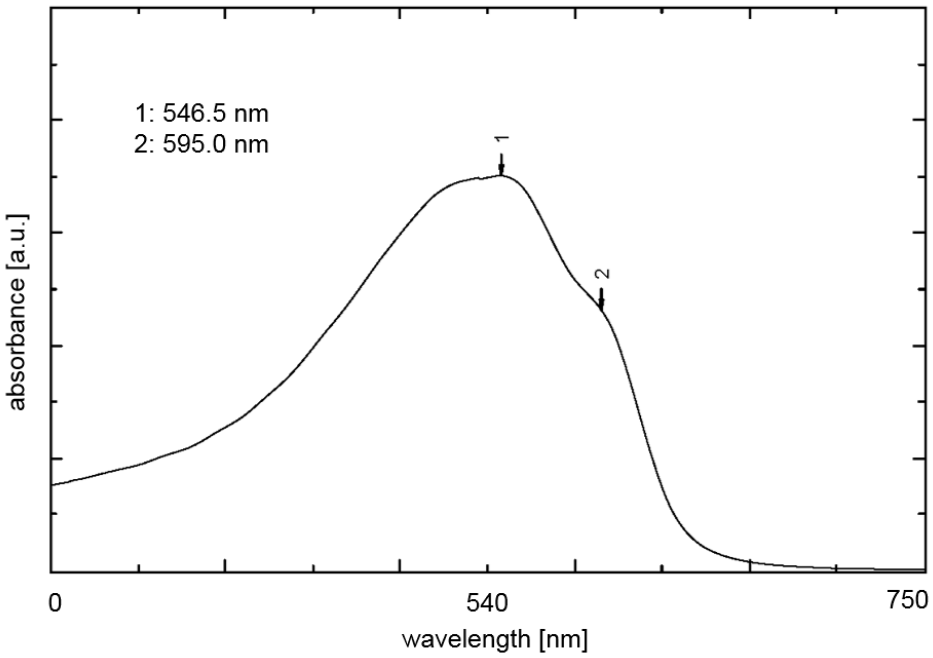

Figure A 63: UV/Vis spectrum of poly(**M6**) in DMSO.

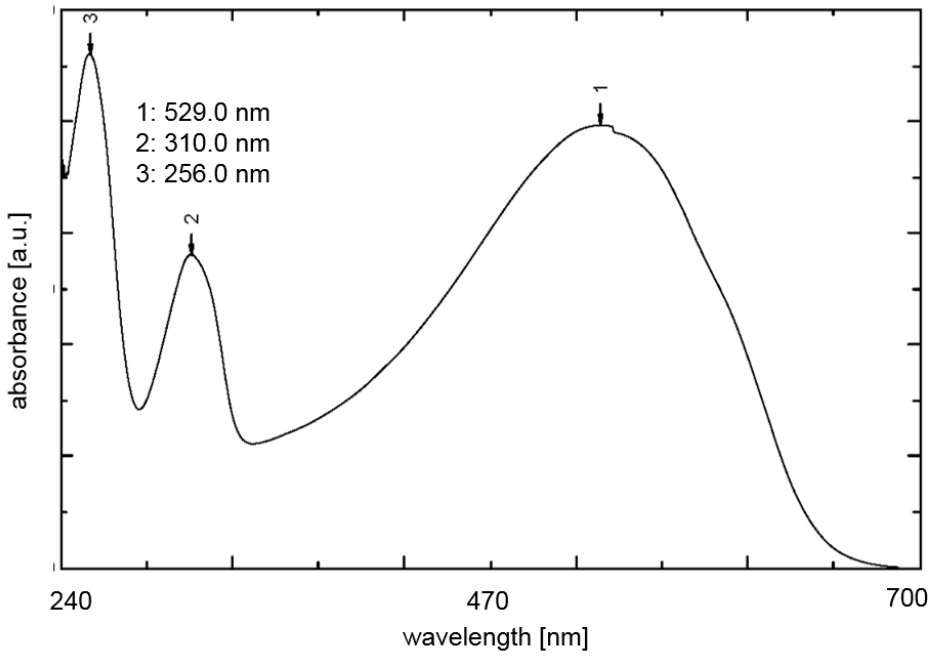

Figure A 64: UV/Vis spectrum of poly(**M9**) in DMSO.

9.2 MOLYBDENUM IMIDO ALKYLIDENE COMPLEXES WITH CHELATING *N*-HETEROCYCLIC CARBENES

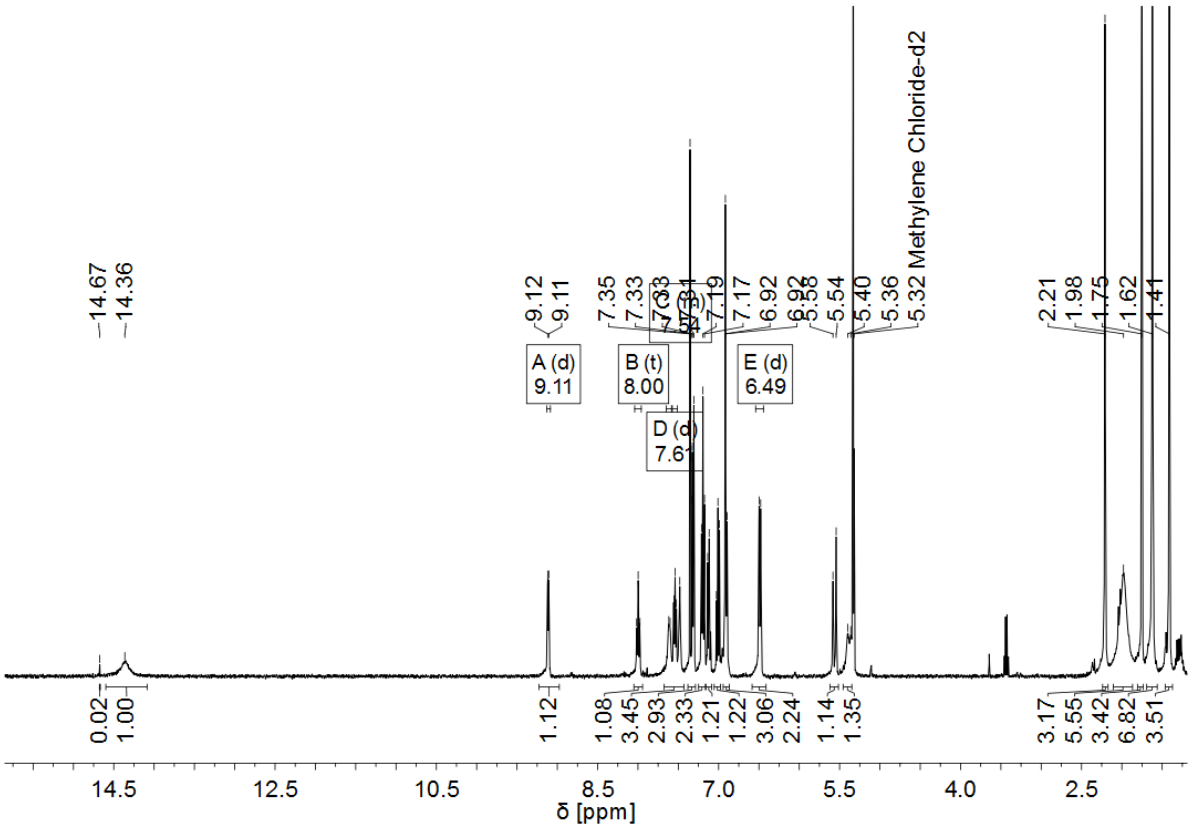

Figure A 65: ^{1}H NMR spectrum of **Mo-12** (400 MHz, CD_2Cl_2).

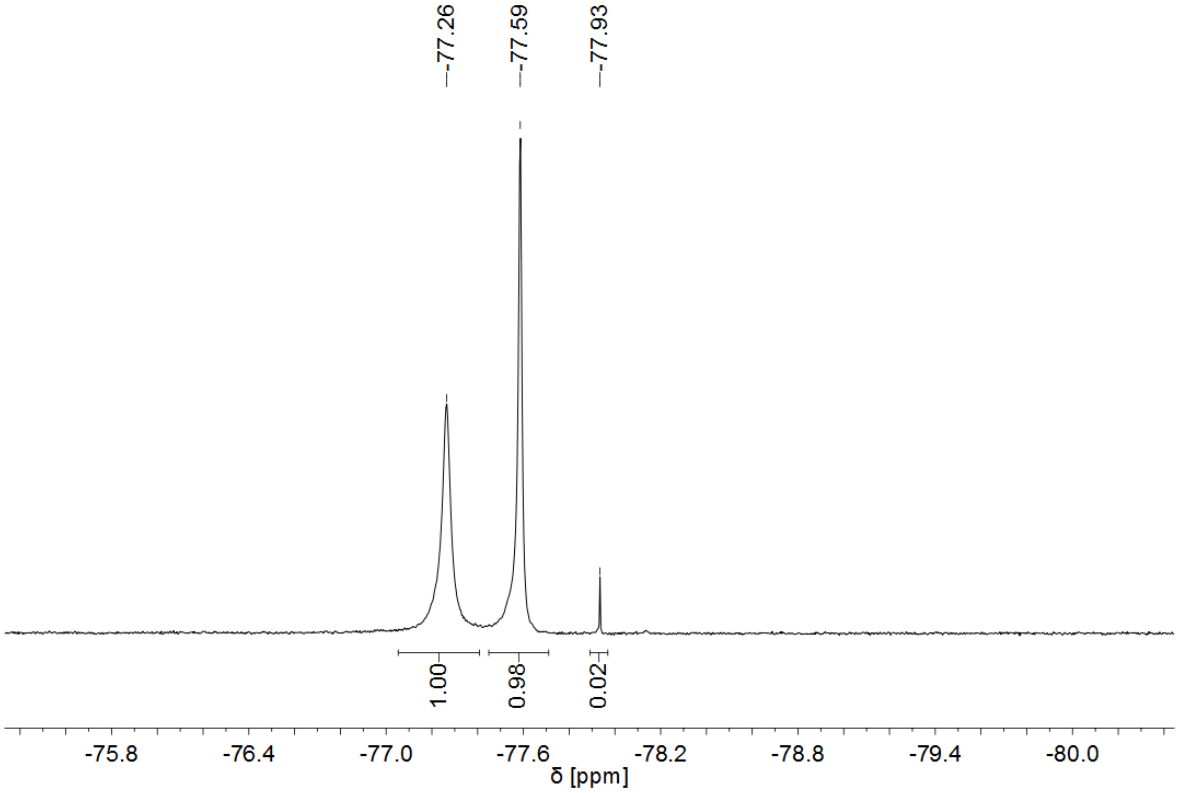

Figure A 66: ^{19}F NMR spectrum of **Mo-12** (376 MHz, CD_2Cl_2).

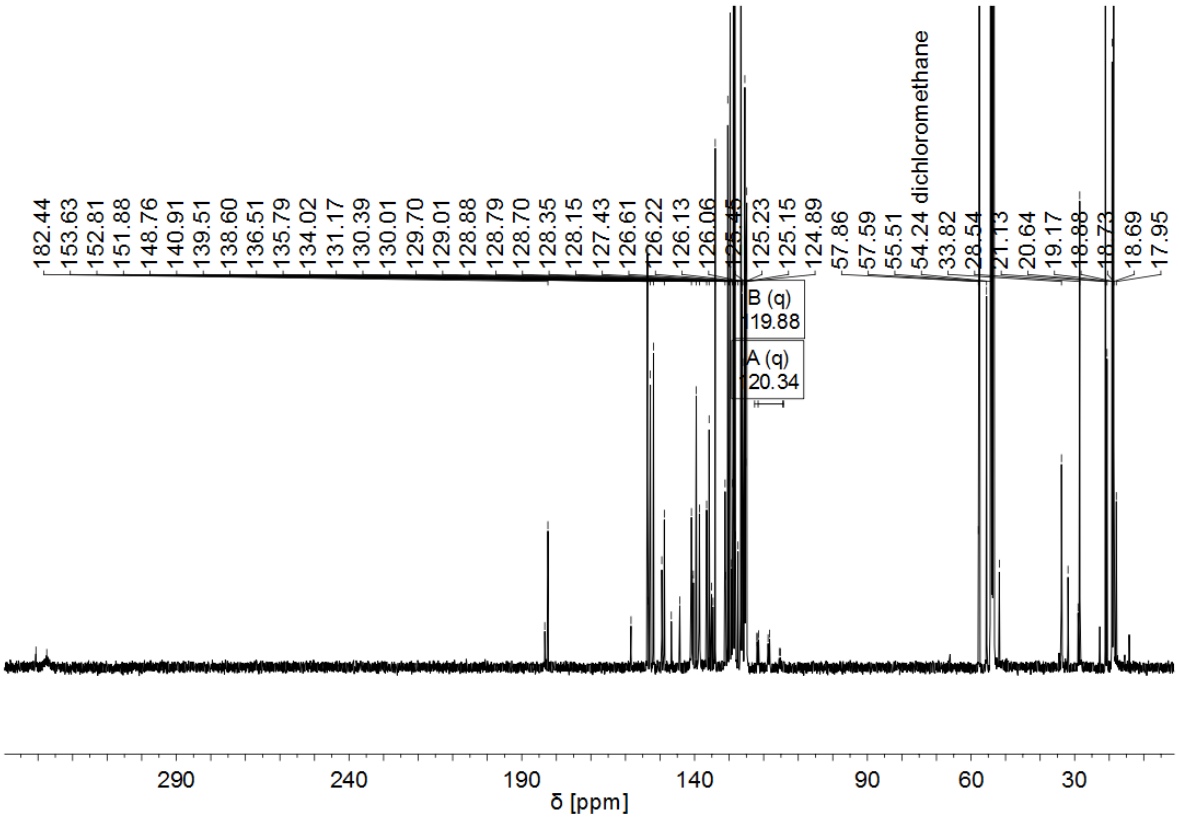

Figure A 67: ^{13}C NMR spectrum of **Mo-12** (101 MHz, CD_2Cl_2).

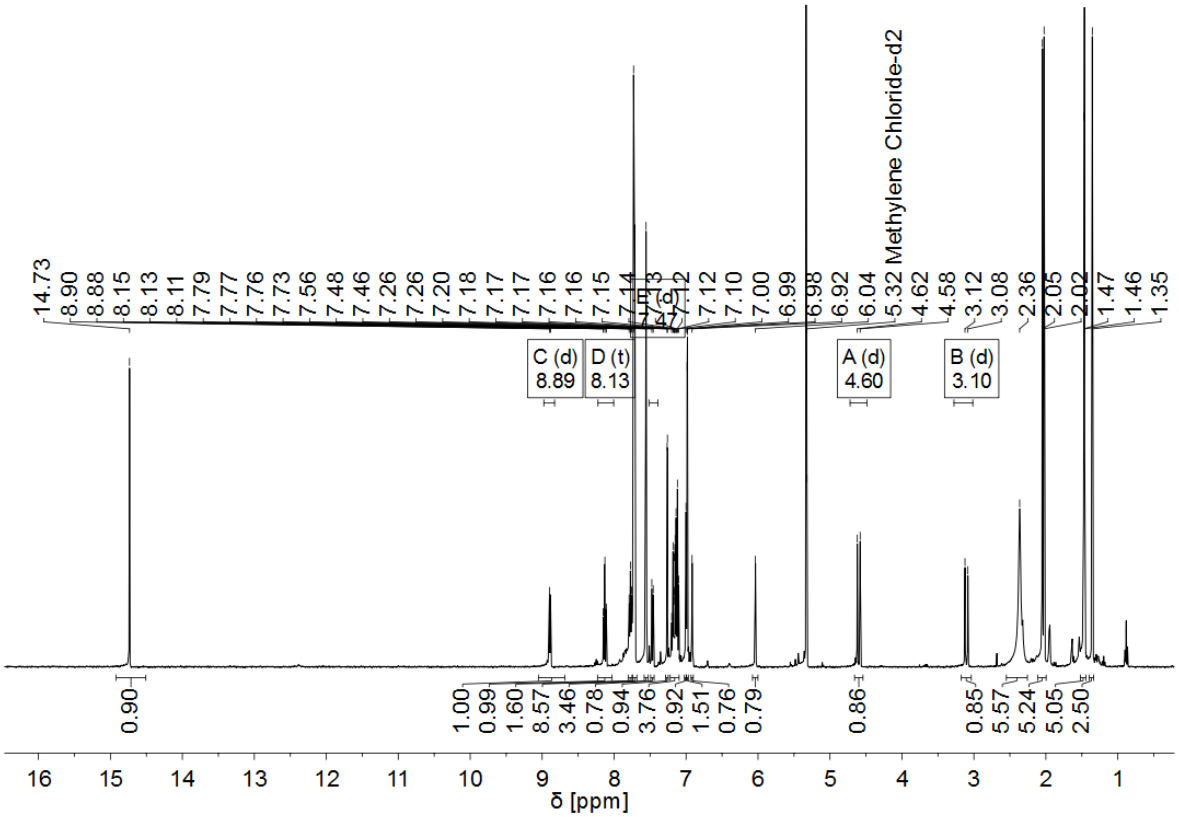

Figure A 68: ^{1}H NMR spectrum of **Mo-13** (400 MHz, CD_2Cl_2).

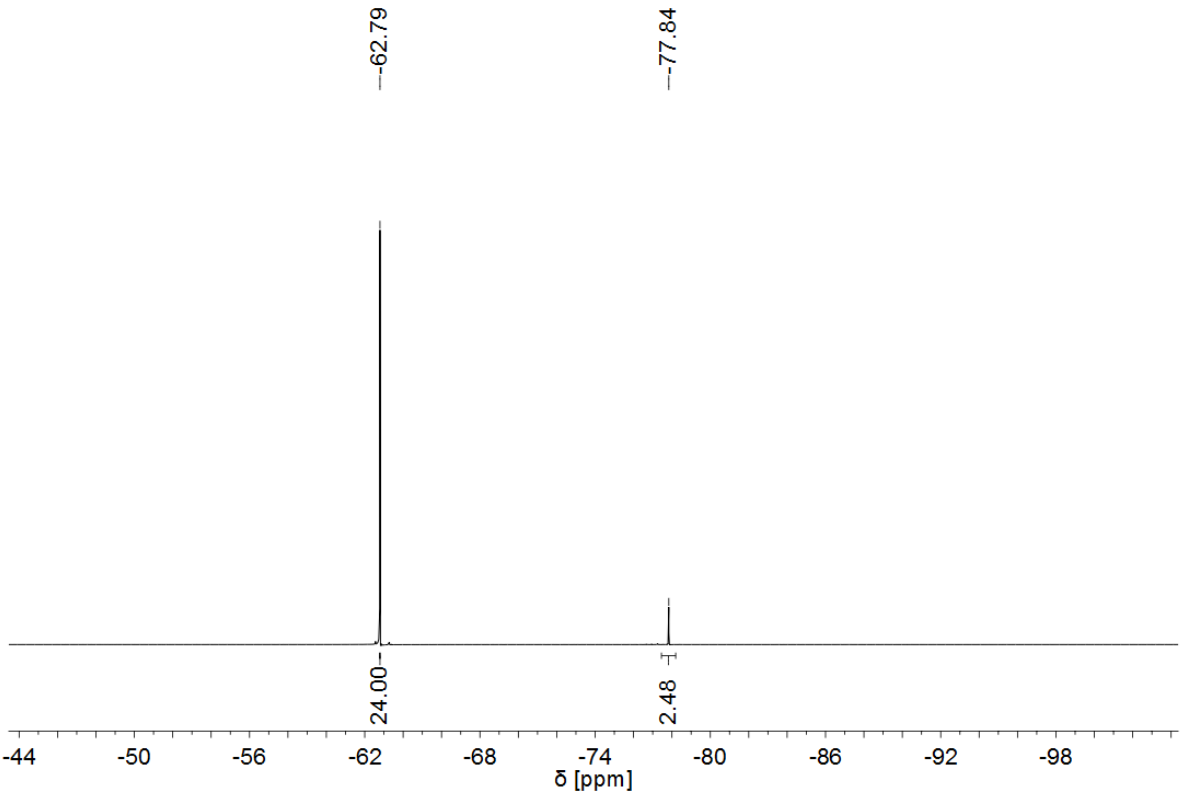

Figure A 69: ^{19}F NMR spectrum of **Mo-13** (376 MHz, CD_2Cl_2).

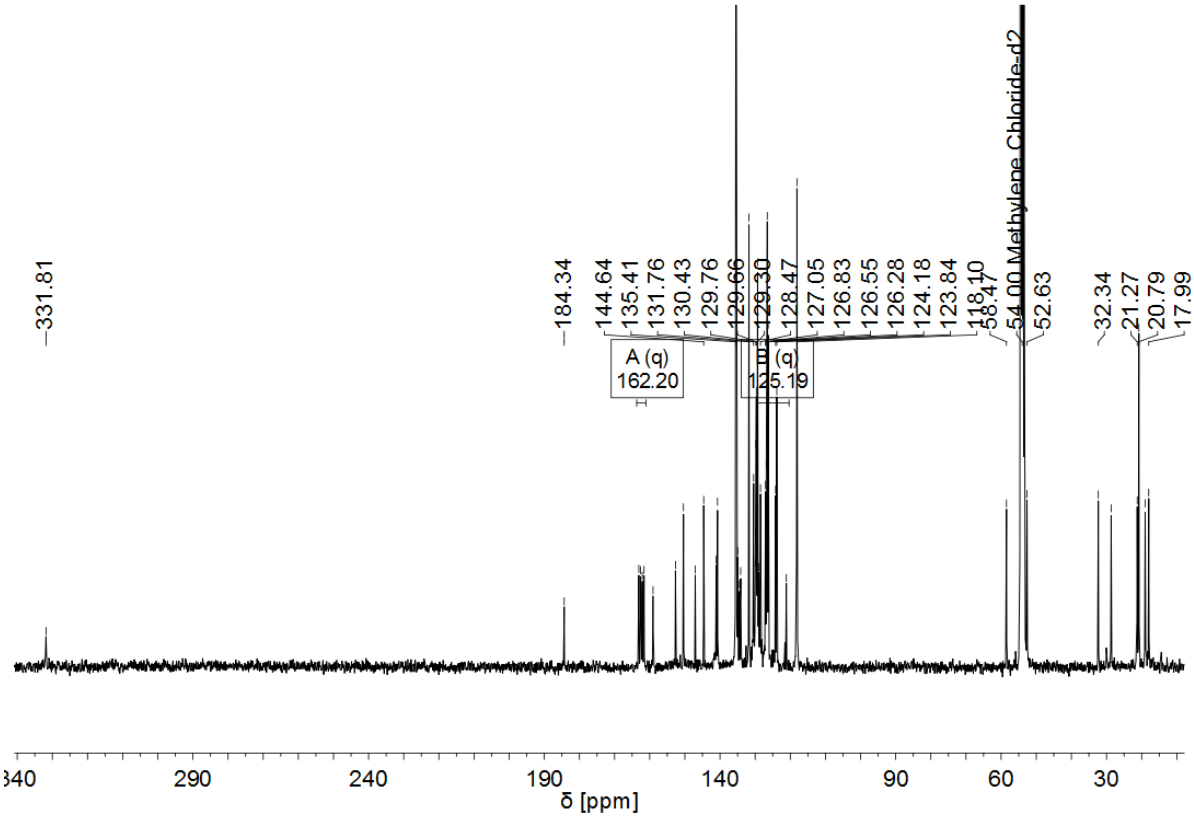

Figure A 70: ^{13}C NMR spectrum of **Mo-13** (101 MHz, CD_2Cl_2).

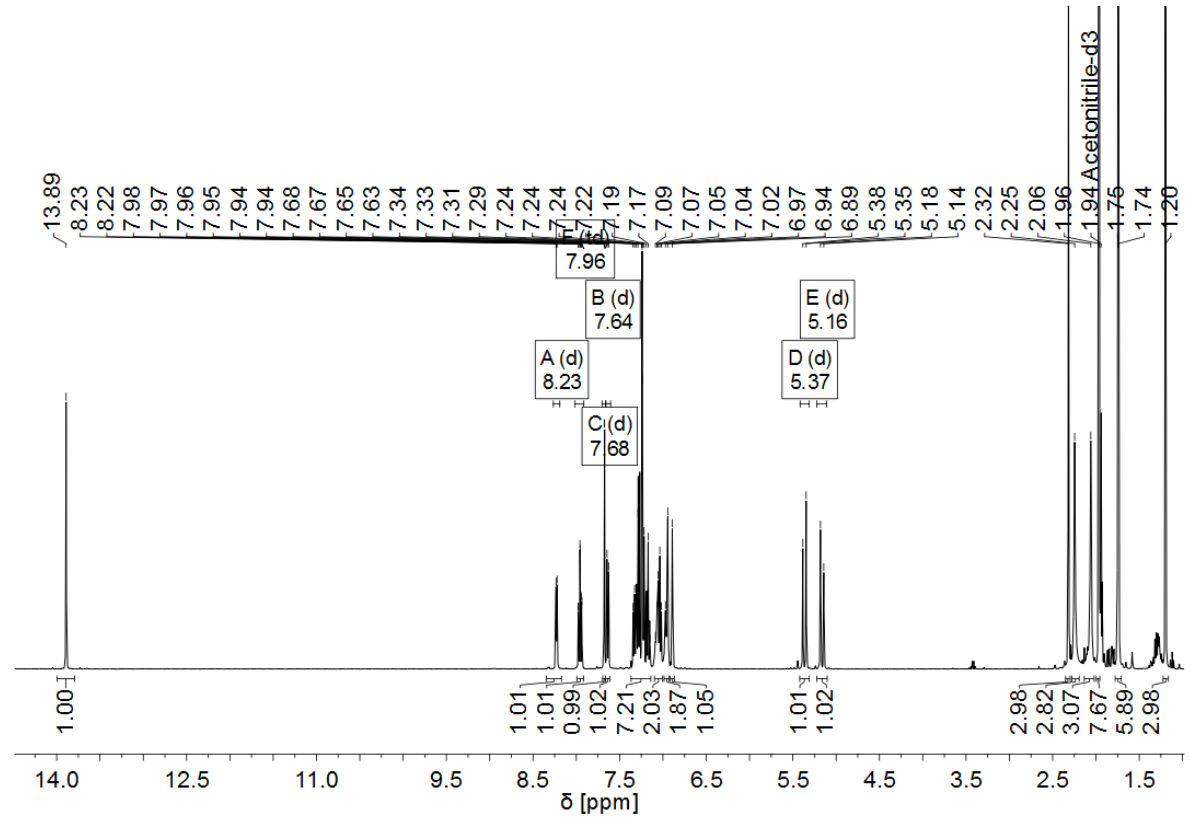

Figure A 71: ^{1}H NMR spectrum of **Mo-14** (400 MHz, MeCN-d3).

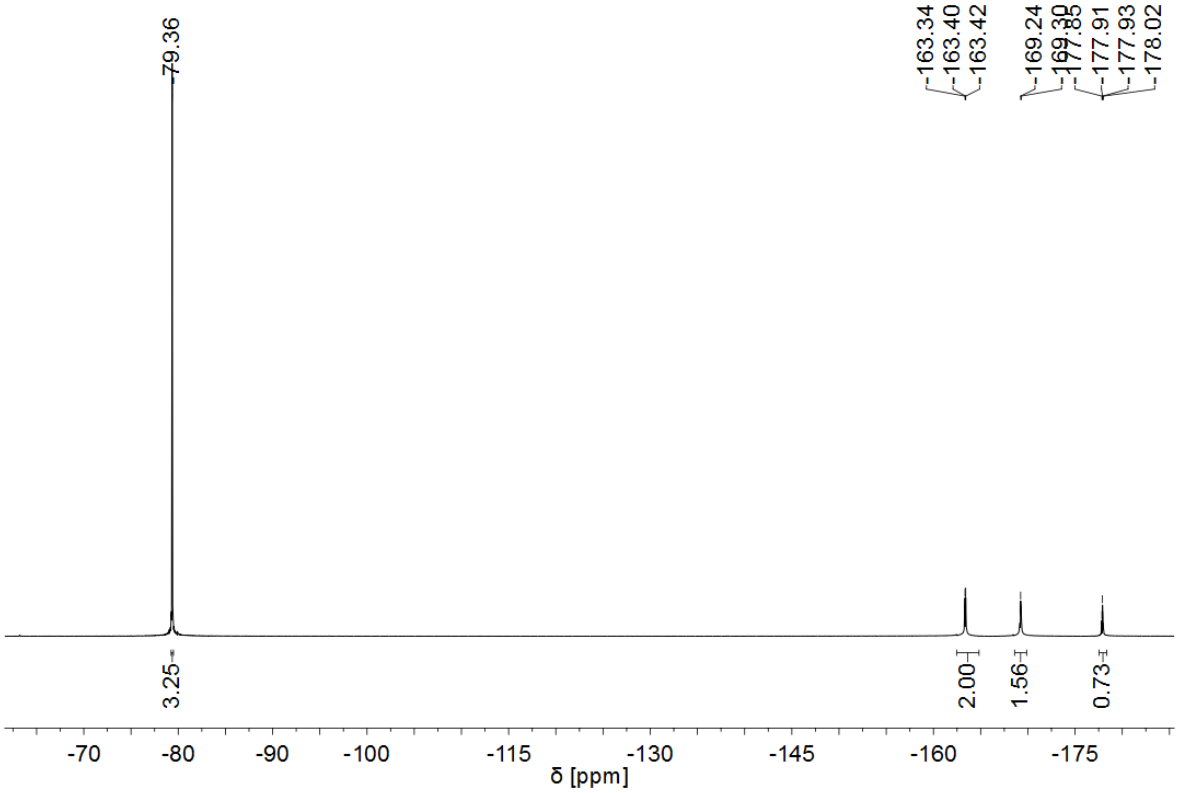

Figure A 72: ^{19}F NMR spectrum of **Mo-14** (376 MHz, MeCN-d3).

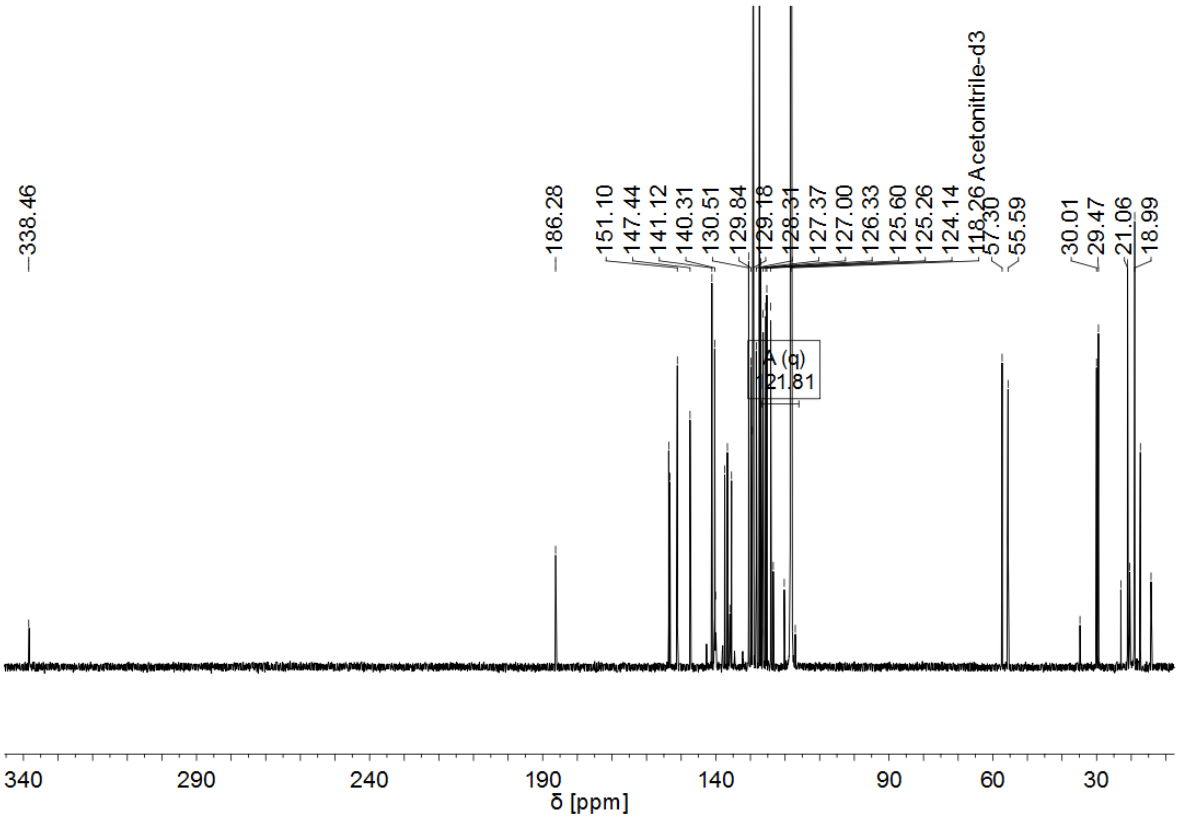

Figure A 73: ^{13}C NMR spectrum of **Mo-14** (101 MHz, MeCN-d3).

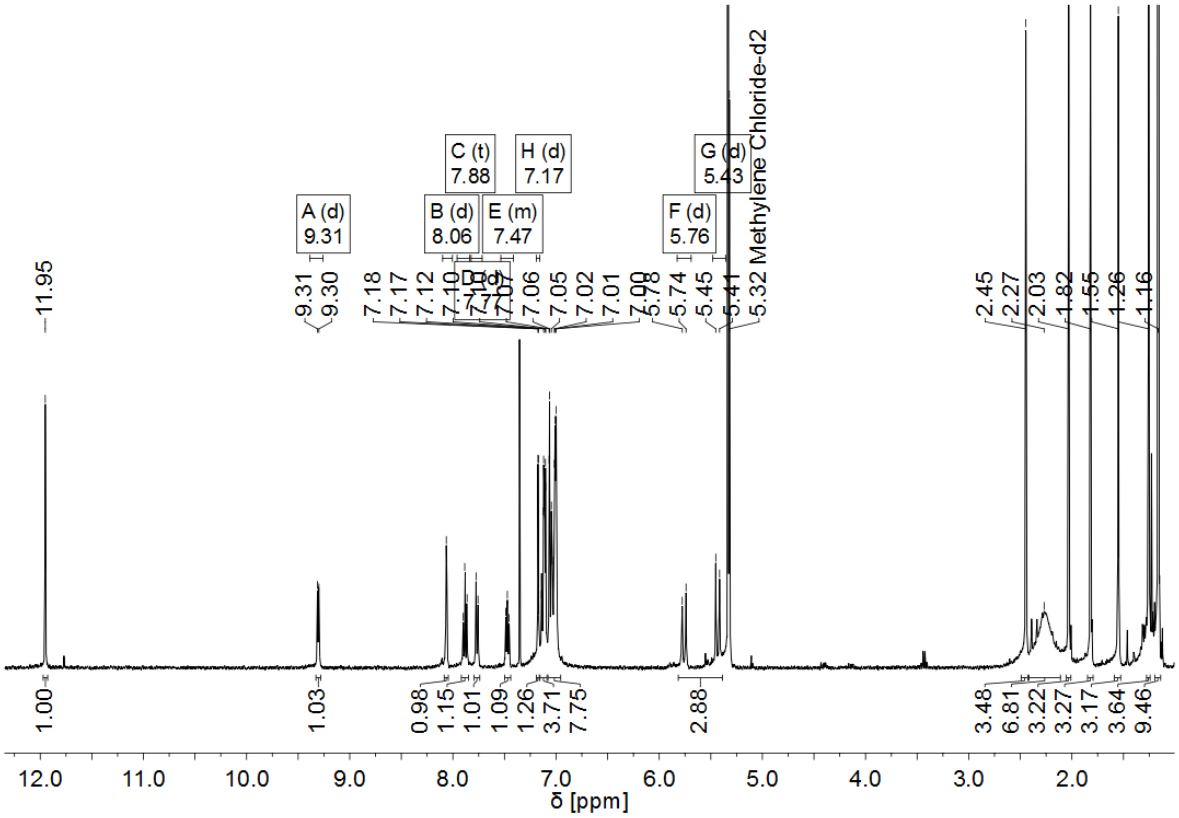

Figure A 74: ^{1}H NMR spectrum of **Mo-15** (400 MHz, CD_2Cl_2).

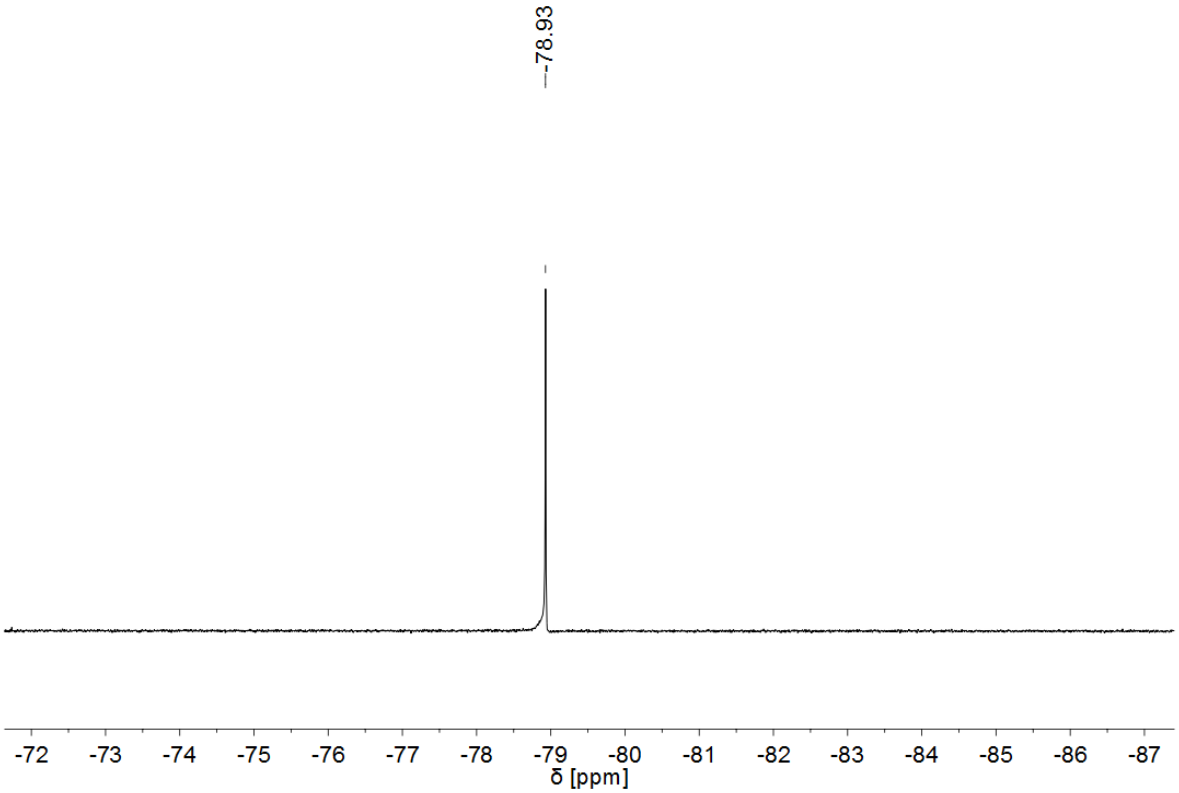

Figure A 75: ^{19}F NMR spectrum of **Mo-15** (376 MHz, CD_2Cl_2).

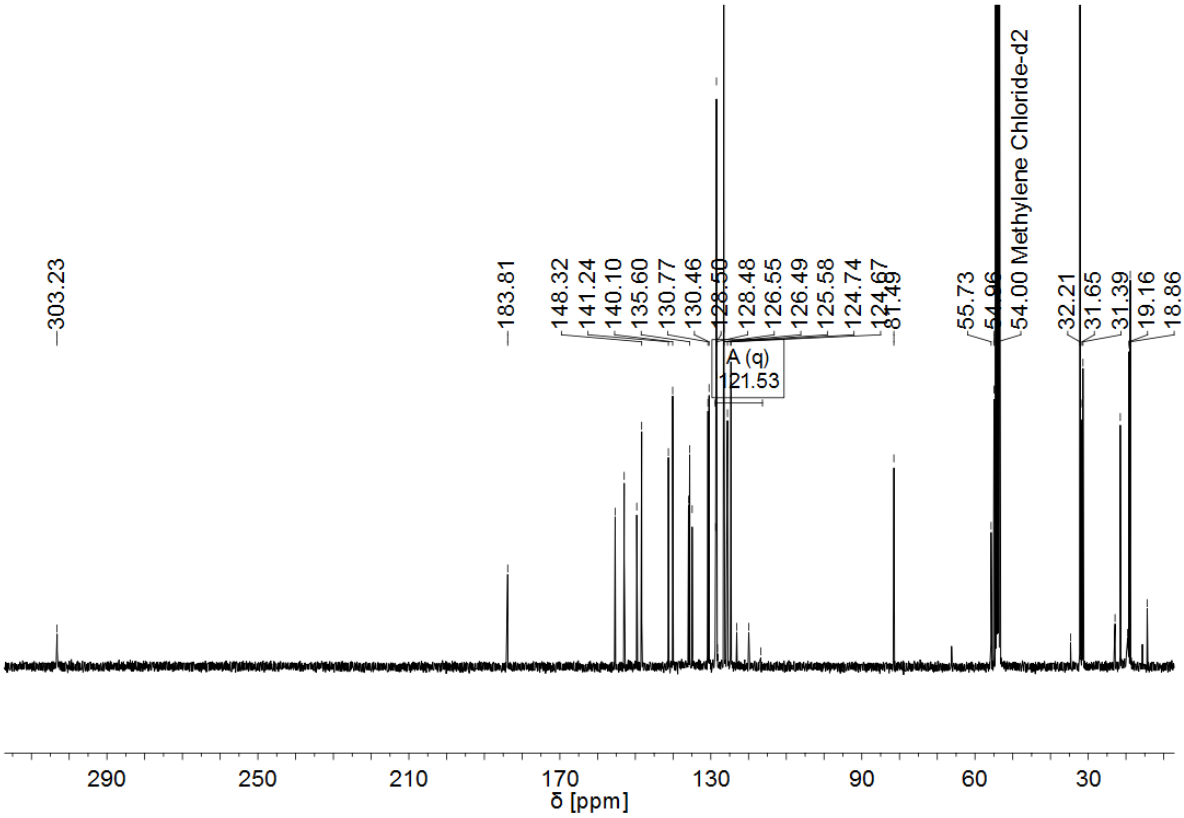

Figure A 76: ^{13}C NMR spectrum of **Mo-15** (101 MHz, CD_2Cl_2).

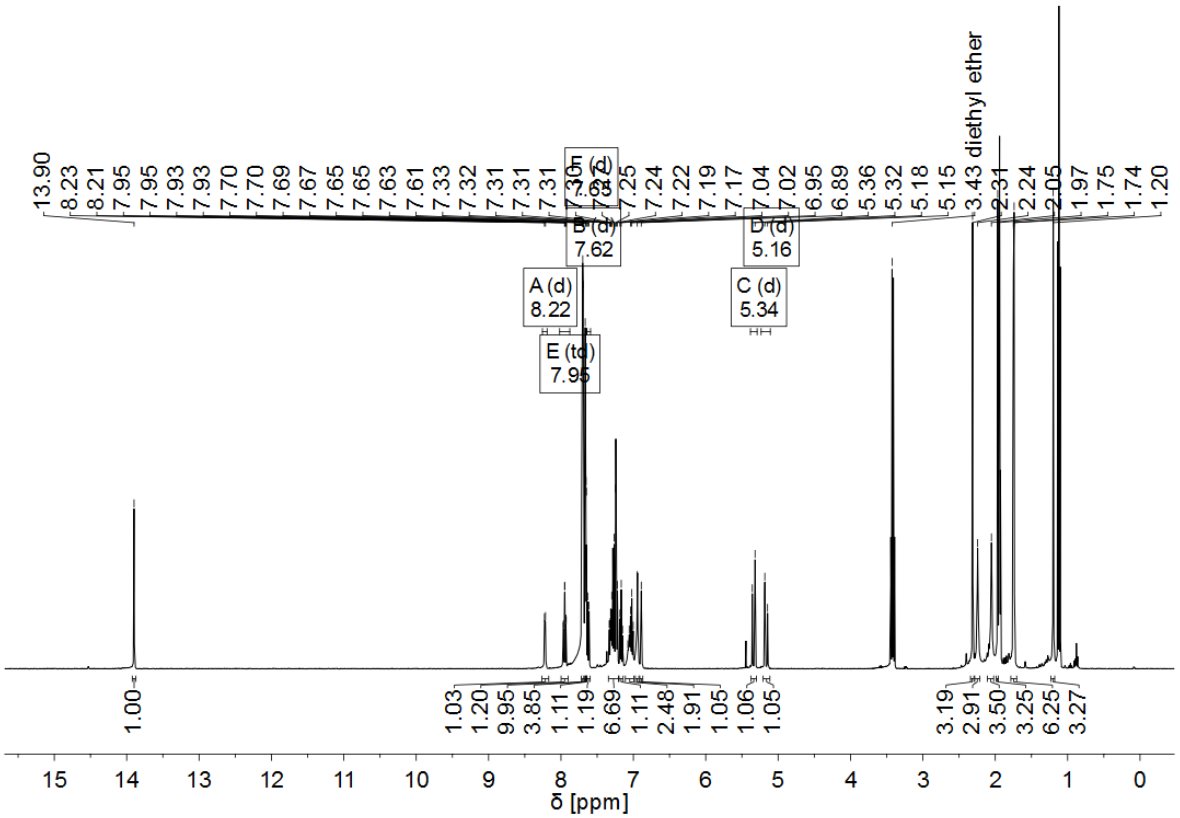

Figure A 77: ^{1}H NMR spectrum of **Mo-16** (400 MHz, CD_2Cl_2).

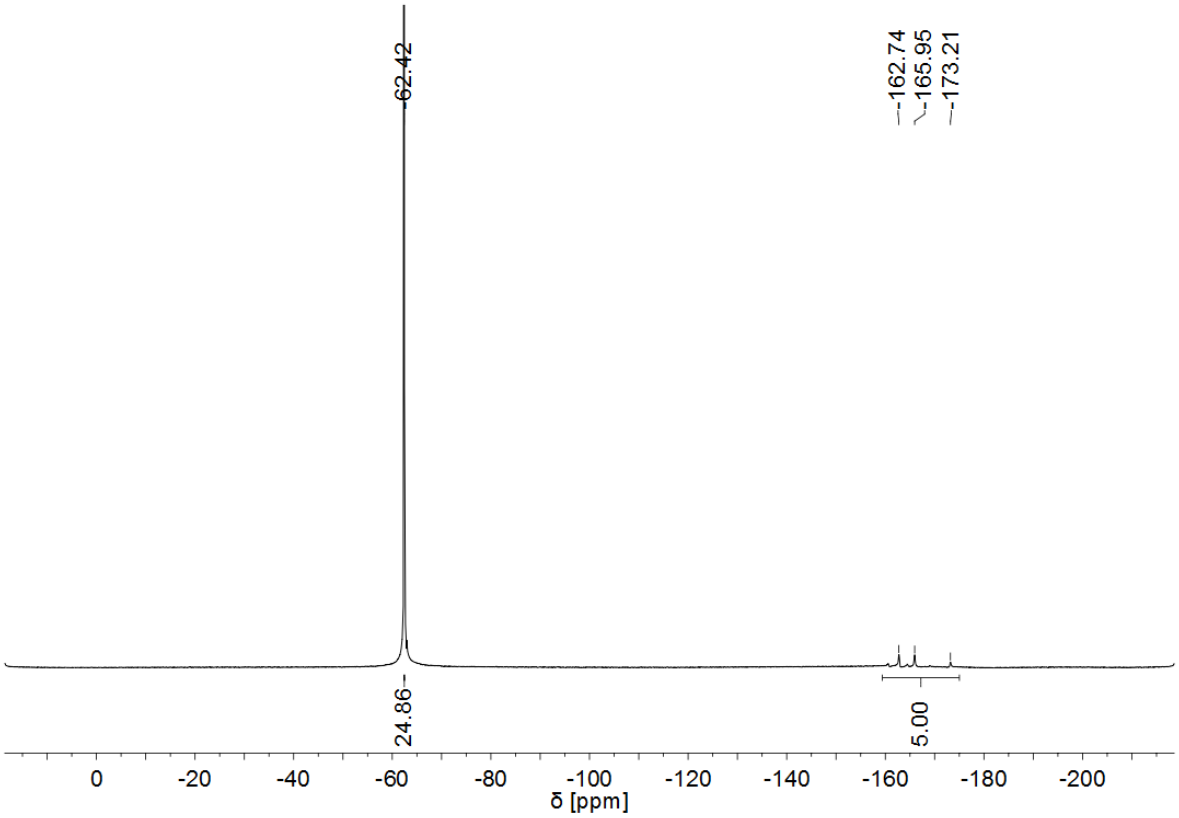

Figure A 78: ^{19}F NMR spectrum of **Mo-16** (376 MHz, CD_2Cl_2).

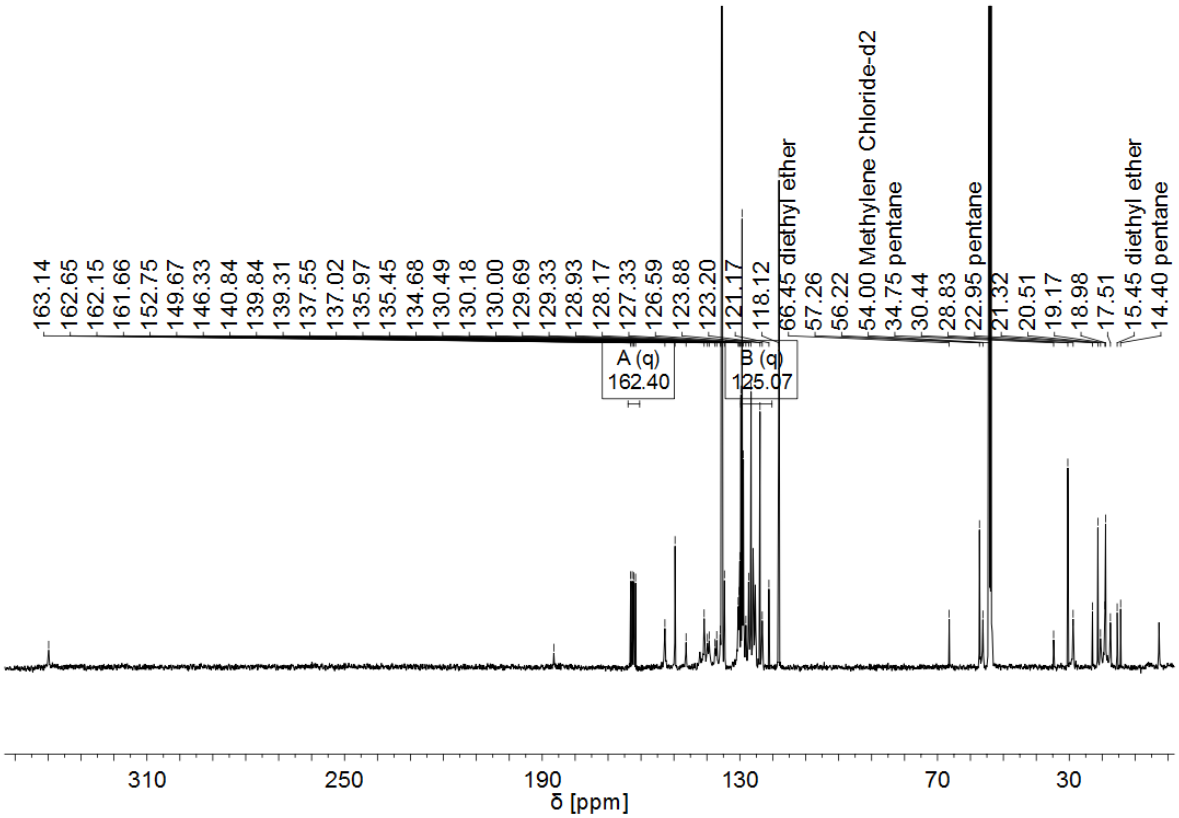

Figure A 79: ^{13}C NMR spectrum of **Mo-16** (101 MHz, CD_2Cl_2).

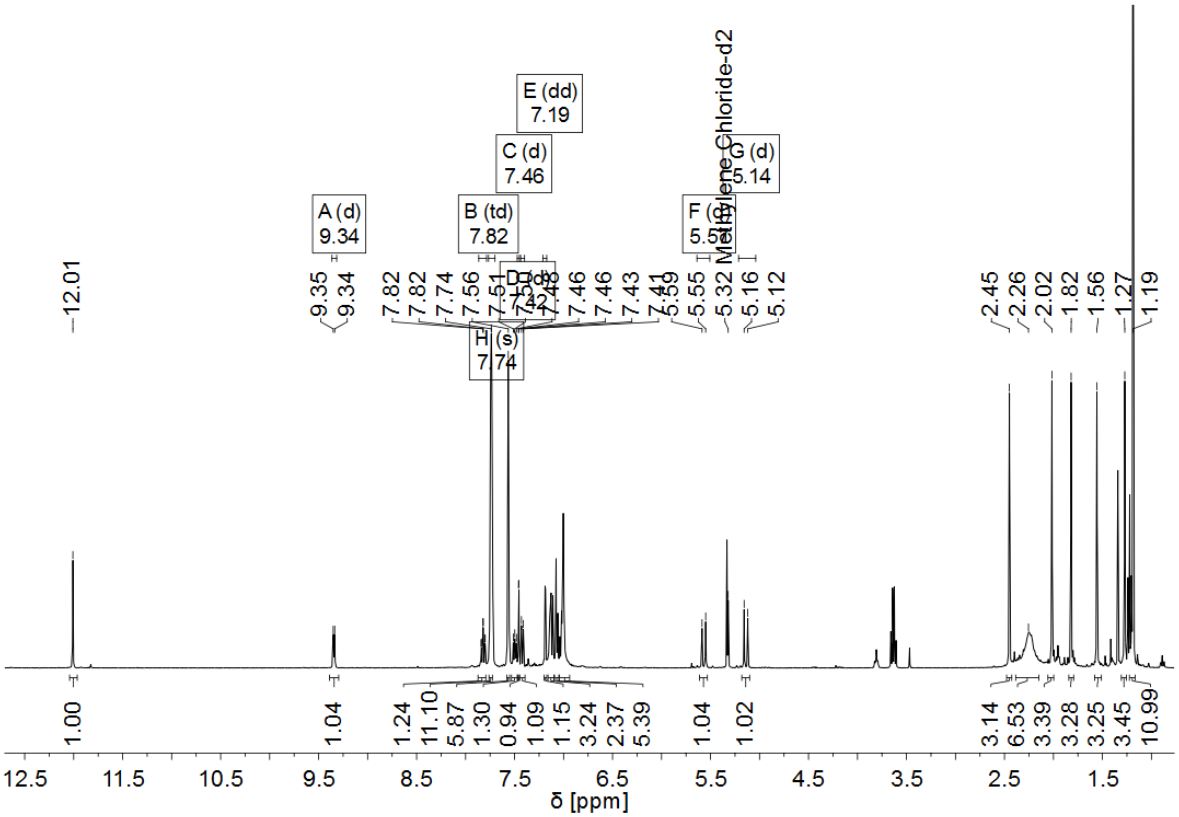

Figure A 80: ^{1}H NMR spectrum of **Mo-17** (400 MHz, CD_2Cl_2).

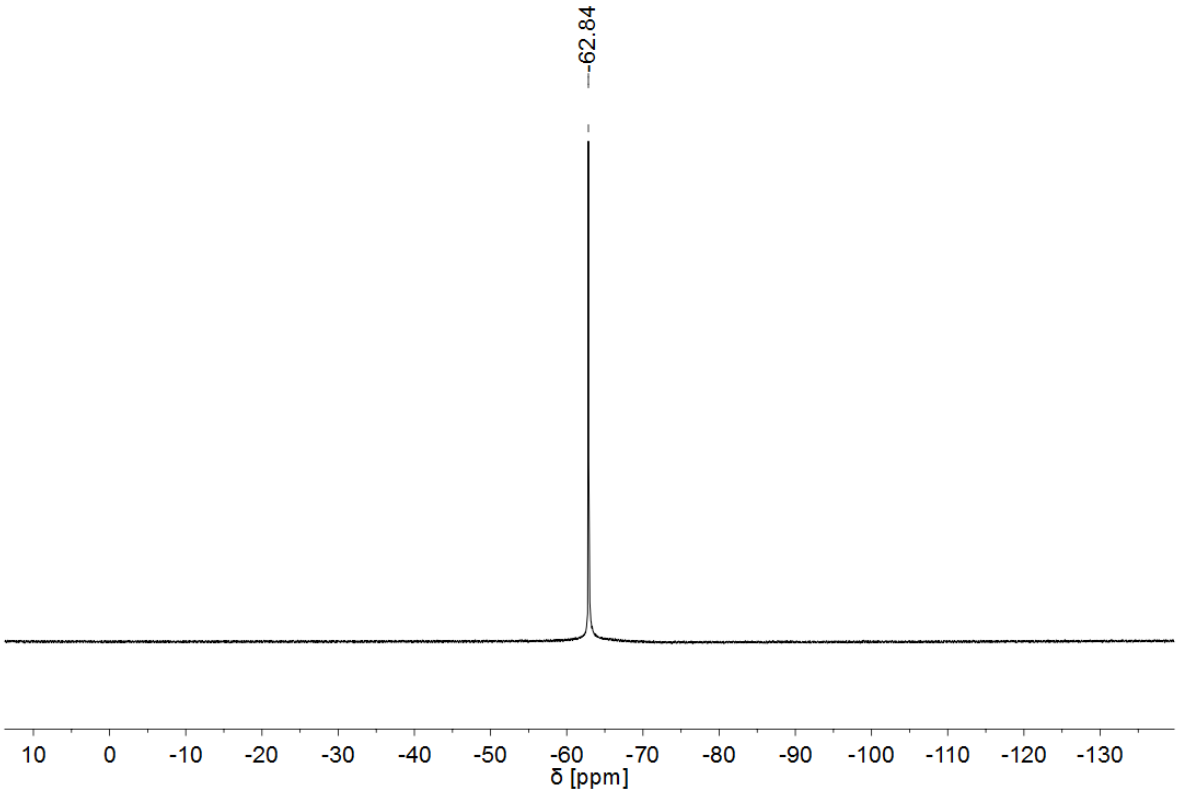

Figure A 81: ^{19}F NMR spectrum of **Mo-17** (376 MHz, CD_2Cl_2).

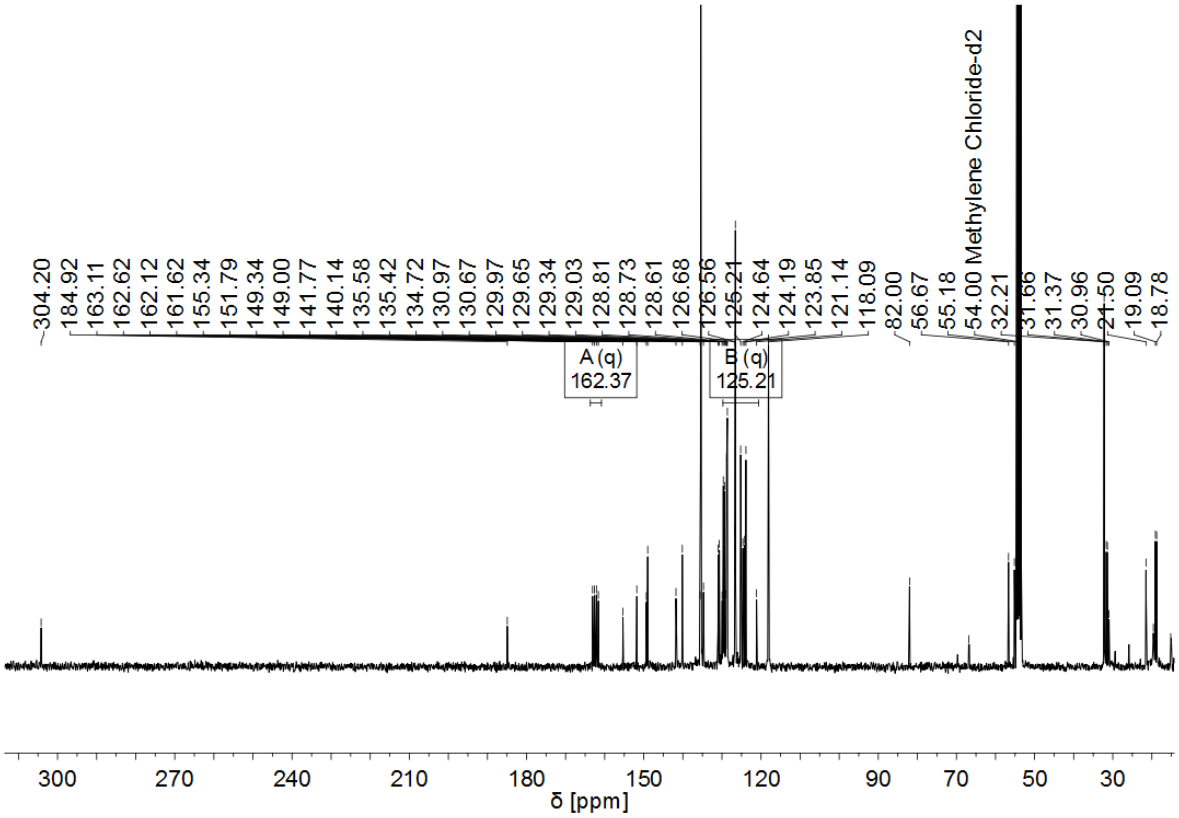

Figure A 82: ^{13}C NMR spectrum of **Mo-17** (101 MHz, CD_2Cl_2).

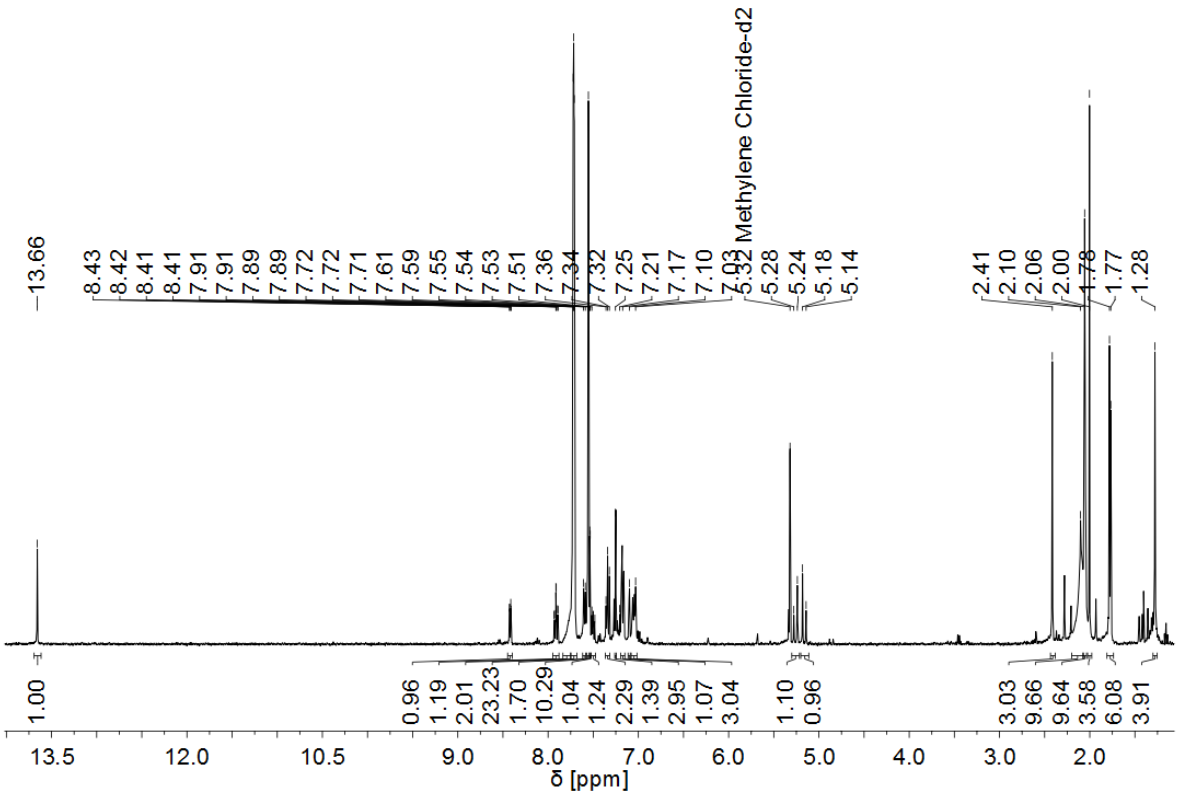

Figure A 83: Crude ^{1}H NMR spectrum of **Mo-18·MeCN** (400 MHz, CD_2Cl_2).

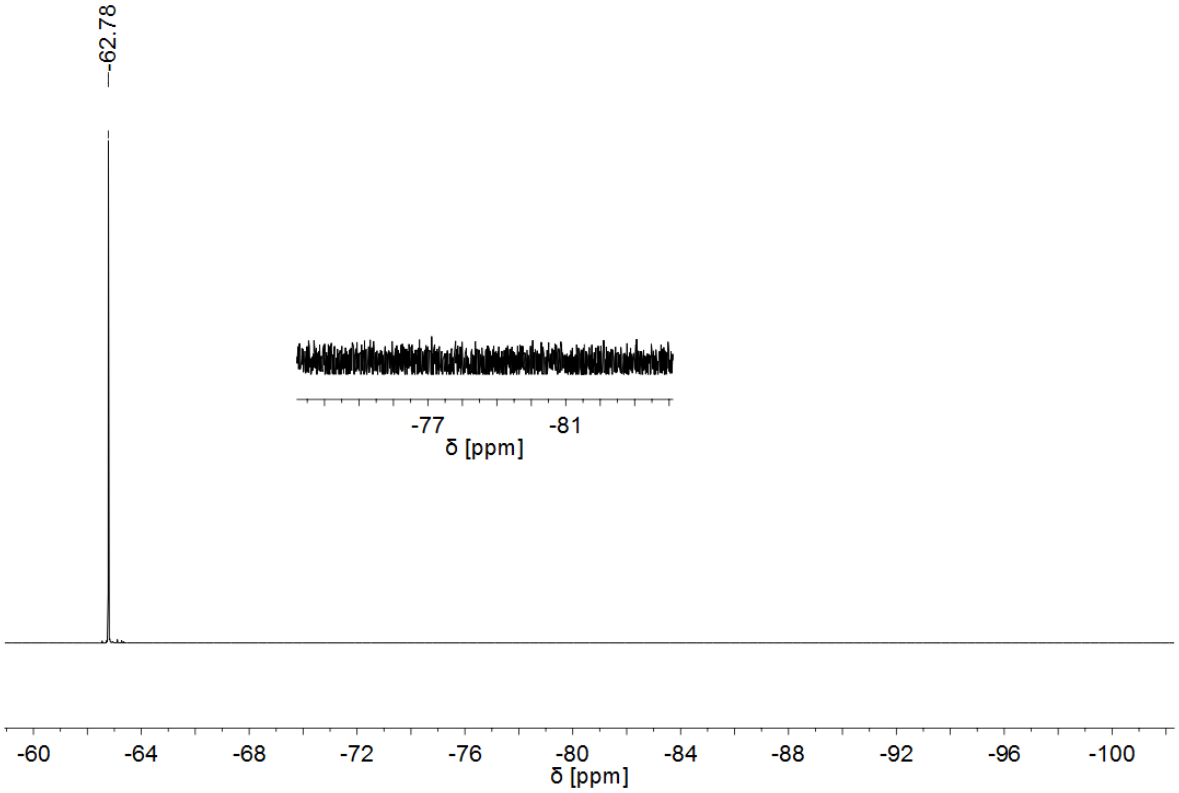

Figure A 84: Crude ^{19}F NMR spectrum of **Mo-18·MeCN** (376 MHz, CD_2Cl_2). No triflate resonance visible.

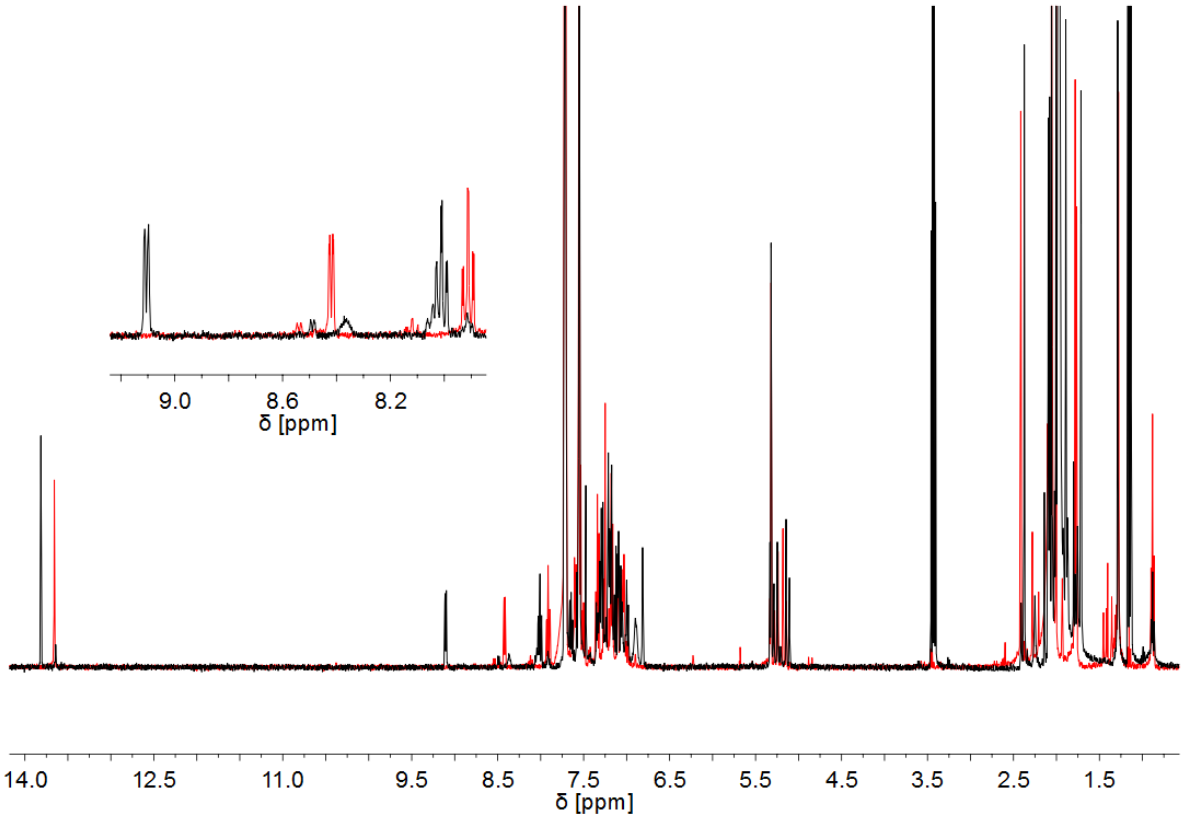

Figure A 85: Stacking of ^1H NMR spectra in CD_2Cl_2. Red: **Mo-18·MeCN**. Black: **Mo-13**.

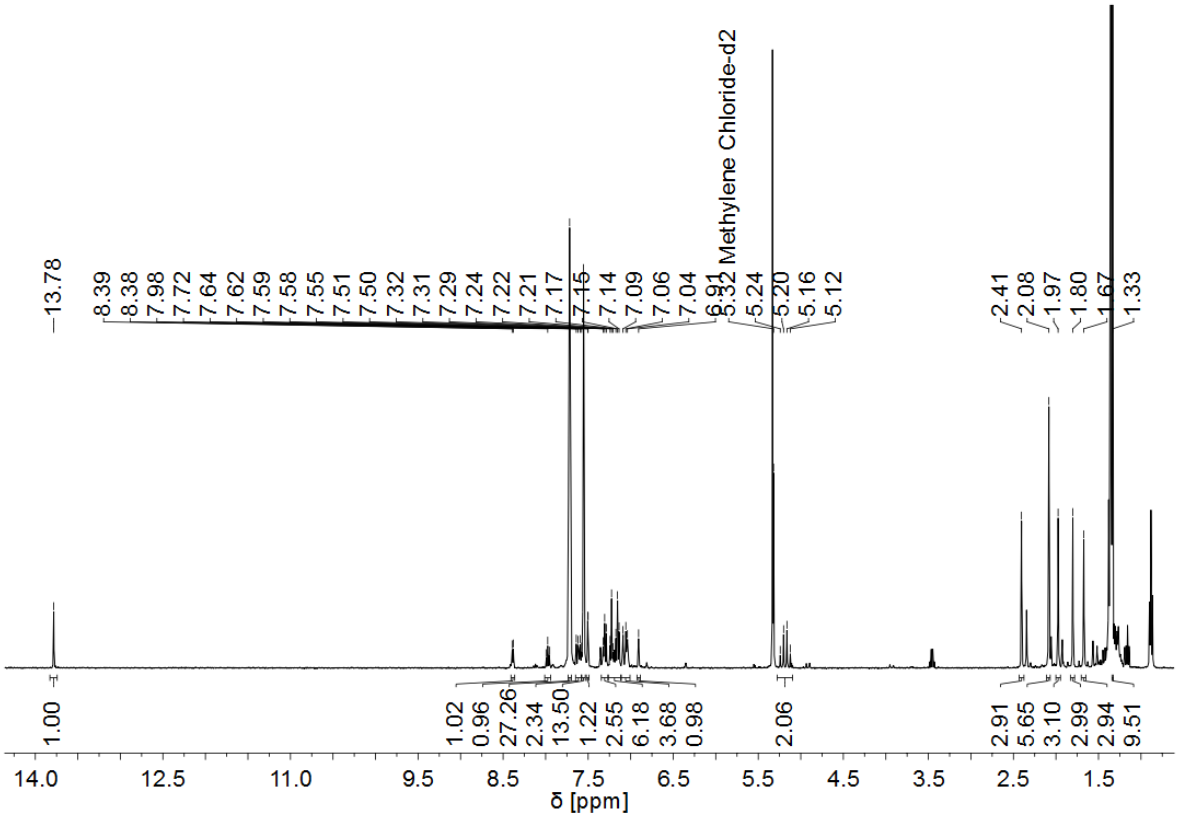

Figure A 86: Crude ^{1}H NMR spectrum of **Mo-18·*t*BuCN** (400 MHz, CD_2Cl_2).

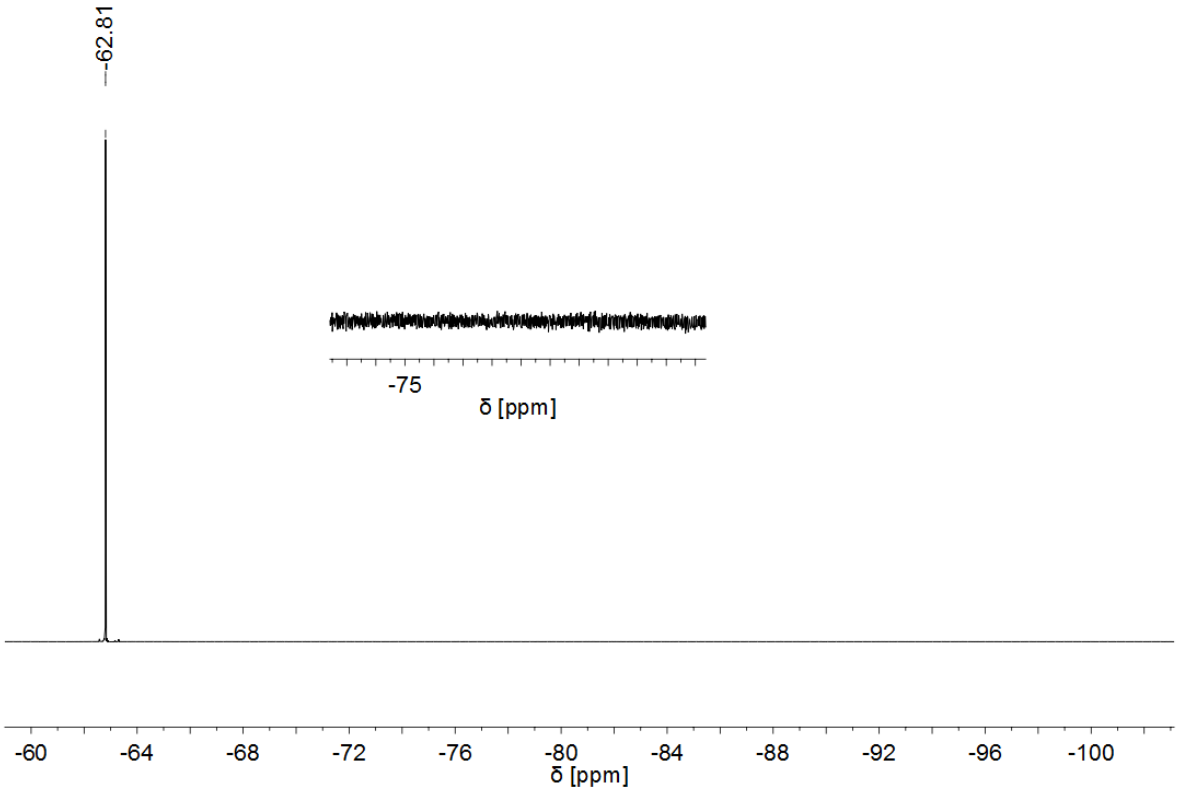

Figure A 87: Crude ^{19}F NMR spectrum of **Mo-18·*t*BuCN** (376 MHz, CD_2Cl_2). No triflate resonance visible.

9.3 (PRE-)CATALYSTS FOR LATENT RING-OPENING METATHESIS POLYMERIZATION OF DICYCLOPENTADIENE

9.3.1 NMR SPECTRA OF NOVEL COMPOUNDS

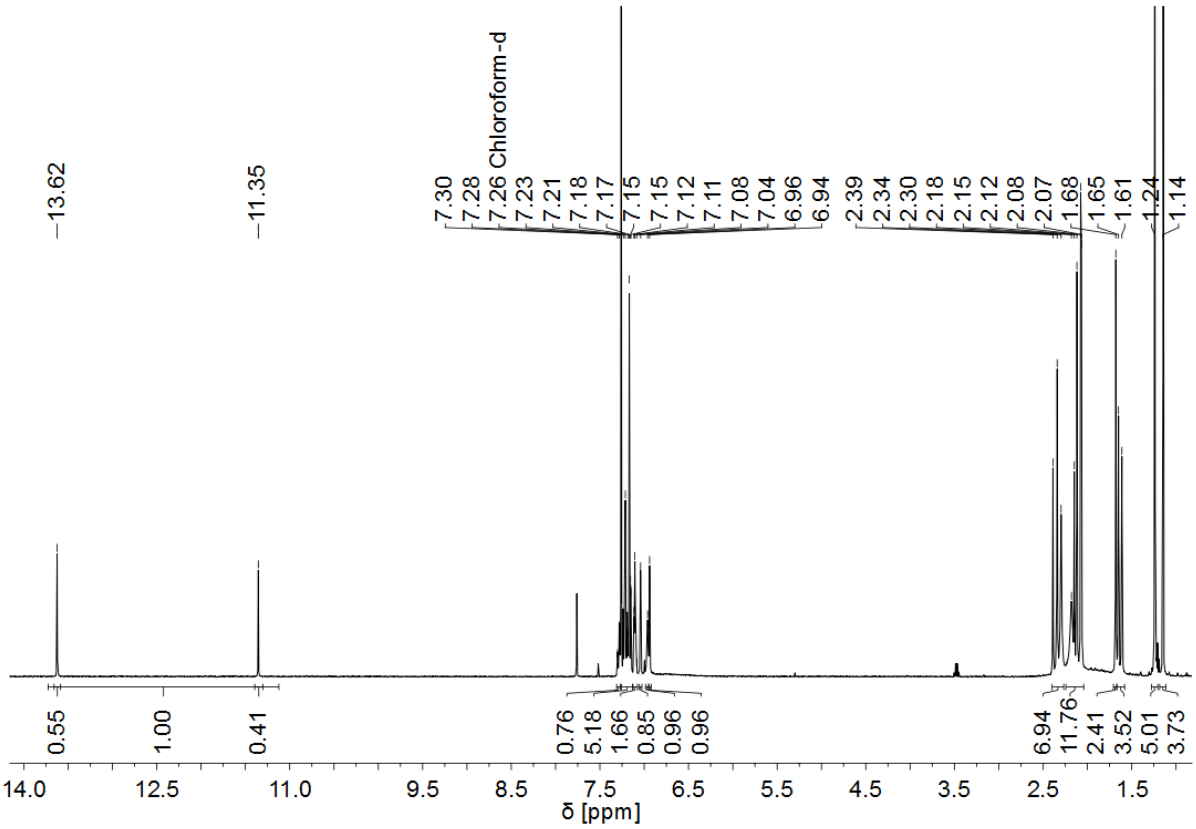

Figure A 88: ^{1}H NMR spectrum of **Mo-19** (400 MHz, $CDCl_3$).

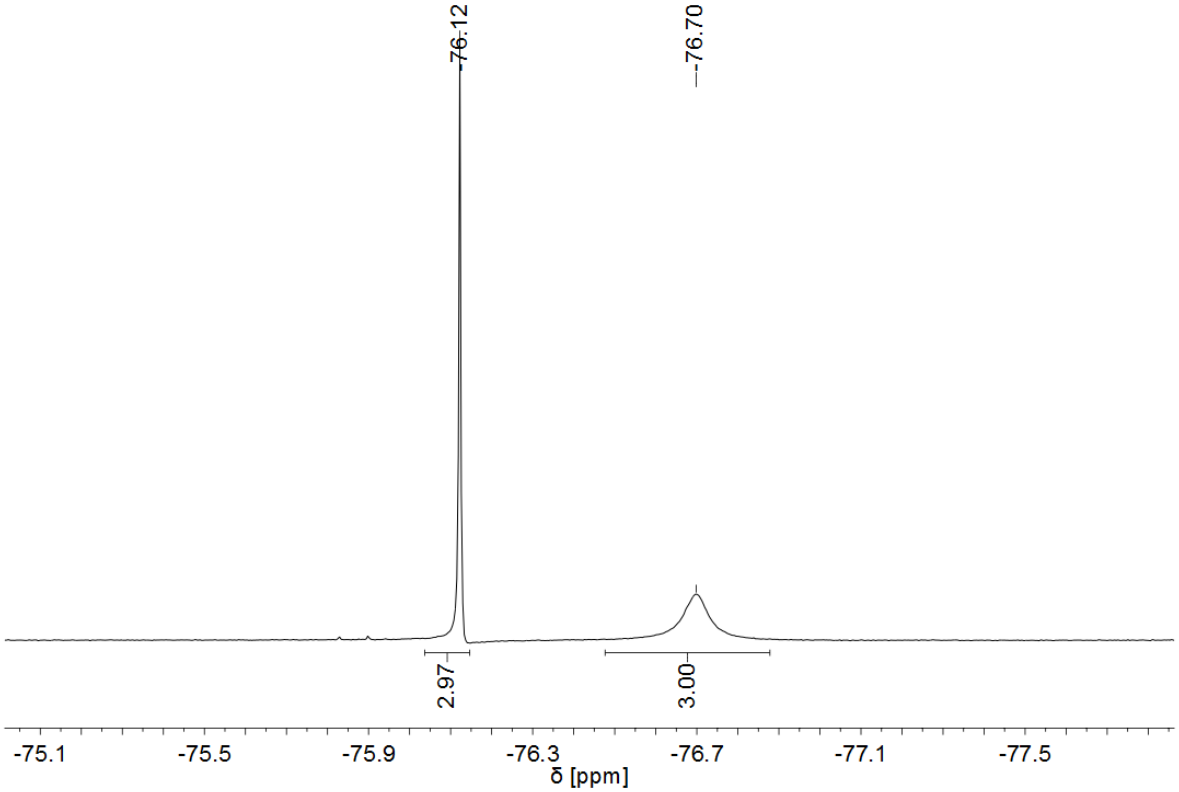

Figure A 89: ^{19}F NMR spectrum of **Mo-19** (376 MHz, $CDCl_3$).

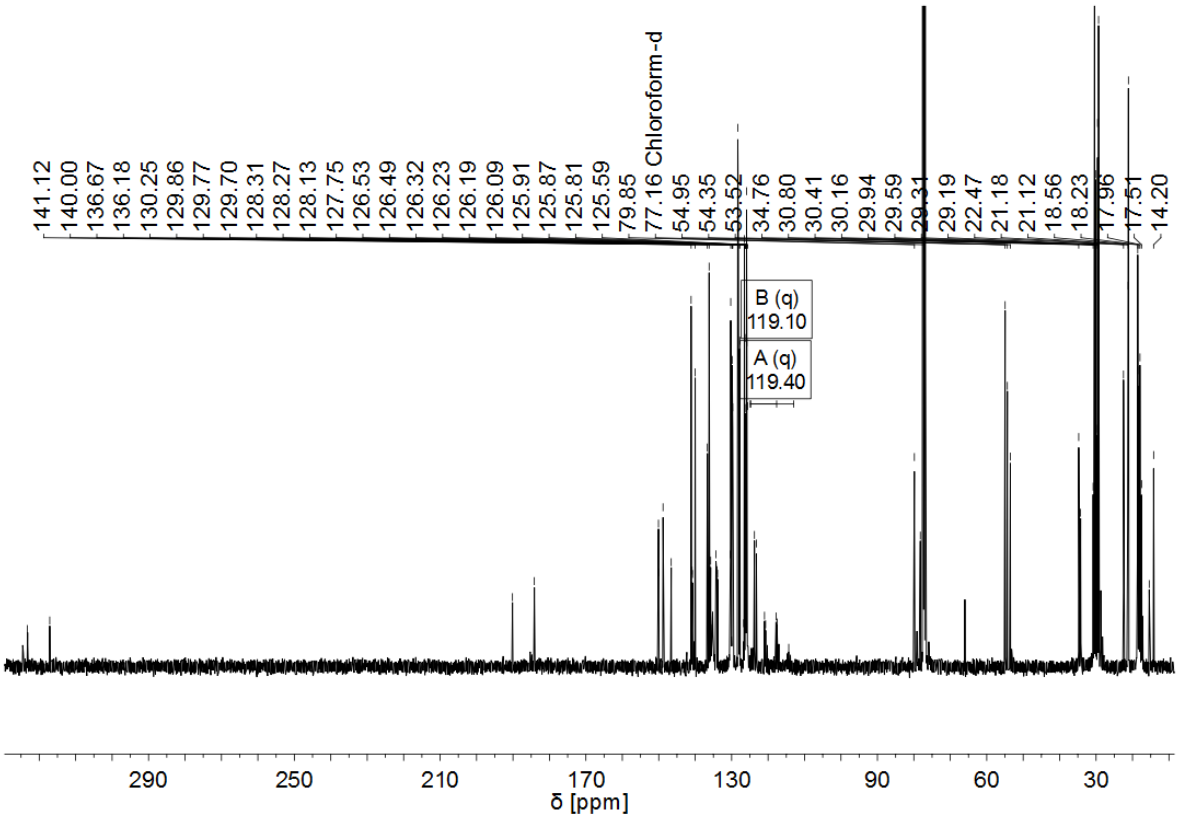

Figure A 90: ^{13}C NMR spectrum of **Mo-19** (101 MHz, $CDCl_3$).

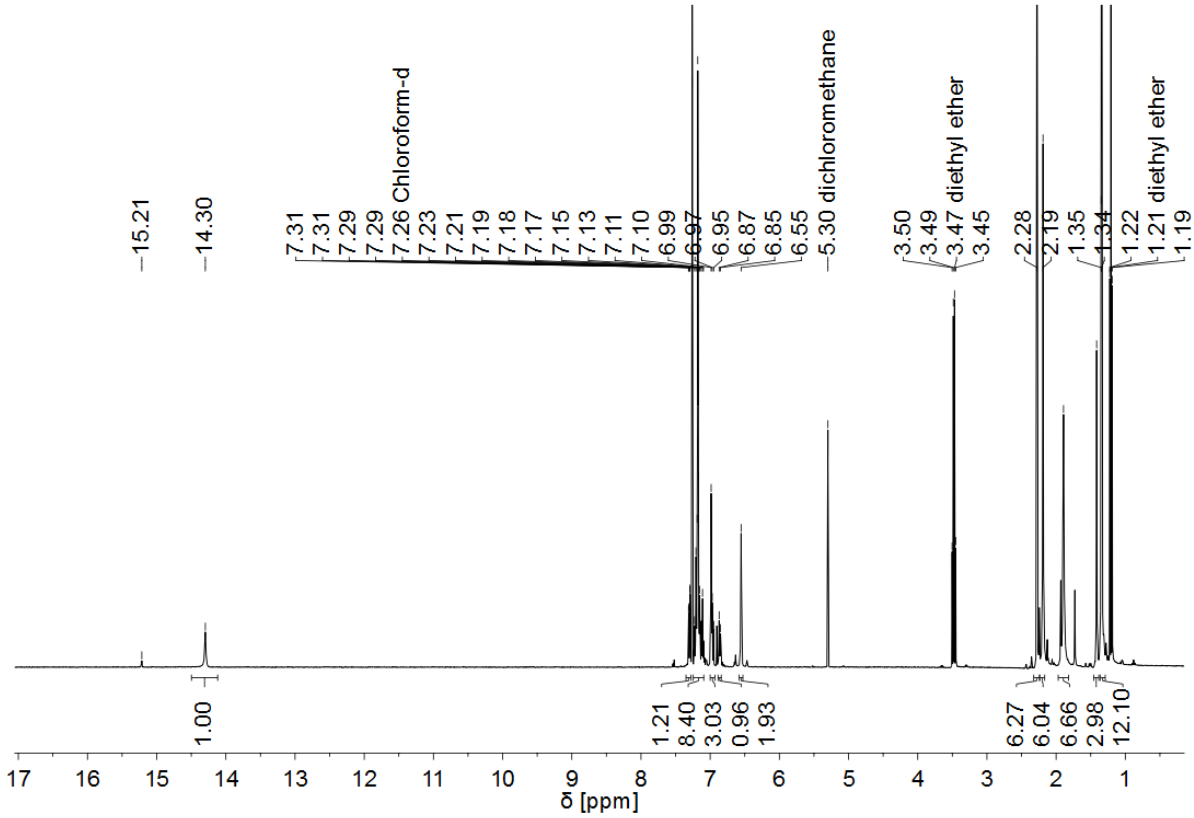

Figure A 91: ^{1}H NMR spectrum of **Mo-20** (400 MHz, $CDCl_3$). Only *syn*-isomer resonances are integrated.

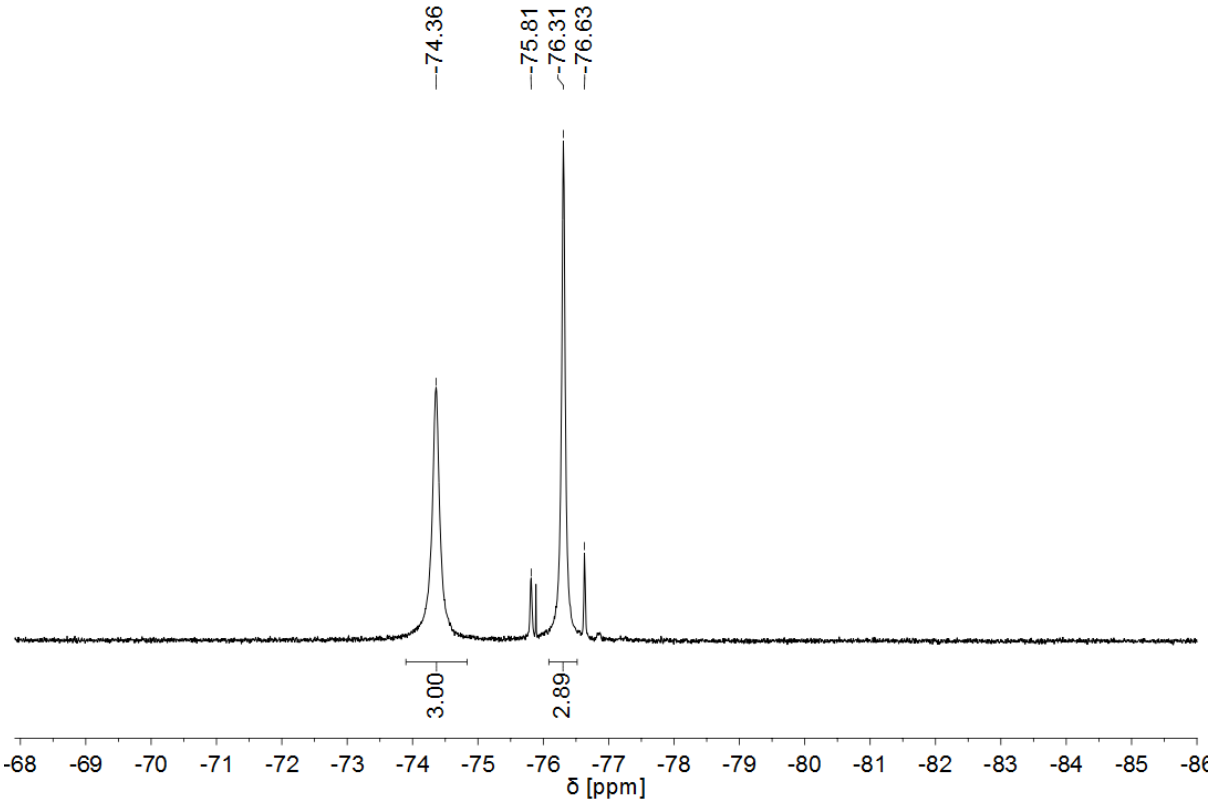

Figure A 92: ^{19}F NMR spectrum of **Mo-20** (376 MHz, $CDCl_3$). Only *syn*-isomer resonances are integrated.

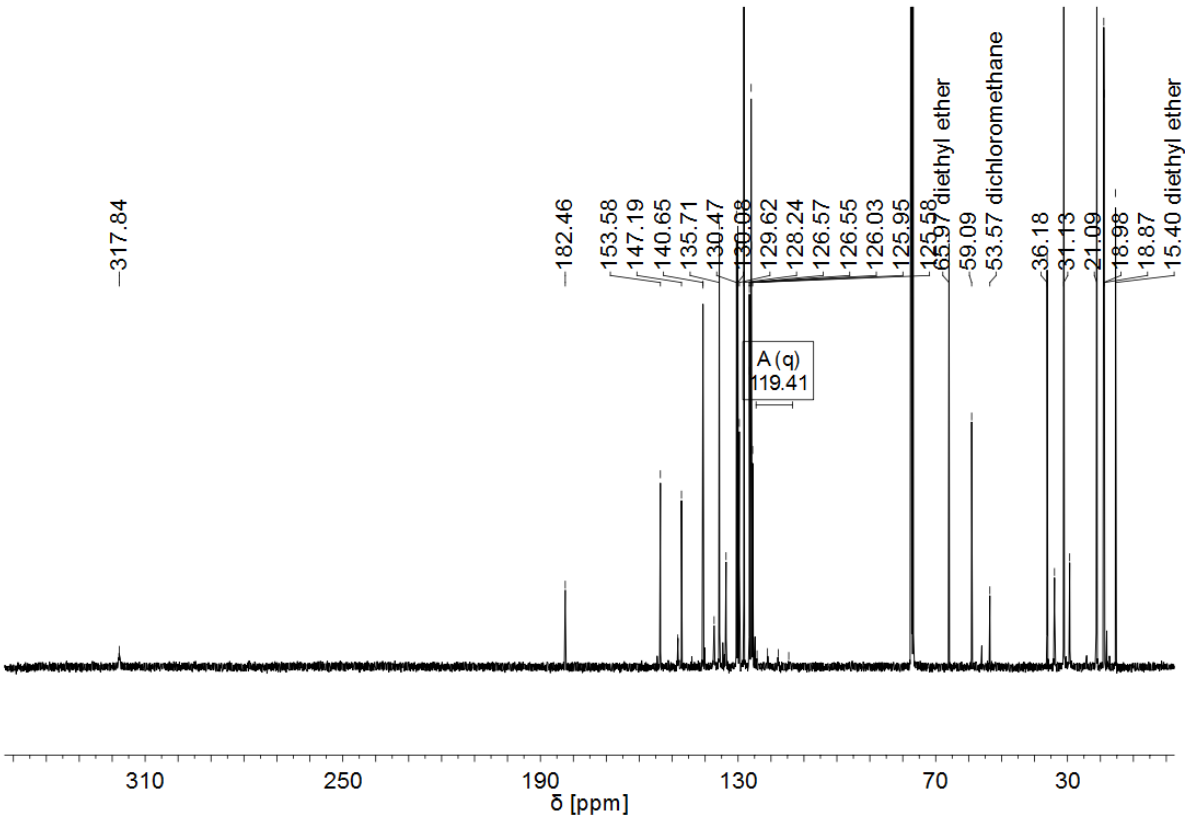

Figure A 93: ^{13}C NMR spectrum of **Mo-20** (101 MHz, $CDCl_3$).

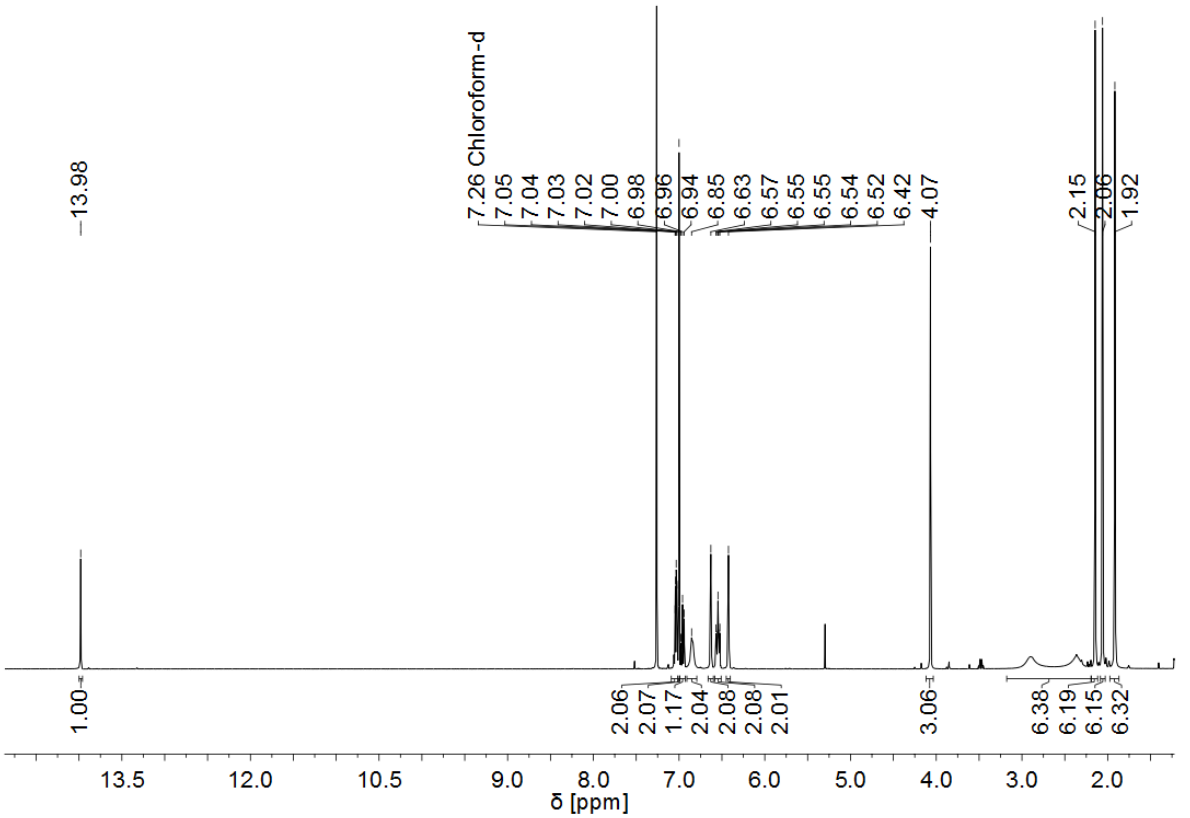

Figure A 94: ^{1}H NMR spectrum of **Mo-24** (400 MHz, $CDCl_3$).

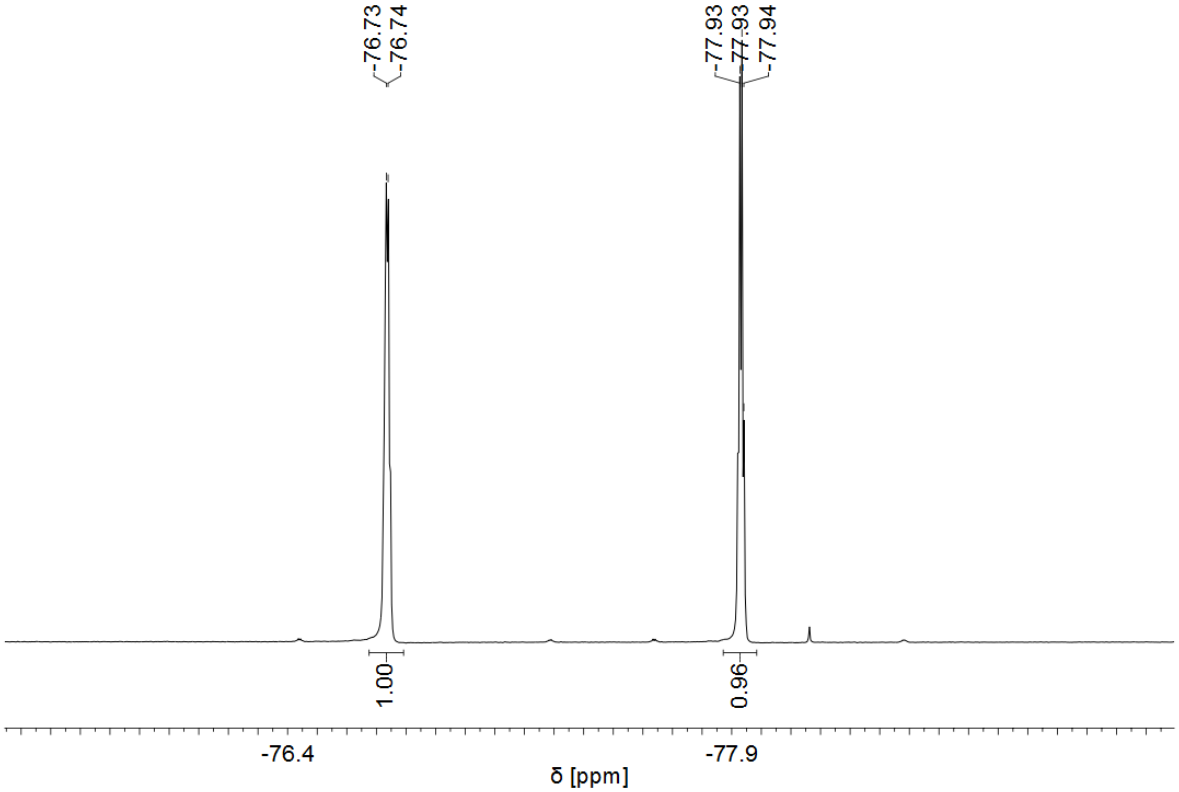

Figure A 95: ^{19}F NMR spectrum of **Mo-24** (376 MHz, $CDCl_3$).

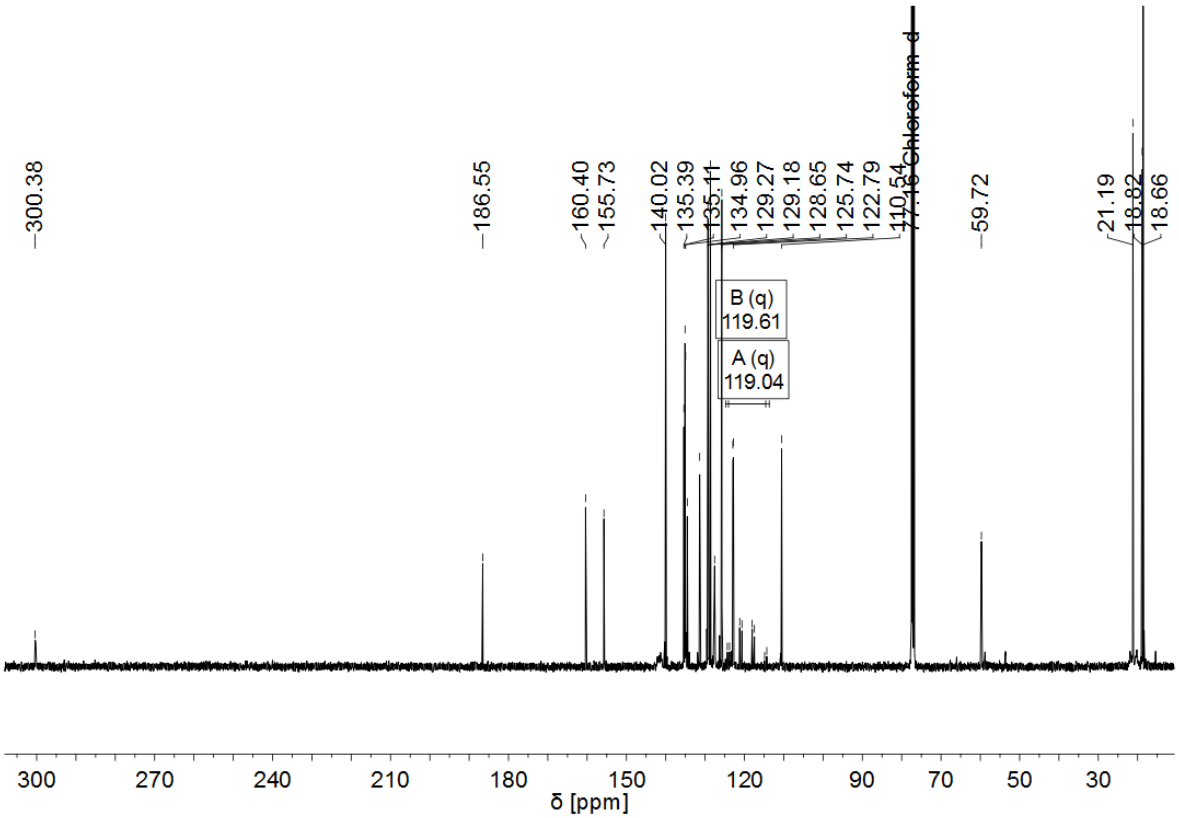

Figure A 96: ^{13}C NMR spectrum of **Mo-24** (101 MHz, $CDCl_3$).

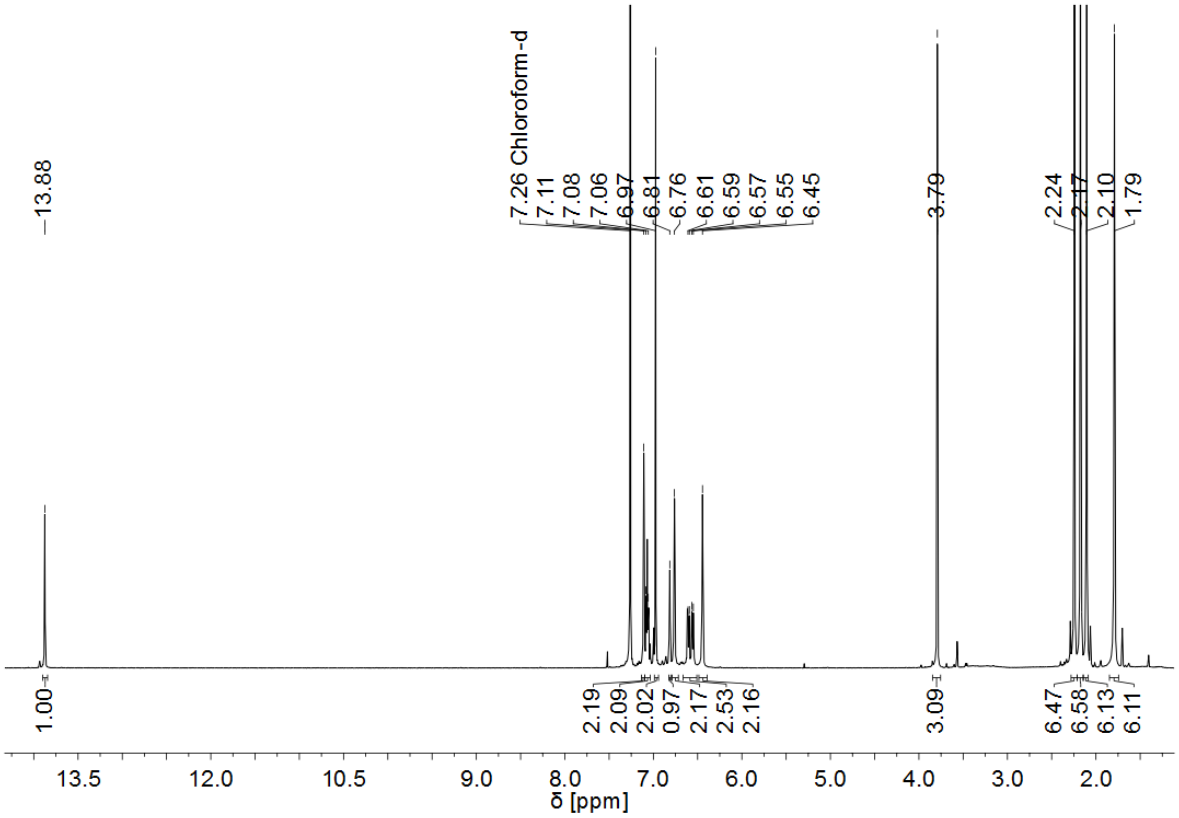

Figure A 97: ^{1}H NMR spectrum of **Mo-25** (400 MHz, $CDCl_3$).

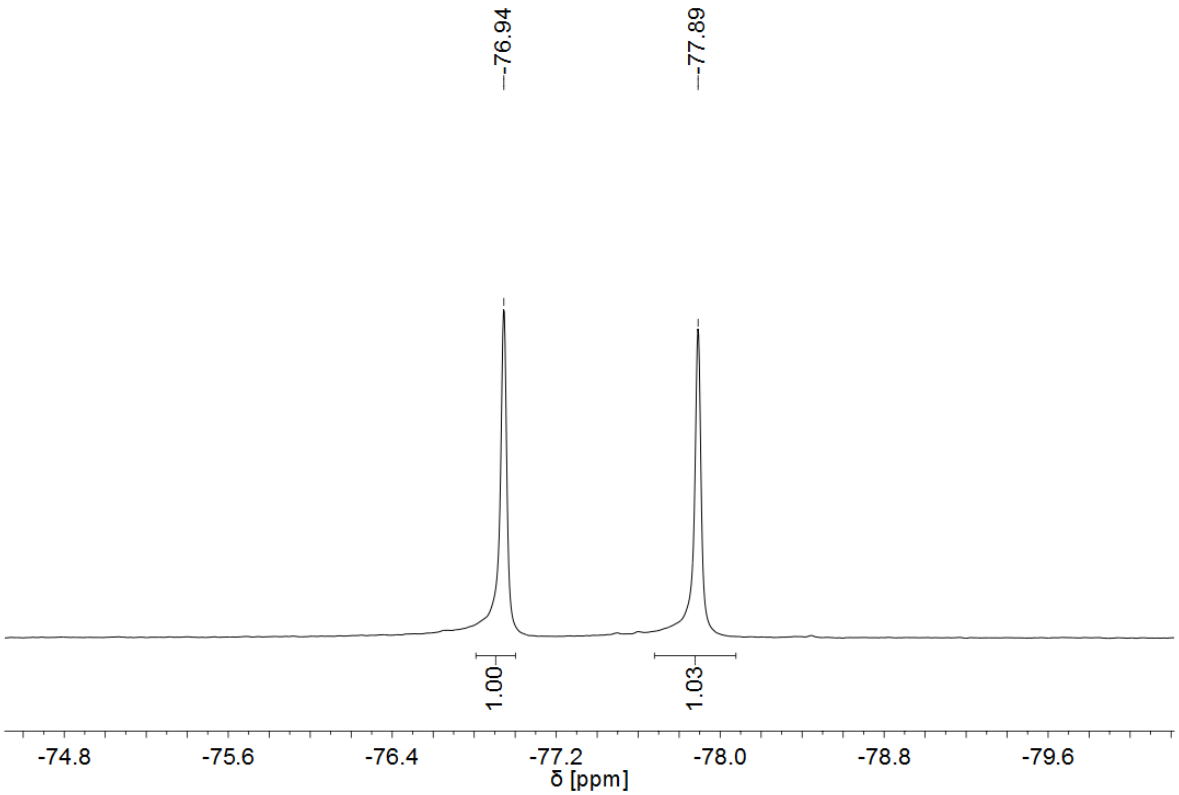

Figure A 98: ^{19}F NMR spectrum of **Mo-25** (376 MHz, $CDCl_3$).

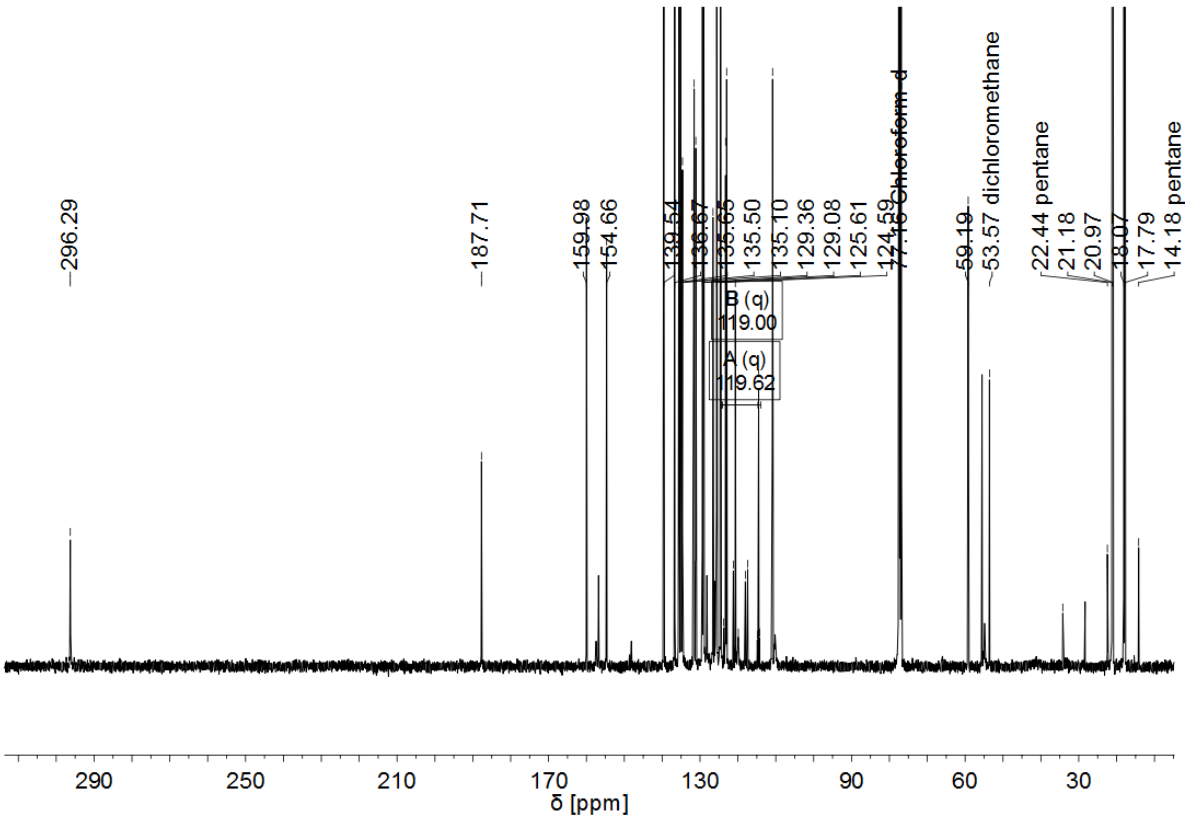

Figure A 99: ^{13}C NMR spectrum of **Mo-25** (101 MHz, $CDCl_3$).

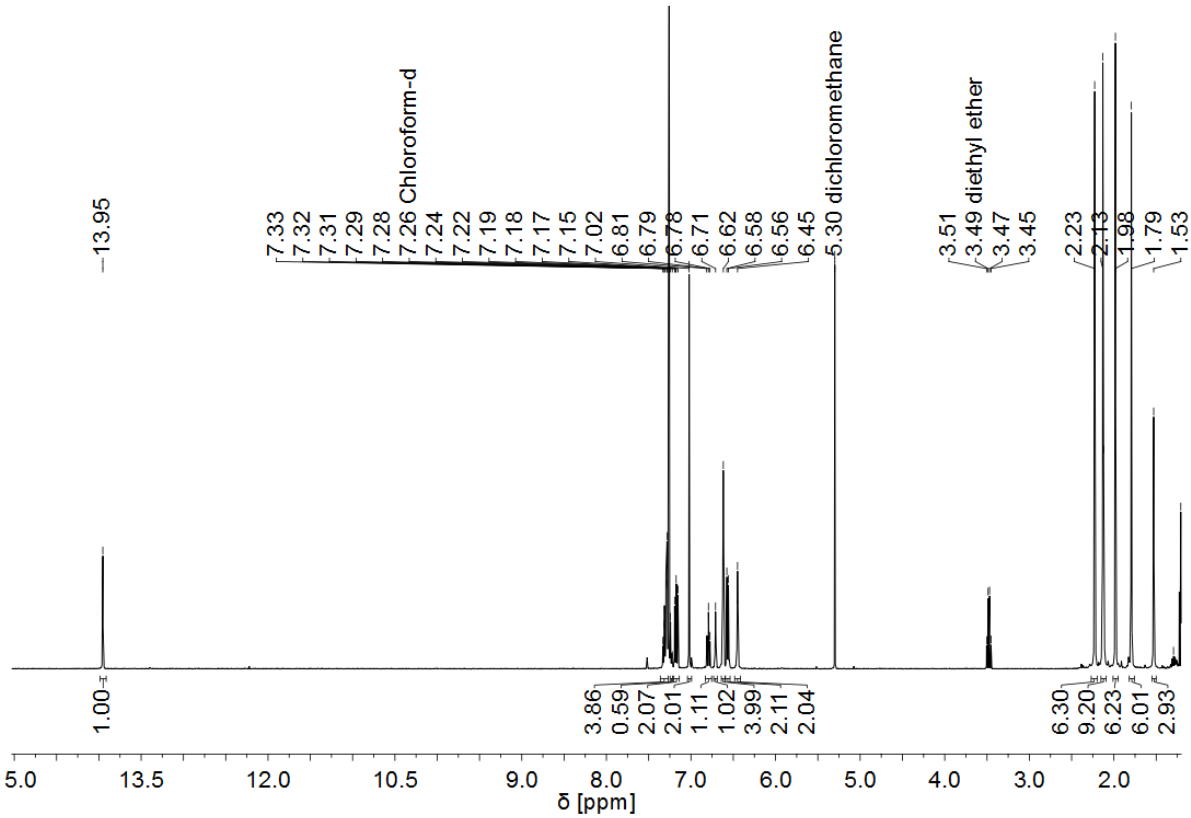

Figure A 100: ^{1}H NMR spectrum of **Mo-26** (400 MHz, $CDCl_3$).

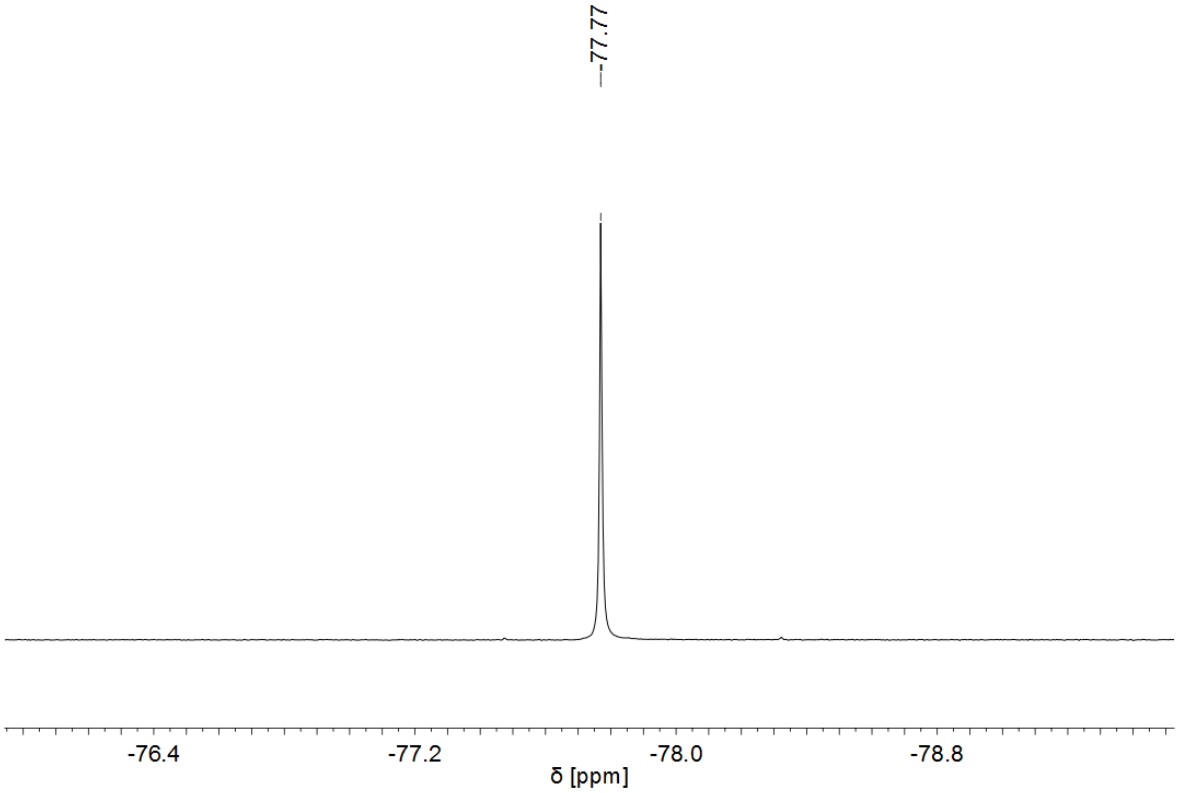

Figure A 101: ^{19}F NMR spectrum of **Mo-26** (376 MHz, $CDCl_3$).

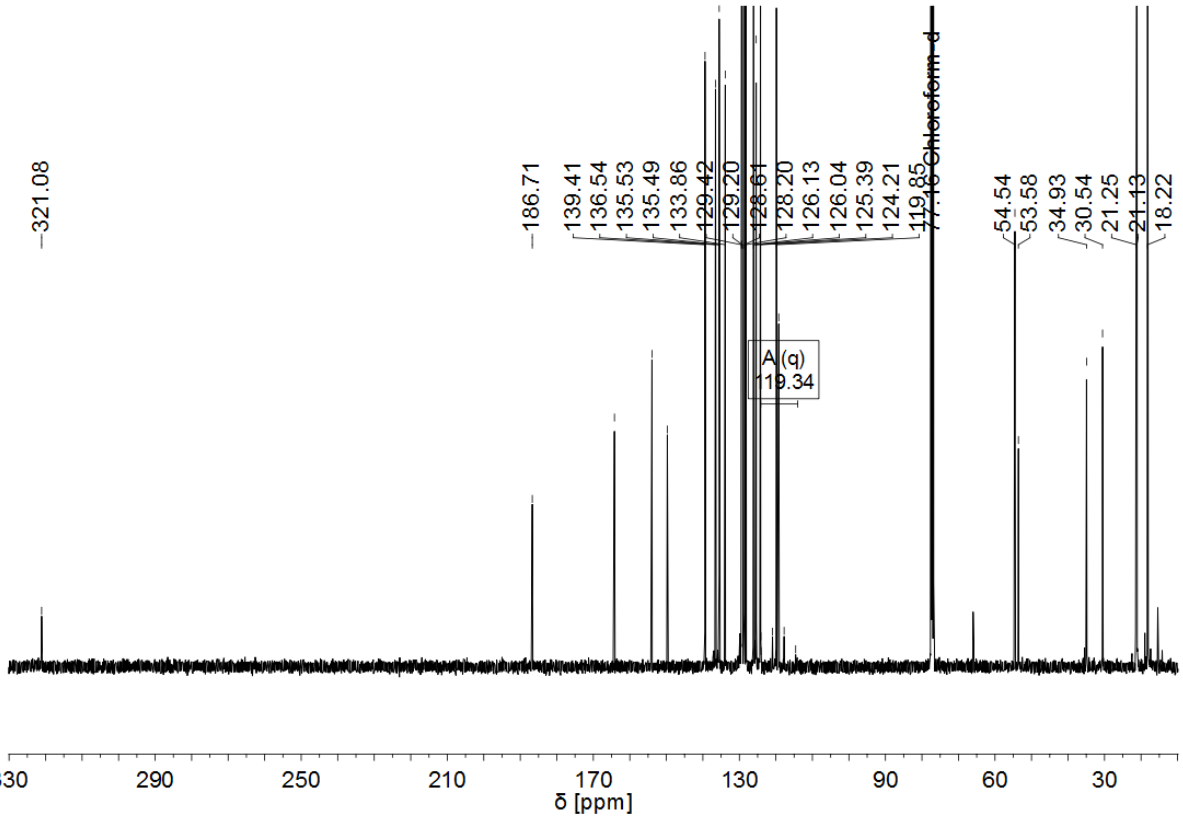

Figure A 102: ^{13}C NMR spectrum of **Mo-26** (101 MHz, $CDCl_3$).

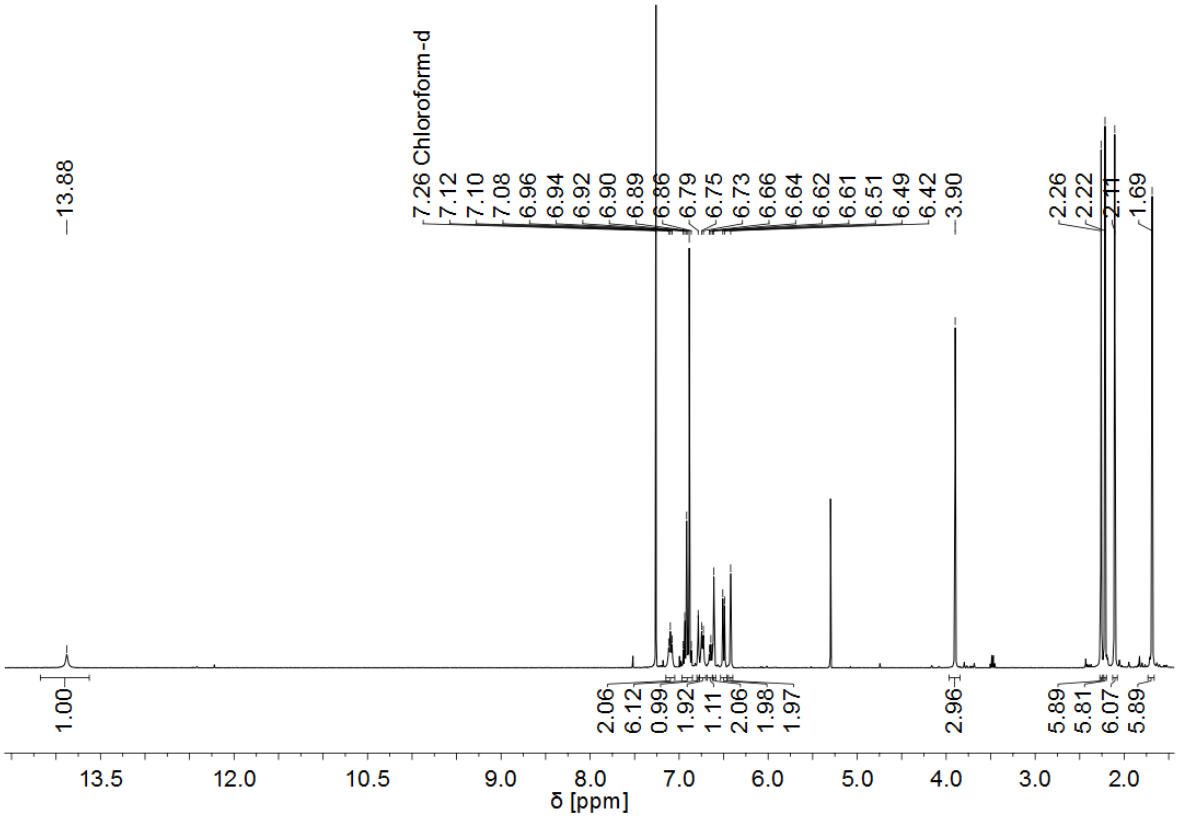

Figure A 103: ^{1}H NMR spectrum of **Mo-27** (400 MHz, $CDCl_3$).

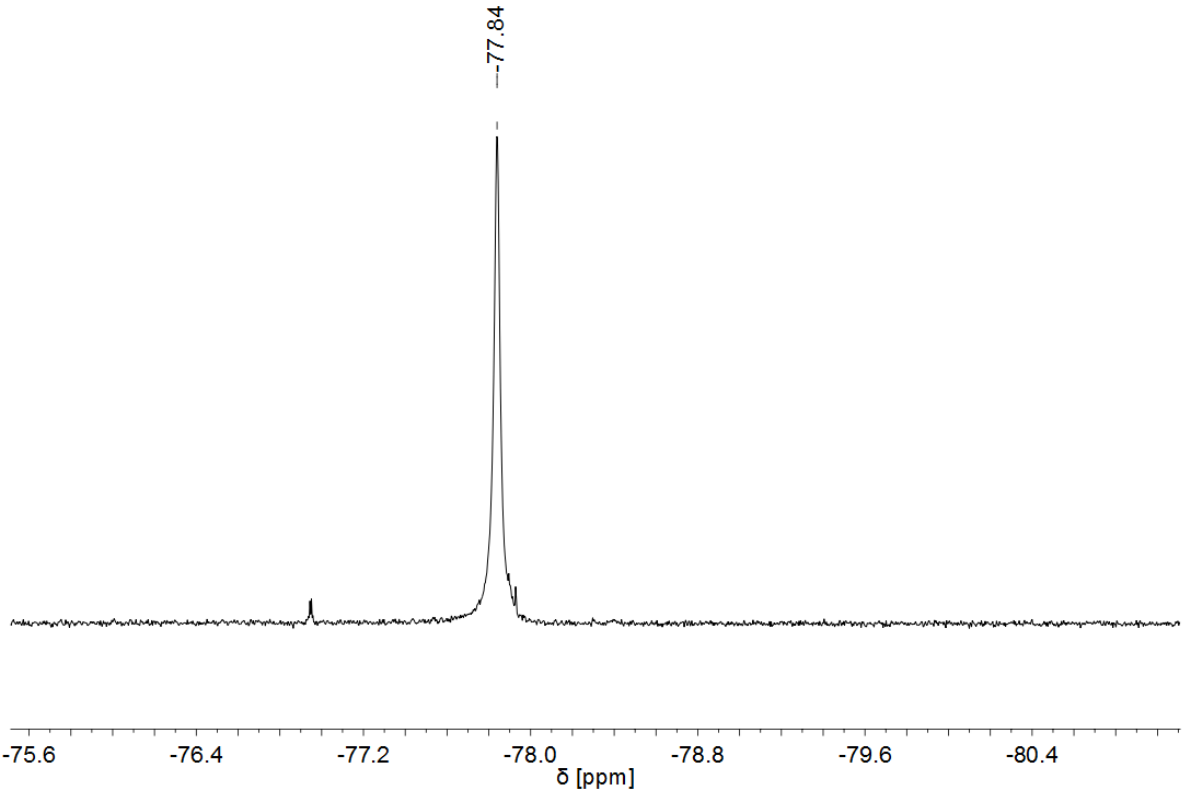

Figure A 104: ^{19}F NMR spectrum of **Mo-27** (376 MHz, $CDCl_3$).

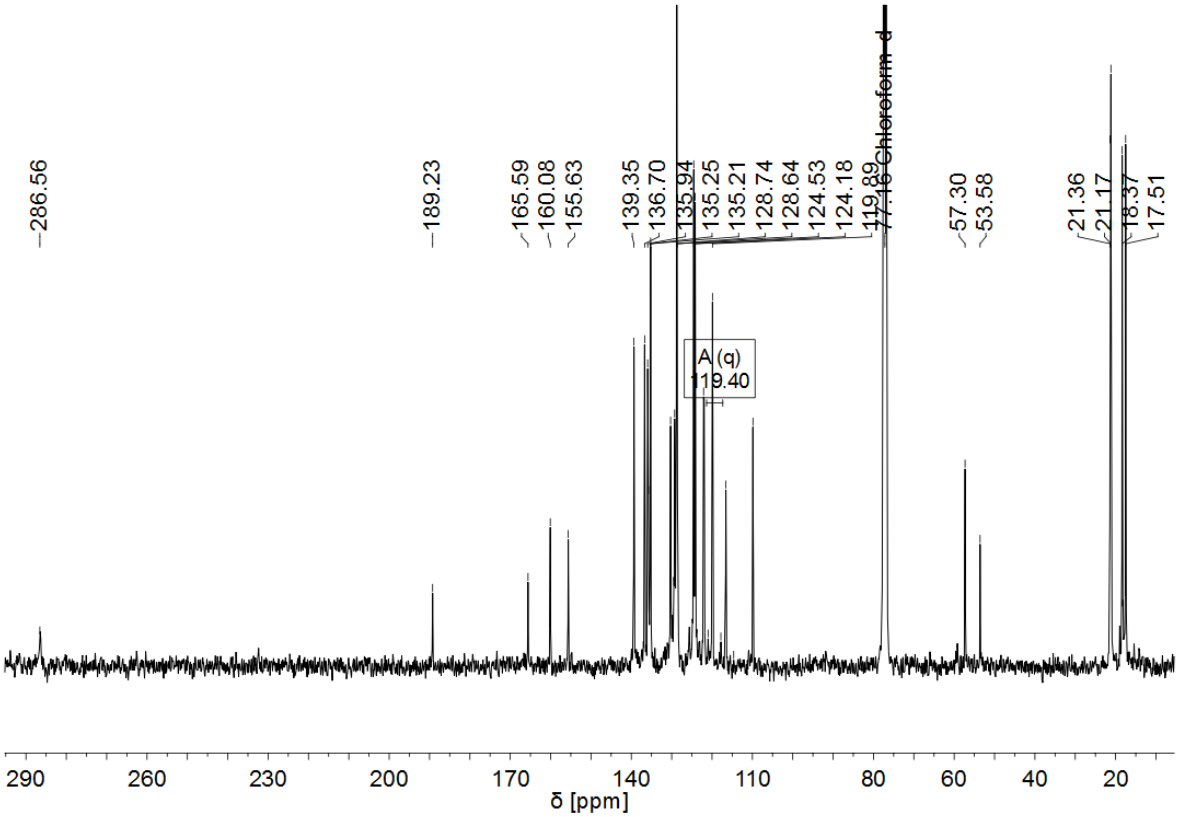

Figure A 105: ^{13}C NMR spectrum of **Mo-27** (101 MHz, $CDCl_3$).

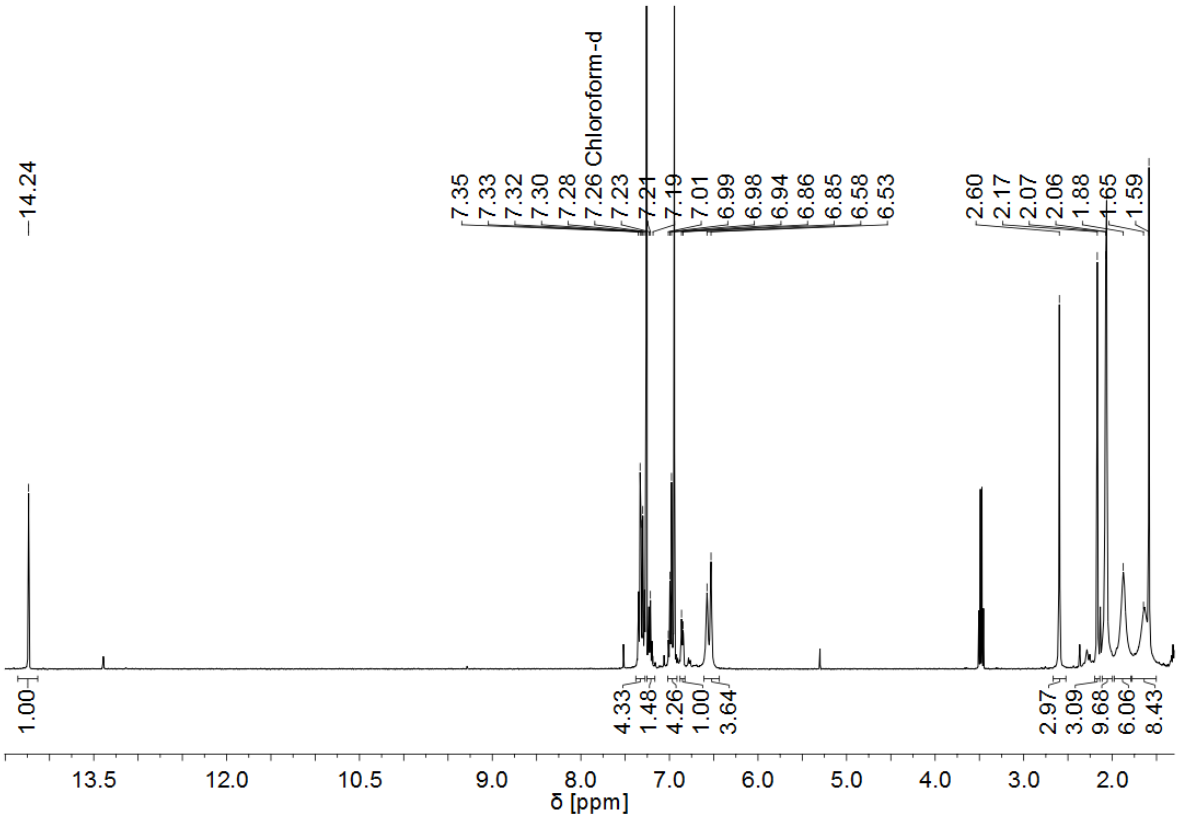

Figure A 106: ^{1}H NMR spectrum of **Mo-28** (400 MHz, $CDCl_3$).

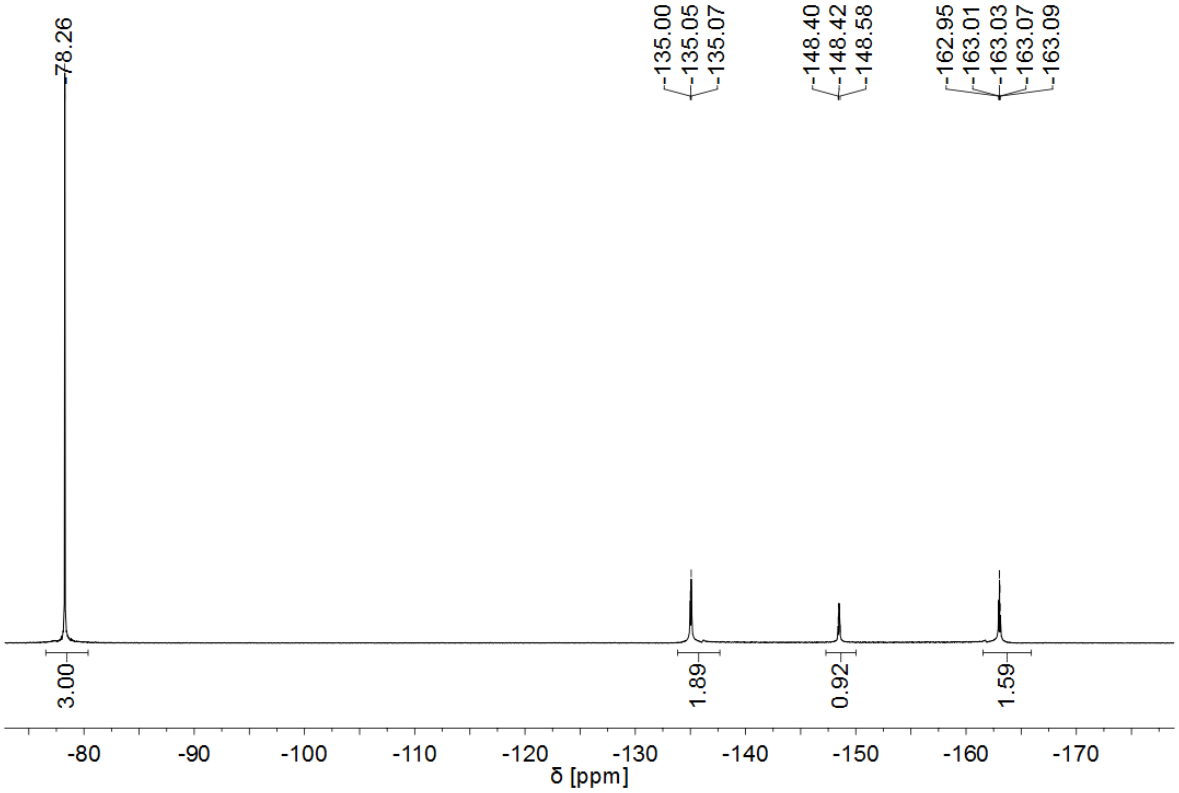

Figure A 107: ^{19}F NMR spectrum of **Mo-28** (376 MHz, $CDCl_3$).

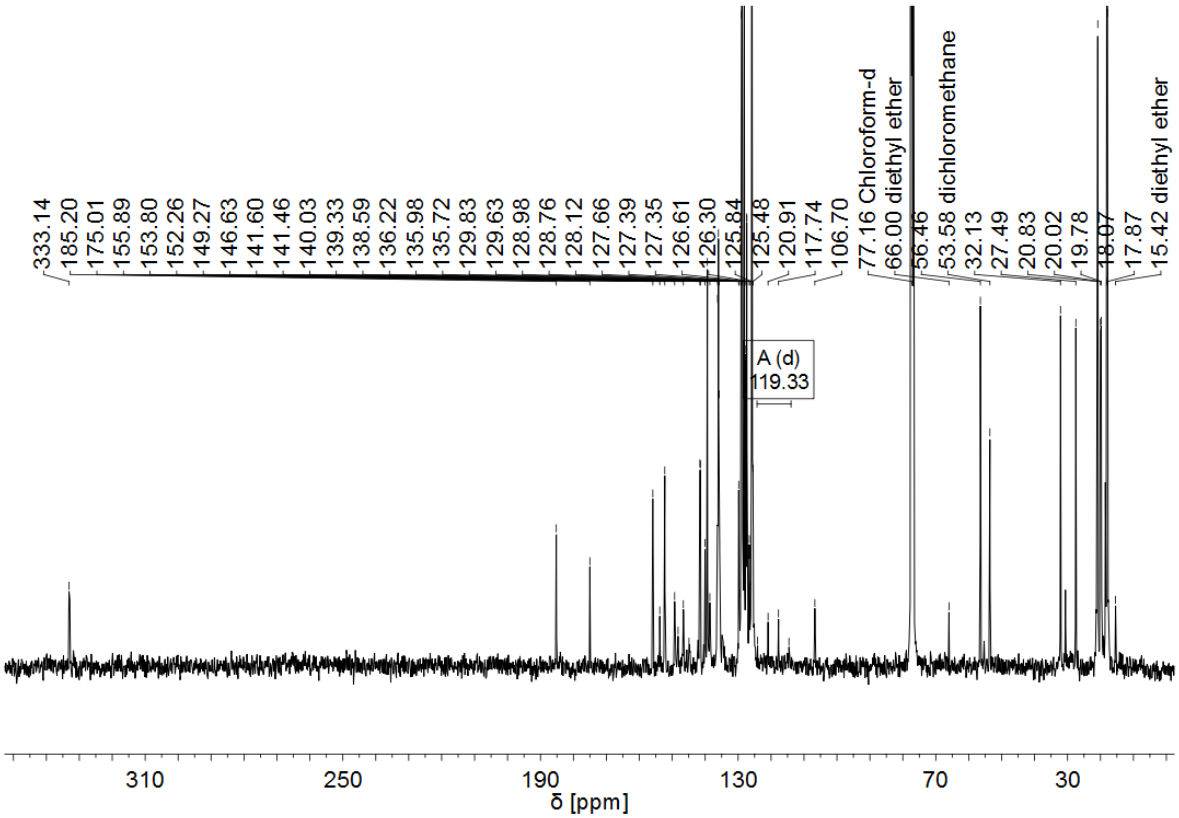

Figure A 108: ^{13}C NMR spectrum of **Mo-28** (101 MHz, $CDCl_3$).

9.3.2 AIR STABILITY TESTS

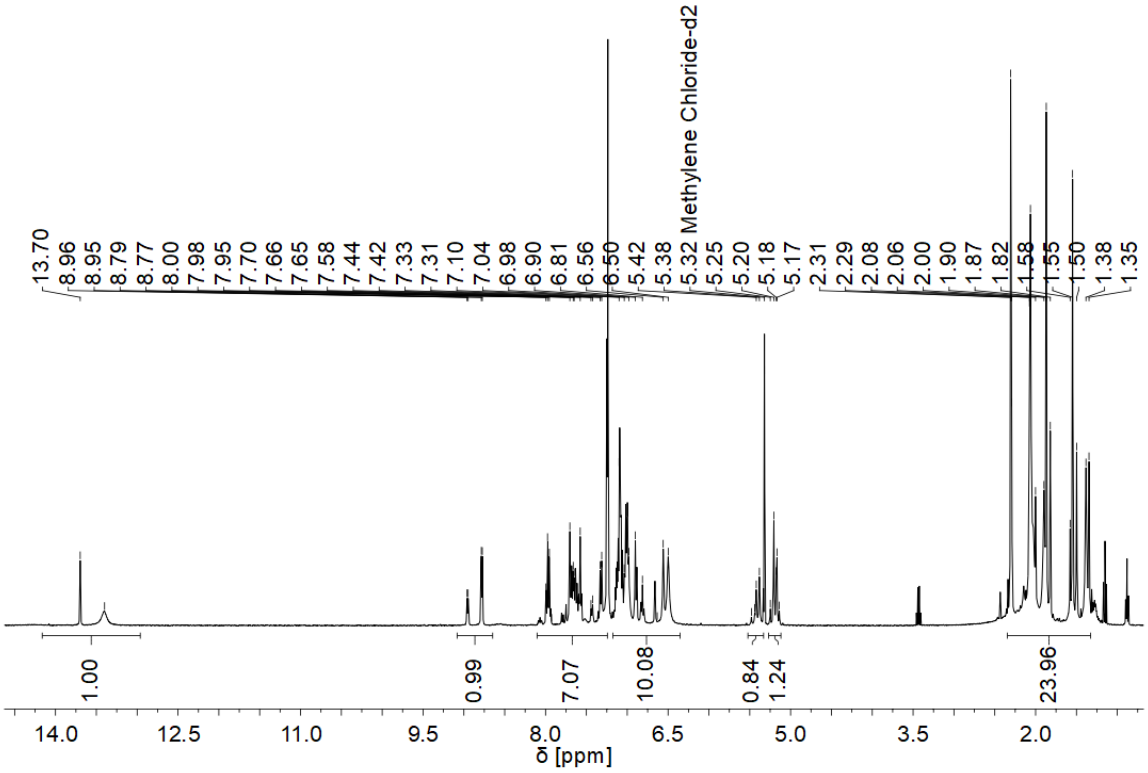

Figure A 109: ^{1}H NMR spectrum of **Mo-12** in CD_2Cl_2 after being stored under air for two hours. No decomposition was observed.

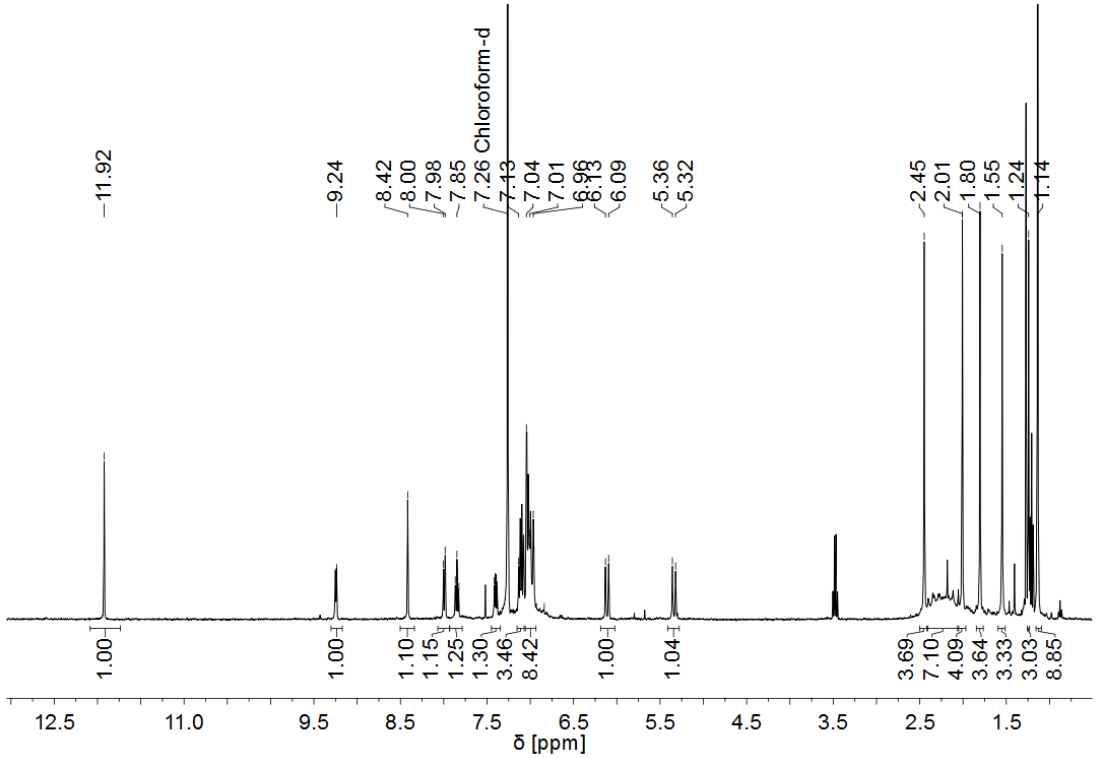

Figure A 110: ^{1}H NMR spectrum of **Mo-15** in $CDCl_3$ after being stored under air for twelve hours. No decomposition was observable.

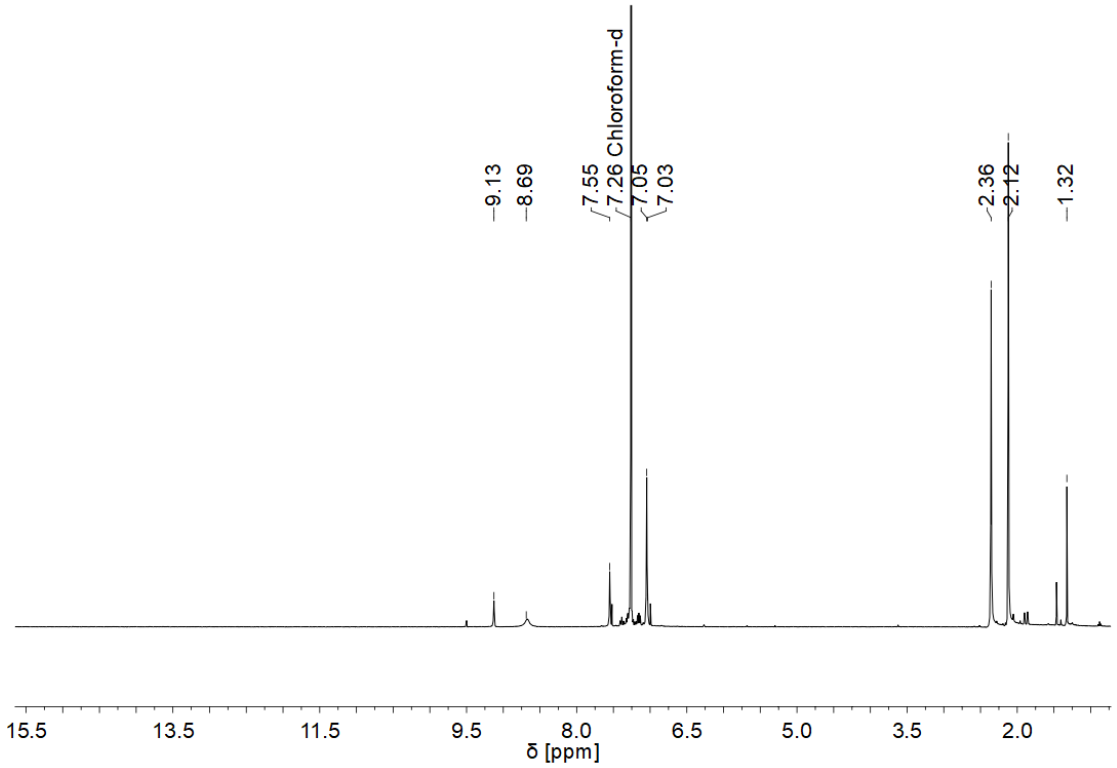

Figure A 111: ^{1}H NMR spectrum of **Mo-21** (precursor complex to **Mo-24**) in $CDCl_3$ after being stored under air for twelve hours. No alkylidene signal was observable.

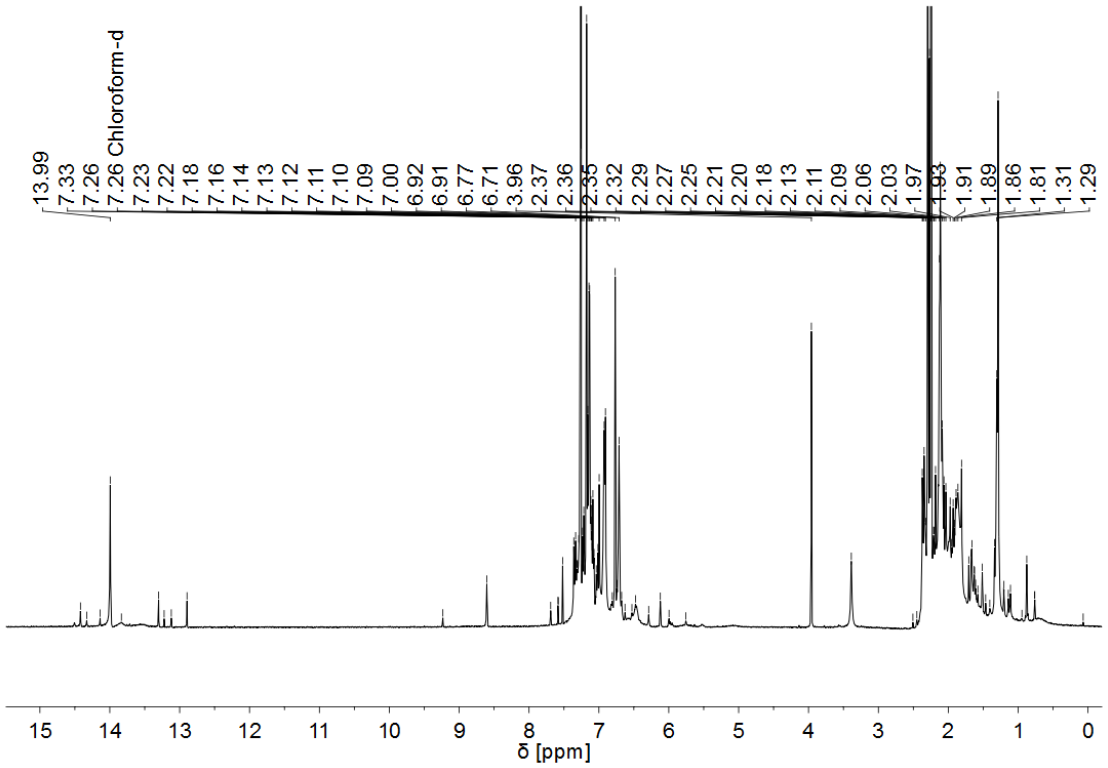

Figure A 112: ^{1}H NMR spectrum of **Mo-22** (precursor complex to **Mo-25**) in $CDCl_3$ after being stored under air for twelve hours. Multiple alkylidene signals were visible.

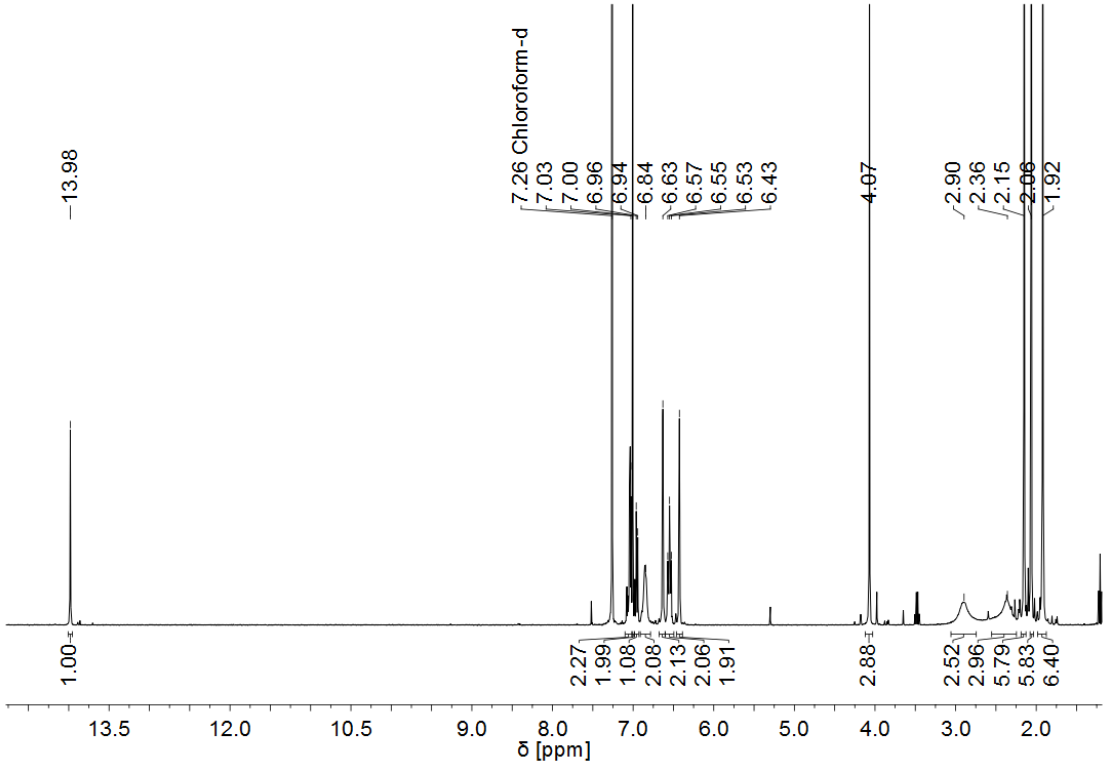

Figure A 113: ^{1}H NMR spectrum of **Mo-24** in $CDCl_3$ after being stored under air for twelve hours. No decomposition was observed.

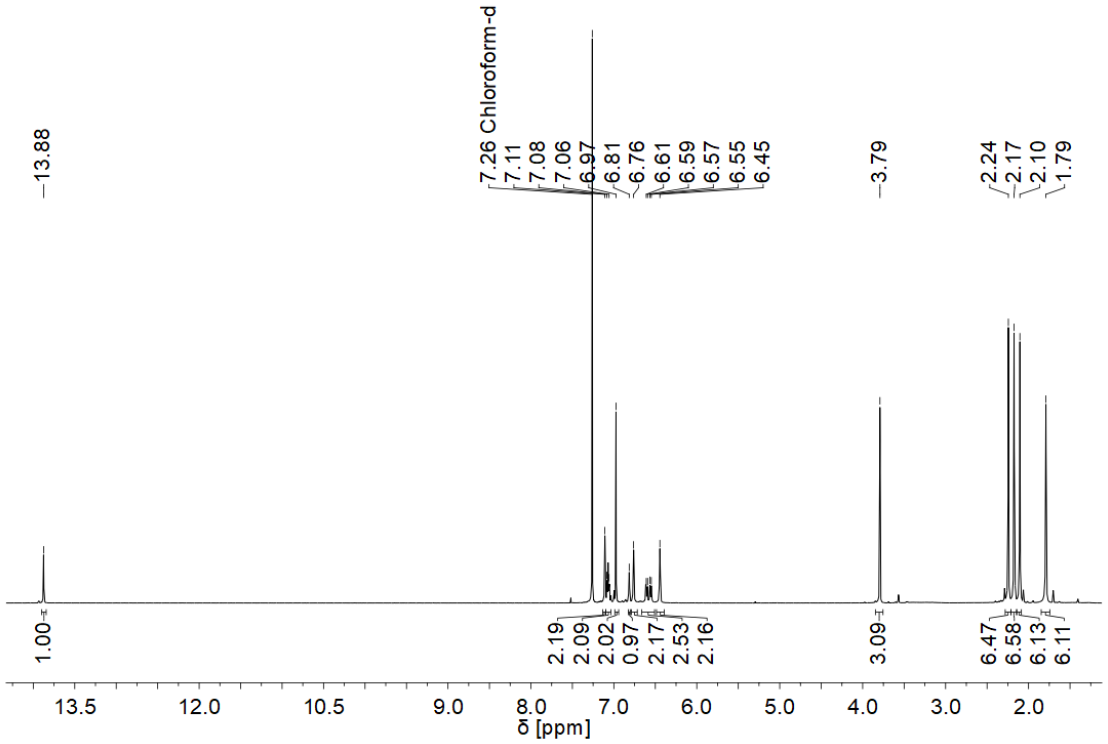

Figure A 114: ^{1}H NMR spectrum of **Mo-25** in $CDCl_3$ after being stored under air for twelve hours. No decomposition was observed.

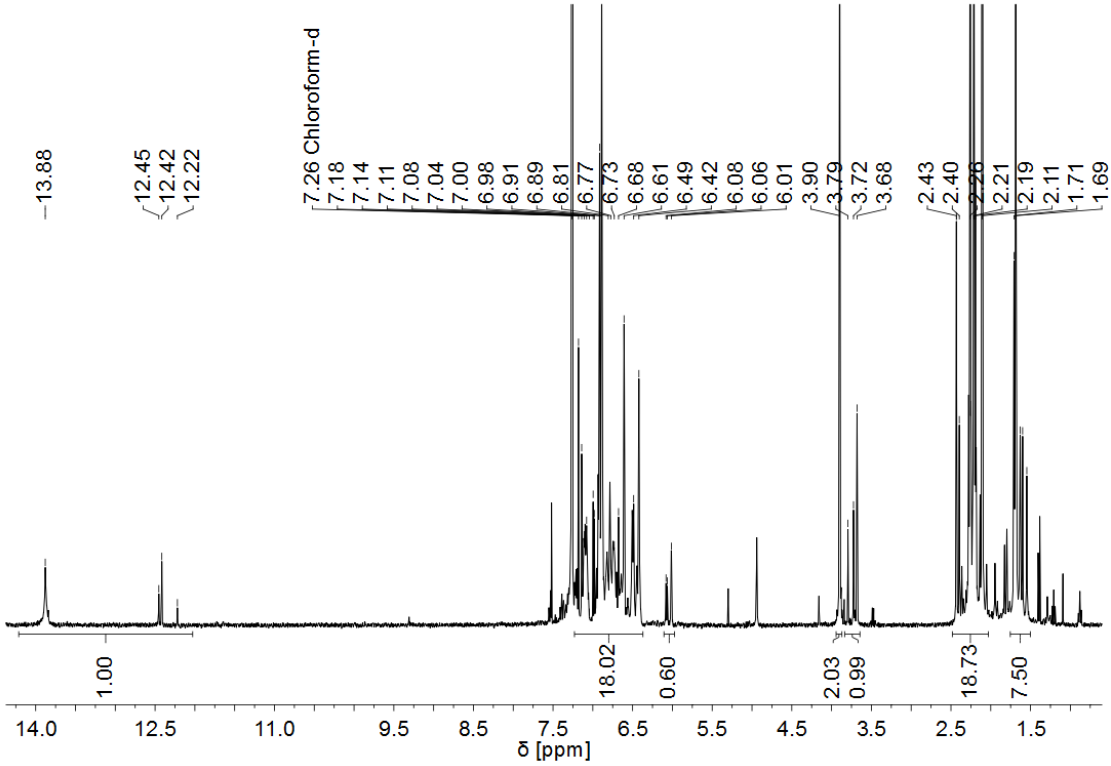

Figure A 115: ^{1}H NMR spectrum of **Mo-27** in $CDCl_3$ after being stored under air for twelve hours. Two additional alkylidene signals were visible.

9.4 SYNTHESIS ROUTES TO CHIRAL MOLYBDENUM IMIDO ALKYLIDENE N-HETEROCYCLIC CARBENE COMPLEXES

9.4.1 REACTIONS WITH MOLYBDENUM IMIDO ALKYLIDENE N-HETEROCYCLIC CARBENE BISTRIFLATE COMPLEXES –CH-ACTIVATION ISSUE

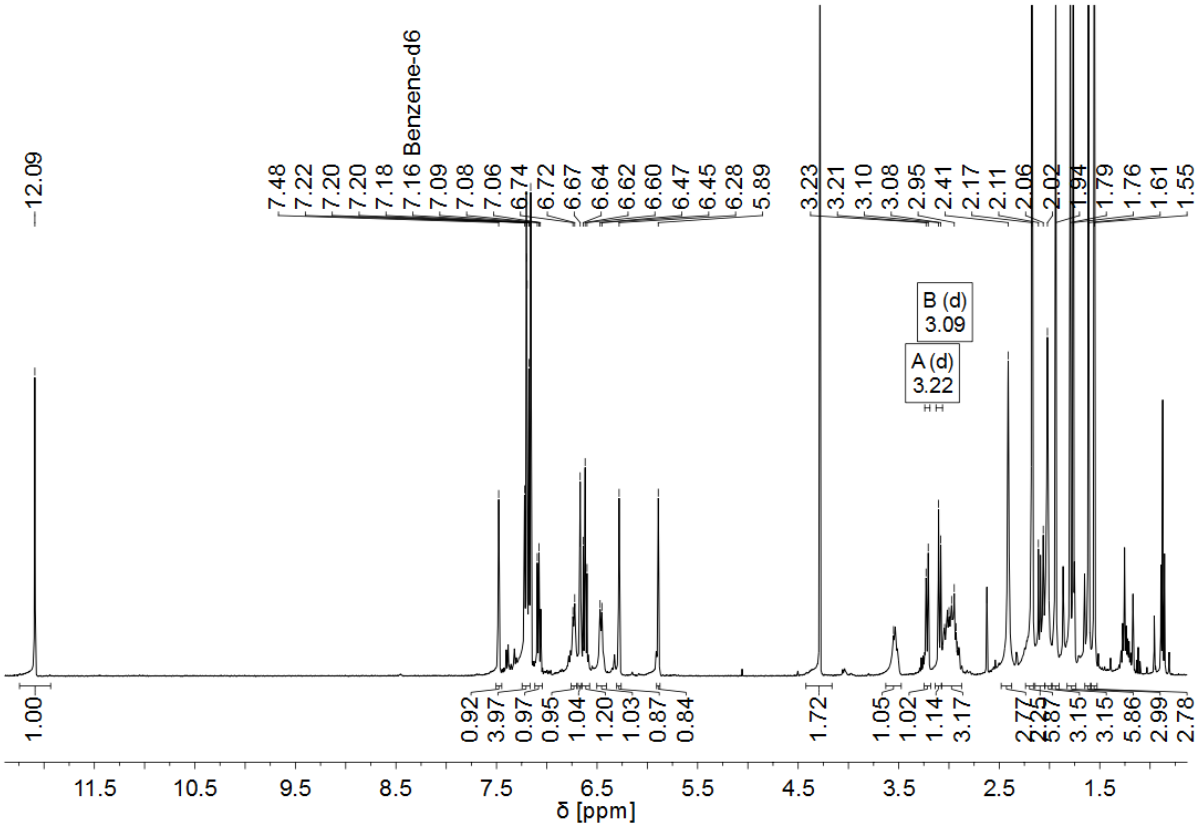

Figure A 116: ^{1}H NMR spectrum of **Mo-29** (400 MHz, C_6D_6).

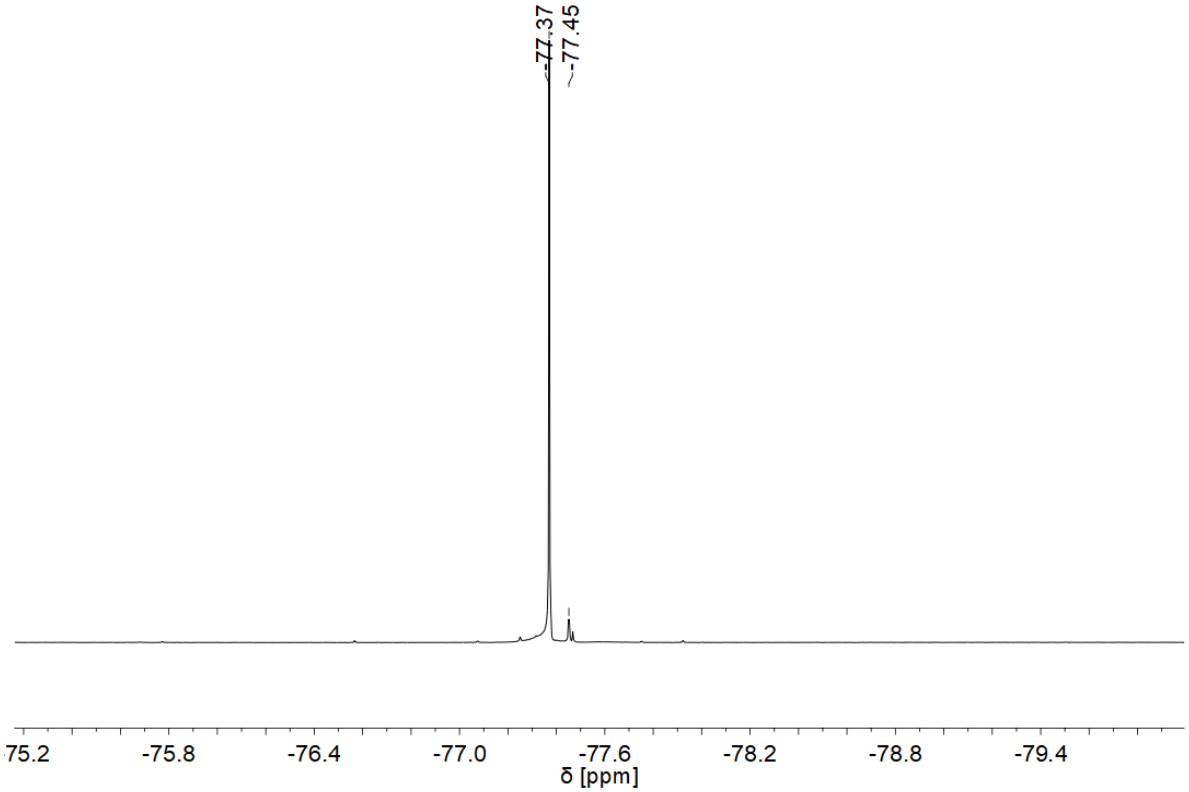

Figure A 117: ^{19}F NMR spectrum of **Mo-29** (376 MHz, C_6D_6).

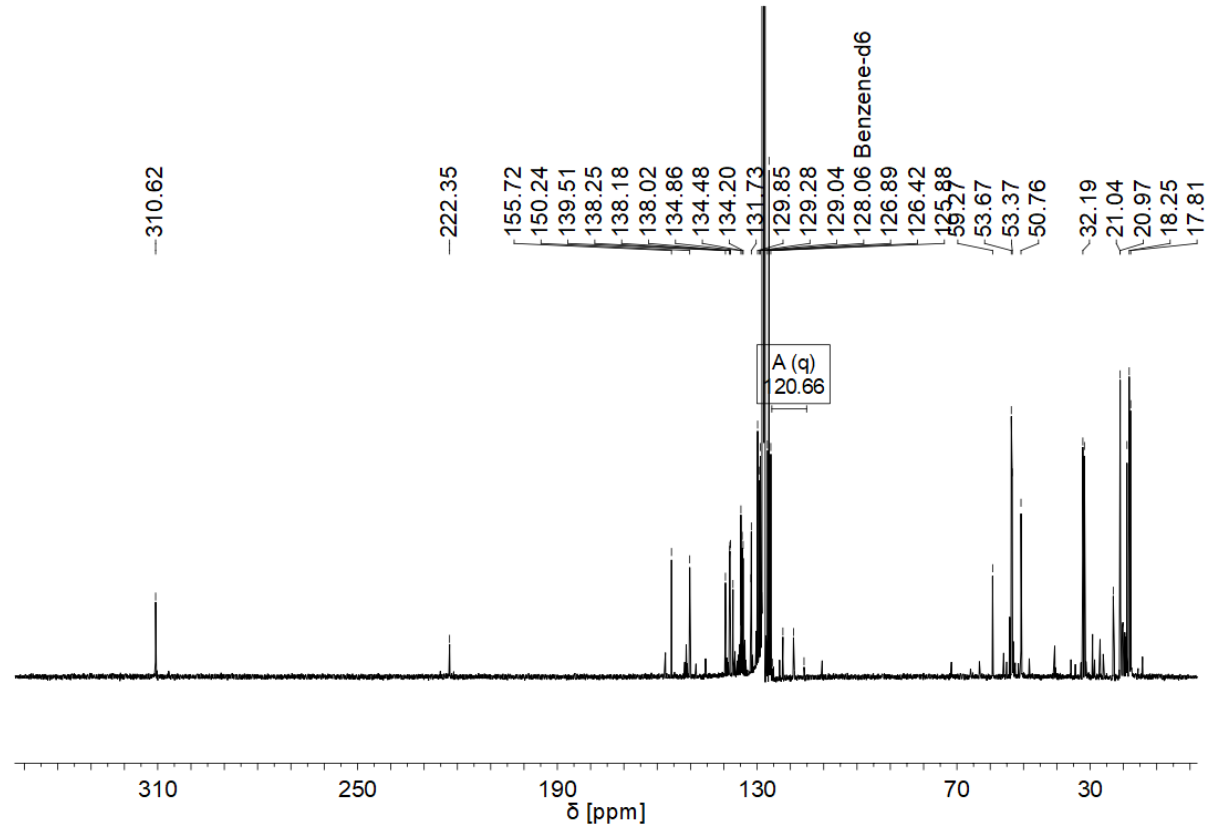

Figure A 118: ^{13}C NMR spectrum of **Mo-29** (101 MHz, C_6D_6).

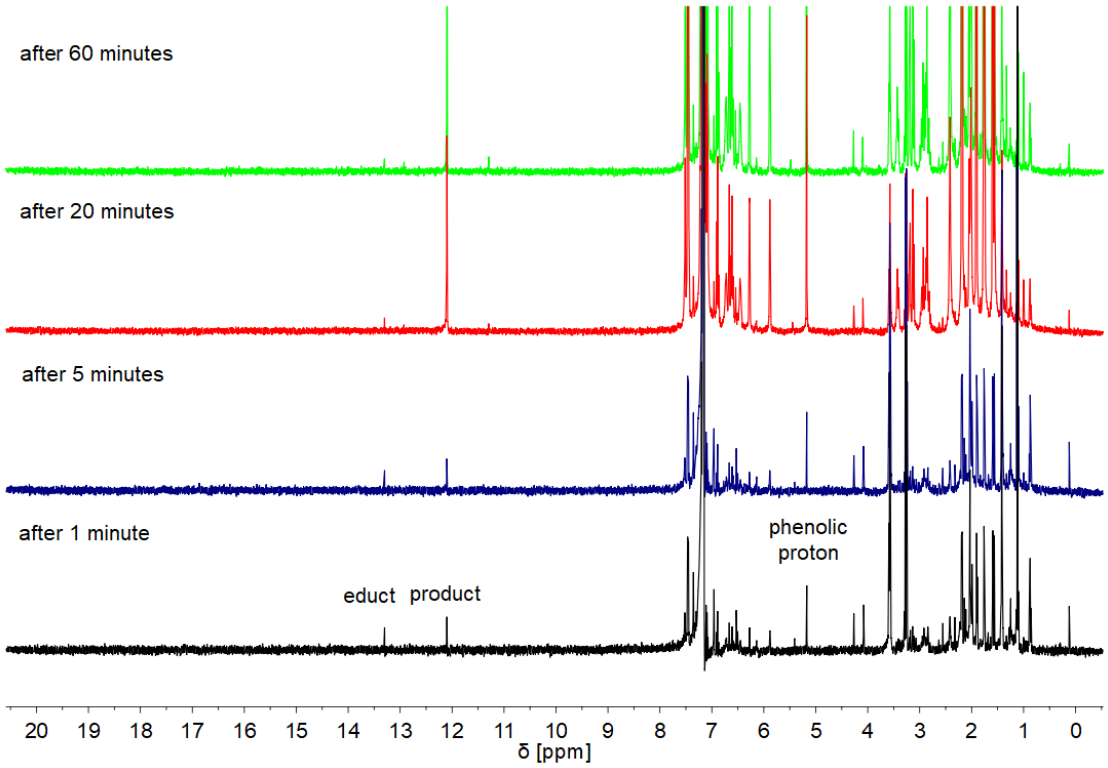

Figure A 119: Stacked ^{1}H NMR spectra of the reaction of 2,6-diphenylphenol with **Mo-1** in C_6D_6 after 1, 5, 20 and 60 minutes.

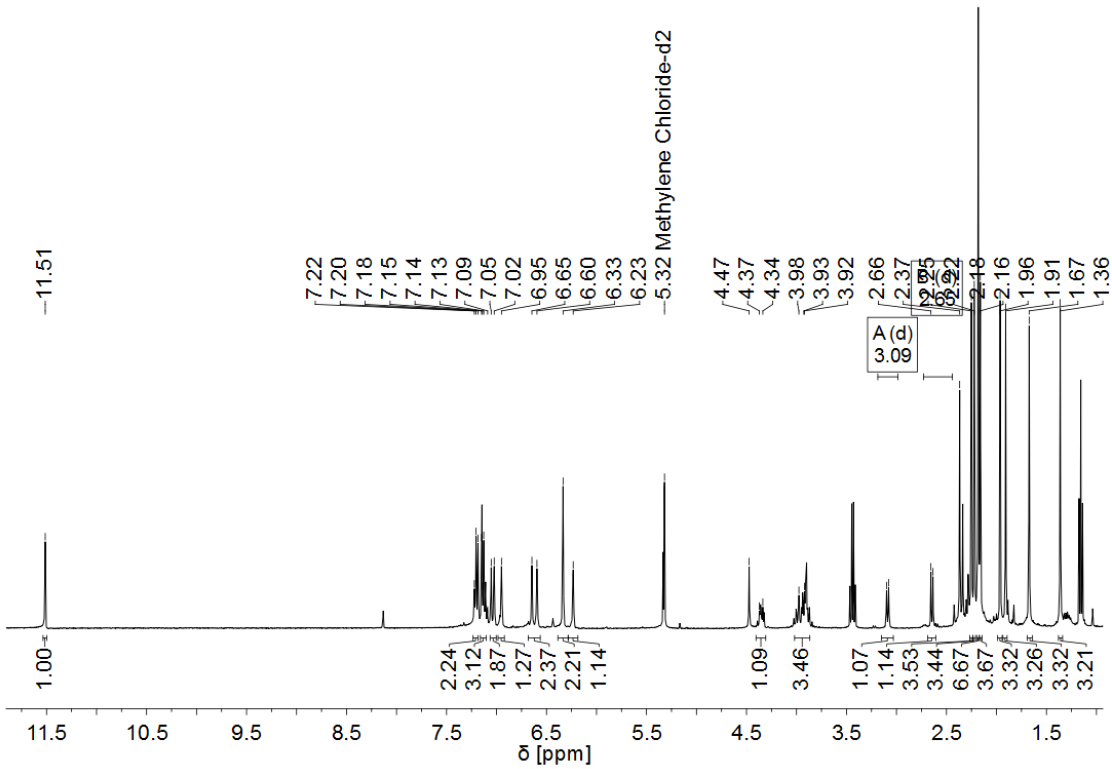

Figure A 120: ^{1}H NMR spectrum of **Mo-31** (400 MHz, CD_2Cl_2).

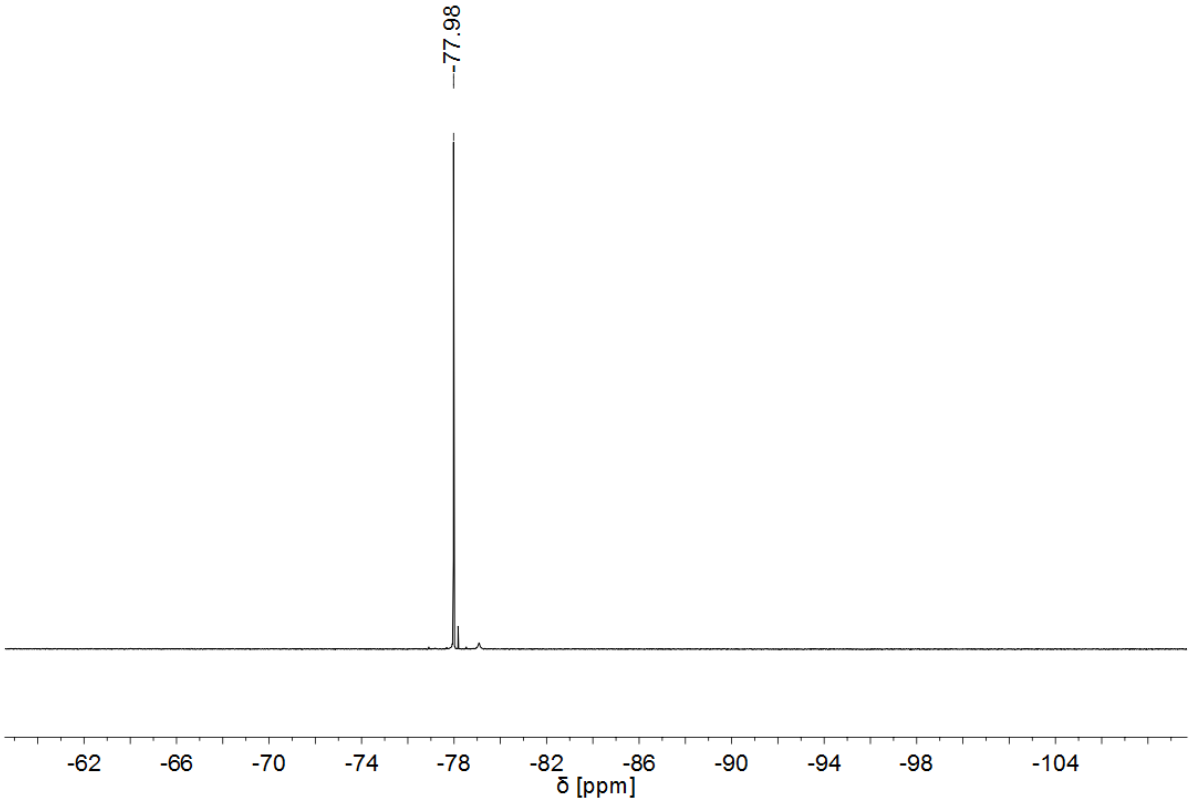

Figure A 121: ^{19}F NMR spectrum of **Mo-31** (376 MHz, CD_2Cl_2).

9.4.2 *Molybdenum Imido alkylidene bispyrrolide N-heterocyclic carbene complexes*

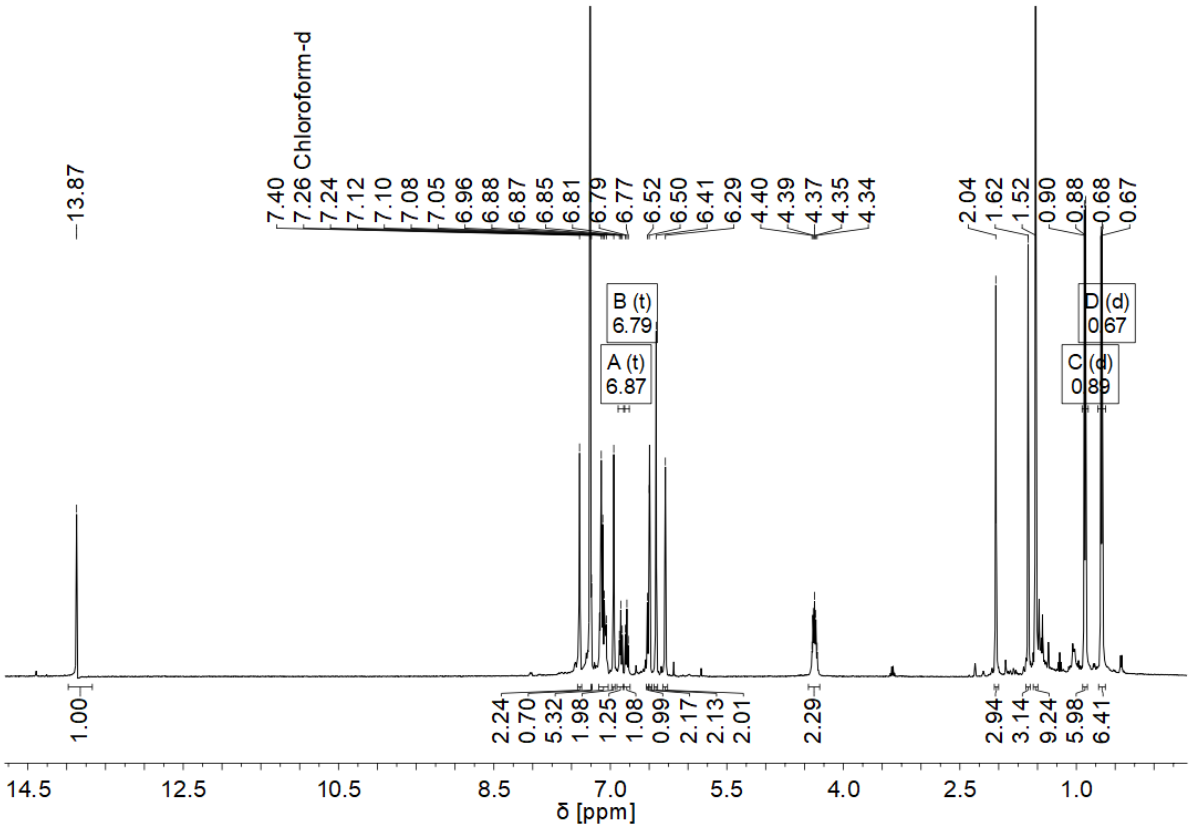

Figure A 122: ^{1}H NMR spectrum of **Mo-71** (400 MHz, $CDCl_3$).

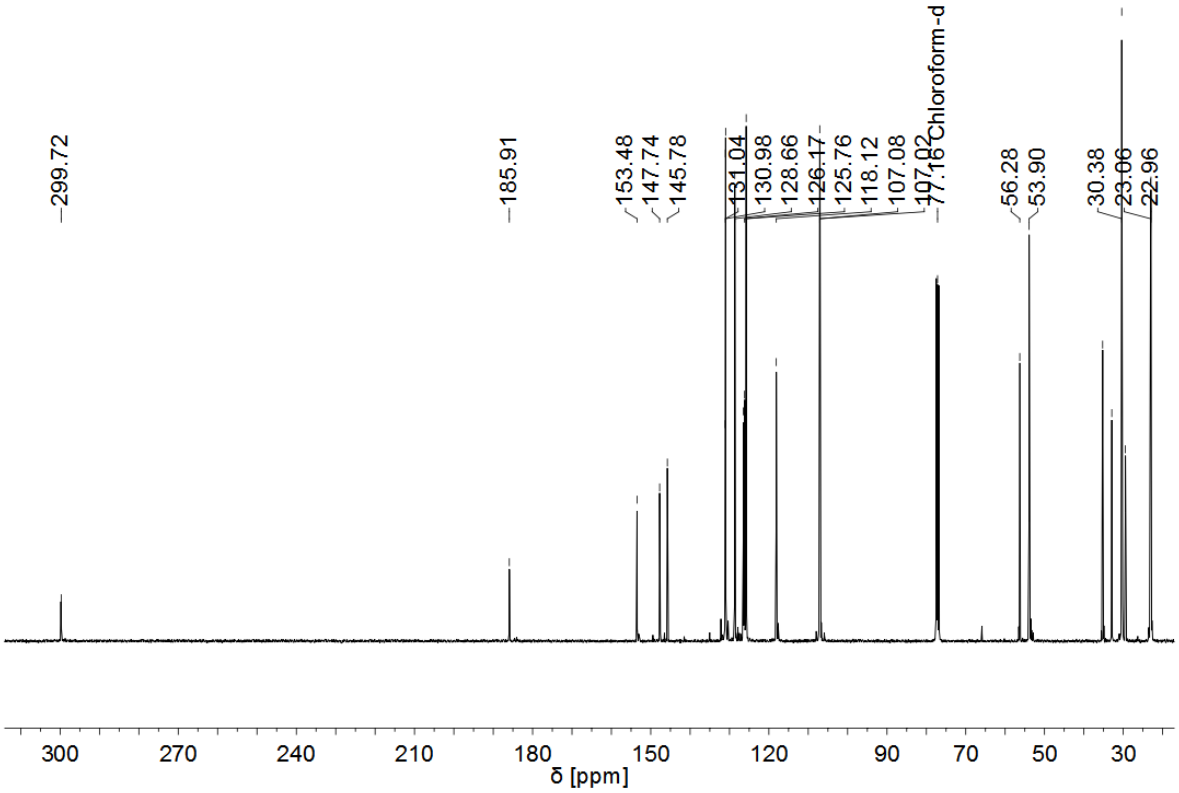

Figure A 123: ^{13}C NMR spectrum of **Mo-71** (101 MHz, $CDCl_3$).

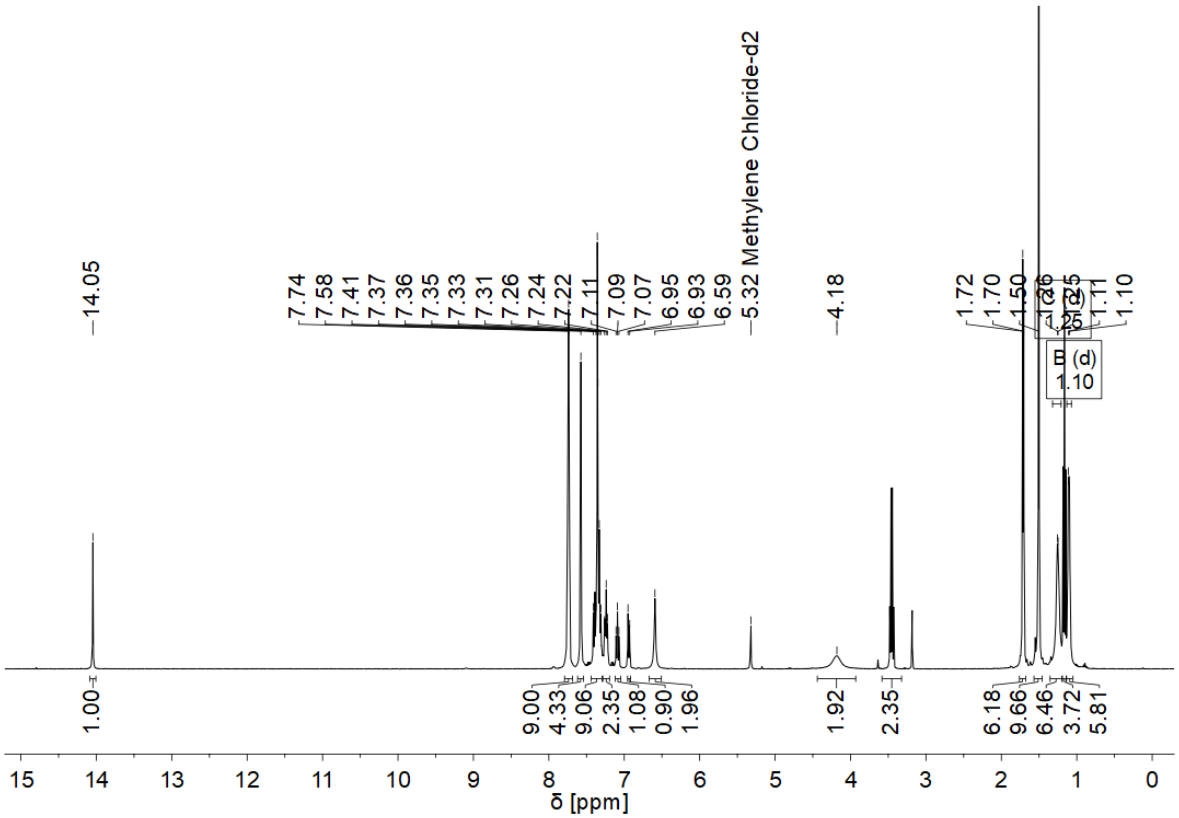

Figure A 124: ^{1}H NMR spectrum of **Mo-72** (400 MHz, CD_2Cl_2).

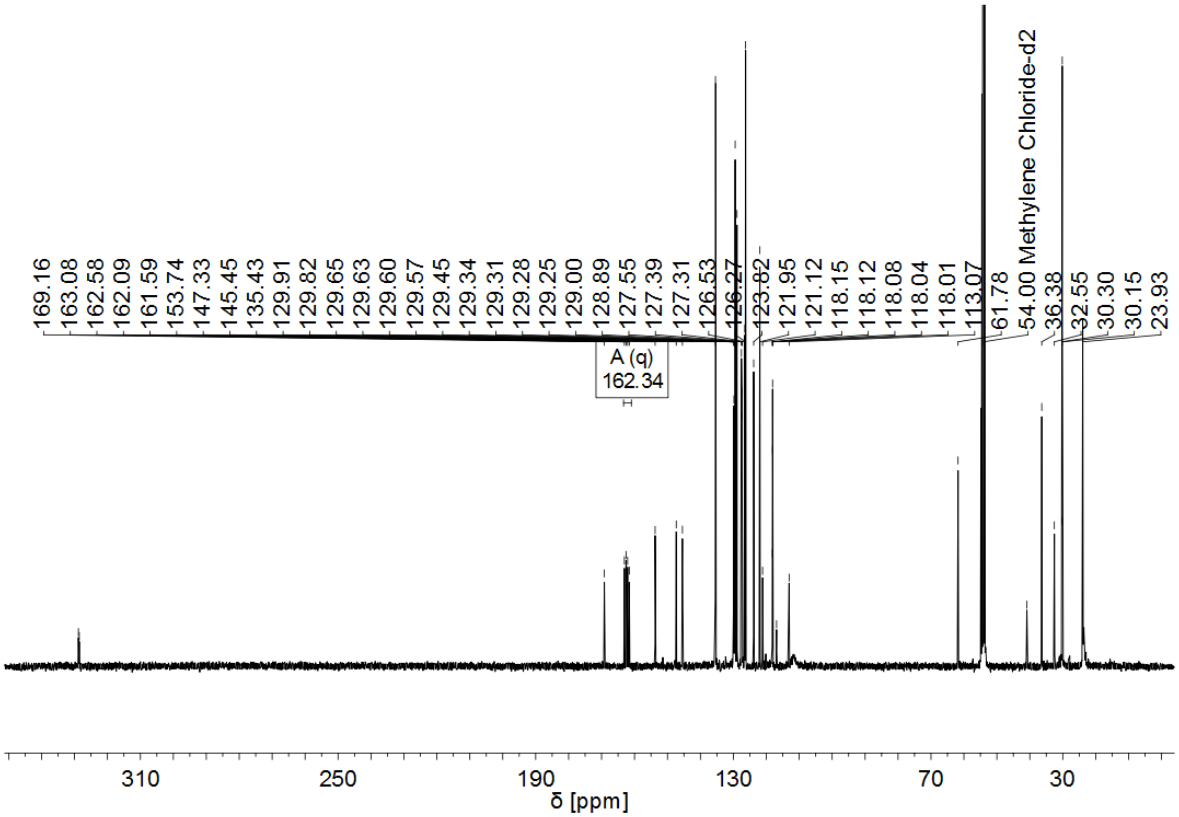

Figure A 125: ^{13}C NMR spectrum of **Mo-72** (101 MHz, CD_2Cl_2).

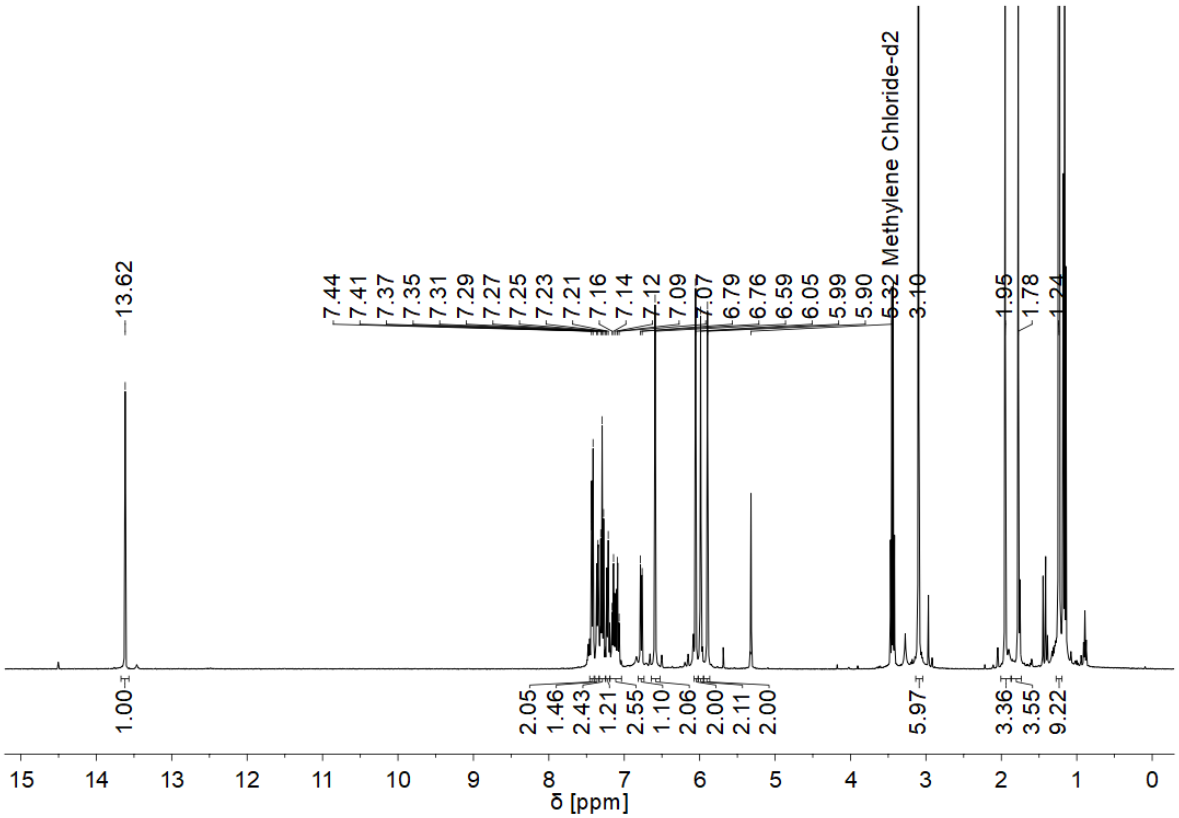

Figure A 126: ^{1}H NMR spectrum of **Mo-73** (400 MHz, CD_2Cl_2).

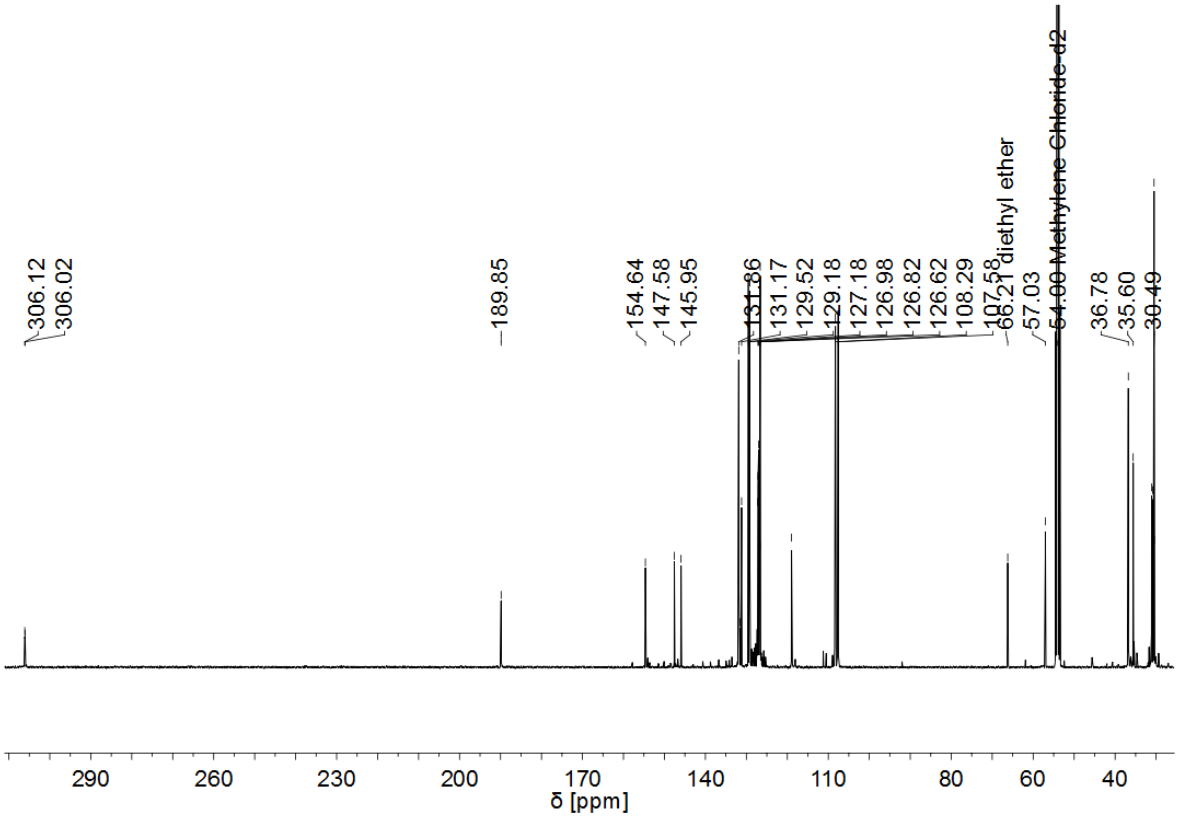

Figure A 127: ^{13}C NMR spectrum of **Mo-73** (101 MHz, CD_2Cl_2).

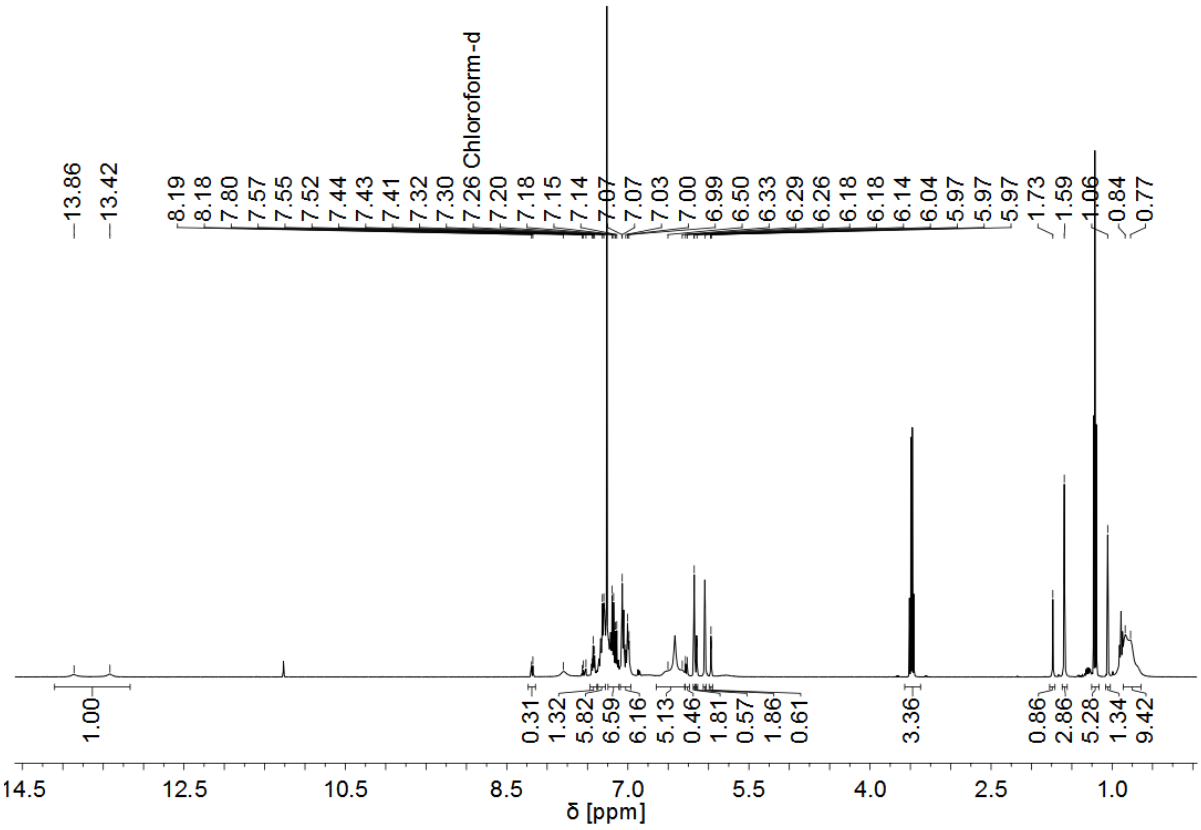

Figure A 128: ^{1}H NMR spectrum of **Mo-75** (400 MHz, $CDCl_3$).

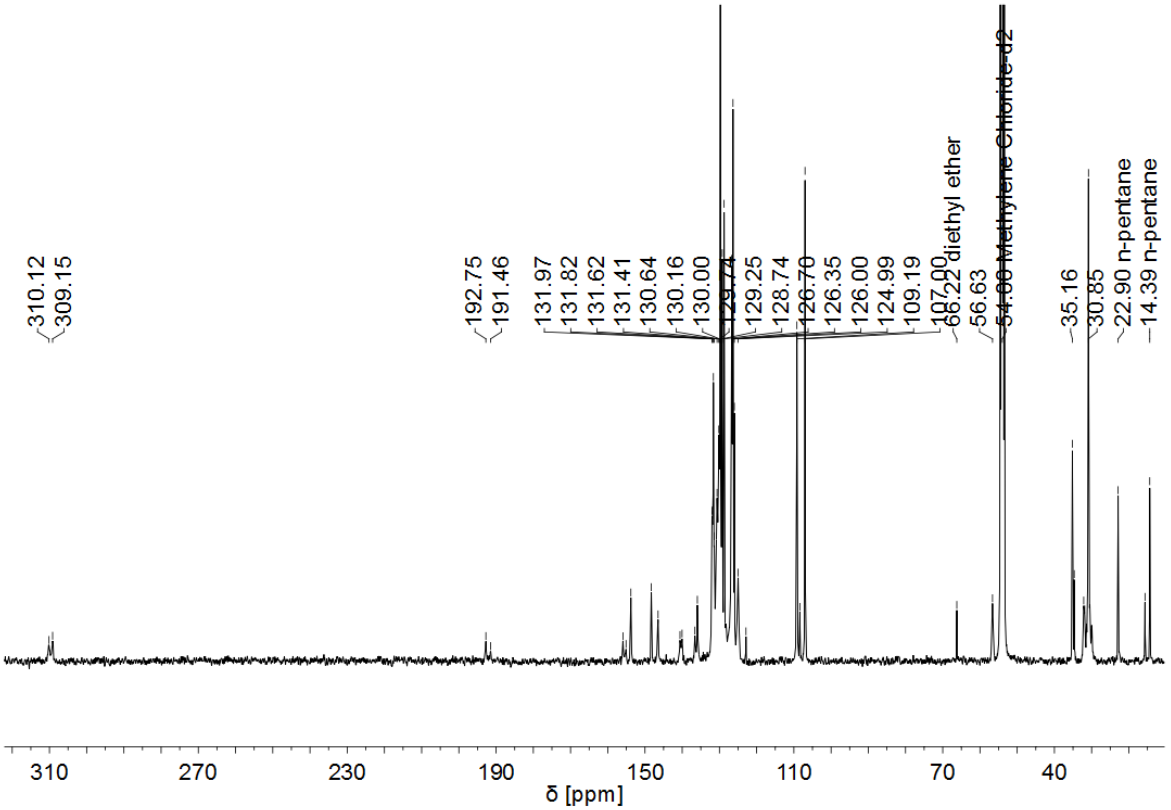

Figure A 129: ^{13}C NMR spectrum of **Mo-75** (101 MHz, CD_2Cl_2).

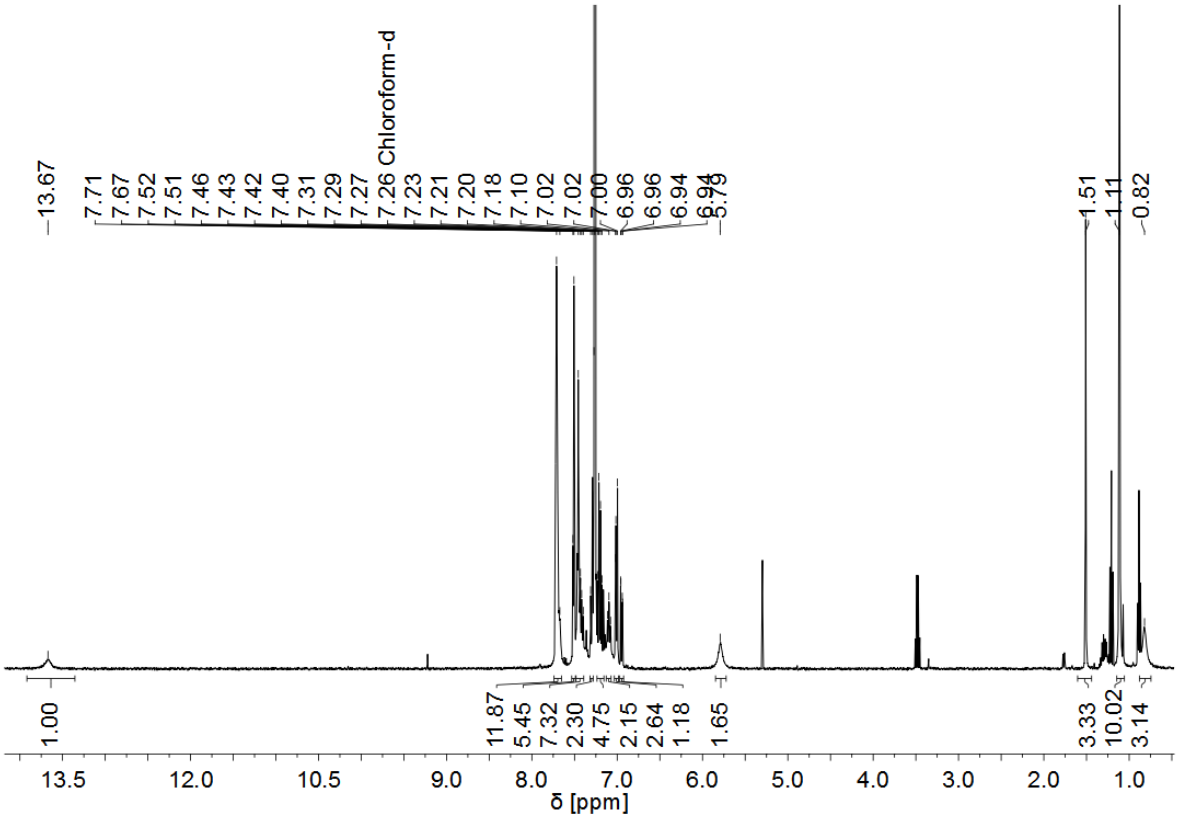

Figure A 130: ^{1}H NMR spectrum of **Mo-76** (400 MHz, $CDCl_3$).

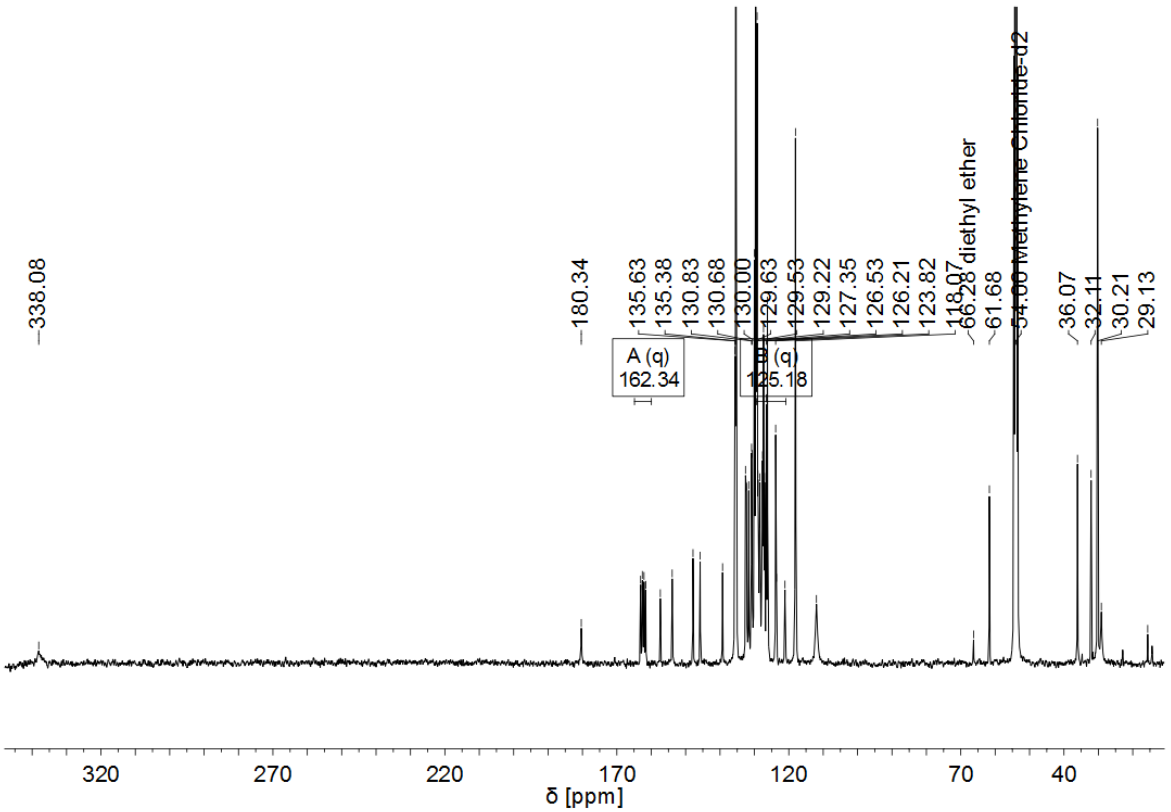

Figure A 131: ^{13}C NMR spectrum of **Mo-76** (101 MHz, CD_2Cl_2).

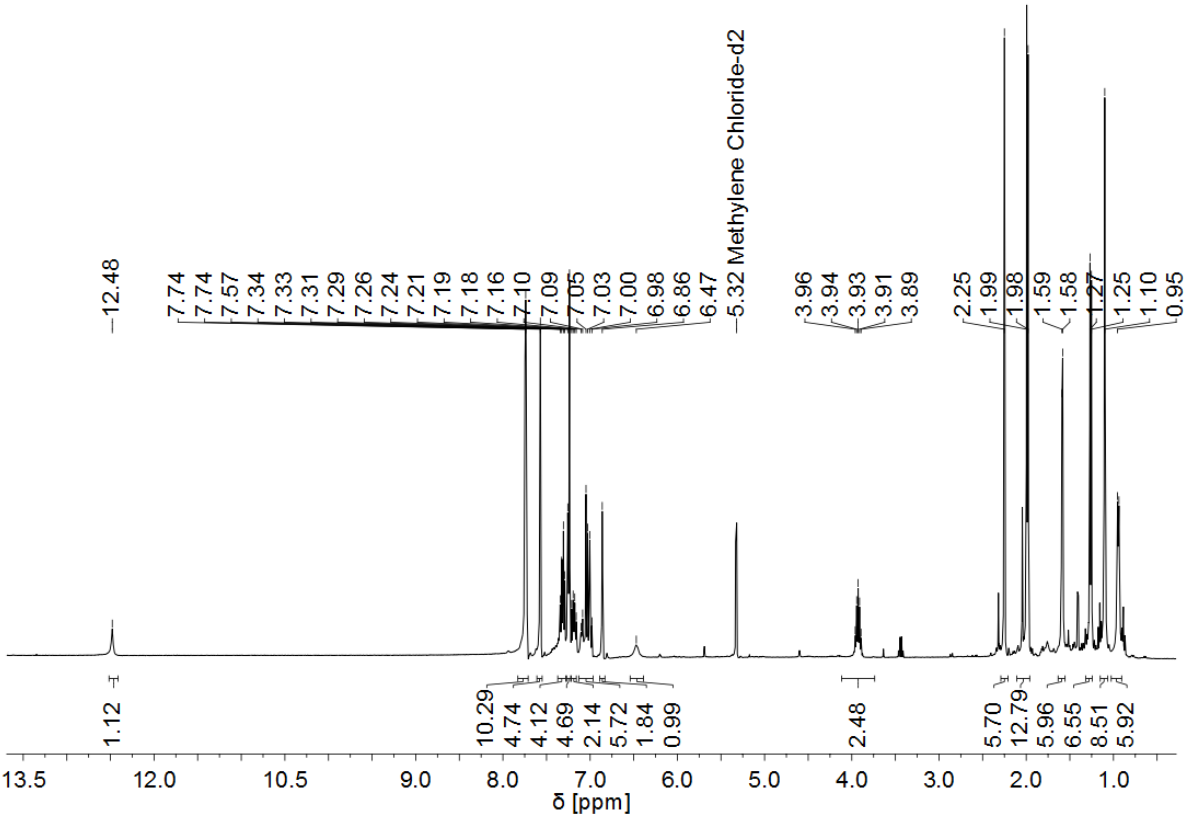

Figure A 132: ^{1}H NMR spectrum of **Mo-77·MeCN** (400 MHz, CD_2Cl_2).

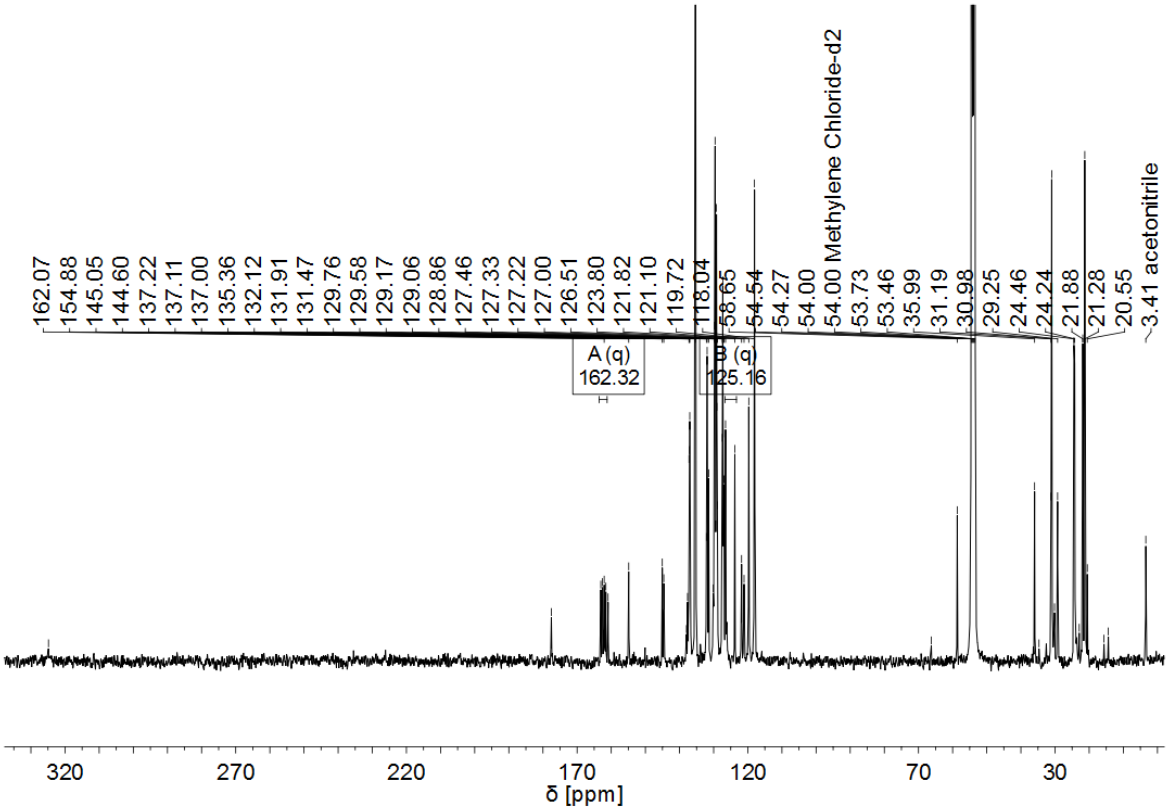

Figure A 133: ^{13}C NMR spectrum of **Mo-77·MeCN** (101 MHz, CD_2Cl_2).

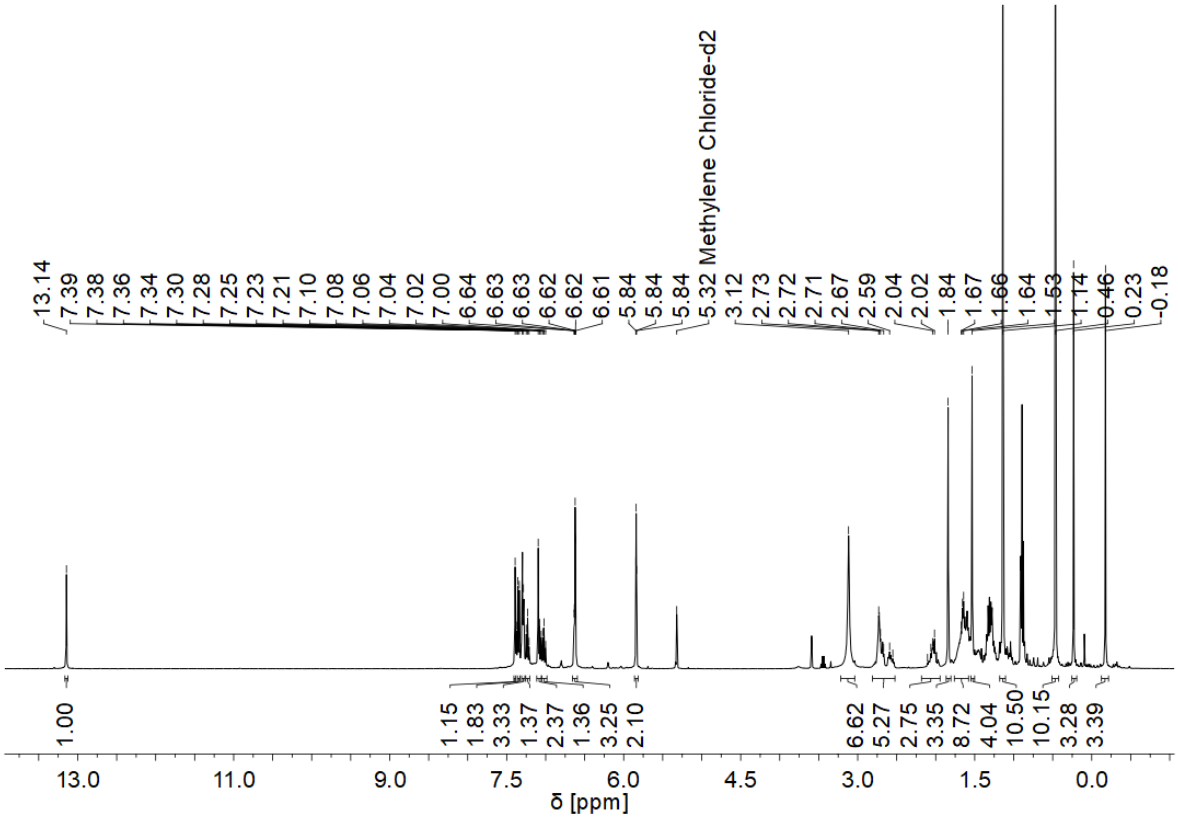

Figure A 134: ^{1}H NMR spectrum of **Mo-78** (400 MHz, CD_2Cl_2).

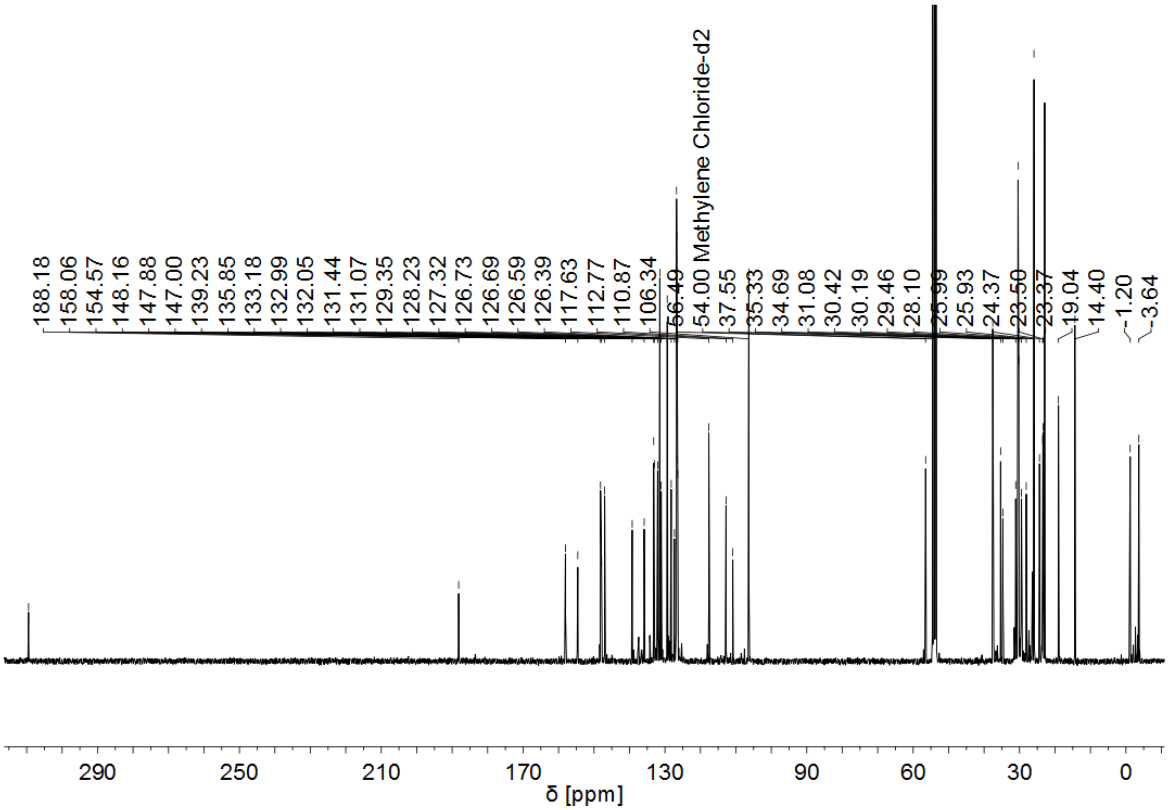

Figure A 135: ^{13}C NMR spectrum of **Mo-78** (101 MHz, CD_2Cl_2).

9.5 INVESTIGATIONS OF STRUCTURE-REACTIVITY RELATIONS IN MOLYBDENUM ALKYLIDYNE *N*-HETEROCYCLIC CARBENE COMPLEXES

9.5.1 SPECTRA OF NOVEL COMPOUNDS

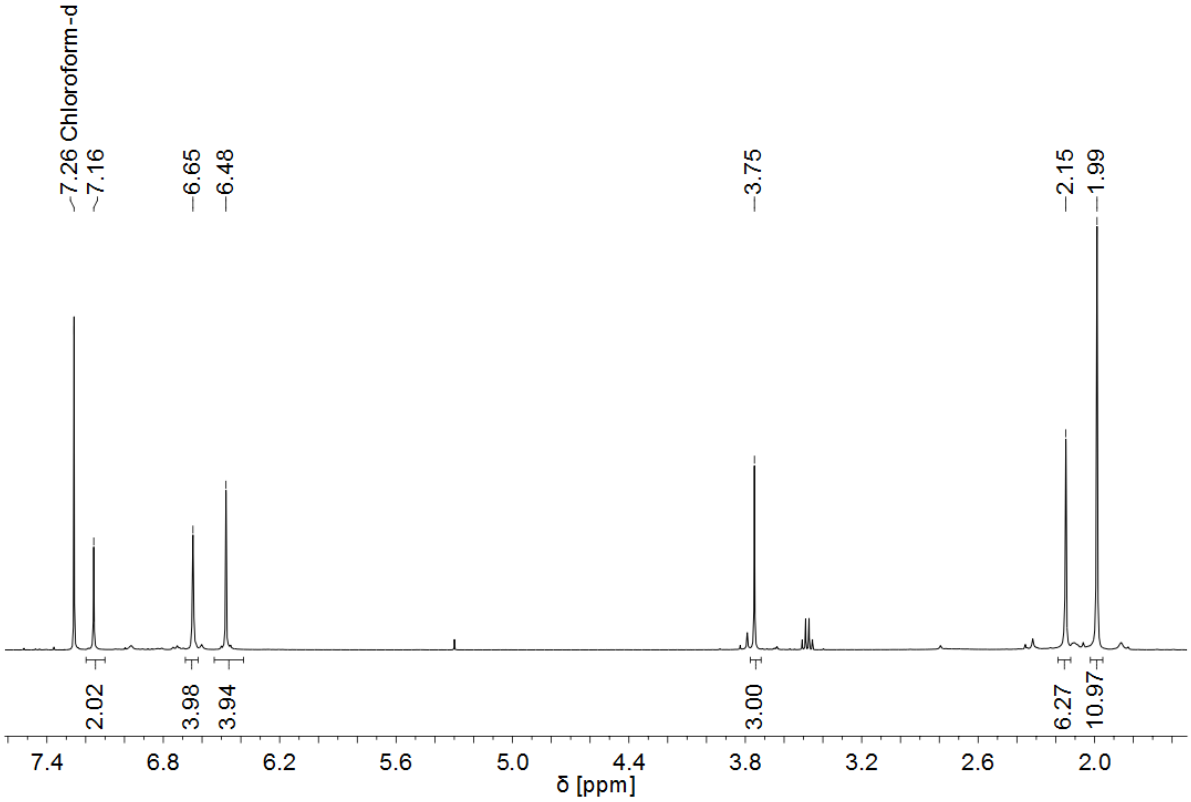

Figure A 136: ^{1}H NMR spectrum of **Mo-91** (400 MHz, $CDCl_3$).

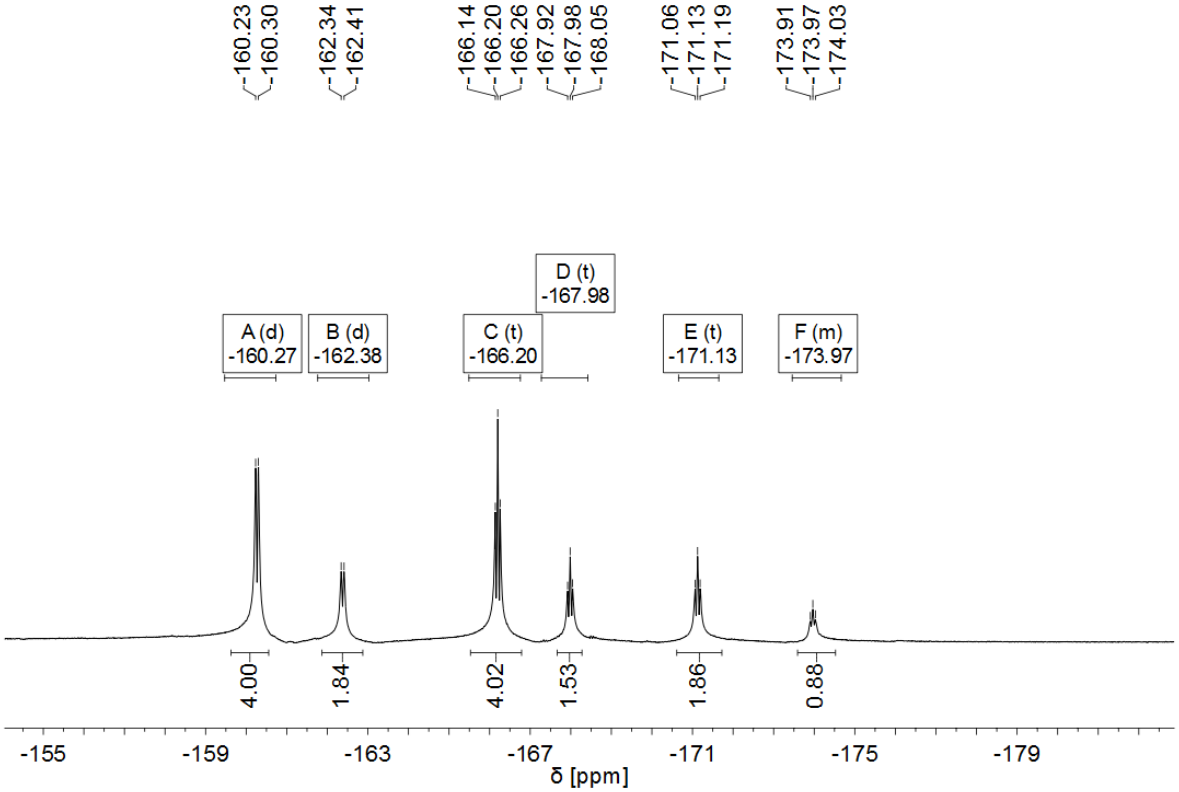

Figure A 137: ^{19}F NMR spectrum of **Mo-91** (376 MHz, $CDCl_3$).

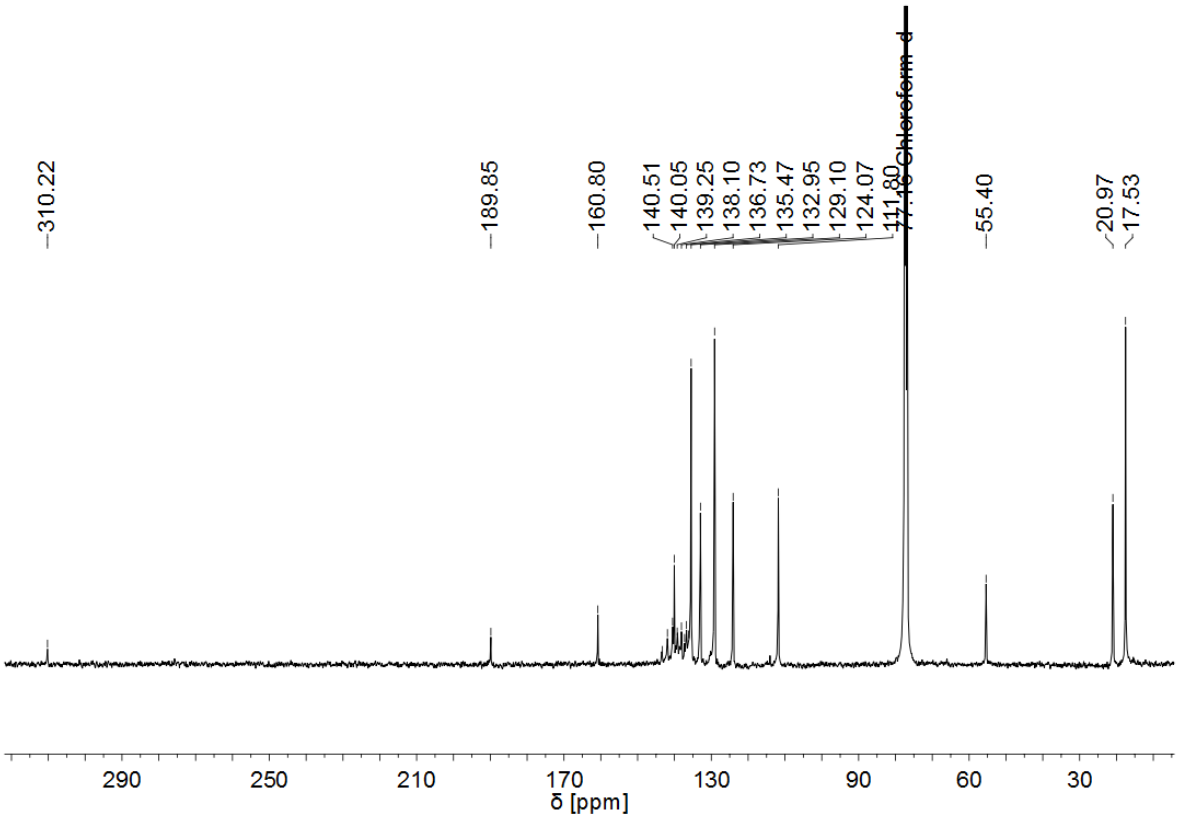

Figure A 138: ^{13}C NMR spectrum of **Mo-91** (101 MHz, $CDCl_3$).

9.5.2 NMR EXPERIMENTS FOR MECHANISTIC INVESTIGATIONS

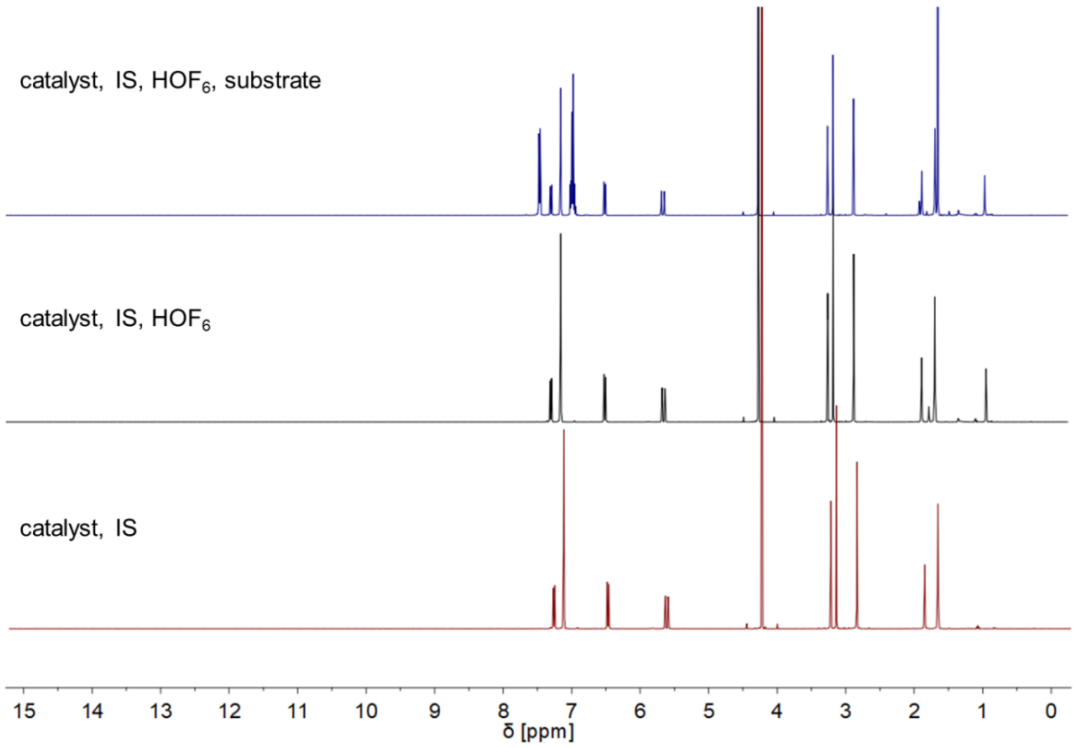

Figure A 139: Stacked ^{1}H NMR spectra in C_6D_6. Catalyst: **Mo-81**. Bottom (red): Catalyst and internal standard (IS). Middle (black): Catalyst, IS and hexafluoro-*tert*-butanol (HOF_6). Top (blue): Catalyst, internal standard, HOF_6 and substrate.

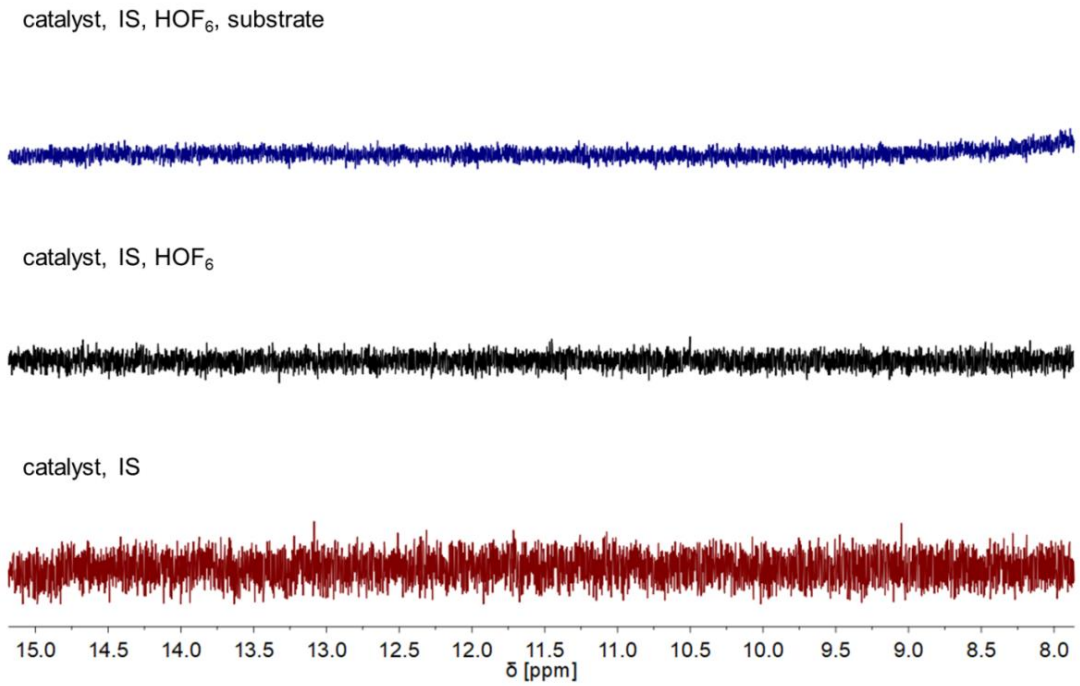

Figure A 140: Zoom into imidazolium proton region of stacked ^{1}H NMR spectra in C_6D_6. Catalyst: **Mo-81**. Bottom (red): Catalyst and internal standard (IS). Middle (black): Catalyst, IS and hexafluoro-*tert*-butanol (HOF_6). Top (blue): Catalyst, internal standard, HOF_6 and substrate.

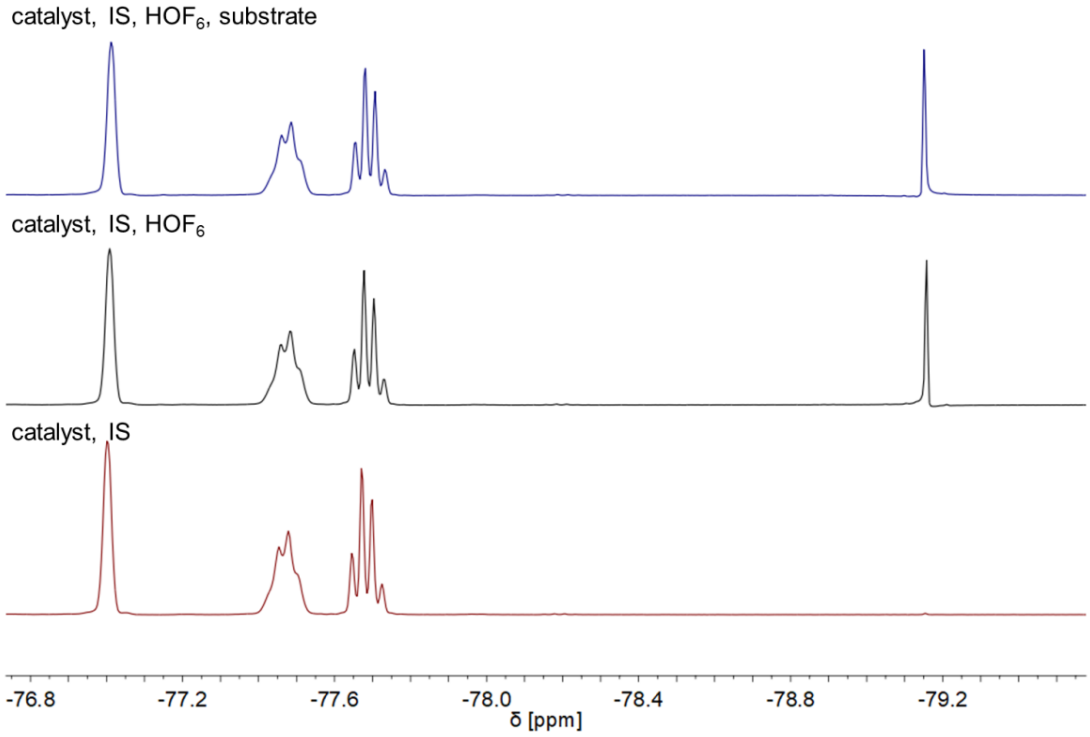

Figure A 141: Stacked ^{19}F NMR spectra in C_6D_6. Catalyst: **Mo-81**. Bottom (red): Catalyst and internal standard (IS). Middle (black): Catalyst, IS and hexafluoro-*tert*-butoxide (HOF_6). Top (blue): Catalyst, internal standard, HOF_6 and substrate.

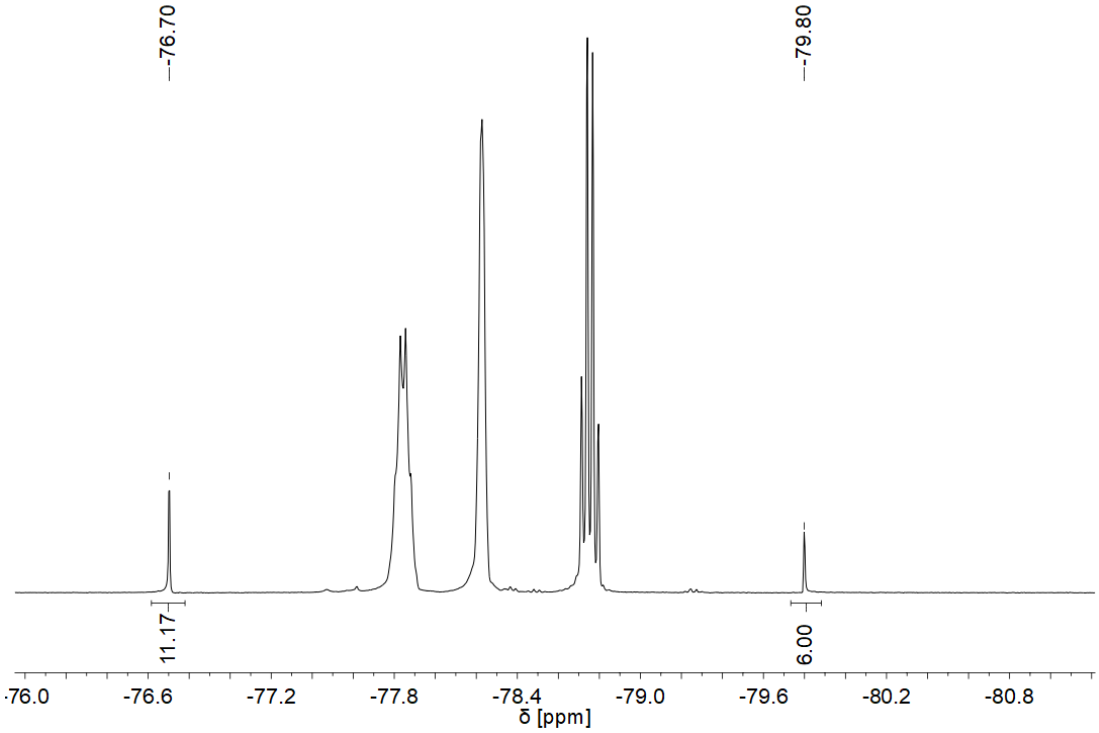

Figure A 142: ^{19}F NMR spectrum of **Mo-81** in MeCN-d3. Integrated signals are tentatively assigned to a species with one partially dissociated hexafluoro-*tert*-butoxide (OF_6) (δ = -79.8 ppm) and two coordinated OF_6 ligands (δ=-76.7 ppm).

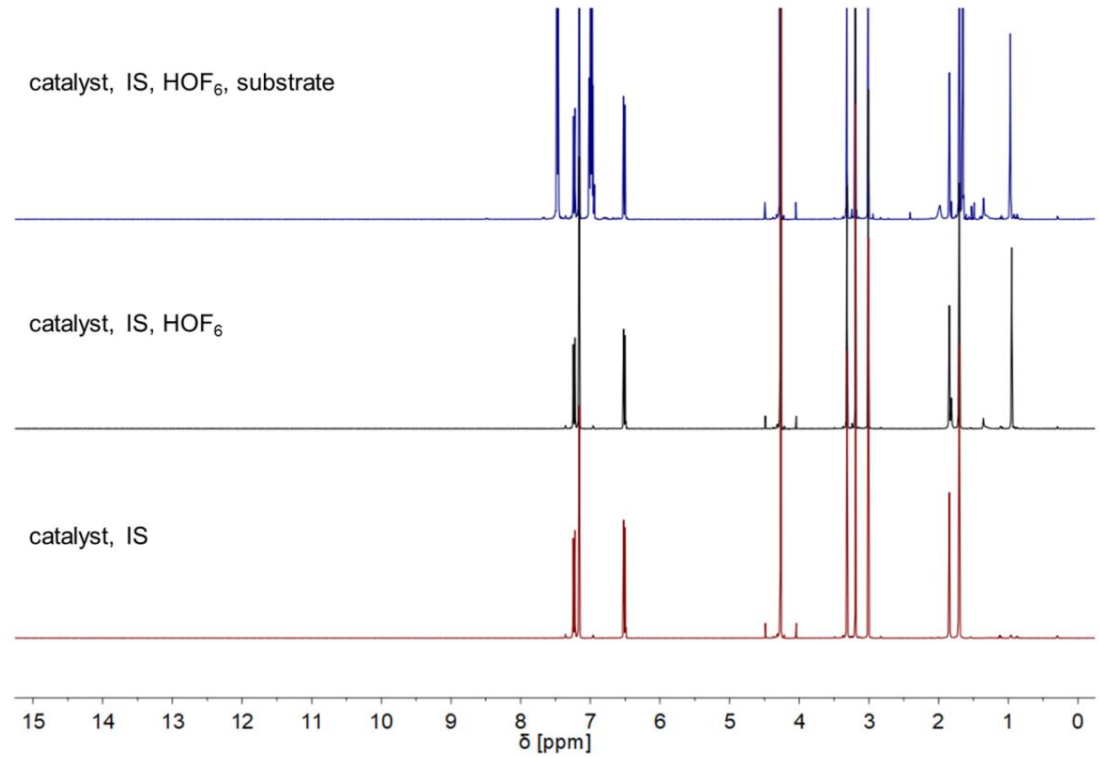

Figure A 143: Stacked ^1H NMR spectra in C_6D_6. Catalyst: **Mo-82**. Bottom (red): Catalyst and internal standard (IS). Middle (black): Catalyst, IS and hexafluoro-*tert*-butanol (HOF_6). Top (blue): Catalyst, internal standard, HOF_6 and substrate.

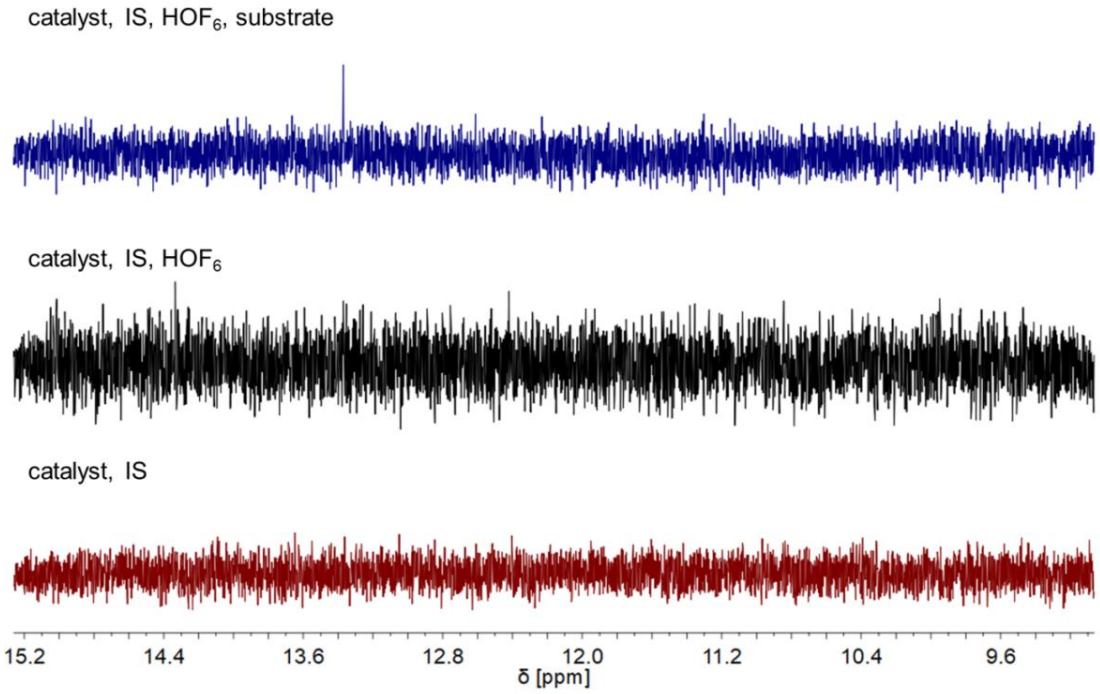

Figure A 144: Zoom into imidazolium proton region of stacked ^{1}H NMR spectra in C_6D_6. Catalyst: **Mo-82**. Bottom (red): Catalyst and internal standard (IS). Middle (black): Catalyst, IS and hexafluoro-*tert*-butanol (HOF_6). Top (blue): Catalyst, internal standard, HOF_6 and substrate.

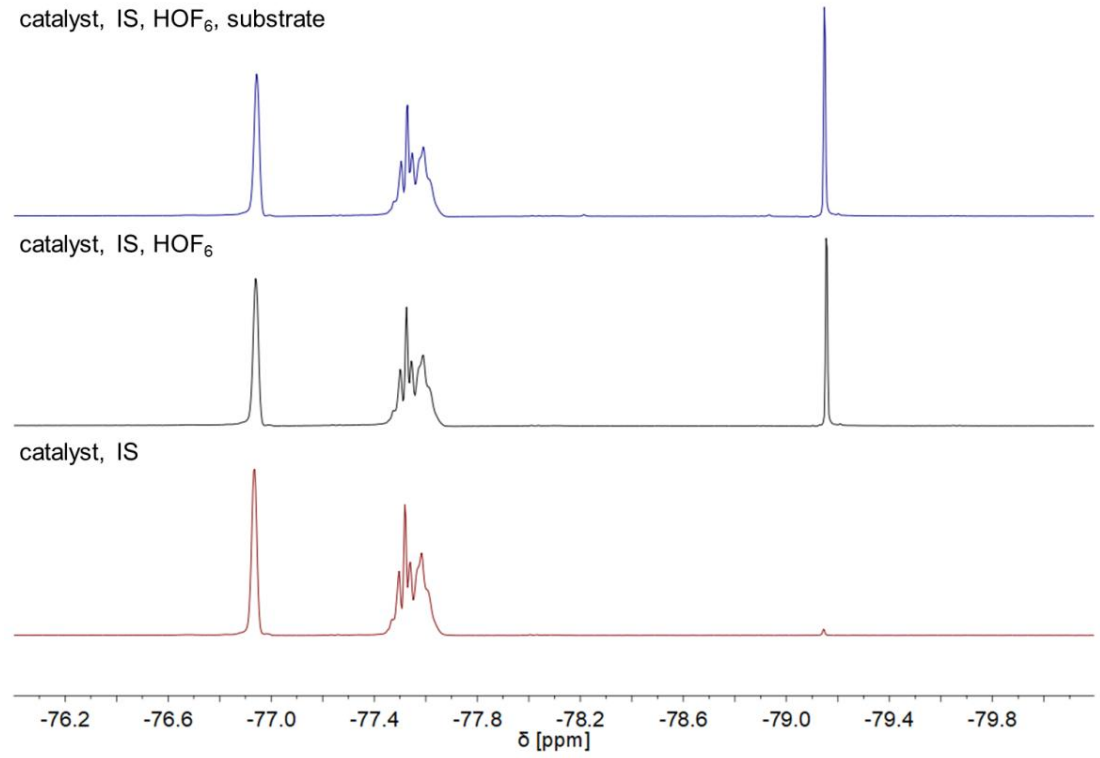

Figure A 145: Stacked ^{19}F NMR spectra in C_6D_6. Catalyst: **Mo-82**. Bottom (red): Catalyst and internal standard (IS). Middle (black): Catalyst, IS and hexafluoro-*tert*-butoxide (HOF_6). Top (blue): Catalyst, internal standard, HOF_6 and substrate.

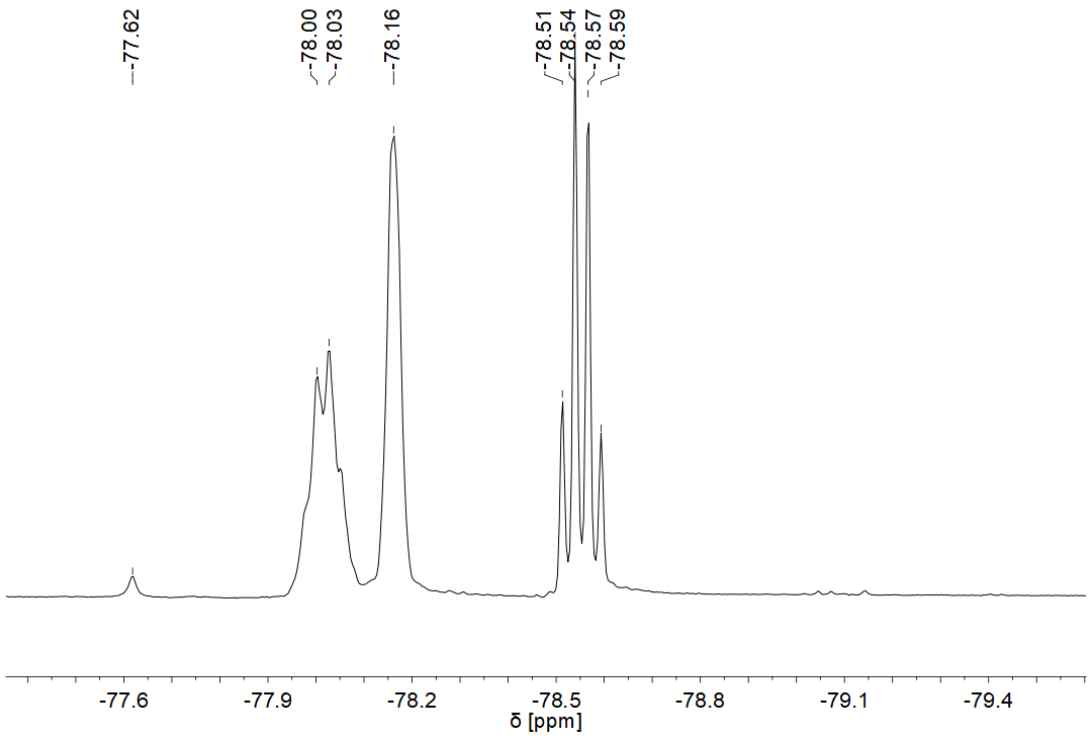

Figure A 146: ^{19}F NMR spectrum of **Mo-82** in MeCN-d3.

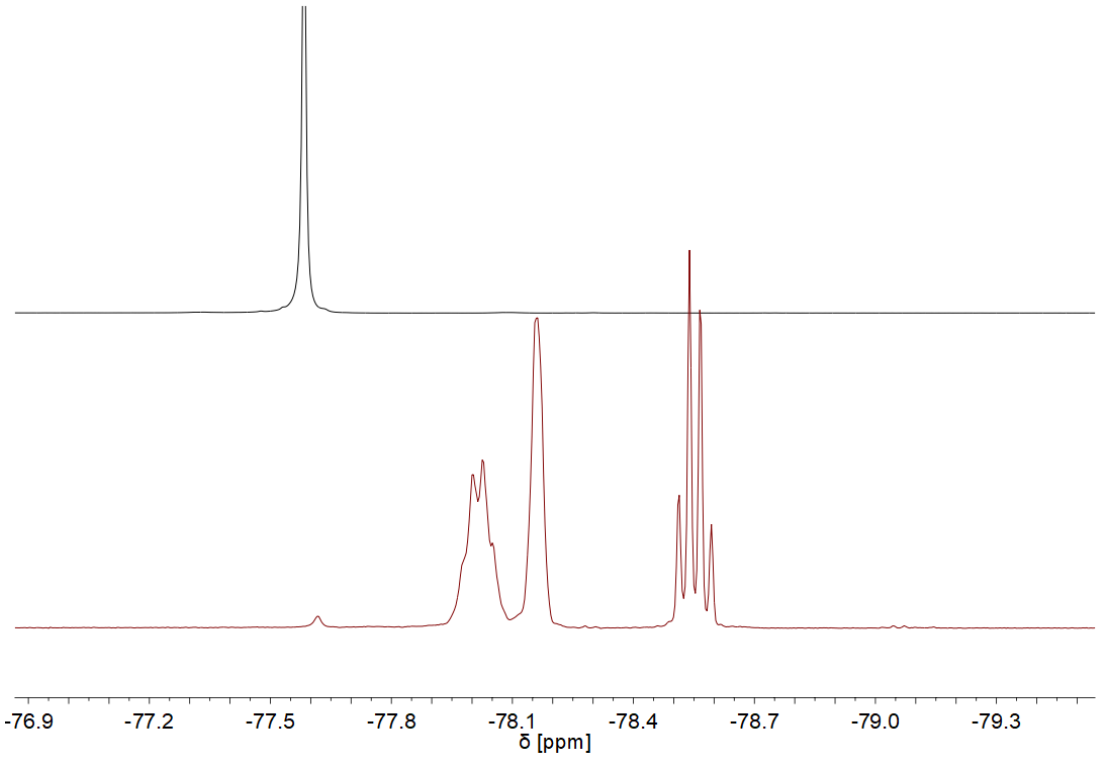

Figure A 147: Stacking of ^{19}F NMR spectra in MeCN-d3. Bottom (red): **Mo-82**. Top (black): **Mo-P11**.

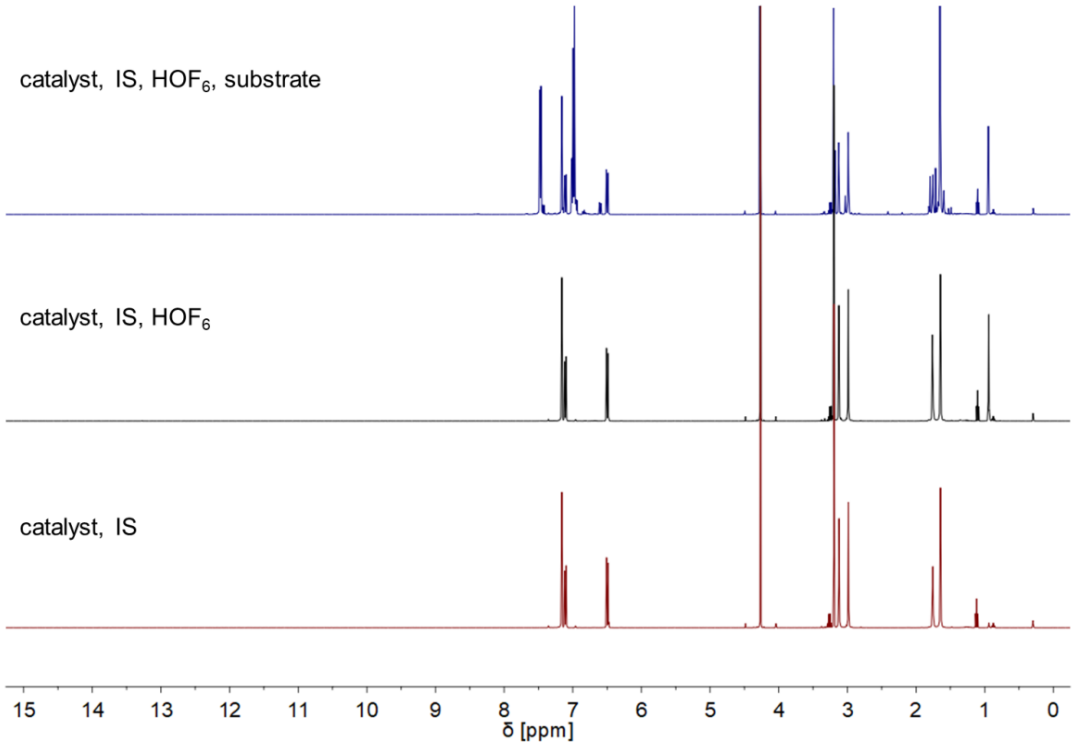

Figure A 148: Stacked ^{1}H NMR spectra in C_6D_6. Catalyst: **Mo-83**. Bottom (red): Catalyst and internal standard (IS). Middle (black): Catalyst, IS and hexafluoro-*tert*-butanol (HOF_6). Top (blue): Catalyst, internal standard, HOF_6 and substrate.

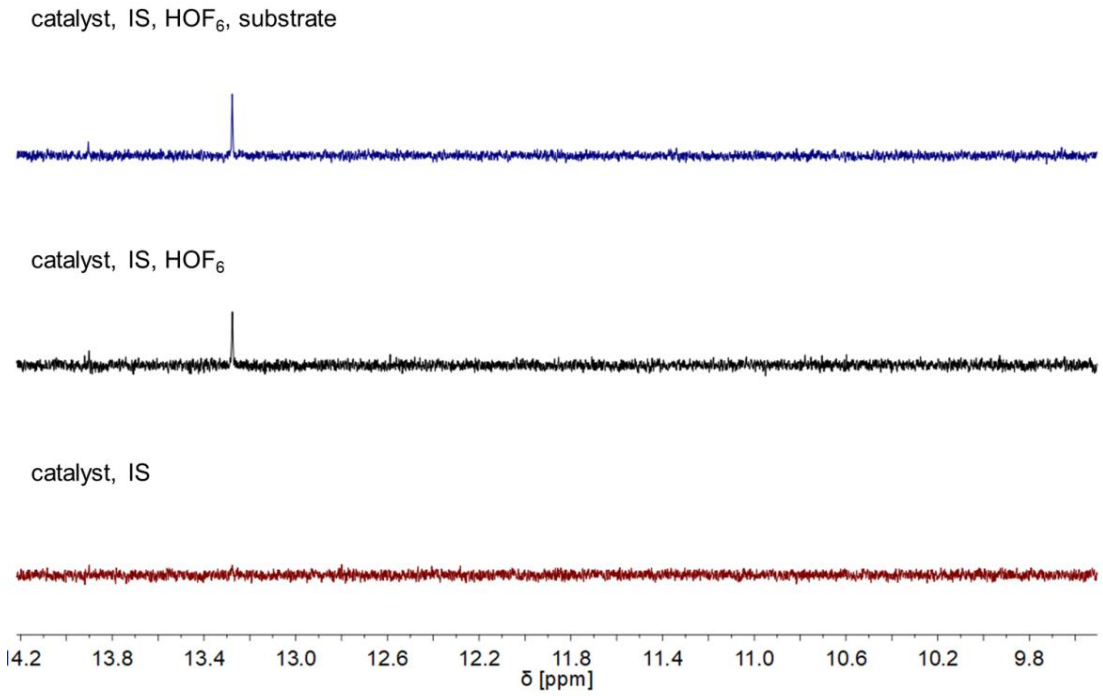

Figure A 149: Zoom into imidazolium proton region of stacked ^{1}H NMR spectra in C_6D_6. Catalyst: **Mo-83**. Bottom (red): Catalyst and internal standard (IS). Middle (black): Catalyst, IS and hexafluoro-*tert*-butanol (HOF_6). Top (blue): Catalyst, internal standard, HOF_6 and substrate.

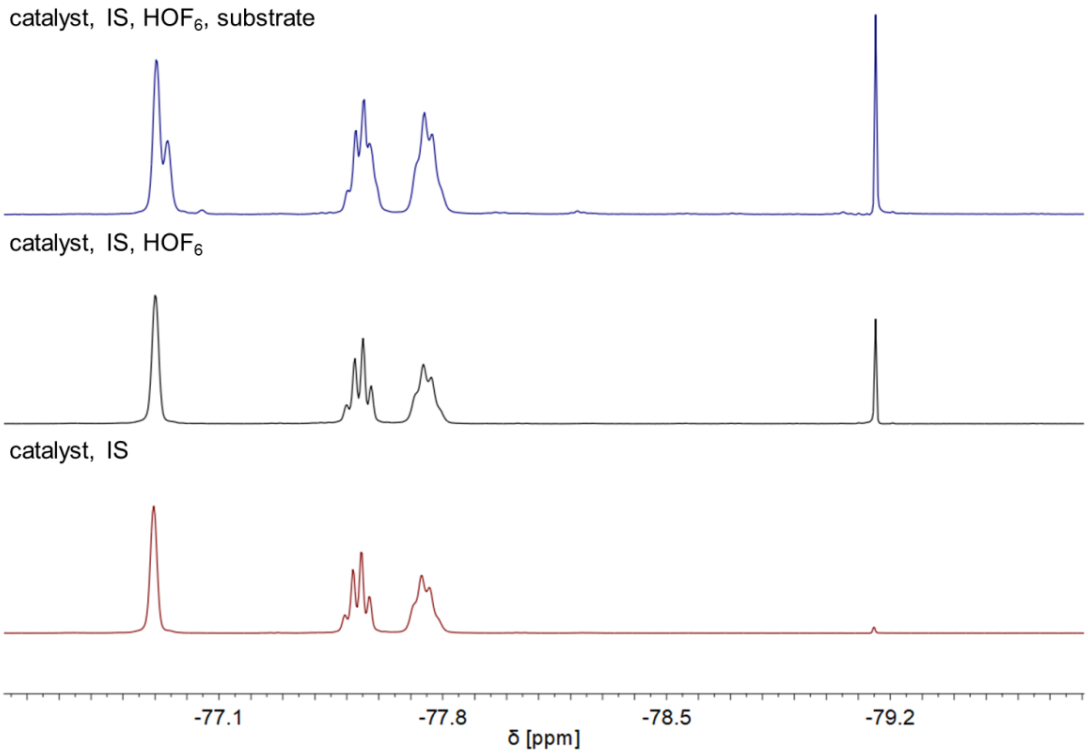

Figure A 150: Stacked ^{19}F NMR spectra in C_6D_6. Catalyst: **Mo-83**. Bottom (red): Catalyst and internal standard (IS). Middle (black): Catalyst, IS and hexafluoro-*tert*-butoxide (HOF_6). Top (blue): Catalyst, internal standard, HOF_6 and substrate.

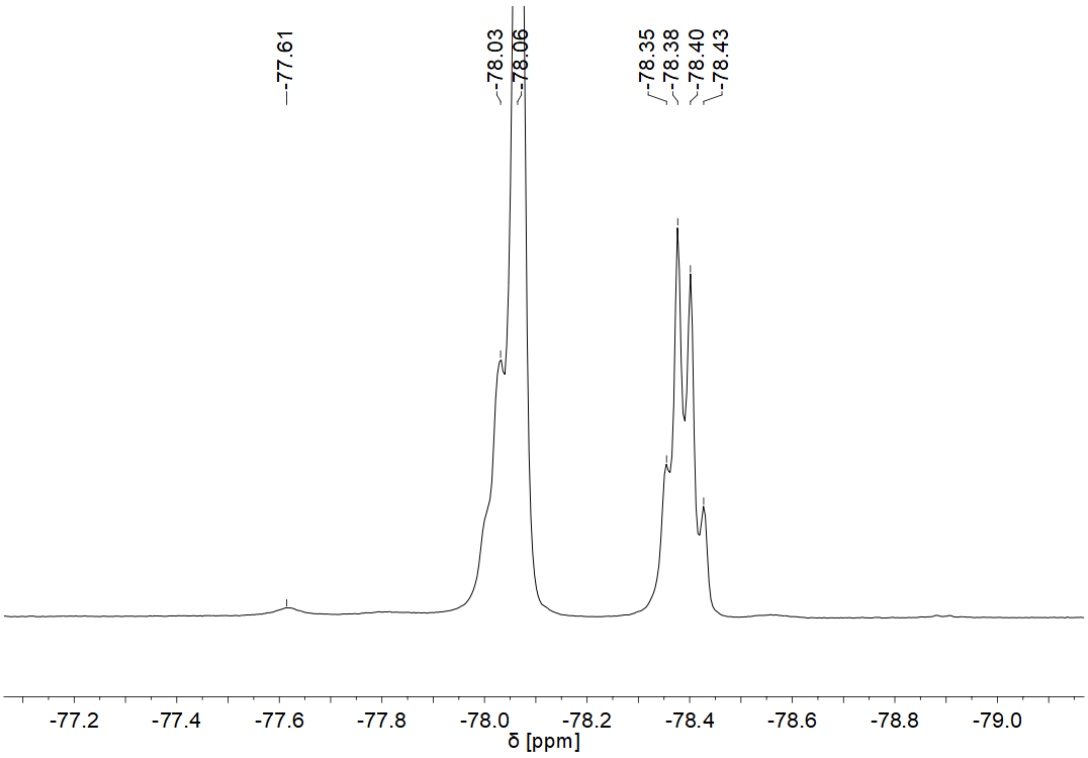

Figure A 151: ^{19}F NMR spectrum of **Mo-83** in MeCN-d3.

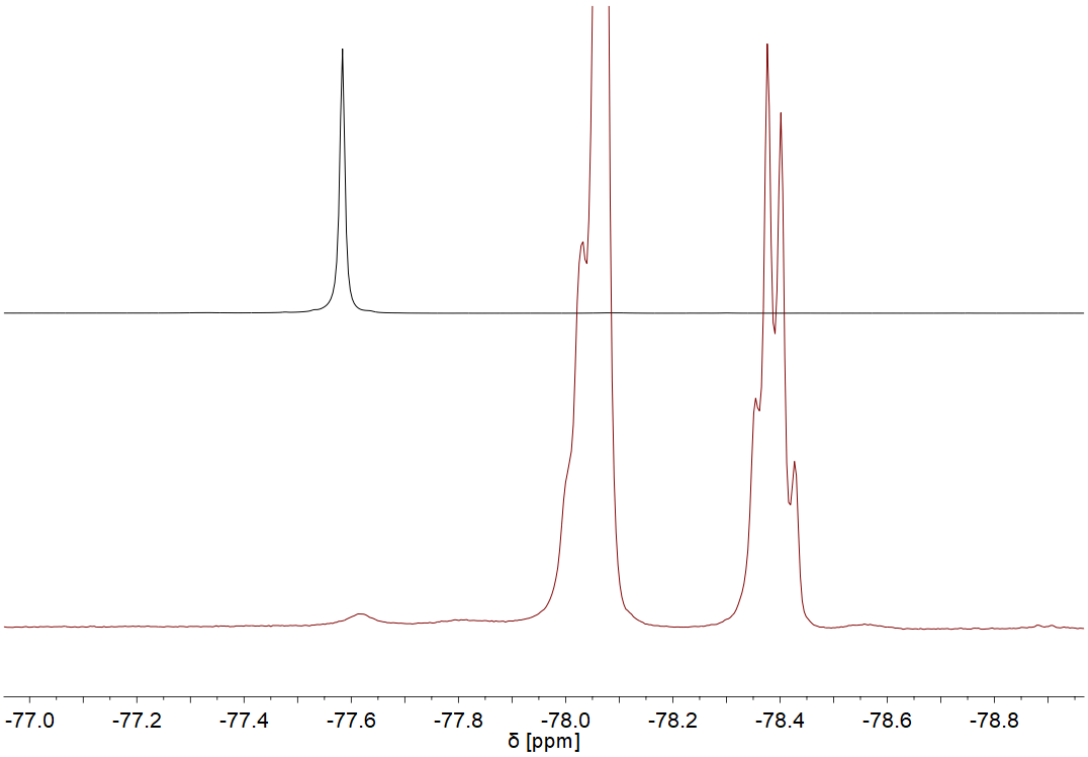

Figure A 152: Stacking of ^{19}F NMR spectra in MeCN-d3. Bottom (red): **Mo-83**. Top (black): **Mo-P11**.

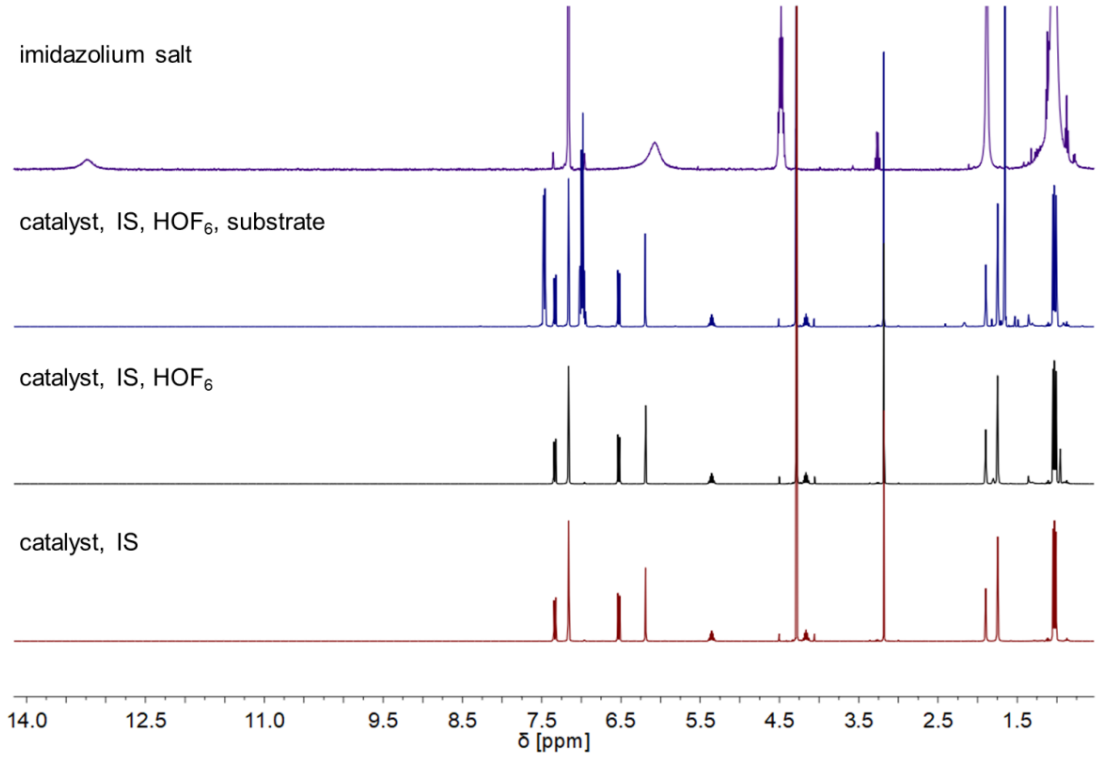

Figure A 153: Stacked ^{1}H NMR spectra in C_6D_6. Catalyst: **Mo-84**. Bottom (red): Catalyst and internal standard (IS). Middle bottom (black): Catalyst, IS and hexafluoro-*tert*-butanol (HOF_6). Middle top (blue): Catalyst, internal standard, HOF_6 and substrate. Top (violet): Corresponding imidazolium salt.

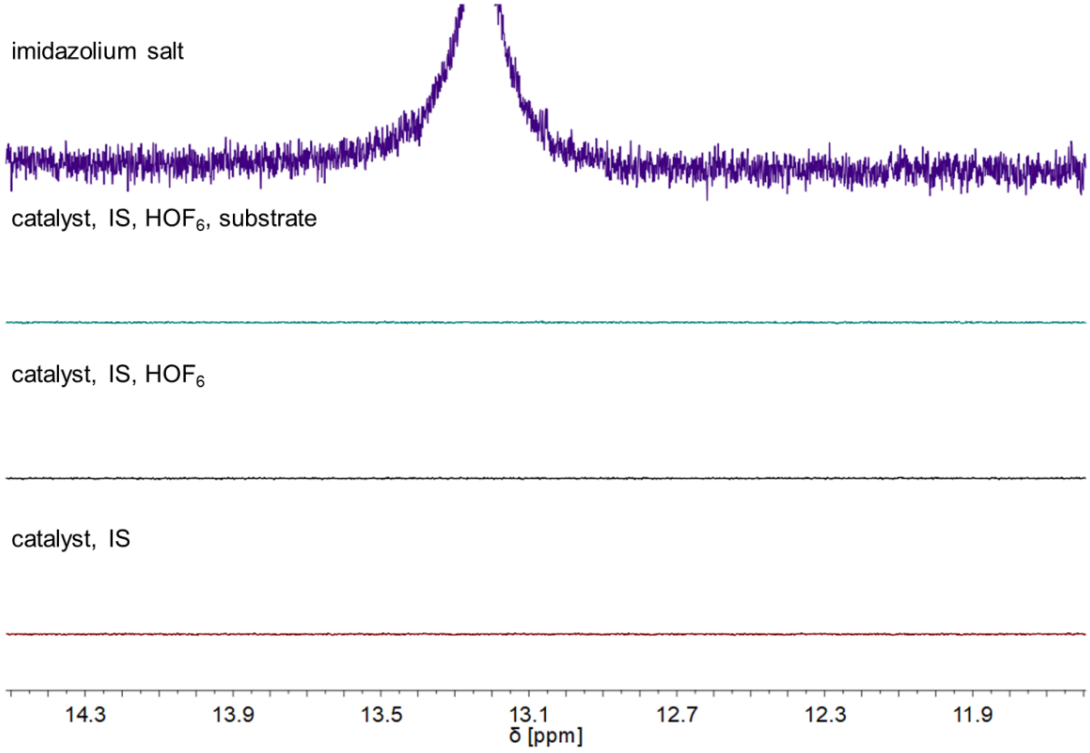

Figure A 154: Zoom into imidazolium proton region of stacked ^{1}H NMR spectra in C_6D_6. Catalyst: **Mo-84**. Bottom (red): Catalyst and internal standard (IS). Middle top (black): Catalyst, IS and hexafluoro-*tert*-butanol (HOF_6). Middle bottom (blue): Catalyst, internal standard, HOF_6 and substrate. Top (violet): Corresponding imidazolium salt.

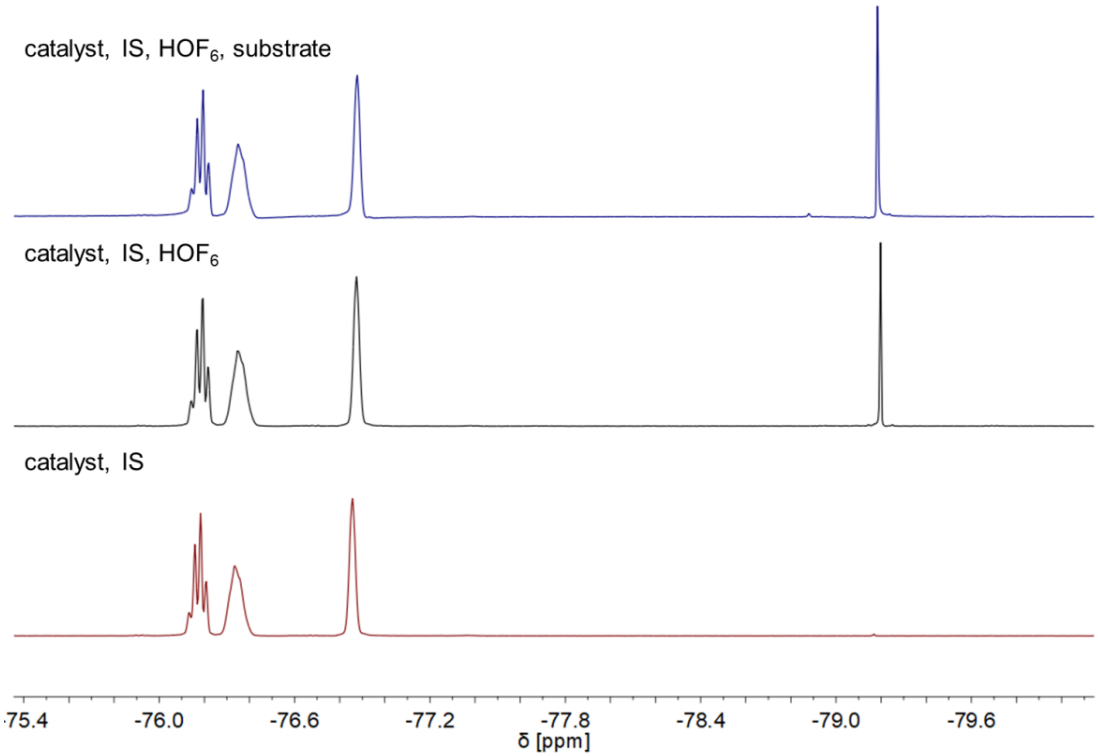

Figure A 155: ^{19}F NMR spectra in C_6D_6. Catalyst: **Mo-84**. Bottom (red): Catalyst and internal standard (IS). Middle (black): Catalyst, IS and hexafluoro-*tert*-butoxide (HOF_6). Top (blue): Catalyst, internal standard, HOF_6 and substrate.

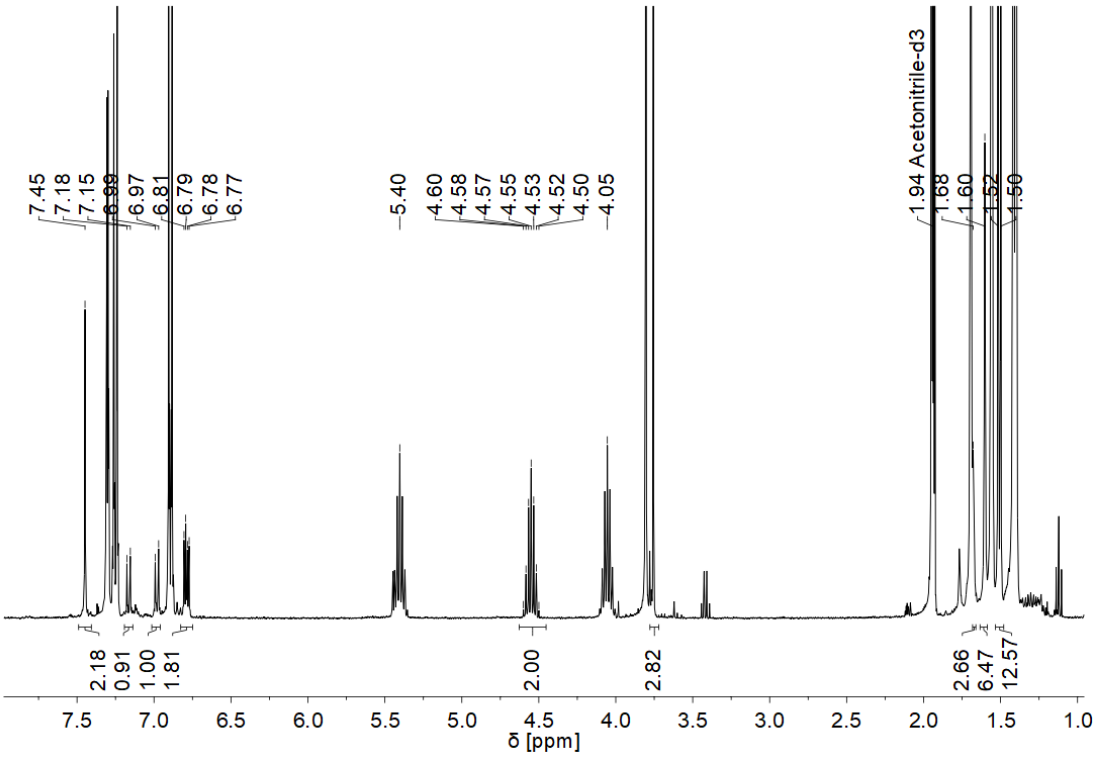

Figure A 156: ^{1}H NMR spectrum of **Mo-84** in MeCN-d3. Only integrals of the new, TBP (trigonal bipyramidal) structure are integrated. All other signals belong to the parent SP (square pyramidal) structure.

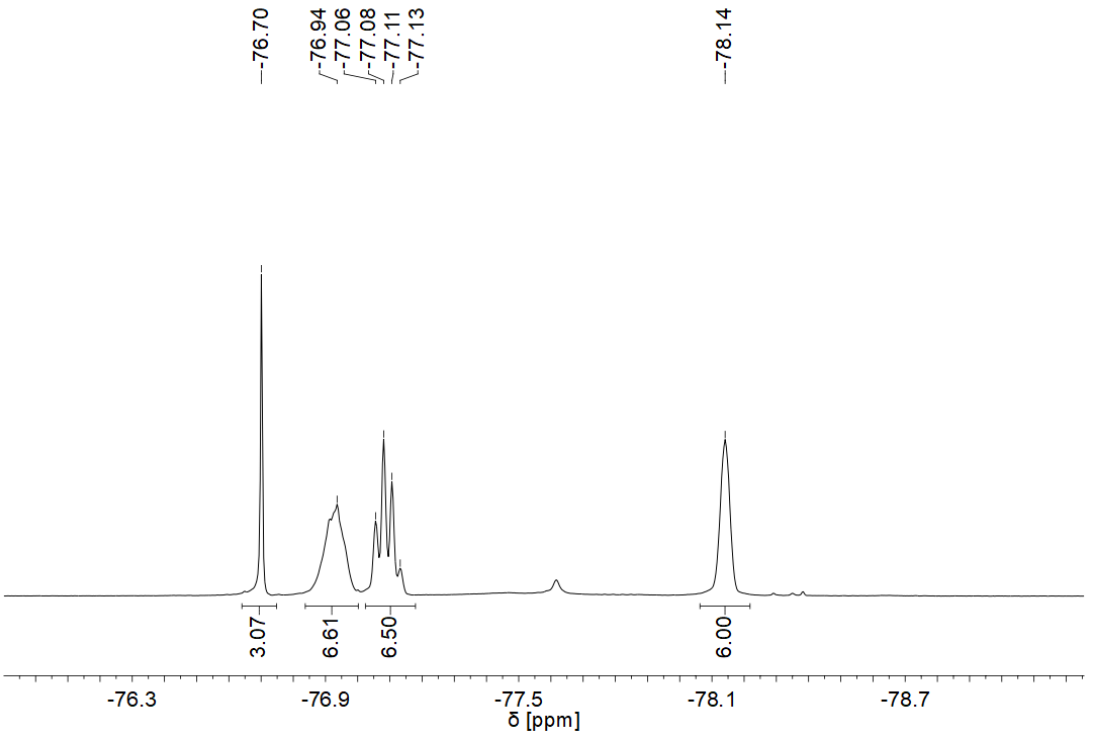

Figure A 157: ^{19}F NMR spectrum of **Mo-84** in MeCN-d3. Resonance at δ = -76.7 ppm belongs to the TBP (trigonal bipyramidal) structure.

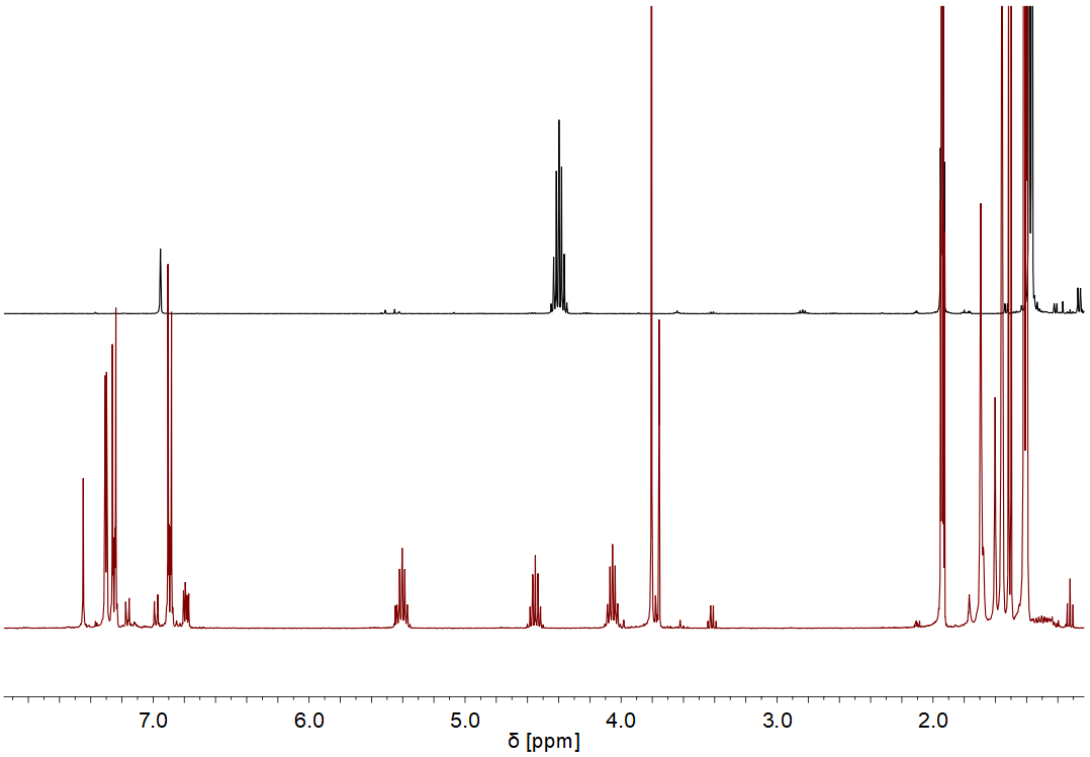

Figure A 158: ^{1}H NMR spectra in MeCN-d3. Bottom (red): **Mo-85**. Top (black): 1,3-diisopropylimidazol-2-ylidene.

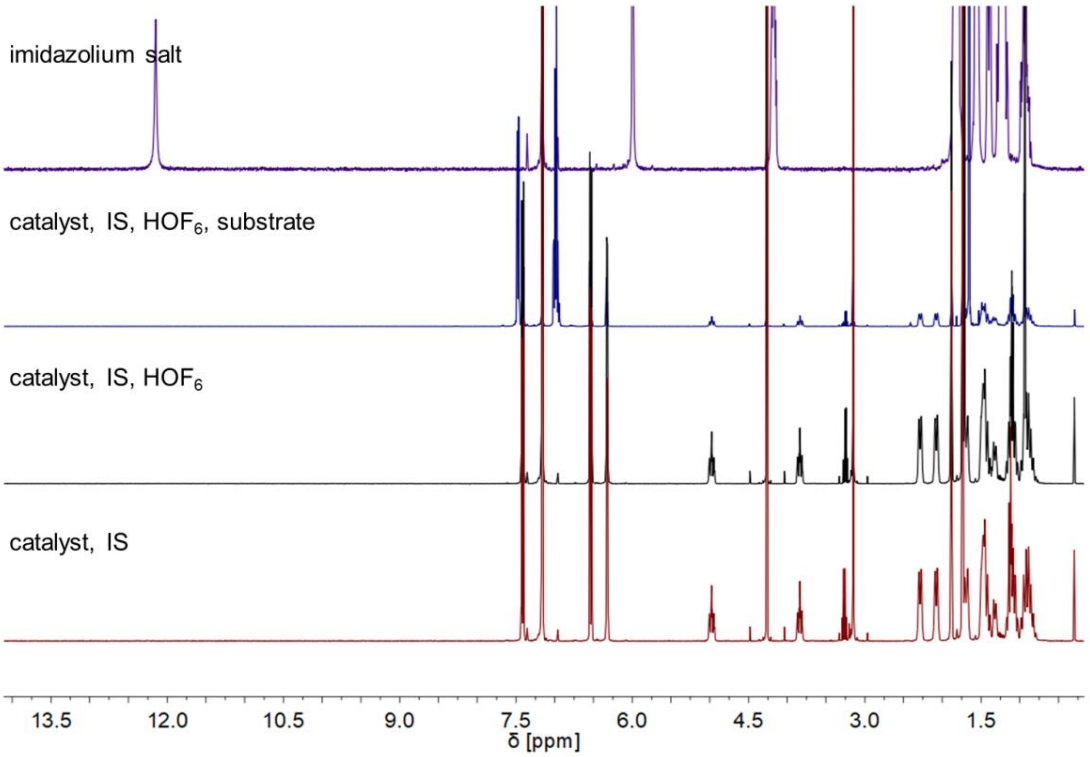

Figure A 159: Stacked ^{1}H NMR spectra in C_6D_6. Catalyst: **Mo-85**. Bottom (red): Catalyst and internal standard (IS). Middle bottom (black): Catalyst, IS and hexafluoro-*tert*-butanol (HOF_6). Middle top (blue): Catalyst, internal standard, HOF_6 and substrate. Top (violet): Corresponding imidazolium salt.

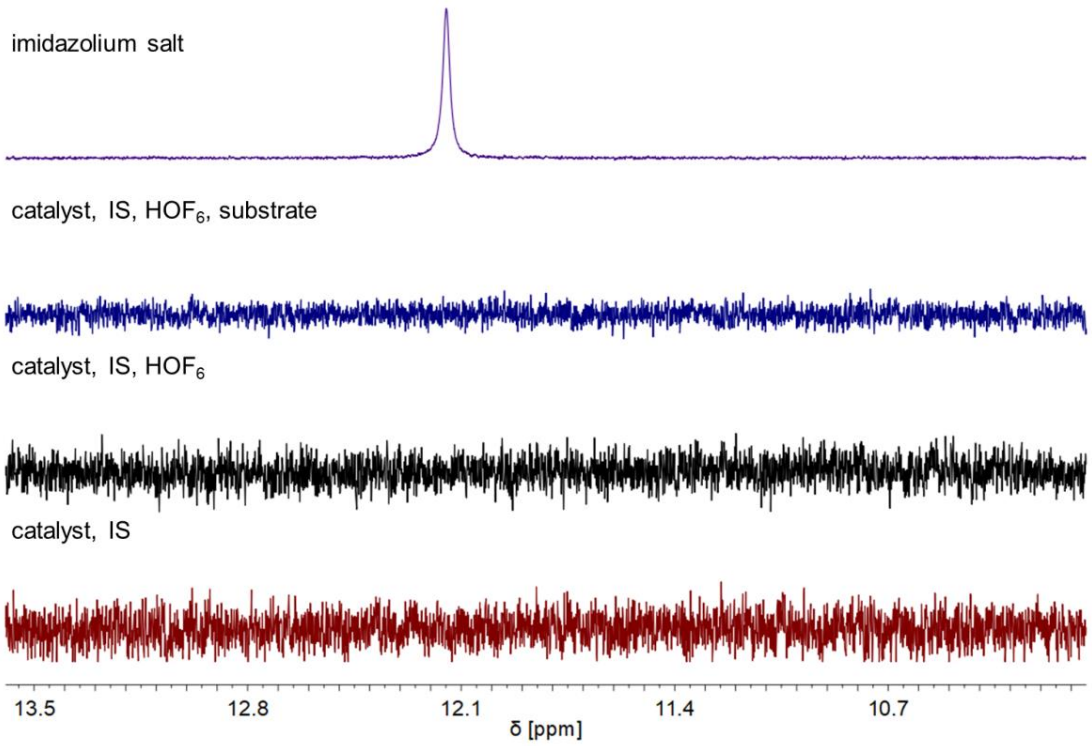

Figure A 160: Zoom into imidazolium proton region of stacked ^{1}H NMR spectra in C_6D_6. Catalyst: **Mo-85**. Bottom (red): Catalyst and internal standard (IS). Middle top (black): Catalyst, IS and hexafluoro-*tert*-butanol (HOF_6). Middle bottom (blue): Catalyst, internal standard, HOF_6 and substrate. Top (violet): Corresponding imidazolium salt.

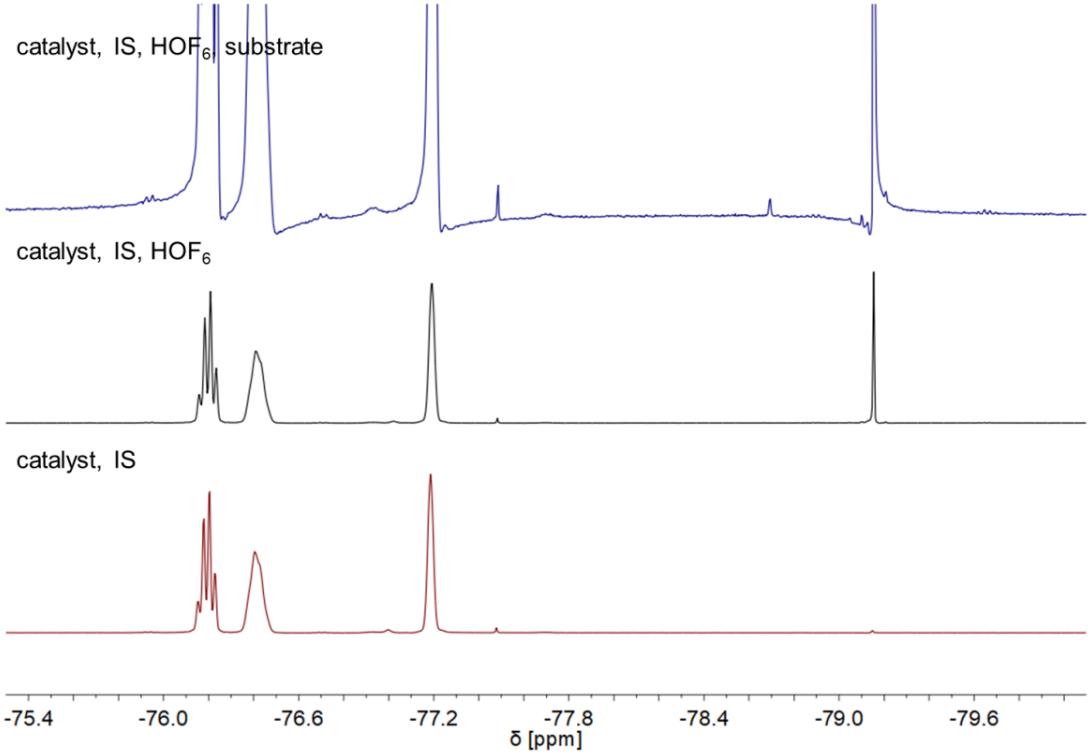

Figure A 161: ^{19}F NMR spectra in C_6D_6. Catalyst: **Mo-85**. Bottom (red): Catalyst and internal standard (IS). Middle (black): Catalyst, IS and hexafluoro-*tert*-butoxide (HOF_6). Top (blue): Catalyst, internal standard, HOF_6 and substrate.

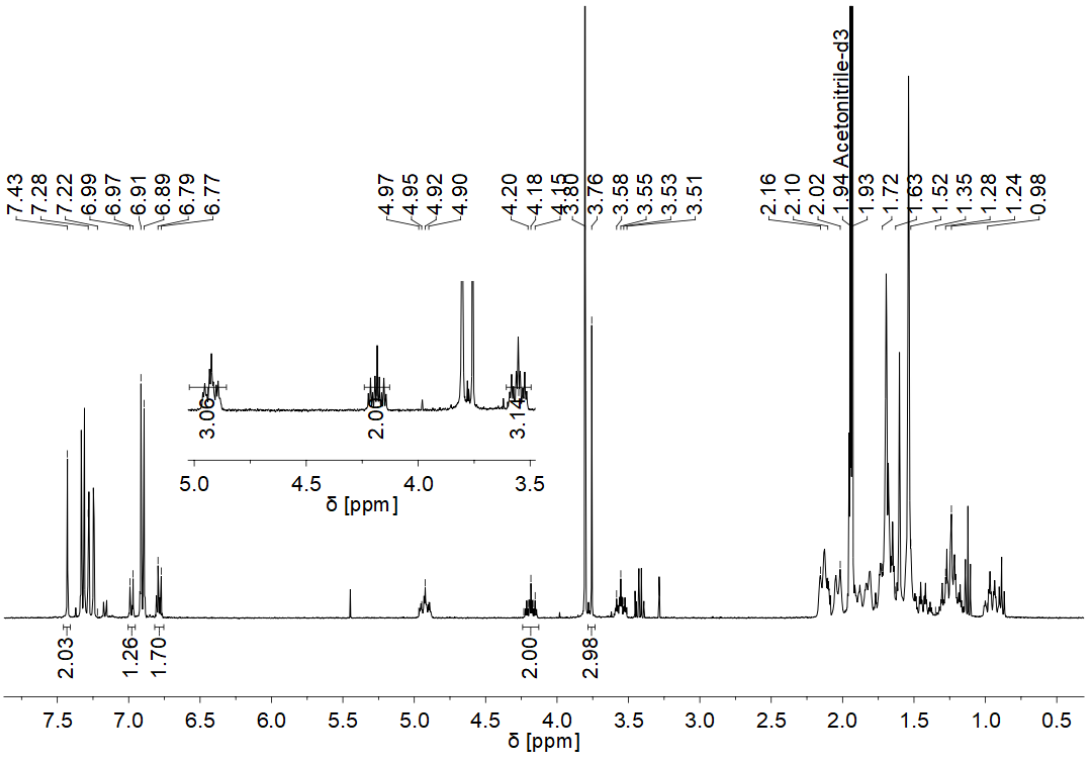

Figure A 162: ^{1}H NMR spectrum of **Mo-85** in MeCN-d3. Integrated signals are assigned to the TBP (trigonal bipyramidal) structure. Not all resonances could unambiguously be assigned.

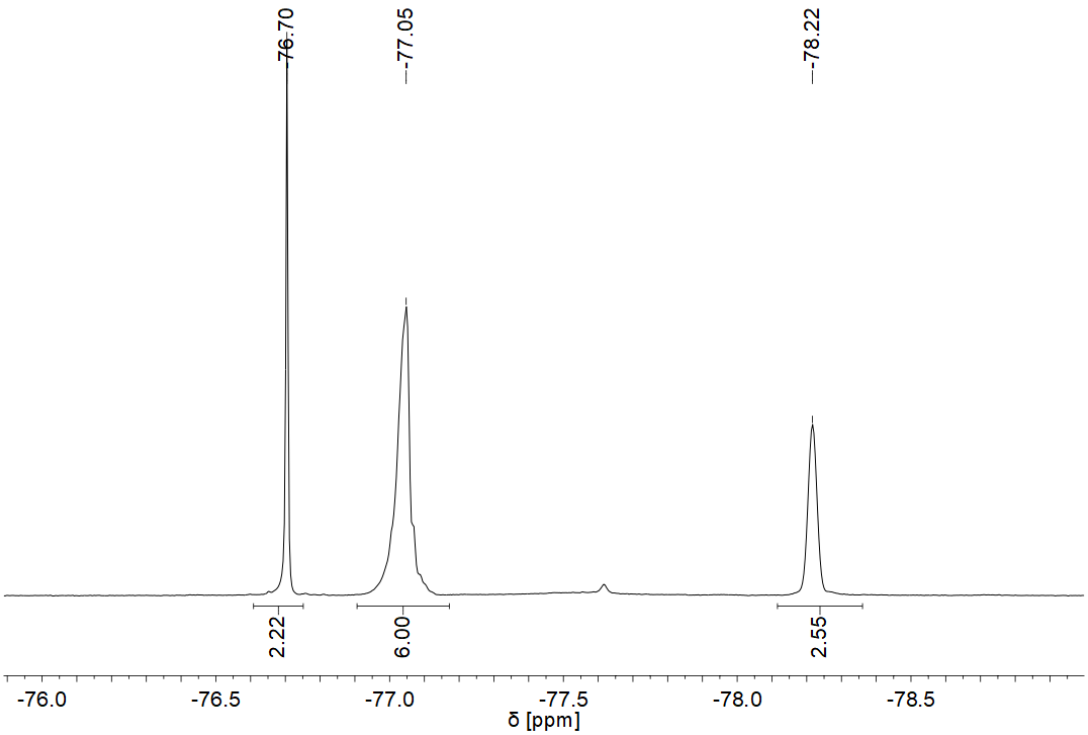

Figure A 163: ^{19}F NMR spectrum of **Mo-85** in MeCN-d3. Resonance at δ = -76.7 ppm is assigned to the TBP (trigonal bipyramidal) structure.

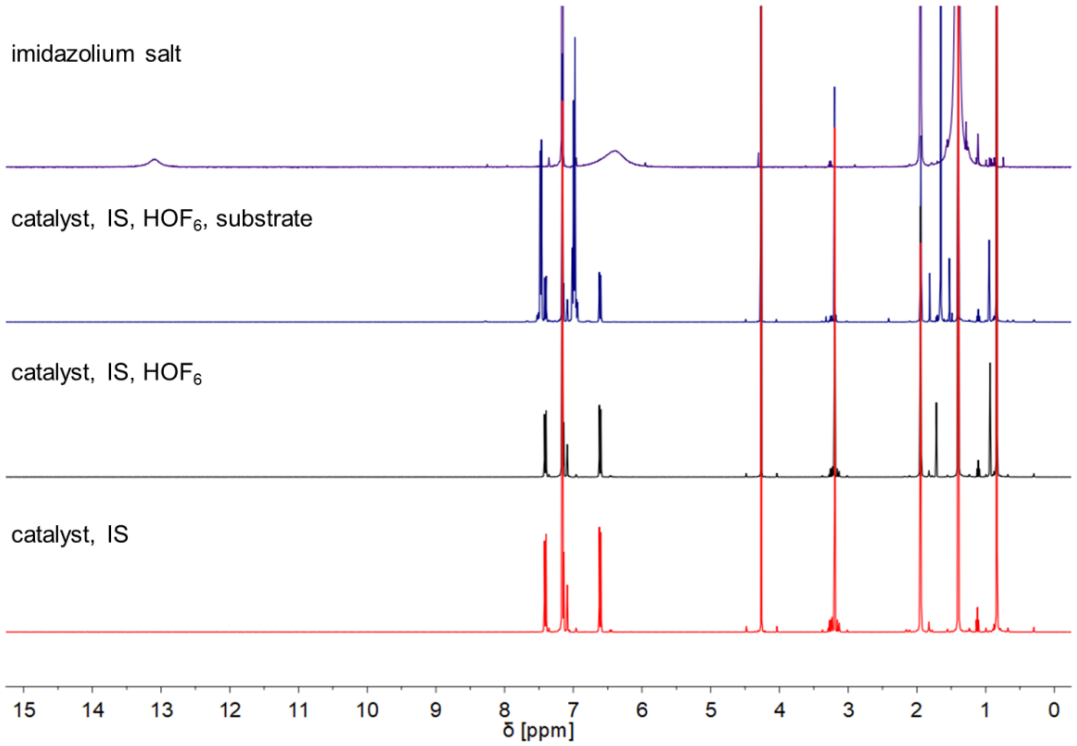

Figure A 164: ^{1}H NMR spectra in C_6D_6. Catalyst: **Mo-86**. Bottom (red): Catalyst and internal standard (IS). Middle bottom (black): Catalyst, IS and hexafluoro-*tert*-butanol (HOF_6). Middle top (blue): Catalyst, internal standard, HOF_6 and substrate. Top (violet): Corresponding imidazolium salt.

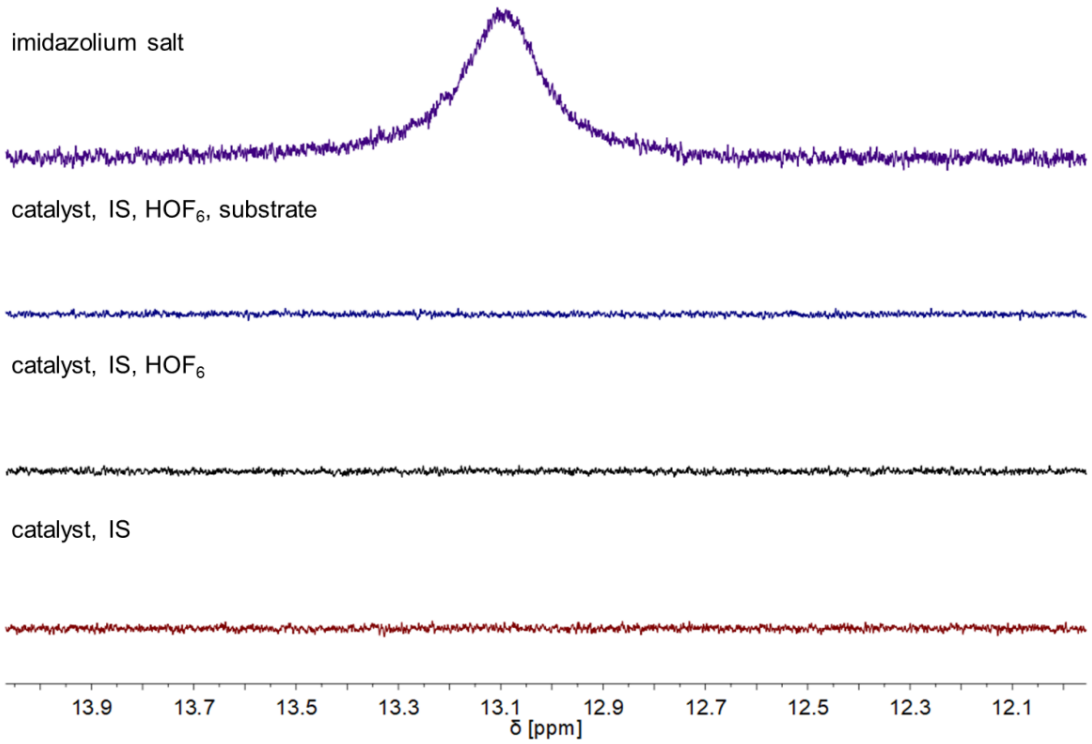

Figure A 165: Zoom into imidazolium proton region of stacked ^{1}H NMR spectra in C_6D_6. Catalyst: **Mo-86**. Bottom (red): Catalyst and internal standard (IS). Middle top (black): Catalyst, IS and hexafluoro-*tert*-butanol (HOF_6). Middle bottom (blue): Catalyst, internal standard, HOF_6 and substrate. Top (violet): Corresponding imidazolium salt.

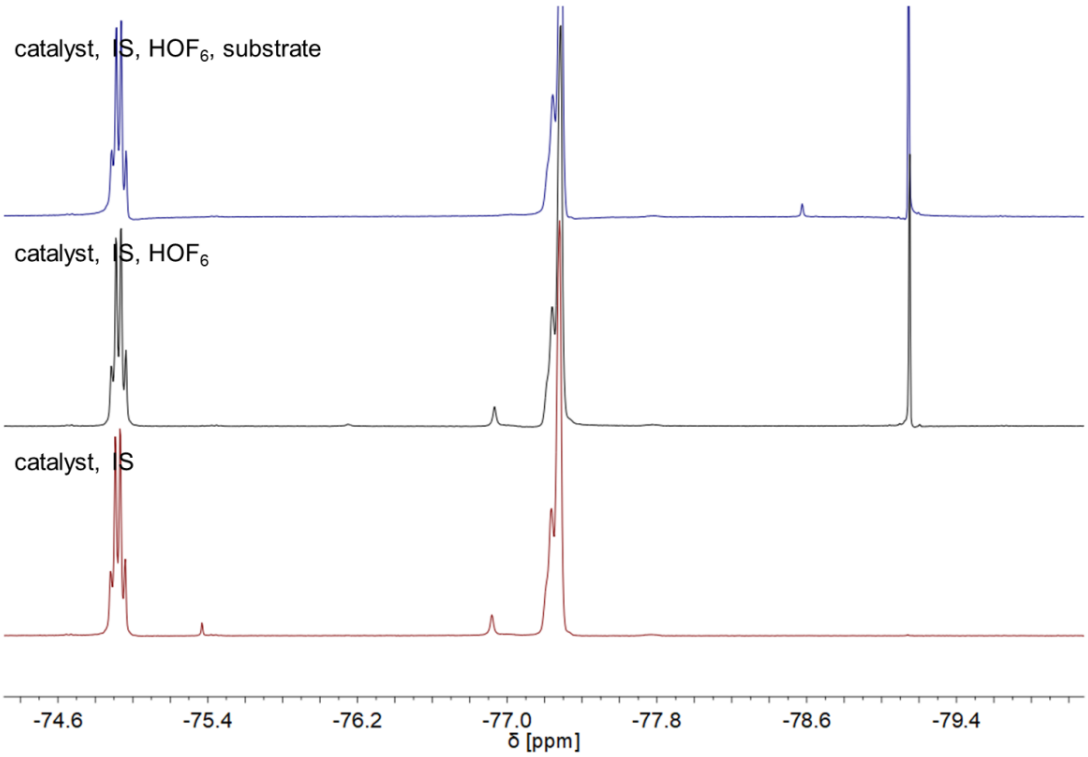

Figure A 166: ^{19}F NMR spectra in C_6D_6. Catalyst: **Mo-86**. Bottom (red): Catalyst and internal standard (IS). Middle (black): Catalyst, IS and hexafluoro-*tert*-butoxide (HOF_6). Top (blue): Catalyst, internal standard, HOF_6 and substrate.

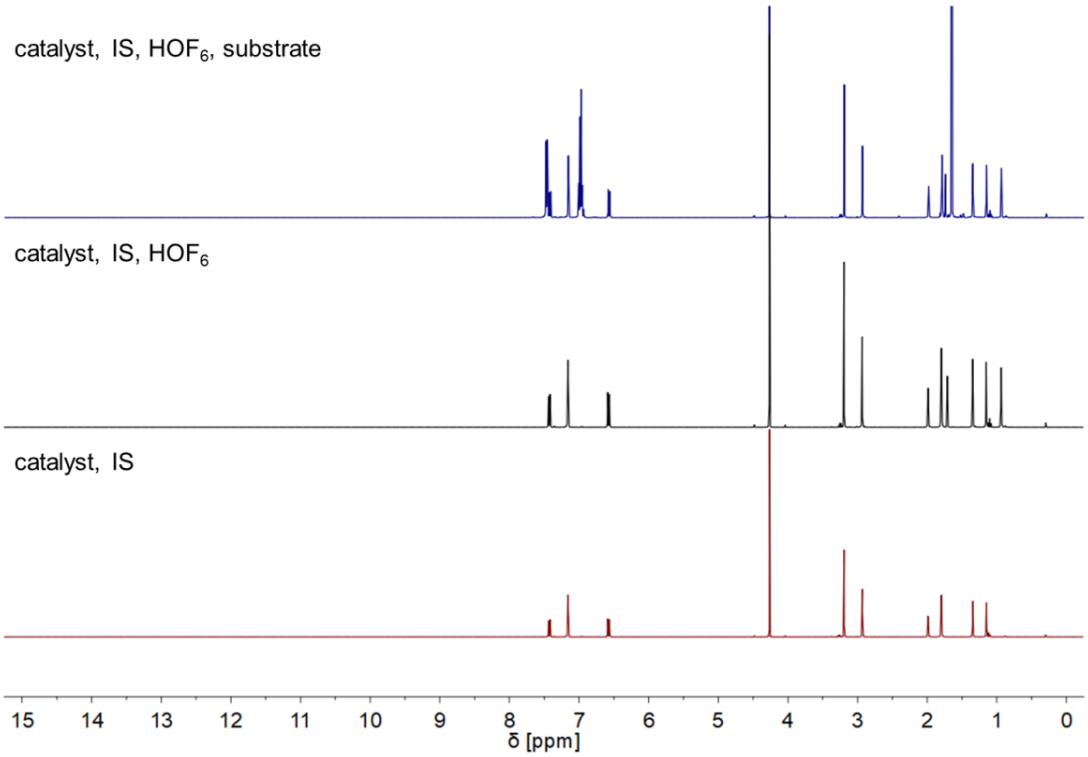

Figure A 167: ^{1}H NMR spectra in C_6D_6. Catalyst: **Mo-87**. Bottom (red): Catalyst and internal standard (IS). Middle (black): Catalyst, IS and hexafluoro-*tert*-butanol (HOF_6). Top (blue): Catalyst, internal standard, HOF_6 and substrate.

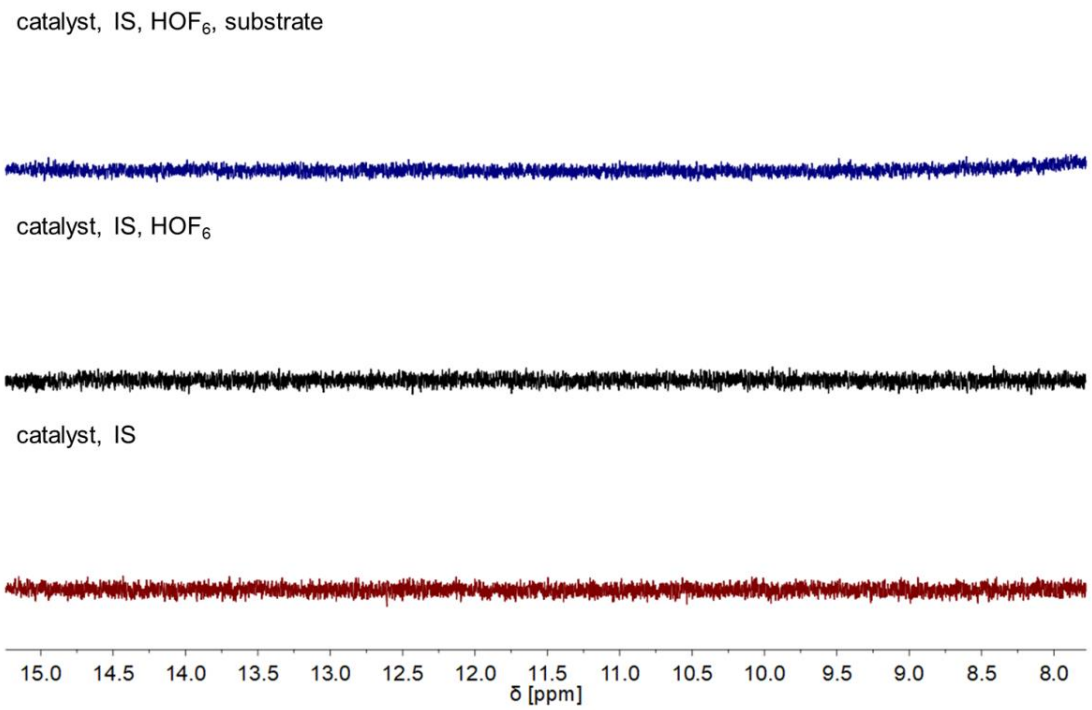

Figure A 168: Zoom into imidazolium proton region of stacked ^{1}H NMR spectra in C_6D_6. Catalyst: **Mo-87**. Bottom (red): Catalyst and internal standard (IS). Middle (black): Catalyst, IS and hexafluoro-*tert*-butanol (HOF_6). Top (blue): Catalyst, internal standard, HOF_6 and substrate.

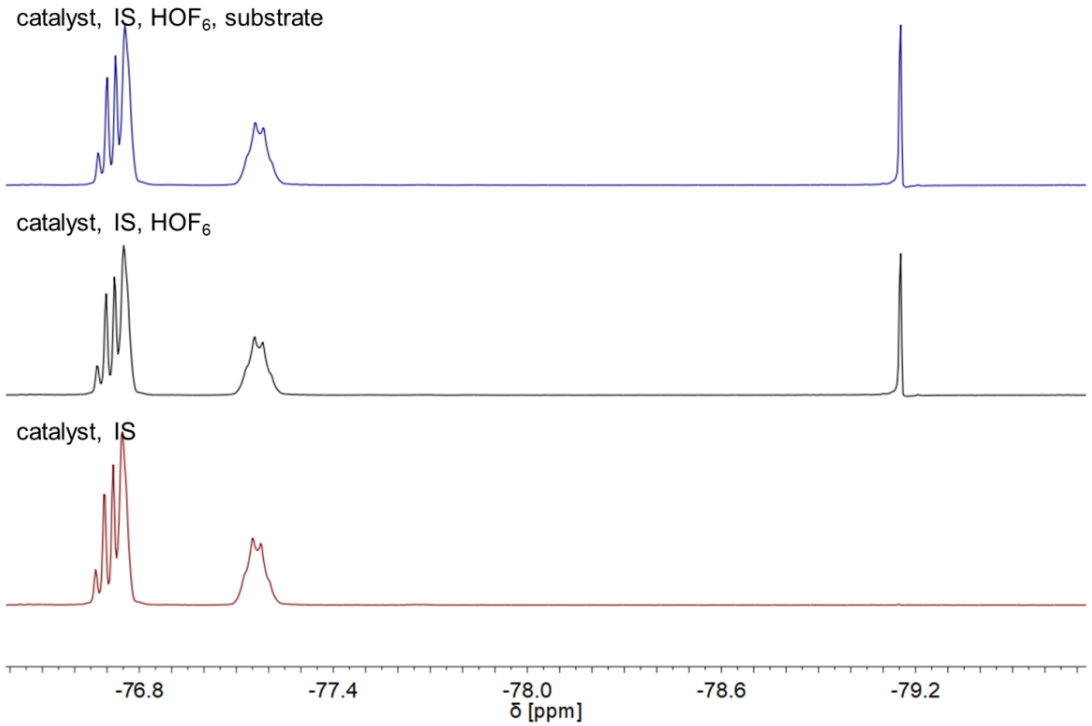

Figure A 169: ^{19}F NMR spectra in C_6D_6. Catalyst: **Mo-87**. Bottom (red): Catalyst and internal standard (IS). Middle (black): Catalyst, IS and hexafluoro-*tert*-butoxide (HOF_6). Top (blue): Catalyst, internal standard, HOF_6 and substrate.

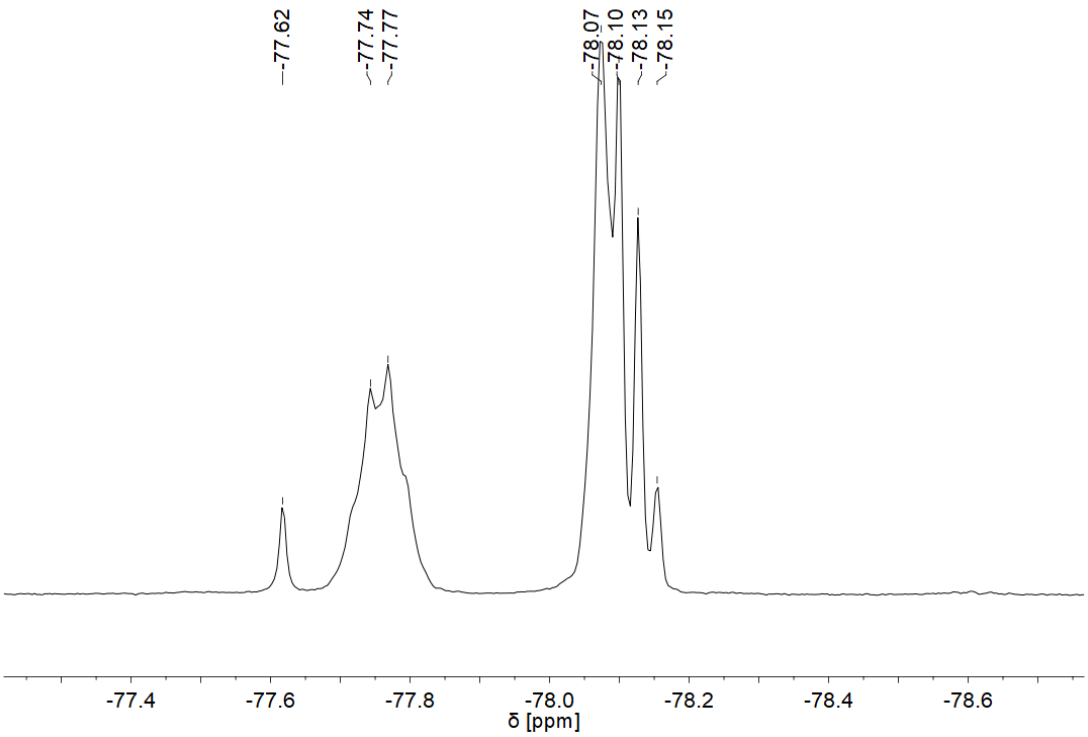

Figure A 170: ^{19}F NMR spectrum of **Mo-87** in MeCN-d3.

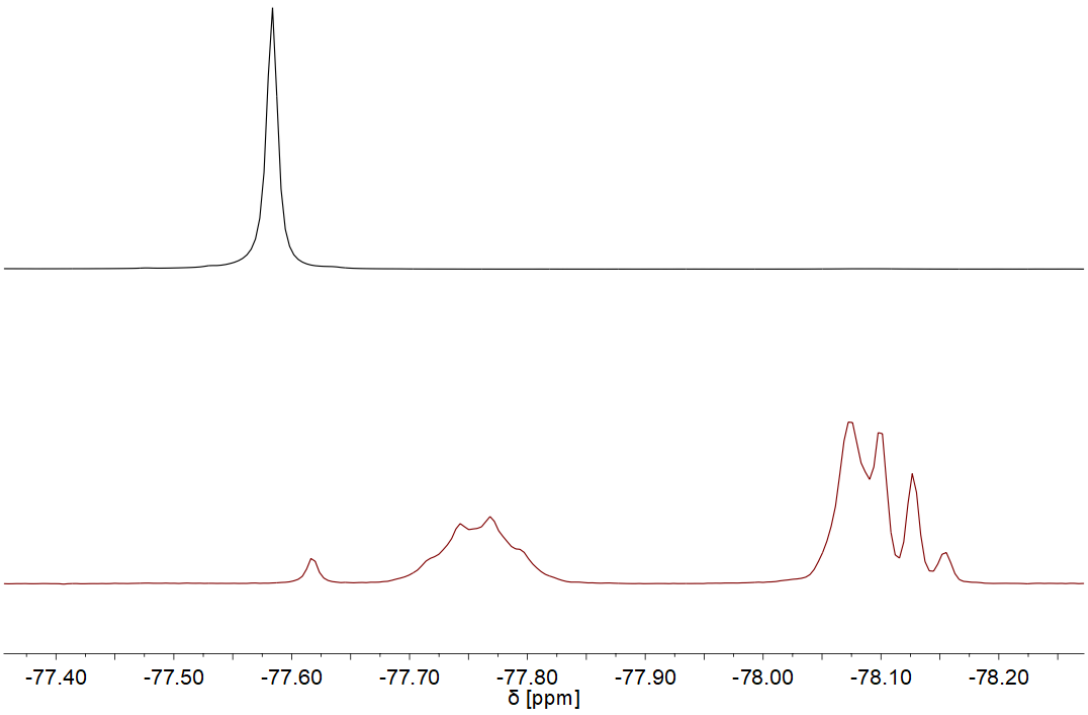

Figure A 171: Stacking of ^{19}F NMR spectra in MeCN-d3. Bottom (red): **Mo-87**. Top (black): **Mo-P11**.

9.6 CURRICULUM VITAE

IRIS ELSER

PROFILE

Ph. D. student at the Institute of Polymer Chemistry, University of Stuttgart, Germany, under the supervision of Professor M. R. Buchmeiser since 2014. Research focus on *organometallic chemistry*, *polymer chemistry* and *catalysis*.

PERSONAL DATA

Name	Iris Elser
Date of Birth	10.07.1989
Place of Birth	Stuttgart, Germany

SCIENTIFIC EDUCATION AND RESEARCH EXPERIENCE

Since 04/2014	Ph.D. student at the Institute of Polymer Chemistry in the group of Professor Dr. M. R. Buchmeiser at the University of Stuttgart, Germany. Focus on ionic metathesis catalysts for various applications.
12/2013	Final Degree: Master of Science (Chemistry) Final Mark: 1.2 (excellent with distinction)
06/2013 – 12/2013	Master Thesis at the Institute of Polymer Chemistry, University of Stuttgart, Germany, under the supervision of Professor Dr. M. R. Buchmeiser. "*Synthesis of Chiral Ionic Ligands for Schrock Type Catalysts*" Final Mark: 1.0
10/2011 – 03/2013	Studies in Chemistry (Master of Science) at the University of Stuttgart, Germany, with a focus on "*Advanced Synthesis and Catalysis"*.
09/2011	Final Degree: Bachelor of Science (Chemistry) Final Mark: 1.5 (excellent)
04/2011 – 08/2011	Bachelor Thesis at the Institute of Polymer Chemistry, University of Stuttgart, Germany, under the supervision of Professor Dr. M. R. Buchmeiser. "*Diazo-Chelated Initiators for ROMP*" Final Mark: 1.1
10/2008 – 03/2011	Studies in Chemistry (Bachelor of Science) at the University of Stuttgart, Germany.

09/1999 – 06/2008	Certificate of General University Qualification Hegel- Gymnasium, 70563 Stuttgart, Germany Final Mark: 1.5

WORKING EXPERIENCE

Since 2014	Supervision of students during their Bachelor thesis
	Teaching assistant in practical courses for Master students in macromolecular chemistry and Bachelor students in basic chemistry

SCIENTIFIC PUBLICATIONS

PUBLICATIONS

2017	"*High Oxidation State Molybdenum N-Heterocyclic Carbene Alkylidyne Complexes: Synthesis, Mechanistic Studies and Reactivity*" M. Koy, I. Elser, J. Meisner, W. Frey, K. Wurst, J. Kästner, M. R. Buchmeiser, *Chem. Eur. J.* **2017**, *23*, 15484-15490.
2017	"*Molybdenum and Tungsten Imido Alkylidene N-Heterocyclic Carbene Complexes Bearing Cationic Ligands for Use in Biphasic Olefin Metathesis*" I. Elser, R. Schowner, W. Frey, M. R. Buchmeiser*, Chem. Eur. J. **2017**, 23,* 6398- 6405.
2017	"*First Neutral and Cationic Tungsten Imido Alkylidene N-Heterocyclic Carbene Complexes*" D. A. Imbrich, I. Elser, W. Frey, M. R. Buchmeiser, *ChemCatChem* **2017**, *9*, 2996- 3002.
2016	"*Molybdenum Imido Alkylidene Complexes Containing N- and C-Chelating N-Heterocyclic Carbenes*" I. Elser, W. Frey, K. Wurst, M. R. Buchmeiser, *Organometallics* **2016**, *35*, 4106- 4111.
2013	"*Ruthenium- Triazene Complexes as Latent Catalysts for UV-Induced ROMP*" D. Wang, J. Unold, M. Bubrin, I. Elser, W. Frey, W. Kaim, G. Xu, M. R. Buchmeiser, *Eur. J. Inorg. Chem.* **2013**, 31, 5462- 5468.

POSTER PRESENTATIONS

2017	"*Molybdenum Imido Alkylidene Complexes with N- and C- Chelating N- Heterocyclic Carbenes*" I. Elser, W. Frey, K. Wurst, B. Kordes, M. R. Buchmeiser, ISOM XXII (International Symposium on Olefin Metathesis and Related Chemistry), Zürich, Switzerland.

2017 "*Synthesis of Molybdenum and Tungsten Imido Alkylidene NHC Complexes Bearing Betaine Type Ligands*" I. Elser, R. Schowner, W. Frey, M. R. Buchmeiser, 50. Jahrestreffen Deutscher Katalytiker, Weimar, Germany.

ORAL PRESENTATIONS

2017 "*Ionic Metal Alkylidenes for Biphasic Metathesis*" I. Elser, R. Schowner, W. Frey, M. R. Buchmeiser, TOCUS, Stuttgart, Germany.

2017 "*Ionic Group 6 Metal Alkylidenes. Olefin Metathesis in Biphasic Reaction Media*" I. Elser, R. Schowner, W. Frey, M. R. Buchmeiser, ISOM XXII (International Symposium on Olefin Metathesis and Related Chemistry), Zürich, Switzerland.